Variable Amplitude Corrosion Fatigue

and

Fracture Mechanics of Weldable High Strength Jack-Up steels

By

Linus Sone Etube

Thesis Submitted for The Degree of Doctor of Philosophy

Department of Mechanical Engineering

University College London

June 1998

0.1 ABSTRACT

The tubular welded joints used in the construction of Offshore structures can experience millions of variable amplitude wave induced stress cycles during their operational life. Fatigue has been identified as the main cause of degradation of structural integrity in these structures. As a result, fatigue is an important consideration in their design.

Jack-up legs are made from a range of high strength steels with yield strengths up to 700MPa. These steels are thought to exhibit fatigue resistance properties which are different when compared with conventional fixed platform steels such as BS 4360 50D and BS 7191 355D. The difference in their behaviour was heightened by the discovery, in the late 80s and early 90s, of extensive cracking around the spud can regions of several Jack-ups operating in the North Sea. It was thought that these steels may be more susceptible to hydrogen cracking and embrittlement. There was the additional requirement to study their behaviour under realistic loading conditions typical of the North Sea environment.

This thesis contains results of an investigation undertaken to assess the performance of a typical high strength weldable Jack-up steel under realistic loading and environmental conditions. Details of the methodology employed to develop a typical Jack-up Offshore Standard load History (JOSH) are presented. The factors which influence fatigue resistance of structural steels used in the construction of Jack-up structures are highlighted. The methods used to model the relevant factors for inclusion in JOSH are presented with particular emphasis on loading and structural response interaction.

Results and details of experimental variable amplitude corrosion fatigue (VACF) tests conducted using JOSH are reported and discussed with respect to crack growth mechanisms in high strength weldable Jack-up steels. Different fracture mechanics models for VACF crack growth prediction are compared and an improved generalised methodology for fast assessment of Offshore structural welded joints is proposed.

To my family

0.2 ACKNOWLEDGEMENTS

I wish to express my deep appreciation for the many fine suggestions offered by the following people from the onset of this research programme.

Firstly, I would like to thank Dr. F P Brennan and Prof. W D Dover for the invaluable supervision and guidance they have given me from the start of this study. Their stimulating discussions are invaluable and I thank them for being my teachers.

I would like to thank everyone in the Department of Mechanical Engineering especially my colleagues Peter Myers, Efrain Rodriguez Sanchez and Farid Ud-din. They all played an important role in providing the conducive environment under which this thesis was produced. The support given by the technical staff, Mr. F Arthur et al, is acknowledged. Their technical discussions and help during the installation of test specimens and general preparation for fatigue testing is highly appreciated.

TABLE OF CONTENTS

0.3 LIST OF TABLES

CHAPTER 1

CHAPTER 2

CHAPTER 3

CHAPTER 4

CHAPTER 5

0.4 LIST OF FIGURES

CHAPTER 1

CHAPTER 2

CHAPTER 3

CHAPTER 4

CHAPTER 5

0.5 NOMENCLATURE

ACPD	Alternating Current Potential Difference
Ag/AgCl	Silver/Silver Chloride reference electrode
AVS	Average Stress
MAVS	Modified Average Stress
TPM	Two Phase Model
SCF	Stress Concentration Factor
UKOSRP	United Kingdom Offshore Steels Research Project
UKCS	United Kingdom Continental Shelf
CLI	Creusot Loire Industrie
UEG	Underwater Engineering Group
UCL	University College London
UTS	Ultimate Tensile Strength
FEA	Finite Element Analysis
JOSH	Jack-up Offshore Standard Load History
WASH	Wave Action Standard History
OPB	Out-of-Plane Bending
PSD	Power Spectral Density (Spectrum)
IPB	In-Plane Bending
CP	Cathodic Protection
L	Tubular joint chord length
D	Tubular joint chord diameter
T	Tubular joint chord thickness
t	brace thickness or time or plate thickness (defined where applicable)
$\alpha, \beta, \gamma, \tau, \theta$	Tubular joint dimensional parameters (except where otherwise defined)

α	Twice the ratio of chord length to chord diameter (2L/D)
β	Ratio of brace diameter to chord diameter (d/D)
γ	Ratio of chord diameter to twice chord thickness (D/2T)
τ	Ratio of brace thickness to chord thickness (t/T)
θ	Angle around tubular joint chord/brace intersection
$\sqrt{Q'_\beta}$	UEG diameter ratio modifying parameter
$\sqrt{Q'_\gamma}$	UEG short chord modifying parameter
ϕ	Angular position or angle of inclination
S, ΔS, $\Delta\sigma$	Stress range
σ_y	Yield strength
N, N_1, N_3	Life (Number of cycles), Initiation life, Through thickness life
D_s	Miners cumulative damage ratio
C, m	Paris law material constants
C_j, m_j	Paris law material constants for a multi-segment da/dN curve
da/dN	Crack growth rate
ΔK	Stress intensity factor range
K_{max}, K_{min}	Maximum and minimum stress intensity factors
a, c	Crack depth (except where otherwise defined), half surface crack length
a_o, a_i	Initial crack depth
a_f	Final crack depth (Except where otherwise defined)
Y(a), Y	Stress intensity factor correction function (Y factor)
K_{ISCC}	Stress intensity factor for stress corrosion cracking
ΔK_{th},	Threshold stress intensity factor range,
ΔK_{eff}	Effective stress intensity factor range
I	Irregularity factor

ε	Spectral bandwidth parameter
S_h, S_{hi}	Equivalent stress, equivalent stress for sea state *i*
erf(x)	Error function of x
$\Gamma(x)$	Gamma function of x
σ	Root Mean Square (RMS) value
K_{IC}	Critical mode I stress intensity factor
H_s, T_D, T_z	Significant wave height, Dominant period, Mean zero crossing period
H_r, T_r, Ω	Non dimensional wave height, Period and frequency ratios
f, f_n, f_p	Frequency, Natural frequency, Peak frequency
$f_{n\beta}$, f_β, Ω_β	Frequency corrected non dimensional parameters
$H_{s\,ext}$, $T_{z\,ext}$	Extreme sea state parameters
$\Phi(f)$	Stress spectrum given by Wirsching's equation
A, φ	Scaling parameters (except where otherwise defined)
$S(f)_N$	Normalised response spectrum
ξ	Damping ratio
C_D, C_m	Drag coefficient, mass coefficient
ν, G, E	Poisson's Ratio, Shear Modulus, Young's Modulus
R	Spudcan radius or chord radius (defined where applicable)
P(x), p(x)	Exceedance of variable x, Probability of occurrence of variable x
Δ, Vc, Vr,	ACPD probe spacing, crack voltage, reference voltage.
M_x d_1	ACPD crack depth modifier, One dimensional ACPD solution
ψ	Crack shape correction (CSC) factor
C_p, p	Empirical retardation parameter, shaping parameter
σ_{op}, K_{op}	Crack tip opening stress, Stress intensity factor corresponding to σ_{op}
M_i	i^{th} spectral moment
S_B, t_B y	Thickness effect parameters

CHAPTER 1

1. LITERATURE REVIEW

1.1 BACKGROUND AND INTRODUCTION TO THESIS

In recent years there has been considerable interest in the use of high strength steels in the construction of Offshore structures. One main reason for this is to satisfy the desire for light weight. This is particularly relevant to Offshore structures because a reduction in weight can lead to the achievement of considerable saving in support substructure. There are other potential benefits to be derived from the use of high strength steels. Fabrication costs for example can be minimised by using reduced plate thicknesses.

Historically, high strength steels have been more extensively used in the fabrication of Jack-up structures when compared with fixed platforms. However the potential benefits of using high strength steels have been recognised by the Offshore industry and a recent review [1.1] has shown that the proportion of higher strength steels used in fixed Offshore structures had gone up to 40% by 1995. This is a five fold increase when compared to 8% in 1988. It is important to note that most of the high strength steels used in fixed structures are limited to topside applications and other less critical parts of the jacket structure where fatigue damage is not a major concern.

This situation is however different for Jack-up platforms which have traditionally been used for short term drilling and maintenance operations. These structures are now being increasingly used as production platforms for marginal field development and in recent designs, extended periods at the same elevation in their fatigue design philosophy are included. BP Harding is a typical example of these new generation of Jack-up platforms. It is designed to operate in a water depth of 100 meters with an intended service life of 35 years.

The main use of high strength steels in Jack-up structures is in the fabrication of the legs. Steels with nominal yield strength in the range of 450 to 700 MPa have commonly been used. The detailed leg structure will vary from one type of Jack-up to another. A review of different designs is presented in [1.2]. In this review the structures were classified according to the Jack-up design, some of which included Le Tourneau, CFEM, MSC, Friede & Goldman and Hitachi designs. In general, each

lattice leg (figure 1.1) is made of three or four longitudinal chord members which may contain a rack plate (figure 1.2) for elevating the hull and a series of interconnecting horizontal and diagonal tubular members (figure 1.3). In some designs, supplementary braces are frequently used between main brace mid-points to increase the buckling resistance of the structure and to provide adequate structural redundancy.

There has been a remarkable increase in the overall size of these structures recently. The main reason for this is to satisfy the requirement to operate in deeper waters in predominantly harsher sectors of the North Sea and world wide. Several Jack-ups are now used for production. This new role requires long term deployment and therefore has significantly limited the opportunity for dry dock inspection and repair where necessary. This has increased the risk of deterioration from long term problems such as fatigue.

The vast majority of research, on the fatigue performance of tubular welded joints, carried out by the Offshore industry [1.3, 1.4] has been focused on conventional fixed Offshore platform steels such as BS 4360 50D [1.5] and BS 7191 355D [1.6] with typical yield strengths in the region of 350 MPa. Fatigue data on higher strength tubular joints is therefore very limited and this has been highlighted in recent reviews [1.2, 1.7]. Consequently the fatigue design guidance that has been developed to date is not applicable to high strength steels and this is reflected in the new guidance published in 1995 [1.8]. In the document the basic design curve is restricted to steels with guaranteed yield strengths of up to 400 MPa for nodal joints and 500 MPa for welded plate connections.

This absence of sufficient guidance on the use of high strength steels Offshore and the lack of fatigue data on high strength steels, in parallel with the increased proportion of higher strength steel grades used in Offshore applications has been the subject of much discussion and concern among academics and the Offshore industry. This concern was strengthened by the discovery of extensive cracking in the spud can region of Jack-ups operating in the United Kingdom Continental Shelf (UKCS) in the period of 1988-1989 [1.9, 1.10]. After the investigation reported in [1.9, 1.10], it was generally accepted that high strength steels are more susceptible to corrosion fatigue

and hydrogen induced stress corrosion cracking (HISCC) when compared with conventional fixed platform steels. The main conclusion drawn from the investigation was that, the generation of hydrogen from the sacrificial anode systems protecting high strength steel structures at levels which are excessively negative (i.e. <-850mV Vs Ag/AgCl), can enhance fatigue crack growth and should be avoided.

Fatigue performance of high strength steels is subject to uncertainty and there is need to investigate their performance further. This will allow the designers of high strength steel marine structures to use these materials with greater confidence. Two principal sources of this uncertainty for high strength Jack-up steels lie in the effect of cathodic protection and variable amplitude corrosion fatigue. An investigation of the effect of cathodic protection on the fatigue performance of a typical high strength Jack-up steel under constant amplitude loading conditions is reported in [1.11]. The study presented in this thesis was aimed at investigating the fatigue performance of the same steel, SE 702 [1.12], under realistic loading and environmental conditions with particular emphasis on the effects of variable amplitude loading under cathodic protection conditions.

The thesis is laid out in six Chapters. The remainder of Chapter 1 contains a review of the current state of knowledge in the fatigue design of Offshore welded structures with particular emphasis on variable amplitude corrosion fatigue.

A Jack-up Offshore Standard load history (JOSH) was developed as part of this investigation. The methodology adopted and how the different factors which affect the fatigue performance of Jack-up steels are modelled and represented in JOSH is presented in Chapter 2.

Chapter 3 follows on to present details of the large scale fatigue testing programme conducted on Y-joints (figure 1.4) using the simulated service loading history, JOSH. The results obtained are presented in this Chapter in the form of fatigue crack initiation and propagation behaviour and S-N data. The results obtained from SE 702 are compared with those obtained from other high strength steels and conventional fixed platform steels such as BS 4360 50D.

Fracture Mechanics (FM) analysis of results are presented in Chapter 4. In this Chapter existing FM models are compared with experimental data and the inherent limitations of the models when applied under variable amplitude conditions are identified.

A generalised fracture mechanics approach for the assessment of fatigue crack growth in high strength steel Offshore installations is proposed and presented in Chapter 5.

The thesis is concluded in Chapter 6 with a statement of the main findings and recommendations from this study. Further work which will add to the existing body of knowledge in this field is also identified and highlighted in Chapter 6.

1.2 REVIEW

Stress analysis for a part containing a crack or crack-like defect and a failure model hypothesis which defines the events of crack extension are the two central ingredients for a fracture theory. This statement emphasises the importance of stress analysis in the process of implementing any fracture mechanics methodology for the assessment of fatigue crack growth. Stress analysis is also a very important step in the design process for Offshore structures as it provides vital information on the level and distribution of critical stresses in each component of the structure. The distribution and level of stresses is important in both stress-life (S-N) and fracture mechanics based methods used both at the design stage and during structural integrity assessment procedures.

This Chapter is concerned with a literature review of appropriate topics related to structural assessment. It is dedicated to the important subjects of stress analysis, fatigue design and the role of variable amplitude corrosion fatigue in the failure of welded connections used in the fabrication of Offshore structures such as Jack-up platforms. It looks at the main sources of stresses in welded joints and reviews the different stress analysis techniques available to the designer for their estimation. The current practice on the design of Offshore welded connections using both S-N analysis

and fracture mechanics is reviewed and the implications of some of the recommendations from the existing design codes are discussed.

1.3 STRESS ANALYSIS OF TUBULAR WELDED JOINTS

Offshore structures are made from welded tubular joints of varying complexity with respect to both size shape and load carrying capacity. These joints can be loaded in any combination of three modes which include axial loading, out-of-plane or in-plane bending (see figure 1.5). Due the complexity of joint geometry and shell behaviour of welded tubular joints which govern load response, local stresses are non uniformly distributed. This non uniform distribution of stress has been demonstrated to occur both on the tubular joint surface and also through the joint thickness. Non uniform stress distribution leads to the existence of stress gradients and sites of stress concentrations, mostly along the chord and brace weld toes. These stress concentration sites represent regions where fatigue cracks are known to originate and propagate to cause structural failure. As an integral step in the design and assessment of Offshore structural components, stress analysis is carried out to determine both the location and magnitude of these critical stresses. This section presents a definition of the stresses involved and the methodologies employed in determining the characteristic stress which is considered to control the fatigue life of tubular welded joints. Great emphasis is placed on experimental techniques and the use of parametric equations.

1.3.1 Definition of Stresses in Welded Connections

In both stress-life (S-N) and fracture mechanics based methodologies for fatigue crack growth analysis, critical stresses have to be determined for each component of the structure. Three main sources of stress have been identified in tubular welded joints: Nominal stresses, geometric stresses and notch stresses.

Nominal stresses arise due to the tubes of the welded joint behaving as beams and columns. These stresses can be calculated by considering the mechanism of load transfer through each tube and intersection using frame analysis and beam bending theory. The nature of such stresses will depend entirely on the dimensions of the joint and the mode of loading.

Geometric stresses on the other hand arise as a result of differences in the load response of braces and chords under the loading configuration. It is known that geometric stresses may cause the tube wall to bend in order to ensure compatibility in the deformation of the chord and brace around the intersection depending on the mode of loading.

A third component of stress in tubular welded joints is due to *notch stresses.* Notch stresses arise from the notch effect or geometric discontinuity of the tube walls introduced by abrupt change in section at the weld toe. These stresses are also commonly referred to as *local stresses* and are a function of weld size and geometry. The greater the weld toe radius and the greater the overall angle of the weld toe, the more restraint there is on localised deformation and the higher the magnitude of local stresses. Unlike nominal and geometric stresses, notch or local stresses are not propagated far through the wall thickness and therefore the resulting three dimensional stress field is highly localised. Due to the complexity and the variety of joint geometries used in the construction of Offshore structures, the weld toe geometry (i.e. the weld toe radius and angle) can not be made identical for each joint configuration. It has been noted [1.13] that even with very tight quality control strategies in manufacturing yards, weld profiles in Offshore structures can not be controlled to such a degree that will lead to consistency in the distribution of notch stress concentrations in tubular joints. These stresses are therefore difficult to measure in a reproducible manner by any criteria. The consequence of this has been the adoption of a characteristic stress for the development of S-N curves. This characteristic stress is known as the *hot spot stress.*

1.3.2 Definition of Hot Spot Stress

The hot spot stress is considered to control the complete fatigue life of a tubular welded joint. It is the stress at the weld toe calculated by manner of a linear extrapolation to the weld toe of the geometric stress. The definition is illustrated in figure 1.6. The hot spot stress excludes the contribution to the stress concentration caused by the notch effect of the weld geometry. This definition is not stated very clearly in many design codes [1.14] and can result in misinterpretation of this important parameter depending on the code used.

The definition of hot spot stress is not clear cut in the DnV rules for the design and construction of Offshore structures [1.15]. The document states that, stress concentration factors may be obtained from relevant tests or analysis. It also indicates that "different stress components may be associated with different SCFs. Different location of 'hot-spots' for the different stress components may be taken into account if relevant documentation on the locations is available". This code also requires the SCF not to be less than 2.5 but fails to emphasise the need for it to be calculable and experimentally reproducible

Another document which attempts to impose a limiting value to the minimum SCF is that produced by Lloyds Register of Shipping [1.16]. Compared to the minimum value of 2.5 recommended by DnV, this document requires that the SCF values are limited to a minimum of 1.5. It also recommends the use of empirical formulae proposed by Wordsworth and Smedley for calculating the brace and chord SCFs for T and X joints while the semi-empirical formulae due to Kuang are recommended for K and KT joints. This document has its limitations regarding the definition of hot-spot stress as it does not spell out the need for the hot-spot stress to incorporate the effects of the overall chord and brace geometry including the stiffening effects of the weld without the influence of the region of rapidly increasing and highly variable non experimentally determinable stress near the weld toe. For particular cases where, due to the joint geometry or loading mode or a combination of both, a particular joint falls outside the validity limits for the formulae indicated above, Lloyds allows the use of estimates for SCFs using equations derived from the punching shear formulae given

for static strength in API RP2A [1.17] and recommends a limiting minimum value of 1.5.

The American Petroleum Institute-RP2A [1.17] defines hot spot strain as "that which would be measured by a strain gauge element adjacent to and perpendicular to the toe of the weld, after stable strain cycles have been achieved". Using this definition the hot spot strain is taken as the absolute peak value obtained by a strain gauge placed near the weld toe. This value is clearly a combination of geometric and notch stresses and is bound to vary from joint to joint depending on the mode of loading. This definition does not therefore offer the necessary consistency required for determining SCFs in tubular welded joints.

The American Welding Society Structural Welding Code AWS D1.1-84 [1.18], offers a different definition of hot spot stress or strain. This design code states that the hot-spot stress or strain is "... stress or strain on the outside surface of intersecting members at the toe of the weld joining them-measured after shakedown in model or prototype connection or calculated with best available theory". This code, like API-RP2A recommends the use of the finite element analysis method to obtain hot-spot stress.

The Norwegian Petroleum Directorate Design rules are even less specific in their definition of hot-spot stress or hot-spot stress concentration factor [1.19]. This code only indicates that the appropriate hot-spot stress for a particular joint should be calculated from the product of the relevant stress concentration factor and the nominal stress.

The British Standard, BS 6235(1982) [1.20] now withdrawn, states that the hot-spot stress or stress concentration factor should be determined by accepted practice. It recommends the use of finite-element analysis, published parametric equations or experimental methods to obtain the hot-spot stress. This standard although now withdrawn presented a significant deviation, though not explicitly from other design codes, in that it implied that the hot-spot stress refers to local deformation stress or geometric stress and not influenced by notch stresses arising from the concentrating

effect of the weld profile. This is the definition that has been adopted as an Offshore standard for stress analysis of Offshore tubular welded joints.

The UK Department of Energy Guidance notes give a clearer definition of hot-spot stress as [1.21], "The greatest value around the brace/chord intersection of the extrapolation to the weld toe of the geometric stress distribution near the weld toe. This hot-spot stress incorporates the overall effects of joint geometry (i.e. the relative sizes of brace and chord) but omits the stress concentrating influence of the weld itself which results in a local stress distribution". This definition of hot-spot stress was a subject of discussion in the United Kingdom Offshore Steels Research Project (UKOSRP) [1.3, 1.4] and was drafted by the review panel set up by the Department of Energy to asses the results of the research programme. It is still used in the latest UK guidance notes [1.8]. This definition of hot-spot stress is now accepted as an Offshore standard for stress analysis of Offshore tubular joints and was used in this study.

Though the guidance available on stress analysis of Offshore welded tubular joints may seem limited as presented above, there is a wide body of literature on stress analysis of tubular welded joints. The recommendations outlined in the codes above depend on the methodologies employed and the degree of accuracy required for any particular joint configuration and loading. These approaches to stress analysis range from classical theoretical methods, through experimental methods on steel and acrylic models to numerical computer intensive methods such as finite element analysis and those based on parametric equations. These categories are covered very briefly in the following section.

1.3.3 Methods of Stress Analysis

Through careful examination and analysis of considerable experimental and theoretical data which was obtained after major research projects into the behaviour of Offshore structures (such as the (UKOSRP), the hot-spot stress at the intersection of welded tubular joints has been accepted to govern fatigue endurance of Offshore structures.

Its determination and evaluation is therefore an important first step at both the design stage and also during structural integrity assessment programmes for Offshore structures.

Stress analysis of tubular welded connections is not the main subject of this thesis. However extensive experimental stress analysis was carried on the tubular welded Y-joints used in this study. The results from the study are presented in Chapter 3. It was felt that a critical look at the background and basic principles behind the development of other methods will assist in the comparison of the results presented in Chapter 3. This knowledge was also thought to represent a suitable platform from which any discrepancies between results obtained using different methods can be adequately explained.

Due to the complexity of joint shapes and the shell behaviour governing load response of tubular joints, stress analysis of tubular welded joint intersections is difficult but a wide range of techniques have been developed and employed in assessing Offshore structures. The methods vary in their degree of accuracy in modelling different geometries and loading cases. This section presents a review of these analysis techniques used to evaluate stresses for fatigue assessment of Offshore structures.

1.3.3.1 Theoretical Methods

A great part of the early analytical studies on stress analysis were based on some version of classical thin shell equations for cylindrical shells such as those presented by Donnel [1.22] and Flugge [1.23]. The first attempts to analyse tubular joints using theoretical methods started in the early part of the 50s and 60s when Bijlaard [1.24] and Toprac [1.25] respectively, used Roark's results to obtain the stress levels at the intersections of T and DT joints. Roark's results were in the form of empirical equations developed for stresses and deflection after studying cylinders subjected to diametrically opposed concentrated loading. Although his work was not directly concerned with tubular joints, his results were used by other researchers like Bijlaard and Toprac to make important contributions in this field. Bijlaard investigated the stresses and deflections in tubular chords caused by load transmitted through different

attachments. He studied T-joints under axial load and assumed that the load was transmitted radially to the chord and distributed uniformly over a square area.

Research in the area of stress analysis continued with important contributions from Hoff et al [1.26], Kempner et al [1.27] and Kellogg [1.28] who used an early analytical approach in 1956 and attempted to construct an analogy with the behaviour of a chord subjected to uniform circumferential line loads. Kellogg's results were later used by Marshall [1.29] to provide correlation for stresses in the chord and brace and he developed a simple method to calculate hot-spot stress.

In 1965, Dundrova [1.30] assumed that the chords were subjected only to forces directly parallel to the brace and obtained a more realistic representation of stresses in a T-joint by imposing compatibility of the displacements in the brace axial direction between the brace and chord. Even though her work did not model the effect of flexural rigidity of the brace wall at the intersection with the chord, it marked the first time the brace was included in the analysis. Her work represented the first nearly complete theoretical analysis that was available in the 60s.

Chen et al [1.31] followed up this approach by using cylindrical shell solutions for both the brace and chord. Their work yielded some good results for T and Y-joints after imposing compatibility of displacements at discrete points along the chord/brace intersection.

During stress analysis assessment of Offshore structures for fatigue evaluation, the distribution of stress around the intersection and also through the joint thickness may be required. Determination of this complex stress field is difficult through the use of theoretical methods especially due to the increasingly complex joint geometries encountered in Offshore structures today. As a result of this, useable theoretical solutions are not generally available even though they have been improved tremendously over the years. These methods have largely been superseded by the more robust numerical methods.

1.3.3.2 Numerical Methods

Several numerical methods were developed and used as early as 1955 through to the early 60s and by the late 60s, the classical solution methods by Kellogg [1.28], Bijlaard [1.24] and Caulkins [1.32] were well established.

Using an analogy of the behaviour of a circular cylinder, subjected to uniform circumferential loads, Kellogg developed a method of obtaining stresses in the chord. The Kellogg method was employed by computing the nominal stresses in the brace and treating this as a live load applied to the surface of the chord at the intersection. The stresses in the chord were then obtained by increasing the load intensity on the chord due to the axial forces in the brace by an appropriate factor and adding this to the load intensity on the chord due to bending stresses in the chord. The stresses obtained by using this method only relate to axial loads applied through the chord and under in-plane-bending conditions. It is therefore not appropriate for loading conditions which include out-of-plane bending. This method has been superseded by finite element analysis, however it is a very quick solution method.

Rodabaugh [1.33] used Bijlaard's theory in the late 70s to analyse K joints. Rodabaugh's results were published in 1980 and as pioneered by Bijlaard, he used a double series to represent displacements in both axial and hoop directions. However in order to increase accuracy, he used a large number of fourier terms in his analysis, 21 terms in the hoop direction and 81 terms in the axial direction. Due to the large number of terms required by this method to attain a higher level of accuracy, it was rather cumbersome at the time and was largely superseded by the more accurate finite element analysis methods.

Caulkins [1.32] published details of a computer program, FRAMETI, in 1968 which was used to analyse tubular joints. FRAMETI used membrane stress theory and cylindrical bending stress theory to evaluate brace and chord behaviour respectively. Different types of joint geometries and loading configurations were incorporated in this program. Which was capable of analysing T and Y-joints under all three modes of loading and K joints under axial loading. Again this is a limited range of joint geometries when compared with the rather wide variety encountered in a typical

Offshore structure. As a result the use of this program for assessing Offshore structures has also been superseded by finite element methods.

1.3.3.3 Finite Element Analysis

Finite element analysis (FEA) is an established technique for structural analysis and has developed very rapidly in recent years. Following the development of microprocessors with very high computing power, finite element analysis emerged in the late 60s and early 70s and has become the only feasible numerical technique for analysing tubular joints with complex geometries for which closed form theoretical solutions are difficult to obtain. The development of finite element analysis method lead to a greater effort being directed towards obtaining correlation methods, first provided by Beale and Toprac [1.34], for determining stresses and strains at intersections of tubular welded joints. The technique is based on the assumption that a complex structure can be discretised into small regular elements of finite size and geometry (finite elements) which can be analysed more easily. By using the appropriate boundary conditions at the nodes, such as compatibility of displacements, the whole structure can be analysed by considering the combined effects of load response of the individual elements in the structure.

The type of elements used will depend on the complexity of the structure or component to be analysed and the level of accuracy required. There are a number of different element formulations available for the analysis of tubular joints. These will not be discussed here but the different categories are outlined.

Facet shell/plate elements, Thin shell elements using Kirchoff assumptions, thin/thick shell elements based on Reissner-Mindlin theory, three dimensional elements and modified three dimensional elements are the widely used element formulations for the analysis of tubular joints. Finite element analysis was used to predict stresses in joints by Reber [1.35] in 1972, Kuang et al [1.36] in 1975, and Gibstein [1.37] in 1978

1.3.3.4 Experimental Methods

Most of the early information on the performance of tubular joints and tubular joint stress behaviour was obtained by experimental measurements on steel models. The increased Offshore activity in the North Sea in the 70s lead to an increased need to predict stresses in tubular joints more accurately and different approaches were being used to determine stresses in tubular welded joints using experimental methods. Experimental methods rely on the measurement of strain and hence stress concentration factors on scaled or full scale models. Experimental methods can be categorised, depending on the modelling medium, into those based on the use of steel models, acrylic models and photoelastic models.

The use of steel models for stress analysis of Offshore structural components is a well established technique. It is usually implemented by extensively strain gauging scaled down models or full-scale replica of tubular welded joints. This method was used extensively in the course of the United Kingdom Offshore Steels Research Project [1.3, 1.4] to study a wide range of T and K joints and the effect of varying their geometric parameters on their behaviour under different modes of loading. This method was used for stress analysis of Y-joints used in this study and a critical review of the method is presented here. Results from this study are presented in Chapter 3 and compared with those predicted by Parametric equations.

In order to attain a high level of correlation with measurable stresses and strains encountered in a typical Offshore structure, steel tubular joints used for stress analysis must be fabricated to standard Offshore procedures to obtain satisfactory results. It is also recommended [1.14] that tolerances on dimensions be based on current Offshore standards and the results interpreted in the light of actual specimen dimensions and geometry. It is known that unrealistically large welds can produce unrepresentative results and care must therefore be taken in the scaling down of weld sizes for scaled down specimens.

The use of experimental stress analysis methods rely on the assumption that the two dimensional strains measured on the surface of the steel model remain linear and therefore two dimensional stresses on the surface of the specimen can be computed

and transformed into principal stresses. This is achieved by multiplying the strains at the gauge locations with the Young's Modulus of the material. This should be done with caution to avoid any unrepresentative results. There are arguments [1.38] that the recommended practice in both AWS D1.1-84 [1.18] and API RP2A [1.17], which considers the hot spot stress as the product of hot spot strain and Young's Modulus, is incorrect as it may lead to underestimation of hot spot stress by up to 30%. This is mainly due the fact that a direct multiplication approach like this does not take into account any deformation resulting from Poisson Ratio effect.

The stresses and stress concentration factor at the weld toe are obtained experimentally by linear extrapolation to the weld toe of the experimentally measured stresses. There are strict guidelines regarding the location of strain gauges and figure 1.7 shows a schematic representation of the locations of the extrapolation gauges. This must be placed at distances from the weld toe in accordance with recommendations of UKOSRP [1.3, 1.4]. The relevant distances and tolerances on positioning the gauges are shown in figure 1.8.

Experimental methods on steel models normally give representative and accurate results if precautions are taken. Results obtained using this technique are therefore commonly used as a bench mark for assessing the accuracy of other methods. However due to the physical size of the gauges, only average strains over the region of interest can be measured. This may pose a serious problem where changes in strain are very small and difficult to measure or on the other extreme where a very steep strain gradient exists. It is also a very time consuming and expensive method because extensive strain gauging is required to give detailed information on the stress distribution in the region of interest. There is also the additional problem associated with the cost of acquiring large loading machines to provide measurable strains in full scale and otherwise stiff specimens. There are two other methods that are very useful and accurate in locating regions of high stress on the surface of joints. They have been successfully used in recent years as an alternative to strain gauging were possible. These include the use of brittle lacquers and thermoelastic methods. The use of these techniques is presented briefly in reference [1.13].

In the 1970s when Offshore activity in the North Sea increased tremendously and the search for more cost effective methods of stress analysis of Offshore tubular joints were being sought after, scaled down acrylic models offered a more cost effective alternative to full scale tests carried out on steel models. This period saw the use of acrylic models by Wordsworth and Smedley [1.39] to investigate the stresses in tubular welded joints.

The use of acrylic models offer some advantages over steel models. Firstly, lower loads are required to produce measurable strains in acrylic models since their Young's modulus is usually a lot smaller than the typical values for steel models. As a result the test rigs designed for applying these loads could be simpler, cheaper and a lot lighter. Secondly, strain gauges can be fitted before assembly making it possible for strains and stresses to be obtained at those locations which will normally be inaccessible in conventional steel models. This makes it easier to use acrylic models to study stress distributions on very complex geometries and ring stiffeners may be added to or removed from the joint as required.

The main disadvantage of using acrylic models is that the tubing may be subject to significant residual stresses which affect the surface of the specimen. They are also susceptible to creep under load and varying temperature. However if enough precautions are taken, such as making estimates of Young's modulus at the same time the strain measurements are made, taking care when selecting the length of tubing and the required model scale, then accurate and representative results can be obtained at a lower cost.

1.3.3.4.1 Photoelastic Methods

Photoelasticity is another experimental technique for strain and stress analysis of tubular joints and is particularly useful for joints with rather complicated geometries. This was developed in parallel with the finite element method and Bouwkamp carried out the first reported tests on tubular welded joints in 1966. This method was also

used by Holliday and Graff [1.40] to carry out three dimensional stress analysis on T-joints.

Using light rays and optical techniques, this method can be used to provide quantitative evidence of highly stressed areas including peak stresses at the exterior and interior of the joint. It can therefore be used to study three dimensional stress patterns in the region of the joint intersection.

One of the more established method of the photoelastic technique is the 'frozen-stress' technique which is used for three dimensional photoelasticity. This technique is employed by heating a model made from birefringent materials to its stress annealing temperature, stressing it by applying appropriate loads and subsequently cooling the model slowly. Once cooled to room temperature, and the load removed, the strains remain 'locked' in the model and can be studied to reveal the stress patterns in the model. This is usually done by dissecting the model and obtaining slices in the regions of interest. Precautions must be taken in obtaining the slices and machining them to avoid local heating and relaxation of the 'frozen stresses'. Any heating may also introduce thermal stresses which are undesirable and may affect the original stress distribution.

This method is known to produce good results provided all the necessary precautions are taken. It was used by Holliday and Graff [1.40] in the early 70s more recently, Fessler et al [1.41, 1.42] used the technique to study a range of tubular joint geometries and obtained detailed information on the distribution of stresses on the surface and also through the chord and brace walls near the intersection.

The most important advantage of the photoelastic method is the ability to study the overall stress field. Such a display can show not only the overall stress distribution but also the sites of high and low stresses thus giving valuable information which can be used for design considerations. On the other hand the manufacturing of the models for photoelastic analysis and the subsequent fringe counting and data analysis can be time consuming and expensive. This represents the main disadvantage of using this method for stress analysis of tubular joints including the fact that the information

obtained may sometimes be unnecessarily too detailed for preliminary design assessments.

1.3.3.5 Parametric Equations

Experimental 'hot-spot' stress has been identified as the stress which governs the fatigue life of Offshore tubular joints and this is the stress upon which the current design guidance are based. The designer has to adopt various analytical methods to estimate 'hot-spot' stresses for the joints being designed. To facilitate this process, Parametric equations were developed.

Based on several independent studies, a few sets of parametric equations have been published. These have varying capabilities in analysing different joint geometries with different degrees of accuracy. These sets of equations include those of Wordsworth and Smedley [1.39] based on a study of acrylic models, equations of Kuang et al [1.36] published in 1977, Gibstein's [1.37] equations published in 1978 after the use of the finite element program NV332 to study stresses in T-joints. They also include other parametric equations such as those proposed by Efthymiou and Durkin [1.43] and the more recent Hellier Connolly and Dover [1.44, 1.45, 1.46] equations. A detailed comparison between experimental measurements and SCFs obtained using parametric equations has been carried out in this thesis. It is reported in detail in Chapter 3. A general review of some of the more widely used parametric equations is presented here.

The Lloyds Register proposed a set of parametric equations which were published in 1991 [1.94]. These were developed for simple tubular joints after completing a project sponsored by the UK Department of Energy to assess methods for deriving SCFs in simple tubular joints. These equations were based on existing database of SCFs previously derived from steel and acrylic models. The equations proposed included design safety factors and influence factors for different loading configurations. An attempt was also made to account for the effect chord length.

1.3.3.5.1 Kuang et al [1.36]

Kuang studied 46 T and Y-joints under the three modes of loading, 39 K joints under balanced axial loading, 37 K joints under in-plane bending and 16 KT joints under balanced axial loading conditions in the inclined braces and a single axial load in the 90° brace using a finite element program, TKJOINT. This work lead to the development of semi-empirical formulae for predicting stresses and stress concentrations in these joints. The full set of Kuang's equations are presented in reference [1.36] but the equations which give the SCFs for out-of-plane bending of T and Y-joints are given in table 1.1. Figure 1.9 shows graphically the variation of SCF with position around the intersection, θ obtained using the hot spot stress concentration factor predicted using Kuang's equations.

In obtaining these equations Kuang assumed fixed chord end conditions to provide the necessary torsional restraint. It should be noted that the stress concentration obtained using Kuang's equation is that at the intersection line of the mid surface between the brace and chord for the Y-joints described in detail in Chapter 3.

1.3.3.5.2 Wordsworth and Smedley [1.39]

The parametric equations developed by Wordsworth and Smedley for stress analysis of T Y KT and X joints including the modified equations were suggested by UEG based on results from acrylic models. The formulae are summarised in [1.39] and the relevant equation for the analysis of Y-joints under out-of-plane bending is given in table 1.2. The predicted SCFs are shown in figure 1.10

It is important to note that no attempts were made to model the effect of the welds and the equations are intended to yield the gross deformation stress concentration factors. The original equations were modified by the Underwater Engineering Group (UEG) as shown in table 1.2.

The reason for the modification was a recognition of the fact that the original equation underestimated the stress concentration factor for joints with $\beta=1.00$. However the

modifying parameter $\sqrt{Q_\beta}$ is assumed to be valid only for DT, X, K, Y and T-joints for estimating the saddle point SCFs. Another geometric modifying parameter, $\sqrt{Q_\gamma}$, was introduced to ensure better prediction for joints with $\gamma \geq 20$. This factor was assumed to apply for all joints.

1.3.3.5.3 Gibstein [1.37]

In 1978 after the use of the finite element program NV332 to study stresses in T-joints, Gibstein proposed a set of parametric equations to predict stress concentrations in T-joints. He studied 17 T-joints with both chord ends rigidly fixed. He also investigated the effect of chord end fixity by varying the end conditions in a separate test which had simply supported chord ends.

Gibstein regarded the Gaussian points closest to the brace chord intersection to be representative of the locations for the 'hot-spot' stresses and did not investigate the effect of the non dimensional parameter, α. However it should be noted that the influence of α was taken from Kuang's formulation and included in the formulation for axial loading of tubular T-joints. He also modified the SCFs for the brace by a factor of 0.8 to ensure correlation between the predicted and experimental results.

1.3.3.5.4 Efthymiou and Durkin [1.43]

Efthymiou and Durkin's paper which presented the proposed set of equations for estimating stresses and stress concentration factors for T, Y and K joints was published in 1985. They were based on a three-dimensional finite element analysis using the program PMBSHELL. Three dimensional curved shell elements, capable of explicitly modelling the tube thickness and weld profile, were used and 150 joints under various loading configurations were studied. At the time of this publication, the most comprehensive and widely used equations were those of Kuang and Wordsworth and Smedley. However at this time designers and classification authorities were still faced with a few problems. Firstly there was a significant difference between the

predictions from these two sets of equations for certain joints and loading configurations, secondly there was limited information on stress concentration factors in stiffened and multi-planner joints, thirdly limited information was available for certain loading configurations in simple K and KT joints and also on joints with overlapped braces.

The set of equations proposed by Efthymiou and Durkin were developed to close up the gap which existed between predicted results from the equations of Kuang and Wordsworth and Smedley and to offer better prediction of SCFs for certain simple K and KT joints and also for joints with overlapped braces. The formulae are summarised in reference [1.43] but the relevant equations for the analysis of Y-joints under out-of-plane bending are presented in table 1.3.

A fixity study was also carried out and the effects of chord end fixity were quantified where relevant including the effect of chord length. It was noted that, if the natural decay of chord deformation resulting from brace loading is interrupted by using short chords, the deformations in the chords and stresses will be reduced. This lead to development of short chord correction factors to be applied to the original equations. Details of these correction factors are given in reference [1.14] but the correction function (F3) relevant to Y-joints used in this study is also given in table 1.3. Figure 1.11 shows the variation of SCF around the intersection of the brace and chord predicted by this equation for the Y-joint used in this study under out-of-plane bending. The results are also compared with experimental results and other parametric equations in Chapter 3.

1.3.3.5.5 Hellier Connolly and Dover [1.45]

Hellier Connolly and Dover carried out an extensive and systematic finite element study of stresses in T and Y-joints which involved nearly 900 thin shell finite element models. A wide range of joint geometries under different modes of loading which included axial loading, in-plane and out-of-plane bending were used for this study. The results, which were compared with a wide range of other techniques and predicted results based on other parametric equations including results from

experimental full scale steel models were published in 1990. They represented a comprehensive set of parametric equations for estimating stresses and stress concentration factors in tubular welded Y and T-joints. A complete summary of these equations is given in reference [1.45] but those relevant to this study are given table 1.4.

The complete set of equations which were presented in the above paper were modified in another paper [1.46] presented in the same year to give the first set of parametric equations capable of predicting the stress distribution around the intersection of the brace and chord. For the Y-joints for instance under out-of-plane bending, the distribution of SCF was found to be symmetrical about the saddle position and the following expression which predicts the distribution of SCF was proposed,

$$S(\phi) = K_{HS} \sin\phi \quad (\text{for } \beta < 0.4) \tag{1.1}$$

$$S(\phi) = K_{HS} \sin^2\phi \quad (\text{for } \beta \geq 0.4) \tag{1.2}$$

where $S(\phi)$ is the characteristic formula for stress concentration factor around the chord brace intersection with a hot spot value of K_{HS}. The variation of SCF around the intersection of the brace and chord predicted by this equation for the Y-joint under out-of-plane bending is presented in figure 1.12. The above equations were adopted for other parametric equations to facilitate the comparison of experimental results with those based on parametric equations as presented in Chapter 3.

1.4 FATIGUE DESIGN

One definition of fatigue given in reference [1.47] is "Failure of a metal under a repeated or otherwise varying load which never reaches a level sufficient to cause failure in a single application". Another definition given in reference [1.48] is, "The process of progressive localised permanent change occurring in a material subjected to conditions which produce fluctuating stresses and strains at some point or points and

which may culminate in cracks or complete fracture after a sufficient number of fluctuations".

These two definitions are not the only variants of the numerous definitions of fatigue found in the vast literature available on fatigue and the behaviour of fatigue cracks. However they give a clear indication that fatigue is a process of cumulative damage. This was recognised well over a hundred years ago and research in this area started as far back as 1838. Codification of the resulting data started around the 1850s when Wohler carried out his now classic experiments which lead to the development of S-N curves. Design for fatigue resistance and fatigue life prediction has since become an important aspect for consideration in a wide range of industries and most especially in the Offshore industry for the design of Offshore structures.

Steel Offshore jackets and Jack-up legs consist mainly of tubular joints which are formed by welding together intersecting brace and chord members. These welded intersections constitute regions of stress concentrations which represent areas that are highly susceptible to crack initiation and subsequent growth which may lead to eventual failure of the structure. This makes fatigue analysis of such structures very important both at the design stage and also during structural integrity assessment programmes.

Fatigue analysis is by no means a rigorous science. And, as a result of the idealisations and approximations employed in the analysis process, any fatigue analysis approach adopted will almost always be associated with some degree of identifiable areas of uncertainty. This will include uncertainties resulting from inadequate understanding of the complete effect on the structure, of the operational environment and the relationship between this and the actual forces, moments and stresses experienced by the structure. The implication of this uncertainty is to introduce a potential for error and at the same time, reduce the level of confidence that may be associated with any exact calculations resulting from any particular fatigue life prediction methodology.

Fatigue analysis, however, is a very important tool for designers to use in the prediction of relative magnitudes of fatigue lives of structures at potentially critical

points. Fatigue analysis methodologies have been shown to yield reliable estimates of fatigue life and two distinct approaches have evolved for use in fatigue life assessment of tubular joints; the S-N approach and the fracture mechanics approach.

1.4.1 The S-N Approach

The Stress life (S-N) approach for assessing Offshore structures is based on available fatigue test data and it has the advantage that it provides an assessment methodology which is based on a single parameter, the 'hot-spot' stress, S. N refers to the life or number of cycles to failure of the joint.

Like 'hot-spot' stress, S, the definition of life, N, for use in S-N design curves has been a subject for consideration in the course of major research programmes such as the UKOSRP [1.3, 1.4], which led to the generation of vast amounts of experimental data that was used to formulate the S-N curves for the Department of Energy Design Guidance notes [1.21] and its revised versions [1.8].

The same definition of 'hot-spot' stress used in the UKOSRP reports [1.3, 1.4, 1.49] was maintained in the Department of Energy's "Background to new fatigue design guidance for steel welded joints in Offshore structures", first published in 1984 [1.50] and other revisions [1.38]. This definition has been discussed in a previous section of this thesis. It is that which is based on a linear extrapolation to the weld toe, of the linear part of the stress distribution near the weld toe but removed from the region of rapidly rising stress immediately adjacent to it.

On the other hand, the definition of life or number of cycles to failure, N, was taken as that which denoted "first through wall cracking, detected either visually or more accurately by noting first loss of internally applied air pressure to the damaged member, or by monitoring the output of strain gauges positioned adjacent to the crack at its deepest part" [1.38, 1.50]. As indicated in these documents, it was felt appropriate to use a measure of life that will result in both detectable and reparable cracks in a structure that is capable of tolerating them without the intervention of catastrophic fracture. Such cracks were also deemed necessary to be "...small enough

for the structure not to have to shed load and thereby (possibly) damage other joints" [1.38]. This life, designated N_3 [1.38], (designated N_2 in reference [1.50]) together with the 'hot-spot' stress, S, are the two parameters used to formulate S-N design curves for Offshore tubular joints.

1.4.1.1 Formulation of the Basic S-N Curves

The S-N approach is well established for the design of Offshore welded tubular joints and connections. Early editions of both API RP2A and AWS D1.1 provided the first guidance on the design of tubular joints against fatigue using S-N curves in the early 70s. Even though the API RP2A was influenced to a large extent by the experience on the behaviour of platforms in the Gulf of Mexico, it has been used extensively to design structures for harsher environments of the North Sea. The curves recommended by the 1972 editions API and AWS were developed on the basis of two concepts.

The first was an attempt to correlate failure to brace nominal stress and the second was based on the 'hot-spot' stress of the joint. Using data obtained from small scale specimens tested in air, under constant amplitude loading conditions, the S-N curve called the 'X curve' was proposed with a note of caution from AWS: "Calculated fatigue lives based on the proposed curves should be viewed with a healthy amount of scepticism and should be used more as design guidance than as an absolute requirement" [1.14].

Though the same data used in producing the API and AWS curves was also the basis of the curves in BS 6235 [1.20], NPD rules [1.19], DnV rules [1.15], including earlier editions of the UK Department of Energy guidance notes, the above statement of caution is a clear indication that there were other factors at the time which were understood to govern fatigue but not yet addressed. This to a large extent, constituted a driving force behind the initiation of extensive research programmes starting with UKOSRP I in 1973. Following the increasing availability of experimental data, design codes have been revised and the guidance on fatigue design modified based on available data. These revisions have not been given here in detail

since they are available in respective codes and other relevant literature. However an indication of how the fatigue guidance offered by the UK Department of Energy Guidance notes has evolved in more recent years is presented with consideration of other relevant factors which affect fatigue performance and how they have been incorporated into the S-N approach at the current state-of-the-art.

After the completion of the first phase of the United Kingdom Offshore Steels Research project (UKOSRP I) in 1984, a major revision of the fatigue Guidance Notes was carried out. Under the section on 'Fatigue-allowable fatigue stresses', a basic T curve was proposed for fatigue design of tubular joints. This curve was based on 64 T, X and K joint test results and recommended for joints having a chord wall thickness of 32mm. The T curve, shown in figure 1.13, was given as;

$$Log_{10}(N) = 12.164 - 3Log_{10}(S) \quad (\text{for } N < 10^7) \tag{1.3}$$

$$Log_{10}(N) = 15.61 - 5Log_{10}(S) \quad (\text{for } N > 10^7) \tag{1.4}$$

The document also addressed the modification to the basic curve for unprotected joints in sea water, thickness effect, effects of weld improvement and treatment for low and high stress cycles.

Since 1984 when reference [1.21] was published, a substantial amount of data on the fatigue behaviour of Offshore welded tubular joints was made available following the completion of other major research projects such as the UKOSRP II [1.4]. The data was assessed by a review panel for fatigue guidance, appointed by the department of Energy in 1987, to ensure that relevant data was used in the revision of the UK Department of Energy Fatigue Design Guidance.

After excluding some categories of the available data [1.38] to ensure that the selected data set covered the widest range of joint geometries and loading configurations, the following design S-N curve was proposed for the UK Department of Energy Design Guidance.

$$Log_{10}(N) = 12.476 - 3Log_{10}(S) \quad (\text{for } N < 10^7) \tag{1.5}$$

This was based on 16mm wall thickness (cf. 32mm for previous revisions) and allowances were made for other relevant factors. This basic design S-N curve for tubular joints was taken to correspond to 2 times the standard deviation of the $Log_{10}(N)$ below the mean S-N line for the 16mm data. An endurance limit was assumed to exist in the high cycle region beyond 10^7 cycles such that;

$$Log_{10}(N) = 16.127 - 5Log_{10}(S) \qquad (\text{for N} > 10^7) \tag{1.6}$$

Equations 1.5 and 1.6 constitute the basic design curve for tubular joints (T' curve). The slope of -1/3 was adopted to retain consistency with previous guidance and other design codes. The existence of an endurance limit was accounted for by a change in slope of the basic curve from -1/3 to -1/5 at 10^7 cycles. The corresponding basic design S-N curves for flat or rolled plates are given by equations 1.7 and 1.8 respectively.

$$Log_{10}(N) = 12.182 - 3Log_{10}(S) \qquad (\text{for N} < 10^7) \tag{1.7}$$

$$Log_{10}(N) = 15.637 - 5Log_{10}(S) \qquad (\text{for N} > 10^7) \tag{1.8}$$

These basic design S-N curves are shown in figure 1.14.

1.4.1.2 The Implication of Other Factors

The design S-N curve (T' curve) given above is for simple tubular joints in air under constant amplitude loading and only represents data on tests carried out using tubular joints with a wall thickness of 16mm. Other relevant factors do affect the fatigue behaviour of welded connections which need to be taken into consideration where relevant. Even though a wide range of these factors had been studied, the data that was available at the time when the above curves were proposed was not considered adequate to be incorporated in the proposed design S-N curves. As a result, some of the data that was available was excluded from the statistical analysis carried out by the review panel for fatigue guidance after the screening process that was employed. Some of the categories that were excluded include the database on variable amplitude

loading and data obtained from tests carried out on specimens with wall thickness less than 16mm. The implication of this is that the current design guidance is very limited for structures under variable amplitude loading. The work for this thesis seeks to address this lack of data on variable amplitude loading through systematic variable amplitude tests carried out on a typical high strength steel, SE 702. It is hoped that the data obtained from this investigation will improve the current knowledge on the variable amplitude corrosion fatigue behaviour of high strength steels and also provide valuable data suitable for the formulation of future guidance.

Despite the exclusion of some of the data sets based on the argument that they were not adequate, allowances were made for these relevant factors to be considered when using the design S-N curves in the design of tubular welded joints. These important considerations and the associated 'penalties' applied to the basic design S-N curve are covered in detail below.

1.4.1.3 Thickness Effects on Fatigue Resistance

Considerable research work into the effect of wall thickness on fatigue resistance of a component or structure has been carried out and documented. This is one of the aspects that was studied by the first phase of the United Kingdom Offshore Steels Research Project [1.3]. A great proportion of the fatigue life of tubular joints is spent in the propagation of fatigue cracks and for a given 'hot-spot' stress, it has been demonstrated that the average growth rate of these cracks is significantly higher in specimens with wall thickness in excess of 32mm. It has also been demonstrated that this effect could be operative for chord wall thickness as high as 75mm. This trend had equally been observed to occur in simpler welded connections such as T-butt welded plates.

This indicates that, instead of an increase in fatigue resistance as wall thickness is increased, a reduction may result for greater wall thickness. This effect has been widely referred to as the 'thickness effect'. It was demonstrated by Wylde et al in

1976 [1.51] and different researchers have since put forward different arguments to explain this phenomenon.

Marshall [1.52] made some studies on size effect on tubular welded joints in the early 80s and suggested that the phenomenon is not only related to plate thickness and that other parameters such as the weld toe and the associated size of the local notch zone could be more important. This view followed on Haibach's findings [1.53] when he investigated the effect of fillet weld throat size on 50mm thick plates in the late 70s. He noted that there was a fall in fatigue strength as a result of an increase in the weld size alone.

Webster et al [1.54] noticed a decrease in fatigue strength by about a third for an increase in plate thickness from 38mm to 100mm. They also observed increases in the weld toe stress concentration factors for thicker joints. Based on this observation, another explanation based on higher local stresses was proposed.

Other researchers [1.55, 1.56, 1.57] argued that the size effect was due to a combination of increased weld toe stresses and to some degree the effect of a lower through thickness stress gradient. This argument focused the size effect on crack growth in the low ΔK region which controls a high proportion of the fatigue life and more significantly so in smaller welded joints.

This is by no means an exhaustive review of studies carried to quantify thickness effects on the fatigue strength of tubular joints. The important thing is that there is a wide acceptance that the effect can be detrimental to fatigue performance. After a review of experimental data a correction factor was proposed. This is expressed as [1.38];

$$S = S_B\left(\frac{t}{t_B}\right)^{-y} \tag{1.9}$$

S_B is taken to be the stress range at the reference thickness, t_B and S, the stress range which results in the same fatigue endurance at a thickness t. This correction factor is

applied as a penalty factor to thickness greater than the reference thickness. y is the thickness correction exponent.

In the earlier edition of the UK Department of Energy Fatigue Guidance notes [1.50, 1.21], the reference thickness was taken as 32mm for tubular joints and 22mm for plates. A value of 0.25 was considered appropriate for the thickness correction exponent, y.

After reviewing further fatigue test data it was demonstrated that thickness effect also occurs in joints with chord wall thickness below the previous limiting thickness of 32mm. A new reference thickness of 16mm was proposed with a conservative thickness correction exponent of 0.3. The effect of thickness on the design S-N curve is demonstrated in figure 1.15.

Marshall's [1.52] and Haibach's [1.53] argument that thickness effect is not only related to plate thickness and that other parameters such as the weld toe and the associated size of the local notch zone could be more important can not be dismissed. However they do not explain the fact that this phenomenon is less pronounced for axial loading than has been observed under situations where bending loads are involved.

As illustrated in figure 1.16 [1.58], there are two likely causes for thickness effect under bending conditions. The first of these is the existence of a lower through thickness stress gradient in a thicker plate. This implies that a fatigue crack of a given size will be subjected to a higher stress in a thicker specimen which may also exhibit a low critical stress intensity factor range. This higher stress level will lead to a higher crack growth rate in the thicker specimen. The second reason for this behaviour is that for a given crack size, a lager surface area or volume of material is subjected to a higher stress level in the thicker specimen. As a result there is a greater probability of initiating a fatigue crack in the thicker specimen which also has a higher probability of containing inherent manufacturing flaws assuming that their distribution per unit volume is uniform. The consequence of these two aspects combined is that even though a fatigue crack has a longer path in a thicker specimen than a thinner one, the

probability of initiating them is higher in thicker specimens where they can also propagate faster due to the presence of a more severe stress field.

1.4.1.4 Environmental effects on fatigue resistance

The environmental conditions experienced by Offshore tubular joints in service can vary depending on the location of the joint in the structure. The environmental influence will depend on whether the joint is in the splash zone, fully immersed and also on the level of any cathodic protection used. Corrosion fatigue and cathodic protection is discussed in greater detail in section 1.5. Only the way this is incorporated in the use of fatigue design S-N curves is reported and discussed here.

It was recognised that the environment could have detrimental effects on fatigue performance of tubular joints relative to air. Based on this and also due to the lack of sufficient experimental data, three recommendations were made in earlier codes regarding the use of design S-N curves and the environment.

A penalty factor of 2 on design fatigue life was recommended for unprotected joints. It was also recommended that the air curve be used for adequately protected joints. The change in slope at 10^7 cycles was not to be applicable to joints under free corrosion. The main reason for this decision was that, free corrosion which leads to pitting may cause fatigue cracks to grow from the resulting pits which act as sites of high stress concentration. This effectively removes the fatigue limit which may exist at low stress levels in a non corrosive environment.

The following curves were proposed for use in the design of joints in a freely corroding environment in the latest proposed revisions to fatigue guidance.

$$Log_{10}(N) = 12.00 - 3Log_{10}(S) \quad (tubulars) \tag{1.10}$$

$$Log_{10}(N) = 11.705 - 3Log_{10}(S) \quad (plates) \tag{1.11}$$

This document also proposed another set of curves for the design of protected joints and plates.

$$Log_{10}(N) = 12.175 - 3Log_{10}(S) \quad (\textit{tubulars}, \text{ for } N < 10^7) \tag{1.12}$$

$$Log_{10}(N) = 16.127 - 5Log_{10}(S) \quad (\textit{tubulars}, \text{ for } N > 10^7) \tag{1.13}$$

$$Log_{10}(N) = 11.784 - 3Log_{10}(S) \quad (\textit{plates}, \text{ for } N < 10^7) \tag{1.14}$$

$$Log_{10}(N) = 15.637 - 5Log_{10}(S) \quad (\textit{platess}, \text{ for } N > 10^7) \tag{1.15}$$

These curves are shown in figure 1.17 together with the air curve and the fatigue design S-N curves for welded joints and plates under freely corroding conditions. These new set of curves effectively represent a factor of 2 on life even for adequately protected joints. The main reason for this change in approach to the design of protected joints was that further fatigue tests carried out before the 1990 revision to the design guidance notes [1.38] under adequate cathodic protection levels did not show trends in fatigue lives comparable to air tests. Corrosion fatigue under cathodic protection conditions is influenced by many factors, some of which have been demonstrated to be different from material to material. Corrosion fatigue crack growth rates under cathodic protection conditions also depends on the level of cathodic protection among other variables. The degree of susceptibility of a particular material will largely depend on the complex interaction between the hydrogen equilibrium in the vicinity of the crack tip and the stress intensity factor. Since the effect of Hydrogen produced under cathodic protection conditions varies for different grades of steel, it is possible that the current reduction factor of 2 on life may not be directly relevant in the design of structures made from higher strength steels. This implication is discussed in greater detail in Chapter 3 where results of the fatigue tests carried in this study are compared with those from previous tests on conventional fixed platform steels such as BS 4360 50D.

1.4.2 The Fracture Mechanics (FM) Approach

The S-N approach has been used extensively to design welded Offshore tubular joints and other welded connections for Offshore applications. This approach however has

it's limitations and one of the most significant shortcomings of the method is that it can not be used in assessing the structural integrity of cracked tubular joints in service.

Crack growth models have been developed for use in fatigue crack growth assessment and at present, fracture mechanics analysis is the most powerful and useful technological tool available for describing and solving fatigue crack problems. It is a simulation with crack growth models for mechanical evaluation of the strengths of cracked bodies or the behaviour of fatigue cracks. The practical use of fracture mechanics has been established for use on large turbine and electric generator rotor components, the atomic power generation and the aircraft industry. Application areas in the Offshore industry have also been identified and reported in the literature [1.59, 1.60 and 1.61]. Some of the existing fracture mechanics models will be reported in detail in Chapter 4 and compared with experimental results from this study.

1.4.2.1 Fatigue crack growth modelling

In the various practical uses of fracture mechanics such as design life prediction and failure analysis, numerical values of fatigue crack propagation rates in a particular environment and operating conditions have to be determined. Often this relies on the use of Fracture Mechanics (FM) fatigue tests to determine the values of certain material constants. Figure 1.18 shows the characteristic sigmoidal shape of the da/dN versus ΔK curve [1.62] in logarithmic scale. This is the typical shape of this curve exhibited by crack growth in air. Unlike corrosion fatigue crack growth where the environment influences crack propagation mechanisms, crack growth in air is mainly governed by deformation controlled mechanisms. This is characterised by three distinctive regions within which the fatigue crack growth rate exhibits distinctively different dependencies on the stress intensity factor range, ΔK.

Region I is characterised by a rapid decrease in crack growth rate with decreasing cyclic plastic zone size. The behaviour of crack growth in this region has been attributed to two forms of resistance to crack growth. These have been described as

extrinsic and intrinsic resistance [1.63, 1.64]. Behaviour in this region is dependent on microstructural features and is of considerable importance in service components.

The rate of crack propagation in region III increases rapidly and terminates with fracture as da/dN increases without bound. This region corresponds to the onset of unstable and rapid crack growth and is characterised by either the materials fracture toughness or in the case of ductile materials by plastic instability. Environment has little effect in this region and deformation mechanisms in this region are similar to those characteristic of monotonic loading.

Crack growth in region II on the other hand has been described as a continuum process not strongly dependent on the microstructure. Region II is characterised by stable crack growth and can be described by the Paris equation;

$$\frac{da}{dN} = C(\Delta K)^m \tag{1.16}$$

where $\frac{da}{dN}$ is the crack growth rate, ΔK is the stress intensity factor (SIF) range and C and m, material constants.

Cracks in region II have been observed to grow by the formation of striations which range in size from 0.05 to 2.5 micrometers [1.64, 1.65]. In 1962, Forsyth [1.65] proposed a model which suggested that striation formation was the result of a cleavage fracture ahead of the crack tip while Laird and Smith in the same year suggested that the striations are formed as a result of alternate blunting and sharpening of the crack tip during cyclic loading. Secondary mechanisms such as brittle intergranular or transgranular microfractures which result in discrete growth increments have also been observed [1.66].

This review on fatigue crack growth only cites early views proposed to explain crack growth and the observed striations. There is abundant literature on crack advance and crack propagation mechanisms in the literature on fatigue. This can not be presented here exhaustively but it is important to note that crack growth in region II forms the basis for linear elastic fracture mechanics analysis as the majority of crack growth in

engineering structures can be considered to lie in this region and most importantly may represent more than 80% of the fatigue life of tubular joints and welded connections.

1.4.2.2 Fatigue life assessment based on FM

The fatigue life of welded tubular joints has been observed to be characterised mainly by the propagation of fatigue cracks. This has lead to what has now become common thinking that defects are always inherently present in welded structures and that crack propagation does represent a substantial percentage of total fatigue life of welded joints.

In fatigue life assessment based on fracture mechanics, the number of fatigue cycles required for a given increase in crack size may be calculated by integration of the Paris equation or the appropriate crack growth law. Using this technique the number of fatigue cycles required to extend a fatigue crack from an initial depth a_i to a depth of a_f is given as;

$$N = \int_{a_i}^{a_f} \left(\frac{1}{C(\Delta K)^m} \right) da \tag{1.17}$$

$$\Delta K = K_{\max} - K_{\min} = Y \Delta \sigma (\pi a)^{\frac{1}{2}} \tag{1.18}$$

The stress intensity factor range, ΔK, is a parameter which expresses the effect of load range on the crack in the form of a stress concentration produced when a crack is introduced into a stressed body. This parameter describes the stress field associated with the cracked body at the crack tip. Y is the modifying shape parameter which depends on the crack geometry and the geometry of the specimen.

In practice calculations depicted by equations 1.17 and 1.18 are more complex and the general fracture mechanics approach to fatigue life calculations will require the selection of a suitable crack growth law, selection of suitable crack growth material constants (C and m), determination of the appropriate stress ranges and considerations

for environmental effects, determination of stress intensity factors and subsequent integration of the selected crack growth law for the actual loading spectrum of interest. This methodology can be heavily dependent on the nature of the load sequence used in the analysis and whether a cycle by cycle approach is preferred in order to account for any sequence effects which may be present. This is discussed in greater detail in Chapters 4 and 5 where the equivalent stress concept is linked to sea state spectra and used to model sea state interaction effects on fatigue crack growth in Offshore structures using a Fracture Mechanics approach. In this section the main stages involved in any FM approach to fatigue crack growth prediction are reviewed.

1.4.2.3 Determination of SIFs

The concept of stress concentration factor becomes inapplicable in the analysis of stresses near the crack tip. To overcome this problem fracture mechanics relies on analysing the stress field in the vicinity of the crack tip, rather than the infinite stress since a stress singularity is presumed to exist at the crack tip. Cracked components may be loaded in one of the following or a combination of modes I, II and III. These modes are shown schematically in figure 1.19. Mode I is characterised by tension normal to the crack faces and is referred to as the opening mode. This mode is the predominant stress situation in most practical loading conditions while modes II and III tend to be less significant with negligible contributions to crack growth.

The stress intensity factor is the parameter adopted to describe the elastic stress field in a cracked body around the crack tip and it is a function of applied stress, the size and shape of the crack and the geometry of the cracked component. For mode I loading for instance, it is expressed as [1.58];

$$K_I = Y(a)\Delta\sigma\sqrt{\pi a} \tag{1.19}$$

For surface cracks in engineering structures, various correction factors have to be used to account for boundary effects, crack shape and loading geometry. The overall correction function, *Y(a)*, may be considered to account for aspects such as a free front surface, finite plate width, crack shape, a non-uniform stress field, presence of

geometrical discontinuity and also effects arising from changes in structural restraint in the component. A variety of solutions have been proposed to model this parameter. It is common to apply the stress distribution and the appropriate boundary conditions in tubular joints to the simpler flat plate solutions to obtain stress intensity factor solutions for cracks in tubular welded joints.

The methods employed include empirical and semi-empirical solutions, adapted plate solutions and numerical methods. Some of these solutions are presented in detail in Chapter 4 where the accuracy of the different solution methods in predicting crack growth under variable amplitude conditions is assessed.

1.5 VARIABLE AMPLITUDE CORROSION FATIGUE

A great deal of effort has been concentrated on the study of the effect of the environment on fatigue resistance of engineering metals for many years. In general air fatigue data is used as a basis for comparing the performance of steels in different environments although it is known that air is not inert with respect to fatigue crack growth. Fatigue crack propagation rates in vacua have been observed [1.67] to be lower than those in air at lower stress levels and it is now well established that a corrosive environment could have serious detrimental effects on the performance of steel components subjected to fatigue.

This section presents a general review of the current state of knowledge on corrosion fatigue and attempts to look at some of the mechanisms that have been identified in the more recent years. The use of fracture mechanics as a tool for assessing corrosion fatigue and the performance of structures and components under realistic variable amplitude loading conditions is covered in Chapters 4 and 5.

1.5.1 Corrosion Fatigue

One definition of fatigue quoted earlier is "Failure of a metal under a repeated or otherwise varying load which never reaches a level sufficient to cause failure in a single application". Corrosion on the other hand could be defined simply as a process by which a metals chemical structure is changed resulting in gradual deterioration by being slowly 'eaten' away in a chemical oxidation-reduction reaction. The interaction of fatigue and corrosion is called corrosion fatigue.

Corrosion fatigue involves unique failure mechanisms which are very complex and depend on the stage of the fatigue process. Different ideas have been proposed to explain the basic mechanism of corrosion fatigue during the initiation stage. However the mechanism which operates during the crack propagation stage is very complicated and not well understood for high strength steels.

Predicting the behaviour of a structural crack entails estimating the load states the structure will have to withstand and obtaining representative loading conditions for such structures is therefore very important. This can be adequately modelled by use of wave power spectra together with the transfer function approach in the frequency domain as discussed in Chapter 2. However if this simulation is carried out in an unrepresentative environment, then misleading results can be obtained.

Environment assisted fatigue is a major cause for concern and contributes significantly towards the failure of structures. The early work of Gough and Sopwith [1.68] had shown that air does decrease fatigue life relative to tests in vacua. They demonstrated that the combined presence of water vapour and oxygen was the cause of atmospheric effects. For tests in aqueous environments the presence of oxygen was demonstrated to be necessary to induce corrosion fatigue. The dissolution of iron in an aqueous solution can be represented as follows [1.69];

$$Fe \rightarrow Fe^{2+} + 2e^{-} \tag{1.20}$$

The resulting free electrons from the above process react with water and dissolved oxygen to give hydroxide ions as shown in the following equation.

$$H_2O + \frac{1}{2}O_2 + 2e^- \rightarrow 2OH^- \qquad (1.21)$$

The corrosion process is effected when the iron ions react with the hydroxide ions resulting in the formation of iron(II) hydroxide as follows;

$$Fe^{2+} + 2OH^- \rightarrow Fe(OH)_2 \qquad (1.22)$$

The above reaction is shown schematically in figure 1.20. Iron(II) hydroxide is not a very stable compound due to the presence of iron(II) ions (Fe^{2+}). This form of the hydroxide is therefore quickly oxidised to produce the more stable iron(III) hydroxide ($Fe(OH)_3$), which is precipitated as a reddish brown substance, the main constituent of rust.

Oxygen is not an absolute requirement for the inducement of corrosion fatigue and the possible role of hydrogen is now thought to play a more significant role in the embrittlement of high strength steels.

The processes of corrosion fatigue and hydrogen embrittlement of Jack-up steels are a complex combination of corrosion and embrittlement chemical reactions. But the overall process can be represented by the following simple reduction -oxidation reaction.

$$\left.\begin{aligned} Fe &\rightarrow Fe^{2+} + 2e^- \quad (oxidation) \\ 2H^+ + 2e^- &\rightarrow H_2 \quad (reduction) \\ Fe + 2H^+ &\rightarrow Fe^{2+} + H_2 \quad (net\ reaction) \end{aligned}\right\} \qquad (1.23)$$

As mentioned before Corrosion fatigue involves unique failure mechanisms which are very complex and depend on the stage of the fatigue process. Different models have been proposed to explain the basic mechanism of corrosion fatigue during the initiation stage. However the mechanism which operates during the crack propagation stage is very complicated and not well understood for high strength steels but increased crack growth rates under CP conditions helps to provide an explanation

that hydrogen embrittlement is a possible mechanism [1.70]. In a recent review [1.71], five main theories which have been proposed to explain this phenomenon were highlighted. Those more plausible include the pressure, decohesion and surface energy theories.

The pressure theory is based on the assumption that atomic hydrogen generated during cathodic protection is absorbed into the microstructure of the steel and diffuses through the metal lattice structure collecting into voids and/or defects within the metal. Subsequent combination of atomic hydrogen at these voids to form hydrogen gas then leads to the formation of 'pockets' of high pressure within the metal. There is evidence to support this theory but the occurrence of hydrogen embrittlement in high strength steels in a relatively low pressure environment [1.72] has led to the view that other mechanisms may be involved in the process of hydrogen embrittlement.

The decohesion and surface energy theories are similar. The decohesion theory suggests that the presence of hydrogen will tend to lower the inter-atomic energy and therefore make it easier for the inter-atomic bonds to be broken resulting in higher than expected crack growth rates. The surface energy theory on the other hand suggests that the presence of hydrogen will decrease the surface energy of newly formed surfaces. This means that the energy required to produce a new surface i.e. produce a fatigue crack is less than expected and therefore higher than expected crack growth rates will prevail in the presence of hydrogen.

Other theories that have been proposed to explain hydrogen embrittlement in high strength steels include the hydride formation and the local plasticity theories. There is little evidence to support the hydride formation theory which suggests that the presence of hydrogen will favour the formation of brittle hydrides in the vicinity of the crack tip leading to the embrittlement of the steel. There is even less evidence to support the local plasticity theory which suggests that the presence of hydrogen tends to reduce the total stress required for dislocation movement. Easy movement of dislocations in the presence of hydrogen implies that high strength steels will show a greater tendency to ductile behaviour thereby reducing the possibility of cleavage

fracture. This contradicts the decohesion and surface energy theories and there is little evidence to this kind of behaviour in high strength steels.

One of the main difficulties in trying to quantify corrosion fatigue and hydrogen embrittlement in high strength steels is the large number of variables involved. Some of these factors are; alloying elements in the structural member, local flow velocity in the corrosive environment, salt content and chemical composition of the corrosive environment, temperature, pH, degree of aeration, and the loading frequency. Some of these aspects and their effects on the fatigue resistance of Offshore structures are covered in greater detail in the following sections. The way they were controlled during the fatigue carried out in this study is presented in Chapter 3.

1.5.1.1 Initiation of corrosion fatigue Cracks

The fatigue life of smooth polished specimens is dominated by fatigue crack initiation. For this type of specimen crack initiation and associated mechanisms are very important. Typically 90% of the air fatigue life of smooth polished specimens may be associated with the initiation of fatigue cracks and only 10% with their growth [1.67]. However, the presence of a corrosive environment can drastically reduce fatigue life by reducing the fatigue crack initiation life to about 10% of the total life.

This is very significant for Offshore structures in which most of the fatigue life of the structural components is considered to be characterised by crack propagation. For this reason initiation mechanisms for these structures are considered not to be as important as is the case with smooth polished specimens. However under variable amplitude loading conditions where there is the possibility of crack arrest as a result of a possible combination of sequence effects and crack tip blunting which may arise from the electrochemical action of the environment, it is important to distinguish clearly between the effects of crack arrest and absence of initiation.

One of the basic mechanisms of corrosion fatigue during the initiation stage can be explained thus:

A corrosive environment is thought to attack the surface of a metal producing an oxide film. Localised cracking of the oxide layer under cyclic loading exposes fresh metal surfaces which subsequently under the same process. This process can cause localised pitting of the metal surface resulting in the production of stress concentration sites. Corrosion fatigue crack initiation and the role of pitting has been the subject of much discussion and Laird and Duquette [1.73] concluded that for steels, "perhaps pits observed at failure were not the cause of corrosion fatigue but rather the result of it".

This conclusion is not applicable to all cases of corrosion fatigue as it is justifiable in some cases and unjustifiable in others. In any case the effect of pitting on the initiation of corrosion fatigue cracks is dependent upon details of pit formation. It is also thought that different mechanisms of initiation are possible and that the mechanism with the fastest kinematics will dominate the fatigue crack initiation process. For example grain boundary attack, hydrogen assisted cracking and localised attack at protruding slip steps are all possible mechanisms for corrosion fatigue crack initiation.

Considerable research work has been carried out on structural steels used for jacket structures and some of the corrosion fatigue crack initiation data for steels such as BS 4360 (50D), BS 7191 (355D), 450F and API X85 are now available. Depending on the operative initiation mechanism, it is possible that high strength Jack-up steels would exhibit an entirely different behaviour under realistic loading and environmental conditions. This comparison is covered in greater detail in Chapters 3.

1.5.1.2 Propagation of Corrosion Fatigue Cracks

As mentioned in the previous section, the fatigue life of Offshore welded tubular joints is dominated by fatigue crack propagation which often represents well over 80% of total life. For Offshore welded tubular joints therefore, crack growth data are of practical significance for corrosion fatigue since Offshore welded tubular joints are assumed to have fabrication defects when they are commissioned. Even under circumstances where this is not the case, defects are developed in these structures

relatively quickly and their service life is determined by how fast they propagate through individual components under the relatively low frequency loading that characterises corrosion fatigue in Offshore structures.

Four main factors have been highlighted [1.3, 1.74] to be the most significant influences on the fatigue life of welded tubular joints; specimen characteristics, environmental effects, component stress state and stress-time interaction effects. Some of the most relevant aspects of specimen characteristics and how this affects the fatigue life of Offshore welded tubular joints are discussed in Chapter 3. The effect of stress states and stress-time interactions are determined by the loading mode and a complex combination of wave loading, wave excitation frequency and structural response for any particular structure. These aspects are covered in Chapter 2. The following two sections review environmental effects and the effect of cathodic protection on the fatigue resistance of tubular welded joints respectively. The way these conditions are modelled for this study to ensure that representative results were obtained is presented in Chapters 2 and 3.

1.5.1.3 Environment and Fatigue Crack Growth

In any crack growth situation in a corrosive environment, it is likely that several crack growth mechanisms are possible with the overall growth rate being controlled by the relative kinematics of the alternative mechanisms. However since fracture mechanics allows conditions for different stressed states at the crack tip to be determined for different specimen geometries and loading conditions, it is possible and convenient to relate crack growth rate data to the crack tip stress intensity factor range, ΔK.

For many systems, air fatigue crack growth occurs only above a certain stress intensity factor range known as the threshold stress intensity factor range, ΔK_{th}. A typical $\log(da/dN)$ vesus $\log(\Delta K)$ curve for this system shows that growth rate per cycle first increases rapidly as ΔK is increased above the threshold value. This then enters a region of linear dependence of $\log(da/dN)$ on $\log(\Delta K)$ and finally becomes very rapid as the maximum stress intensity factor approaches the critical value. This is

the characteristic sigmoid shape of air fatigue crack growth rate curves. This typical pattern is shown in figure 1.18 and has been observed to be different from other systems under corrosion fatigue conditions.

Fatigue crack growth behaviour in a corrosive environment is more complex and in contrast to air fatigue crack growth, crack growth for systems that stress corrode show a definable stress intensity factor below which crack growth will not occur. This is termed the stress intensity factor for stress corrosion cracking, K_{ISCC}. For this kind of system, the crack growth rate curve first rises steeply and frequently reaches a plateau value that is independent of K before rising again as K approaches the critical stress intensity factor K_{IC} [1.67].

The steady state corrosion fatigue crack growth rate as a function of crack tip stress intensity factor range, ΔK can be grouped into three different categories as shown in figure 1.21. These three different categories depend on the interaction between the effect of the corrosive environment and the alternating stress that is independent of any existing corrosion mechanism. That is, the relationship between K_{ISCC} if it exists and ΔK_{th}. In any case, the deviation of crack growth rate for the corrosive environment from the air crack growth rate curve, which is used as a reference, will represent the materials sensitivity to the corrosive environment.

As mentioned above, the three categories of crack growth depend on their relationship with K_{ISCC}. The three types of responses to corrosion fatigue can therefore be defined with respect to K_{ISCC}. The first category is true corrosion fatigue and corresponds to a system which is relatively immune to stress corrosion cracking and shows the synergistic effect of the corroding environment and the alternating stress that is independent of any stress corrosion mechanism. This effect is manifested by an increased crack growth rate and a lower threshold stress intensity factor range.

The second category is characteristic of a system for which the critical stress intensity factor for stress corrosion cracking, K_{ISCC}, is significantly lower than K_{IC}. This type of system will exhibit greater sensitivity to stress corrosion cracking which will be

stronger or weaker depending on whether K_{max} is greater or lower than K_{ISCC}. This is typical of a stress corrosion fatigue situation.

The third category as shown schematically in figure 1.21, is a combination of stress corrosion fatigue and true corrosion fatigue with one of them dominating depending on whether K_{max} is greater or less than K_{ISCC} respectively.

As mentioned before, corrosion fatigue is quite complex and there may exist several possible mechanisms with the overall crack growth rate being determined by the relative kinematics of the different mechanisms. A multi-segment type da/dN Vs ΔK dependence shown in figure 1.22 has been thought to be applicable even for lower strength steels. The exact type of behaviour will also depend on additional factors such as the type of loading and the level of cathodic protection in the system. Some of these aspects are covered in the following section and discussed in greater detail in Chapter 3.

1.5.1.3.1 Effects of CP on Fatigue Crack Growth

Cathodic Protection (CP) is the most widely used method for preventing corrosion. It is a remedial measure that was originally thought to improve corrosion fatigue life to levels comparable to that in air. Cathodic protection is achievable in two ways. One of these methods involves attaching a sacrificial anode to the structure to be protected and the other requires the application of a cathodic potential or current to the structure to be protected by use of an external current generator. This method is referred to as the impressed current method. The impressed current method was used for corrosion fatigue tests carried out in this study and is described in detail in Chapter 3.

Depending on the method adopted, the difficulty in maintaining a uniform cathodic potential over the entire structure and the actual levels of these potentials are known to have considerable effect on the fatigue crack propagation rates of materials

exposed to corrosive environments under cathodic protection conditions. This behaviour was observed on SE 702 and the results are presented in Chapter 3.

The actual levels of cathodic protection used in fatigue tests can be classed simply into three categories. Under-protection (free corrosion), adequate protection and over-protection. These categories are a function of the relative magnitudes of the protection potential and the equilibrium potential for the free corrosion of bare steel in sea water, This dependence on electrode potential is shown schematically in figure 1.23. The equilibrium potential for free corrosion of bare steel in sea water is approximately $-650mV$ with respect to Ag/AgCl reference electrode and adequate cathodic protection is said to be achieved when the protection potential reaches a level which is just sufficient to prevent dissolution of iron ions in the aqueous solution. This adequate CP level has been identified to be around $-850mV$ and has been used in a wide range of fatigue tests as part of the UKOSRP programmes. The fatigue tests carried out in this study have assessed the effect of CP on High strength steels and presented in Chapter 3.

Fatigue tests carried out under free corrosion potentials ($-600mV$ to $-700mV$) have been shown to produce shorter fatigue lives when compared to air tests [1.75, 1.76, 1.77, 1.78, 1.79]. These tests showed similar environmental reduction factors between 2 and 3 with the larger reduction factors occurring at lower stresses suggesting a possible effect from a greater exposure time characteristic of tests carried out at lower stress ranges.

There seems to be general agreement that moderate cathodic protection can produce a corrosion fatigue performance of initially smooth specimens of the lower strength structural steels comparable to that in air [1.67]. However the effect of moderate cathodic protection potentials on welded tubular joints is far less conclusive as the data for tubular joints seem to exhibit inconsistency. For example there was some discrepancy between the sea water tests carried out as part of the UKOSRP II [1.4] programme when compared in terms of environmental reductions factors with results obtained from the UKOSRP I [1.3] plate joint tests. It has been noted [1.74] that

individual tubular joint test programmes show a trend towards longer lives at low stresses with a cathodic protection level of $-850mV$.

The influence of cathodic overprotection on fatigue crack growth rates is even less conclusive as the data for tests conducted using cathodic potentials in excess of $-1000mV$ are limited especially on high strength steels and primarily on medium strength steel plate specimen tests. Previous research however suggests that very negative cathodic potentials may have a detrimental effect on the fatigue performance of BS 4360 50D in sea water. Tests on API-X65 steel also show that cathodic overprotection can result in accelerated crack growth rates when compared to free corrosion and air fatigue crack growth data [1.80, 1.81].

In general, the effects of both under protection and over protection are of considerable importance for crack growth in a corrosive environment under cathodic protection conditions especially due to the fact that different materials may show different responses to these two extreme conditions. For instance it is known that some steels may be subject to hydrogen embrittlement cracking depending on the level of protection potential used. There is evidence that cathodic polarisation may be of little benefit in reducing corrosion fatigue crack growth rates and that cathodic overprotection may be decidedly detrimental especially for high strength steels. A review of UK and other design guidance suggests that cathodic protection potentials more negative than $-850mV$ may be detrimental to steels with strength levels above 700 MPa and that in some instances even $-800mV$ may be detrimental to steels with yield strengths higher than 800 MPa [1.82]. This dependence of crack growth rates is presented further in Chapters 3 and 4 where the effects of cathodic protection on both fatigue crack initiation and propagation are discussed for a typical high strength steel, SE 702.

Tests on API X65 pipeline steel have shown that high cathodic protection potentials can increase crack growth rates by as much as 50 times over those observed in air [1.67]. This effect may be worse for high strength steels which are thought to be more susceptible to hydrogen embrittlement cracking. Data on the effects of variable amplitude loading is limited for these class of steels

1.5.2 Analysis of variable amplitude loading

The current guidance on fatigue assessment and design of welded connections and welded Offshore tubular joints is still rather limited with respect to the variable amplitude loading experienced by Offshore structures in service.

The available design S-N curves are based on constant amplitude tests, while in-service loading experienced by Offshore structures has both variable amplitude and frequency content. A number of tests have been carried out [1.4, 1.83, 1.84] using variable amplitude loading. However the data was not incorporated in the proposed S-N curves. The effect of environmental loading (variable amplitude loading) on fatigue performance and crack propagation in high strength steels is an important aspect of this work and has been covered in greater detail in Chapters 2 and 3. However a brief review of current guidance on the design of Offshore structures against variable amplitude fatigue using S-N curves is given here.

The current edition of API RP 2A LRFD [1.17], under the section on Fatigue analysis recommends that "the wave climate should be derived as the aggregate of all sea states to be expected over the long period. This may be condensed into representative sea states characterised by wave energy spectra". This document further adds that the stress response calculated for each location should be combined into the long term stress distribution used in calculating the cumulative damage ratio. The approach outlined in this document does not make any allowances for any sequence or sea state interaction effects which may be present under service loading conditions where several sea states of different significant wave heights may characterise the long term distribution of stresses in a structure. This aspect of variable amplitude corrosion fatigue in Offshore structures is reported in greater detail in Chapters 3 and 4 where the results of fatigue tests carried out for this study are presented in terms of a sea state sequence and the variations in crack growth rates accounted for.

The earlier editions of the Norwegian Petroleum Directorate Design Rules does not provide any specific guidance on the effect of variable amplitude loading. The document recommends a similar damage summation model to that in API RP 2A. i.e.

$$D_s = \sum\left(\frac{n}{N}\right) \tag{1.24}$$

The damage summation level D_s recommended by this code is however, unlike API, "taken equal to 1.0 for any part of the structure unless otherwise specified by the NPD".

The same damage summation rule was recommended by AWS with a damage summation level of one third for critical joints. Similarly, DnV recommends the use of Miners rule for the determination of cumulative damage. It indicates that the calculated damage summation failure limit should range from 0.1 to 1.0. This is a very conservative level and is relevant to practical situations were inspection and maintenance operations are limited. The DnV rules also requires that, in establishing the long term distribution of stress range, variable loads arising from influences such as waves, wind, current etc. should be accounted for.

Lloyds register of shipping also recommends the use of miners rule with a summation level "normally taken as 1.0"

The recommendations proposed by UK Department of Energy guidance notes were based on variable amplitude tests carried out on welded plates with respect to a best fit constant amplitude curve from tests on similar joints. The document recommends the use of a damage summation level of unity for both tubular and plate joints.

Overall, the effect of miners rule on an S-N curve is shown in figure 1.24. Thus even in present day, constant amplitude loading is generally assumed when analysing the behaviour of tubular joints. At present Miners rule is generally accepted and any other fatigue damage prediction method requires an assumption on the accumulation of damage resulting from variable amplitude stress cycles of any stress sequence. Variable amplitude used within the context of existing methods and codes based on S-N curves seems to be based on a fundamental assumption that individual cycles from a variable amplitude process cause the same damage as if each individual cycle were part of a constant amplitude series. This has been an aspect for discussion by many researchers and different explanations have been proposed to account for the effect of

variable amplitude loading in fatigue crack growth mechanism. This is discussed in greater detail in Chapter 4..

The effect of loading conditions on corrosion fatigue crack growth can be understood only by attempting to study the effect this has on the crack tip, a region of rapidly deforming material where new surfaces are being created at a rate that is not easily definable. This sort of approach is very difficult and not well understood for variable amplitude loading conditions where the stress time behaviour and the crack tip stress intensity factor range both determine crack growth rate.

However by calculating the relevant strain rate for the crack tip using the crack opening displacement for each cycle it has been shown that, the strain rate will initially be very high but decreases with increasing load for monotonic loading [1.67]. In a similar way, triangular wave forms give an initially high strain rate which decreases as the maximum load is approached. Unloading is however known [1.67] to be affected by factors such as reversed plastic flow, crack closure crack extension and crack tip profile. For sinusoidal loading on the other hand the strain rate will be zero at the minimum stress, reach a maximum during the loading cycle and fall to zero again at the maximum stress. Hence in a cyclic loading situation the region at the crack tip will experience high strain rates with the continual generation of new surface if the crack is growing.

The relationship between crack tip strain rate and variable amplitude loading fatigue cycles is not as clear as the case for constant amplitude wave forms due to possible sequence effects or load interaction effects which could be quite significant. A number of possible models have been proposed to explain the variability in crack growth rates observed under variable amplitude loading and to predict fatigue crack growth under these conditions. In each of these models, discussed in Chapter 4, separate mechanisms involved are not necessarily exclusive as a number of them may be operating simultaneously.

The following section presents an established method used in analysing a variable amplitude load sequence. This is very important as it is used to identify the significant events in the sequence which are directly relevant to fatigue damage. These analysis

methods are referred to as cycle counting. Cycle counting methods can be broadly classified into two categories - conventional and theoretical methods.

1.5.2.1 Conventional Methods of Cycle Counting

Cycle counting is the process of reducing a complex variable amplitude load history into a number of constant amplitude stress excursions which can be related to available constant amplitude test data. This is a necessary step which needs to be carried out in order to predict fatigue crack growth in components subjected to variable amplitude loading. The method of cycle counting used often depends on the occurrences in the particular sequence which are considered to be significant in terms of fatigue damage. Several counting methods have been developed in this respect. The more commonly used methods include rainflow counting, range counting and peak counting. One of the most important considerations in cycle counting is that the basis of the counting method needs to be compatible with the understanding of the relevance of stress fluctuations to the fatigue process. Some of these methods are discussed below.

1.5.2.1.1 Rainflow Counting

The rainflow method of cycle counting derived its name from an analogy used by Matsuishi and Endo in their early work [1.85] on cycle counting. It has since become a generic term that describes any cycle counting method which attempts to identify closed hysteresis loops in the stress-strain response of a material subjected to cyclic loading. A number of different rainflow counting techniques can be identified which vary in principle from the original rainflow method [1.85, 1.86, 1.87, 1.88, 1.89]. These include other methods such as range-pair counting, hysteresis loop counting and ordered overall range counting. The main advantage of using this method of cycle counting is that it identifies closed hysteresis loops in the material stress-strain response and thus represents the most accurate method for local strain type analysis. When used in conjunction with the predicted stress-strain response of a material, this

method of cycle counting provides insight into the effect of a given strain history on the materials response. When the stress-strain response of the material is considered, the mean stress of the hysteresis loops can also be determined.

1.5.2.1.2 Peak Counting

Peak counting [1.90] can be implemented in a number of ways depending on the way the significant events, peaks, are counted. The method is based on the identification of local maximum and minimum stresses in the continues sequence. *Positive and Negative Peak Counting* is implemented for example by counting positive peaks above and negative troughs below zero which fall into prescribed stress increments. Using this technique implies that troughs which are negative peaks above or positive peaks below zero are not taken into account directly.

Peak counting can also be implemented by setting a datum at the lowest stress in the sequence and counting only the positive peaks present. This method is known as *Positive Peak Counting*. By using this approach it is assumed that all minima occur at the datum level. This method will amplify small variations in stress and increase overall excursions of stresses in the sequence. The distortion introduced by using this method can be avoided by using *Net Peak Counting*. To implement Net Peak Counting, peaks are measured from the preceding trough root which is taken as the datum. When the *Positive and Negative Peak Counting* method is used in conjunction with this method, the zero stress line is taken as the datum when it is reached.

In an alternative peak counting method, only one count of the highest peak, positive or negative, is made between two successive zero crossings. This is known as the *Zero-Crossing Peak Counting* and ignores all peaks smaller than the highest between zero-crossings. This means that significant load excursions may be ignored by using this method leading to considerable distortion of the original sequence.

1.5.2.1.3 Range Counting

Simple Range Counting [1.90] requires that only the stress or strain ranges between successive reversals are counted. This method can be used to record information on the actual stress ranges that have occurred. However it does not give any information on the actual peaks unless the stress returns to zero between cycles. In determining the number of cycles in a sequence, if both positive and negative ranges are included, each range is assumed to form one-half cycle. In this way positive and negative ranges are paired to form complete cycles which are assumed to have the same mean. This method of cycle counting will not retain the sequence of stress variations. It may also be difficult to pair negative and positive ranges.

The difficulty of assuming a mean level in the Simple Range Counting method can be overcome by also counting the mean value associated with each range. When range counting is implemented in this way it is referred to as *Range-Mean Counting*.

An alternative implementation of range counting is *Range-Pair Counting*. Unlike Simple Range Counting and Range-Mean Counting methods, Range-Pair Counting is independent of the smallest variations neglected. Also, the inability to pair all Ranges is removed as a count is not made unless the ranges pair. This means that the overall sequence may be heavily distorted by using this method although a great part of the sequence can also be retained due to the pairing conditions.

Range counting is quite popular mainly because it can be easily implemented to extract the required load ranges from any known sequence. It is however important to point out here that although Range Pair Counting for example is capable of showing good agreement with total excursion of the original sequence by retaining a great part of the sequence as a result of the pairing conditions, it can also lead to loss of a considerable part of the overall sequence. It is also thought that the main disadvantage of this counting method is that it can produce a large number of small cycles for wide band sequences. Since fatigue damage is largely influenced by larger fluctuations in stress, any analysis based on range counting may be unconservative for long term fatigue damage assessment.

1.5.2.1.4 Level-Crossing Counting

This is a cycle counting method where a count is made when the load, stress or strain in the sequence crosses a specified level [1.90]. In this method the stress axis of the sequence is divided into a number of increments as required and a count is made each time a positively sloped portion of the stress history crosses an increment located above the reference level. Similarly, a count is made each time a negatively sloped portion of the sequence crosses an increment located below the reference stress level. For this type of cycle counting, the reference level can be arbitrarily selected but when zero is used as the reference level it is known as *Zero-Crossing Counting*. Like the previous methods, the individual crossings have to be combined to form complete cycles. In this way, the most damaging combination in terms of fatigue are obtained by first forming the largest cycles. Zero-crossing counting is significant for Offshore structures as it is used to establish sea state statistics. It is also more conservative in terms of fatigue damage as it leads to the identification of large cycles.

Like other cycle counting methods the level-crossing counting method does not lead to a complete reproduction of the original sequence and will lead to a misplacement of load excursions in the sequence. The implication of this is that the effect of a particular cycle or half-cycle may be incorporated into a fatigue damage analysis before it actually occurs. This is particularly relevant for the counting methods like rainflow counting which aim to be more conservative by combining the most damaging fatigue cycles first. Where sequence effects are insignificant, this will have very little implications on the accuracy of fatigue crack growth prediction. However this is not always the case especially for Offshore structures where sea state interaction effects are most likely to be too significant to be ignored in any crack growth prediction model.

1.5.2.2 Theoretical Methods of Cycle Counting

Conventional cycle counting methods described above require the generation of the variable amplitude sequence of interest. This is usually a lengthy process but it is not a problem when dealing with sequences used in variable amplitude fatigue test

programmes as these are readily available for cycle counting. This approach to cycle counting is however difficult to implement when dealing with service loading experienced by Offshore structures in the North Sea for example. The need to calculate equivalent stresses under conditions like this without a pre-knowledge of the loading sequence lead to the development of fast assessment methods [1.13] for use during structural integrity assessment procedures. The way these methods can be incorporated into a more robust methodology to fatigue crack growth assessment in Offshore structures is presented and discussed in Chapter 5. The background knowledge of these fast assessment procedures is presented here.

1.5.2.2.1 Wirsching Equation

Wirsching's work [1.91] in the development of fast assessment equations was the first of its kind. He assumed that the equivalent damage from a broad band signal, D_{BB}, can be related to that due to a narrow band signal, D_{NB}, such that;

$$D_{BB} = \lambda D_{NB} \tag{1.25}$$

Where $\lambda = a + (1-a)(1-\varepsilon)^b$, $a = 0.926 - 0.033m$ and $b = 1.587m - 2.323$. ε is the band width parameter and m is the material's Paris law exponent.

Using Wirsching's approach, the equivalent stress, S_h, for both broad and narrow band signals with root mean square, σ, can be calculated by using a Gamma function, $\Gamma(x)$, such that;

$$S_h = 2\sqrt{2\sigma}\left[\lambda\Gamma\left(\frac{m}{2}+1\right)\right]^{\frac{1}{m}} \tag{1.26}$$

where $\Gamma(x) = 2\int_0^\infty u^{2x-1}\exp(-u^2)du$ and u is an arbitrary function or variable.

1.5.2.2.2 Chaudhury and Dover Equation

A similar equation was also proposed by Chaudhury and Dover [1.92]. This is given as;

$$S_h = 2\sqrt{2\sigma}\left[\frac{\varepsilon^{m+2}}{2\sqrt{\pi}}\Gamma\left(\frac{m+1}{2}\right)+0.75I\Gamma\left(\frac{m+2}{2}\right)\right]^{\frac{1}{m}} \tag{1.27}$$

Where I is the irregularity factor and all the other variables are previously defined. Equation 1.27 was considered a better alternative to Wirsching's equation since it was developed after an extensive study of the distribution of peaks in typical Offshore power spectra. Chaudhury and Dover's equation is based on the assumption that the equivalent stress range for typical Offshore spectra lies between a narrow and broad band solution. It is essentially a semi theoretical solution given as the sum of two standard distributions.

1.5.2.2.3 Hancock Equations

Hancock proposed two different equations. These are given as [1.93];

$$S_h = 2\sqrt{2\sigma}\left[I\Gamma\left(\frac{m}{2}+1\right)\right]^{\frac{1}{m}} \qquad (Equation\ A) \tag{1.28}$$

$$S_h = q\sigma\left[\Gamma\left(\frac{m}{h}+1\right)\right]^{\frac{1}{m}} \qquad (Equation\ B) \tag{1.29}$$

Where $q = \sqrt{2}(2-\varepsilon^2)$, and $h = 2-\varepsilon^2$

He assumed a Weibull distribution of peaks and used curve fitting to develop empirical parameters which depended on the spectral properties and resulted in the best fit to the Weibull distribution. The main difference between the two equations is that equation A is a function of the irregularity factor while equation B depends on the

bandwidth parameter. They both therefore accounts for the spectral bandwidth of the PSD used.

1.5.2.2.4 Kam and Dover Equations

The theoretical cycle counting equation proposed by Kam and Dover [1.13] is of the following form;

$$S_h = \left(2\sqrt{2\sigma}\right)\left[Eq1 + Eq2\right]^{\frac{1}{m}} \tag{1.30}$$

Where $Eq1 = \frac{\varepsilon^{m+2}}{2\sqrt{\pi}}\Gamma\left(\frac{m+1}{2}\right) + \frac{I}{2}\Gamma\left(\frac{m+2}{2}\right)$,

$$Eq2 = I\int_0^{\infty} erf(x)\left(\frac{\varepsilon x}{I}\right)^{m+1}\exp\left\{-\left(\frac{\varepsilon x}{I}\right)^2\right\}d\left(\frac{\varepsilon x}{I}\right)$$

$$erf(x) = \frac{2}{\sqrt{\pi}}\int_0^x \exp\left(-u^2\right)du \text{ and } \Gamma(x) = 2\int_0^{\infty} u^{2x-1}\exp\left(-u^2\right)du$$

All the variables are as previously defined. On close examination of the above equation, it can be shown that it is based on the same assumption as the original Chaudhury and Dover equation. The main difference between the Kam & Dover equation and the Chaudhury & Dover equation is that the former does not assume a value 0.25 for the error function ($erf(x)$) as in the latter. This is demonstrated below.

The difference between equations 1.27 and 1.30 lies in the way the second part of the second term (Eq2) of equation 1.30 is analysed. Suppose this part of the equation is represented by *III*, then

$$III = I\int_0^{\infty} erf(x)\left(\frac{\varepsilon x}{I}\right)^{m+1}\exp\left\{-\left(\frac{\varepsilon x}{I}\right)^2\right\}d\left(\frac{\varepsilon x}{I}\right) \tag{1.31}$$

By replacing $erf(x)$ with ¼, equation 1.31 can be rewritten as;

$$III = I\left(\frac{1}{4}\right)\int_0^{\infty}\left(\frac{\varepsilon x}{I}\right)^{m+1}\exp\left\{-\left(\frac{\varepsilon x}{I}\right)^2\right\}d\left(\frac{\varepsilon x}{I}\right) \tag{1.32}$$

This equation can now be rearranged to give;

$$III = I\left(\frac{1}{4}\right)\int_0^{\infty}\left(\frac{\varepsilon x}{I}\right)^{2\left(\frac{m+2}{2}\right)-1}\exp\left\{-\left(\frac{\varepsilon x}{I}\right)^2\right\}d\left(\frac{\varepsilon x}{I}\right) \tag{1.33}$$

At this point recalling that $\Gamma(x)=2\int_0^{\infty}u^{2x-1}\exp(-u^2)du$, $\Gamma(x)$ can be substituted into equation 1.33. This allows *III* to be expressed as a function of the Gamma function, $\Gamma(x)$. Using $\left(\frac{m+2}{2}\right)$ in place of x and $\left(\frac{\varepsilon x}{I}\right)$ in place of u in the standard Gamma function gives;

$$III = I\left(\frac{1}{4}\right)\Gamma\left(\frac{m+2}{2}\right) \tag{1.34}$$

Re-substituting this into the original equation (1.30) gives;

$$S_h = \left(2\sqrt{2\sigma}\right)\left[\frac{\varepsilon^{m+2}}{2\sqrt{\pi}}\Gamma\left(\frac{m+1}{2}\right)+\frac{I}{2}\Gamma\left(\frac{m+2}{2}\right)+I\left(\frac{1}{4}\right)\Gamma\left(\frac{m+2}{2}\right)\right]^{\frac{1}{m}} \tag{1.35}$$

$$\Rightarrow S_h = \left(2\sqrt{2\sigma}\right)\left[\frac{\varepsilon^{m+2}}{2\sqrt{\pi}}\Gamma\left(\frac{m+1}{2}\right)+\left(\frac{I}{2}+\frac{I}{4}\right)\Gamma\left(\frac{m+2}{2}\right)\right]^{\frac{1}{m}} \tag{1.36}$$

$$\Rightarrow S_h = \left(2\sqrt{2\sigma}\right)\left[\frac{\varepsilon^{m+2}}{2\sqrt{\pi}}\Gamma\left(\frac{m+1}{2}\right)+0.75I\Gamma\left(\frac{m+2}{2}\right)\right]^{\frac{1}{m}} \tag{1.37}$$

Equation 1.37 is identical to the equation originally proposed by Chaudhury and Dover (equation 1.27). Thus the fundamental difference between Chaudhury & Dover and Kam & Dover equations lies in the way the function, $erf(x)$, is approximated.

The Kam and Dover equation has undergone a detailed investigation and has been shown [1.13] to be more accurate in determining the equivalent stress from a stress spectrum without cycle counting. This accuracy was determined by comparing predicted results with those obtained using conventional rainflow cycle counting. Details of these results are given in [1.13]. This section highlights how this more accurate theoretical method can be used together with a proposed sea state probability distribution function to predict equivalent stresses directly. This approach has very wide implications for fatigue analysis of Offshore structures under service conditions as it will allow equivalent stresses to be estimated for multi-sea state loading over any period of interest. Details of this approach are presented in Chapter 5 together with the derivation of the sea state probability distribution function and how it can be used together with fast theoretical assessment equations to determine any equivalent stresses required.

1.6 SUMMARY

Stress analysis and fatigue design of tubular welded connections has been reviewed in this Chapter. Despite the availability of all the methods discussed for determining the stresses and stress concentration factors in tubular welded joints, the method adopted for any particular design will depend on the constraints of time, cost, and the accuracy required.

Photoelastic methods have been superseded by finite element analysis. Finite element analysis is also an expensive technique though this depends on the element formulation used in the analysis and the computational time required for the accuracy needed. As already mentioned, the use of strain gauge measurements on steel models is known to be the most reliable way of determining stress concentration factors. However this method is time consuming and also represents an expensive way of determining SCFs.

The use of parametric equations, which are based on finite element analysis and validated by experimental results, can represent a very quick way of checking SCFs

before any detailed analysis is carried out where necessary. A summary of the recommended parametric equations for the joint geometry used in this study is shown in table 1.5 This method provides an expedient analysis method for simple planar tubular joint designs.

However, each set of parametric equations is limited in application in one of three ways; There are restrictions in the types of joint geometry that can be analysed using these equations, restrictions on parametric validity range and restrictions on the loading configuration covered by any particular set of parametric equations. These restrictions constitute a limitation in the use of parametric equations to determine stress concentration factors in tubular welded joints used in Offshore structures. As a result, the design of more complex joint geometries still requires the use of some form of finite element analysis since the currently available parametric equations are limited in applicability in the design of more complex joints.

On the subject of fatigue design of welded Offshore structures, the two approaches available are the S-N approach and the fracture mechanics approach. The S-N method relies on the use of available experimental data. However due to the inherent scatter associated with the limited experimental data available, large factors of safety or reduction factors on life are still applied to give conservative results and also to account for different factors which are known to control the fatigue performance of a welded joint. Currently there is no guidance available on the use of high strength steels and it is hoped that data obtained from this study will provide useful information which can be used towards the formulation of future guidance. As more reliable experimental data becomes available this method of fatigue design will also become increasingly more reliable and cost effective. This is demonstrated by the modification of the reduction factors on life as more data becomes available to give less conservative estimates and narrow down the largely unnecessary safety margins recommended by the previous fatigue design guidance. At the same time, as more material data becomes available, the potential for using fracture mechanics analysis for both design and also for structural integrity analysis and inspection scheduling for Offshore structures will gain more ground. At this point, fracture mechanics analysis remains the most powerful and useful scientific tool for describing and solving fatigue

crack problems. This is an important aspect for this thesis. The use of fracture mechanics and the different models available for the analysis of Offshore structures will be discussed in greater detail in Chapters 4 and 5.

Corrosion fatigue has been reviewed here in general and particular attention has been given to some of the mechanisms that have been proposed to explain corrosion fatigue crack initiation and propagation as observed in recent years. The use of cycle counting has also been reviewed. Different fracture mechanics models used to predict fatigue crack growth rates and to model the different observations of crack growth retardation and acceleration observed during variable amplitude loading conditions are covered in Chapters 4 and 5.

Through this review it is apparent that one of the main difficulties in trying to quantify variable amplitude corrosion fatigue is the large number of variables involved which almost always operate as a combination to influence fatigue crack growth at any one time. Some of these variables include material properties determined by the alloying elements present, the nature of the corrosive environment determined mainly by its chemical composition and additional factors such as flow velocity, temperature., pH and degree of aeration, the magnitude of cyclic loads applied and also the loading frequency. These factors can however be adequately controlled in a laboratory to carry out tests under realistic loading and environmental conditions as described in Chapter 3. A considerable amount of data is now available for fixed platform structural steels such as 50D. There is significantly less fatigue data available on high strength Jack-up steels and this investigation, on SE 702, seeks to address part of this shortfall, especially under simulated service conditions.

1.7 REFERENCES

[1.1] Billingham, J, Healy, J and Spurier J, "*Current and Potential use of High Strength Steels in Offshore Structures*", Publication No. 95/102, Marine Technology Directorate Limited, London 1995.

[1.2] Stacey A, Sharp J V and King R N, "*High Strength Steels used in Offshore Installations*", Proceedings of the Fifth International Conference on Offshore Mechanics and Arctic Engineering, American Society of Mechanical Engineers, Vol. III, New York, 1996.

[1.3] *United Kingdom Offshore steels Research Project-Phase I: Final Report*, Ed. Peckover R, Health and Safety Executive Report OTH 88 282, Her Majesty's Stationary Office, London 1988.

[1.4] *United Kingdom Offshore steels Research Project-Phase II: Final Summary Report*, Ed. Peckover R, Health and Safety Executive Report OTH 87 265, Her Majesty's Stationary Office, London 1987.

[1.5] BS 4360: 1990, *Weldable Structural Steels,* British Standards Institution, London 1990.

[1.6] BS 7191: 1989, *Weldable Structural Steels for fixed Offshore Structures,* British Standards Institution, London 1989.

[1.7] Sharp J V, Billingham J and Stacey A, "*Performance of High Strength Steels Used in Jack-ups*", Proceedings, Sixth International Conference, The Jack-up Platform, Design, Construction & Operation, Ed. Boswell L F, D'Mello C and Supple W J, London, 1997.

[1.8] Health and Safety Executive (1995), *Offshore Installations: Guidance on Design Construction and Certification*, Fourth Edition, Third Amendment, HSE Books, Sudbury, Suffolk, UK.

[1.9] Davey, V S, "*Hydrogen Assisted Cracking of High Strength Steels in the Legs of Jack-up Rigs*", Recent Developments in Jack-up Platforms, Ed. Boswell L. F. and D'Mello C.

[1.10] *Hydrogen Assisted Cracking in High Strength Steels*, Health and Safety Executive Report OTH 91 351, Her Majesty's Stationary Office, London, 1992.

[1.11] Myers P, *Corrosion Fatigue Fracture Mechanics of High Strength Jack Up Steels*, Ph.D. Thesis submitted to London University, Feb. 1998

[1.12] Baron, G. "*Super Elso SE702*", Creusot Loire Industrie, February 1989

[1.13] Kam J C, "*Structural Integrity of Offshore Tubular Joints Subject to Fatigue*", Ph.D. Thesis ,Department of Mechanical Engineering, University College London, 1989

[1.14] *Design of tubular joints for Offshore structures*, Vol. 2, Published by UEG Offshore Research, 1985.

[1.15] Det Norske Veritas, *Rules for the design, construction and inspection of fixed Offshore structures*, DnV, 1977 (plus 1982 amendments)

[1.16] Lloyds Register of Shipping, *Fatigue Analysis of Fixed Steel Platform welded tubular joints*, Fatigue Appendix, Issue 5 July 1980

[1.17] American Petroleum Institute, *Recommended Practice for Planning, Designing and Constructing fixed Offshore Platforms*, API RP2A 20th edition, 1993.

[1.18] American Welding institute, *Structural Welding Code*, AWS D1.1-84, 1984

[1.19] Norwegian Petroleum Directorate, *Regulations for the Structural Design of Fixed Structures on the Norwegian Continental Shelf*, 1977.

[1.20] British standards Institution, *Code of practice for fixed Offshore structures*, BS 6235: 1982

[1.21] Department of Energy, *Offshore Installations Guidance on Design and Construction*, HMSO, London, April 1984

[1.22] Donnell L H, "*Stability of thin walled tubes under torsion*", National Advisory Committee on Aeronautics (NASA)", Report No. 479, 1934

[1.23] Flugge W, "*Statik and Dynamik der schalen*", Springer, Berlin, 1934

[1.24] Biljaard P P, "*Stresses from radial loads in cylindrical pressure vessels*", The Welding Journal 33(12), Research Supplement 1954, 615S-623S.

[1.25] Toprac A A et al, "*Welded tubular connections: an investigation of stresses in T joints*", Welding Journal, Jan. 1966.

[1.26] Hoff N J et al, "*Deformation and stresses in circular cylindrical shells caused by pipe attachments*", Knolls Atomic Power Laboratory Reports KAPL 921, 922, 923, 924, 925, 926 and 1025, Nov. 1953

[1.27] Kempner et al, "*Tables and curves for deformation and stresses in circular cylindrical shells under localised loading*", Journal of Aeronautical science, Vol. 24 No 2, Feb. 1957, pp. 119-129.

[1.28] Kellogg M W, *Design of Piping Systems*, 2nd edition, Wiley. 1956

[1.29] Marshall P W, "*General consideration for tubular joint design*", Proceedings of Welding Institute Conference on welding in Offshore construction, Newcastle, Feb. 1974

[1.30] Dundrova V, "*Stresses and intersection of tubes, Cross and T joints*", Technical report from Structures Fatigue Research Laboratory, Department of Civil Engineering, University of Texas, Austin, Jul. 1965.

[1.31] Chen T Y, Chen Z and Wang Y Q, "*The Stress Analysis and Experimental Research of Tubular Joints of Offshore Drilling Platforms*", Journal of Engineering Resource Tech., Trans. ASME, Mar. 1984, Vol. 106

[1.32] Caulkins D W, *Parameter study for FRAMETI elastic stress in joints*, CDG Report 15 shell, Sept. 1968d

[1.33] Rodabaugh E C, "*Review of data relevant to the design of tubular joints for use in fixed Offshore platforms*", Welding Research Council Bulletin No. 256, Jan. 1980

[1.34] Beale L A and Toprac A A, *Analysis of T, Y and K welded tubular connections*, Welding Research Council Bulletin 125, Oct. 1967

[1.35] Reber J B, "*Ultimate strength design of tubular joints*", Paper OTC 1664, Offshore Technology Conference Texas, 1972

[1.36] Kuang J G, Potvin A B and Leick R D, "*Stress concentration in tubular joints*", Paper Society of Petroleum Engineers, 1977

[1.37] Gibstein M B, "*Parametric stress analysis of T joints*", Paper 26, European Offshore steels research Seminar, Cambridge, UK, Nov. 1978.

[1.38] Background to new fatigue design guidance for steel joints and connections in Offshore structures, 1990.

[1.39] Wordsworth A C and Smedley G P, "*Stress concentrations at unstiffened tubular joints*", Paper 31, European Offshore steels research Seminar, Cambridge, UK, Nov. 1978.

[1.40] Holliday G H and Graff W J, "*Three dimensional photoelastic analysis of welded T connections*", Proceedings of Offshore Technology Conference, Texas 1971.

[1.41] Fessler H, "*Comparison of Stress Distribution in a Single Tubular Joint Using 3D Finite Element, Photoelastic and Strain Gauge Techniques*",

Proceedings, International Offshore Technology Conference, ASME Houston, 1983, paper OTC 4646.

[1.42] Elliot K, Fessler H, "*Photoelastic study of hot-spot stresses in tubular joints*": Final report, Cohesive Programme of Research and Development into the Fatigue of Offshore Structures, July 83 - June 85, Final Reports, edited by Dover WD et al UK, 1986.

[1.43] Efthymiou M and Durkin S, "*Stress concentrations in T/Y and gap/overlap K joints*", Behaviour of Offshore Structures, Elsevier Science Publishers B V, Amsterdam, 1985-Printed in the Netherlands.

[1.44] Connolly M P, Hellier A K, Dover WD and Sutomo J, "*A parametric study of the ratio of bending to membrane stress in tubular Y and T joints*", International Journal of Fatigue, 12 No 1, 1990, pp. 3-11.

[1.45] Hellier A K, Connolly M P and Dover W D, "*Stress concentration factors for tubular Y and T joints*", International Journal of Fatigue, 12 No 1, 1990, pp. 13-23.

[1.46] Hellier A K, Connolly M P, Kare R F and Dover W D, "*Prediction of stress distribution in tubular Y and T joints*", International Journal of Fatigue, 12 No 1, 1990, pp. 25-33.

[1.47] L P Pook in *The Role of Crack Growth in Metal Fatigue*, Book 307, published by The Metals Society, 1983, ISBN 0 904357 63 5

[1.48] *Fatigue design handbook*, 2nd edition, ed. Richard Rice, associate eds. Brian N leis, Battelle and Drew V Nelson. Published by the Society of Automotive Engineers, Inc.

[1.49] N M Irvine, *Review of stress analysis techniques used in UKOSRP*, Safety and Reliability Directorate, United Kingdom Atomic Energy Authority.

[1.50] Background to new fatigue design guidance for steel welded joints in Offshore structures. First published in 1984.

[1.51] Wylde J G, Mcdonald A, "*The influence of Joint Dimensions on Fatigue strength of Welded Tubular Joints*", Paper 42, Proceedings, Behaviour of Offshore Structures, International Conference, London August 1979.

[1.52] Marshall P W, "*Size effects in tubular welded joints*", Proceedings, ASCE Structures Congress 1983, Houston, Oct. 1983.

[1.53] Haibach E, Oliver R, Ritter W, "*Fatigue strength of angular fillet welds fabricated from 50mm plate*", Paper 7, European Offshore Steels Research Seminar, Cambridge, Nov. 1978

[1.54] Webster S E, Walker E F, "*The effect of section thickness on the fatigue performance of welded and cast steel joints*", Proceedings, 2nd International Conference On Fatigue and Fatigue Threshold, Ed. Beevers C.J, Sept. 1984.

[1.55] Berge S "*On the effect of plate thickness in weldments*", Engineering Fracture Mechanics. Volume 21, No. 2, 1985, pp. 423-435.

[1.56] Gurney T R, "*The Influence of Thickness on Welded Joints*", Proceedings, International Conference on Offshore Mechanics and Arctic Engineering, ASME, The Hague, 1989.

[1.57] Gurney T R, "*The Influence of Thickness on the Fatigue Strength of Welded Joints*", Paper 41, Proceedings, 2nd International Conference, Behaviour of Offshore Structures, London 1979.

[1.58] Fracture Mechanics Methodology, Evaluation of Structural Components Integrity, Ed. George C S and Luciano De Oliveira Faria, Martinus Nijhoff Publishers, 1984.

[1.59] Rhee H C and Salama M M, "*Opportunities for application of fracture mechanics for Offshore structures*", Fracture Mechanics in Offshore Industry, Reprinted from Applied Mechanics Reviews, Vol. 41, No. 2, February 1988, ASME Book No. AMR032.

[1.60] Dharmavasan S and Dover W D, "*Nondestructive evaluation of Offshore structures using fracture mechanics*", Fracture Mechanics in Offshore Industry, Reprinted from Applied Mechanics Reviews, Vol. 41, No. 2, February 1988, ASME Book No. AMR032.

[1.61] Machida S, Yajima H, Toyosada M, Hagiwara Y and Kajimoto K, "*Japanese research activities in Offshore fracture mechanics applications*", Fracture Mechanics in Offshore Industry, Reprinted from Applied Mechanics Reviews, Vol. 41, No. 2, February 1988, ASME Book No. AMR032.

[1.62] Monahan C C, "Early Fatigue Crack Growth in Offshore Structure", PhD Thesis, Department of Mechanical Engineering, University College London, May 1994.

[1.63] Beevers C J, Bell K, Carlson R L et al "*A model for fatigue crack closure*", Engineering Fracture Mechanics, 19, pp. 93-100, 1984.

[1.64] Bates R C and Clark W G (1969) "*Fractography and fracture mechanics*", American Society for Metals Transactions Quarterly, 62, pp. 380-9.

[1.65] Forsyth P J E, "*A two stage process of fatigue crack growth*", Proceedings, Crack Propagation Symposium, Vol. 1,Cranfield College of Aeronautics, Cranfield, UK, 1962.

[1.66] Beevers C J, Cooke R J,Knott J F et al (1975), "*Some considerations of the influence of sub-critical cleavage growth during fatigue crack propagation in steels*", Metal Science, 9 119-26.

[1.67] Congleton J and Craig I H, "*Corrosion Fatigue*", Corrosion Processes, edited by R N Parkins, Applied Sceince publishers LTD (1982), London and New York

[1.68] Gough H J and Sopwith D G, J. Inst. Metals, 56, 55-89 (1935).

[1.69] Design and Operational Guidance on Cathodic Protection of Offshore Structures, Subsea Installations and Pipelines, Marine Technology Directorate Limited, 1990, ISBN 1 870553 04 7.

[1.70] Saenz de Santa Maria M, Proctor R, "*Environment Cracking (Corrosion Fatigue and Hydrogen Embrittlement) of X-70 Linepipe Steel*", Fatigue and Crack Growth in Offshore Structures, Proceedings IMechE, C137/86, 1986.

[1.71] Cotis R A, "*Stress Corrosion Cracking in High Strength Steels*", Corrosion, Ed. Shrier, Jarman, Burstein 3rd Edition, 1994.

[1.72] Oriana R A, Josephic P H, Acta Metall Vol. 22, 1974.

[1.73] Laird C and Duquette D J, *Corrosion Fatigue, Chemistry, mechanics and Microstructure*, NACE 2 pp. 88-117, 1972.

[1.74] Austin J A, *The Role of Corrosion Fatigue crack growth Mechanisms in Predicting Fatigue life of Offshore Tubular Joints.*, Ph.D. Thesis, Department of Mechanical Engineering, University College London, October 1994.

[1.75] Mohaupt, U H et al, "*Fatigue crack development, thickness and corrosion effects in welded plate to plate joints*", paper TS 3, Proceedings of the 3rd International Conference On steel in marine structures, Delft, 1987.

[1.76] Vosikovsky, O, Bell R, Burns D J and Mohaupt, U H, "*Effects of corrosion fatigue and thickness on corrosion fatigue life of welded plate T joints*", paper TS 44, Proceedings of the 3rd International Conference on Steel in Marine Structures, Delft, 1987.

[1.77] Proceedings of CANMET workshop on Cathodic Protection: a + or - in corrosion fatigue, Halifax, Canada, 1986.

[1.78] Berge S, Astrup O C, Simonsen T and Lian B "*Effect of seawater and cathodic protection in fatigue of welded low carbon micro-alloyed steel*",

paper TS 39, Proceedings of the 3rd International Conference On steel in marine structures, Delft, 1987.

[1.79] Iwasaki T, Wylde J Gand Booth G S, "*Fatigue tests on welded tubular joints in air and sea water*", Fatigue and crack growth in Offshore structures, proceeddings of the IMECHE, 1986-2,1986.

[1.80] Vinas-Pich J, "*Influence of environment loading and steel composition on fatigue of tubular connections*", Ph.D. thesis, Department of Mechanical Engineering, University College London, January 1994.

[1.81] Smith A T, *The Effects of Cathodic Over-protection on the Corrosion Fatigue Behaviour of API 5L X85 Grade Welded Tubular Joints*, Ph.D. Thesis, City University, London 1995.

[1.82] Laws P A, *Corrosion Fatigue Performance of Weldable High Strength Low Alloy Steels for Use Offshore*, Ph.D. Thesis, Cranfield University, 1993.

[1.83] Tilly G P and Nunn D E, "*Variable Amplitude Fatigue in Relation to Highway Bridges*", Proceedings, Institution of Mechanical Engineers, Vol. 194, 1980.

[1.84] Gurney T D, *Summary of Variable Amplitude Fatigue Data for Welded Joints*, The Welding Institute Report No. 3707/3887/1A/87, November 1987.

[1.85] Matsuishi M and Endo T, "*Fatigue of Metals Subjected to Varying Stress*", paper presented to Japan Society of Mechanical Engineers, Fukuoka, Japan, March 1968

[1.86] American Society for Testing and Materials, Annual Book of ASTM Standards, Section 3: Metals Test Methods and analytical Procedures, Vol. 03.01-Metals Mechanical Testing; Elevated and Low Temperature tests, ASTM, Philadelphia, 1986, pp. 836-848.

[1.87] Endo T et al, "*Damage Evaluation of Metals for Random or Varying Loading*", Proceedings of the 1974 symposium on Mechanical Behaviour of Materials, Vol. 1, The Society of Materials Science, Kyoto, Japan, 1974, pp. 371-380,

[1.88] Anzai H and Endo T, "*On-site Indication of Fatigue Damage Under Complex Loading*", International Journal of Fatigue, Vol. 1, No. 1, 1979, pp. 49-57.

[1.89] Endo T and Anzai H, "*Redefined Rainflow Algorithm: P/V Difference Method*", Journal of Japan Society of Materials Science, Vol. 30, No. 328, 1981, pp. 89-93.

[1.90] Bathgate R G "*Service Load Analysis and Random Load Fatigue*", Department of Mechanical Engineering, City University.

[1.91] Wirsching P H, "*Fatigue Under Wide Band Random Stresses*", Journal of the Structural Division, ASCE, July 1980, pp. 1593-1606

[1.92] Chaudhury G K and Dover W D, "*Fatigue Analysis of Offshore Platforms Subject to Sea Wave Loading*", International Journal of Fatigue, Vol. 7, No. 1, 1985, pp. 13-19.

[1.93] Hancock J W and Gall D S, "*Fatigue Under Narrow and Broad Band Stationary Loading*", Part I and II, Cohesive Programme of Research and Development into the Fatigue of Offshore Structures, 1983-85, Final Reports.

[1.94] Smedley P and Fisher P, "*Stress Concentration Factors for Simple Tubular Joints*", Proceedings, First International Offshore and Polar Engineering Conference, 11-16, August 1991, pp. 475-483.

1.8 TABLES AND FIGURES

Table 1.1: Kuang's parametric equations for Y-joints.

Equation	Application	Validity range
$1.020\beta^{0.787}\gamma^{1.014}\tau^{0.889}\sin^{1.557}$	chord SCF	$\beta \le 0.55$
$0.462\beta^{-0.619}\gamma^{1.014}\tau^{0.889}\sin^{1.557}\theta$	chord SCF	$\beta \ge 0.55$
$1.522\beta^{0.801}\gamma^{0.852}\tau^{0.543}\sin^{2.033}\theta$	brace SCF	$\beta \le 0.55$
$0.796\beta^{-0.281}\gamma^{0.852}\tau^{0.543}\sin^{2.033}\theta$	brace SCF	$\beta \ge 0.55$

Table 1.2: Wordsworth and Smedley's parametric equations for Y-joints.

Equation	Application	Validity range
$\beta\gamma\tau\left(1.6-1.15\beta^5\right)\sin^{\left(1.35+\beta^2\right)}\theta$	chord SCF	$8 \le \alpha \le 40$ $0.13 \le \beta \le 1.0$ $12 \le \gamma \le 32$ $0.25 \le \tau \le 1.0$ $30^0 \le \theta \le 90^0$
$\beta\gamma\tau\left(1.6-1.15\beta^5\right)\sin^{\left(1.35+\beta^2\right)}\theta\left(Q_\beta' Q_\gamma'\right)^{\frac{1}{2}}$	(UEG modified) chord SCF	$8 \le \alpha \le 40$ $0.13 \le \beta \le 1.0$ $12 \le \gamma \le 32$ $0.25 \le \tau \le 1.0$ $30^0 \le \theta \le 90^0$
$Q_\gamma' = 1$ for $\gamma \prec 20.0$ and $Q_\beta' = \frac{480}{\gamma(40-0.833\gamma)}$ for $\gamma \ge 20.0$		
$Q_\beta' = 1$ for $\beta \le 0.6$ and $Q_\beta' = \frac{0.3}{\beta(1-0.833\beta)}$ for $\beta \succ 0.6$		
$\sqrt{Q_\beta'}$ is assumed to be valid only for DT, X, K, Y and T-joints $\sqrt{Q_\gamma'}$, was introduced to ensure better prediction for joints with $\gamma \ge 20$.		

Table 1.3: Efthymiou and Durkin's parametric equations for Y-joints

Equation	Application
$\beta\gamma\tau\left(1.7-1.05\beta^3\right)\sin^{1.6}\theta$	chord SCF
$\tau^{-0.54}\gamma^{-0.05}\left(0.99-0.47\beta+0.08\beta^4\right)*\beta\gamma\tau\left(1.7-1.05\beta^3\right)\sin^{1.6}\theta$	brace SCF
$F3=1-0.55\beta^{1.8}\gamma^{0.16}\exp\left[-0.49\gamma^{-0.89}\alpha^{1.8}\right]\quad(\text{for }\alpha<12)$ short chord correction factor	

Table 1.4: Hellier Connolly and Dover's parametric equations.

Equation	Application
$K_{SC}=0.315\alpha^{0.054}\gamma^{\left(1.12-\frac{0.0939}{\theta^2}\right)}\tau\exp\left[\frac{-0.00139}{\beta^4}+0.654\sin^2\theta\right]$	chord saddle SCF
$K_{HSC}=0.255\alpha^{0.013}\gamma^{\left(1.24-\frac{0.224}{\theta}\right)}\tau\exp\left[\frac{-0.00135}{\beta^{4.1}}+0.923\sin\theta\right]$	chord hot spot site
$K_{SB}=0.0788\alpha^{0.091}\beta^{\frac{0.132}{\theta}}\gamma^{0.902}\tau^{0.957}\exp\left[\frac{-0.211}{\beta^{1.2}}+2.62\sin\theta\right]$	brace saddle SCF
$K_{HSB}=0.103\alpha^{0.005}\beta^{\left(-\frac{0.227}{\theta}\right)}\gamma^{0.848}\tau^{0.469}\exp\left[\frac{-0.232}{\beta^{1.2}}+2.59\sin\theta\right]$	brace hot spot site
Validity limits $6.21\le\alpha,\ 0.20\le\beta\le0.80,\ 7.60\le\gamma\le32.0,\ 0.20\le\tau\le1.0,\ 35^o\le\theta\le90^o$	

Table 1.5: Recommended parametric equations for Y-joints under OPB

Location	Words	Efthy	Kuang	UEG	LR	UCL
Chord side	√	√	X	√	√	√
Brace side	√	√	X*	√	√	√

Key	
Words	Wordsworth and Smedley Equations [1.39]
Efthy	Efthymiou and Durkin Equations [1.43]
Kuang	Kuang Equations [1.36]
UEG	UEG Equations [1.14]
LR	Lloyds Register Equations [1.94]
UCL	UCL Equations (HCD) [1.45]
√	Recommend the parametric equation
√c	Recommend the parametric equation - Note equation is generally conservative
N/A	There is no parametric equation for this load case
X	Not recommend the parametric equation, since it fails to meet the acceptance criteria
X*	The equation cannot be recommended since there are less than 15 steel and acrylic joints in the SCF database

Figure 1.1: Typical lattice leg structure of a Jack-up platform

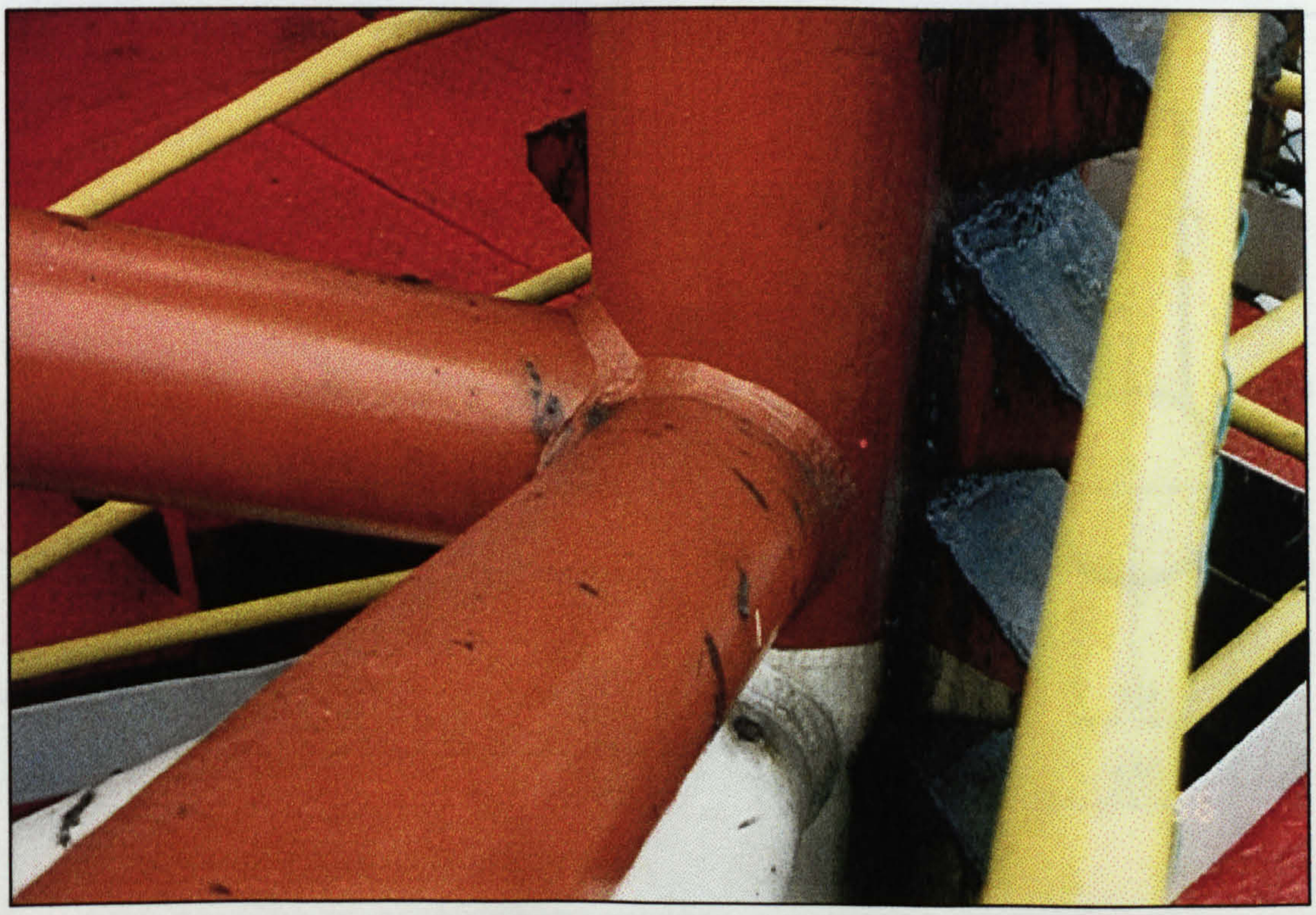

Figure 1.2: Typical Jack-up leg chord with rack plate

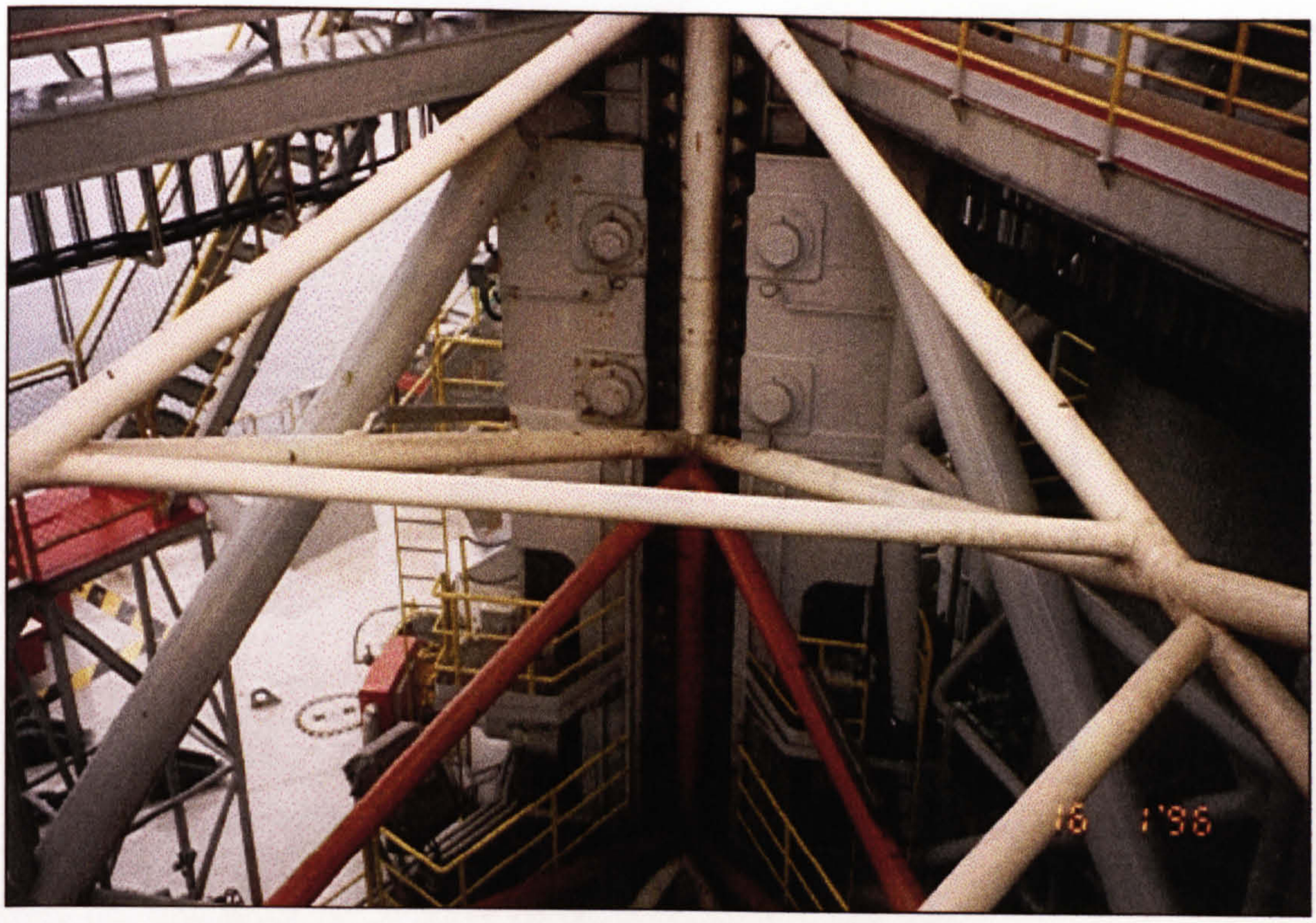

Figure 1.3: Jack-up leg structure showing interconnecting tubular members

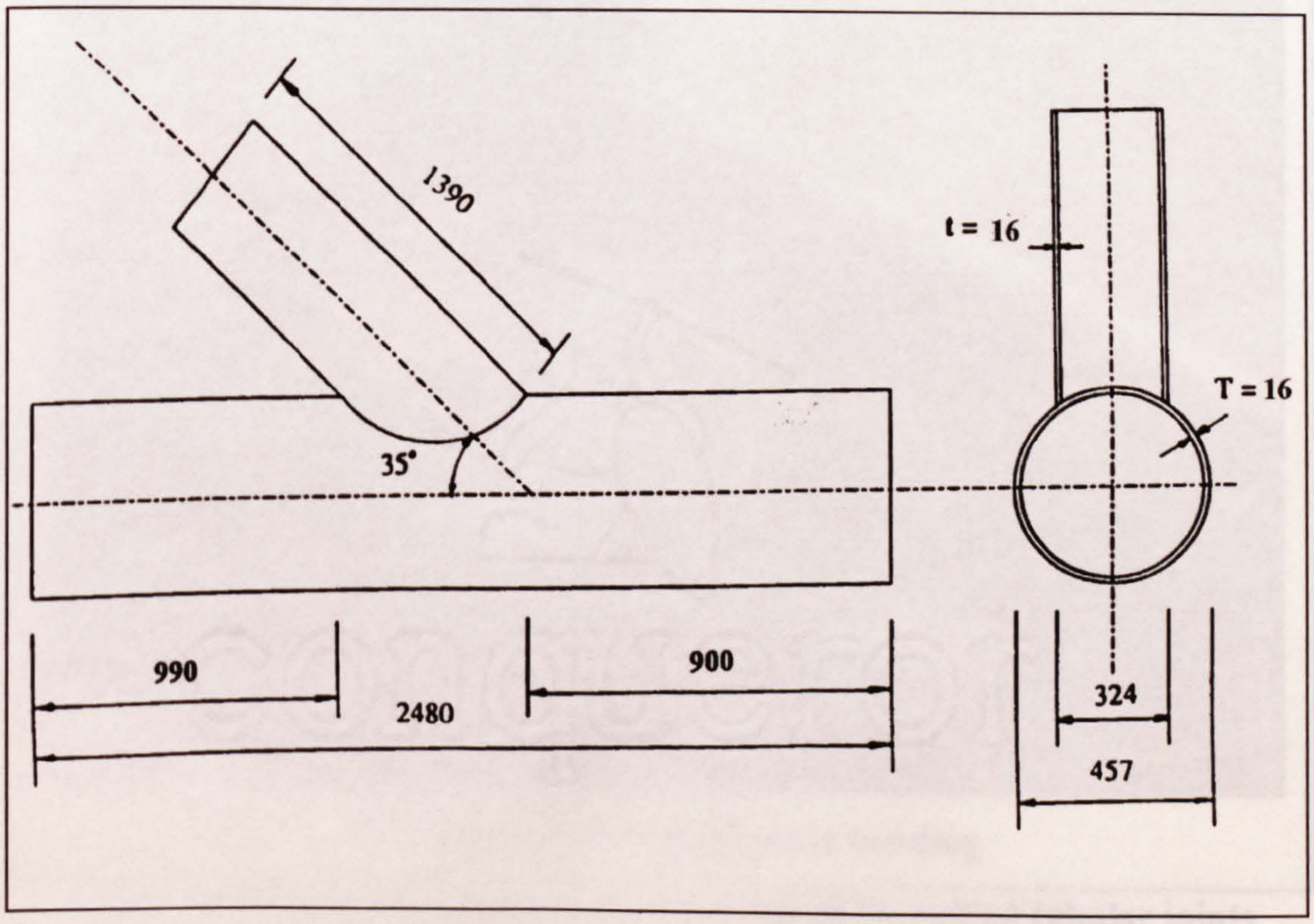

Figure 1.4: Dimensions of Y-joint used in the fatigue tests

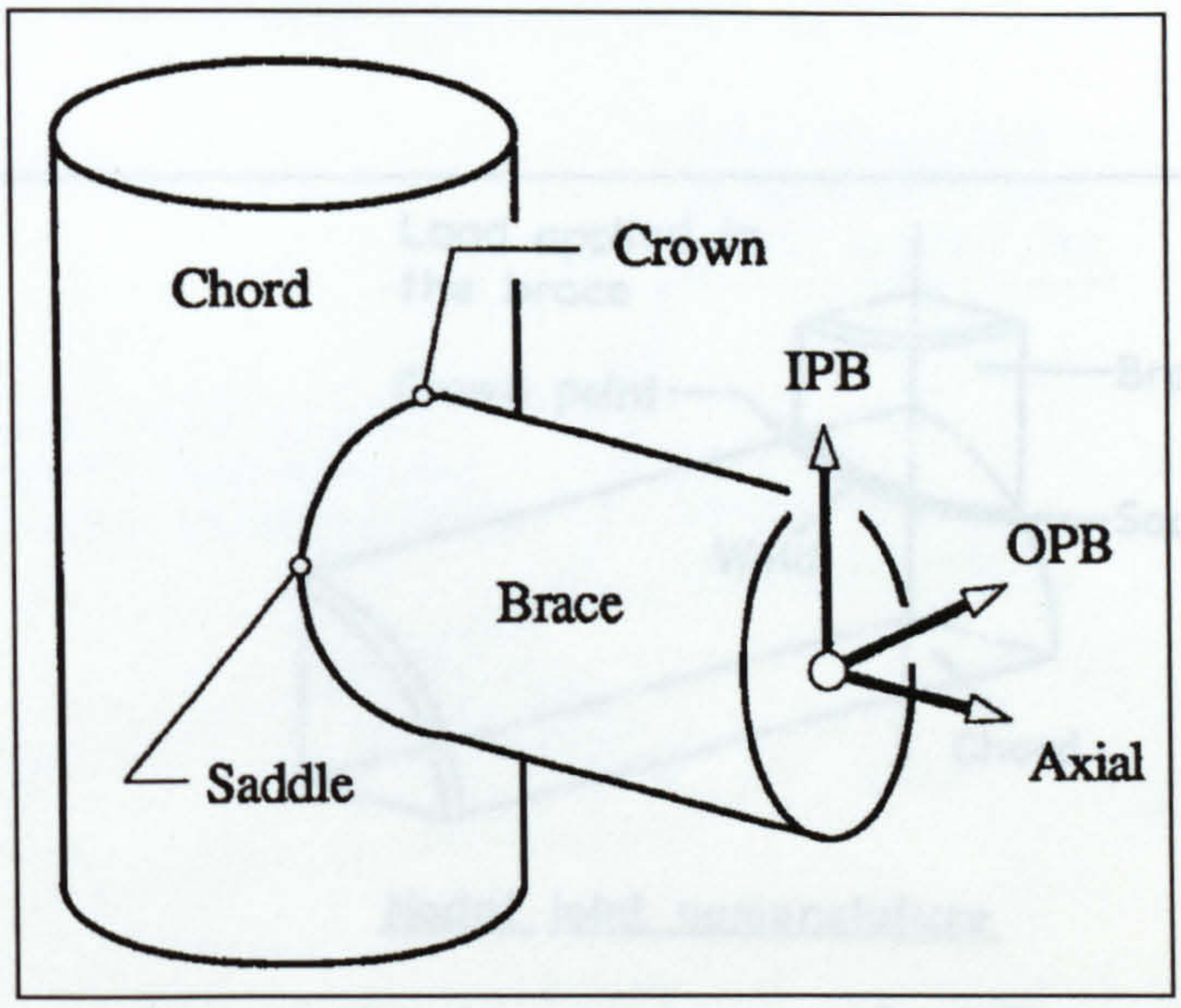

A: Definition of in-plane bending (IPB), out-of-plane bending OPB and axial loading of a welded tubular joint

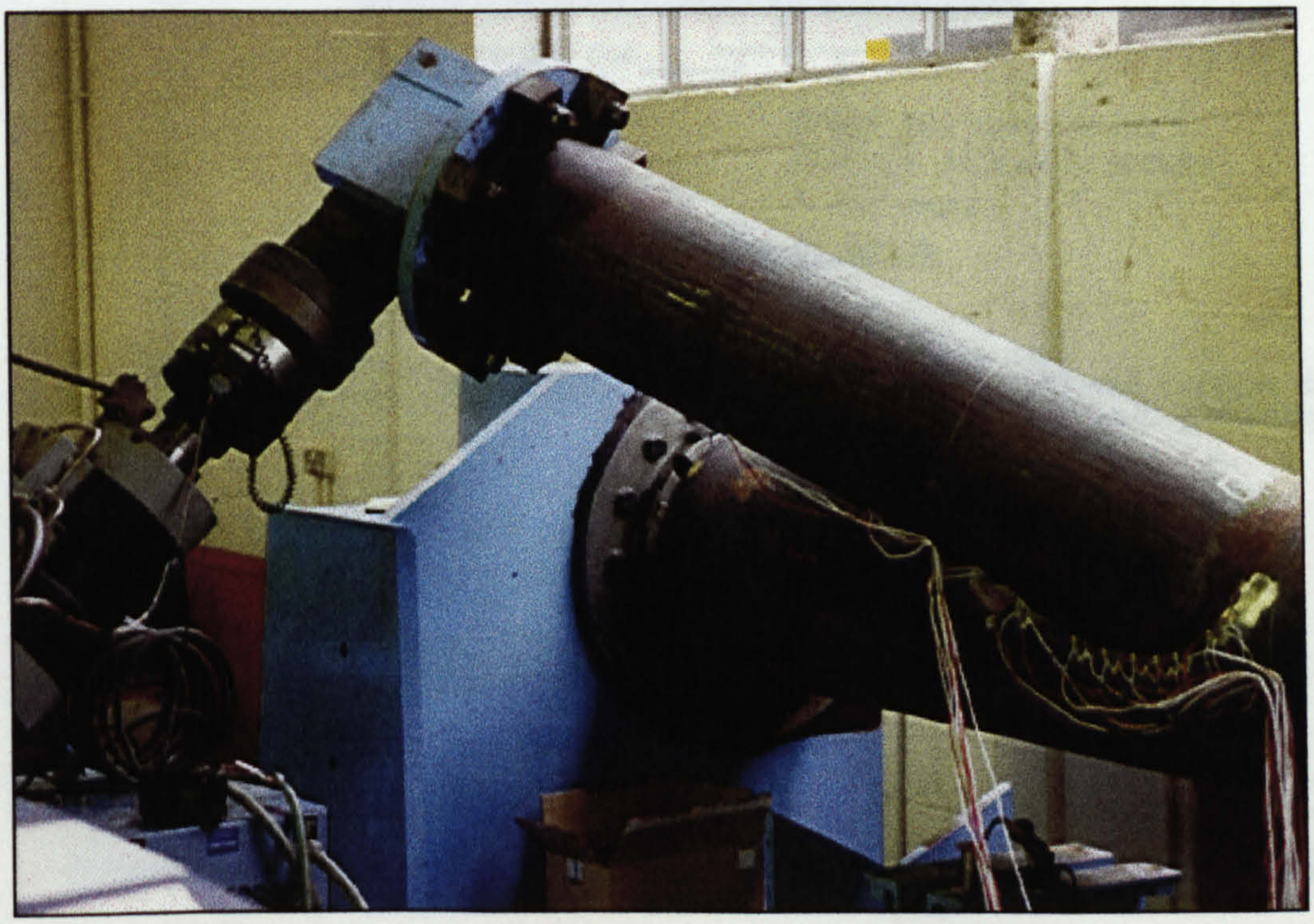

B: Y-joint under out-of-plane bending

Figure 1.5: Typical Loading modes experienced by welded tubular joints

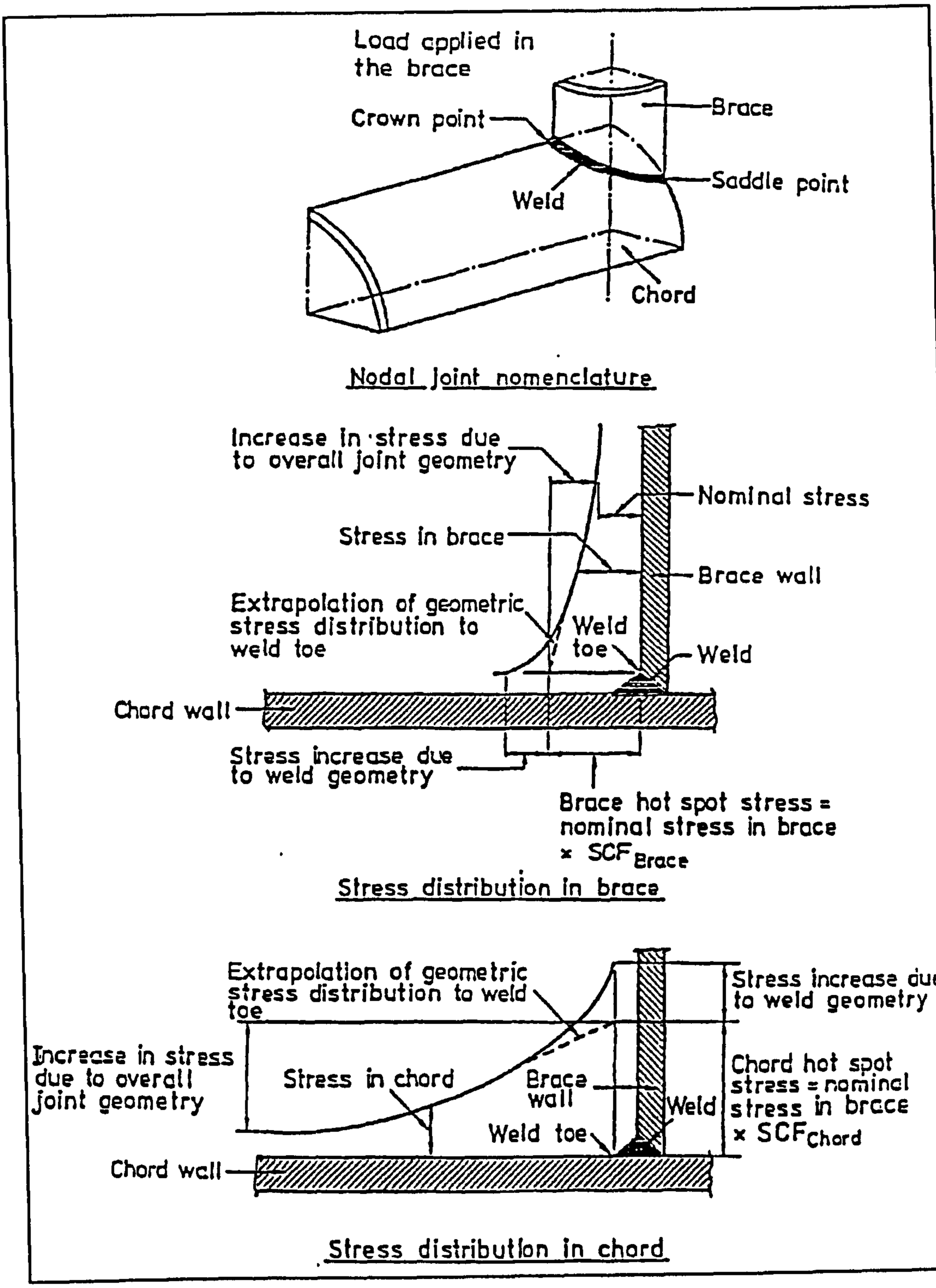

Figure 1.6: Schematic definition of hot spot stress in tubular joints [1.38]

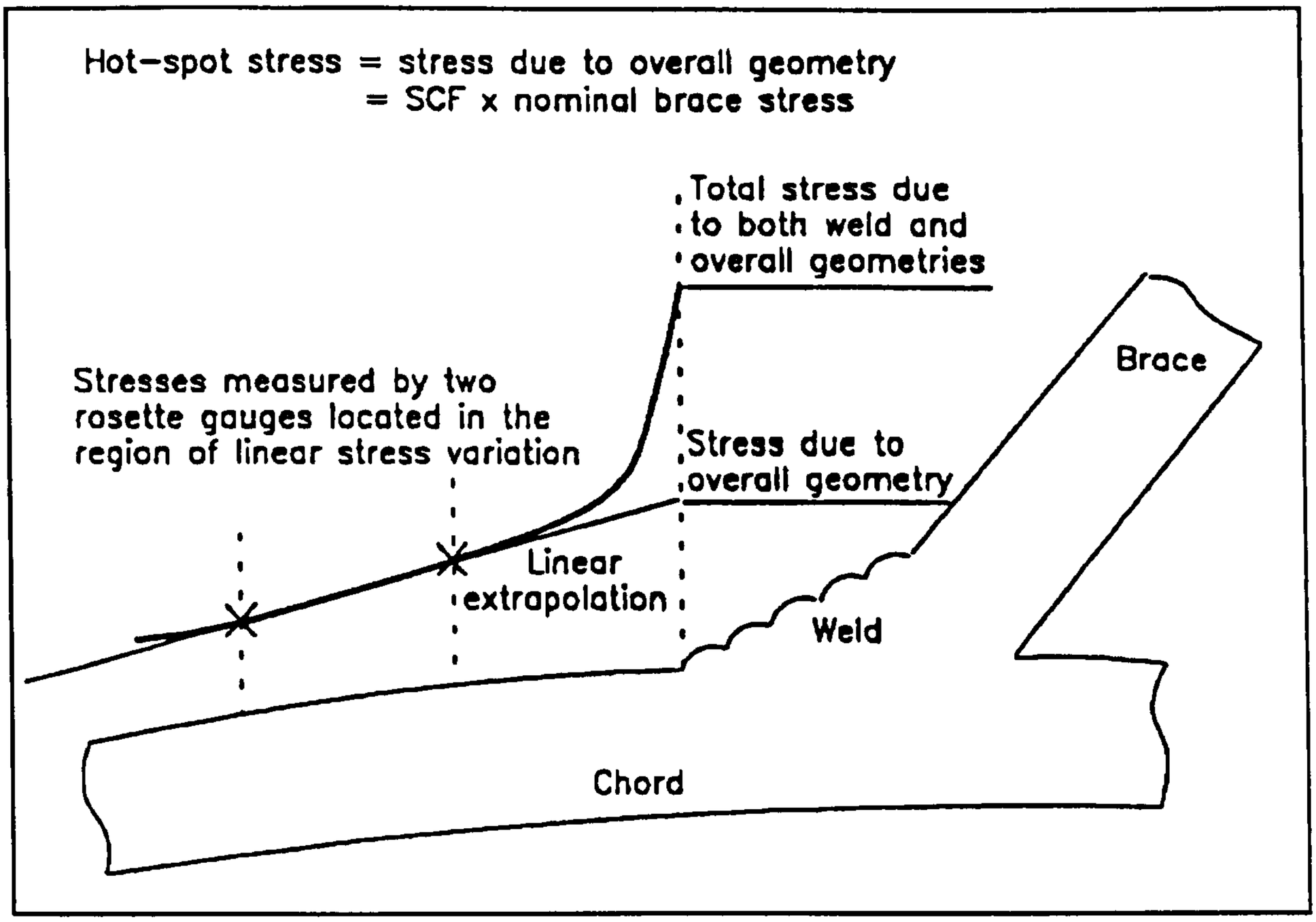

Figure 1.7: Locations of strain gauges on tubular joints to measure SCF [1.74]

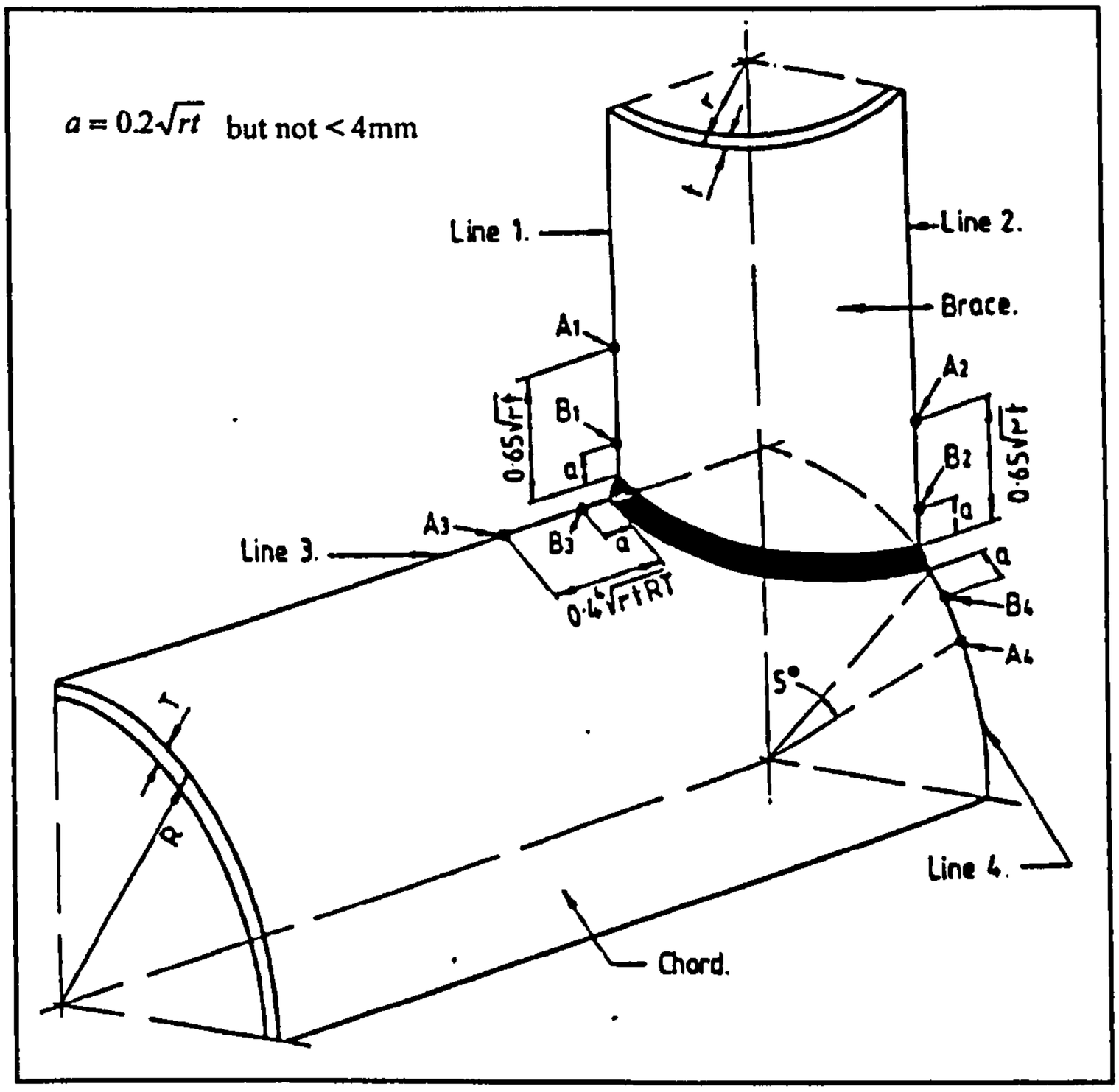

Figure 1.8: Recommended locations of strain gauges from joint weld toe [1.49]

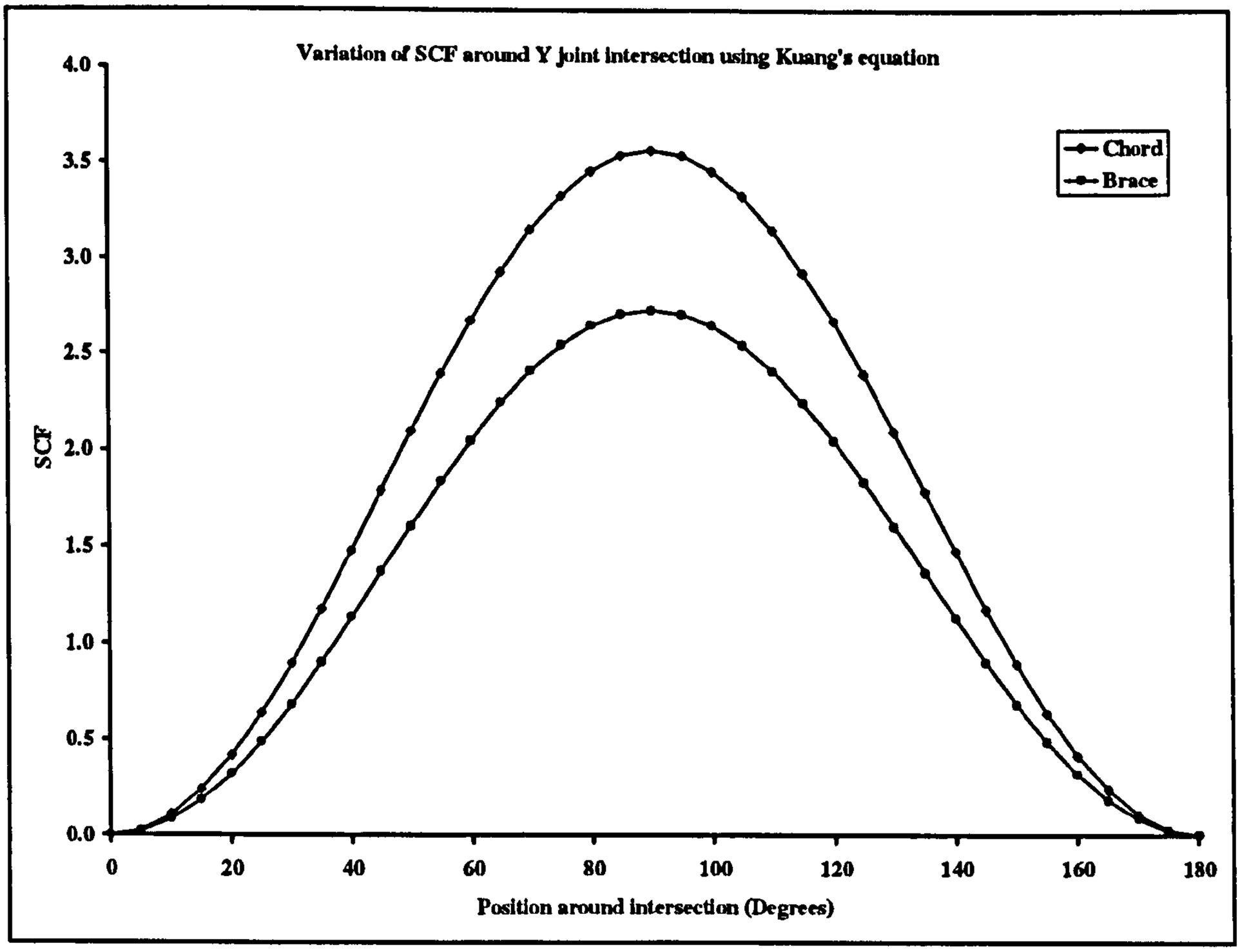

Figure 1.9: SCFs predicted using Kuang's equation

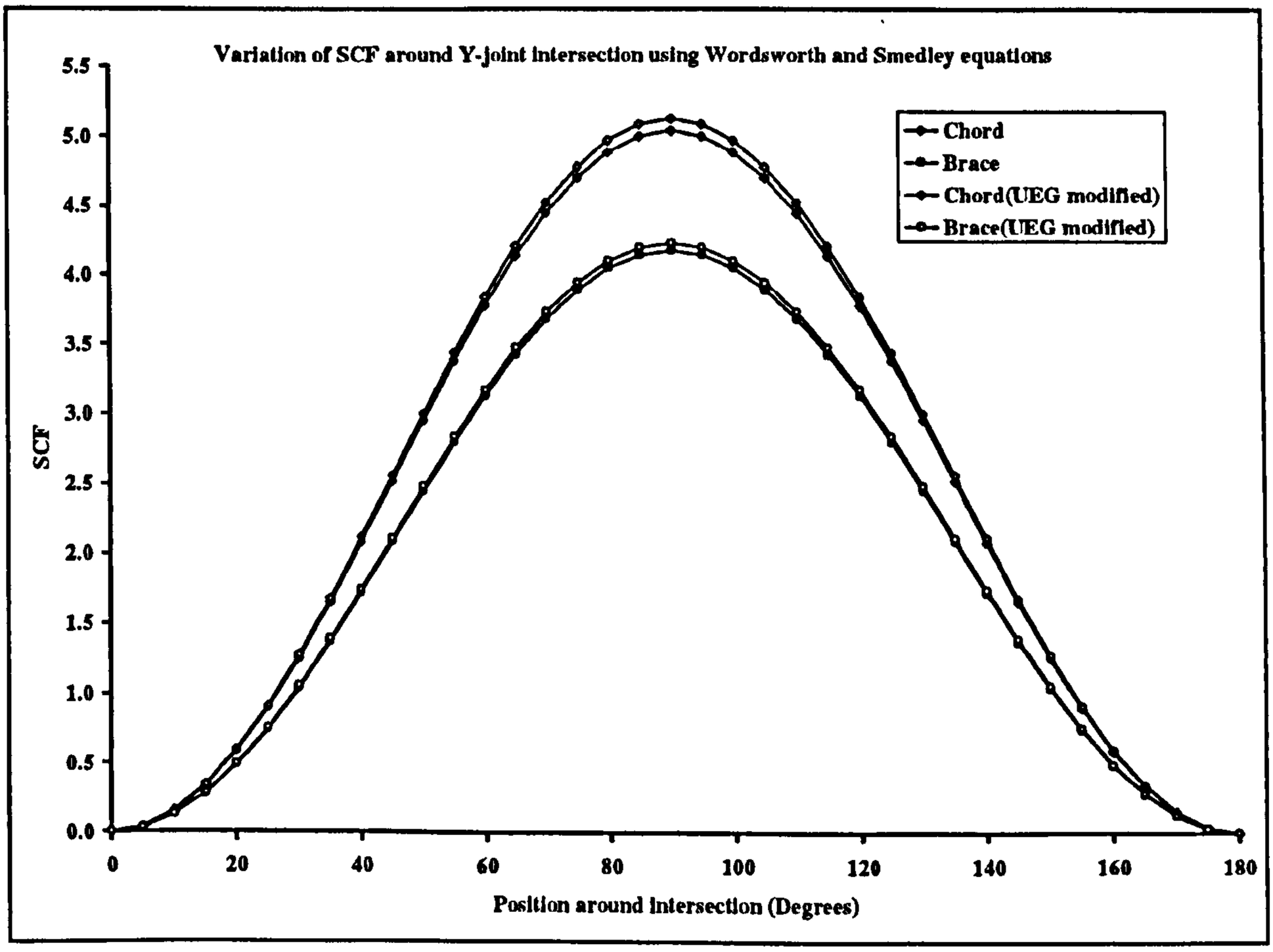

Figure 1.10: SCFs predicted using Wordsworth and Smedley's equation

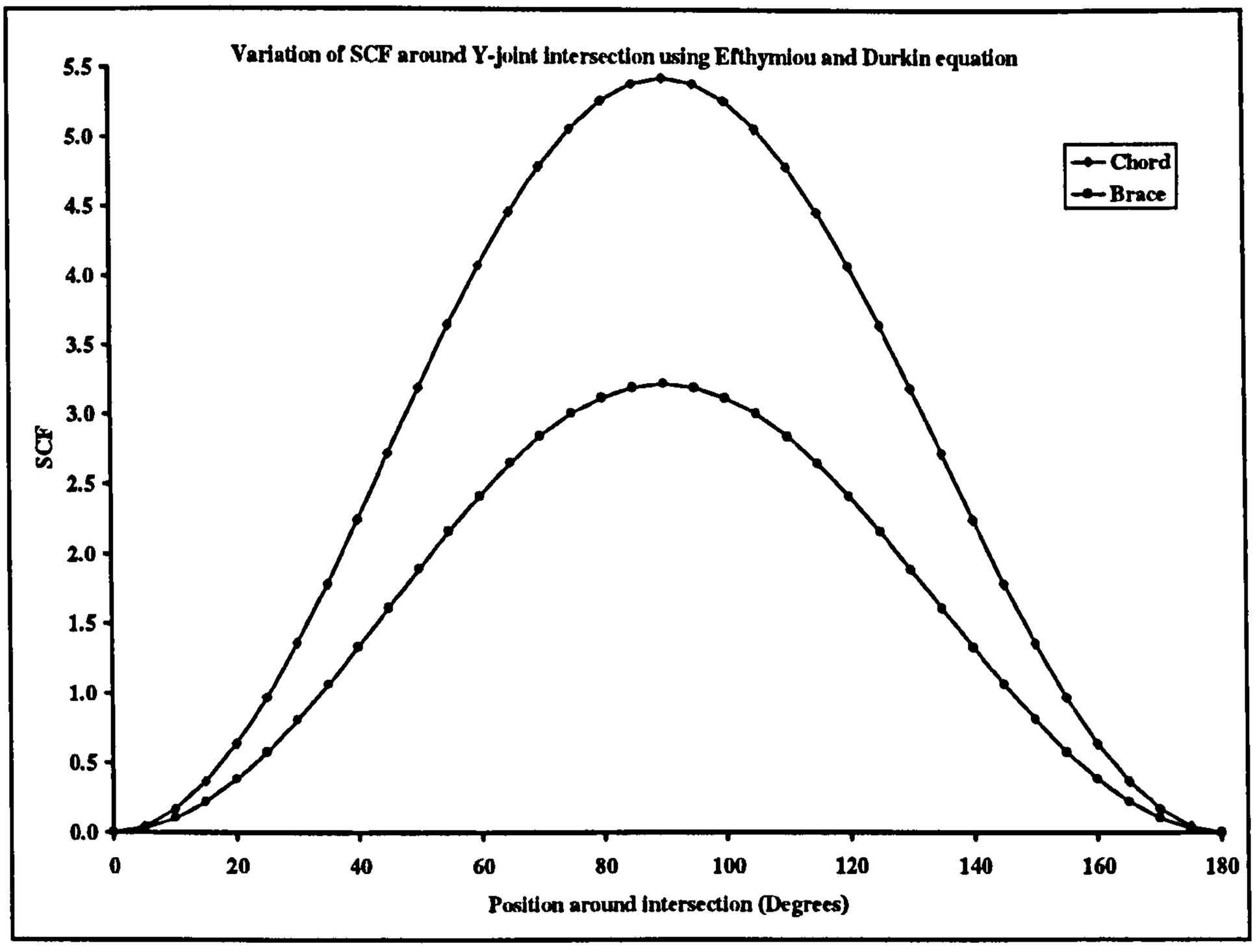

Figure 1.11: SCFs predicted using Efthymiou and Durkin's equation

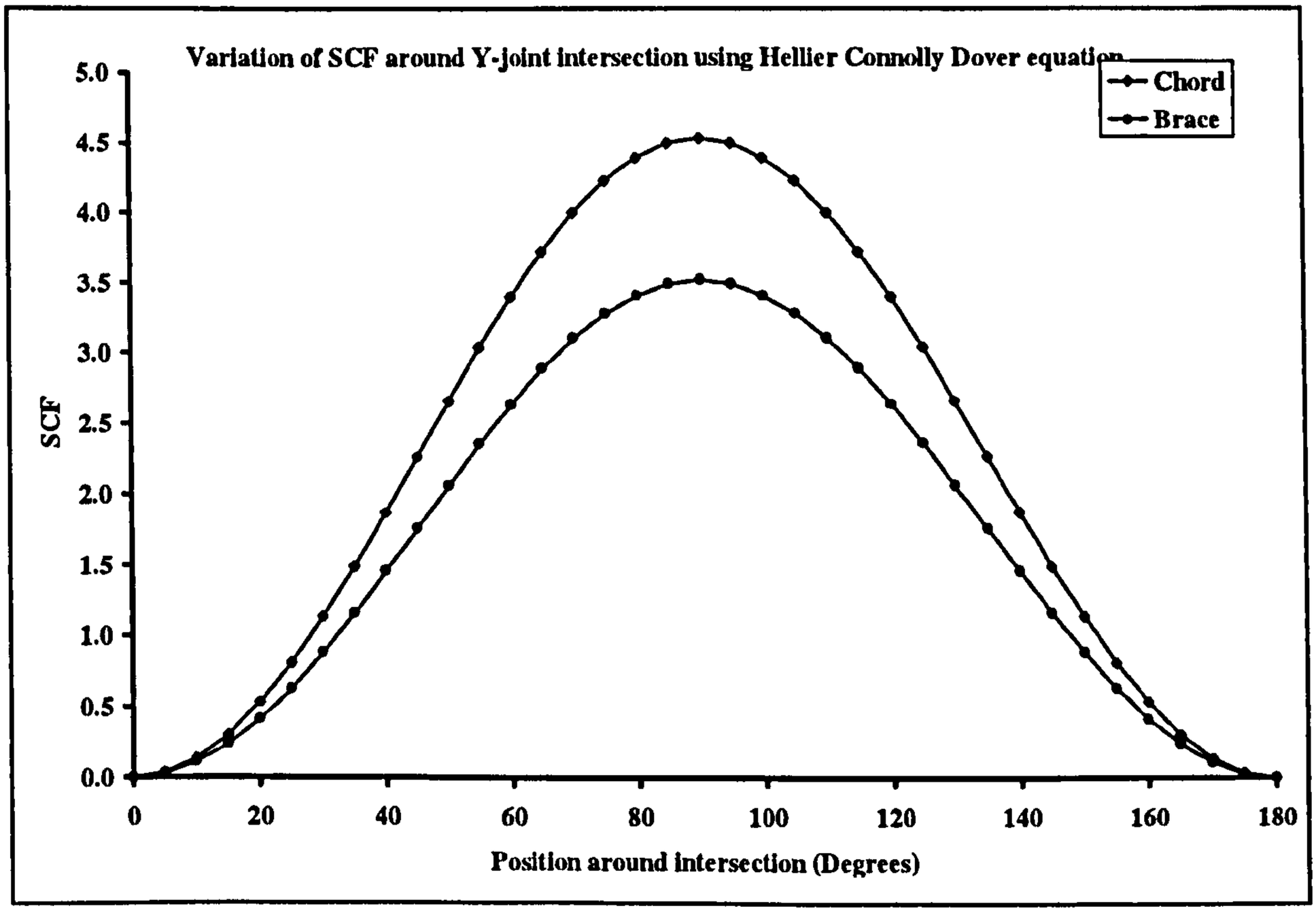

Figure 1.12: SCFs predicted using Hellier Connolly Dover equation

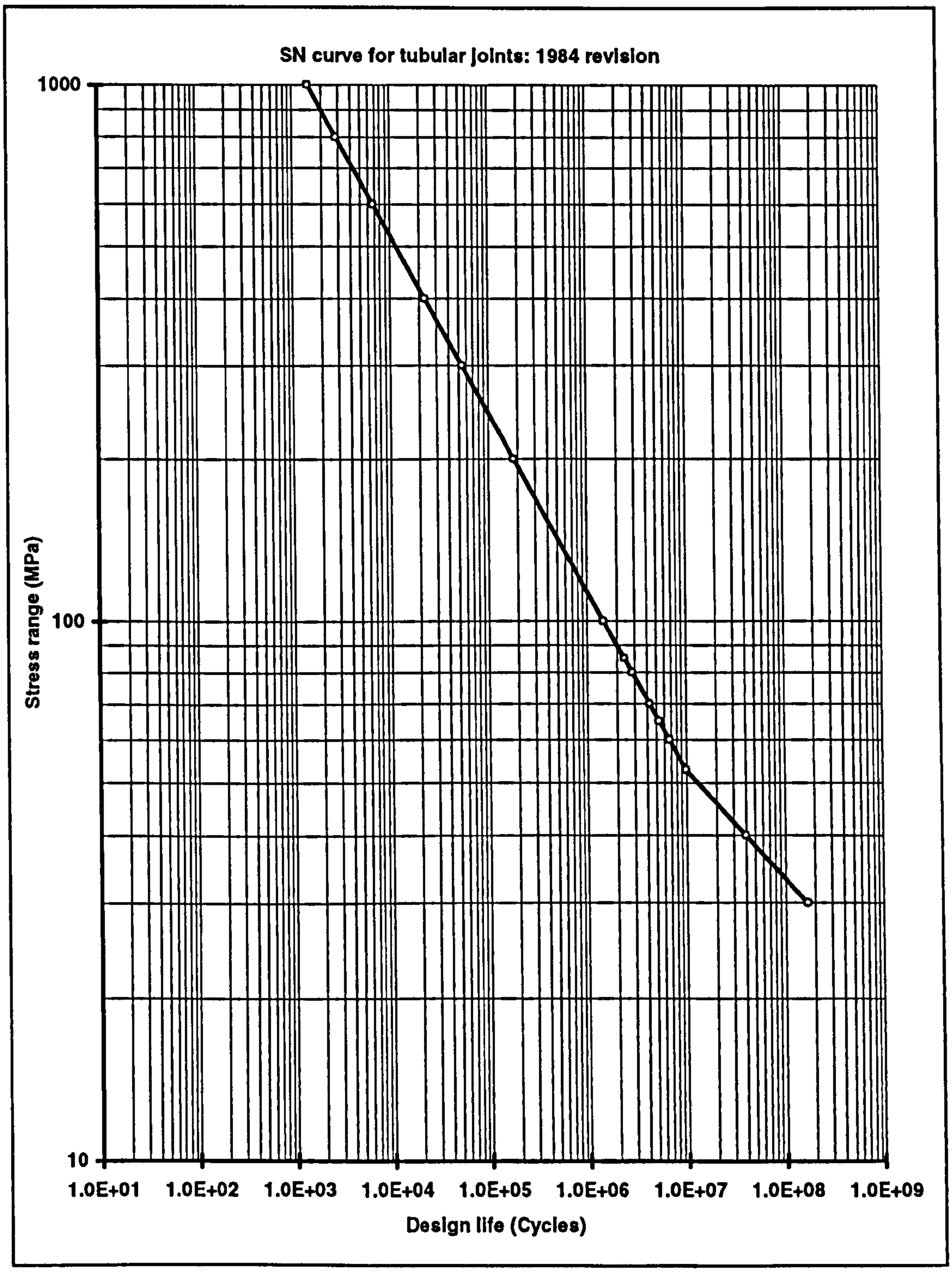

Figure 1.13: UK Dept. of Energy early design curves for tubular joints.

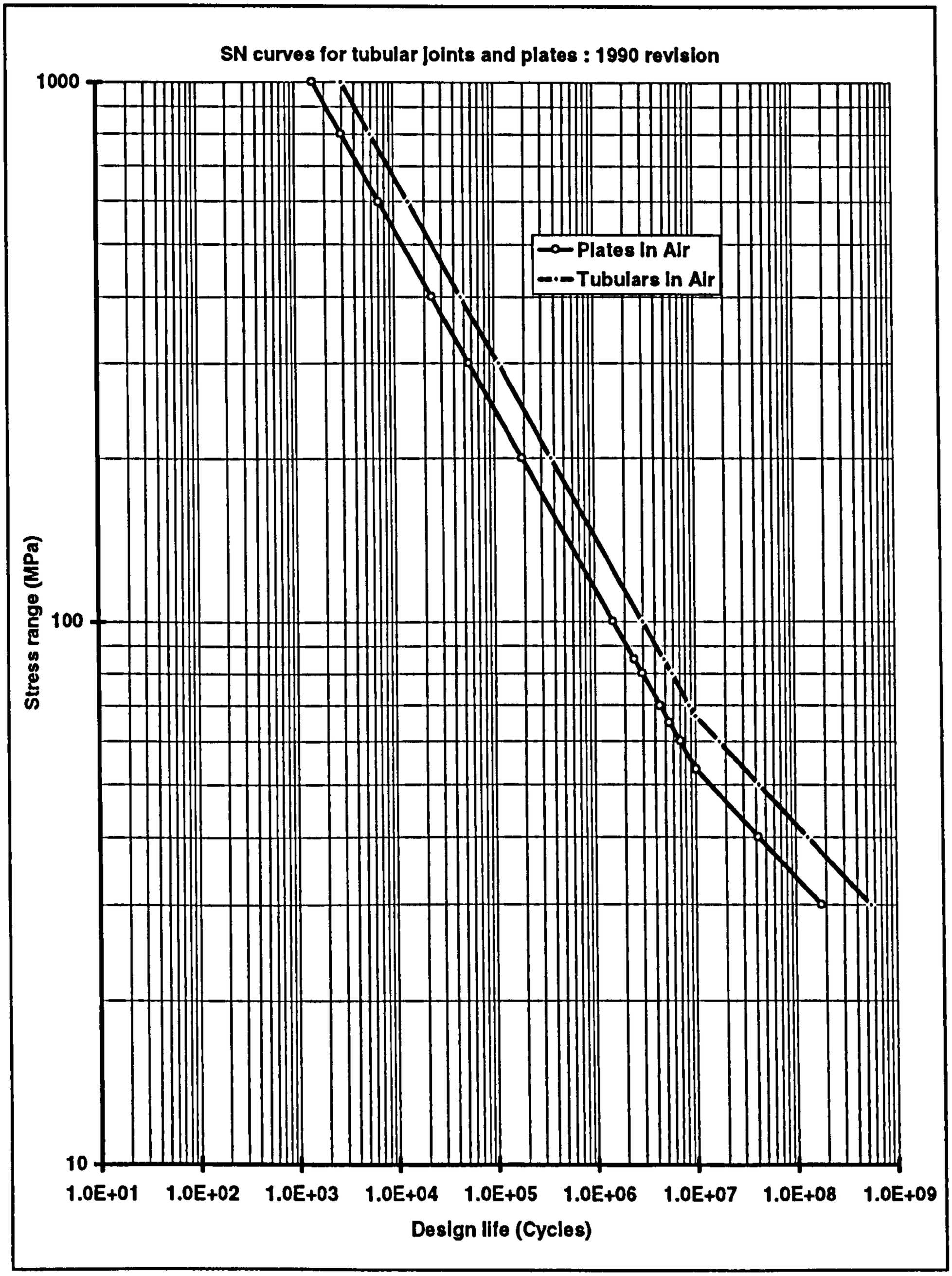

Figure 1.14: UK Department of energy basic design curves (1990 revision)

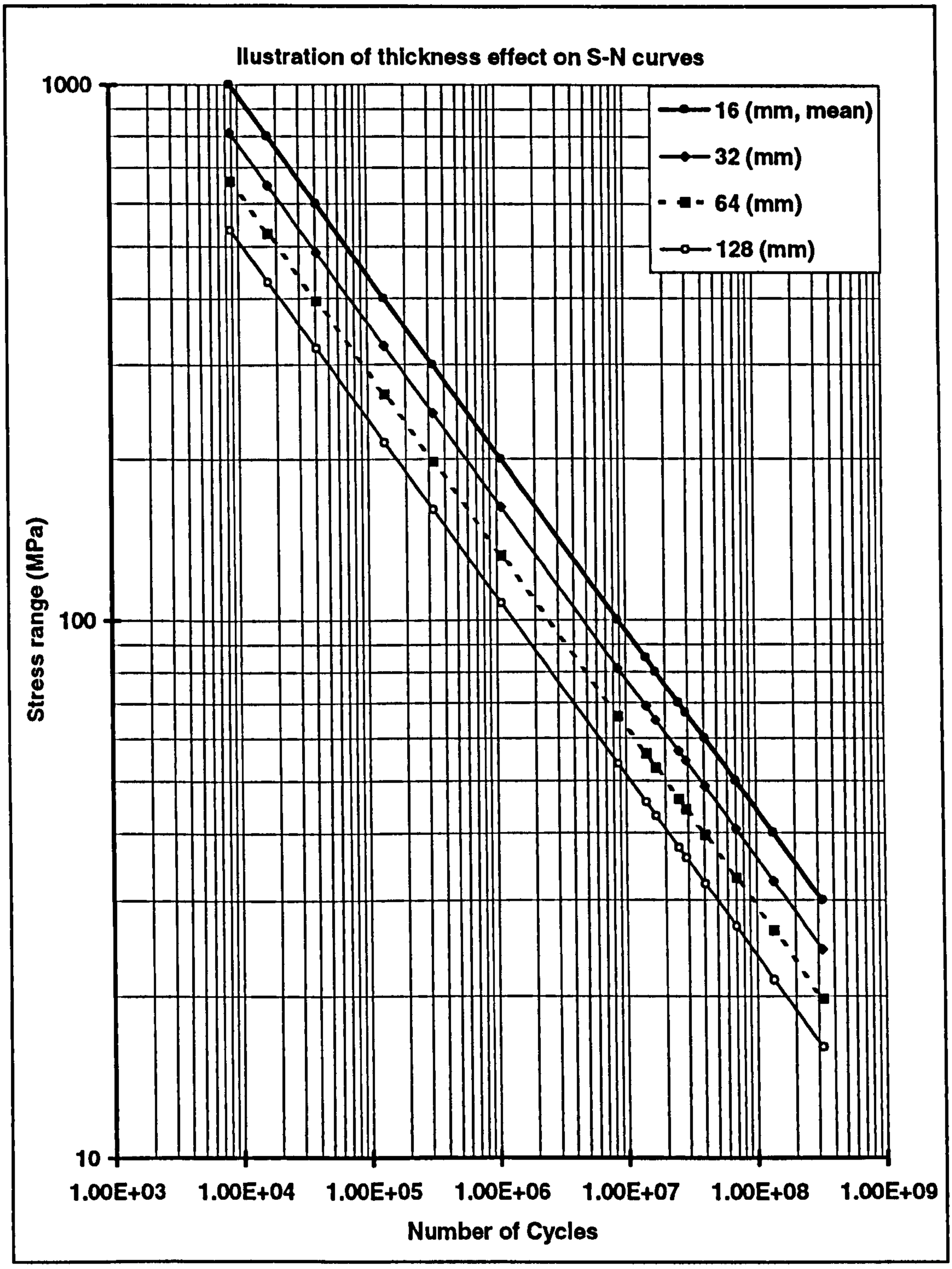

Figure 1.15: Thickness effects on basic design curves

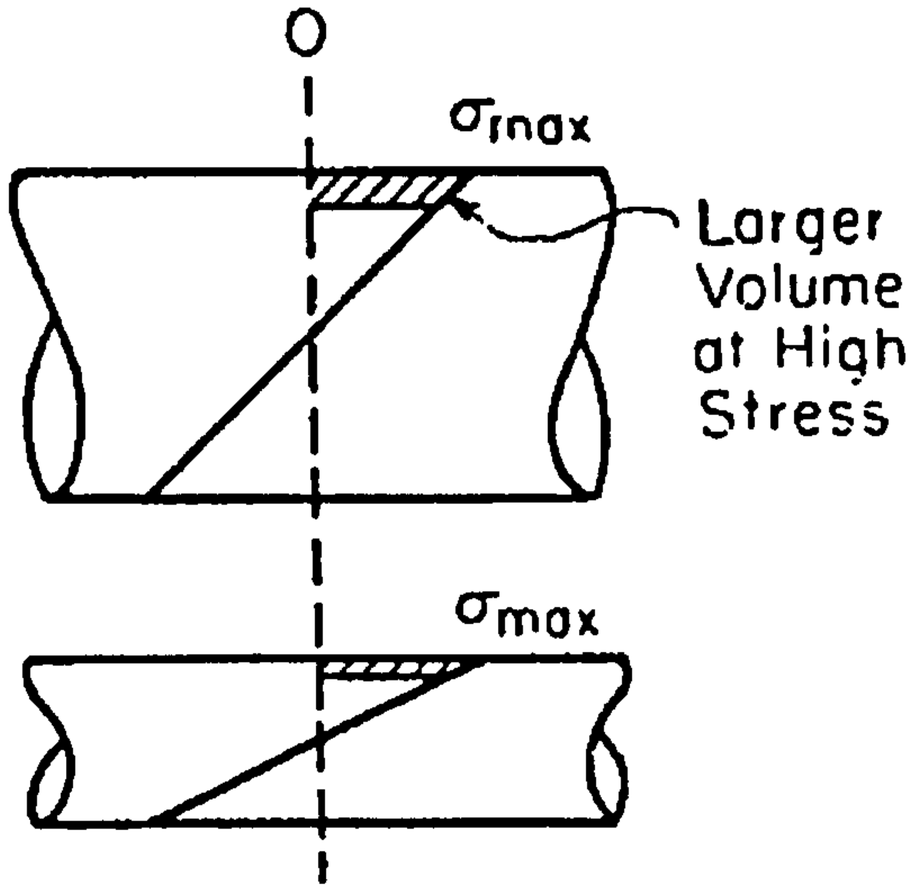

A: Illustration of a changing through thickness stress gradient and the effect of surface area and volume on fatigue

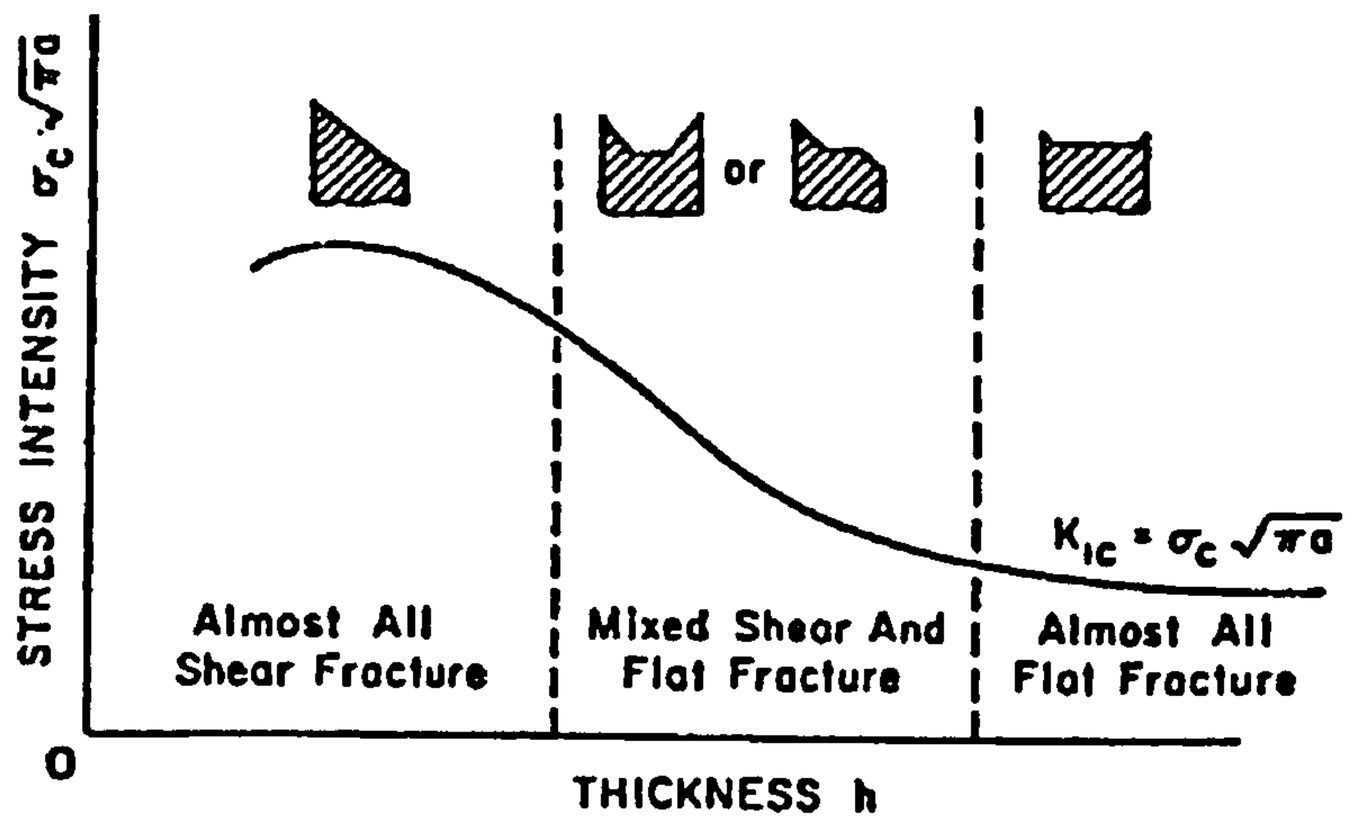

Effect of thickness on stress intensity factor and mode of fracture

Figure 1.16: Schematic illustration of thickness effects [1.58]

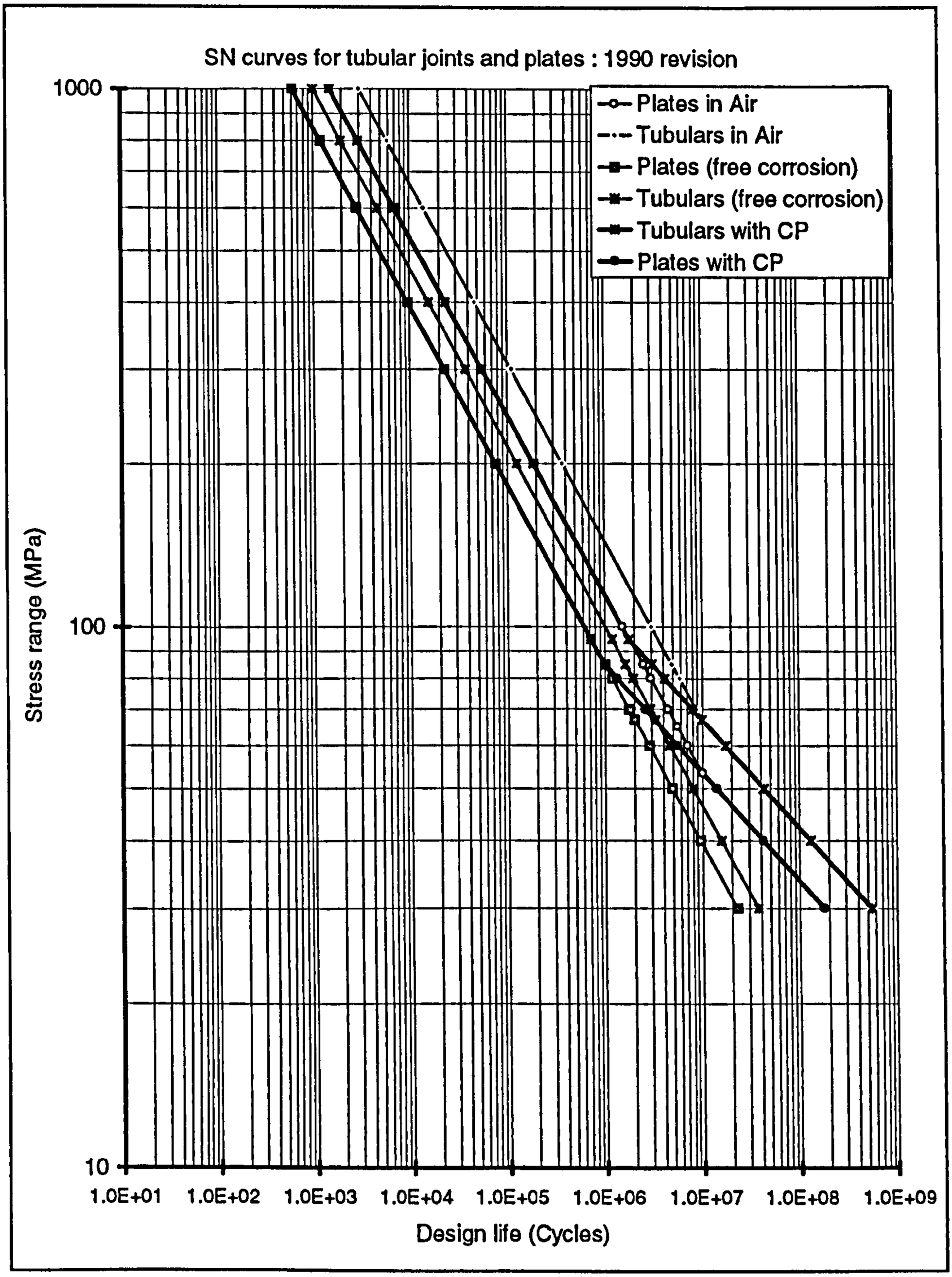

Figure 1.17: Environmental effects on basic design curves (1990 revision)

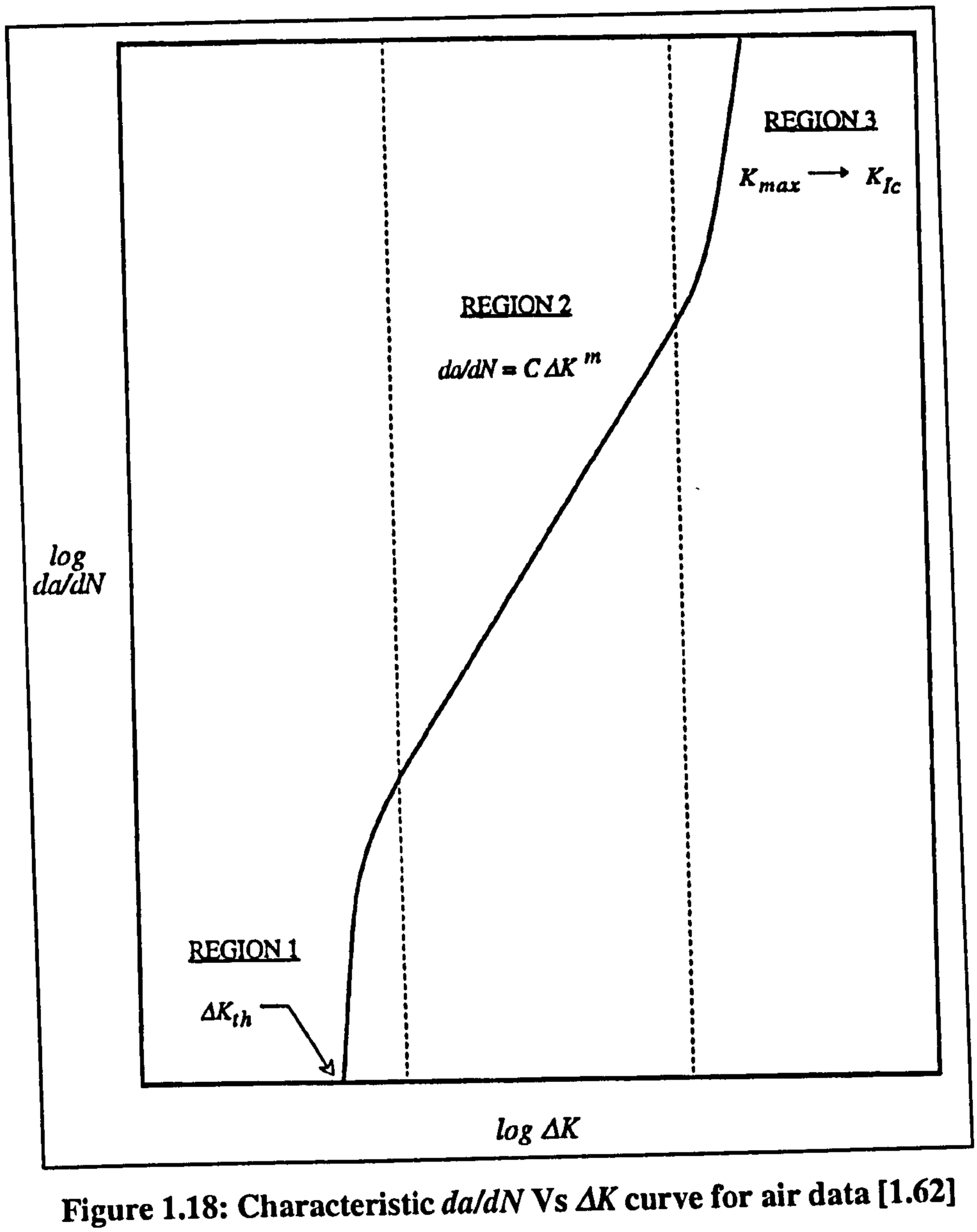

Figure 1.18: Characteristic *da/dN* Vs ΔK curve for air data [1.62]

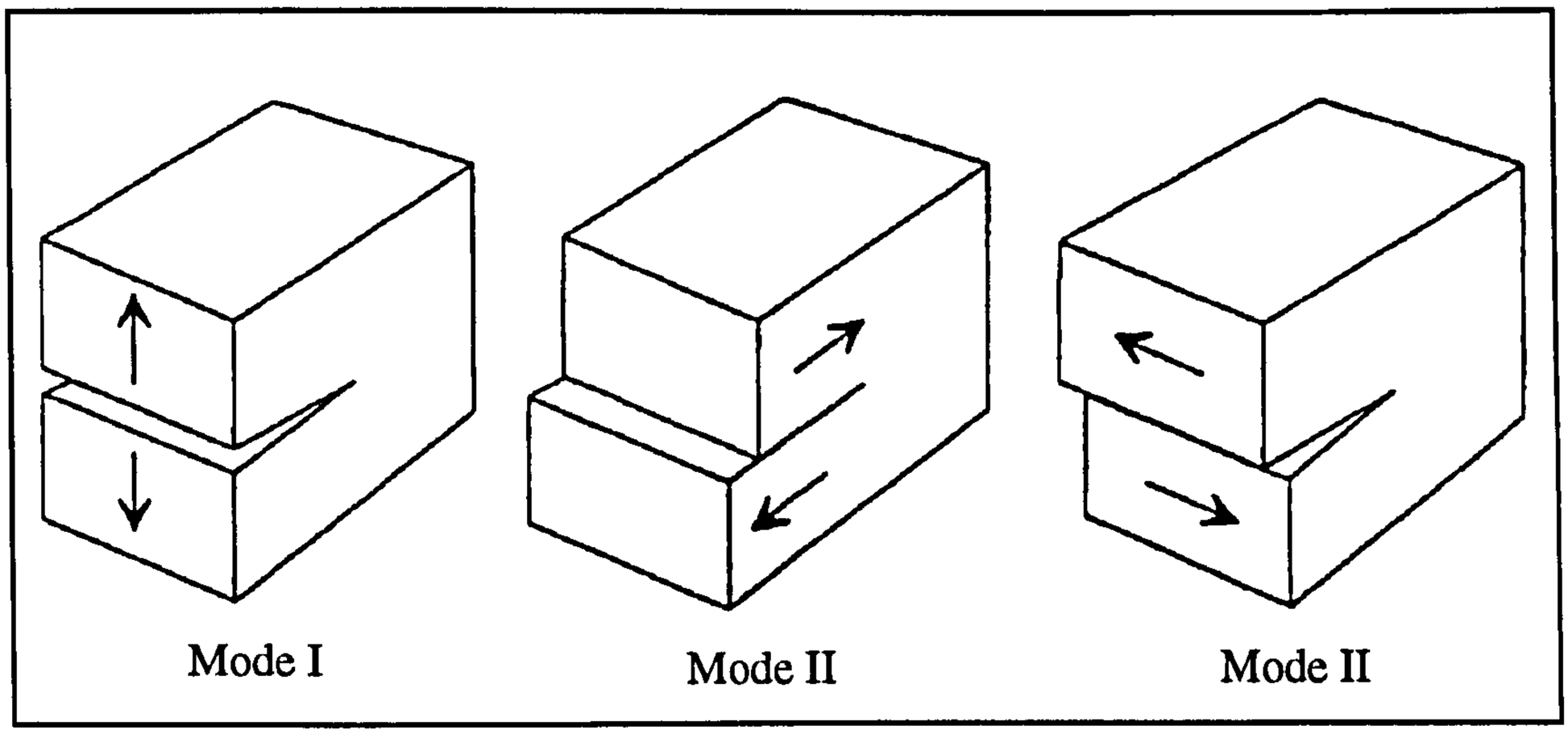

Figure 1.19: Different modes of crack opening

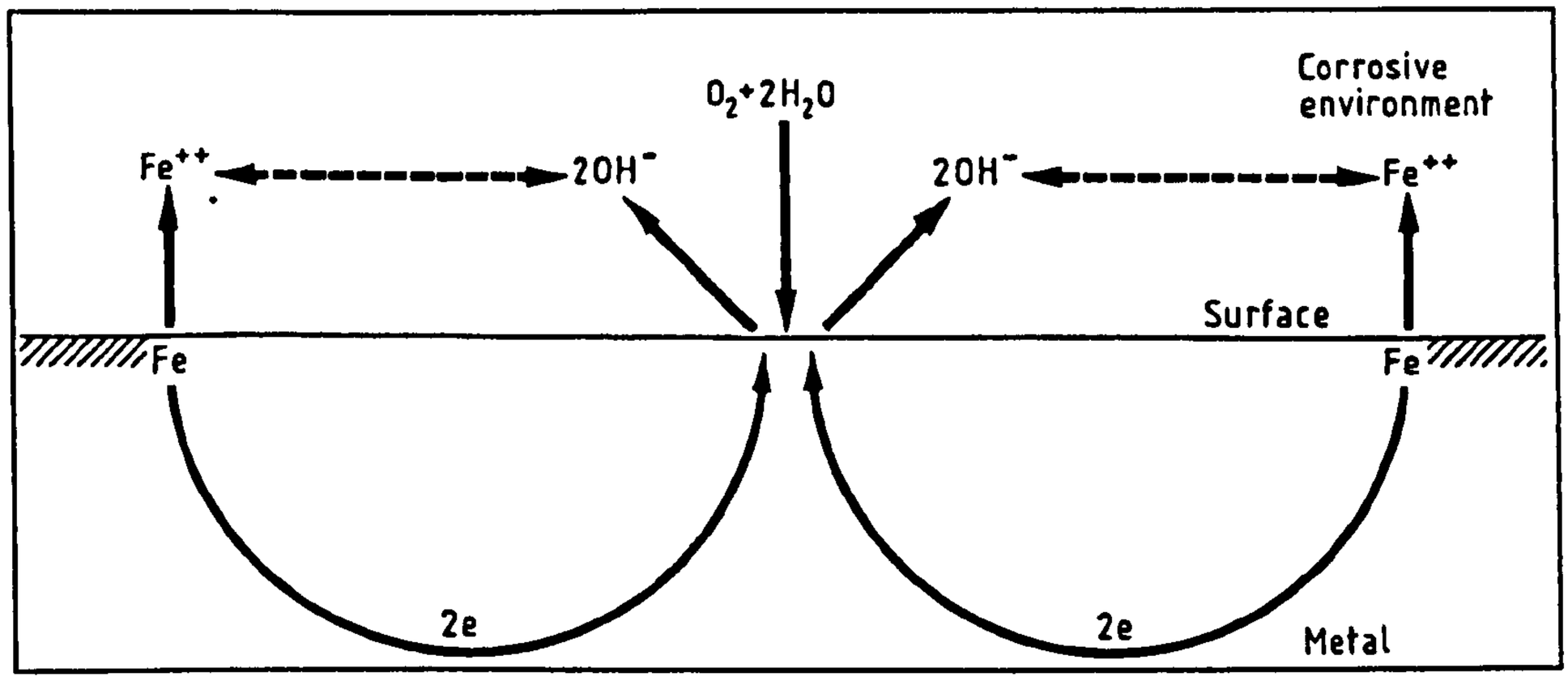

Figure 1.20: Schematic Illustration of the corrosion process [1.69]

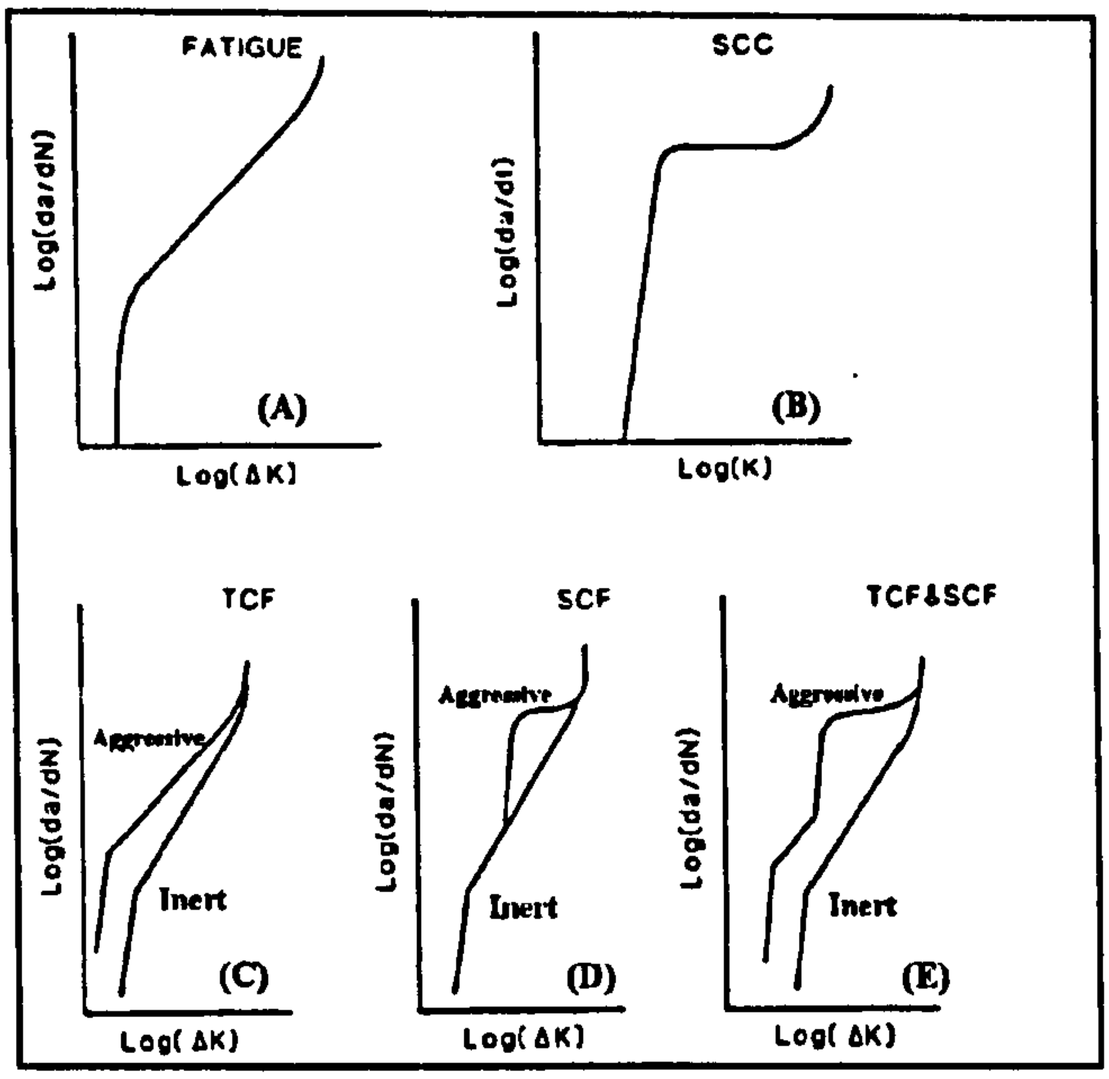

Figure 1.21: Illustration of basic types of corrosion fatigue behaviour

(A): typical air data, (B): Effect of K_{ISCC}, on stress corrosion cracking,

(C): True corrosion fatigue, (D): Stress corrosion fatigue

(Obtained from ref. [1.67])

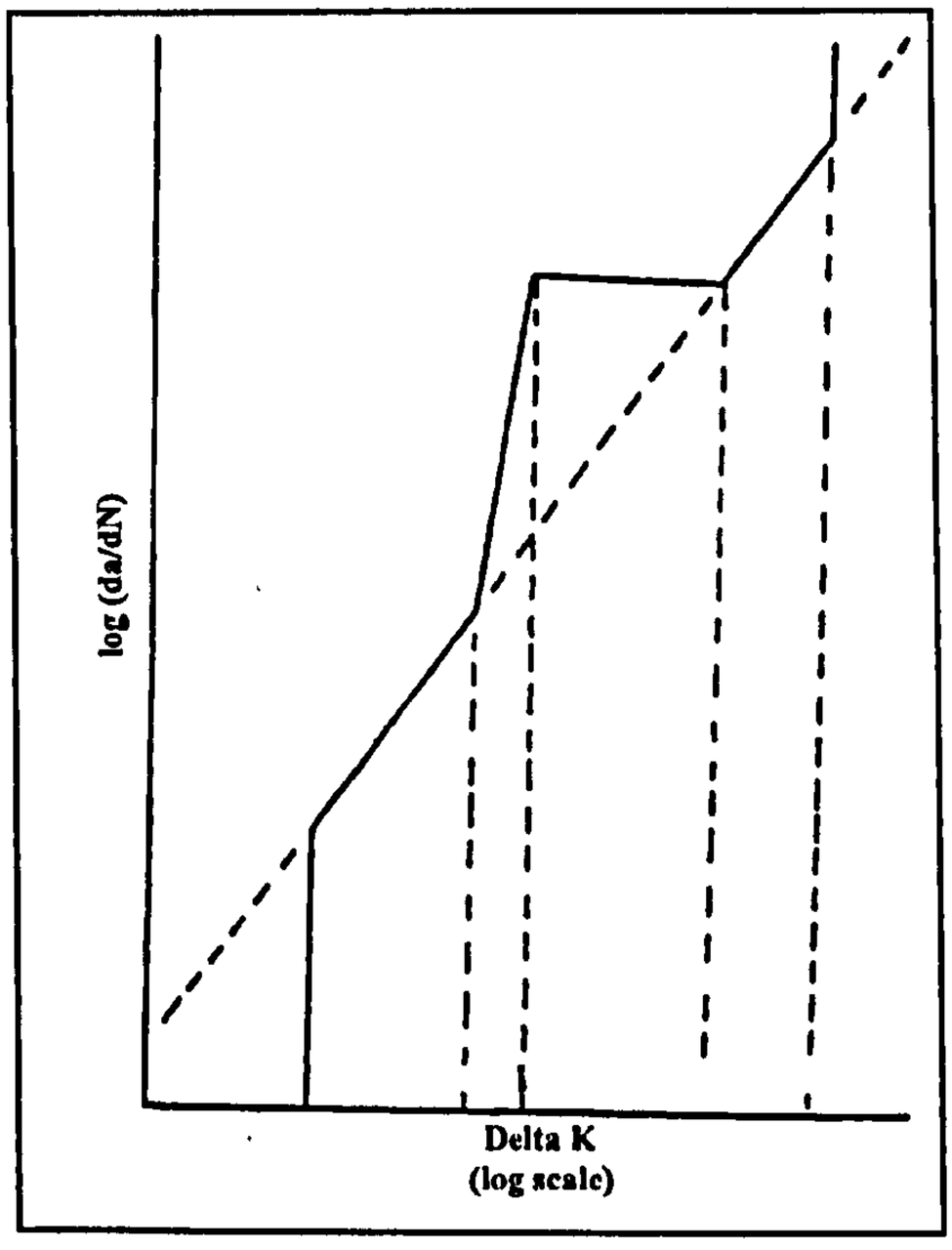

Figure 1.22: Multi-segment corrosion fatigue crack growth rate curve

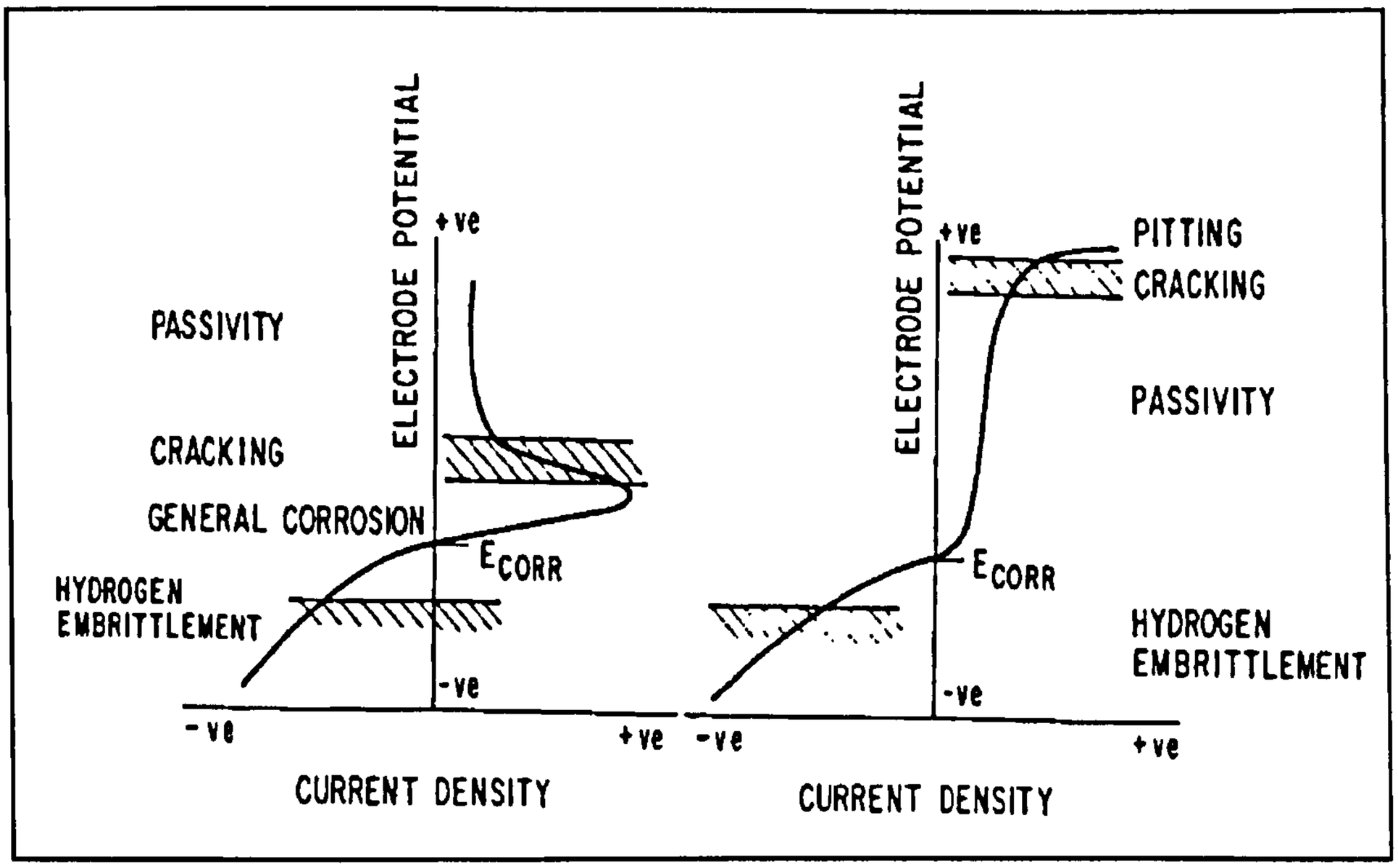

Figure 1.23: Effect of electrode potential on corrosion fatigue [1.67]

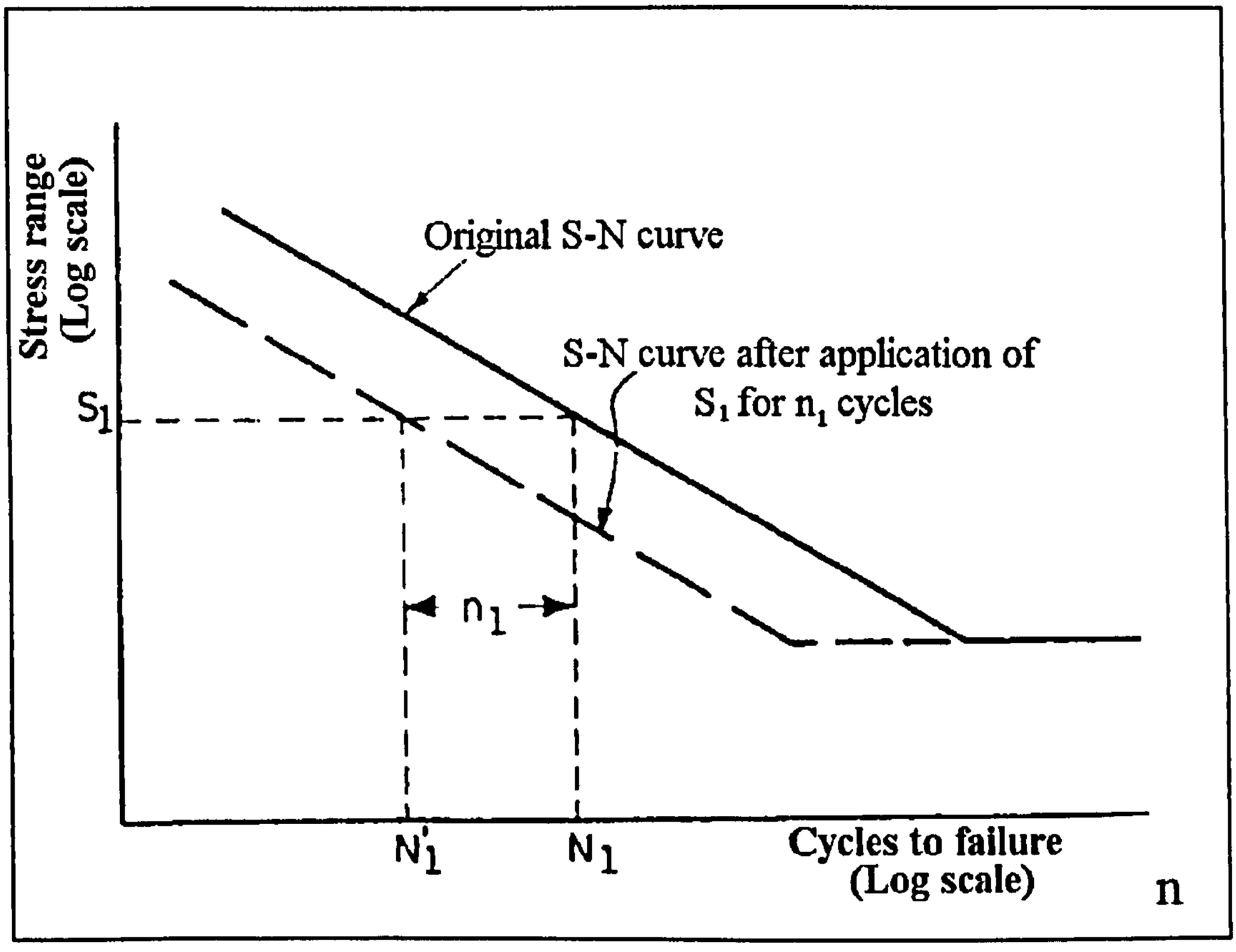

Figure 1.24: Effect of Miners damage summation rule on S-N curves

CHAPTER 2

2. SERVICE LOAD SIMULATION FOR JACK-UPS

2.1 INTRODUCTION

Jack-up platforms unlike fixed jacket structures are self elevating platforms which have conventionally been used extensively in the North Sea to drill both exploratory and production wells and for other short term Offshore operations. As highlighted in Chapter 1, many of these platforms are now designed to operate in deeper waters as production platforms. The TPG 500 production Jack-up design [2.1] and the production platform used for the marginal Siri field [2.2] are examples of Jack-up platforms designed for use as production platforms. Their use as production platforms for marginal field development means long term deployment. This change of use increases the potential risk of eventual fatigue failure as established for conventional fixed platforms. Typical examples of fatigue failure are represented by incidents such as Ranger 1 (1979) where the mat/column connection failed due to fatigue and the Pool 145 (1982) where fatigue was the cause of failure.

The introduction of the safety case regulations [2.3] for structures on the United Kingdom Continental Shelf (UKCS) is designed in part to minimise such risk of structural failure. It requires the owner or operator of an Offshore installation to demonstrate that all hazards with the potential to cause an accident have been identified and sufficient measures taken to reduce the risk to a level that is reasonably practicable. This risk may be associated to potential material failure due to fatigue. This makes material selection for critical parts of the structure at the design stage an integral part of the risk reduction process. This can only be satisfactorily achieved through adequate guidance but as highlighted in Chapter 1 and in a recent review [2.4], fatigue design guidance for high strength steels under sustained North Sea conditions is limited.

There is therefore a need for adequate understanding of their fatigue behaviour under realistic variable amplitude loading and environmental conditions as highlighted in Chapter 1.

In-service loading of Jack-ups is mainly due to wave and/or wind action with variable amplitude and frequency content. As Jack-ups move into deeper waters fatigue

loading becomes more sensitive to the dynamic response of the structure. This means that the effects of dynamics and structural response become more important and must be modelled if realistic results are to be obtained.

It has since been recognised that predicted fatigue lives for Offshore structures should be confirmed by large scale tests under simulated service loading. This provides important information on the crack growth mechanisms in these steels under realistic loading and environmental conditions. This knowledge will contribute significantly towards the development of an appropriate design code for use by Offshore designers of Jack-ups. It will also enable Jack-up designers to assess the validity of the adaptation of the damage calculation procedure of fixed jacket structures and also for in-service integrity assessment.

This Chapter covers the relevant methodology used [2.5] in the course of the investigation to ensure that realistic results of the kind mentioned above were obtained for this study on high strength steels used in Offshore structures. It looks at the influences on fatigue resistance of structural steels used in the construction of a typical Jack-up structure. The environmental loading and structural response interaction are discussed and emphasis is placed on how the relevant factors were modelled to produce the Jack-up Offshore Standard load History (JOSH). These factors especially include wave loading, Jack-up structural dynamic response and the effect of a corrosive environment. As a bench mark for validating the analytical results presented, model results are compared with service measurements made on a typical Jack-up platform operating at two different locations in the North Sea. This Chapter also presents and discusses the advantages and disadvantages of previous simulated load histories and further emphasises the significance of JOSH in the fatigue analysis of high strength steel Jack-up structures.

2.2 FATIGUE LOADING IN JACK-UP STRUCTURES

Fatigue is the main source of structural degradation of structures in the North Sea and this has been the focus of many major research programmes. These have been

discussed in Chapter 1. Due to the fact that fatigue is sensitive to very many factors which may be different in each application area, previous research experience and understanding of the fatigue performance of conventional fixed platform steels such BS 4360 50D and BS 7191 355D which have been heavily researched can not be easily extrapolated to predict the behaviour of high strength Jack-up steels. These steels are thought to be more susceptible to hydrogen embrittlement which may result from the cathodic reactions for typically protected Jack-up structures in the North Sea. In order to increase the understanding of the fatigue performance of these steels under loading conditions in the North Sea environment, it is very important that the relevant factors which influence their performance in service are identified and included in the analysis to obtain realistic and representative results.

Jack-up platforms exhibit non linear dynamic response in different sea states and can be exposed to different wave loading conditions at different locations in the North Sea. For a typical Jack-up structure used as a mobile drilling unit, transportation loading for moving from one location to another can be very important. This led to the proposal [2.6] that transition loads should be included in any simulated Jack-up Offshore Standard load History. Four simulation options were envisaged as shown in figure 2.1. The most suitable simulation option for production Jack-up platforms is that which in detail would only contain transportation loading at the beginning of the loading sequence. This is relevant to Jack-ups used for production since it is representative of a situation were the transportation loads are experienced by the structure while it is towed to the installation site.

Data on typical transit loads experienced by Jack-up platforms is very limited as this depends on the method of transportation to the installation site. Figures 2.2 and 2.3 show typical Jack-up transportation modes. Self propelling Jack-ups are transported as shown in figure 2.2, whereas dry toe is implemented by transporting the Jack-up on a carrier as shown in figure 2.3. In both cases the Jack-up rig legs may be fully elevated as shown in figures 2.2 and 2.3. Depending on the weather conditions and the turbulence of the sea, large bending moments can be induced on the legs during transportation. For production Jack-ups, this would represent only a small proportion of total fatigue damage experienced by the structure during its design life except under

circumstances where transportation loads are severe enough to cause leg failure or plastic deformation due to static loading. This type of static loading is however difficult to quantify for inclusion in a typical load history for a production Jack-up. The characteristics of fatigue loading, under service conditions, which apply to Offshore structures such as Jack-up platforms are dependent on three broad categories of influences, namely the wave loading regime, structural features and environmental conditions. These features are covered in detail in this Chapter. The way they were modelled to produce realistic results in a major fatigue testing programme carried out on a typical high strength weldable Jack-up steel, SE 702, is presented and discussed.

2.3 CRITICAL REVIEW OF PREVIOUS LOADING MODELS

Fatigue testing of specimens and structures started well over a hundred years ago. As demonstrated in a comprehensive review on fatigue [2.7], codification of the resulting data can be said to have started around the 1850s when Wohler carried out his now classic experiments which lead to the determination of S-N curves. Repeated loading tests were carried out around the middle of the last century and laboratory testing of specimens continued since then through the 1920s and 40s resulting in the accumulation of a considerable amount of empirical data.

By the mid 1950s which is considered by most as the beginning of the era of modern fatigue testing, three main trends had emerged. These included structural fatigue testing, tests to study fatigue crack growth and the development of design codes from the experimental fatigue data available.

Research work into the fatigue behaviour of different structures continued. The Comet accidents of 1954 had a very significant effect on the study of fatigue as this stimulated extensive fatigue testing of aircraft structures.

With the development of servo-hydraulic actuators and microprocessors, the whole art of fatigue testing entered a new phase which saw an era with the potential for testing structural components by applying increasingly complex fatigue loads. The

ultimate aim from this period and on was to simulate service loading conditions and carry out fatigue tests under simulated realistic service loading conditions.

The original idea as it remains today was to produce standardised load histories intended for use in fatigue testing and simulation so as to allow for comparison of results and also to provide guidance for laboratories undertaking the tests. This was done with the objective of increasing the general understanding of variable amplitude fatigue testing, compare performance of crack growth prediction methods and attempt to justify the degree of validity of the extrapolation of linear damage accumulation models to the more complex real life variable amplitude loading regimes.

The development of standardised load histories for fatigue testing of Offshore structural components has progressed rather slowly and did not receive great attention until more recent years. On the other hand standardised load spectra were developed for the aircraft and automotive industries by the late 1960s. By the early 70s aircraft components were being tested using standardised load sequences. A well known example is FALSTAFF (Fighter Aircraft Loading Standard For Fatigue) [2.8].

Attention was turned to the development of standardised load histories for testing welded Offshore tubular structures in the early 80s and through into the 90s. This period saw the development of the COLOS (Common Load Sequence for the European Coal and Steel Community Research Programme II) [2.9] and the associated C-12-20 series, the UKOSRP II (the United Kingdom Offshore Steels Research Programme II) double peaked spectrum [2.10, 2.11], the Hart/Wirsching algorithm [2.12, 2.13] and the WASH sequence [2.14] which followed. Some of these models including their advantages and disadvantages are covered in greater detail in this section highlighting the main differences between these models and the JOSH model.

2.3.1 COLOS/C-12-20 Series [2.9]

The Common Load Sequence for fatigue evaluation of Offshore Structures (COLOS) was developed to be used for the European Coal and Steel Community Research

Programme III. This sequence and the associated C-12-20 series represent a single narrow band stress spectrum with constant RMS. The overall spectrum was built up using seven stationary Gaussian spectra of different RMS values. All stationary spectra were stepped by about 5% of the peak load in order to produce a random distribution of peaks.

The forcing loads developed by this sort of load history has peaks which can be defined by a Raleigh distribution. The main draw back with this sequence is the fact that only the forcing loads are taken into consideration while dynamic effects are ignored. For structures operating under conditions with significant resonance effects, this load sequence was not very representative of real life loading and the frequency control was far from being accurate. This type of spectrum would therefore not be appropriate for use in the Variable Amplitude Corrosion Fatigue testing of Jack-up steel tubular joints since the frequency content under these realistic conditions is very important.

2.3.2 UKOSRP II Double Peaked Spectrum [2.11]

This double peaked spectrum was developed for random load fatigue testing in the UKOSRP II. It was based on data obtained from the Forties Bravo platform and other relevant data as to the general content of Offshore loading histories [2.11]. The UCL double peak spectrum is basically the same and the frequency content of the resulting load history was represented by the double peak power spectrum. Like the COLOS/C-12-20 sequences, this sequence did not completely model the realistic load history since it was based on a single stormy sea state and some features which could be represented by other sea states were missing. The resulting time history from this spectrum could be pseudo-random since a suitable pseudo-random generator was developed at UCL using a binary shift register. However this sequence did not model the long term variation in sea state RMS and therefore was not representative of real life wave induced stress history. As a result it could not be used directly for the fatigue testing of Jack-up steels without introducing the necessary modifications which would allow for Jack-up specific response characteristics to be accounted for.

2.3.3 Hart/Wirsching Algorithm [2.12]

The most sophisticated simulation of North Sea stress histories was available early in 1986 which modelled the long term variation in sea state RMS. This was a modification of the fatigue loading spectrum proposed by Wirsching to produce a new spectrum more similar in appearance to the long term stress history of deep water structures. This was based upon the original relationship proposed by Wirsching [2.13] and given as:

$$\Phi(f) = AH_s^{2\varphi}\left[\frac{\exp\left(\frac{-1050}{(2\pi T_D f)^4}\right)}{T_D^4(2\pi f)^5\left(\left[1-\left(\frac{f}{f_n}\right)^2\right]^2+\left[\frac{2\xi f}{f_n}\right]^2\right)}\right] \tag{2.1}$$

Where: $\Phi(f)$ is the stress spectral density function expressed as a function of wave frequency, f. The natural frequency of the structure is given by f_n and ξ is the damping factor while A and φ are scaling factors. H_s is the significant wave height of a wave with dominant period T_D.

For this spectrum the three lowest sea states for the original spectrum were omitted and the three highest stress states were combined into one. The long term random history was simulated by use of a discrete Markov chain model which allowed the sequence of sea states to be adequately modelled. A realistic sequencing of sea states represented the major difference between this model and previous models, most of which relied on using power spectra based on the extreme storm sea conditions.

2.3.4 WASH Sequence [2.14]

The Hart proposal was by far, the most realistic simulation for the fatigue testing of Offshore structures by the end of 1986. Around this same period research work undertaken to develop WASH was in progress.

The basic philosophy of the WASH model [2.14, 2.15, 2.16] is the same as the Hart proposal but there are three main features that are unique to the WASH model:

1. The signal generation mechanism in WASH was designed as a 'standard'. The randomness in the generated load history was produced using the pseudo-random binary sequence technique (PRBS).

2. The duration of each sea state was also taken into account in the Markov chain modelling. This was done by defining a state transition matrix which contains the probabilities for each sea state to move up or down one state, or to remain at the current state. This makes the modelled sea state sequence a more realistic and consistent simulation of the monitored service behaviour.

3. The WASH model makes use of realistic sea states obtained from monitored service data.

The implementation of features 1 and 2 is covered in greater detail in reference [2.17] but aspects relevant to the work presented in this thesis are discussed in section 2.5.

2.4 THE JOSH MODEL

The WASH model is the state of the art in the simulation of realistic service loading for fatigue testing of fixed Offshore structural materials. However it cannot be applied directly to Jack-ups, since resonance effects turn to dominate the power spectral density functions for typical Jack-up platforms [2.18].

The main differences between these two models is that the JOSH model takes into account the dynamic response characteristics of the more dynamically sensitive Jack-up platforms. This model also relies on the use of a representative combination of sea state data observed in service from a typical Jack-up site in the North Sea. The Jack-up structural response data used in the generation of JOSH was also modelled and validated with data obtained from service measurements.

2.5 GENERATION OF JOSH

The JOSH model like the WASH model relies on the use of advanced simulation techniques to generate the realistic loading history. These include the Markov chain technique for simulating the random sea state sequence and the pseudo random binary sequence technique for simulating the stationary random load history for each sea state. Both these techniques and their implementation in JOSH are discussed below.

2.5.1 The Pseudo Random Binary Sequence Technique

The random load history within the duration of any particular sea state is generated from the corresponding power spectral density function for that sea state. Four different methods can be used in this process. These four methods include the random range generator, the Markovian load range generator, Fourier summation random walk technique and the pseudo random binary shift technique. The last method was used in the WASH framework [2.14, 2.16] and the same procedure is maintained for this study. A schematic diagram of this technique is shown in figure 2.4. This method has the advantage over other methods in that it makes use of a shift register of a certain length. Although only discrete frequencies occur in the pseudo random binary signal generated in this way, they are so closely spaced that the characteristics of broad band random loading typical for Offshore structures are approximately preserved. This excellent frequency control of the generated signal is the major advantage of this technique since this is very important for corrosion fatigue.

The detailed procedure used in implementing this technique is given in [2.17] and [2.19]. In its mathematical form it relies on using output points from a shift register which is filtered through a filter function, $h_x(\tau)$. This filter function contains weights which are used to amplify the desired frequency content for any given sea state power spectral density function. In order to reproduce the loading characteristics which are relevant to any particular power spectral density function, the filter function is taken as the inverse discrete Fourier transform of the transfer function, $H_x(f)$, obtained from the white noise spectrum, $S_\varepsilon(f)$, relevant to the power spectral density function (PSD), $S_x(f)$. This is expressed as;

$$S_x(f) = \left|H_x(f)\right|^2 S_\varepsilon(f) \tag{2.2}$$

The second step involves the generation of the filter function which is given in the angular frequency domain as;

$$h_x(\tau) = \int_0^\infty H_x(\omega) e^{-i\omega\tau} d\omega \tag{2.3}$$

The white noise signal generated by the shift register is then finally filtered to give the required loading history, $n_x(t)$, such that;

$$n_x(t) = \int_0^\infty h_x(\tau)\varepsilon(t-\tau)d\tau \tag{2.4}$$

This method of simulating service loading has been demonstrated [2.17] to give very good simulation for any given power spectrum. Previous studies have also shown that the feed back loop size does not show any significant effect on either the sequence root mean square value or the weighted average stress range ratio. It therefore offers a considerable advantage over other simulation techniques not only in reproducing the frequency content of the power spectrum but also in maintaining the long term statistics so that they are representative of the PSD.

2.5.2 The Markov Chain Technique

After generating a pseudo random loading sequence from any particular sea state power spectral density function using the pseudo random binary shift technique, the next step is to reproduce the long term behaviour for a combination of naturally occurring multiple sea states. This is where the Markov chain technique becomes very important.

The long term distribution of naturally occurring sea states is a random process in its own right where the occurrence of each sea state follows the long term probability distribution of sea states. It is therefore possible that based on these long term probability distributions a state transition matrix can be obtained which contains the probabilities for each sea state to either move up or down one sea state or to remain in

its original state. Where the occurrence of any individual sea state does not affect the long term probability distribution of all the sea states. It can be stated mathematically that [2.16, 2.17];

$$\Pi(p+1) = T^{i}\Pi(p) = T^{i.p+1}\Pi(0) \tag{2.5}$$

Where $\Pi(p)$ is a matrix containing the probability of occurrence of each sea state after p transitions and T^{i} is the transpose of the Markov chain matrix which allows the state transition matrix after a large number of transitions to represent the long term probability distribution of sea states such that

$$\Pi(p+1) = \Pi(p) = \Pi(\infty) \tag{2.6}$$

The state transition matrix is obtained from the individual sea state characteristics such as the significant wave height and their average duration which are discrete approximations of their exponential conditional distribution.

2.6 JACK-UP DYNAMIC RESPONSE

Wave loading regime, structural features and environmental conditions were identified as the three main categories of influences which determine the fatigue performance of structural steels used in the construction of Offshore structures such as Jack-up platforms. The way these features were modelled to produce realistic results in this study is presented in this section. The methodology used in the analysis to account for the above effects and generate the representative stress response PSDs used to produce JOSH is presented and discussed.

2.6.1 The Transfer Function Approach

Figure 2.5 shows a typical Jack-up platform while figures 2.6 and 2.7 show simplified Jack-up models. Detailed mathematical modelling was carried out to investigate the behaviour of this theoretical model under wave excitation. As a benchmark for

comparison of results, modelled results have been compared with service measurements carried out on a typical Jack-up platform in-service at typical North Sea sites [2.18, 2.20]. The methodology used to determine model response is presented here.

At this point it is important to distinguish between dynamic loading and dynamic response. Dynamic loading varies with time and/or direction. Dynamic response which must result from this depends on the ***stiffness***, ***mass*** and overall ***damping*** of the structure.

The governing equation of the dynamic behaviour of the structure represented by the simple theoretical model is given as:

$$M\ddot{X} + C\dot{X} + KX = F(t) \tag{2.7}$$

M, C and *K* are the mass, damping and stiffness matrices respectively. While X, $\dot{X}$ *and* $\ddot{X}$ represent the displacements, velocity and acceleration vectors at time, *t* respectively.

M, C and *K* are multi-dimensional square matrices which may be obtained by use of a finite element approach to analyse the mathematical model.

The model used here is a two dimensional 22 degree of freedom system. The approach relies on the fact that if the forcing function is variable in nature, the response will also be variable [2.21]. A transfer or receptance function can then be derived which is independent of the forcing function but which relates the input forcing function to the output response. For this analysis a complex 22 by 22 receptance matrix is obtained as follows;

by substituting $X = X_o e^{j\omega t}, \dot{X} = j\omega X_o e^{j\omega t}$ and $\ddot{X} = -\omega^2 X_o e^{j\omega t}$ into equation 2.7 gives;

$$X = \frac{1}{(K - M\omega^2) + j(C\omega)} F \quad \text{or} \quad X(t) = H(j\omega)F(t) \tag{2.8}$$

$$H(j\omega) = \frac{1}{(K - M\omega^2) + j(C\omega)} \tag{2.9}$$

where $H(j\omega)$ is the complex transfer (or receptance) matrix. Figures 2.8 and 2.9 show respectively, how the solution for the first and second modes of response converge as the number of elements in the model are increased.

It is important here to consider the physical interpretation of the transfer function matrix. Each element $H_{(ij)}$ relates the deflection in freedom i on the structure due to an excitation force in freedom j when all other freedoms are unrestrained and unforced i.e.

$$H_{(ij)} = \frac{X_i}{F_j} = \frac{\text{Deflection in freeom } i}{\text{Force in freedom } j} \tag{2.10}$$

For random loading such as that experienced by Offshore structures, the response in each of the n degrees of freedom may be calculated as;

$$S_{x_i x_i}(f) = \sum_{r=1}^{n}\sum_{s=1}^{n} H_{ir}H_{is}S_{F_rF_s}(f) \tag{2.11}$$

where: $S_{x_i x_i}$ is the spectral density of the response $x_i(t)$ in freedom i of the structure and $S_{F_rF_s}$ is the cross spectral density between the force in freedom r and the force in freedom s

Fatigue loading in Offshore structures is such that many forces on the structure are caused by the same basic wave and wind action. This implies that the cross-correlation functions will not be zero. However analysis which superimposes responses in such a way that the cross correlation functions and hence the cross spectral densities are assumed negligible leads to satisfactory and conservative estimates. Using this approach simplifies equation 2.11 to;

$$S_{x_i x_i}(f) = \sum_{r=1}^{n}\left(H_{ir}H_{ir}S_{F_rF_r}(f)\right) \tag{2.12}$$

$$\Rightarrow S_{x_i x_i}(f) = \sum_{r=1}^{n} \left(|H_{ir}|^2 S_{F_r F_r}(f) \right) \tag{2.13}$$

This is a realistic approach and represents the effect due to each individual random force. When applied directly to an Offshore structure with a well defined transfer function *H(f)*, which is a summation of the overall nodal effect of the n degrees of freedom, together with a relevant forcing spectrum $S_{yy}(f)$, a representative response spectrum, $S_{xx}(f)$, of the structure can be obtained thus;

$$S_{xx}(f) = |H(f)|^2 S_{yy}(f) \tag{2.14}$$

This approach, depicted in figure 2.10, yields a frequency domain solution which can be transformed into a time sequence using the approach [2.22] presented in section 2.5. The time domain is the more useful form for fatigue testing of Offshore structures. For the work presented in this thesis, it was important that a representative Jack-up transfer function was obtained. To ensure this, results obtained by analysing the model were compared with data obtained from in-service field measurements. The model transfer function agreed very closely with the service data obtained for the same Jack-up operating at two different sites in the North Sea [2.5]. The following sections present the way the important parameters which affect the dynamic response of Jack-ups were accounted for in the analysis. An alternative approach based on a direct integration type analysis to obtaining a generalised representative spectrum was also considered. This method was not studied further because it was thought that the approximation errors were significant and did not reproduce service conditions adequately.

2.6.2 Modelling of Structural Parameters

The characteristics and influences of fatigue loading which apply to Offshore structures such as Jack-up platforms have already been highlighted and the importance of modelling these effects lies in the necessary requirement to obtain realistic results. The importance of the wave loading regime used in the analysis is discussed in the previous section and this section covers the effects of structural features and how

these were modelled to generate representative results. Consideration of a typical in-service Jack-up platform used as a benchmark to validate the model results was thought to be a necessary starting point for the analysis and this is introduced in this section.

2.6.2.1 Study of an in-service Jack-up platform

The in-service Jack-up considered for this study is the Maersk Guardian. This Jack-up was built in 1986 and is owned by Maersk Drilling. It is an independent 3-legged self elevating cantilever Jack-up with a leg length of 156.77m. Its legs are triangular and it can operate in a maximum water depth of about 106m. The Maersk Guardian has an electric rack and pinion jacking system with a speed of about 0.46m/min. It also has a helideck just over 25m diameter with a refuelling system of 14440 gallons and provides accommodation for 94 persons [2.23].

The Maersk Guardian Jack-up platform is considered to have features that are representative of a wide range of Jack-up platforms deployed in the North Sea. A comprehensive structural measurement programme was carried out on this platform during the winter of 1988-1989 in the southern North Sea (Silver Pit) [2.18] and during the winter of 1990-1991 in the central North Sea (Ekofisk complex) [2.20]. Due to the availability of these service data, the Maersk Guardian Jack-up platform was selected as a benchmark for comparing modelled structural response characteristics of a typical Jack-up under wave excitation in the North Sea with service measurements.

The most important parameters determining dynamic effects of a structure are namely;

1. Excitation frequency,
2. Natural frequency,
3. Effective mass of structure,
4. Effective stiffness of structure and
5. The overall damping of the structure.

The first parameter depends on the nature of the excitation spectrum and is not covered in this section . The second parameter is a function of the third and fourth. The nature of a structures complex transfer function depends on all these parameters as shown in equation 2.8. The last three of which are of particular interest as they represent physical properties of the structure. These are covered in greater detail in the following sections.

2.6.2.2 Effective Mass of Structure and Mass Matrix

The mass matrix was modelled by considering the details of structural mass and its distribution. This included the topside mass (or deck mass) and the distribution of mass per unit length of legs. These details were obtained from the Maersk company and represented typical structural data on the Maersk Guardian Jack-up platform. The actual values are not presented here because of confidentiality.

An important addition to the normal structural mass, the added mass, was also considered. Because of the uncertainty and variability of the increase in mass resulting from marine growth, the effect of increase in mass due to marine growth was not modelled. This is assumed to be negligible compared to the overall mass of a typical Jack-up platform.

The added mass was taken to consist of two components.

1. Mass of water contained within the submerged part of the structure, M_{am}
2. Mass of externally entrained water, M_{em}

These two components were determined using the method of equivalent Jack-up leg sections. This relies on using an equivalent cylindrical leg section which has the same structural and hydrodynamic properties as the actual Jack-up legs. Using this approach the two components of added mass were obtained as follows.

$$M_{am} = \rho \pi a^2 \tag{2.15}$$

$$M_{em} = \frac{M_{am}}{(C_m - 1)} \tag{2.16}$$

C_m, is the mass coefficient of the structure. This was taken as 2 for this analysis. This value was based on information supplied by the Maersk Company on the Maersk Guardian Jack-up. The density of sea water is ρ and a is the equivalent radius.

2.6.2.3 Stiffness of Structure and Stiffness Matrix

This was derived from the generalised stiffness matrix based on the equivalent leg structure with coupled springs at the relevant nodes to model the effect of leg structure-soil interaction. The details of the approach adopted in selecting the stiffness of the linear springs used in the model are presented in a section 2.6.3.

2.6.2.4 Damping of Structure and Damping Matrix

The overall damping of the structure was considered to have two contributing components.

1. Structural damping.
2. Hydrodynamic damping.

The structural damping is the most difficult to determine and cannot be determined analytically. However there are documented values and typical values for spring steel for example range from 0.4% to 0.8% [2.21].

Hydrodynamic damping is also important and the methodology used is based on obtaining damping due to motion in-line with the flow. Hydrodynamic damping is non linear and complete modelling requires non linear analysis. However, linearisation yields satisfactory results for large structures under the action of small waves [2.21]. This is more applicable to inertia rather than drag dominated loading. Non linear effects are more severe in the latter.

The damping matrix used in this analysis was obtained using Rayleigh damping coefficients, the first two natural modes of vibration and a damping ratio of 4% (Silver Pit location). Previous research [2.24] has shown that estimates of damping calculated using the spectral peaks and the half power bandwidth method range from 2% to 5% over a wide range of representative sea states

2.6.3 Modelling of soil-structure interaction

Soil structure interaction is a very important aspect in Jack-up dynamic response and this area has attracted a lot of research interest [2.18, 2.20, 2.24, 2.25, 2.26, 2.27, 2.28, 2.29]. A site assessment is usually required to determine the soil properties. Even after a site assessment the values obtained are subject to variability and it is common practice to consider a parametric study to ensure that the worst combination of values are chosen to produce conservative solutions.

There are two established methods for modelling the soil to study the problem of soil-structure interaction. One of them relies on the use of a finite element approach. This method is more expensive but has the advantage in that, variation of soil properties with depth can be analysed.

The second approach relies on the use of a lumped mass model. For this method the foundation is assumed to be rigid and the springs representing the soil are assumed to perform as uncoupled elements. This method is very satisfactory and is the more popular approach used in modelling soil structure interaction. Based on this approach, formulae have been derived using elastic theory, which relate spring constants to the shear modulus, G, and Young's Modulus, E of the soil. The derived formulae are based on the spring constant of a rigid circular base on an elastic half space and given by;

$$K_v = \frac{4GR}{1-\nu} = \frac{2ER}{1-\nu^2} \tag{2.17}$$

$$K_h = \frac{32GR(1-\nu)}{7-8\nu} = \frac{16ER(1-\nu)}{(7-8\nu)(1+\nu)} \tag{2.18}$$

$$K_\theta = \frac{8GR^3}{3(1-\nu)} = \frac{4ER^3}{3(1-\nu^2)} \tag{2.19}$$

$$K_\varphi = \frac{16GR^3}{3} = \frac{8ER^3}{3(1+\nu)} \tag{2.20}$$

K_V, K_h, K_θ and K_φ are the vertical, horizontal, rotational and torsional springs' stiffness respectively. ν is Poisons ratio and R, the radius of circular base. This was taken as the spudcan radius.

This second approach was adopted for this analysis. The horizontal and rotational springs were considered sufficient to model the soil structure interaction. The Poisons ratio is known to vary between 0.3 for dry granular soils to 0.5 for soft saturated clays [2.21]. It is also known that any errors caused by using a value of Poisons ratio equal to 0.5 for all calculations is small compared to other uncertainties. This is because there is very little variation as the Poisons ratio changes from 0.1 to 0.5. This trend is shown in figures 2.11 and 2.12. The variation of vertical and horizontal stiffness with Poisons ratio is shown in figure 2.11 while the effect of Poisons ratio on the rotational stiffness is shown in figure 2.12. In both cases the sensitivity of stiffness to changes in Poisons ratio between 0.1 and 0.5 for a particular spudcan radius is minimal. Some of the in-service results used in the validation of the model were measured on the Maersk Guardian Jack-up [2.18] while at the Silver Pit Location. This site has a sandy soil structure and a for Poisson's ratio of 0.4 was considered representative of the soil type. Table 2.1 presents quoted values [2.21] of Young's modulus for different soil types and the value assumed for this analysis is typical of loose sandy soil which lies in the range of 40MPa to 80MPa..

The stiffness of the springs used to model soil-structure interaction was the main parameter that was varied to ensure a close match in the peak frequency of the model and measured transfer functions. The actual values used are presented in a separate section and on the transfer function plots at the end of this Chapter.

2.7 MODELLING OF WAVE LOADING

In-service loading of Jack-ups is mainly due to wave and/or wind action, these are dynamic in nature. More generally dynamic loading is considered to be all loading which has an appreciable variation with time. For many design purposes it is adequate to consider variable loads in terms of an equivalent static load. The validity of such assumptions depends on two main factors. The form of the structure and the nature of the load.

The design wave approach is based on this methodology and is applied by defining a wave of large height and period range whose probability of occurrence is such that it represents the maximum wave that the structure will encounter within the return period. This approach is only realistic from the view point of designing against static structural failure due to a large wave and does not permit fatigue damage to be considered within the design. The design wave approach is not satisfactory for smaller waves with excitation frequencies that will lead to structural resonance.

The second approach is based on a design to a statistical wave description. In this approach, the occurrence of waves incident on the structure is expressed in terms of a probability of occurrence of waves with specific wave heights, period and direction. This method allows for adequate characterisation of fatigue inducing loads. It however relies on the linearity of superposition of wave components. This assumption yields satisfactory results for inertia dominated loading such as that experienced by a typical Jack-up platform.

Due to a combination of the form of the Jack-up structure and the nature of the loads it experiences in service, any analysis using an equivalent static load without the necessary consideration of variability would be inadequately representative. The methodology used here is a frequency domain analysis using spectral density functions and the transfer function approach, presented in section 2.6.1, to model the response spectrum. The main reasons for using this approach are:

1. The successful use of wave power spectra to describe water surface elevation;
2. The existence of short periods during which wave statistics of the random sea may be assumed not to change (sea states);

3. The ease of handling non linear effects;
4. And the resulting physically interpretable solution.

Considerable research work has been done on modelling ocean waves. Some of the better known one-dimensional wave spectra that have been developed to describe ocean waves include the Bretchneider spectrum, JONSWAP spectrum, Pierson-Moskowitz (PM) spectrum [2.30] and the modified version of the PM spectrum. The modified PM spectrum was chosen for this study. This form was adopted by Det Norsk Veritas and has been successfully used to analyse threaded tension leg platform tethers in the North Sea [2.31]. It expresses the wave power spectral density $S_{yy}(f)$ as a function of significant wave height H_s, mean zero crossing period T_z, and wave frequency f, such that;

$$S_{yy}(f) = \frac{H_s^2 T_z}{8\pi^2}(fT_z)^{-5}\exp\left[-\frac{1}{\pi}(fT_z)^{-4}\right] \tag{2.21}$$

This spectrum is based on extensive oceanographic data and has been adopted as the most appropriate expression of water surface behaviour for a fully developed open sea. It may be used to generate a force spectrum and hence the stress spectrum directly [2.21]. This method of analysis relies on the use of the transfer function approach presented in section 2.6.1. This method was preferred over the alternative method based on the linear wave theory and a direct integration type analysis.

The main advantage of this approach is that it allows for a site independent transfer function to be determined. The transfer function can then be subsequently used to obtain the response spectrum which is transformed into a load history in the time domain as described in section 2.5.1. However, using this approach directly with the PM spectrum as given in equation 2.22 can lead to an inaccurate representation of the frequency content of the generated time history. This is due to the fact that most of the wave energy in wave spectra measured at typical Jack-up sites is concentrated at frequencies slightly higher than that predicted by equation 2.22. This peak frequency effect is shown clearly in figures 2.13 and 2.14 for data obtained from the Silver Pit and Ekofisk locations respectively.

A peak frequency correction parameter, β, was therefore incorporated into the PM spectrum to account for this effect giving an alternative form of equation 2.22 as,

$$S_{yy}(f) = \frac{H_s^2 T_z}{8\pi^2}\left((f-\beta)T_z\right)^{-5}\exp\left[-\frac{1}{\pi}\left((f-\beta)T_z\right)^{-4}\right] \qquad (2.22)$$

Equation 2.23 is more accurate and yields a wave energy spectrum closer to the measured spectra for both locations used in this study. The relationship between β, and the peak frequency of the wave energy spectrum is a linear one. It is a site dependent parameter and its magnitude depends on sea state parameters such as the significant wave height and mean zero crossing period. The values of β for the Ekofisk and Silver Pit locations were found using a curve fitting method to be 0.016 and 0.044 respectively.

2.8 SELECTION OF SEA STATES

The importance of the wave loading regime used in the analysis and the effects of structural features and how these were modelled to generate representative results have been introduced and discussed. This section introduces a study of the environmental influences on the stress PSD and highlights the importance of using representative sea states and modelling the effects of the corrosive environment to study the variable amplitude corrosion fatigue behaviour of high strength Jack-up steels.

A detailed examination of oceanographic data for the North Sea, observed over a period of five years has shown that the distribution of significant wave height, H_s, is more accurately described by the Gumbel distribution as illustrated in [2.14]. The Gumbel distribution is given as:

$$P(x) = 1 - \exp\left[-\exp(-x)\right] \qquad (2.23)$$

Where $P(x)$ is the exceedance of the variable x.

Observed sea state data was found [2.14] to be well fitted by the following expression:

$$P(H_s) = 1 - \exp\left[-\exp\left(\frac{1.9 - H_s}{1.06}\right)\right] \tag{2.24}$$

The associated mean zero crossing period T_z for a wave of significant height H_s is given as:

$$T_z = \sqrt{\left[8(H_s + 2.6)\right]} \tag{2.25}$$

This modelled distribution agrees very closely with sea state data observed at typical Jack-up locations in the North Sea. Table 2.2 shows the distribution of significant wave height and mean zero crossing period for the Bery/Frig location in the North Sea. The sea states used for the JOSH model are presented in table 2.3.

2.9 DISCUSSION

The JOSH model [2.5, 2.22] relies on the use of advanced simulation techniques to generate the service loading history. Details of the implementation procedure have been presented in section 2.5. This simulation procedure relies on the use of the transfer function approach presented in section 2.6.1 and illustrated in figure 2.10.

The Jack-up transfer function $H(f)$, used to generate the response spectrum, $S_{xx}(f)$, was obtained using the procedure outlined in section 6.3.1. As shown in figures 2.15 and 2.16 there is a very close match in the model and service transfer functions for 4 and 5.5%, damping respectively using data obtained from the Silver Pit and the Ekofisk complex in the North Sea. The sensitivity of the normalised transfer function to changes in damping is not very high as seen in figures 2.15, 2.17 and 2.18 for the data obtained from the Silver Pit location. The corresponding results for the Ekofisk complex are shown in figures 2.16, 2.19 & 2.20.

Peak frequency matching of the transfer functions was carried out by varying the stiffness of the rotational and translational springs used to model the effect of leg-foundation interaction. For this investigation three cases were studied:

1 fixed
2 pinned and
3 model based on a rotational and translational spring system.

A rotational spring stiffness of 5.576×10^{10} Nm / rad was seen to give the best agreement between the service and peak frequency of about 0.24Hz as shown in figure 2.15 for the data obtained from the Silver Pit location.

For the data obtained at the Ekofisk complex, a rotational spring stiffness of 2.365×10^{10} Nm / rad was used together with a damping ratio of 5.5%. Both these values compare very well with those presented in references [2.18] and [2.20] respectively. In reference [2.20] a similar approach was used with values of 2.7×10^{10} Nm / rad for rotational stiffness and a mean damping ratio of 5.5%. This value was obtained with a standard deviation confidence range of 1.2% implying that the most likely damping estimates were between 4.3 and 6.7%. This is confirmed by the model results obtained for this study for both cases with 4.0% and 5.5% damping for the Silver Pit location and Ekofisk complex respectively.

The service transfer functions were obtained in each case from the measured wave elevation and response spectra for each site considered. These are shown in figures 2.13 and 2.21 for the silver pit location and in figures 2.14 and 2.22 for the Ekofisk complex. Figures 2.13 and 2.14 show the measured wave elevation spectra for the respective locations compared with those predicted by the PM spectrum and the modified PM spectrum. The measured service response spectra for the Silver Pit and Ekofisk locations are shown in figures 2.21 and 2.22 respectively. Using these spectra it was possible to obtain the corresponding service transfer functions for the two sites by using equation 2.14. The service transfer functions were compared with those predicted by using the Pierson Moskowitz (PM) spectrum with a peak frequency correction. This comparison is shown in figure 2.23 for the Silver Pit location and in figure 2.24 for the Ekofisk location. The agreement in the normalised transfer

functions was good especially for frequencies higher than 0.1Hz. Below 0.1Hz the discrepancy in the transfer functions was greater. This effect is either due to inaccuracies in measuring the energy of the ocean waves at very low frequencies and/or as a result of non linear effects which are not accounted for in the model.

It was observed that the effect of the translational spring constant on the transfer function is negligible. This is illustrated in figure 2.25 which shows that the model transfer function is identical for cases 2 and 3 using identical rotational springs. The overall effect of varying the rotational spring stiffness on the normalised transfer function is shown in figure 2.26. Figure 2.26 shows that as the spring constant is increased, the normalised transfer function for case 2 approaches that for case 1 as expected.

A sensitivity analysis was carried out to quantify the effect of water depth on the model transfer function. Results obtained from this study show that the nature of the transfer function is very sensitive to the operating water depth. For the Silver Pit location, the results obtained from the sensitivity study on the rotational transfer function are shown in figure 2.27. Overall, the magnitude of the rotational transfer function was found to increase exponentially with water depth as shown in figure 2.28. The results obtained on the sensitivity of the translational transfer to changes in water depth are shown in figure 2.29. Figure 2.29 shows that the effect on the magnitude of the translational transfer function is less severe as the water depth is increased. For the rotational transfer function, a 5% and 30% increase in water depth lead to about 25% and 250% increase in the magnitude of rotational transfer function respectively. The effect of increasing water depth on the translational transfer function on the other hand is not as significant as the effect on the rotational transfer function. This is shown in figure 2.30 and it can be seen from this figure that the translational transfer function exhibits an approximately linear dependence on water depth. An equivalent increase in water depth of 5% and 30% only leads to an increase in magnitude of about 9% and 45% respectively.

It was observed that though the magnitudes of the rotational and translational transfer functions increase with depth at different rates, they are equivalent when normalised for any particular water depth. In a similar manner, normalising the PSD preserves

the frequency content of any resulting time history but allows for the magnitude of the peaks to be varied as required by applying a suitable scaling factor to meet the needs of any testing conditions. This is the best way of varying the testing time for a particular joint instead of altering the frequency content of the load history which is understood to be very important for corrosion fatigue behaviour of Offshore structures.

The response spectra used to generate JOSH were based on the model transfer function and the modified PM spectra for the different sea states used. In a similar manner the predicted response spectra for the Maersk Guardian Jack-up platform at the Silver Pit and Ekofisk locations were compared with those measured at the respective locations. Figures 2.31 and 2.32 show this comparison. The overall prediction of the distribution of energy across the frequency range of interest in both cases is good. However there are slight discrepancies in both cases possibly due to a combination non linear effects which are not accounted for in the model and noise in the measured data.

2.10 SUMMARY

This Chapter has introduced and discussed the relevant analytical work that was carried out to ensure that realistic results are obtained for this study. The influences on fatigue resistance of structural steels used in the construction of a typical Jack-up leg structure have been presented. The methodology used for the work presented in this thesis to model these relevant influences has also been presented. This Chapter has also introduced and discussed the results of a comparative study between model and service data and demonstrated the level of agreement between the two sets of data.

Further details of JOSH are presented in Chapter 3 together with the large scale fatigue testing programme undertaken in this study using the simulated sequence.

2.11 CONCLUSIONS

The following conclusions can be drawn from this analysis.

A mathematical model has been successfully used to obtain a representative transfer function for a typical Jack-up platform.

Comparison of the model transfer function has been demonstrated to agree very closely with that obtained from service data.

Using the established transfer function approach and a suitable wave energy spectrum, a representative response spectrum can be obtained from which the time history of the loading can be derived in a similar manner as in the WASH model

The complex leg -soil interaction can be adequately modelled using springs and assuming a rigid foundation. This requires the use of well known soil properties or the use of conservative estimates. The effect of the translational spring is insignificant and the leg-soil connection can be satisfactorily treated as pinned.

Jack-up response is very sensitive to water depth and as a result, it is very difficult to produce any single load history that will be representative of service loading conditions for Jack-ups operating in different water depths. Increasing the water depth changes the resonant frequency and magnitude of peaks and also the frequency content of the resulting time history. However most operating sites in practice cover extensive areas of similar water depth. The JOSH model provides a suitable frame work for generating any representative service load history applicable to all sites within a range of water depths.

Due to the variability of the nature of the stress PSDs obtainable for a particular structure depending on the operating environment as highlighted by conclusion 5, an approach has been proposed based on results obtained from this study which is expected to eliminate the lengthy analysis procedure covered in section 2.6. This approach relies on the use of non dimensional parameters to describe the normalised stress PSD of any particular structure for any set of sea states. The proposed normalised PSD approach is presented and discussed in Chapter 5.

2.12 REFERENCES

[2.1] Thomas P A, "*TPG 500 Production Jack-up Design: Why Is It Different From A Drilling Jack-up?*", Sixth International Conference, The Jack-up Platform Design, Construction & Operation, Ed. Boswell L F, D'Mello C and Supple W J, Sept. 1997.

[2.2] Baerheim M, Manschot D and Nortvedt T, "Use of a Jack-up as a Permanent Installation for the Marginal Siri Field", Sixth International Conference, The Jack-up Platform Design, Construction & Operation, Ed. Boswell L F, D'Mello C and Supple W J, Sept. 1997.

[2.3] Health and Safety Executive (1992) Offshore Installations (Safety Case) Regulations, HSE Books, Sudbury, Suffolk, UK.

[2.4] Sharp J V, Billingham and Stacey A, "*Performance of High Strength Steels used in Jack-ups*", Sixth International Conference, The Jack-up Platform Design, Construction & Operation, Ed. Boswell L F, D'Mello C and Supple W J, Sept. 1997.

[2.5] Etube L S, Brennan F P and Dover W D, "*Modelling of Jack-up Response for Fatigue Testing of Weldable High Strength Jack-up Steels Under Simulated Service Conditions*", Sixth International Conference, The Jack-up Platform Design, Construction & Operation, Ed. Boswell L F, D'Mello C and Supple W J, Sept. 1997.

[2.6] Kam J C P, Dover W D and Dharmavasan S, "Fatigue testing technology for large scale Offshore structures", Handbook of Fatigue Crack Propagation in Metallic Structures, Ed. Andrea Carpinteri, Vol. 2.

[2.7] Pook L P, *The Role of Crack Growth in Metal Fatigue*, Book 307, published by The Metals Society, 1983, ISBN 0 904357 63 5

[2.8] "*FALSTAFF (Description of a Fighter Aircraft Loading Standard For Fatigue Evaluation)*", Fraunhofer-Institut für Betriebsfestigkeit, Darmstadt, 1976

[2.9] Schutz W, Bergmann, Heuler and Huck, "*The Common Load Sequence for Fatigue Evaluation of Offshore Structures -Background and Generation*", IABG Report TF-1892, 1985

[2.10] *United Kingdom Offshore steels Research Project-Phase II: Final Summary Report*, Ed. Peckover R, Health and Safety Executive Report OTH 87 265, Her Majesty's Stationary Office, London 1987.

[2.11] Irvine N M, "*The development of a broad-band loading sequence for use in the variable amplitude fatigue testing of UKOSRP-II*', Safety and Reliability Directorate, United Kingdom Atomic Energy Agency (UKAEA).

[2.12] Hart W H and Lin N K, "*A proposed stress history for fatigue testing applicable to Offshore structures*",. International Journal of Fatigue, 8 No 2 (1986) pp. 91-93.

[2.13] Wirsching P W, "*Probability-based fatigue design criteria for Offshore structures*", International Journal of Fatigue 2, April 1980 pp. 77-83

[2.14] Pook L P and Dover W D, "*Progress in the development of a Wave Action Standard History (WASH) for fatigue testing relevant to tubular structures in the North Sea*", American Society for Testing and Materials: Symposium on the Development of Standard Load Spectra, 29 April 1987.

[2.15] Schutz W and Pook L P, "*WASH (Wave Action Standard History) A Standardized Stress-time History for Offshore Structures*", Developments in Marine Technology 3, Steel in Marine Structures, Ed. Noordhoek C and Back J, Elsevier, Amsterdam 1987, pp. 161-178.

[2.16] Kam J C P "*Wave Action Standard History (WASH) for Fatigue testing of Offshore structures*", International Journal of Applied Ocean Research, Vol. 14, No. 1, July 1992.

[2.17] Kam J C P, *Structural Integrity of Offshore Tubular Joints Subject to Fatigue*, Ph.D. Thesis ,Department of Mechanical Engineering, University College London, 1989.

[2.18] Brekke J N, Campbel R B, Lamb W C and Murff J D, "*Calibration of a Jackup Structural Analysis Procedure Using Field Measurements from a North Sea Jack-up*", Proceedings, Offshore technology Conference, (OTC 6465), Houston, Texas, May 7-10 1990.

[2.19] Newland D E, *An Introduction to Random Vibrations, Spectral & Wavelet Analysis*, Published by Longman Group Ltd, ISBN 0582 21584 6.

[2.20] Weaver T O and Brinkmann C R, "*Calibration of Dynamic Analysis Procedure Using Measurements from a North Sea Jackup in a severe storm*", Offshore Technology Conference (OTC 7840), May 1995.

[2.21] Hallam M G, Heaf N J and Wootton L R, *Dynamics of Marine Structures*, published by CIRIA Underwater Engineering Group, ISBN: 0-86017-023-3

[2.22] Etube L S, Brennan F P and Dover W D, "*Service Load simulation for Fatigue Testing of Jack-up steels*", Recent Advances in Corrosion Fatigue, Sheffield, April 1997.

[2.23] *Mobile Drilling Units of the World*, Offshore Publications Limited, ISBN 1 870945 29 8

[2.24] Hambly E C, Imm G R and Stahl B, "*Jack-up Performance and Foundation Fixity Under Developing Storm Conditions*", Proceedings, Offshore technology Conference, (OTC 6466), Houston, Texas, May 7-10 1990.

[2.25] Watanabe Y, "*Development and Field Tests on Prototype of Leg Penetration Monitor System to Avoid the Punch-Through Accidents of Jackup Rigs*", Proceedings, Offshore technology Conference, (OTC 6469), Houston, Texas, May 7-10 1990.

[2.26] Cox W R, McClure S C, Alan C, and Sorenson K H, "*Settlement of Mat-Supported Mobile Units in Very Soft Clays*", Proceedings, Offshore technology Conference, (OTC 6468), Houston, Texas, May 7-10 1990.

[2.27] Siciliano R J, Hamilton J M, Murff J D and Phillips R, "*Effect of Jack-up Spud Cans on Piles*", Proceedings, Offshore technology Conference, (OTC 6467), Houston, Texas, May 7-10 1990.

[2.28] Stewart W P, White R M, Rapoport V and Devoy S D, "*On-Bottom Stability of Jackups*", Proceedings, Offshore technology Conference, (OTC 6125), Houston, Texas, May 1-4 1989

[2.29] Arnesen K, Dahlberg R, Kjeoy H, Carl Carlsen S A. "*Soil-Structure-Interaction Aspects for Jack-up Platforms*", Proceedings, BOSS.

[2.30] Pierson W J, Moskowitz L, "*A proposed spectral form for fully developed wind seas based on the similarity theory of S A Kitaigorodskii*", Journal of Geophys. Res. Vol. 69 no 24, pp5181-5190, 1964.

[2.31] Brennan F P and Dover W D, "*Fatigue of threaded tension leg platform tethers*" Proceedings of the fourth International Offshore and Polar Engineering Conference. Osaka, Japan, April 10-15, 1994.

2.13 TABLES AND FIGURES

Table 2.1: Typical values of Young's modulus for different soil types.

Soil type	Young's modulus (MPa)
Sand, loose round	20 - 50
Sand, loose angular	40 - 80
Sand, medium dense round	50 - 100
Sand, medium dense angular	80 - 150

Table 2.2: Scatter diagram for a typical Jack-up location in the North Sea.

state	Hs	Zero crossing period (s)							
		2.5	3.5	4.5	5.5	6.5	7.5	8.5	9.5
1	0.25		1	1					
2	0.75	3	32	34	13	6	1		
3	1.25		30	82	46	17	4	1	
4	1.75		3	66	67	28	13	1	1
5	2.25			21	77	37	45	3	
6	2.75			2	49	40	16	4	1
7	3.25				19	48	16	7	1
8	3.75				4	39	17	7	2
9	4.25					15	19	5	2
10	4.75					4	19	5	1
11	5.25					1	19	5	1
12	5.75						6	4	1
13	6.25						4	6	
14	6.75						1	3	1
15	7.25							2	1
16	7.75							1	1
17	8.25							1	

Table 2.3: Summary of sea states used for JOSH.

sea state number	significant wave height (m)	mean zero crossing period (s)
1	1.25	5.5
2	1.75	5.9
3	2.25	6.2
4	2.75	6.5
5	3.25	6.8
6	3.75	7.1
7	4.25	7.4
8	4.75	7.7
9	5.25	7.9
10	6.25	8.4
11	7.25	8.9
12	8.00	9.2

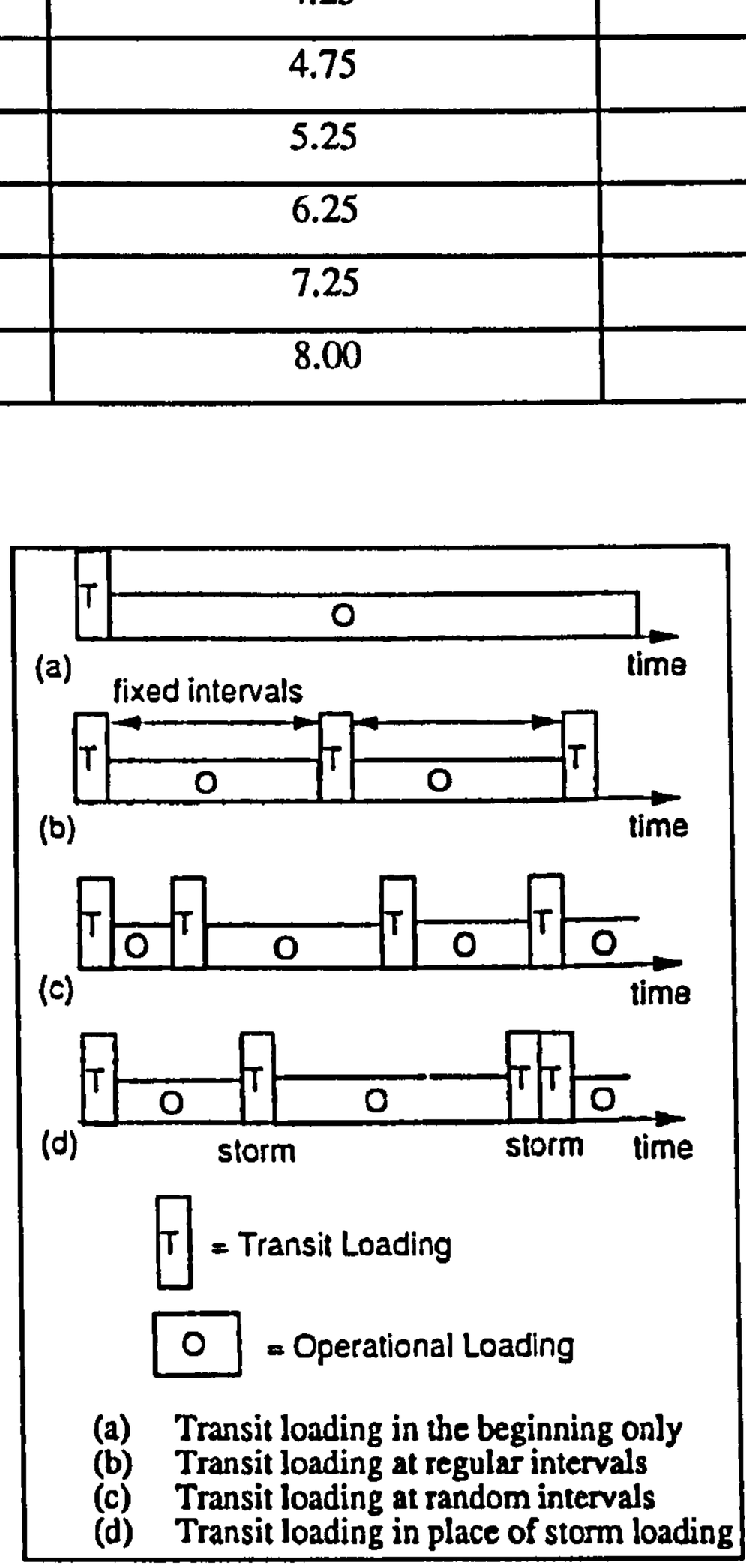

Figure 2.1: Options for simulating transit loading in Jack-ups [2.6]

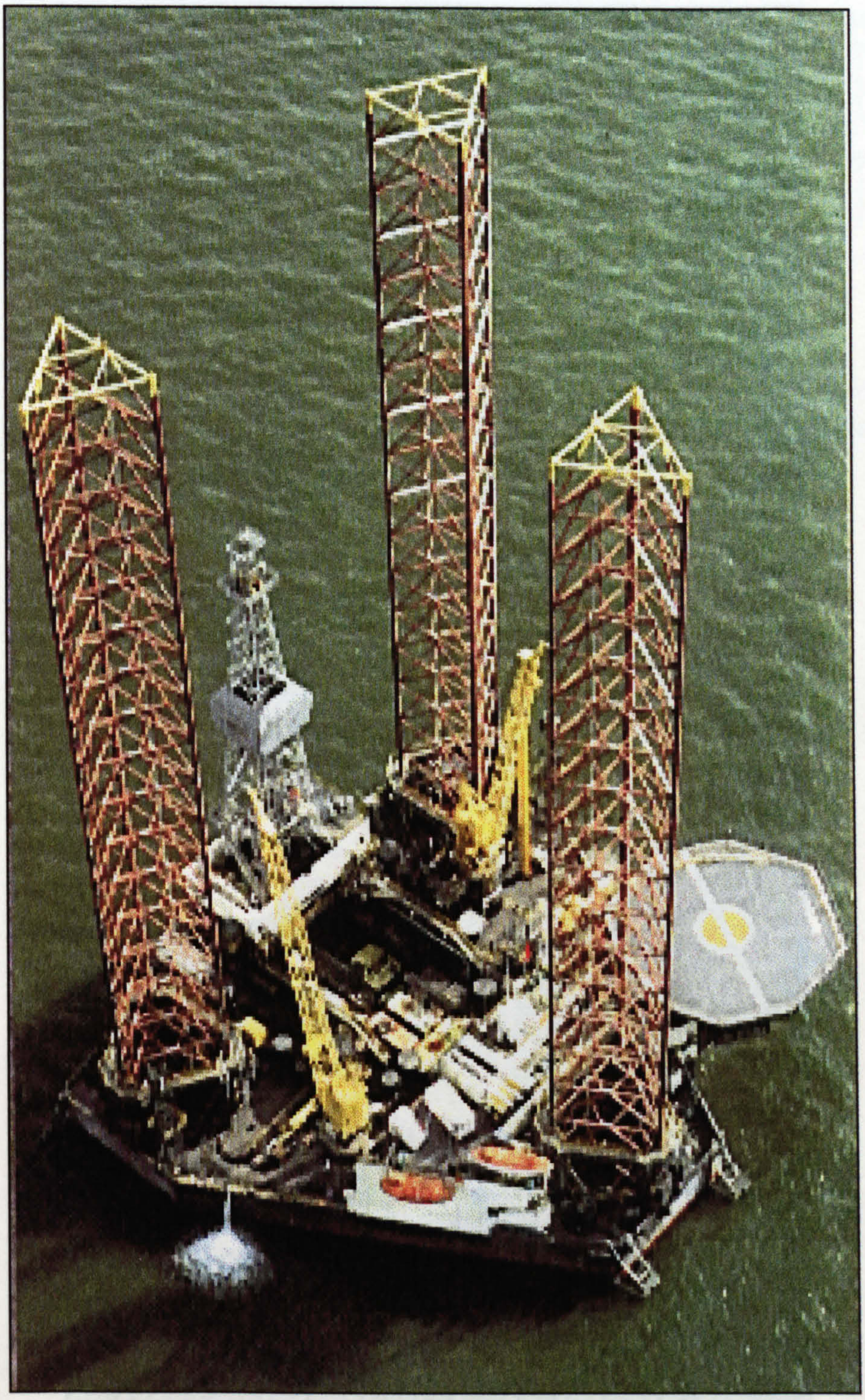

Figure 2.2: Wet transport of a self propelling Jack-up

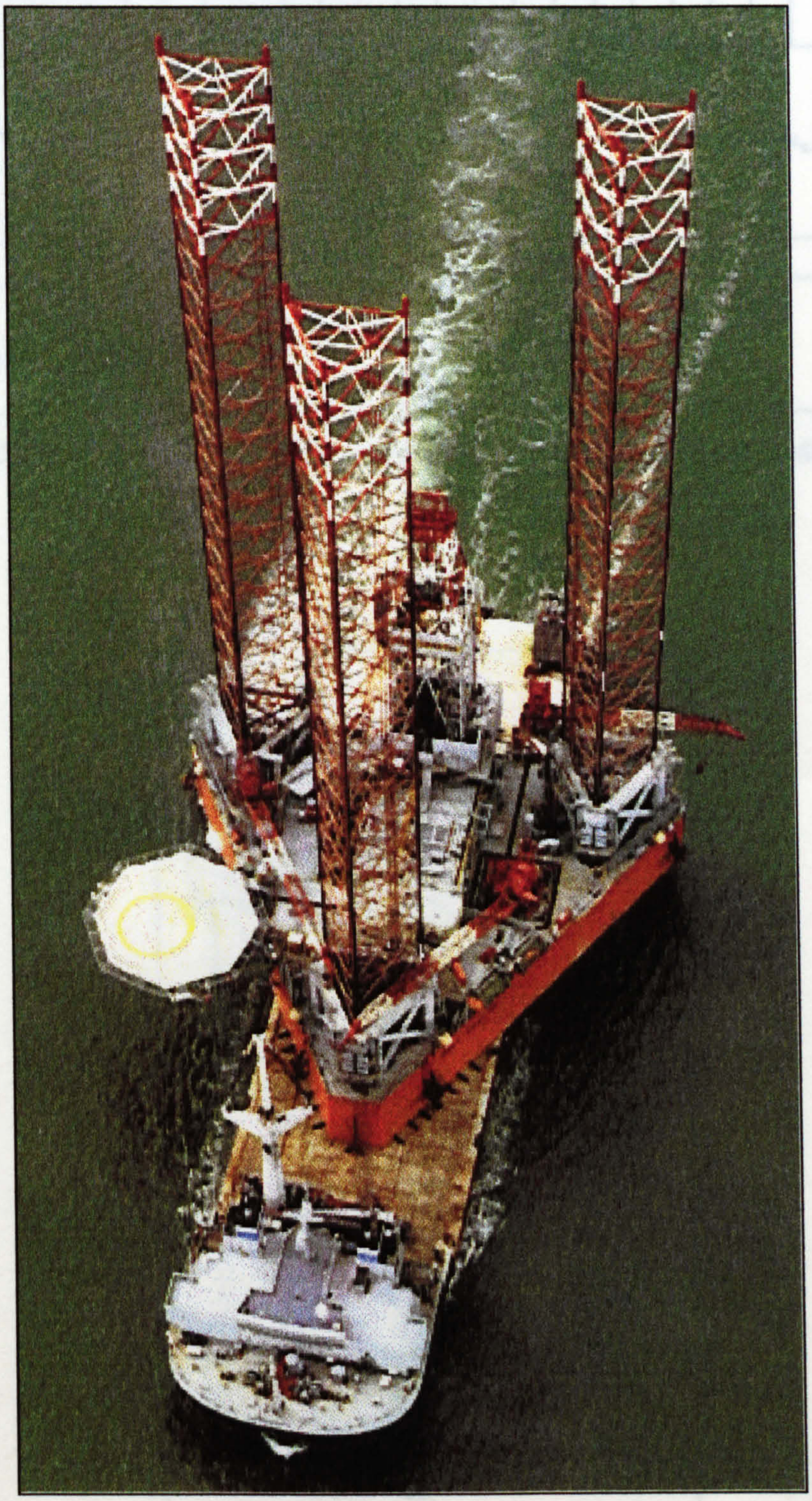

Figure 2.3: Dry transport of a jack-up using a low loader

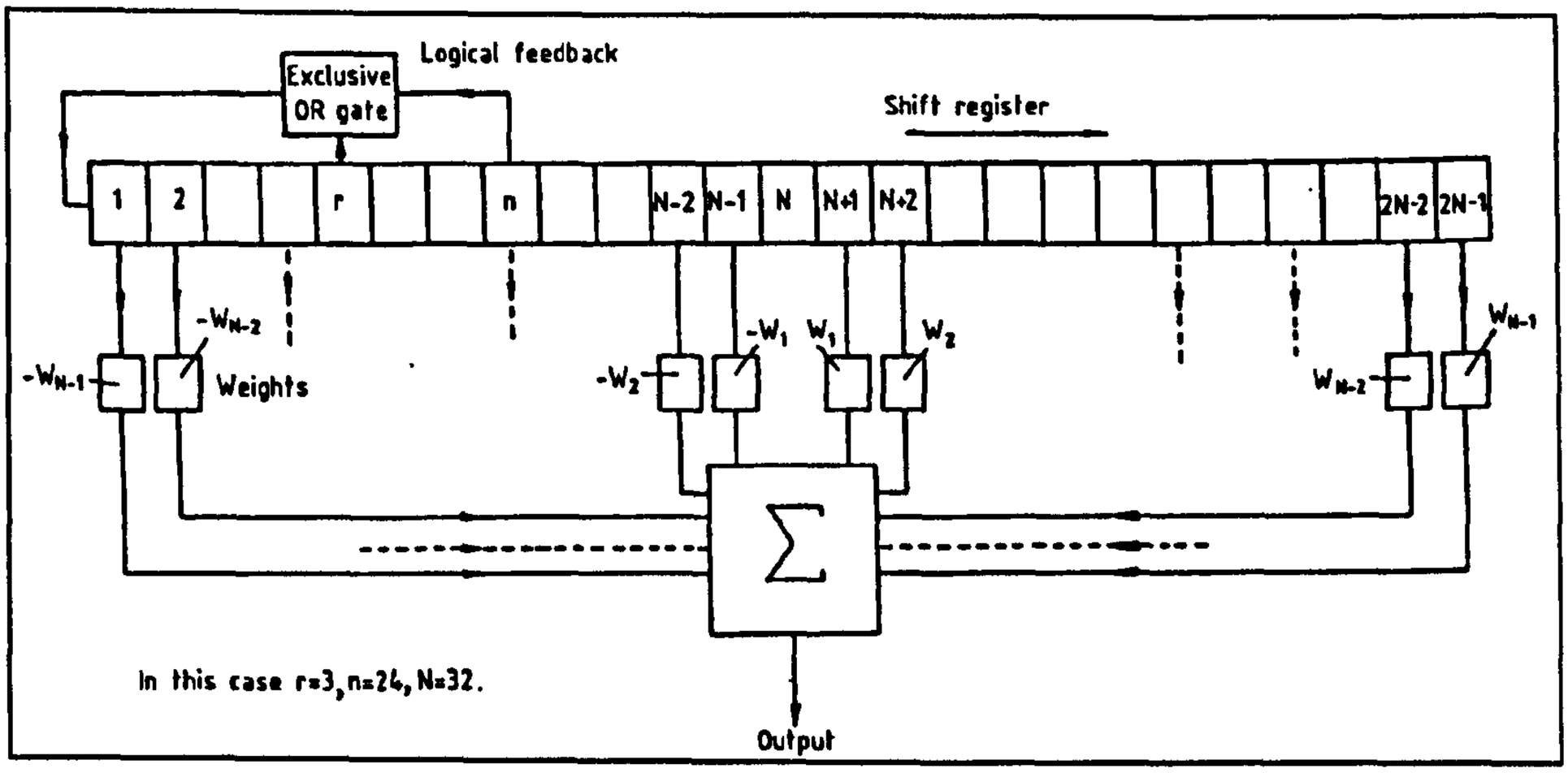

Figure 2.4: Schematic illustration of pseudo random signal generation [2.17]

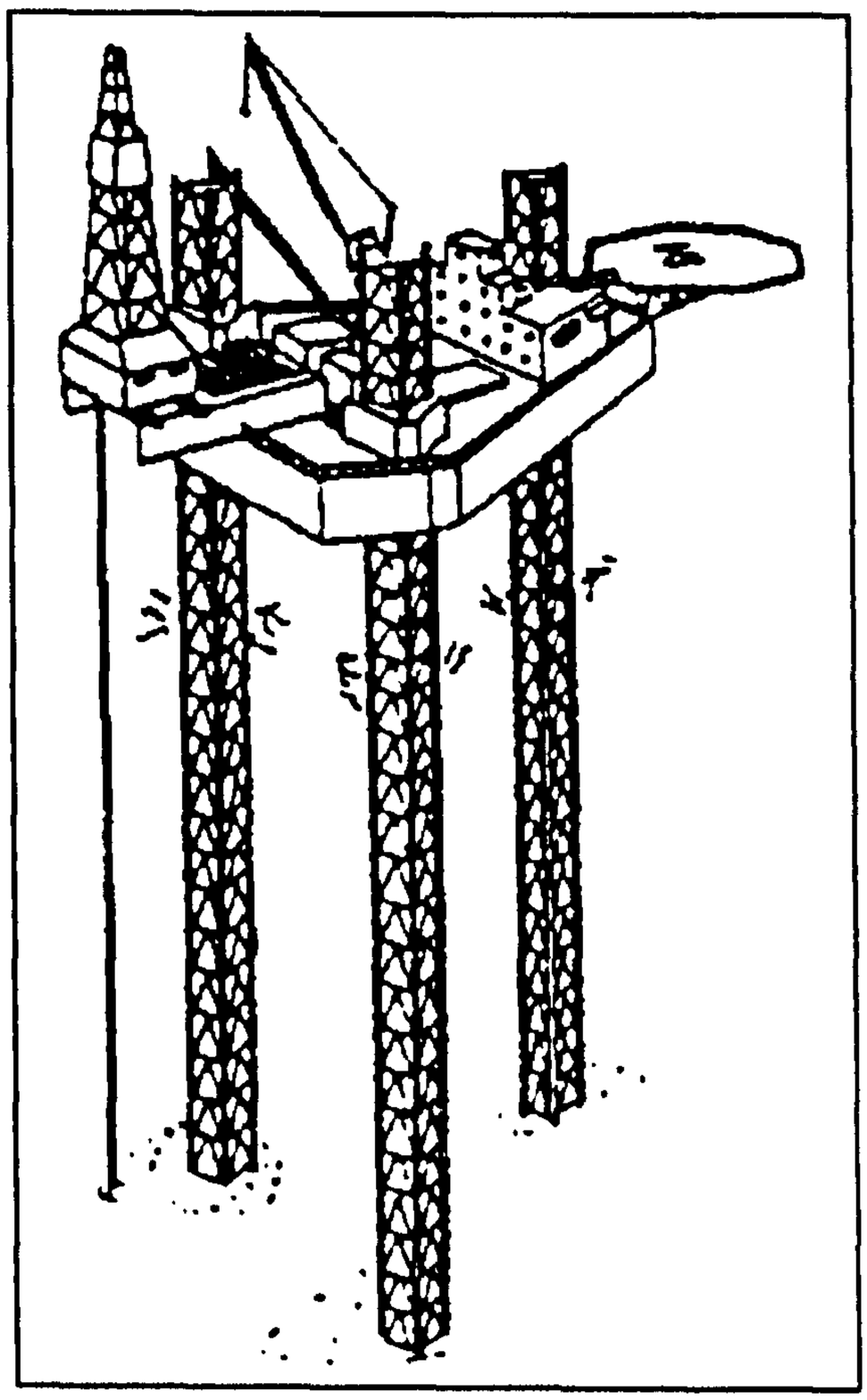

Figure 2.5: Typical Jack-up platform

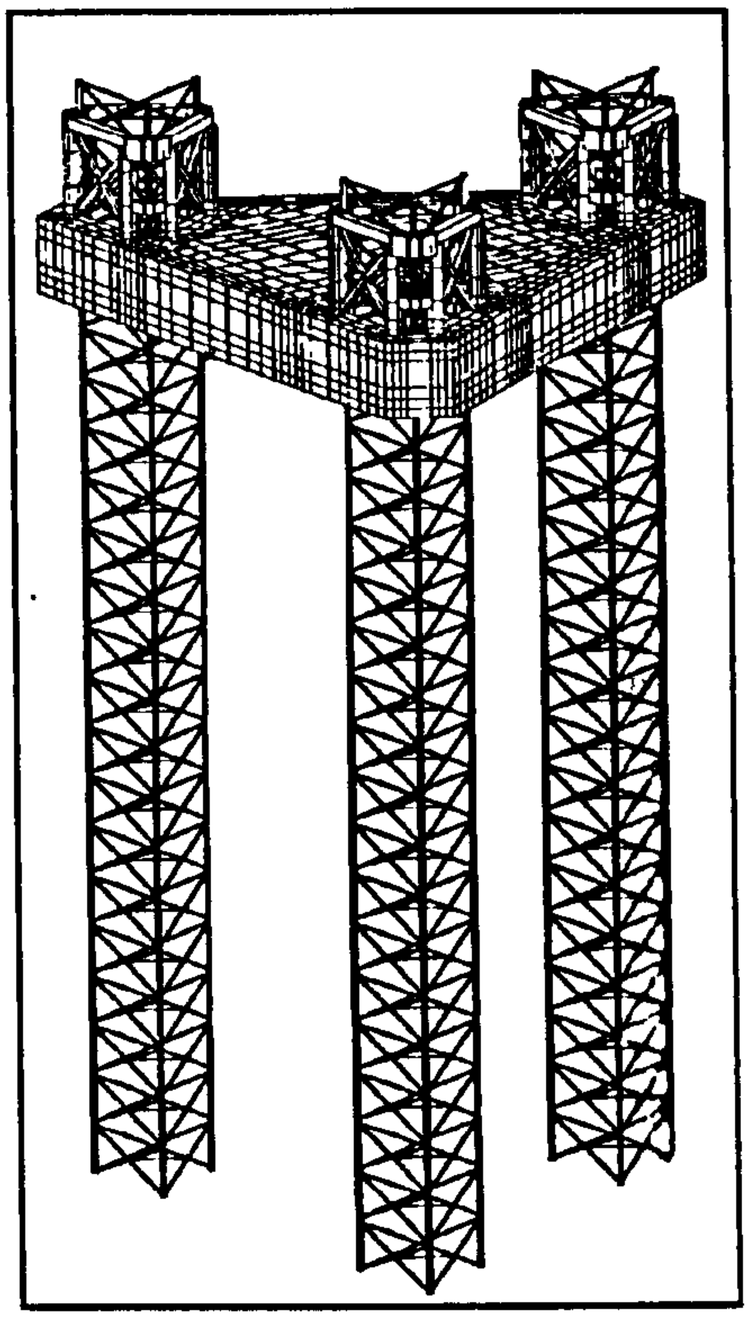

Figure 2.6: Simplified model of Jack-up platform

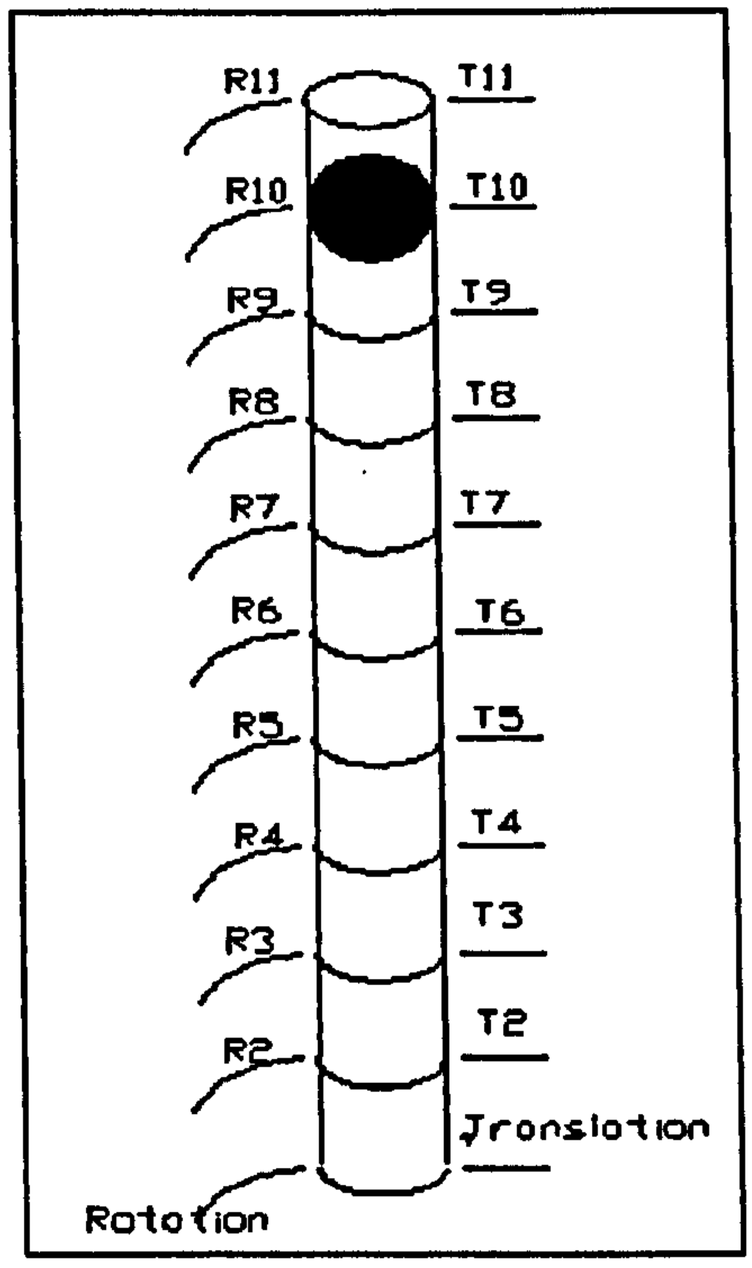

Figure 2.7: Model leg elements and nodes

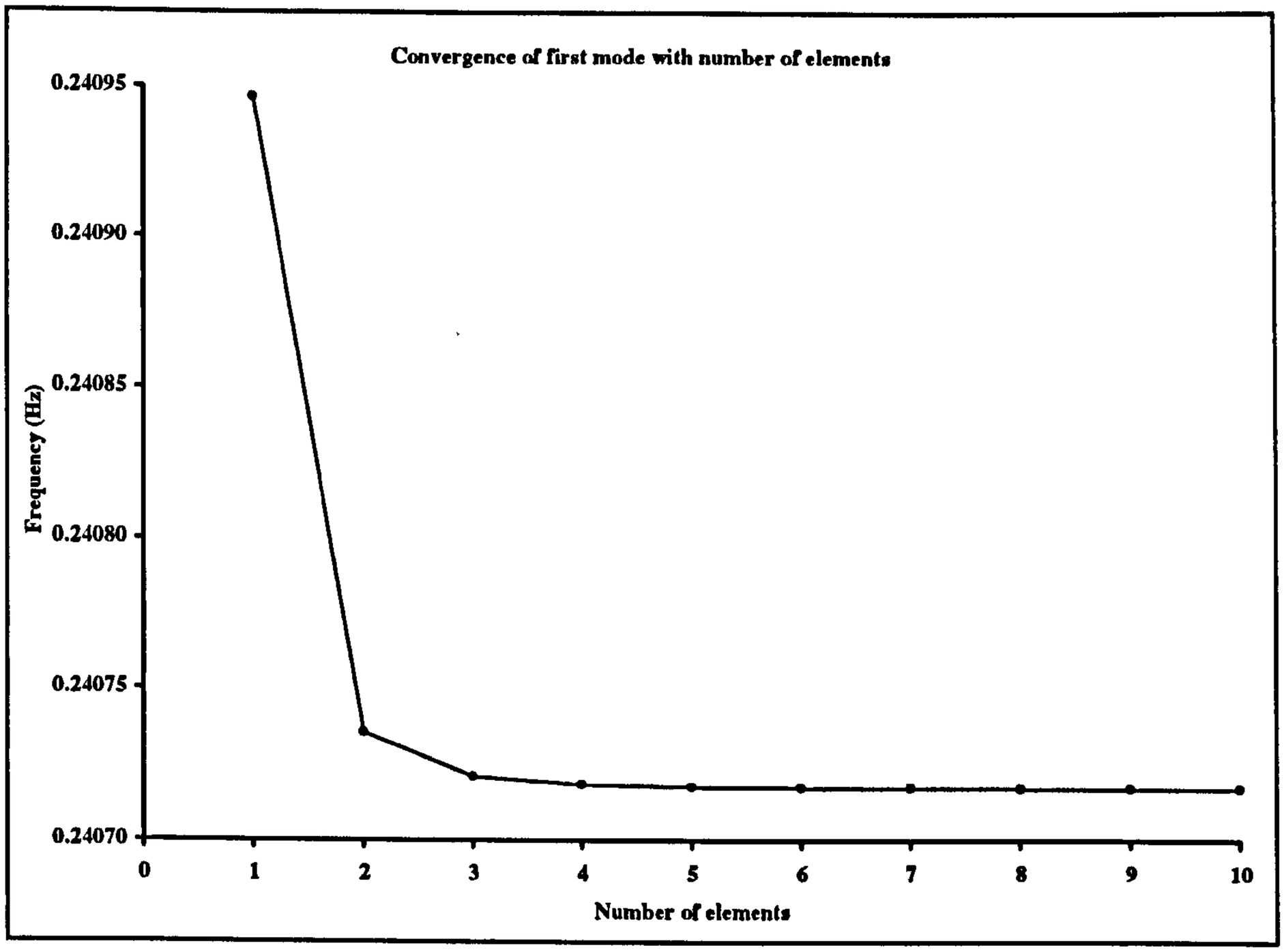

Figure 2.8: Principal mode convergence

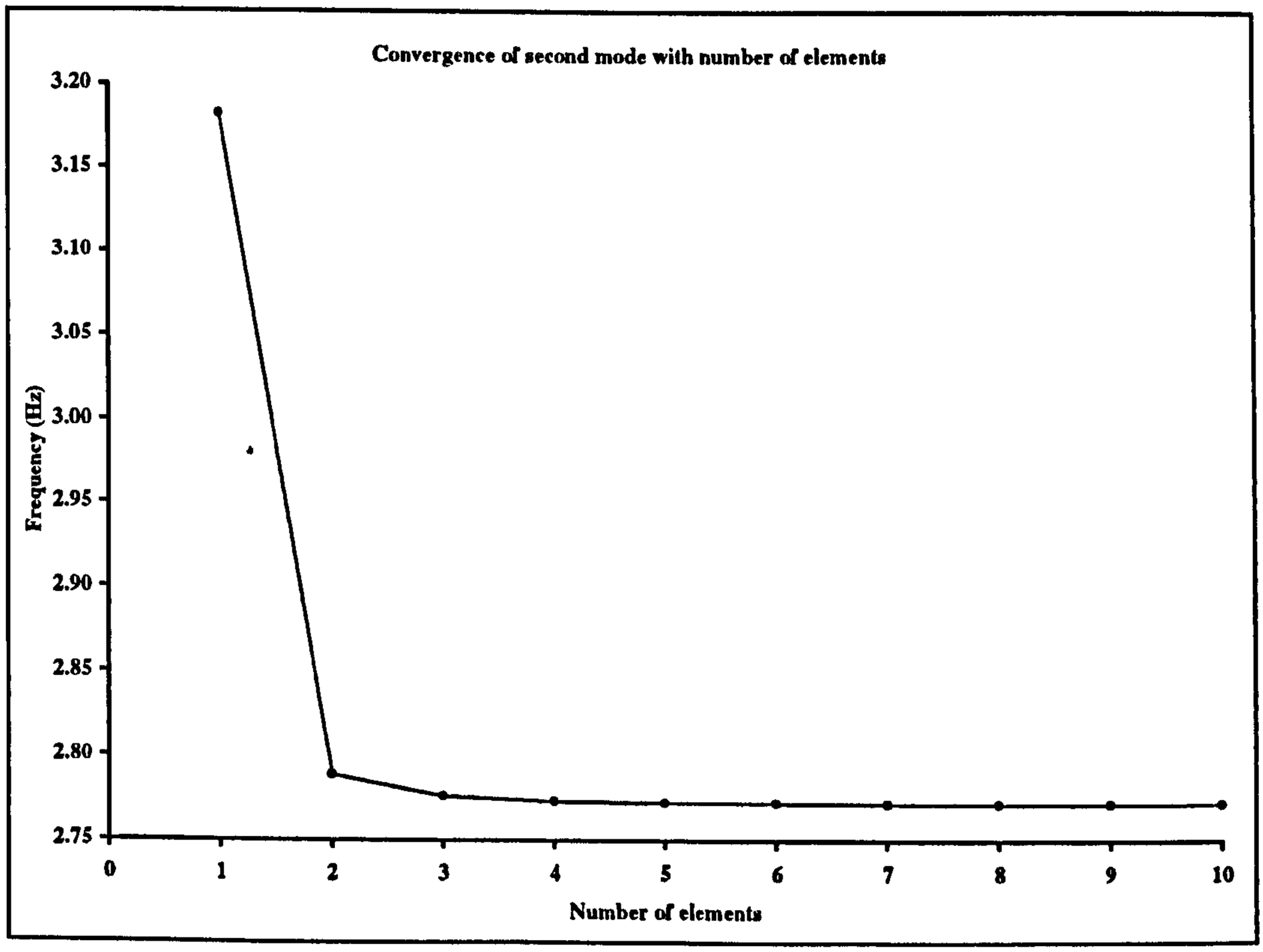

Figure 2.9: Second mode convergence

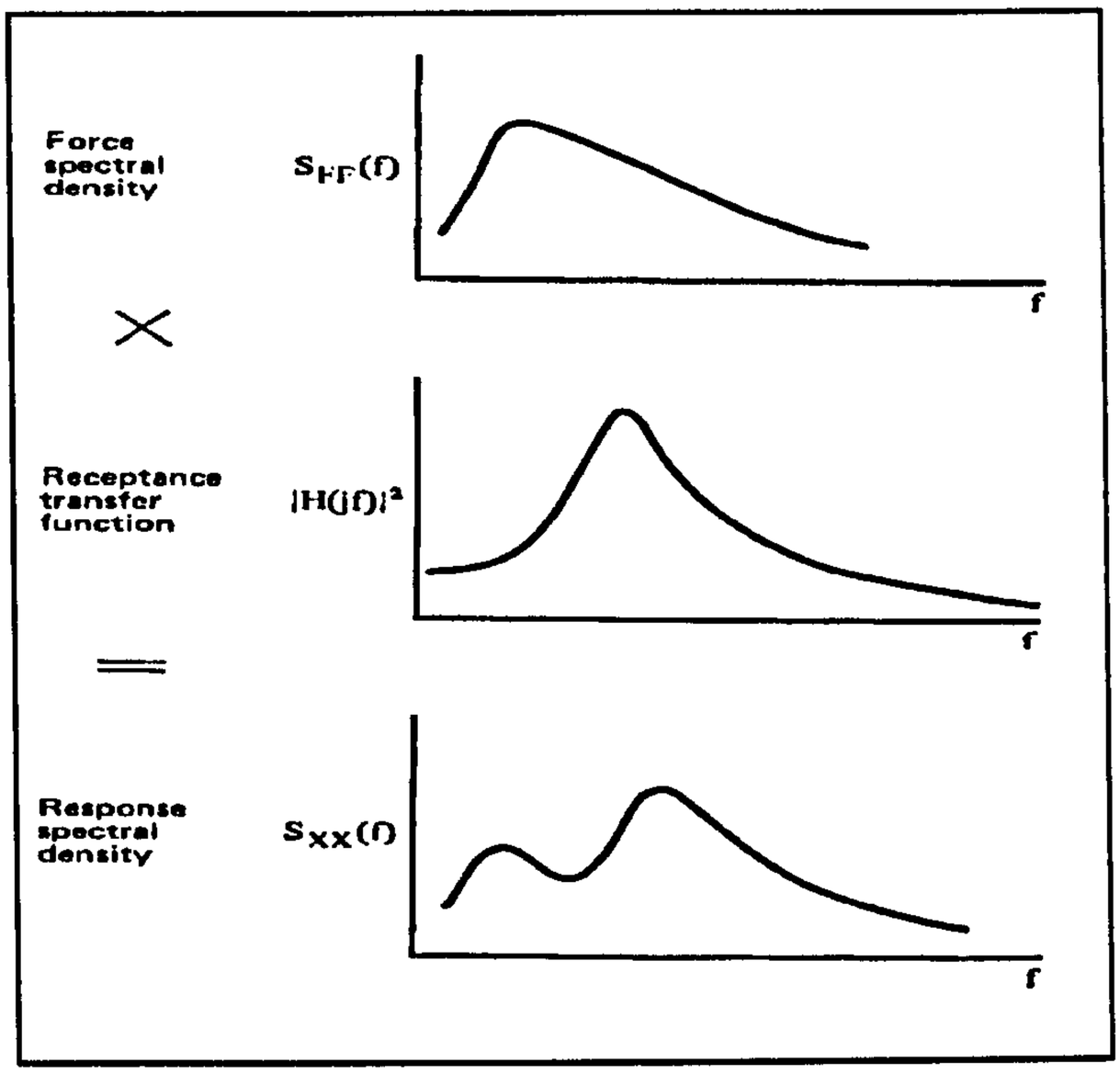

Figure 2.10: Schematic illustration of the transfer function approach [2.21]

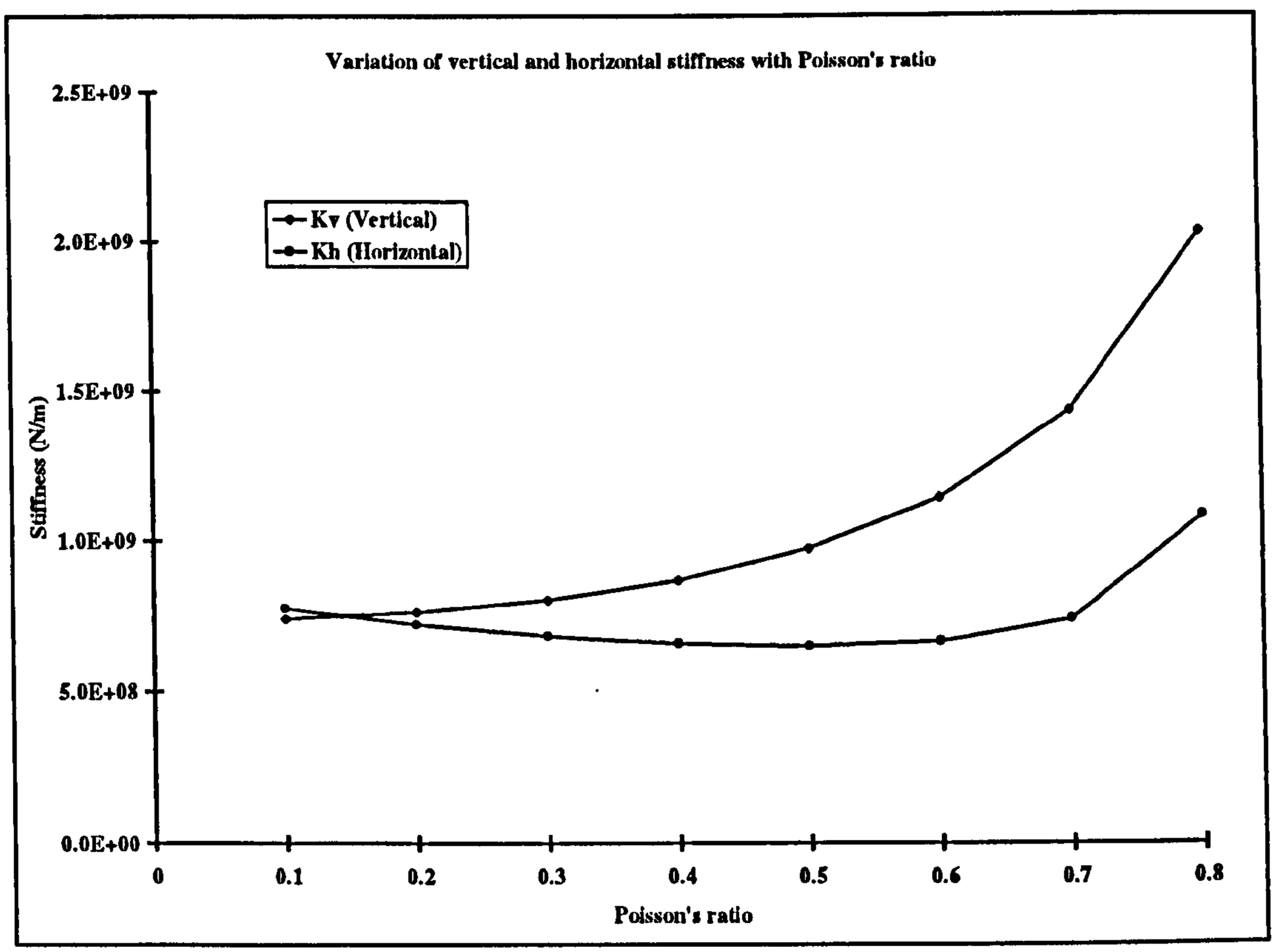

Figure 2.11: Variation of vertical and horizontal stiffness with Poisson's ratio

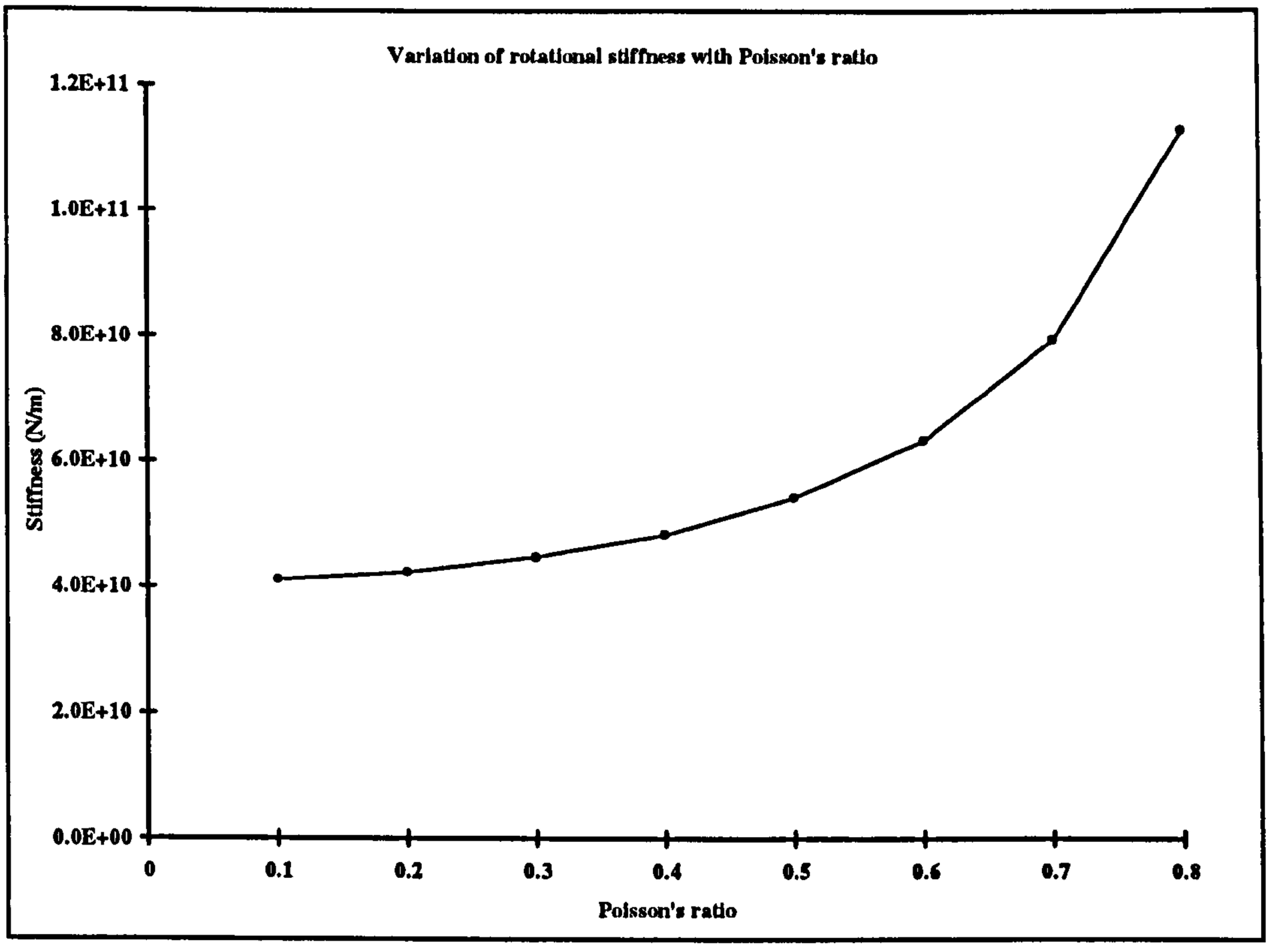

Figure 2.12: Variation of rotational stiffness with Poisson's ratio

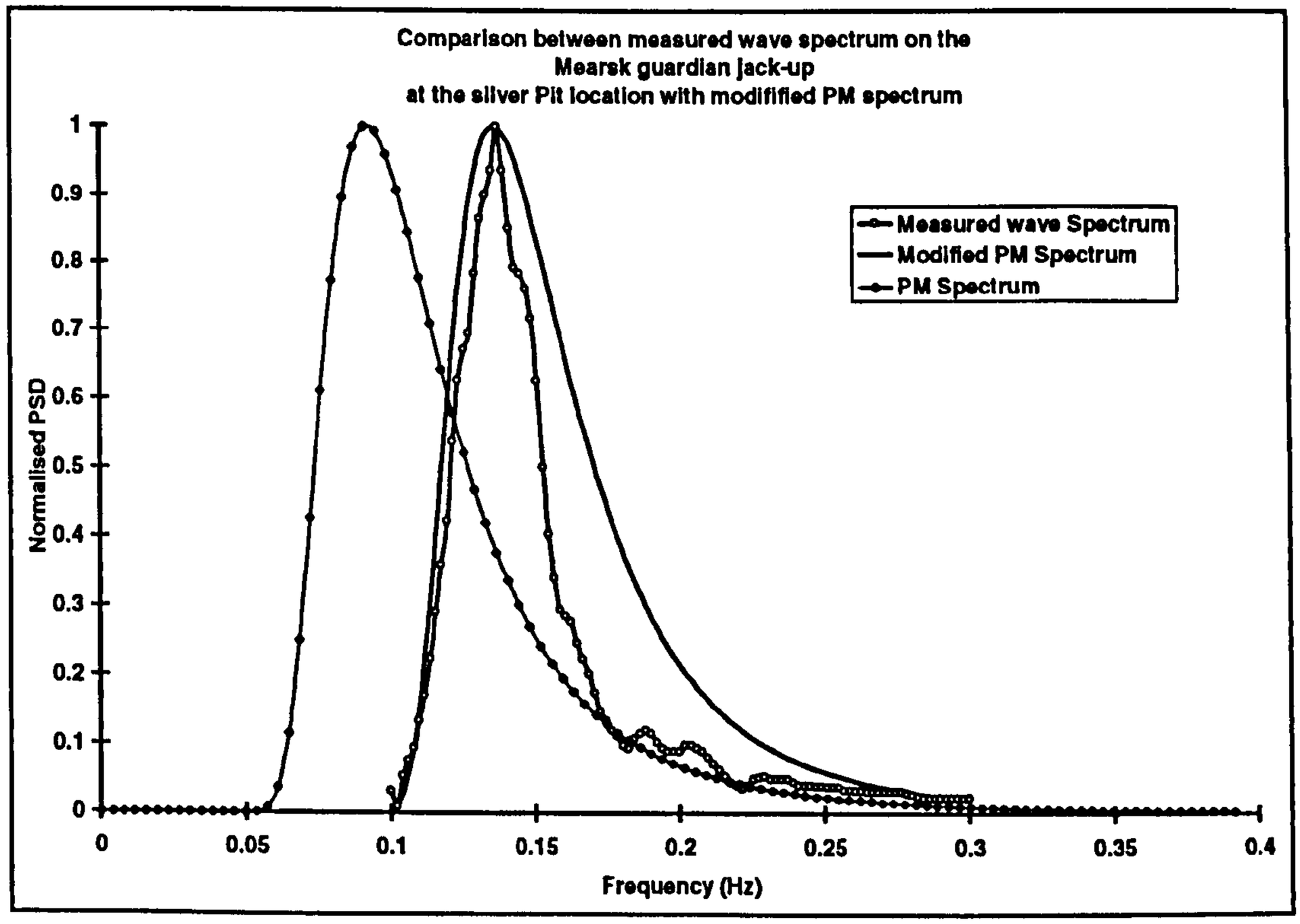

Figure 2.13: Comparison of measured wave spectrum at Silver Pit with modified PM spectrum.

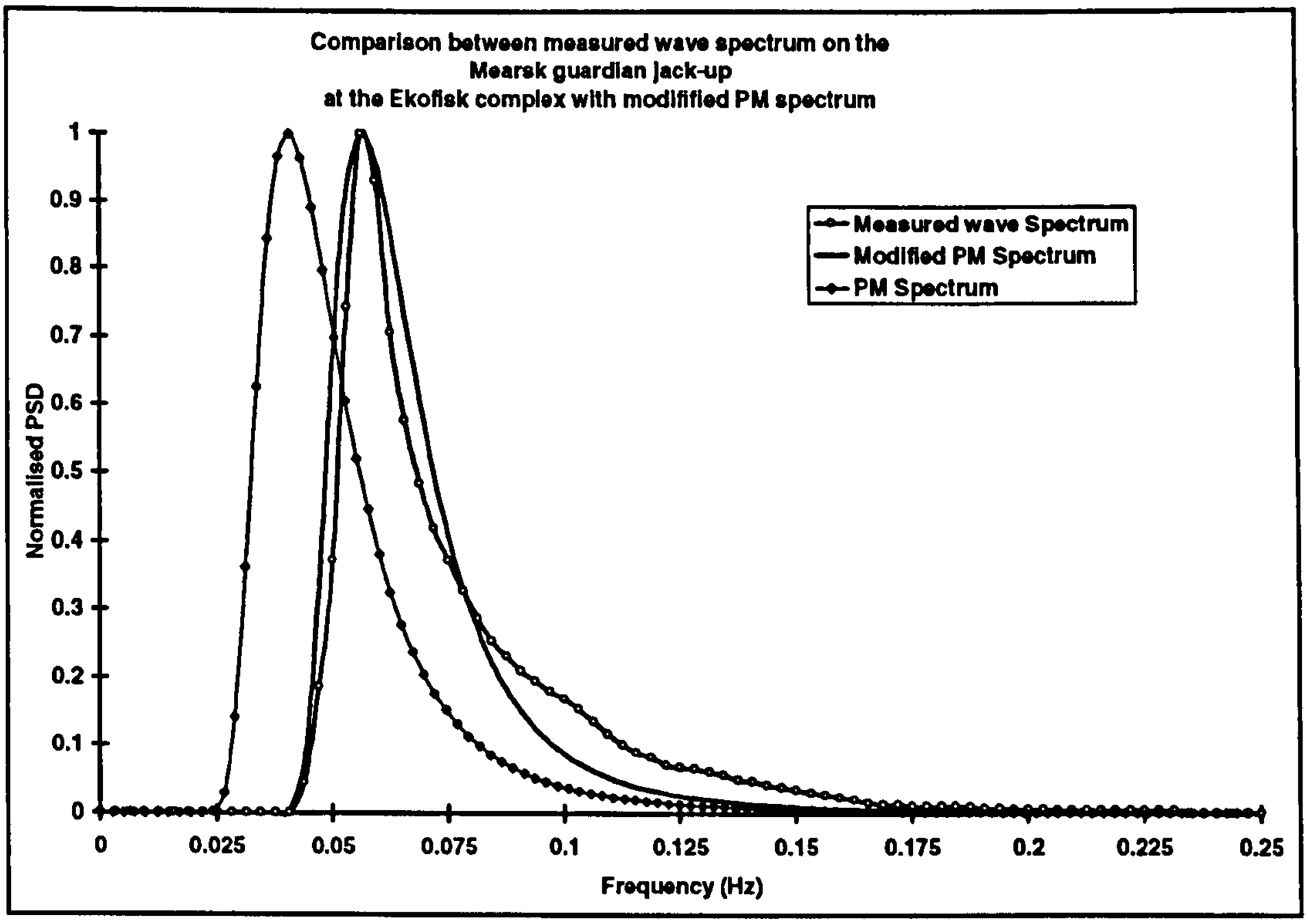

Figure 2.14: Comparison of measured wave spectrum at Ekofisk with modified PM spectrum.

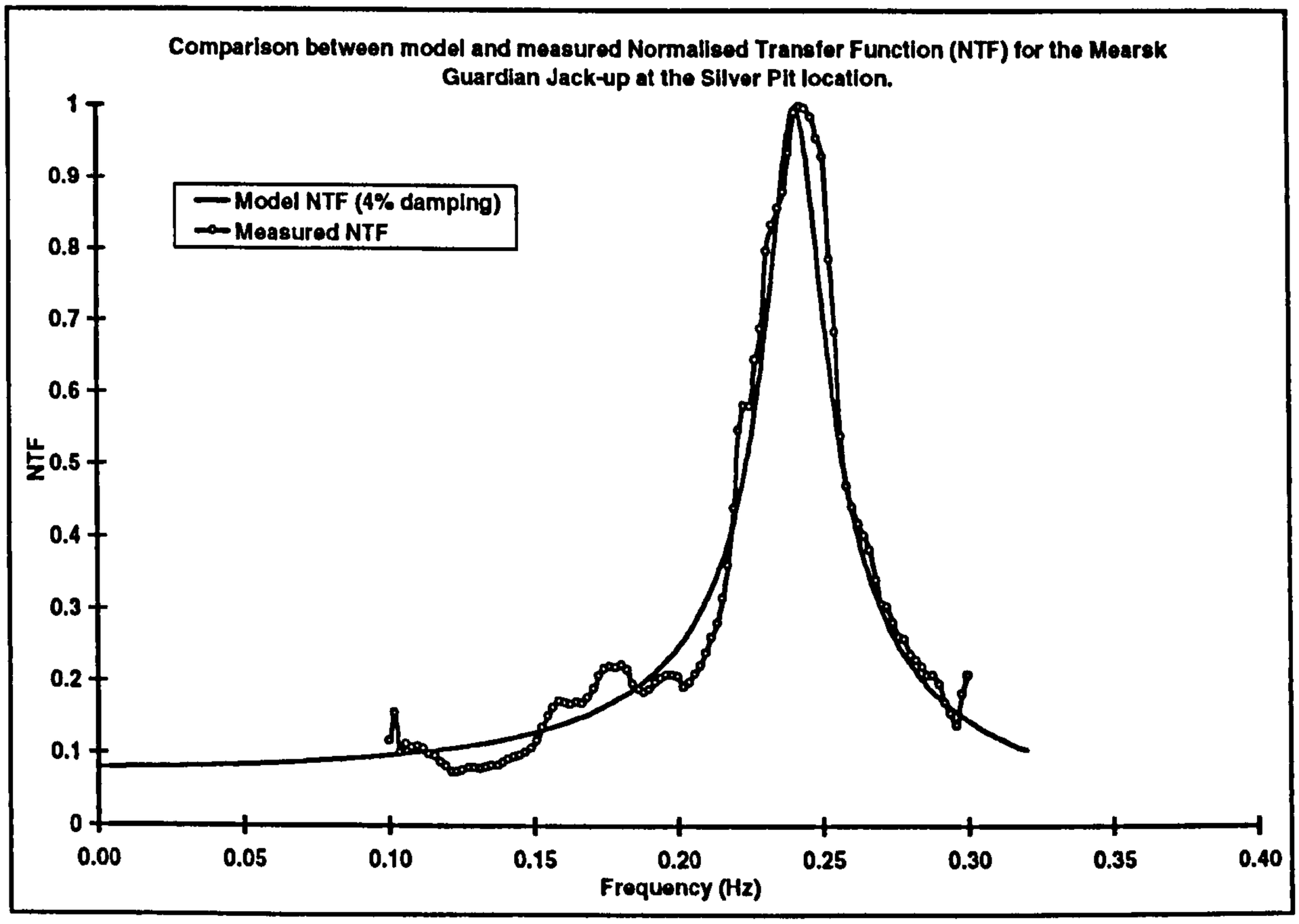

Figure 2.15: Model and measured service NTF for the Silver Pit location with 4% damping

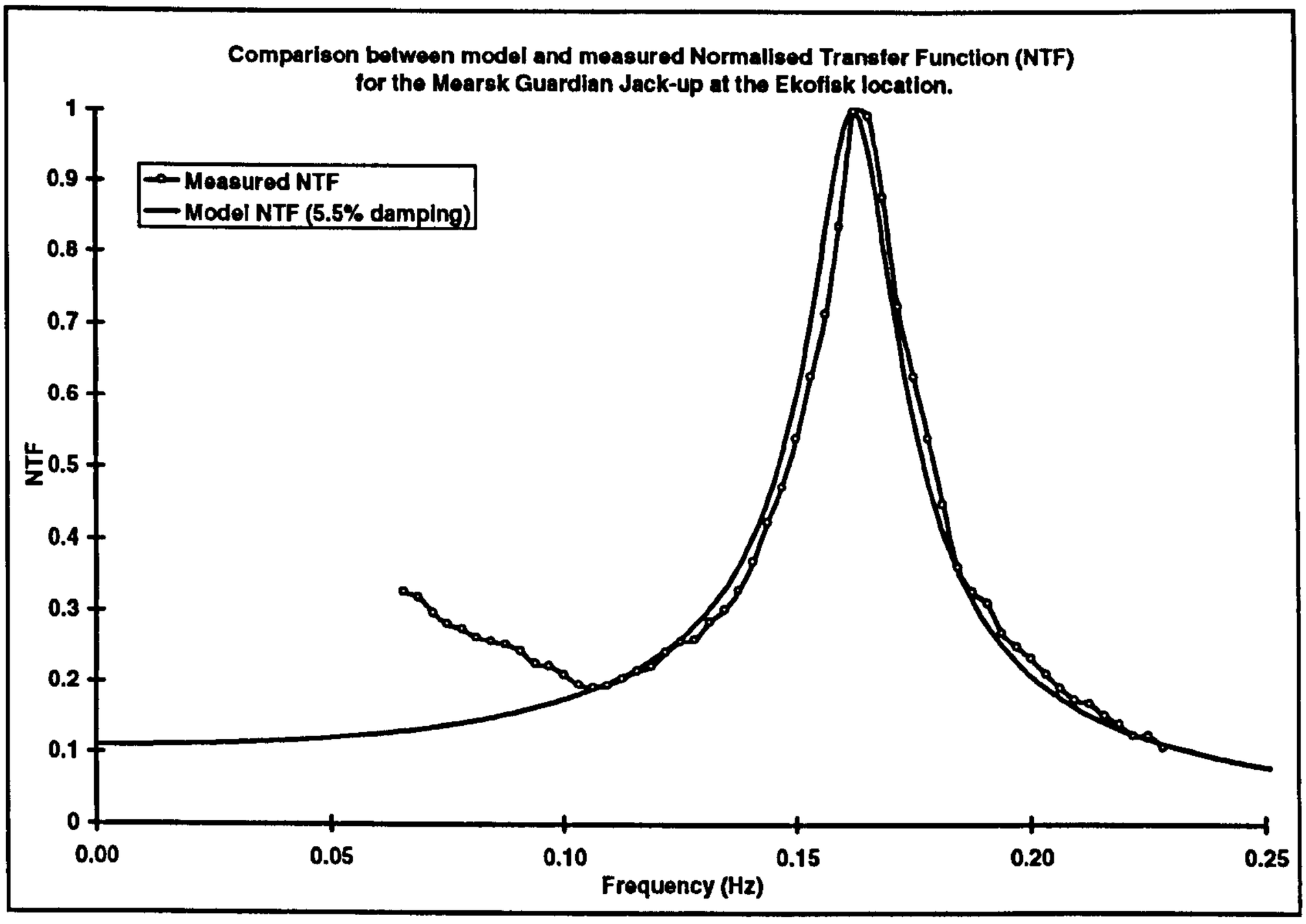

Figure 2.16: Model and measured service NTF for the Ekofisk complex with 5.5% damping

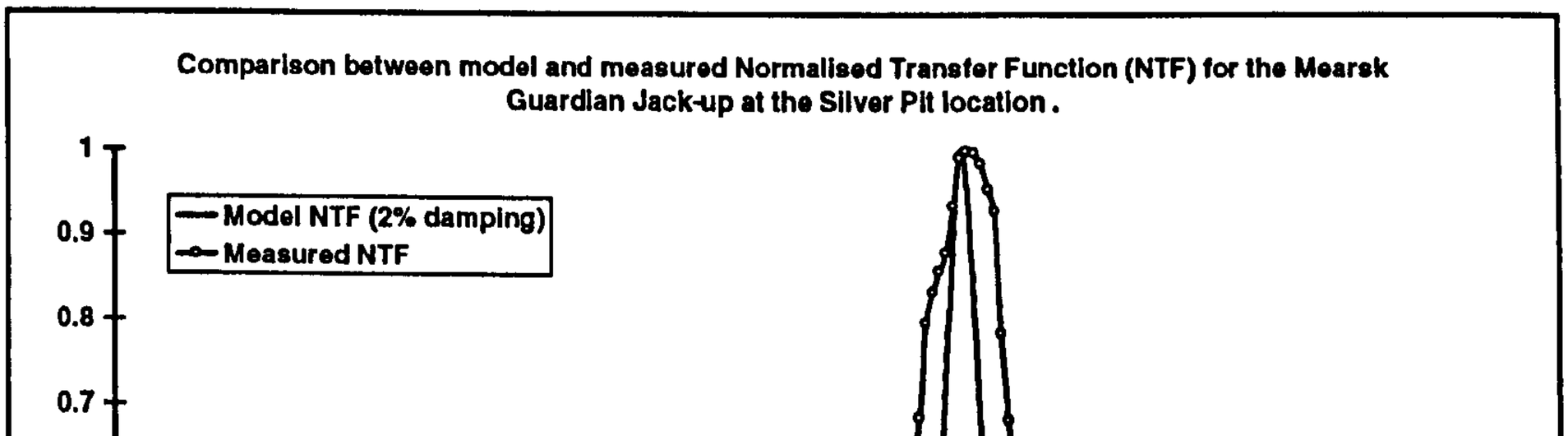

Figure 2.17: Model and measured service NTF for the Silver Pit location with 2% damping

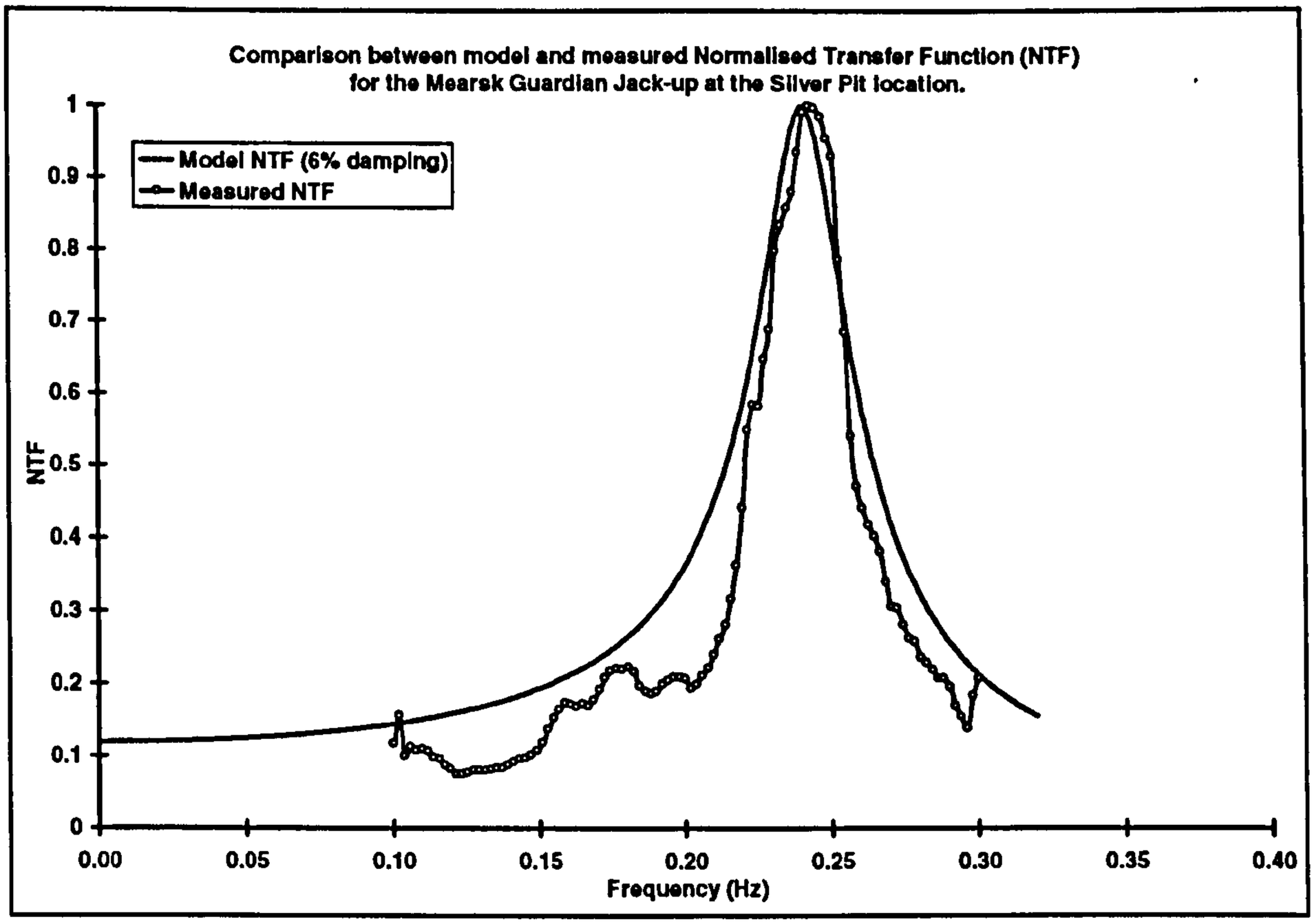

Figure 2.18: Model and measured service NTF for the Silver Pit location with 6% damping

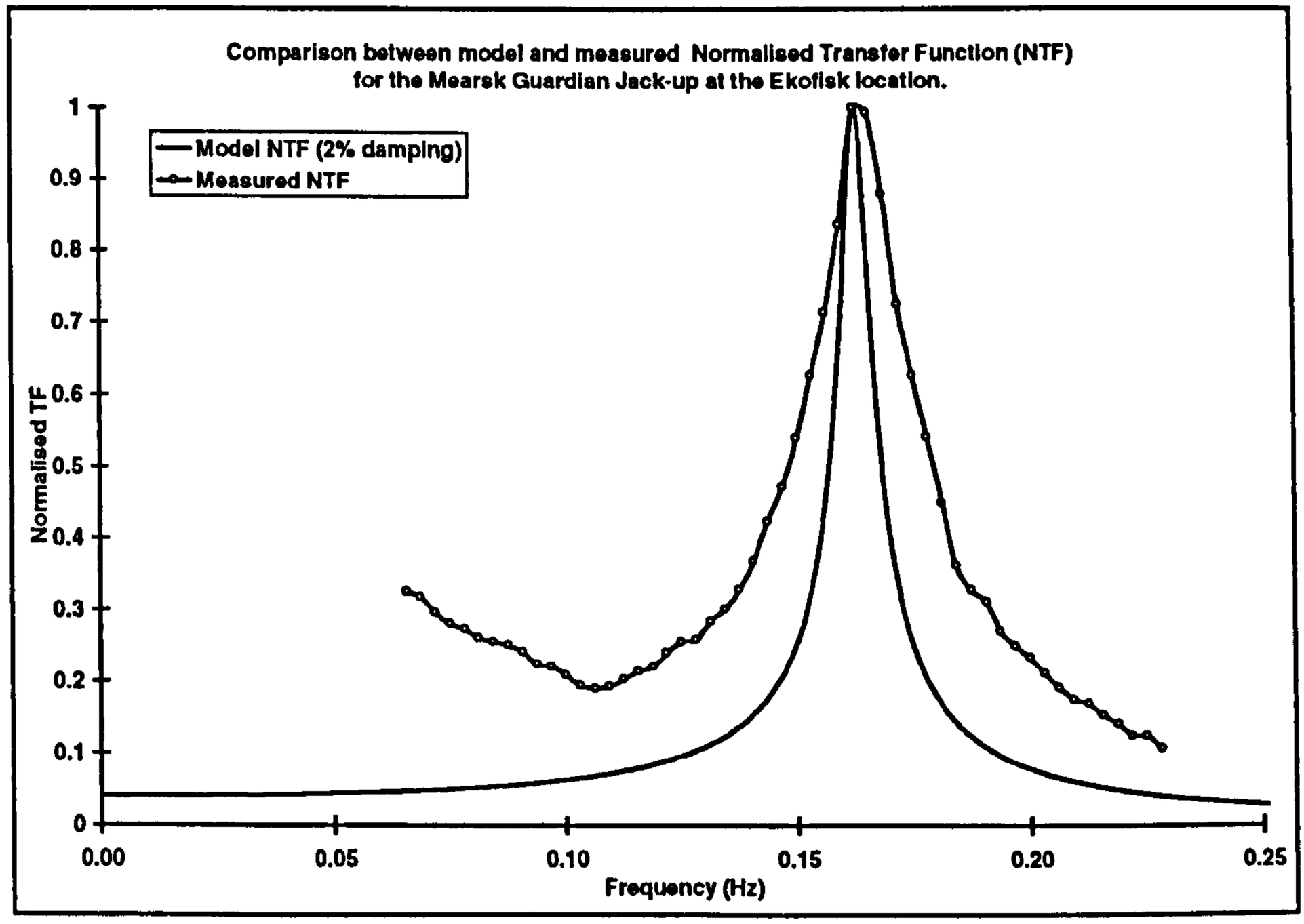

Figure 2.19: Model and measured service NTF for the Ekofisk complex with 2% damping

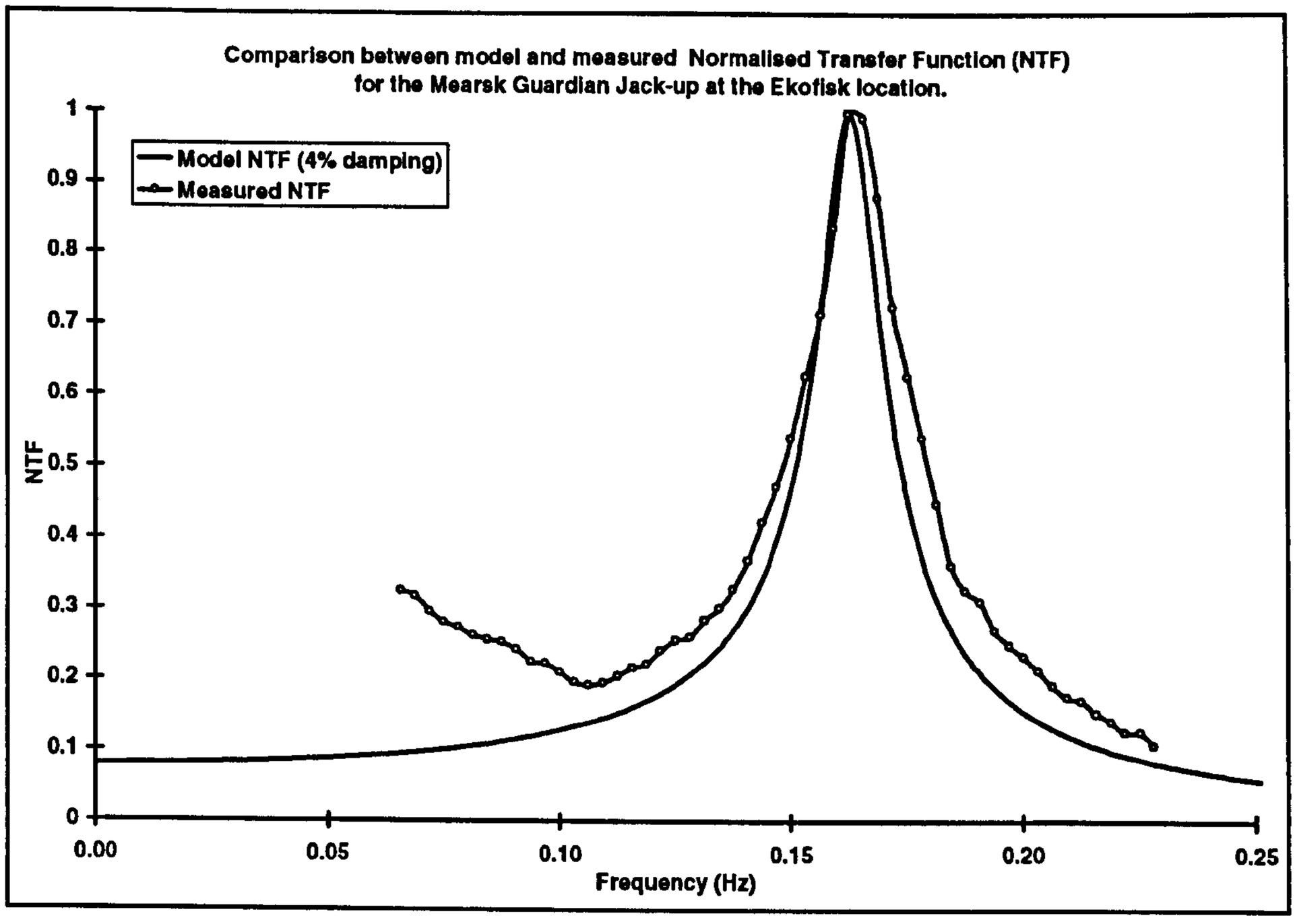

Figure 2.20: Model and measured service NTF for the Ekofisk complex with 4% damping

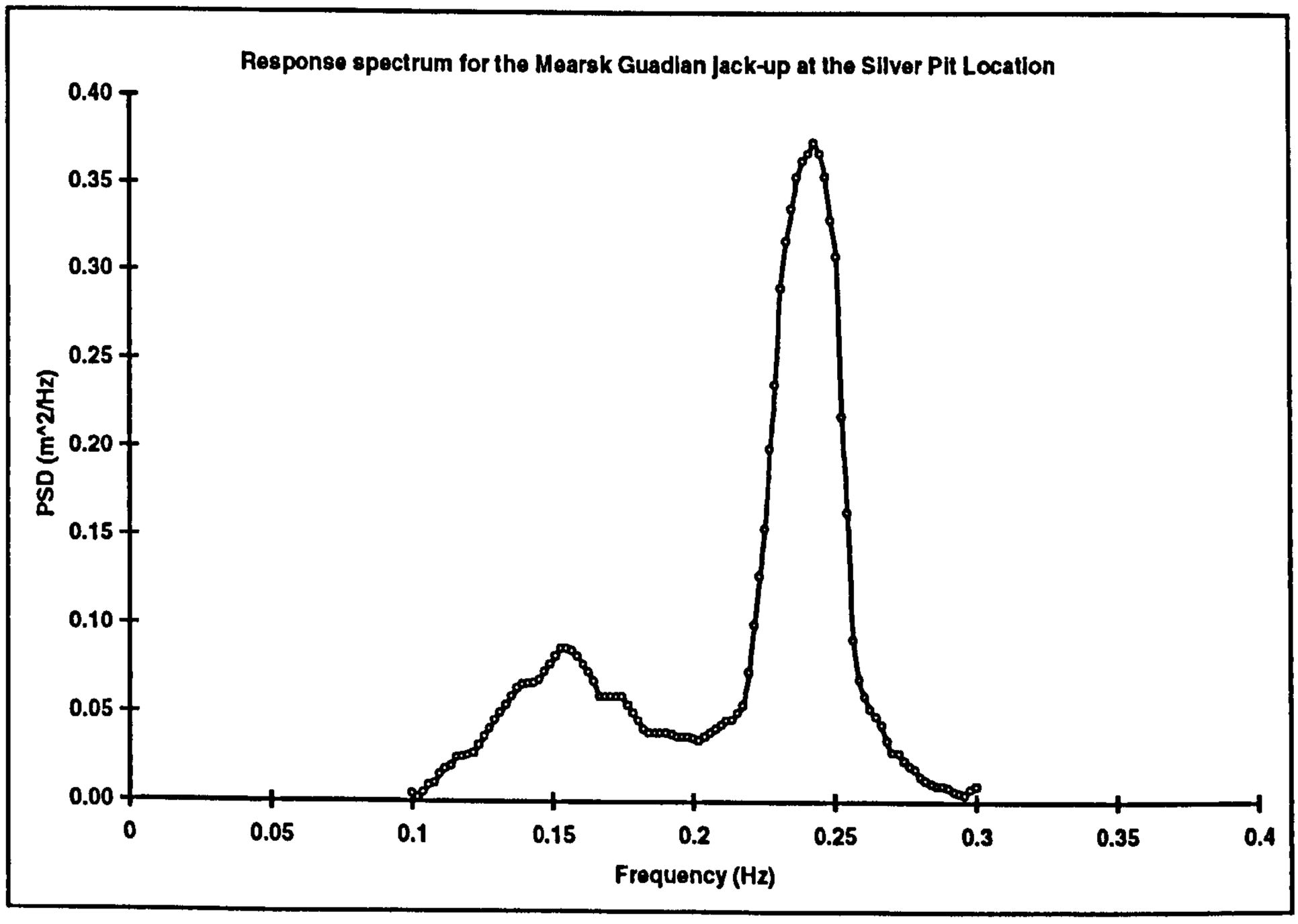

Figure 2.21: Measured service response spectrum at the Silver Pit location

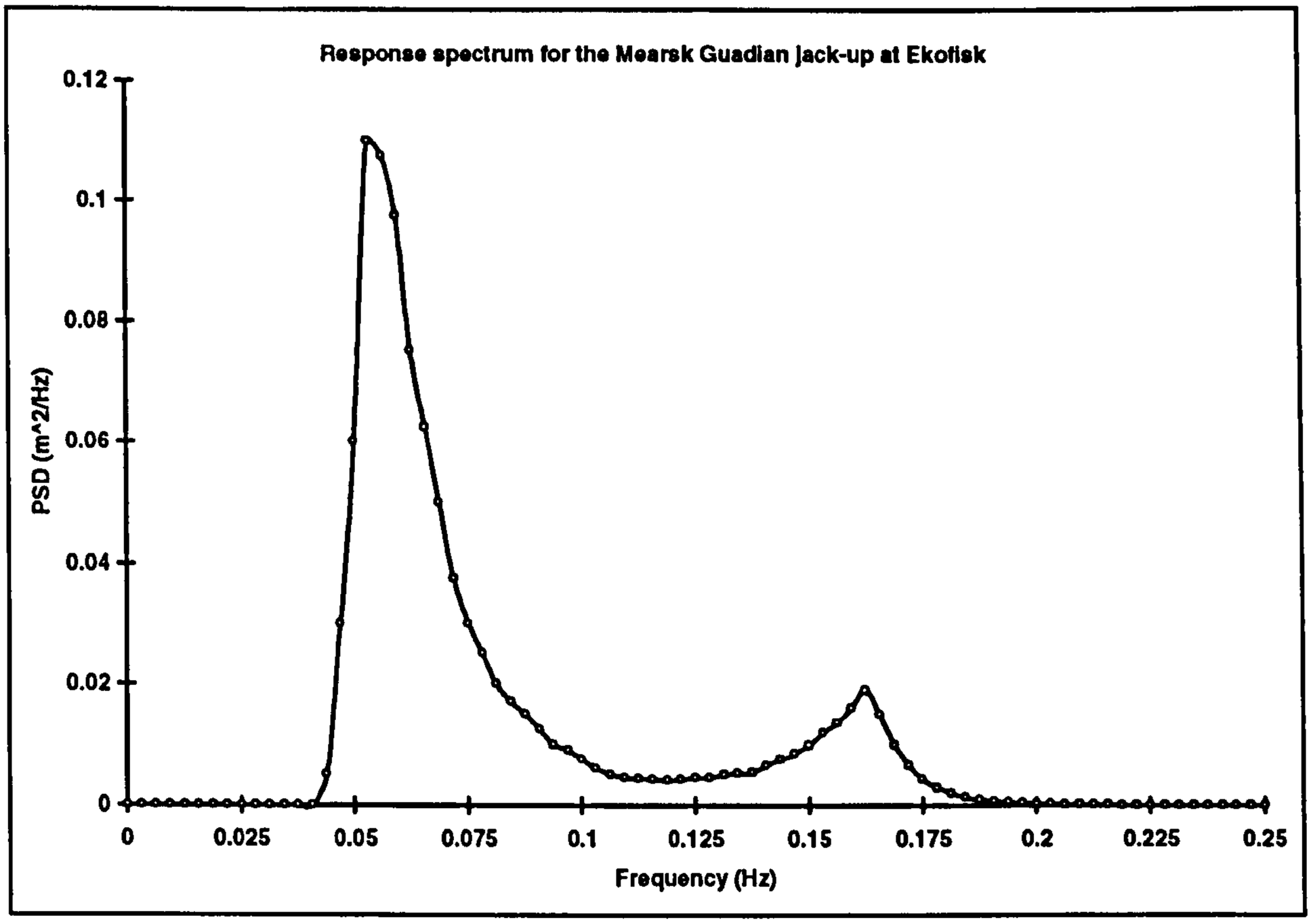

Figure 2.22: Measured service response spectrum at the Ekofisk complex

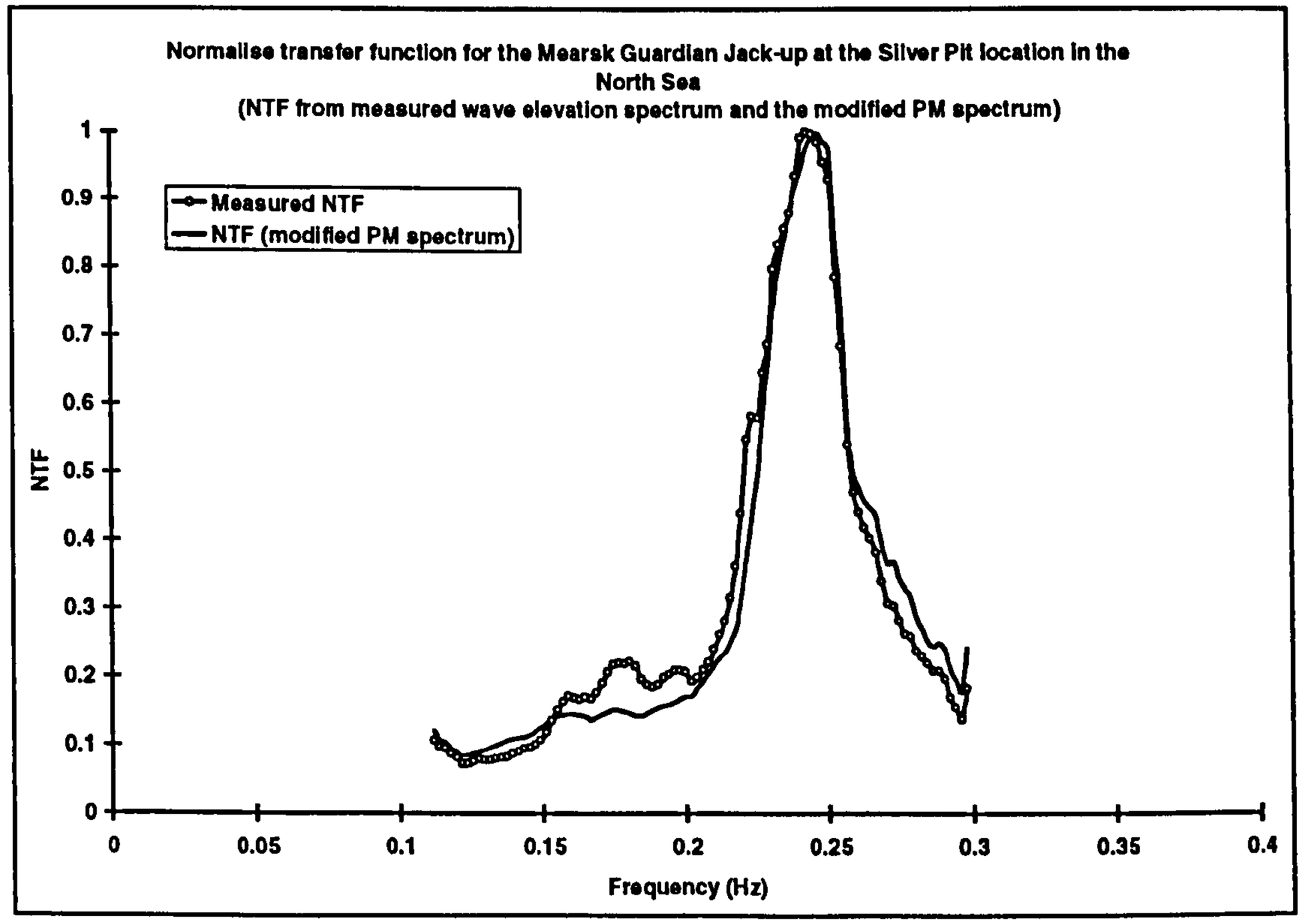

Figure 2.23: NTF for measured and modified PM spectra for Silver Pit

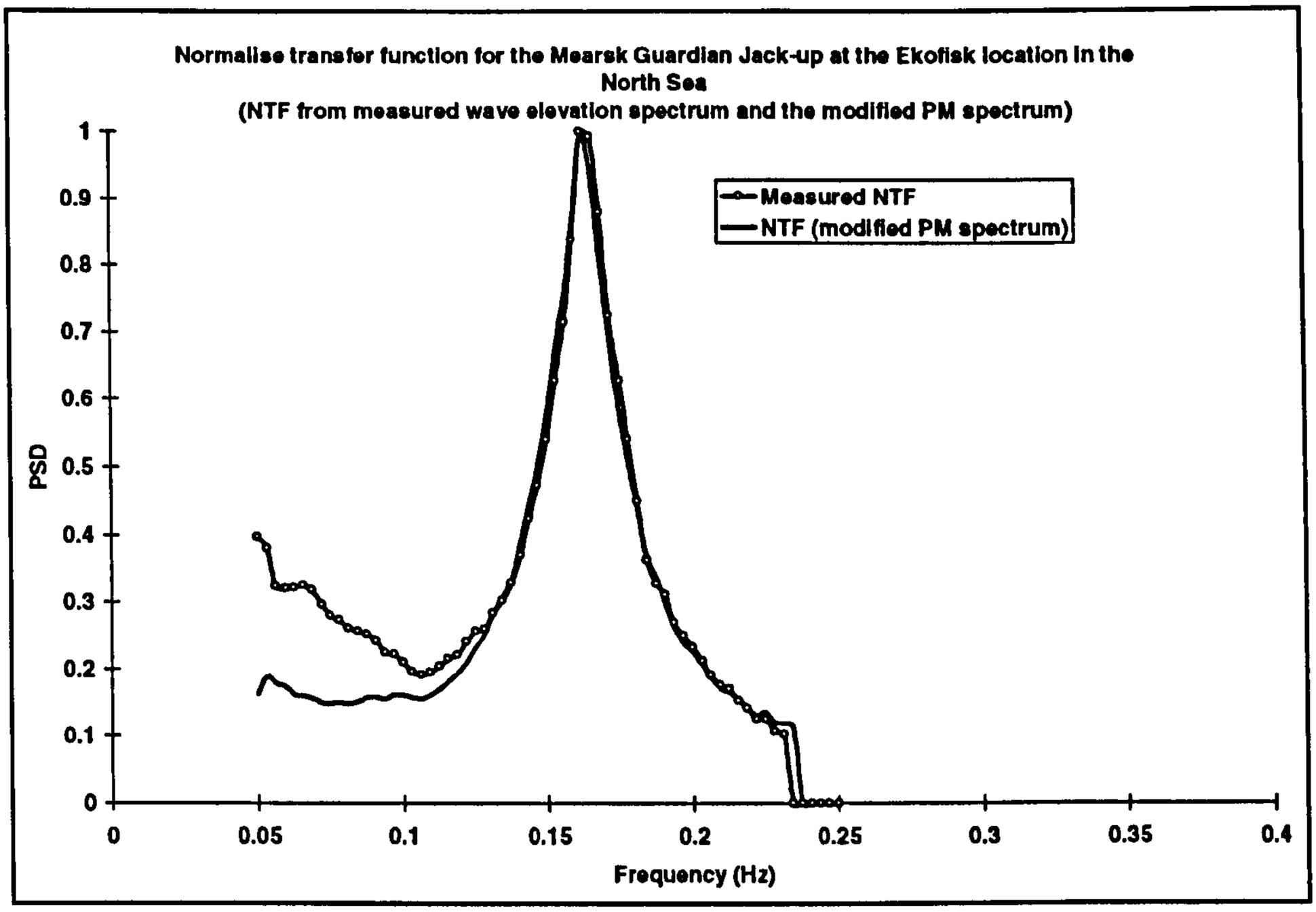

Figure 2.24: NTF for measured and modified PM spectra for Ekofisk complex.

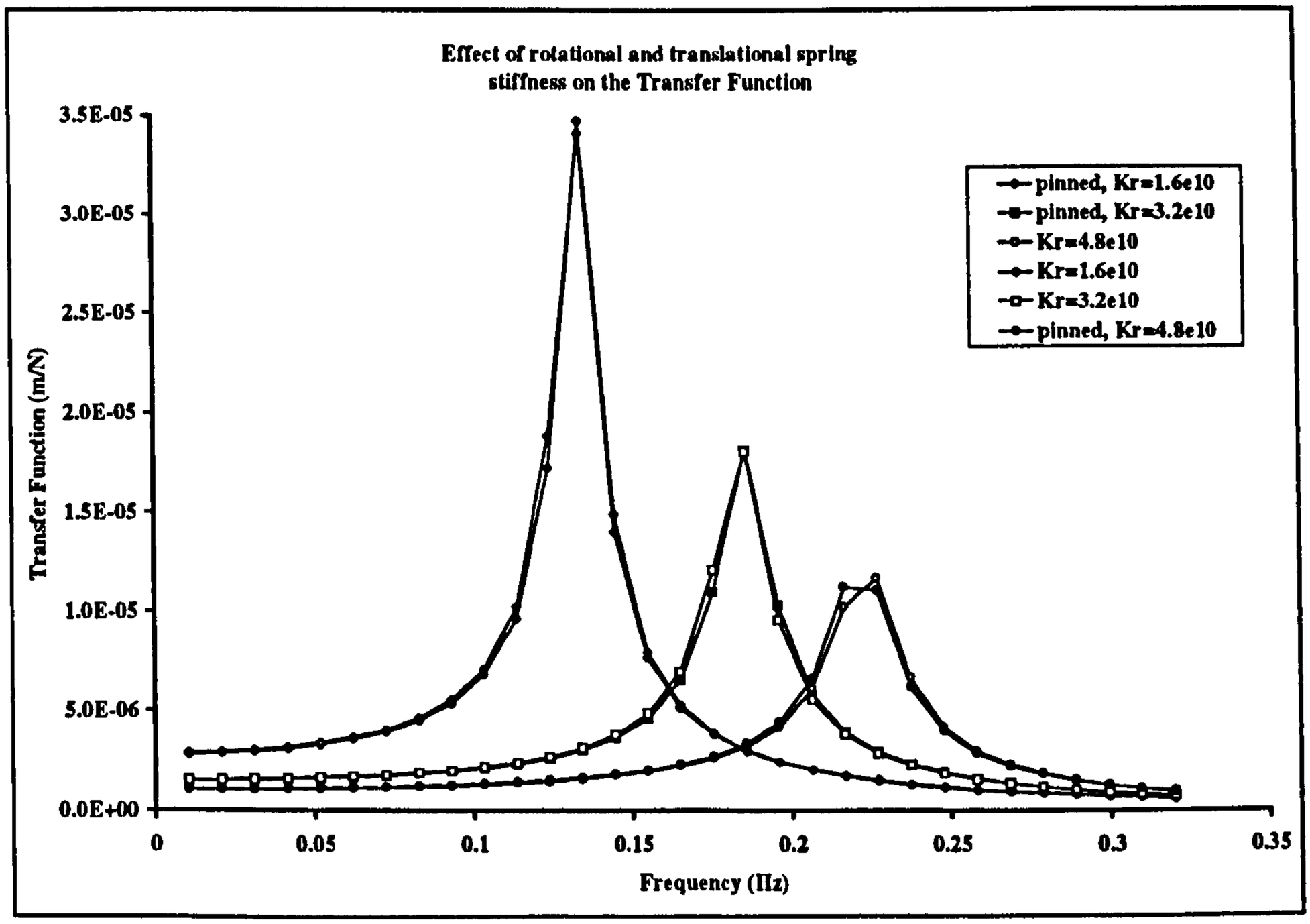

Figure 2.25: Effect rotational and translational stiffness on the transfer function

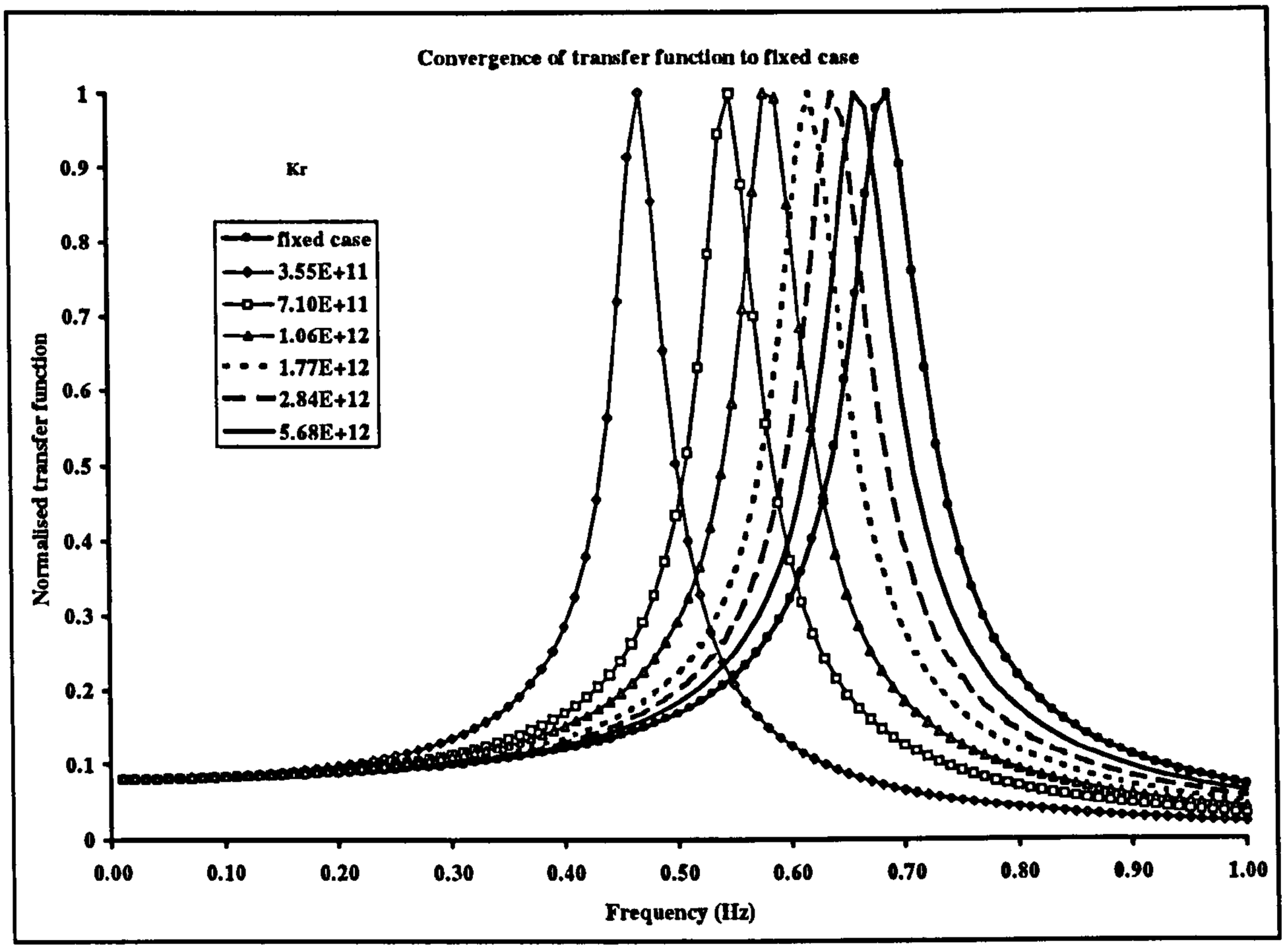

Figure 2.26: Convergence of transfer function to fixed case

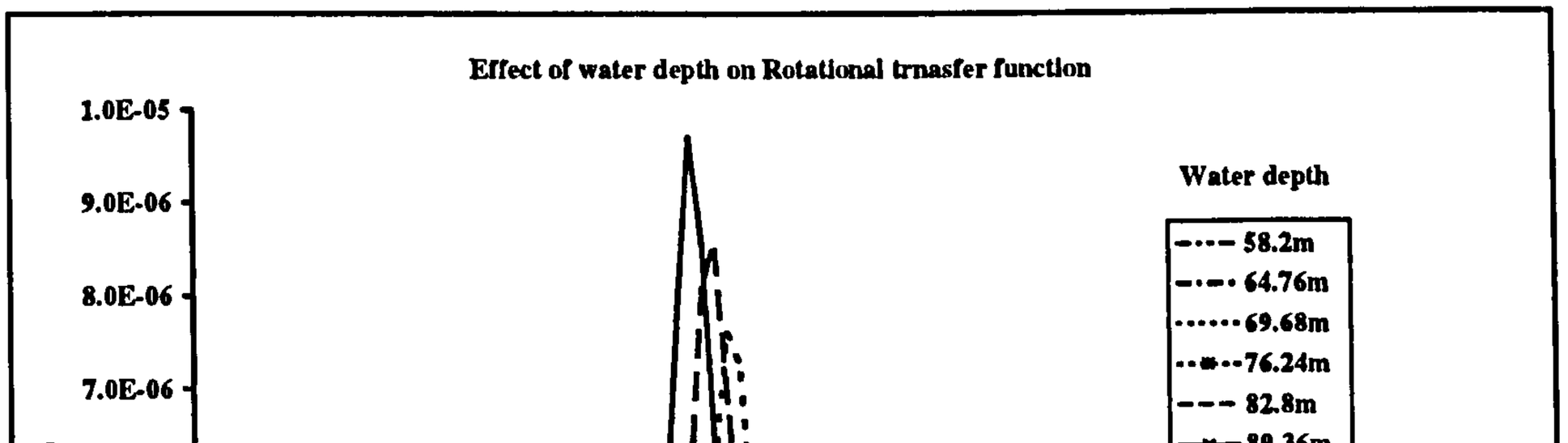

Figure 2.27: Effect of water depth on rotational transfer function

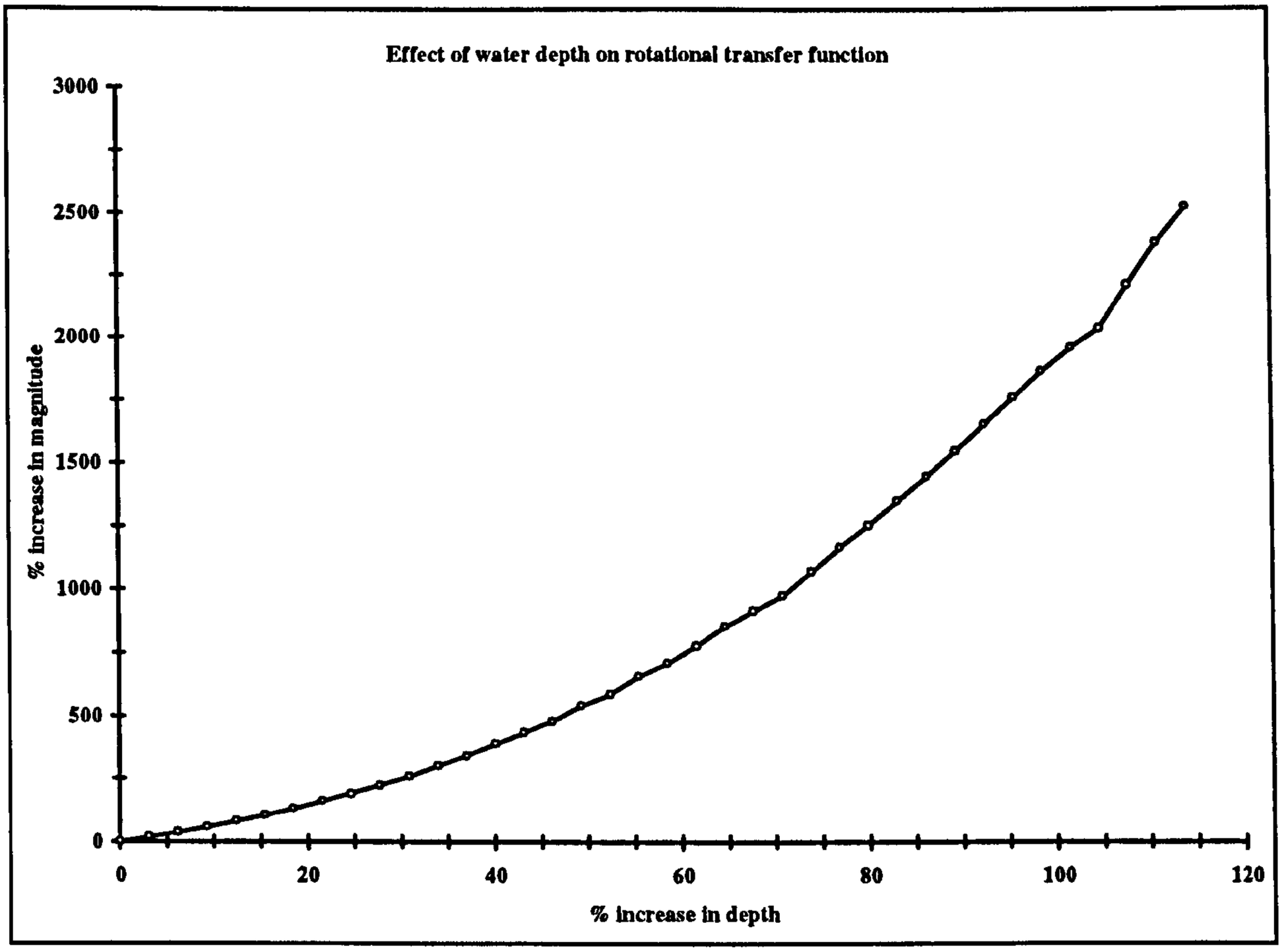

Figure 2.28: Sensitivity of rotational transfer function to water depth

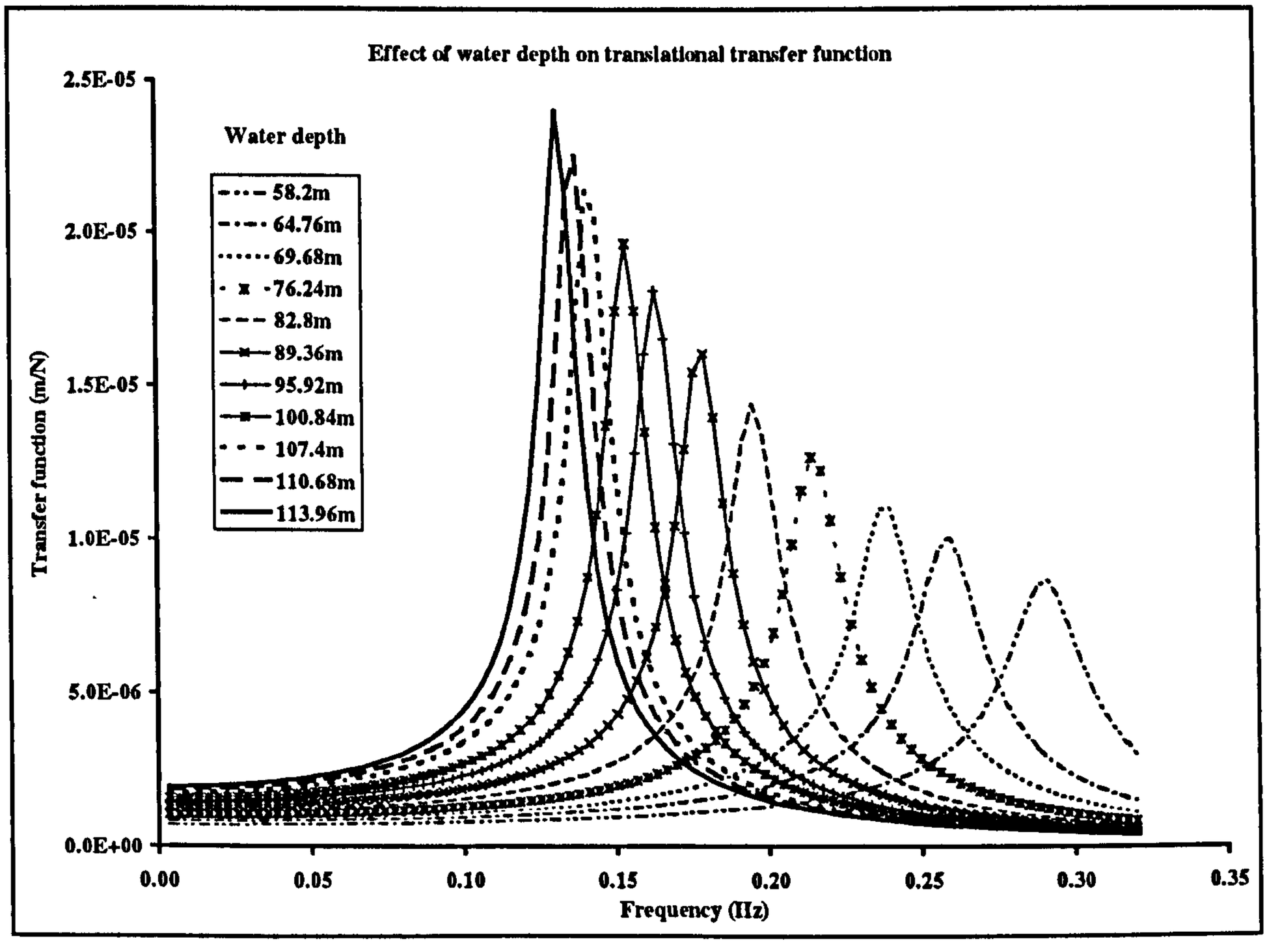

Figure 2.29: Effect of water depth on translational transfer function

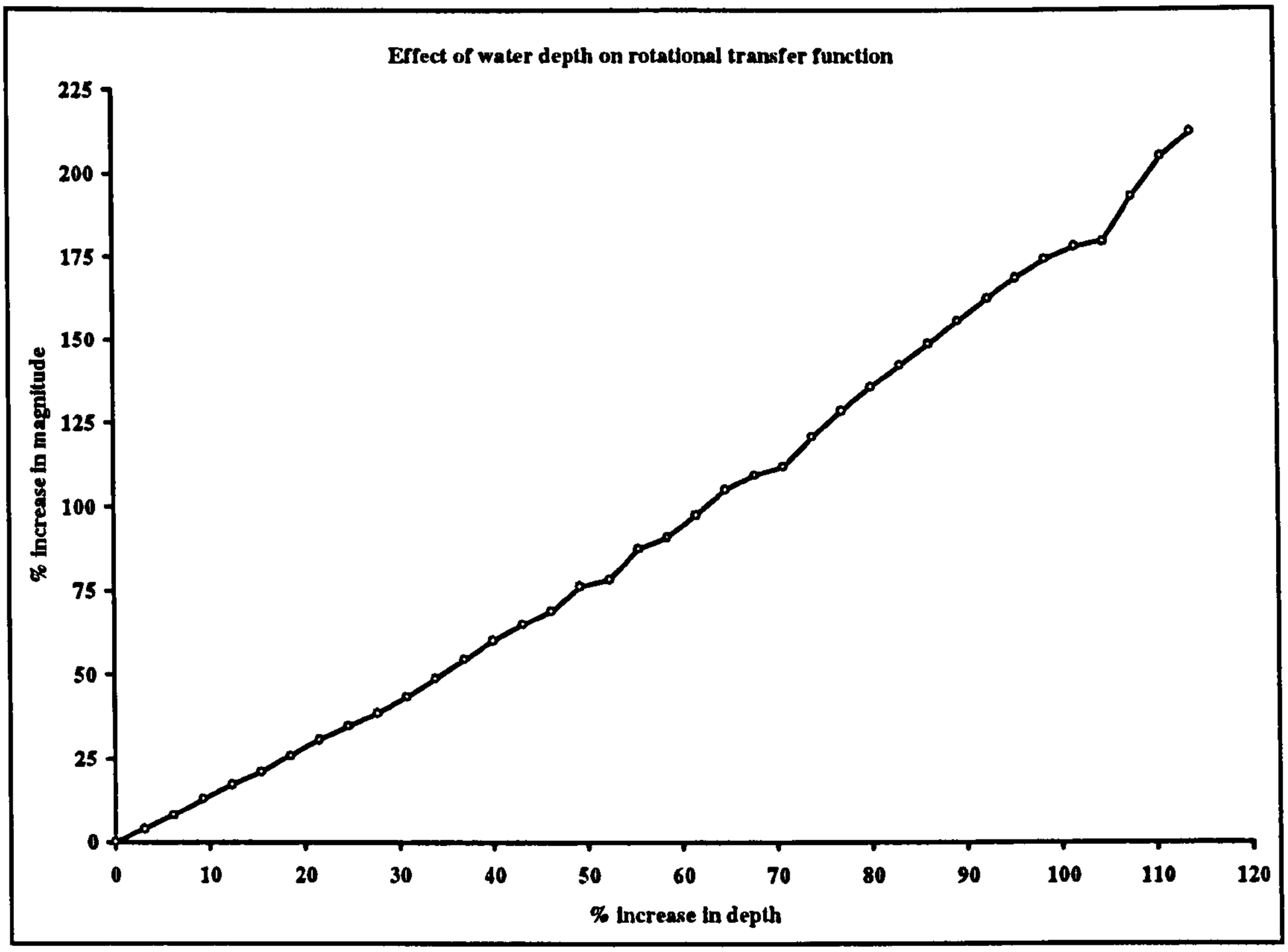

Figure 2.30: Sensitivity of translational transfer function to water depth

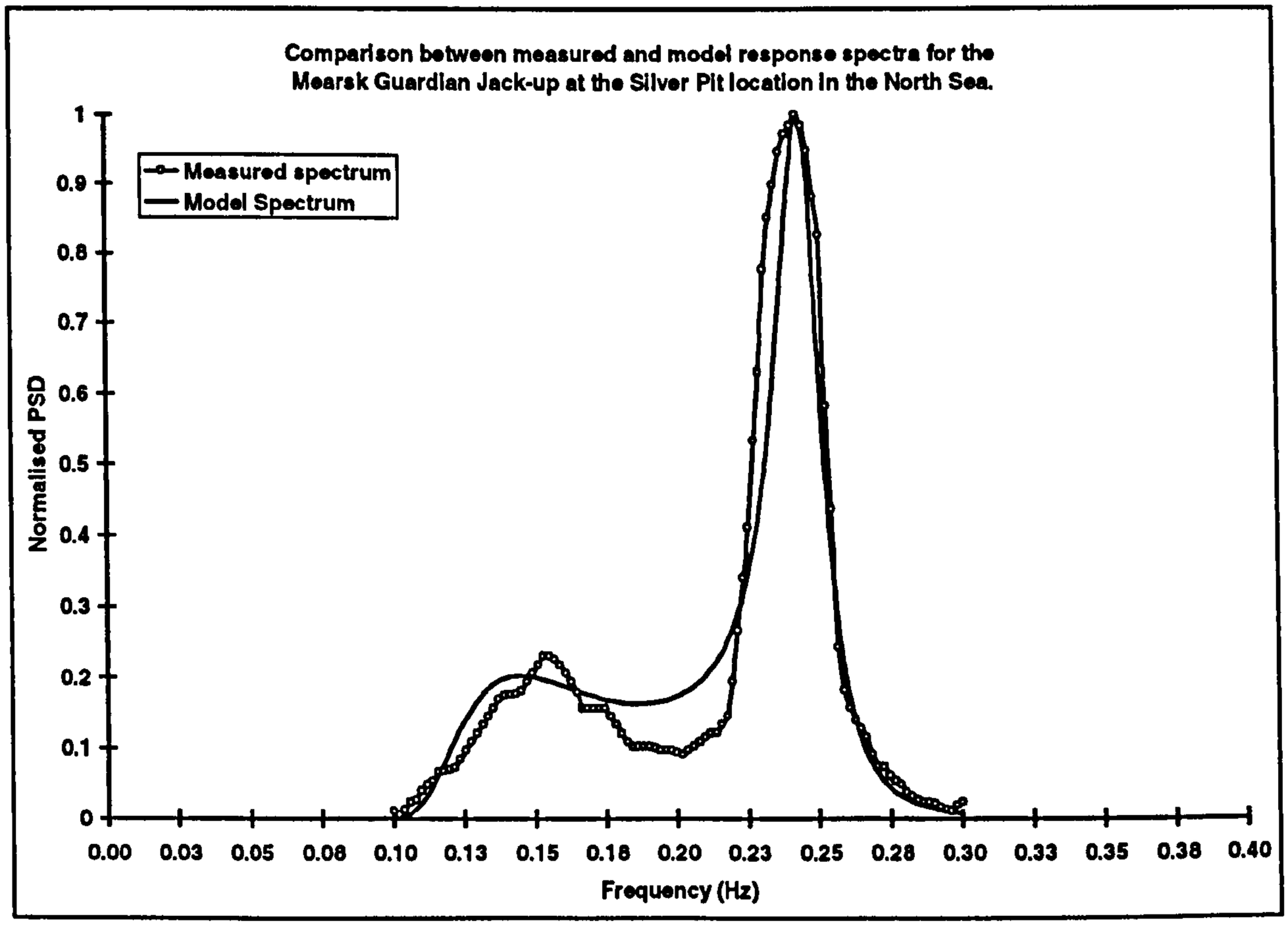

Figure 2.31: Measured and model PSD for the Silver Pit Location

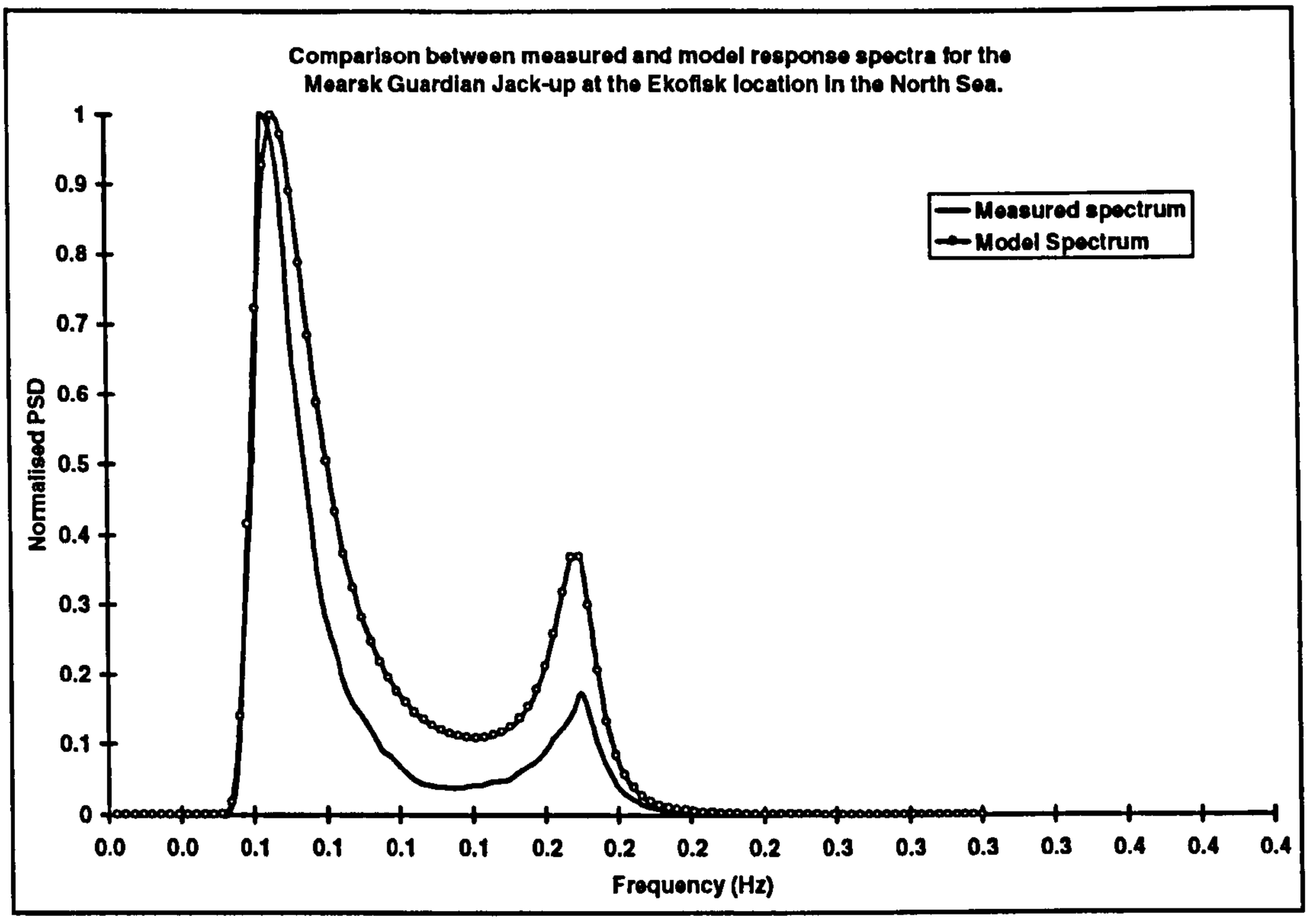

Figure 2.32: Measured and model PSD for the Ekofisk complex

CHAPTER 3

3. LARGE SCALE FATIGUE TESTING OF SE 702

3.1 INTRODUCTION

Fatigue tests on large scale tubular welded joints have been performed for many years to characterise the fatigue behaviour of steels used Offshore. Conducting these tests can be very expensive. The large expense is justified on the grounds that crack growth behaviour in tubular welded joints is complex and can not be reproduced by carrying out fatigue tests on simple welded specimens.

For several years a large number of these tests have been conducted on conventional fixed platform steels such as BS 4360 50D [3.1] and BS 7191 355D [3.2]. However, in recent years, there has been a steady increase in the use of high strength steels in the construction of Offshore structures. They are used in the construction of jack-up lattice structures to increase strength to weight ratio.

The lack of fatigue data on high strength steels under these applications as highlighted in Chapter 1 is an incentive for carrying out this investigation. The main objective of the study was to investigate the fatigue performance of high strength steels used in the construction of Offshore structures under realistic loading and environmental conditions. This was done firstly by developing a simulated service loading history for a typical Jack-up platform operating in the North Sea environment. This aspect of the study was covered in Chapter 2. Secondly the simulated history was used to carry out variable amplitude fatigue tests using large scale welded tubular Y-joints made from a typical high strength steel, SE 702.

The objective of this study was to assess the effect of realistic variable amplitude loading and cathodic protection (CP) on the fatigue crack growth behaviour and subsequent fatigue life of SE 702. This is a typical high strength steel used in the construction of Jack-up rig legs. A total of one air test and three corrosion fatigue tests were carried out under simulated environmental conditions using the simulated Jack-up Offshore Standard load History, JOSH.

This Chapter presents details of the testing programme and the results obtained from the study. The results are presented in the form of initiation behaviour, fatigue crack growth rates and stress life (S-N) data. These results are compared with results from

previous studies [3.3, 3.4, 3.5 3.6 and 3.7] on lower strength steels, those obtained from a parallel study [3.8] on SE 702 and other high strength steels. The parallel study investigated the effect of cathodic protection on the same steel by conducting constant amplitude tests on large scale welded T-joints.

3.2 TEST SPECIMEN CONSIDERATION

Large scale welded Y-joints made from SE 702 were used for this study. This section describes the geometry in detail. The mechanical and chemical properties of SE 702 are also presented.

3.2.1 Properties of SE 702

The steel, SE 702, is a member of the Super Elso (SE) family of steels. It is Creusot Loire Industrie's (CLI) equivalent of the A517GrQ standard. The quoted chemical properties of the material are given in table 3.1. These are compared with independent chemical analysis [3.9] results carried out on a piece of the material cut from one of the Y-joints used during the tests. The independent chemical analysis results are given in table 3.2. As shown from tables 3.1 and 3.2, the chemical properties of the batch of steel from which the joints were made meets the specified standard for each of the alloying elements except for manganese which is higher than the guaranteed maximum. This difference in the percentage of Manganese present in the steel was not thought to be particularly relevant to its fatigue performance since Manganese acts as a de-oxidising agent.

The specified mechanical properties for SE 702 are given in table 3.3. These were also compared with results from tensile tests carried out at Cranfield University [3.10] using specimens made from the same batch of steel used in the fabrication of large scale Y-joint specimens. The results from Cranfield are given in table 3.4. These results compare well with the specified mechanical properties but they generally show that the actual mechanical properties of the steel are better than those specified in

table 3.3. One of the conclusions made from the results obtained at Cranfield University was that SE 702 had a uniform fine grained microstructure with a good combination of mechanical properties. It is of high strength and it was noted that it has good ductility and excellent low temperature toughness. Other measurements were made on the parent metal, weld metal and the heat affected zone obtained from the qualification weld sample. These included hardness measurements and a summary of the results obtained is compared with specified values in table 3.5. Further details of the tests carried out can be obtained from reference [3.10]. Vickers Hardness values for the parent plate were approximately 250HV. This value was considered acceptable for SE 702 and it has been suggested [3.11] that carbon steel with Vickers hardness values in this range should have an ultimate tensile strength in the region of 800MPa. This agrees with the values shown in table 3.4.

3.2.2 Consideration of test specimen geometry

A typical Jack-up leg structure (figure 3.1) is made from steel tubes into a three dimensional space frame. The tubes are normally welded together at the intersections within the structure leading to the formation of tubular welded joints. These joints are usually made from different materials of generally high strength. Each lattice leg is composed of longitudinal chord members which may contain a rack plate for elevating the hull. Generally horizontal and diagonal tubular members are used to connect the chord.

Depending on the overall structural requirements and the degree of structural redundancy employed, a complex combination of joint geometries may therefore result. These geometries will usually be a combination of planar and multi-planar joints as shown in figure 3.2. Due to the practical difficulties involved in testing full scale multi-planar joints in the laboratory, planar joints are more commonly used. However it has been established that the fatigue performance of these joints is governed by the magnitude and the distribution of hot spot stresses around the intersection. This invariably implies that once the fatigue behaviour of simple planar joints under known hot spot stresses is understood and the stress distribution in the

more complex joints known, it is possible to relate them and therefore have a good understanding of the performance of more complex joint geometries.

The joint geometry used for this study is of the Y configuration shown in figure 3.3. A summary of the detailed dimensions of the joint is given in table 3.6. The Y-joint dimensional parameters are also given in table 3.7. The specimen dimensions were chosen to allow direct comparison with earlier tubular joint test programmes performed at UCL using lower strength steels.

3.2.3 Fabrication of SE 702 Specimens

It was important that the welding was representative of that used in the construction of Offshore structures as this is known to have a significant effect on the resulting fatigue life of welded tubular joints. The joints were fabricated by a welding contractor (PAUMECA S. A. of Le Breuil, France) with experience in the fabrication of Offshore structures. PAUMECA has been involved in the construction of Offshore structures such as the BP Harding Jack-up platform.

The chord and brace tubes were made by seam welding two halves of rolled 16mm thick plate. The welding was carried out by using a Gas Metal Arc Welding (GMAW) process with a heat input of less than 2.5kJ/mm. Post weld heat treatment (PWHT) was applied to the seam welds with preheating temperature of 125°C. Figure 3.4 shows the seam weld on the brace and the brace/chord intersection string weld. As shown in figure 3.4, the weld quality was good and no weld toe grinding was employed.

All welds successfully passed a full ultrasonic inspection in accordance with the French standard NFP22-471 [3.12]. The Dime Test was performed on all welds and no weld completely failed the test.

3.3 EXPERIMENTAL SET-UP

This section describes the experimental facilities used in this study. This includes details of test rigs used, fatigue testing software and data acquisition system. Information on the instrumentation used for the control of load and environmental conditions is also presented.

3.3.1 Details of Test Rig

A purpose built reaction frame was available and this was used for the entire test programme. This was designed to allow for out-of-plane bending (OPB) tests on Y-joints. Figure 3.5 shows a typical set-up for an out-of-plane bending test. The load is applied using a 250KN hydraulic actuator as shown in figure 3.5.

3.3.2 Test control and data acquisition

The actuator was controlled with an INSTRON mini-controller via an advanced fatigue testing software, FLAPS [3.13]. All tests conducted were performed under load control. In this mode the specimen is subjected to load cycles of a pre-defined amplitude as contained in the relevant sequence file regardless of any change in stiffness of the specimen.

The FLAPS system is able to generate different types of wave forms and also has the necessary capability to play back any developed realistic load sequence.

It also has the facility for obtaining crack growth data in the course of a fatigue test. Fatigue crack development was monitored by taking Alternating Current Potential Difference (ACPD) [3.14] crack depth measurements at fixed points around the chord brace intersection where the fatigue crack was expected to occur. This technique, details of which are presented in the following section, is an established non destructive inspection (NDI) technique. It has been successfully applied to the non destructive inspection of different welded joints of varying geometry including other

components [3.15]. By choosing suitable inspection intervals it was possible to use this technique to follow crack growth from initiation ,N_1, to through wall penetration, N_3.

ACPD measurements were performed using a U10 Crack Microguage [3.14] together with a 144 channel ACM3 switching unit. Two channels were used for each measurement site, one channel for measuring the crack voltage and the other for measuring the reference voltage. It was therefore possible to monitor crack growth at 72 different sites around the chord brace intersection.

3.3.2.1 The ACPD Method

The alternating current potential difference (ACPD) technique was first developed at UCL [3.16, 3.17, 3.18] for non destructive inspection of welded tubular joints. The technique has been successfully used in monitoring fatigue crack growth in metals [3.15, 3.18] and it has also proved to be a success in the non destructive inspection (NDI) of other components.

When a high frequency alternating current flows through a ferrous material, the current flow is concentrated in a thin skin along the surface of the material [3.16]. This is referred to as the skin effect and the depth of this 'thin skin', which depends on the frequency of the alternating current, f , the permeability, μ , and conductivity of the material, σ , is given as

$$\delta = \left[\mu\sigma\pi f\right]^{-\frac{1}{2}} \tag{3.1}$$

This skin depth is significantly smaller for a high frequency alternating current than typical cracks encountered in engineering structures and this is what the ACPD technique relies on.

As illustrated in figure 3.6, when a surface breaking crack interrupts a uniform AC field, the current flows down one face of the crack and up the other face to join the main stream. Assuming that the potential gradient on the crack faces is the same as

that on the surface of the specimen, the AC potentials, V_r and V_c measured away from the crack and across the crack respectively can be related to the distances over which the measurement is made such that;

$$\left.\begin{aligned} &V_r \propto \Delta \\ &and \\ &V_c \propto (\Delta + 2a) \end{aligned}\right\} \tag{3.2}$$

Where Δ is the distance between the probe terminals and a is the depth of crack to be measured. Rearranging the above equations gives the so called 'one dimensional' crack depth d_1 as;

$$d_1 = a = \frac{\Delta}{2}\left[\frac{V_c}{V_r} - 1\right] \tag{3.3}$$

A specialised crack detection and sizing instrument, crack microgauge [3.14], was developed to apply this principle to the sizing of fatigue cracks.

The one dimensional solution given above was based on an infinitely long crack in an infinite plate. This solution was found to produce some discrepancies in crack depth estimates for semi-elliptical cracks compared with optical measurements obtained through destructive sectioning and required correction for cracks of finite size in specimens of finite dimensions. This problem was investigated and Dover et al [3.18] established that it can be solved as a 2-dimensional Laplacian problem. By using this method together with conformal mapping techniques and other numerical methods such as Fourier series analysis, the 2-dimensional solution was expressed in terms of the 1-dimensional solution and an appropriate modifying factor, M_x such that;

$$d_2 = M_x d_1 \tag{3.4}$$

M_x is a function of $\frac{d_1}{\Delta}$, $\frac{2a}{\Delta}$ and the distance along the crack length on the surface of the specimen from the deepest point, x. The accuracy of this technique in sizing fatigue cracks is well established and it has been successfully used in many applications such as [3.15]. The main advantage of this method over other non

destructive inspection techniques is that it does not require any calibration to give accurate and easily interpretable results. This is the method used to obtain crack growth data in this study.

3.3.3 Simulation of Environmental Conditions

Previous research and understanding of the effect of a corrosive environment on the fatigue performance of structural steels was introduced and reviewed in Chapter 1. Three main categories of $\frac{da}{dN}$ *vs* ΔK behaviour were discussed. These three different categories were noted to be a function of the severity of the corrosive environment and the interaction of cyclic loading. This observed behaviour represents the significance of carrying out fatigue tests in the appropriate environment as misleading results may be obtained if the corrosive environment is not representative of the environment - loading system for which the results are intended. This section reiterates the importance of modelling both the loading and environmental conditions.

The loading is modelled by use of wave power spectra together with the transfer function approach as described in Chapter 2. However if the simulated loading is applied to test specimens in an unrepresentative environment, then misleading results can be obtained. The processes of corrosion fatigue and hydrogen embrittlement of jack-up steels are a complex combination of corrosion and embrittlement chemical reactions. The effects of these chemical reactions, service loading and the influences of any cathodic protection system have to be modelled in the laboratory to obtain representative results.

3.3.3.1 Sea Water Environment

All the corrosion fatigue tests were carried out under simulated environmental conditions. The welded intersection, where the fatigue crack was expected to grow, was immersed in sea water. This was achieved by the use of an environment chamber around the chord / brace intersection. Artificial sea water made to ASTM D1141

[3.19] was circulated from a reservoir through a closed loop passing through the environment chamber. The fully aerated sea water was maintained between temperature limits of 8°C and 10°C using an external refrigeration system. The pH of the sea water was also monitored in the course of each test and maintained between 7.8-8.2.

3.3.3.2 Cathodic Protection System

Cathodic protection (CP) normally used in service to reduce the rate of corrosion to a value that will allow the structure to attain its design life, was applied and maintained at a steady level ($-800mV$ and $-1000mV$) with respect to Ag/AgCl reference electrode for all the corrosion fatigue tests.

Prior to the application of fatigue loading, each joint was subjected to a 'soak time' where the joint was submerged in sea water with the cathodic protection (CP) switched on and maintained at the appropriate level. A soak time of two weeks was implemented to achieve polarisation of the specimen and allow hydrogen to diffuse through the steel.

The length of time required to achieve a uniform through thickness hydrogen concentration is dependant on the diffusion coefficient for the material and the thickness of the specimens used. The two week soak time was used to allow for easy comparison of results from this study with previous studies undertaken at UCL which employed a two week soak time. Another consideration is that the soak time for tubular joints is less critical when compared with that for simple specimen tests. For simple specimens, the fatigue tests may only last a day or two while typical large scale tubular joint tests on the other hand can last for several months. This makes the through thickness hydrogen concentration gradient at the commencement of loading less critical. For this study it is also worth noting that after the two week soak time, the surface of the specimen is still charged with hydrogen for a further period before crack initiation.

The effect of soak time on the fatigue performance of Se 702 was investigated at Cranfield University [3.10] by carrying out tests employing a soak time of 2 and 8 weeks. Although other researchers have noted that there can be significant differences, the study concluded that varying the soak time from 2 to 8 weeks had very little effect on the results obtained for SE 702.. This confirms that results from the UCL large scale tests conducted with a soak time of 2 weeks can be directly compared with those employing a soak time of 8 weeks. This comparison is done in Chapter 4 where fatigue crack growth rate results from Cranfield are compared with those obtained from this study.

3.4 STRESS ANALYSIS OF Y-JOINTS

Extensive stress analysis of the joints used for this study was carried out before each test. Two methods were used in this process. Experimental stress analysis using strain gauges and parametric equations. This section presents the procedure employed and compares the results obtained

3.4.1 Experimental stress analysis procedure

The hot spot stress concentration factor for each joint was measured experimentally using strain gauges. In order to obtain accurate results for the stress concentration factors, 2mm rosette gauges were used for all the tubular joints tested. The gauges were placed around the brace/chord intersection as shown in figure 3.7 in accordance with recommendations of UKOSRP II [3.4] to obtain strains and stresses on the surface of the joint near the intersection.

At each measurement site the gauges were placed 10 and 20mm from the chord weld toe. These distances were determined from figure 3.8 which gives details of the linear regions recommended for positioning strain gauges for T and X joints. The region of linearity was assumed to apply equally well to Y-joints. The measurements from the

two positions at each site were linearly extrapolated to the weld toe to obtain the appropriate hot spot stresses.

Three rosette gauges were also placed on the brace. One close enough to the brace toe to measure the effect of the stress field determined by the combined deformation of the chord/brace intersection. The other two gauges were placed 500mm and 800mm from the brace toe away from the region of rapidly increasing stress influenced by a combination of loading and chord/brace deformation. These two gauges were used to measure the experimental nominal stresses and the extrapolated value to the brace weld toe, of the stresses measured by these gauges was used to obtain the appropriate stress concentration factors.

Using these three gauges, it was possible to measure the variation of stress along the brace with applied load and this was compared with results from simple beam bending type analysis. Three different sets of measurements were taken for each site and average values of stress concentration factors determined.

The effect of load path on the measured stress concentration factors was also investigated. This was considered very important since it was the only way of checking for any stress hysteresis effects. This was also used as a measure of the chord end fixity and to ensure that there was no twisting of the chord within the fixed end castilations. This was carried out by increasing the applied load from 0% to 10%, from 10% back to 0% and up again to 10%. For the first two stages of loading intermediate measurements were made at 6% load. For all three stages of loading the measured stresses were very repeatable as shown in figures 3.9, 3.10, 3.11 and 3.12 for tests LEYOPB1A, LEYOPB2C, LEYOPB3C and LEYOPB4C respectively.

3.4.2 Experimental stress analysis results

A summary of stress concentration factors obtained for the joints is given in table 3.8 where they are compared with values predicted using parametric equations. The experimental measurements were very consistent and an average SCF of 4.47 was

obtained. This value is typical for Y-joints under out-of-plane bending with dimensions shown in figure 3.3.

3.4.3 Use of Parametric Equations

Figure 3.13 shows how the stress concentration factors predicted by the various parametric equations compare with the experimental values obtained for all the Y-joints tested. The Parametric equations of Efthymiou and Durkin, Kuang, Wordsworth and Smedley and the UEG modified versions of Wordsworth and Smedley do not predict the variation of stress concentration factors around the intersection. The Hellier Connolly Dover equation which predicts the variation of stress concentration factors around the intersection for a given chord saddle hot spot stress concentration factor was used in all cases to produce the trends shown in figure 3.13.

For all the parametric equations used, the Hellier Connolly Dover (HCD) equation appears to give the best agreement with the experimental results after considering the scatter shown in Figure 3.14. The HCD equation predicted a hot spot stress concentration factor of 4.54 compared with the measured value of 4.6 for the first joint LEYOPB1A. Efthymiou and Durkin equation and the equations of Wordsworth and Smedley over predicted the hot spot stress concentration by 18% and 9.5% respectively. Even the UEG modified versions of Wordsworth and Smedley equation over predicted the chord SCF by 11.3%. The only equation which under predicted the chord saddle hot spot SCF is Kuang's equation, which gave a value of 3.57, 22.4% less than the measured average value of 4.6.

The stress concentration factors measured on the other three Y-joints varied very slightly from the first. The actual hot spot values obtained were 4.3, 4.6 and 4.4 for LEYOPB2C, LEYOPB3C and LEYOPB4C respectively. The percentage differences of these values from the first are 6.52%, 0% and 4.34% respectively. These results are consistent with a very small scatter.

3.5 EXPERIMENTAL FATIGUE TESTING

Three major variables in the current test programme are the hot spot stress used, the applied levels of cathodic protection (CP) and the type of loading.

The effect of CP on hydrogen embrittlement is particularly relevant to high strength steels. It is thought that CP could have a greater effect on the corrosion fatigue behaviour of SE 702 steel than on lower strength steels such as BS 4360 50D and BS 7191 355D. A review of UK and other design guidance suggests that potentials more negative than $-850mV$ (Ag/AgCl) may be detrimental to steels with strength levels above 700MPa. In a recent study it was highlighted that in some instances, even $-800mV$ may be harmful to steels with strength levels above 800MPa [3.20]. A study on the effect of CP on the fatigue performance of SE 702 has been carried out [3.8] using constant amplitude loading. The results from reference [3.8] are compared with those obtained from this study on the effect of environmental loading under CP conditions later in this Chapter.

3.5.1 Test Parameters and the JOSH Sequence

A summary of the test parameters for the entire test programme undertaken in this study is given in table 3.9. The equivalent stresses indicated on this table were obtained after rainflow cycle counting of the sequence used in each case.

In each case the sequence was simulated [3.21] from 4000 transitions of 12 sea states. Each transition was taken to last for a period of 10 minutes. The sea state PSDs used are shown in figure 3.15. The output turning points for the whole sequence, part of which is shown in figure 3.16, were scaled to ±100%. The sea states used are summarised in table 3.10 and their distribution in JOSH is shown in figures 3.17 and 3.18.

All variants of JOSH are based on the same sea state PSDs. The normalised power spectral density functions, $S(f)_N$ for the JOSH sea states have been demonstrated [3.22] to be given as (chapter 5);

$$S(f)_N = \frac{4H_r^2 T_r^{-4} \Omega^{-5} \xi^2}{\left[(1-\Omega^2)^2 + (2\xi\Omega)^2\right]} Exp\left[\frac{1}{\pi}\left(\left(f_n T_{z_{ext.}}\right)^{-4} - \left(fT_z\right)^{-4}\right)\right] \qquad (3.5)$$

Where f_n is the natural frequency of the structure, ξ is the damping ratio. H_r, T_r and Ω are non dimensional parameters given as;

$$H_r = \frac{H_s}{H_{s_{ext.}}},\ T_r = \frac{T_z}{T_{z_{ext.}}} \text{ and } \Omega = \frac{f}{f_n} \qquad (3.6)$$

The distribution of sea states in the sequence (JOSH1A) used for the air test (LEYOPB1A) is different from that in the sequence (JOSH2C) used for the corrosion tests. This is shown in figure 3.18. The reason for this difference is that some of the non damaging lower sea states were removed. For this sequence the first two sea states (sea states 1 and 2) were clipped to increase the effective equivalent stress of the sequence and to ensure that the maximum stress did not exceed the yield strength of the material.

Figure 3.19 shows the distribution of stress ranges for both JOSH1A and JOSH2C together with the stress range distribution in part of the JOSH2C sequence used in the first corrosion test (LEYOPB2C). These distributions are normalised with respect the total number of rainflow stress ranges in each sequence in figure 3.20 and with respect to the most probable occurring stress range in figure 3.21. Further details of the sequence are also shown in table 3.11.

As highlighted in Chapter 1, large scale fatigue testing is a necessary requirement for the research into the fatigue behaviour of Offshore structural steels. They are necessary to increase the general understanding of variable amplitude fatigue performance of Jack-up steels and also to provide justification for the environmental reduction factors proposed by a few design codes which offer the available limited guidance on the design of tubular welded joints used under variable amplitude loading conditions. The limited guidance available on the effects of variable amplitude loading stem from the fact that there is limited experimental data available and this is the primary justification for carrying out these rather expensive large scale tests.

Most of the analysis presented in Chapter 2 was carried out to ensure that a representative loading history or sequence is produced. This section presents the details of the large scale fatigue tests carried out using the developed Jack-up Offshore Standard load History, JOSH.

The frequency content of sea state PSDs was reproduced in the generated sequence as shown by the out put from a spectrum analyser in figure 3.22. The air test however was carried out at an average higher frequency (5 times the frequency represented by the sea state PSDs) while the corrosion fatigue tests were run with the frequency content represented in the JOSH sequence.

3.6 FATIGUE TEST RESULTS

The results of the fatigue tests are presented here. Fracture mechanics analysis of results is presented in Chapter 4. In Chapter 4, the experimental Y factors and crack growth rates obtained are presented and compared with predictions using existing fracture mechanics models. In this section the results are presented in the form of initiation data, crack shape evolution curves, crack growth curves, crack aspect ratio evolution and the fatigue life of each specimen presented in S-N format. These results are compared with those obtained from tests conducted on lower strength steels and other high strength steels.

3.6.1 Fatigue Crack Initiation

Inspection of the ACPD data collected during the early portion of each test has shown the ACPD technique to be capable of detecting crack growth increments of less than 0.1mm. This detection capability is important when it comes to determining the point of initiation of each defect.

The definition of initiation, N_i was taken as the attainment of a 0.1mm deep fatigue crack. Early crack growth data from the four tests conducted for this study are shown

in figures 3.23 to 3.26. Figure 3.23 shows results obtained from the air test, LEYOPB1A. From this figure it can be seen that the initiation life for the air test is about 620500 cycles which corresponds to the first data point collected after the attainment of a crack 0.1mm deep. The corresponding results obtained for the corrosion tests (LEYOPB2C, LEYOPB3C and LEYOPB4C) are shown in figures 3.24, 3.25 and 3.26 respectively. It was possible to monitor the progress of a fatigue crack from initiation and as it propagated through the specimen. The initiation lives were determined graphically from plots such as those shown in figures 3.23 to 3.26. The initiation data obtained for the Y-joints is summarised in table 3.12. These results were compared with those obtained from constant amplitude tests [3.8] conducted on T-joints made from SE 702 and shown in table 3.13.

The initiation to total life ratio, N_I/N_3,, was used to measure the importance of the initiation period to the overall fatigue life. Welded tubular joints generally exhibit short initiation and long propagation lives. Austin [3.6] carried out a series of variable amplitude tests on BS 4360 50D steel using the WASH sequence. The trend noted from his study was for lower N_I/N_3 ratios for higher equivalent stress levels. This effect is not so clear from the results obtained from this study. The total number of data points is limited even when the results from the T-joint tests are included. There is further difficulty involved with comparing the T-joint results directly as the type of loading is different. This makes it difficult to draw firm conclusions on any existing trends in terms of initiation to total life ratio.

The results from Y-joints are compared with those obtained from constant amplitude tests reported in [3.8] (table 3.13) for the same steel, SE 702, in terms of initiation to total life ratio. The values for Y-joints under variable amplitude loading are lower than those for T-joints. The only discrepancy is from LEYOPB1A as shown in figure 3.27. The main reason for the difference in initiation to total life ratios (figure 3.27) is the presence of very damaging stress ranges from severe sea states which are present in the JOSH sequence. This is further supported by results from T5 when compared with LEYOPB1A carried out at the same hot spot stress range. It is also apparent that the CP level has an effect on the initiation to total life ratio for both joint types. This is shown in figure 3.28. Figure 3.28 shows that the tests carried out at a CP level

of $-1000mV$ have a higher initiation to total life ratio in both cases when compared with those carried out at the CP level of $-800mV$.

3.6.2 Crack shape evolution Curves

ACPD crack depths measured around the chord/brace intersection were collected for each test. This information was used to monitor crack shape evolution in the welded joints. The early crack shape evolution curves obtained for the four tests are shown in figures 3.29, 3.30, 3.31 and 3.32. The results shown in these figures are for tests LEYOPB1A, LEYOPB2C, LEYOPB3C and LEYOPB4C respectively. The crack shape evolution curves obtained on completion of the tests are also shown in figures 3.33, 3.34, 3.35 and 3.36 for the respective tests. The ACPD crack depth for the deepest point along the crack length was used to obtain experimental crack growth data for each test.

3.6.3 Crack Growth Curves

The crack growth curves for all the tests are shown in figures 3.37 to 3.40. The results obtained for the air test (LEYOPB1A) are shown in figure 3.37 while the results from the corrosion tests are presented in figures 3.38, 3.39 and 3.40 for tests LEYOPB2C, LEYOPB3C and LEYOPB4C respectively. All the crack growth curves are compared in figure 3.41. The curves shown in figure 3.41 show that fatigue crack growth under variable amplitude loading conditions is not steady and this was anticipated since the variable amplitude load sequence used to conduct the tests (JOSH) consisted of multiple sea states with varying degrees of severity. The sequence used in each case had significant variability in amplitude and frequency content. A 'stair case' type crack growth curve was consistently obtained for each of the tests as shown in figure 3.41. In each case regions of accelerated growth were found to coincide with the 'storm' in the load sequence which resulted in high stress intensity factor ranges.

The corrosive environment used for the sea water tests also plays an important role in the fatigue crack growth process. This influences the mechanism by which cracks propagate and can lead to irregular behaviour. This is highlighted by the difference in the crack growth curves when variable amplitude tests are compared with those obtained from constant amplitude loading conditions in sea water with cathodic protection. The crack growth curves obtained under constant amplitude conditions for the tests reported in [3.8] are shown in figure 3.42. It can be seen from figure 3.42 that fatigue crack behaviour in a corrosive environment (with CP) is somewhat more complex when compared with air tests. The main difference is the existence of distinct regions where the crack growth curves take on different linear slopes for the corrosion tests. This behaviour was also found in a more pronounced manner and following a distinctive pattern which could be linked to significant fatigue damage related events in the sequence for the variable amplitude tests.

3.6.4 Crack aspect ratio evolution

The surface crack length was measured at similar intervals to crack depth measurements for each of the four tests conducted. This was done by using crack shape evolution data presented in section 3.6.2. By using this information it was possible to determine the evolution of crack aspect ratio. The results obtained are shown in figures 3.43, 3.44, 3.45 and 3.46 for LEYOPB1A, LEYOPB2C, LEYOPB3C and LEYOPB4C respectively. The results from all the tests are compared in figure 3.47. This figure shows that the results from the air test are more regular when compared with those obtained from the corrosion tests. These results are discussed further in Chapter 5 where they are used to develop a new Y factor model which can be used in the analysis of fatigue crack growth in Offshore structures.

3.6.5 S-N Data

The end of each test was defined as the attainment of a through wall fatigue crack. The experimental fatigue life (N_3) of each specimen is given in table 3.14. The stress range indicated is the sequence equivalent stress range derived from rainflow counted fatigue cycles. The fatigue lives predicted by the T Design Curve for Air and Sea Water environments together with the mean of the 16mm 50D joint data used during the formulation of the fatigue design guidance are also included in table 3.14 for comparison.

The results obtained for the study on the Y-joints are compared with those obtained from T-joints in figure 3.48. These results are later compared with the design S-N curves for air and Sea Water with CP conditions and the mean line for 16mm thick specimens made from BS 4360 50D. The fatigue performance of SE 702 is further compared in section 3.8 with other medium and high strength steels tested both in air and sea water.

3.7 MATERIAL EXAMINATION

A materials investigation was performed in parallel with this programme at Cranfield University. The role of Cranfield University was to examine and metallurgically characterise the welded quenched and tempered properties of SE 702, used in the large scale fatigue testing programme. Paris law type tests on SE 702 in air and in sea water under different cathodic protection potentials were also conducted. This part of the study also included a metallographic investigation of fracture surfaces from the tubular joints used in the study presented in this thesis.

The investigation has been reported separately [3.10]. The main findings from the microscopic examination of the steel showed that SE 702 has a uniform fine grained microstructure with a good combination of mechanical properties suitable for use in Jack-up structures. It was also observed that SE 702 parent plate metal showed

superior fatigue performance characteristics when compared with conventional BS 4360 50D carbon manganese steels and other high strength steels used Offshore.

A study on the effect of cathodic protection on fatigue crack growth rates in SE 702 was also carried out. Standard three point bend (SENB) specimens were used and it was observed that higher cathodic protection potentials enhance fatigue crack growth rates in SE 702. Typically results from Cranfield showed that fatigue crack growth rates were increased by a factor of 3 when the CP level was increased from $-830mV$ to $-1080mV$ (Ag/AgCl). The results were compared with other high strength steels and it was noted that SE 702 shows similar behaviour with similar high strength steels but that its performance is generally superior to that of BS 4360 50D type steels.

It was also concluded from the investigation that varying the soak time from 2 to 8 weeks had very little effect on the results obtained. This confirms that results from the UCL large scale tests conducted with a soak time of 2 weeks can be directly compared with those employing a soak time of 8 weeks. This comparison is done in Chapter 4 where fatigue crack growth rates in the large scale specimens are compared with those from compact tension tests conducted at Cranfield university.

3.8 DISCUSSION OF RESULTS

The results obtained from this study are compared with design S-N curves for air and sea water under adequate cathodic protection conditions. These curves are shown in figure 3.49. The mean line for data obtained from previous test programmes on lower strength steels such as BS 4360 50D is also shown in figure 3.49 for easy comparison of the fatigue performance of high strength steels with conventional fixed platform steels.

On superimposing the results from SE 702 on to the design curves shown in 3.49, It can be seen from figure 3.50 that the SE 702 data points all lie above the air design curve. One interesting observation can be made on comparing Y-joint results with those obtained using T-joints made from the same steel. This comparison is shown in figure 3.50. In figure 3.50, it can be seen that all the Y-joint data lie to the right of T-

joint data. This indicates that Y-joints under out-of-plane bending may exhibit a nominally better fatigue resistance than T-joints under axial loading. It is difficult to draw any conclusions from this observation as the T-joints were tested under constant amplitude while the Y-joints were tested under variable amplitude loading conditions. However, axially loaded T-joints are known to exhibit a more severe response to fatigue loading when compared with Y-joints under out-of-plane bending. This observation was also made by Vinas-Pich [3.5] and is reflected by the existing database for tests under different modes of loading as shown in figure 3.51.

The SE 702 results are also compared with those of Austin [3.6] and Vinas-Pich [3.5] obtained on tubular welded joints made from BS4360 50D steel. Both of these test programmes were conducted using variable amplitude loading under corrosion conditions with CP. The geometry of the test specimens used by Austin was nominally identical to the SE 702 T-joint test specimens reported in [3.8] while those of Vinas-Pich were of the same geometry as the Y-joints used for this study. Both Austin and Vinas-Pich used the WASH sequence. This comparison is shown in figure 3.52. As seen from figure 4.52, SE 702 shows a tendency to lie at the upper end of the scatter band. The lower strength steel data points all lie below the air design curve whilst the SE 702 data points all lie above this line. This is increasingly so for the tests conducted at lower stresses. The data suggest that high strength steel joints may have longer fatigue lives at lower stress levels but there is insufficient data to identify a clear trend.

The effect of cathodic protection on the fatigue performance of SE 702 is shown in figure 3.53 where the air tests are compared with those carried out in simulated sea water with CP. The fatigue performance of SE 702 was observed to be influenced by the level of CP applied. Increasing the CP level form $-800mV$ to $-1000mV$ resulted in a shorter life at a given stress level for both the T and Y-joints. For the constant amplitude loaded T-joints at 225MPa for example, the life at $-1000mV$ corresponded to approximately 70% of the life at $-800mV$ (see table 3.13). A similar ratio of 73% was obtained from the variable amplitude Y-joint tests conducted at an equivalent hot spot stress range of 200MPa (see table 3.14). This reduction factor on life observed for the large scale tubular joint tests is however less severe

when compared with a reduction factor of 3 in crack growth rate for the fatigue crack growth specimens (SENB) tested at Cranfield University [3.10]. The results from Cranfield showed that fatigue crack growth rates were increased by up to a factor of 3 when the CP level was increased from $-830mV$ to $-1080mV$ (Ag/AgCl). SE 702 tubular joint results are compared with results from a database of cathodically protected joints in figure 3.53. Again the results lie well within the existing scatter and showing a general tendency of better fatigue performance when compared directly with lower strength steels of similar joint geometry.

There is a limited amount of S-N data for welded joints manufactured from higher strength Offshore steels relative to medium strength structural steels and none appear to be directly relevant to the joint geometries frequently used in the fabrication of jack-up platforms. Data for welded plates with yield strengths up to 540 MPa are reported in [3.23]. Tests were performed on T-butt joints in sea water with cathodic protection and under free corrosion. The results indicate that the performance of these joints is comparable to that of conventional structural steels.

Data from tests conducted on high strength steel tubular joints in air with chord thicknesses of 5 mm to 78 mm have been thickness corrected to 16 mm using a thickness exponent of 0.3 [3.24]. These results are compared with SE 702 data together with the T' design curve in figure 3.54. It can be seen from Figure 3.54 that some points fall below the T' design line. Data for tubular DT joints manufactured from Le Tourneau MM X85 high strength steel with a nominal yield strength of 590 MPa [3.25] were generated in a study funded by the Health and Safety Executive. These results are also included in Figure 3.54 and are seen to lie above the T' curve.

A very small number of tests have been performed on high strength steel tubular joints in sea water. The HSE study included a programme of constant amplitude corrosion fatigue tests [3.25]. Four specimens were tested, giving a total of eight results. Two welding methods representative of actual fabrication methods were used, namely flux cored arc welding (FCAW), entailing weave welding, and shielded metal arc welding (SMAW), yielding string welds. The tests were conducted in air and in synthetic sea water at a cathodic protection level of $-1000mV$ Ag/AgCl under out-of-plane bending at an R-ratio of 0.05. The sea water temperature was maintained between

8°C and 10°C. These conditions are similar to those used for the work presented in this thesis as a soak time of two weeks was equally employed prior to testing. The mode of cracking in the in-air SMAW specimens differed from that observed in tubular joints of conventional structural steel in that the cracks propagated in a plane that was approximately parallel to the chord surface, rather than perpendicular to it. This behaviour was attributed to the presence of manganese sulphide inclusions in the parent material [3.7]. These results are compared with SE 702 data in figure 3.55. The data has been thickness corrected to 16mm using a thickness exponent of 0.3, as recommended in [3.26]. The graph shows that some of the data points lie above the S-N curves. Some of the tests were conducted under free corrosion conditions and it can be seen from figure 3.55 that their performance is not necessarily poorer than that of cathodically protected joints. However, the joints were manufactured from materials with different strengths and direct comparisons are difficult, particularly since the number of data points is low.

The characteristic 'stair case' type crack growth curves obtained for the Y-joint tests (figure 3.41) suggest that crack growth under variable amplitude conditions is not uniform. This observation may make it more difficult to predict fatigue crack growth in Offshore structures where multi sea state type loading prevails. A sea state based [3.27] fracture mechanics approach has therefore been proposed. This approach is presented in detail in Chapter 5.

3.9 SUMMARY

This Chapter has presented details of variable amplitude fatigue tests conducted on full scale tubular welded Y-joints fabricated from a 700 MPa yield strength steel, SE 702. SE 702 is a typical high strength steel used in the construction of Jack-Up rig legs. A total of one air test and three corrosion fatigue tests with cathodic protection were carried out under simulated environmental conditions using the simulated Jack-up Offshore Standard load History, JOSH.

The objective of this study was to assess the effect of realistic variable amplitude loading and cathodic protection (CP) on the fatigue crack growth behaviour and subsequent fatigue life of high strength steels.

Details of the material used have been presented. The results obtained from the investigation have been presented in the form of initiation data, crack shape evolution curves, crack growth curves, crack aspect ratio evolution and S-N data. These results have been compared with results from previous studies and those obtained from a parallel study on SE 702. The parallel study investigated the effect of cathodic protection on the same steel under constant amplitude loading conditions. The following conclusions can be drawn from this study.

3.10 CONCLUSIONS

The fatigue life results from the current investigation suggest that tubular joints fabricated from SE 702 are at least as good as conventional fixed platform steels. They have the potential for better performance and may offer the benefit of longer fatigue lives at lower stress levels. However the limited number of tests conducted in the course of this study make it difficult to draw firm conclusions on any existing trends in the fatigue behaviour of high strength steels.

It is also possible that, increasing the cathodic protection level from $-800mV$ to $-1000mV$ may lead to a shorter fatigue life. For hot spot stress levels of around 200-225MPa a factor on life of around 30% was observed for tests conducted using variable amplitude loading and this was consistent with results obtained from a separate investigation on the same steel under constant amplitude loading conditions. However there was no evidence to suggest that SE 702 is any more susceptible to hydrogen embrittlement than other high strength steels of similar grade.

On the whole the results from this investigation are encouraging. There are potential benefits to be gained by using high strength steels in the fabrication of Offshore structures and especially Jack-up platforms used for production. The minimum number of tests conducted show that SE 702 may be used under these applications

without necessarily increasing the risk of fatigue failure due to hydrogen induced stress corrosion cracking and embrittlement since the results show that high strength steels are no worse than conventional fixed platform steels such as BS 4360 50D. No evidence has been found to support the abolition of a change in slope for multi-sea state loading as was found for lower strength steels. However further tests at lower stress levels will have to be performed to confirm this. It is recommended that further tubular joint fatigue tests be carried out on this and other high strength steels to quantify the potential benefits and identify clearly any existing trends in their performance.

3.11 REFERENCES

[3.1] BS 4360: 1990, *Weldable Structural Steels,* British Standards Institution, London 1990.

[3.2] BS 7191: 1989, *Weldable Structural Steels for fixed Offshore Structures,* British Standards Institution, London 1989.

[3.3] *United Kingdom Offshore steels Research Project-Phase I: Final Report,* Ed. Peckover R, Health and Safety Executive Report OTH 88 282, Her Majesty's Stationary Office, London 1988.

[3.4] *United Kingdom Offshore steels Research Project-Phase II: Final Summary Report*, Ed. Peckover R, Health and Safety Executive Report OTH 87 265, Her Majesty's Stationary Office, London 1987.

[3.5] Vinas-Pich J, *Influence of environment loading and steel composition on fatigue of tubular connections*, Ph.D. thesis, Department of Mechanical Engineering, University College London, January 1994.

[3.6] Austin J A, *The Role of Corrosion Fatigue crack growth Mechanisms in Predicting Fatigue life of Offshore Tubular Joints.*, Ph.D. Thesis, Department of Mechanical Engineering, University College London, October 1994.

[3.7] Smith A T, *The Effects of Cathodic Over-protection on the Corrosion Fatigue Behaviour of API 5L X85 Grade Welded Tubular Joints*, Ph.D. Thesis, City University, London 1995.

[3.8] Myers P, *Corrosion Fatigue Fracture Mechanics of High Strength Jack Up Steels*, Ph.D. Thesis submitted to London University, Feb. 1998

[3.9] Stanger Science & Environment, Acrewood Way, St. Albans, Herts. AL4 0JY. *"Chemical Composition of Steel Sample ED3639453"*, 5 November 1997.

[3.10] Billingham J, Spurrier J, Healy J and Kilgallon P, "*Corrosion Fatigue Fracture Mechanics of Jack-up steels*", Project Report, University of Cranfield, 1998.

[3.11] Baron, G. "*Super Elso SE702*", Creusot Loire Industrie, February 1989

[3.12] Norme Francais, NFP22-471, *"Assemblages Soudés. Étendues des controles non destructifs."*1986

[3.13] Technical Software Consultants Ltd., "*FLAPS PLUS USER GUIDE* ", Manual No. M5873R Issue F, 1991.

[3.14] Technical Software Consultants Ltd, "*ACFM Crack Microguage - Model U10 User Manual*", April 1991, Milton Keynes

[3.15] Michael D H, Collins R and Dover W D, "*Detection and Measurement of Cracks in Threaded Bolts with an AC Potential Difference Method*", Proc. Roy. Soc. London, A385, pp145-168, 1983

[3.16] Dover W D, Collins R, "*Recent Advances in the Detection and Sizing of Cracks Using Alternating Current Field Measurements (ACFM)*", British Int. Jnl. Of NDT, November 1980, pp291-295.

[3.17] Collins R, Dover W D, Michael D H, "*The use of AC Field Measurements for Non Destructive Testing*", Research Technique in NDT Vol. 8, edited by R S Sharpe, Academic Press 1985.

[3.18] Dover W D, Charlesworth F D W, Taylor K A, Collins R and Michael D H, "*The Use of AC Field Measurement to Determine the shape and size of a crack in a metal*", Eddy Current Characterisation of Materials and Structures, Edited by Birnbaun G and Free G, American society of Testing Materials Publications, STP 722, pp401-427, 1982.

[3.19] American Society for Testing and Materials, *"Specification for Substitute Ocean Water."*, ASTM D 1141-75, 1980.

[3.20] Laws, P.A., *Corrosion Fatigue Performance of Welded High Strength Low Alloy Steels for Use Offshore*, PhD Thesis, Cranfield University,1993.

[3.21] Etube L S, Brennan F P and Dover W D, "*Service Load simulation for Fatigue Testing of Jack-up steels*", *Recent Advances in Corrosion Fatigue*, Sheffield, April 1997.

[3.22] Etube L S, Brennan F P and Dover W D, "*Modelling of Jack-up response for fatigue testing of weldable high strength Jack-up steels under simulated service conditions*", Sixth International Conference on the Jack-up Platform, City University, September 1997.

[3.23] The Welding Institute, *Update on Survey on Corrosion Fatigue Tests*, Health and Safety Executive Report OTH 92 392, Her Majesty's Stationary Office, London.

[3.24] Stacey A, Sharp J V and King R N, "*High Strength Steels used in Offshore Installations*", Proceedings of the Fifth International Conference on Offshore Mechanics and Arctic Engineering, American Society of Mechanical Engineers, Vol. III, New York, 1996.

[3.25] Smith A T and Dover W D, "*Corrosion Fatigue of API 5L X85 Grade Welded Tubular Joints with Applied Cathodic Protection of* $-1000mV$ ", Draft Final Report, 20th June 1994 Revised 11th November 1994.

[3.26] Background to new fatigue design guidance for steel joints and connections in Offshore structures, 1990.

[3.27] Etube L S, Brennan F P and Dover W D, "*Prediction of Fatigue Crack Growth in Offshore Structures Using a Sea State Equivalent Stress Concept*", International Society of Offshore and Polar Engineering Conference, Montreal, Canada, May 1998.

3.12 TABLES AND FIGURES

Table 3.1: Quoted chemical composition of SE 702

Element	Specified
C	≤ 0.14
Mn	≤ 0.9
Si	≤ 0.3
S	≤ 0.004
P	≤ 0.01
Ni	≤ 1.5
Cr	≤ 0.7
Mo	≤ 0.55
B	≤ 0.003
V	≤ 0.05
Cu	-
Sn	-
Al	-
Ti	-
Co	-
Nb	-
As	-
Pb	-

Table 3.2: Independent chemical analysis results for SE 702

Element	CLI Analysis	UCL Analysis
C	0.125	0.12
Mn	1.1	1.05
Si	0.256	0.25
S	<0.0005	<0.001
P	0.007	0.009
Ni	1.404	1.34
Cr	0.467	0.51
Mo	0.474	0.48
B	0.0012	
V	0.008	0.02
Cu	0.185	0.19
Sn	0.003	
Al	0.069	0.08
Ti	0.003	<0.01
Co	0.011	0.01
Nb	0.004	<0.01
As	0.007	
Pb	0.003	

Table 3.3: Quoted mechanical properties of SE 702

Material	σy (MPa)	UTS (MPa)	Elongation (%)
SE702	700 min	790 / 940	16

Table 3.4: Measured mechanical properties of SE 702

Specimen No.	σy (MPa)	UTS (MPa)	Reduction in Area (%)	Elongation (%)	Yield Ratio (σy/UTS)
1	755	823	66	21	0.92
2	744	813	61	20	0.91
3	744	807	65	20	0.92
4	750	816	64	20	0.92
5	750	815	64	20	0.92
Average	748	815	63	20	0.92

Table 3.5: Hardness data for SE 702

		Weld Metal		CGHAZ		Parent
	Specimen	CAP	ROOT	CAP	ROOT	plate
Average	1	305	249	392	311	253
	2	305	253	389	300	260
Range	1	276 - 336	245 - 251	373 - 409	262 - 363	242 - 268
	2	260 - 336	247 - 258	363 - 401	272 - 345	243 - 274
Sample Size	1	10	4	8	10	11
	2	10	4	9	10	11

Table 3.6: Detailed dimensions of Y-joint

	Length(mm)	**Diameter(mm)**	**Thickness(mm)**
Chord	2480	457	16
Brace	1390	324	16
Brace angle = 35 degrees			

Table 3.7: Y-joint dimensional parameters

Parameter	Definition	Value
Alpha, α	2L/D	10.85
Beta, β	d/D	0.71
Gamma, γ	D/2T	14.28
Tau, τ	t/T	1.0
Theta, θ	degrees	35

Table 3.8: Summary of measured Y-joint SCFs

Method	Predicted SCF	Test ID/Percentage difference in measured and predicted SCF			
		LEYOPB1A (Y1)	LEYOPB2C (Y2)	LEYOPB3C (Y3)	LEYOPB4C (Y4)
HCD	4.53	-2.20	5.07	-1.54	2.86
Mod. W&S	5.12	9.57	16.01	10.16	14.06
W&S	5.04	8.13	14.68	8.73	12.70
E&D	5.43	14.73	20.81	15.29	18.97
Kuang	3.57	-29.69	-20.45	-28.85	-23.25
Measured		**4.63**	**4.3**	**4.6**	**4.4**

Table 3.9: Summary of fatigue test parameters

Test	Test ID	Equivalent stress range (MPa)	CP (mV)	Type of environment
Y1	LEYOPB1A	180	Air	Air
Y2	LEYOPB2C	260	-800mV	Sea water
Y3	LEYOPB3C	200	-800mV	Sea water
Y4	LEYOPB4C	200	-1000mV	Sea water

Table 3.10: Summary sea states used in JOSH

sea state number	significant wave height (m)	mean zero crossing period (s)
1	1.25	5.5
2	1.75	5.9
3	2.25	6.2
4	2.75	6.5
5	3.25	6.8
6	3.75	7.1
7	4.25	7.4
8	4.75	7.7
9	5.25	7.9
10	6.25	8.4
11	7.25	8.9
12	8.00	9.2

Table 3.11: Summary of parameters of JOSH

Parameter	JOSH1A	JOSH2C		
	LEYOP1A	LEYOP2C	LEYOP3C	LEYOP4C
Sea states used	3-12	1-12	1-12	1-12
Maximum stress (MPa)	701.48	975.38	783.42	783.42
Minimum stress (MPa)	21.23	21.12	20.53	20.53
RMS (based on rain flow ranges) (MPa)	81.62	111.75	89.34	89.34
Clipping ratio	8.59	8.73	8.76	8.76
Equivalent stress range (MPa)	180.29	250.0	200.0	200.0
Total number of cycles(Rain flow)	280744	532025	532025	532025

Table 3.12: Summary of initiation data for Y-joints

Test No.	Conditions	N_1	N_3	N_1/N_3
Y1	180MPa (Air test	620,500	2,130,000	0.291
Y2	260MPa (-800mV)	10,000	380,000	0.026
Y3	200MPa (-800mV)	50,000	1,545,000	0.032
Y4	200MPa (-1000mV)	180,000	1,140,000	0.158

Table 3.13: Summary of initiation and S-N data for T-joints [3.8]]

Test No.	Conditions	N_1	N_3	N_1/N_3
T1	400MPa (Air)	13,000	74,000	0.176
T2	300MPa (Air)	24,000	180,000	0.133
T3	225MPa (-1000mV)	115,000	194,000	0.292
T4	225MPa (-800mV)	105,000	548,000	0.192
T5	180MPa (-1000mV)	Run Out	-	-
T5(retest)	300MPa (-1000mV)	-	130,000	-
T6	300MPa (-800mV)	<10,000	138,000	<0.072

Table 3.14: Summary of S-N data

Test	Stress (MPa)	Environment	Experimental N_3	50D Mean N_{3p}	Reduction Factor N_{3p}/N_3
Y1	180	Air	2,130,000	1.500.000	0.67
Y2	250	CP=-800mV	380,000	560,000	1.47
Y3	200	CP=-800mV	1,545,000	1,090,000	0.71
Y4	200	CP=-1000mV	1,140,000	1,090,000	0.96

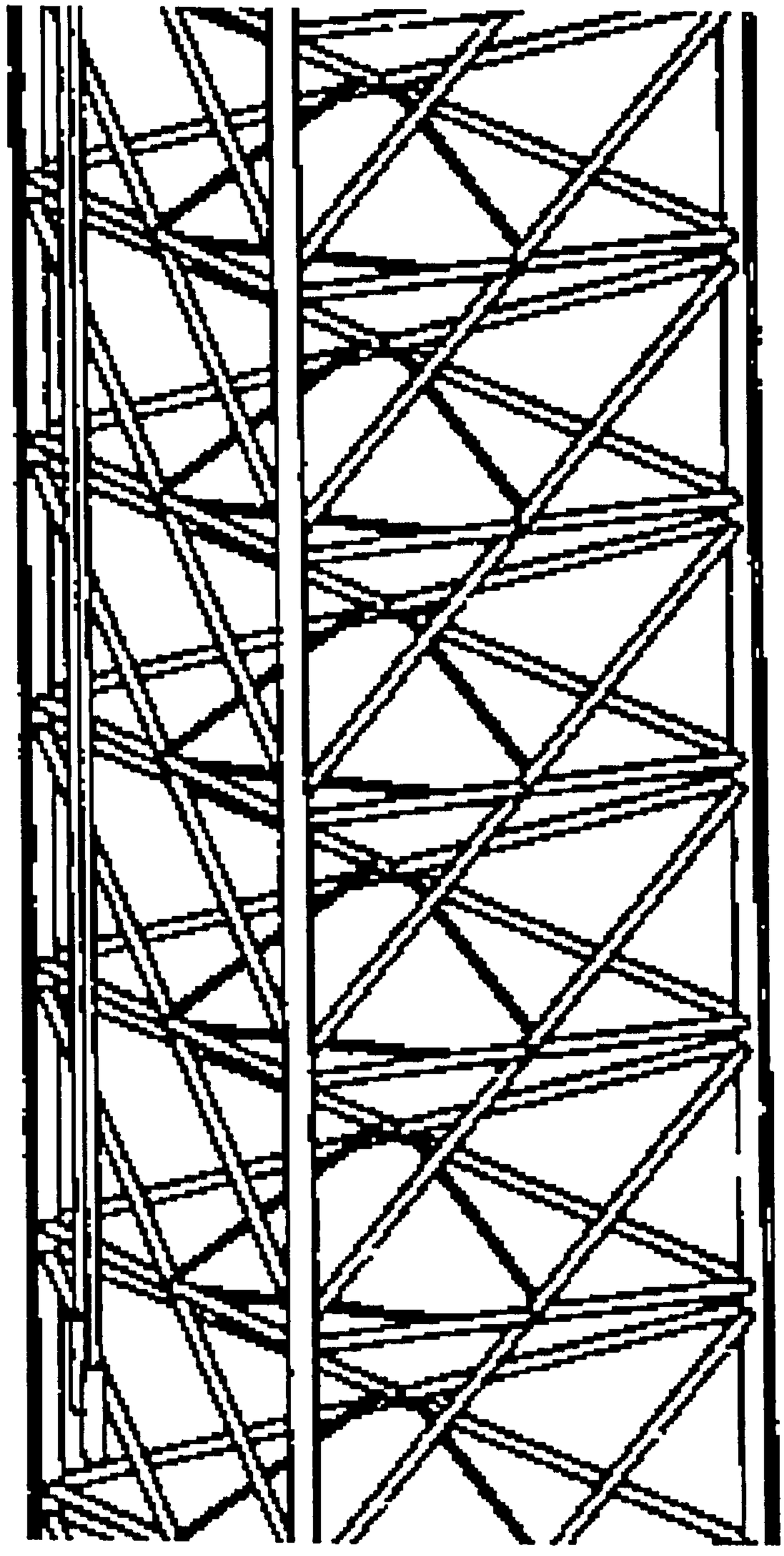

Figure 3.1: Part of a typical Jack-up leg showing interconnecting tubulars

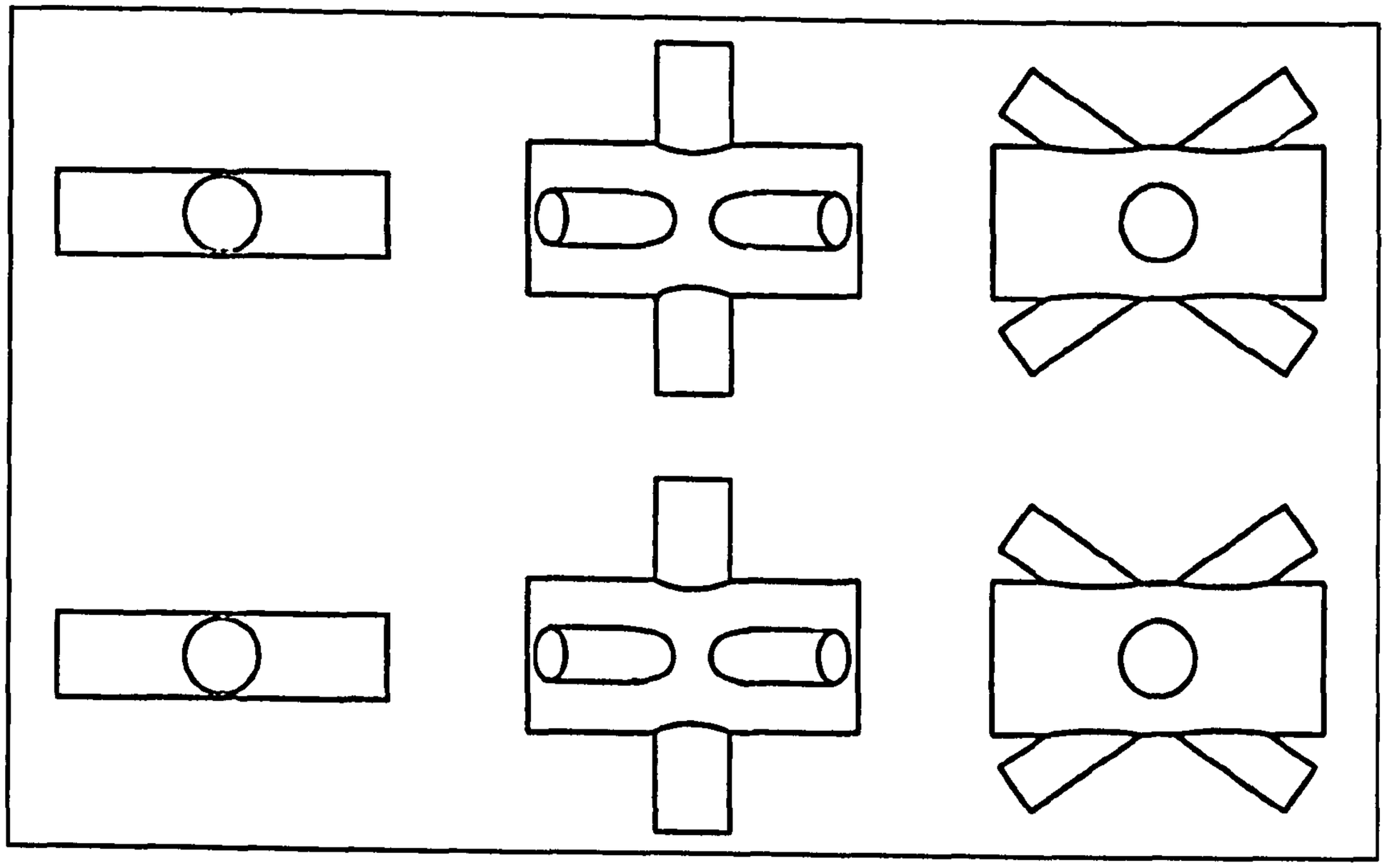

Figure 3.2: Typical planar and multi-planar joints used Offshore

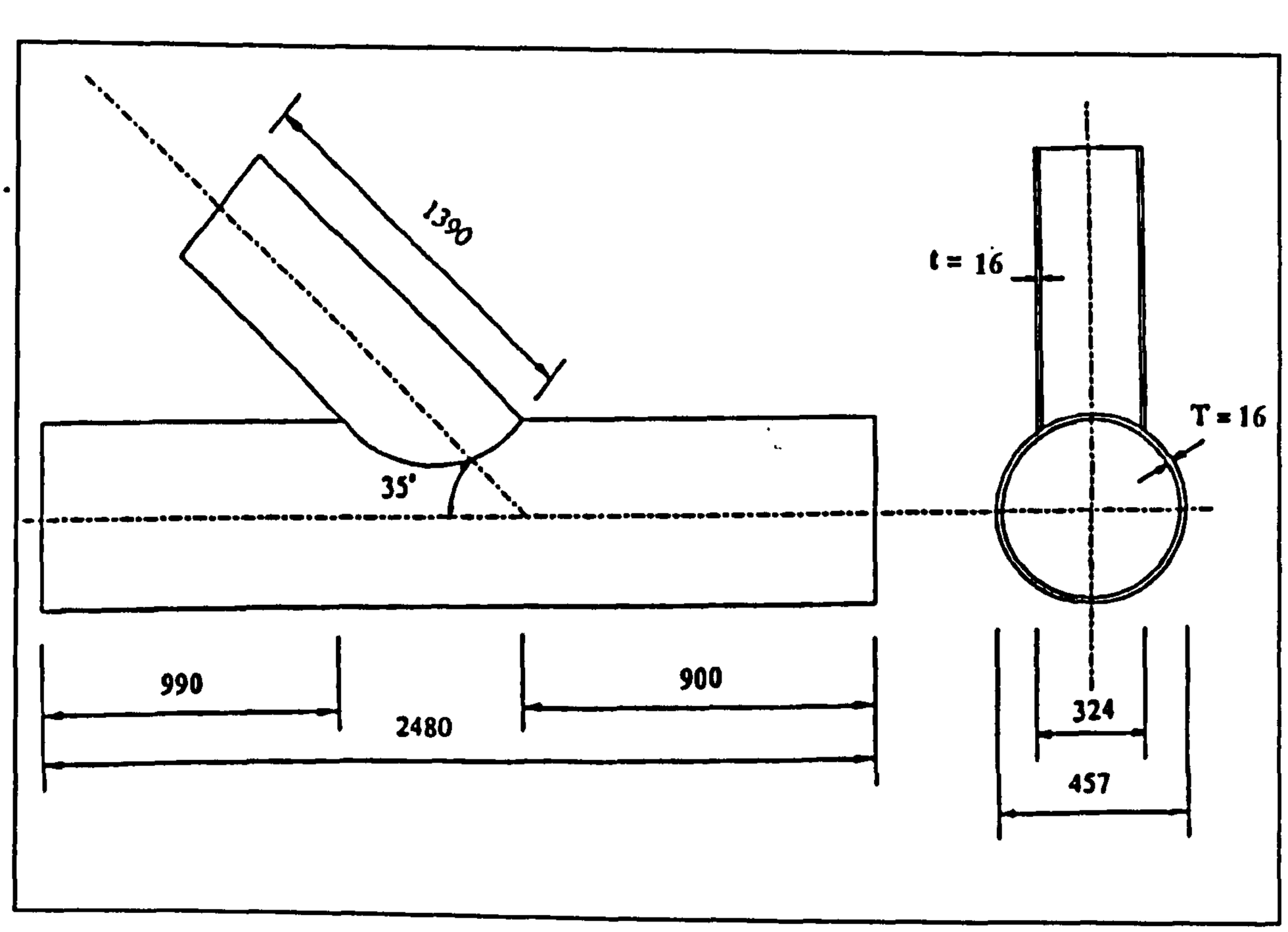

Figure 3.3: Detailed geometry of Y-joint used for large scale fatigue testing

Figure 3.4: Illustration of brace seam weld and intersection weld on Y-joint

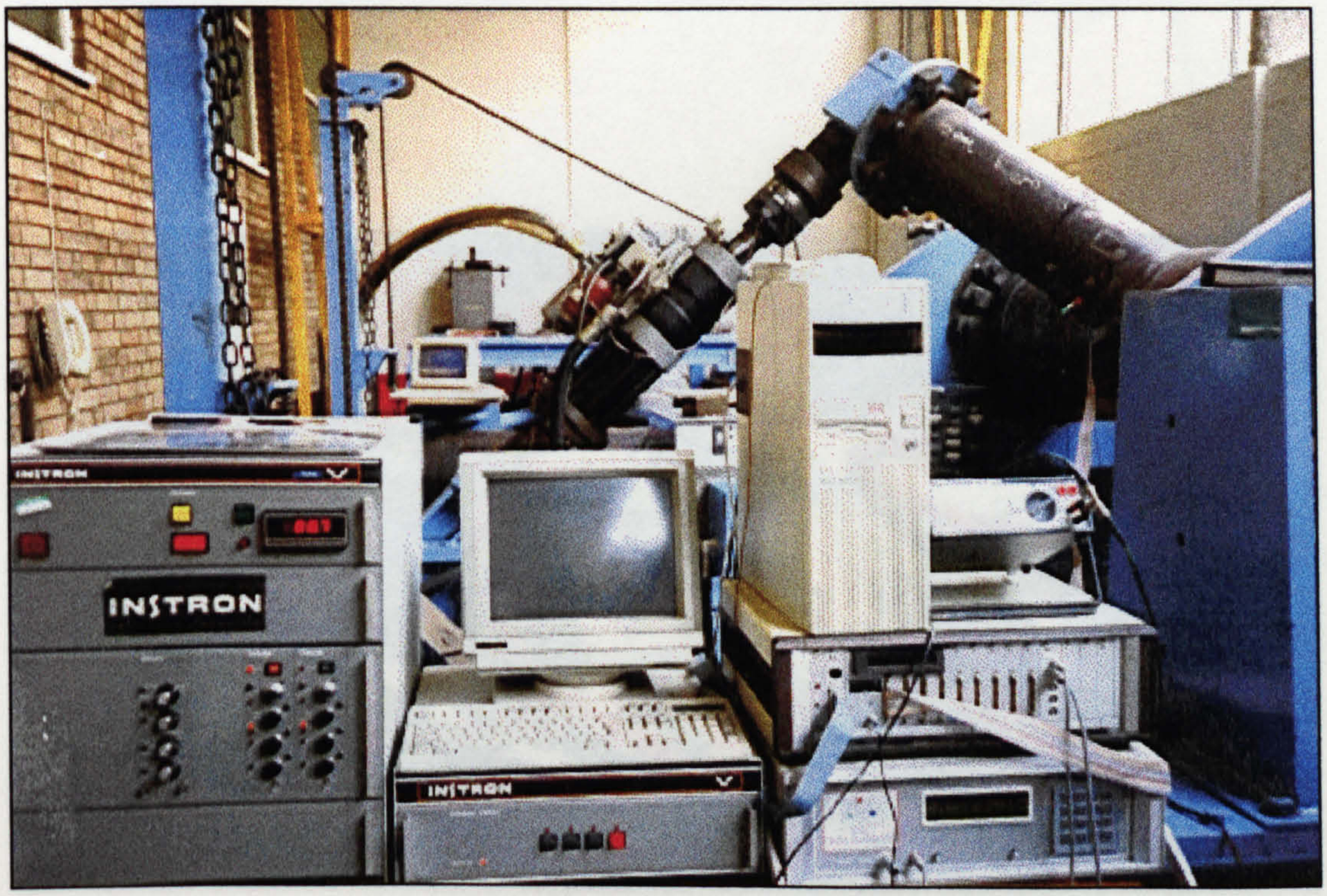

Figure 3.5: Experimental set-up for Y-joint under OPB mode

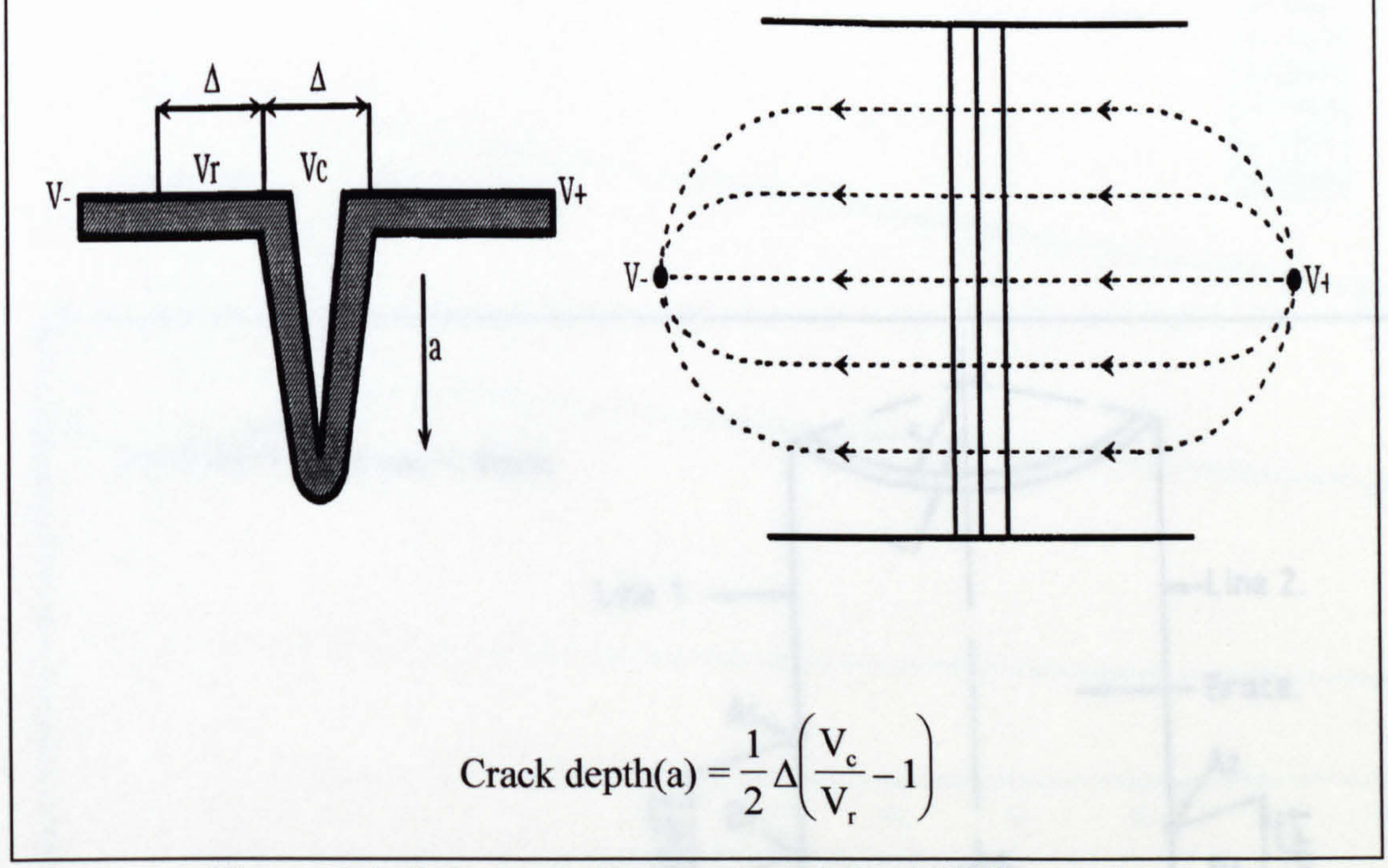

$$\text{Crack depth(a)} = \frac{1}{2}\Delta\left(\frac{V_c}{V_r} - 1\right)$$

Figure 3.6: Schematic illustration of the ACPD technique

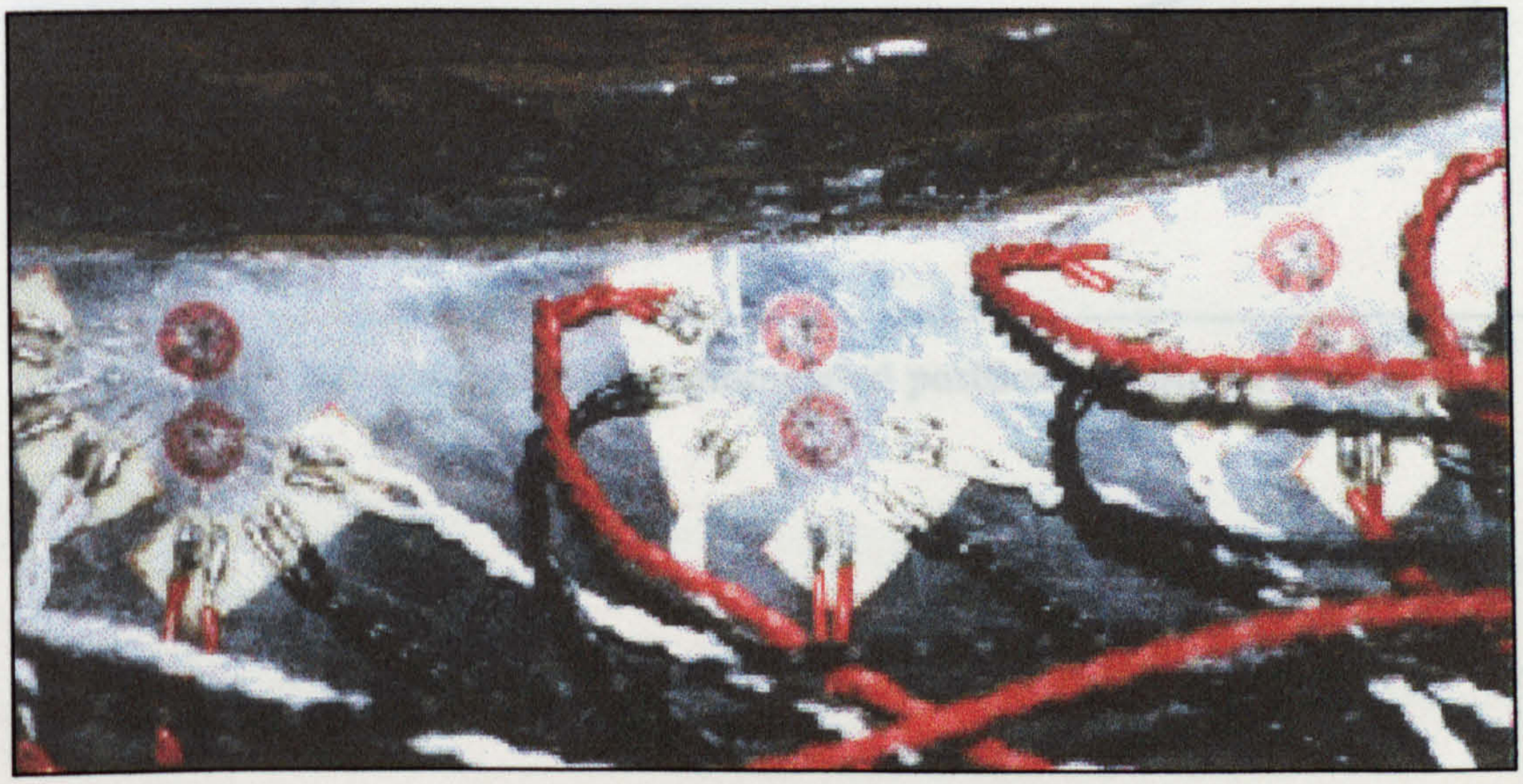

Figure 3.7: Location of strain gauges for experimental stress analysis

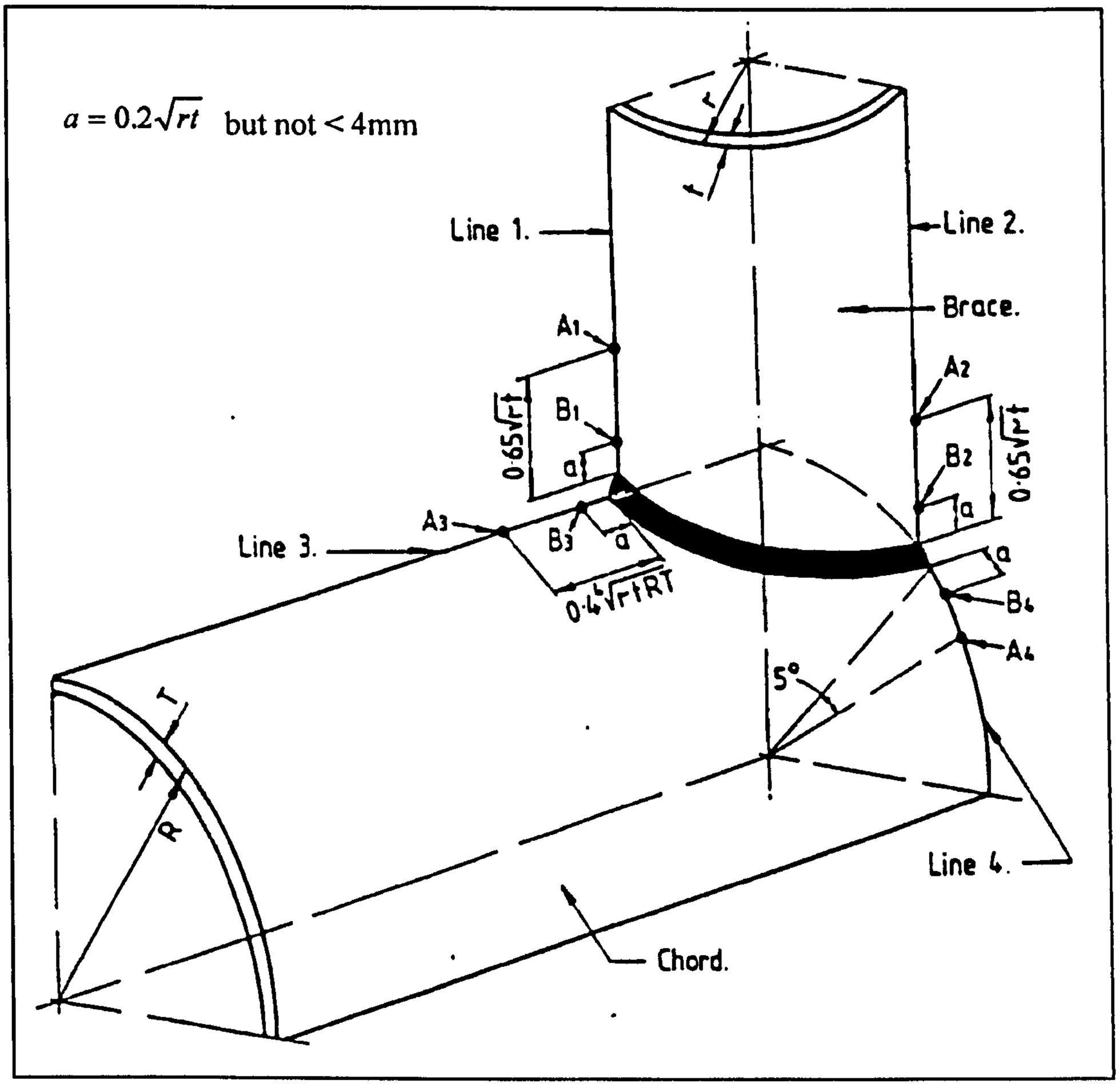

Figure 3.8: UKOSRP II recommended positions for strain gauges.

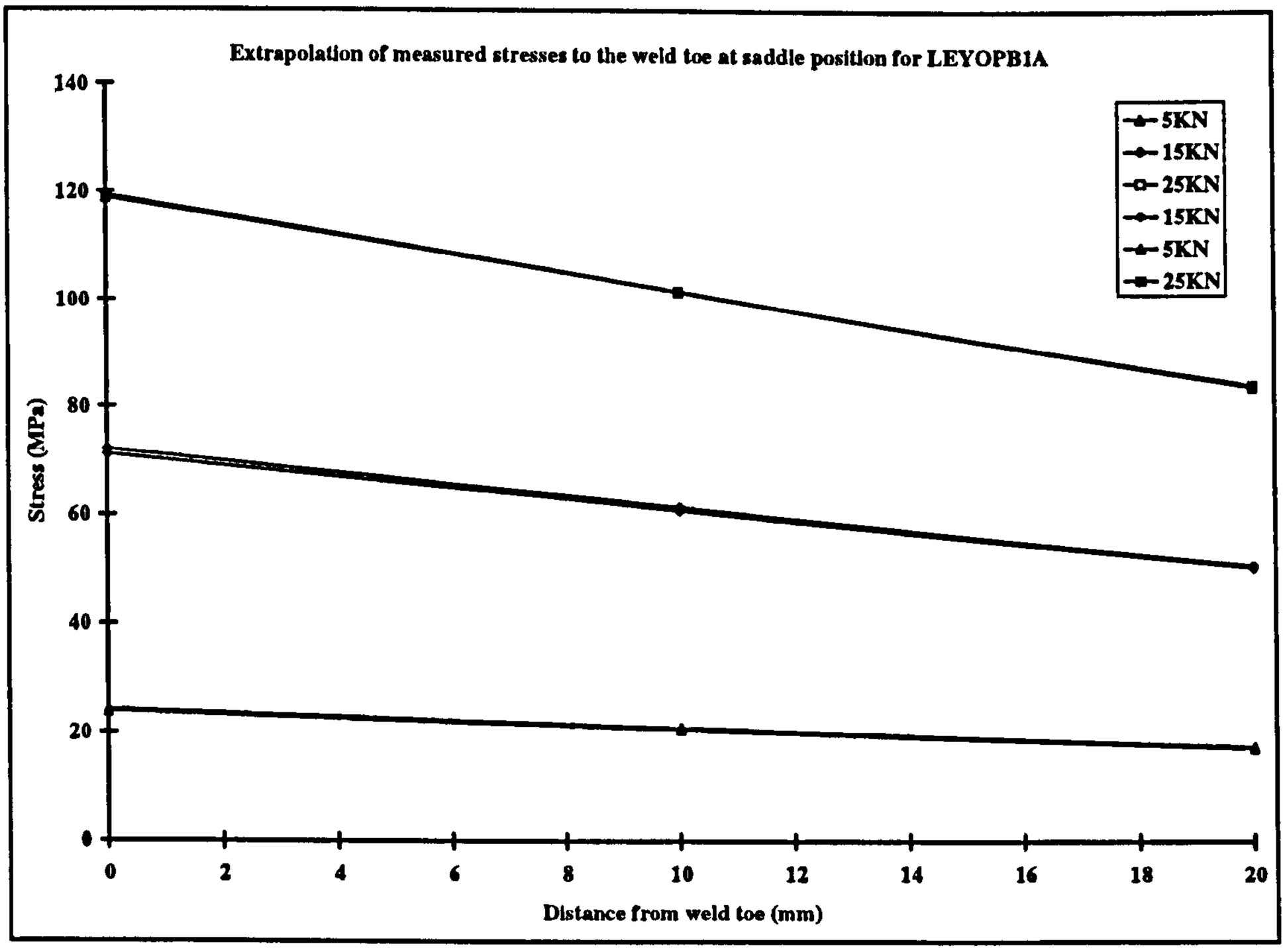

Figure 3.9: Extrapolation of measured stresses to the weld to for LEYOPB1A

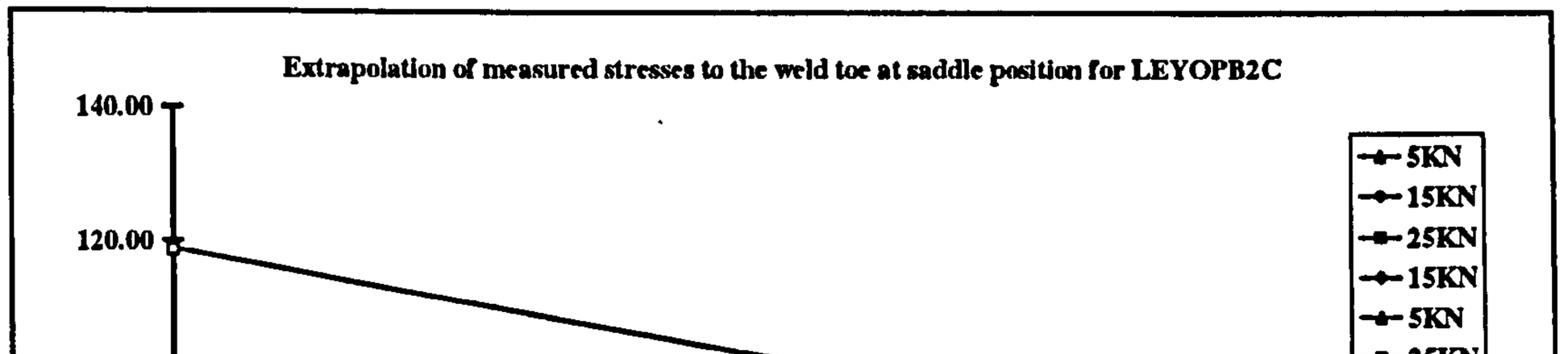

Figure 3.10: Extrapolation of measured stresses to the weld to for LEYOPB2C

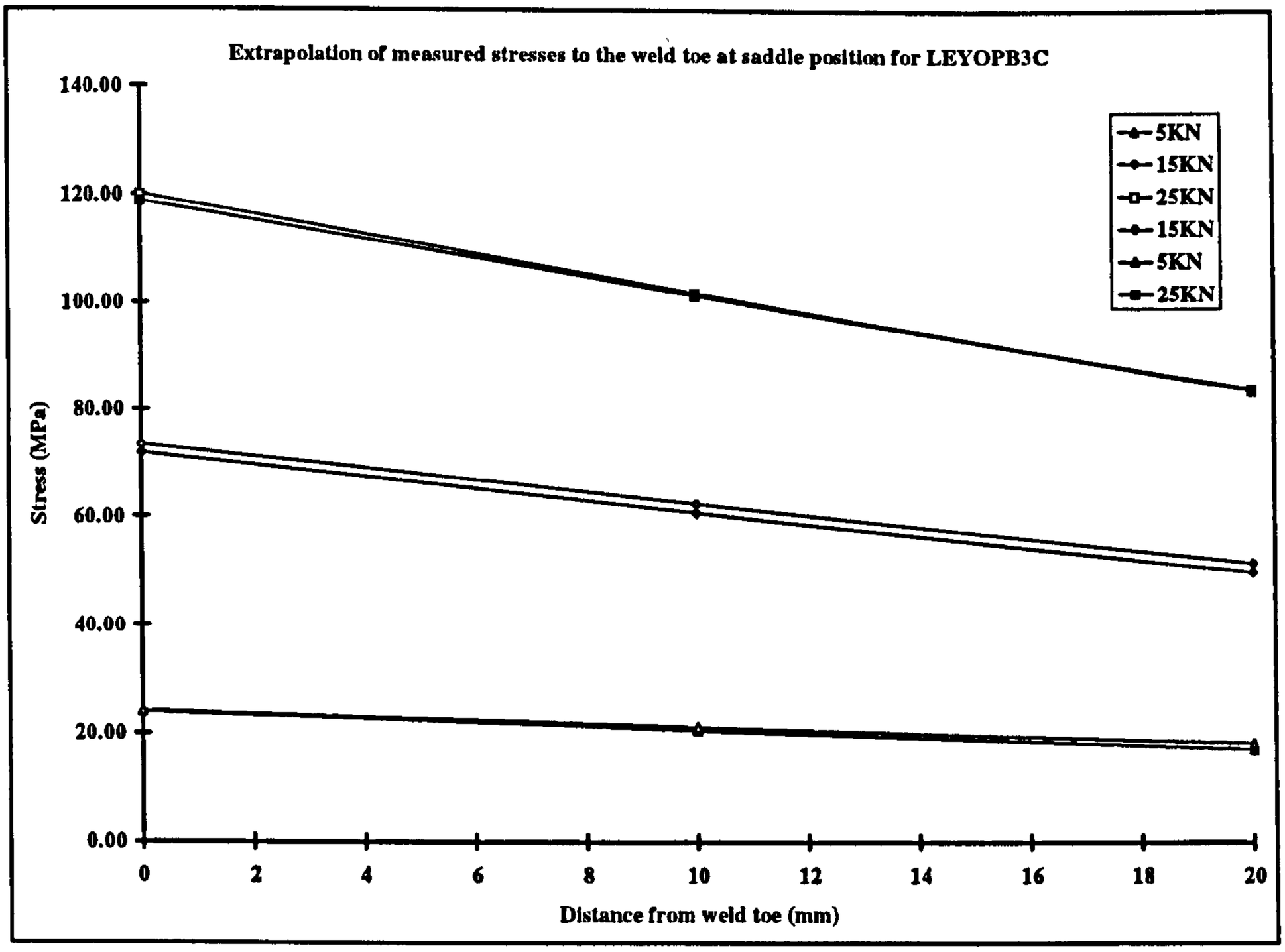

Figure 3.11: Extrapolation of measured stresses to the weld to for LEYOPB3C

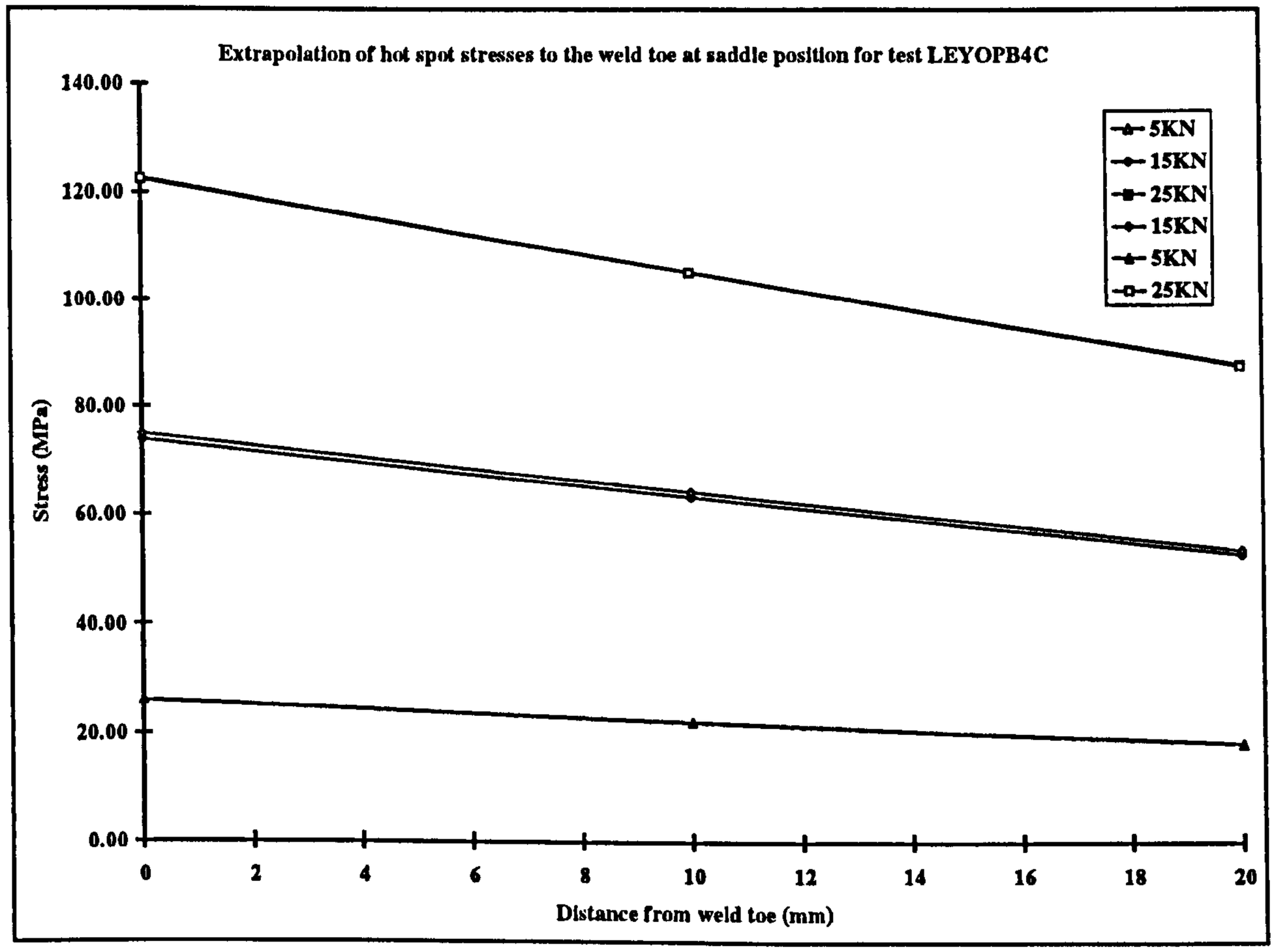

Figure 3.12: Extrapolation of measured stresses to the weld to for LEYOPB4C

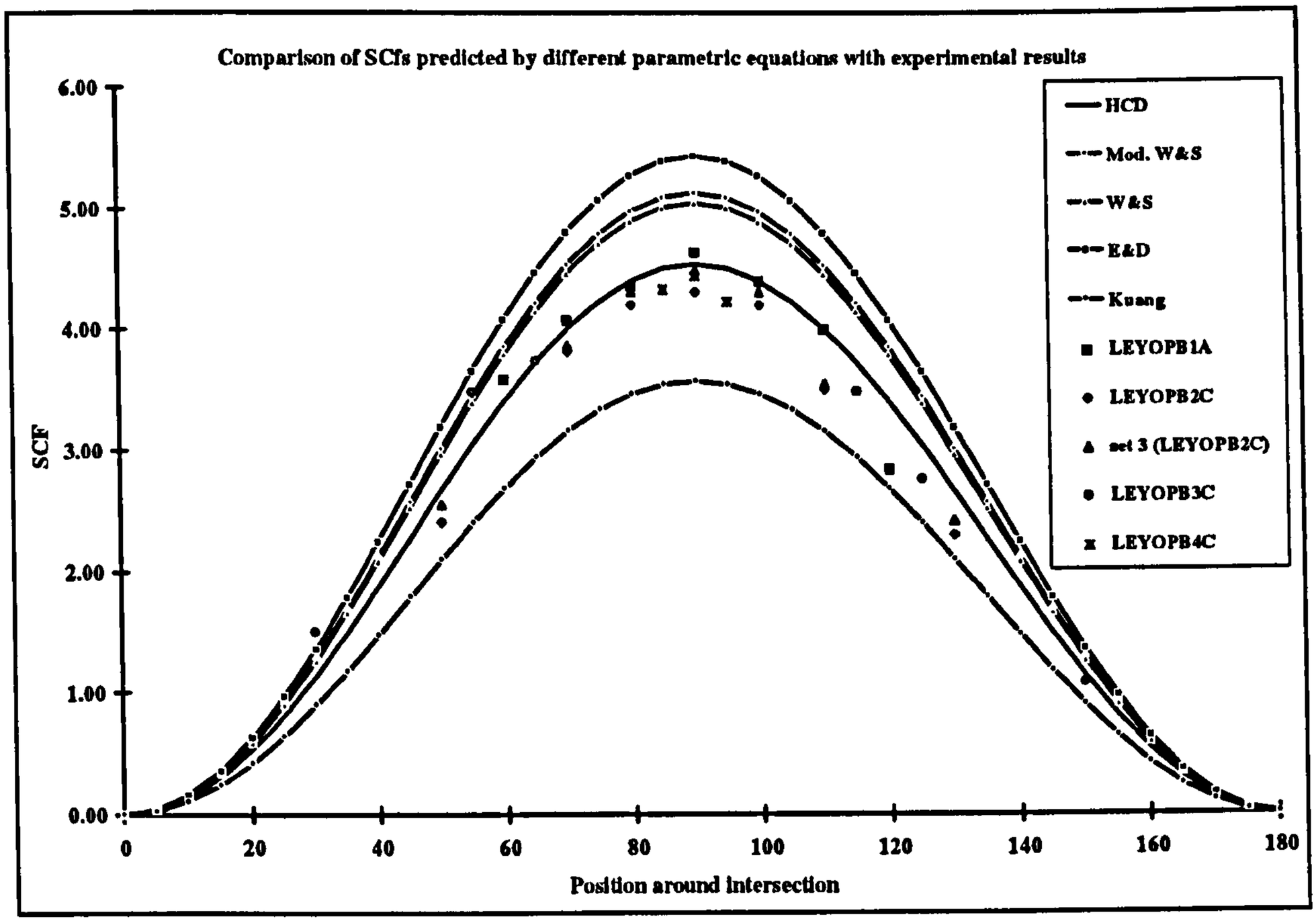

Figure 3.13: Comparison of measured and predicted SCFs for Y-joints

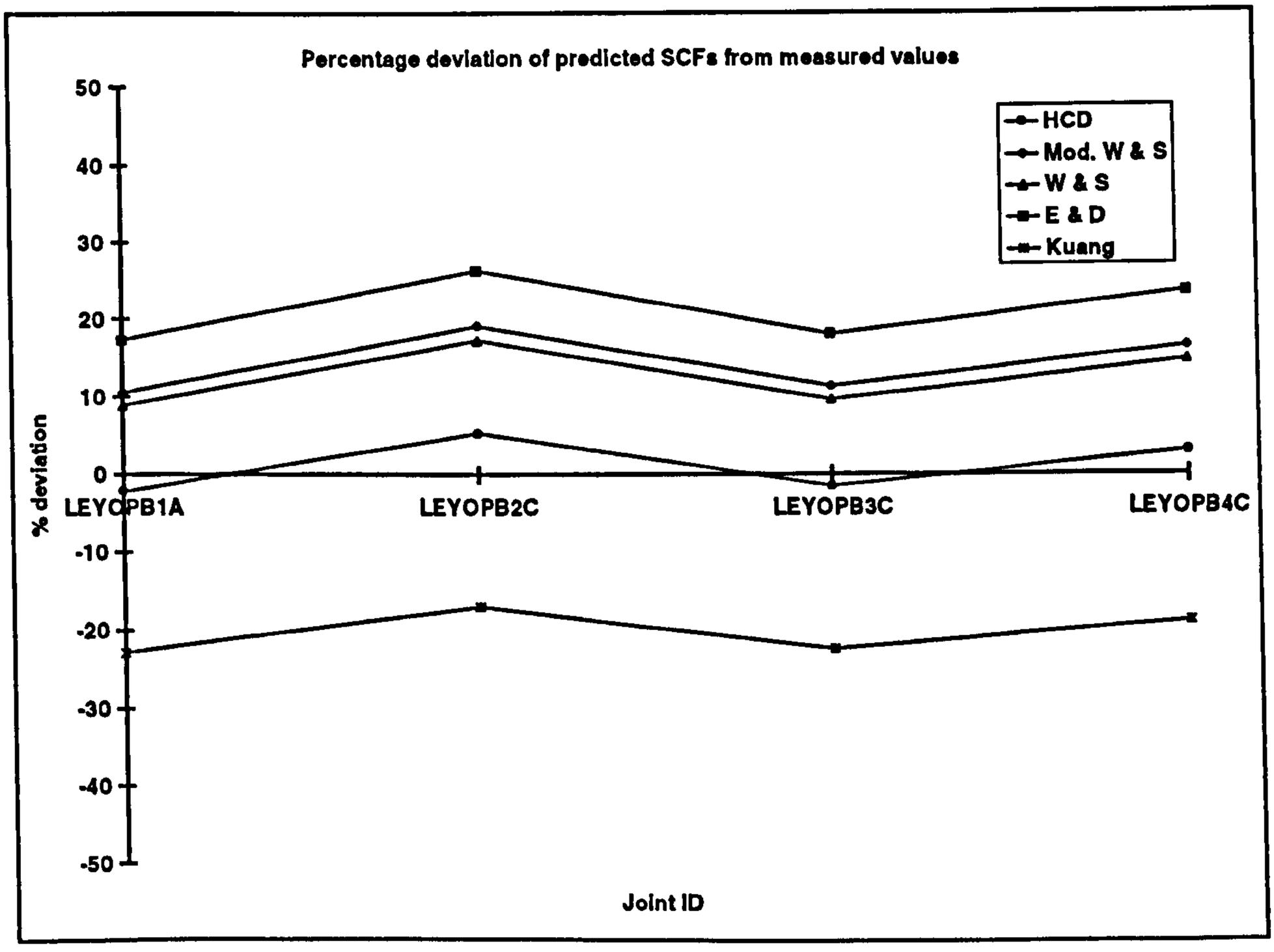

Figure 3.14: Deviation of predicted SCFs from experimental values

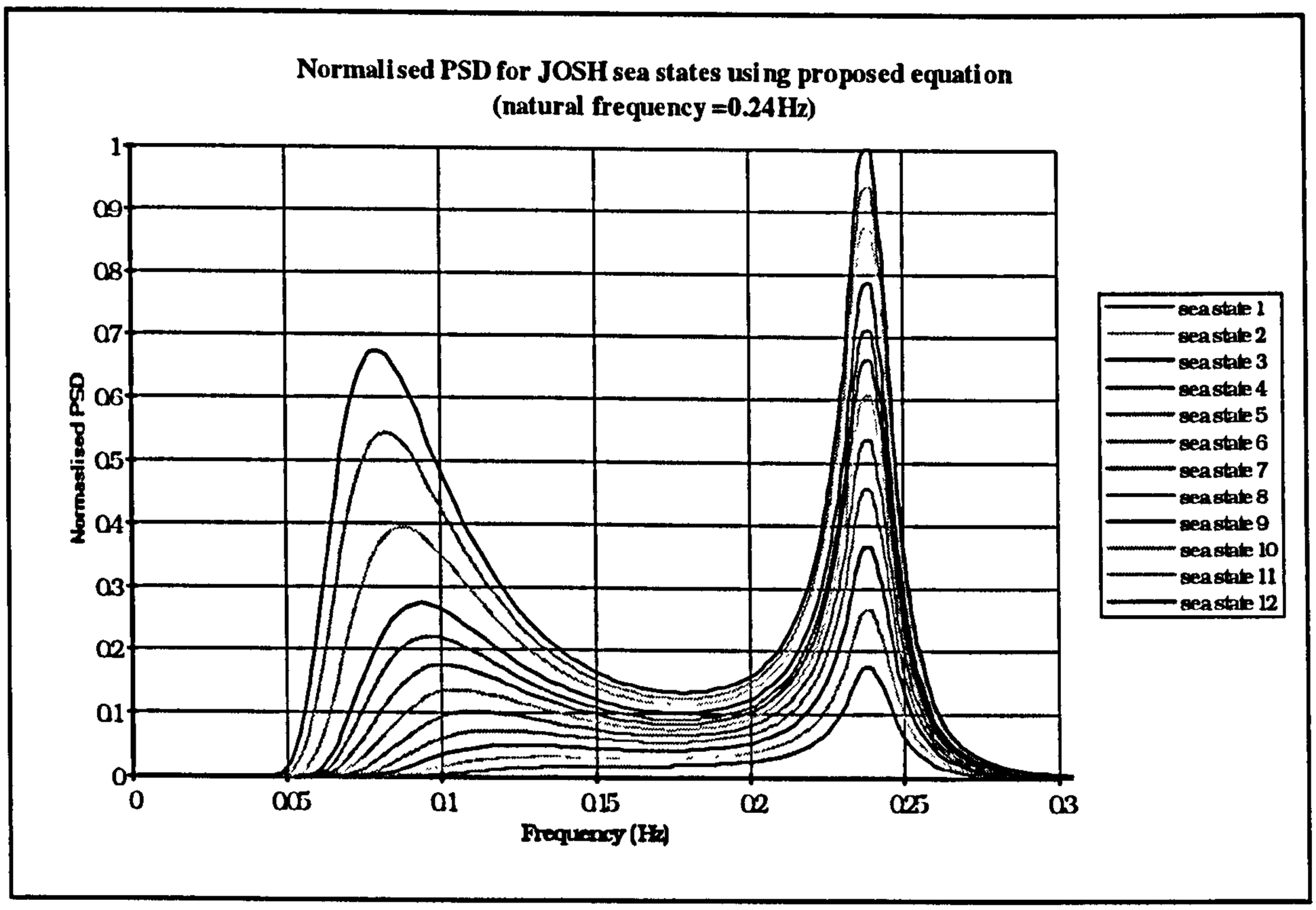

Figure 3.15: Normalised PSDs for the 12 sea states used in JOSH

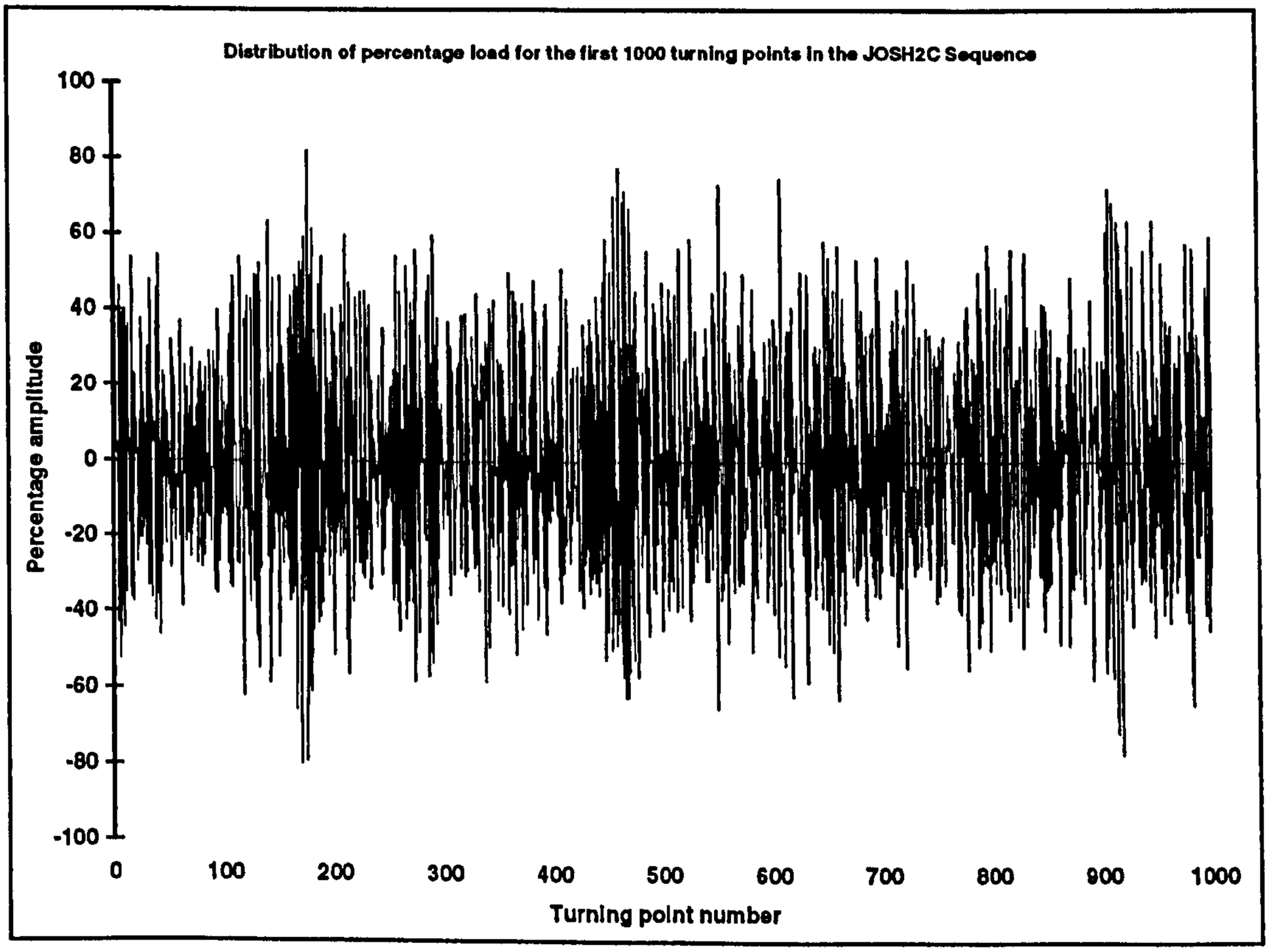

Figure 3.16: The 1st 1000 of over a million turning points in JOSH (JOSH2C)

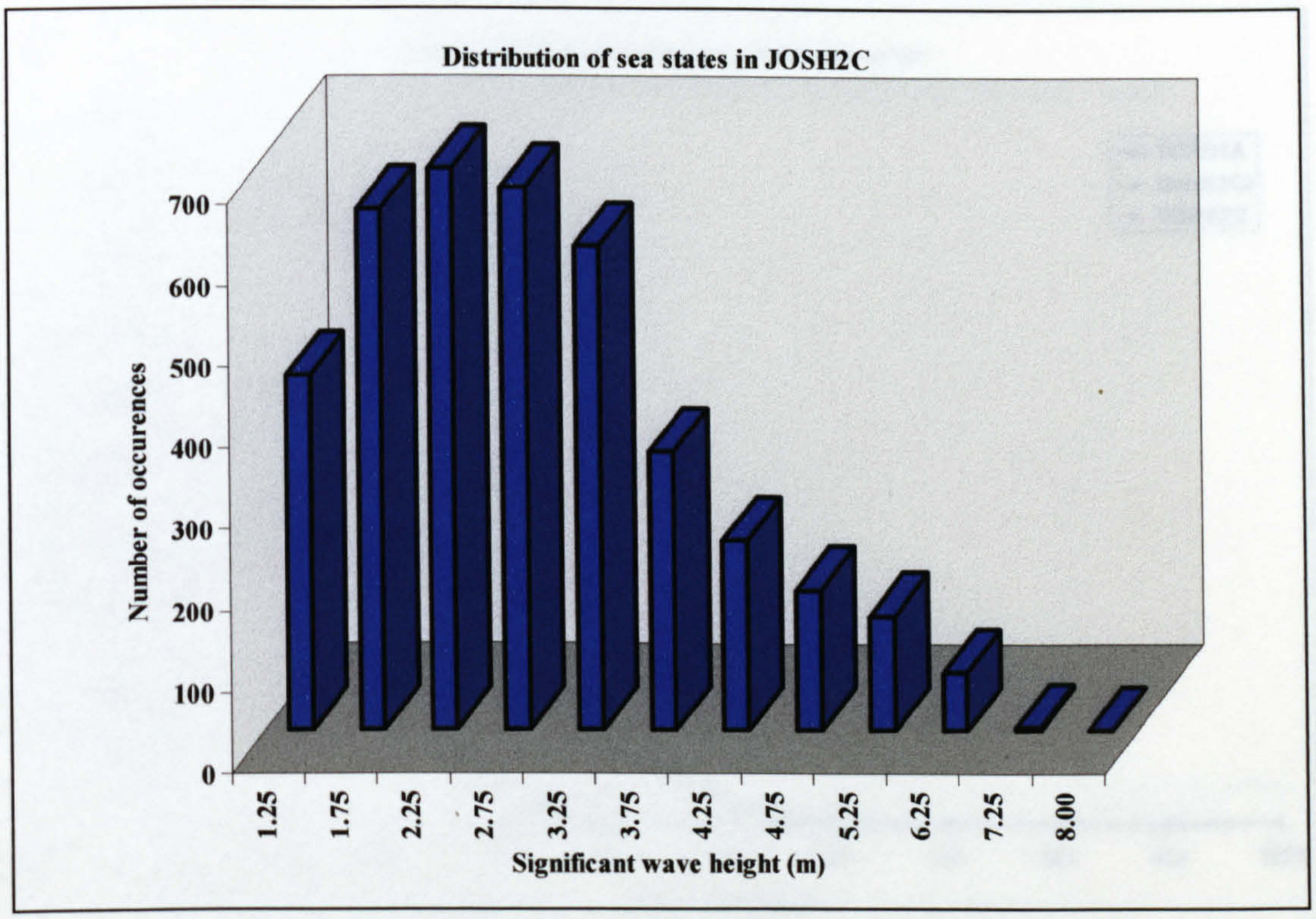

Figure 3.17: Distribution of sea states in JOSH2C

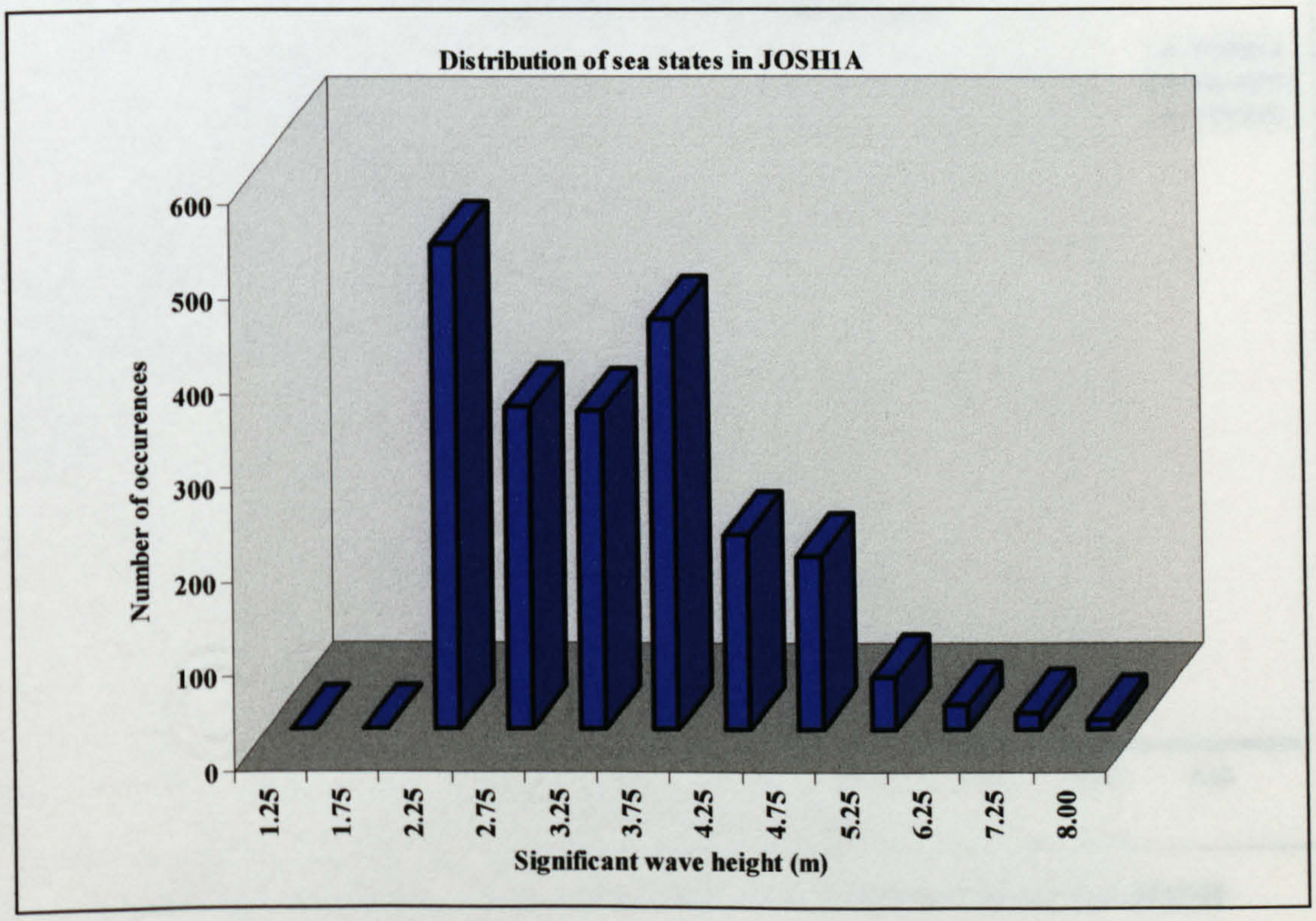

Figure 3.18: Distribution of sea states in JOSH1A

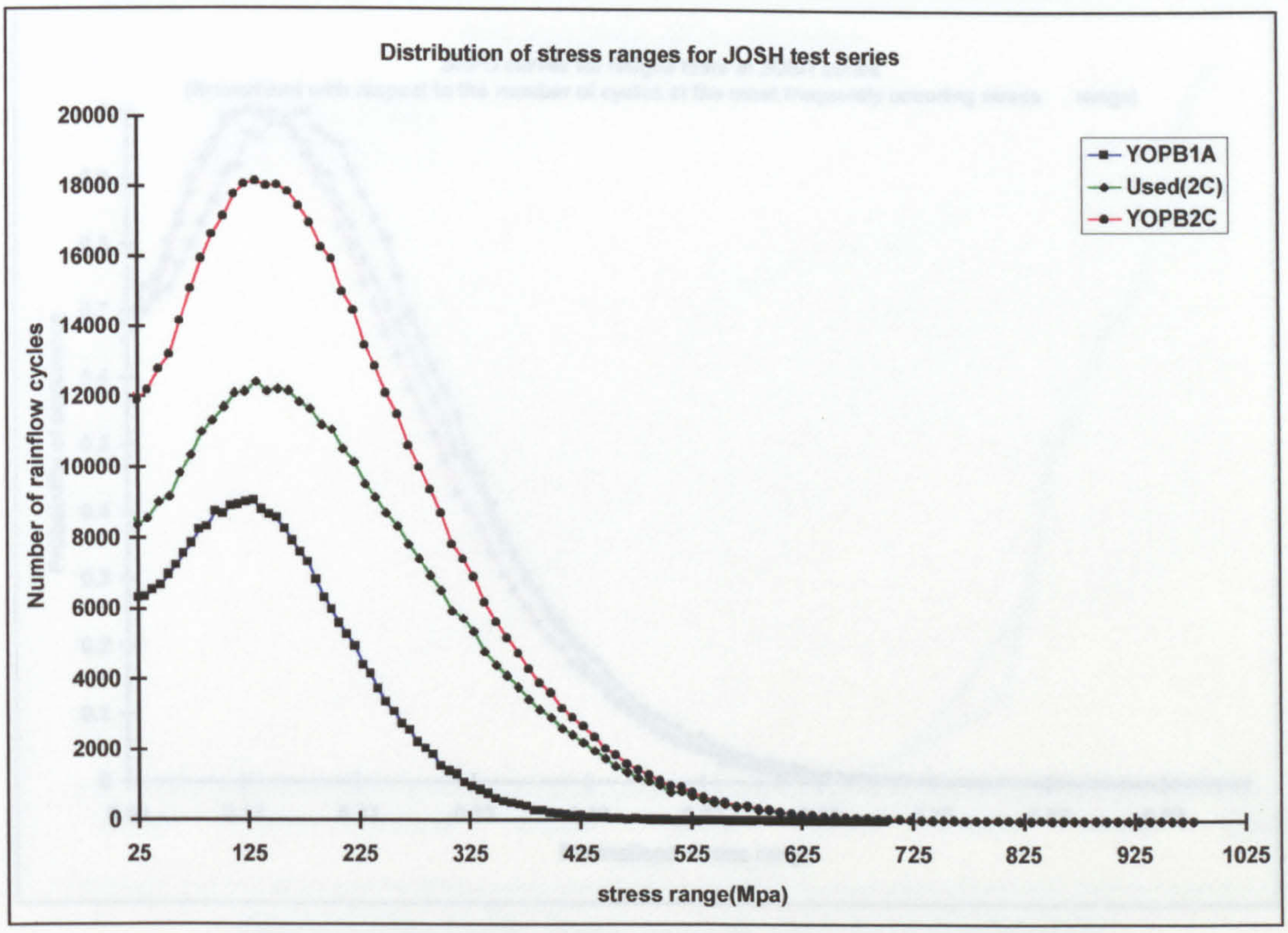

Figure 3.19: Stress range distribution curves for JOSH

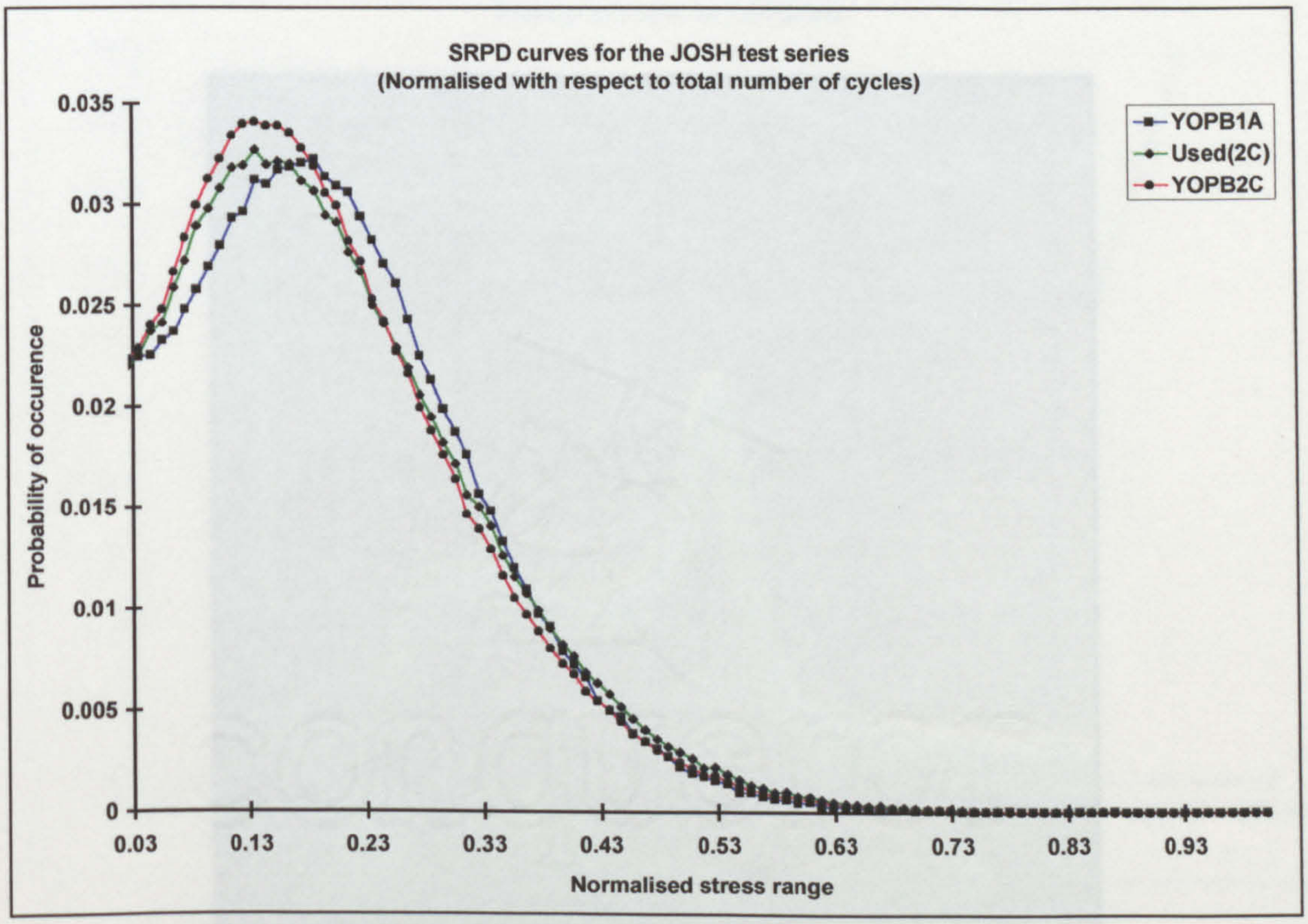

Figure 3.20: Stress range probability distribution curves for JOSH

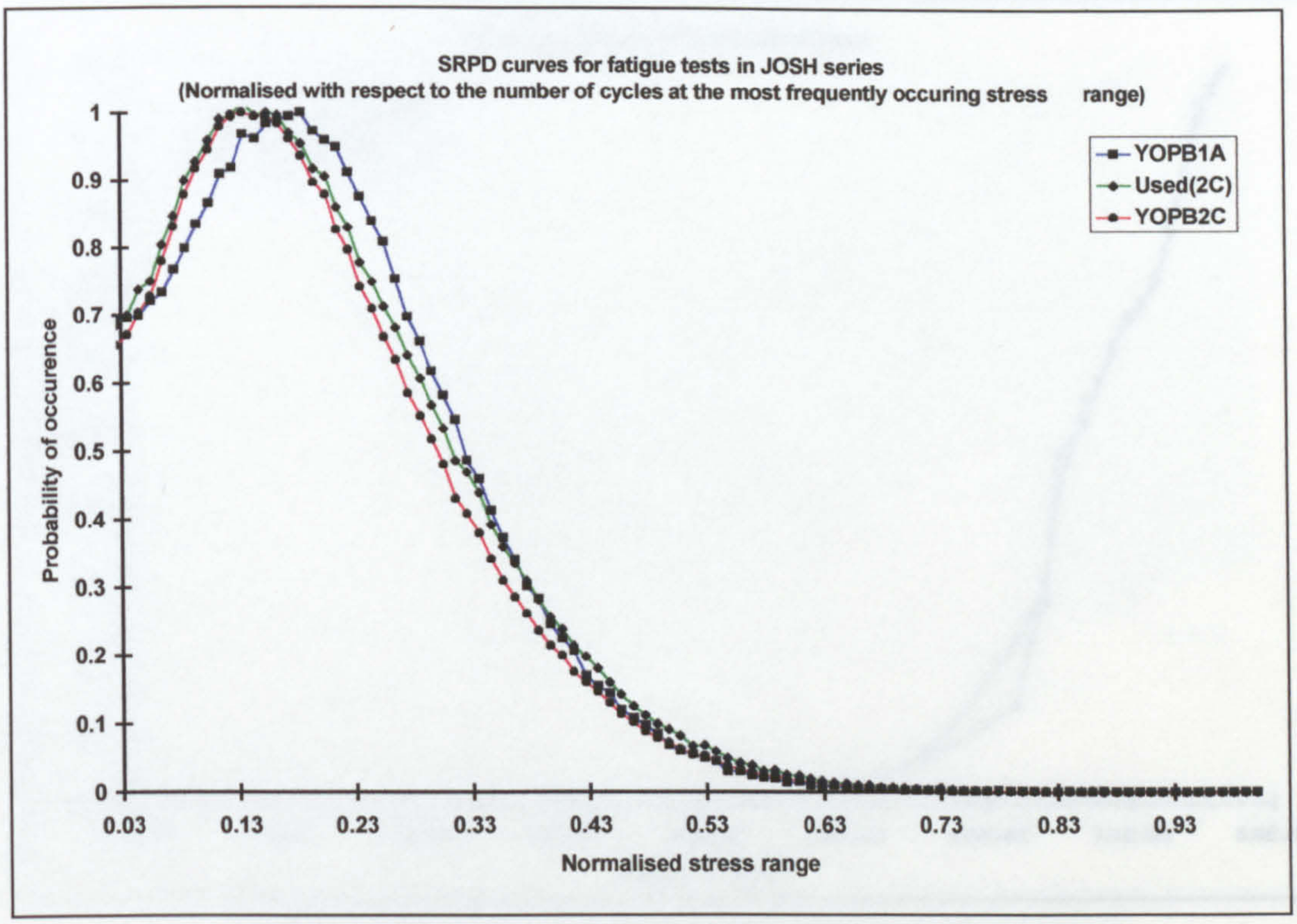

Figure 3.21: Normalised SRPD curves for JOSH

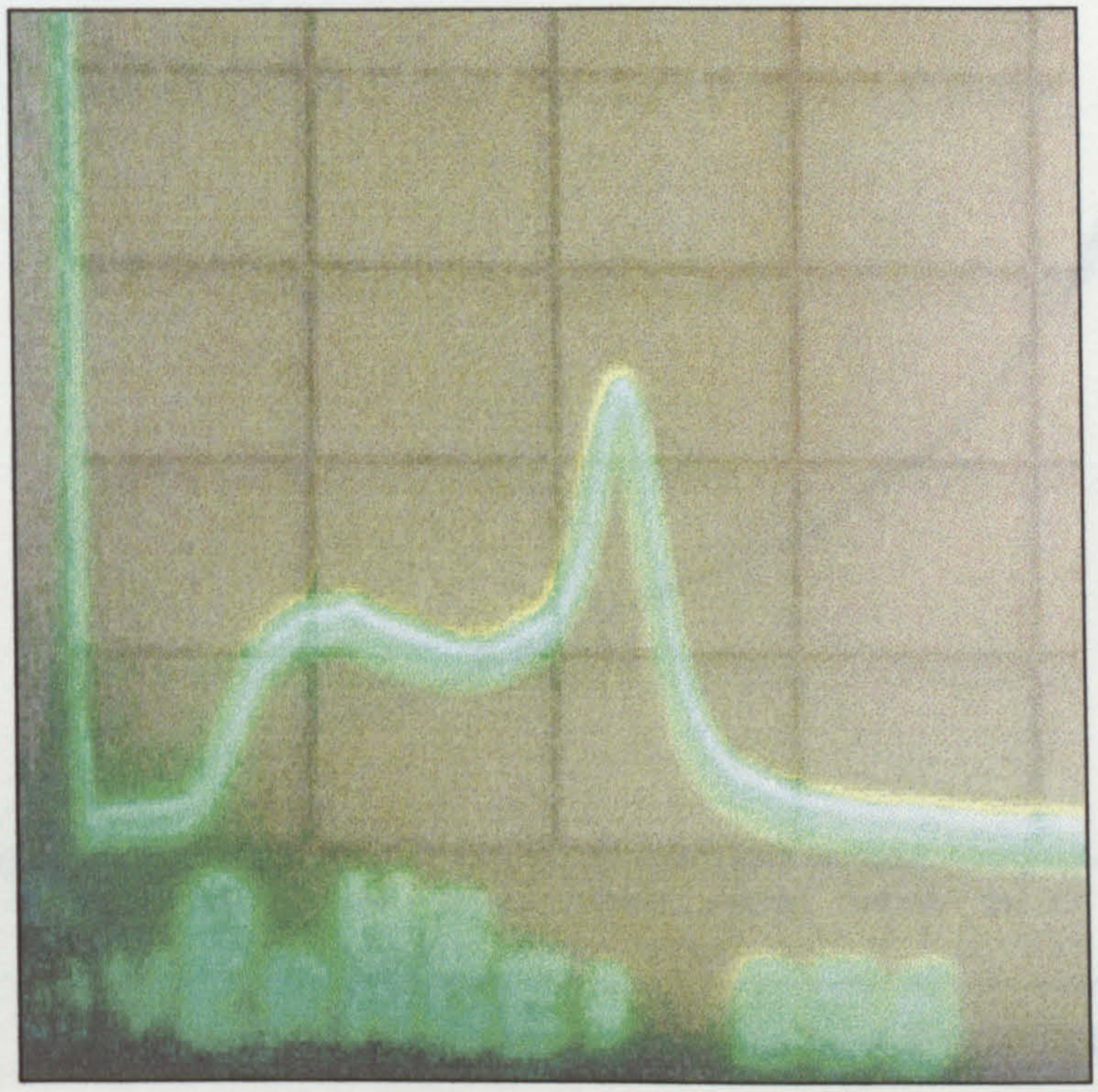

Figure 3.22: PSD obtained from spectrum analyzer during a fatigue test

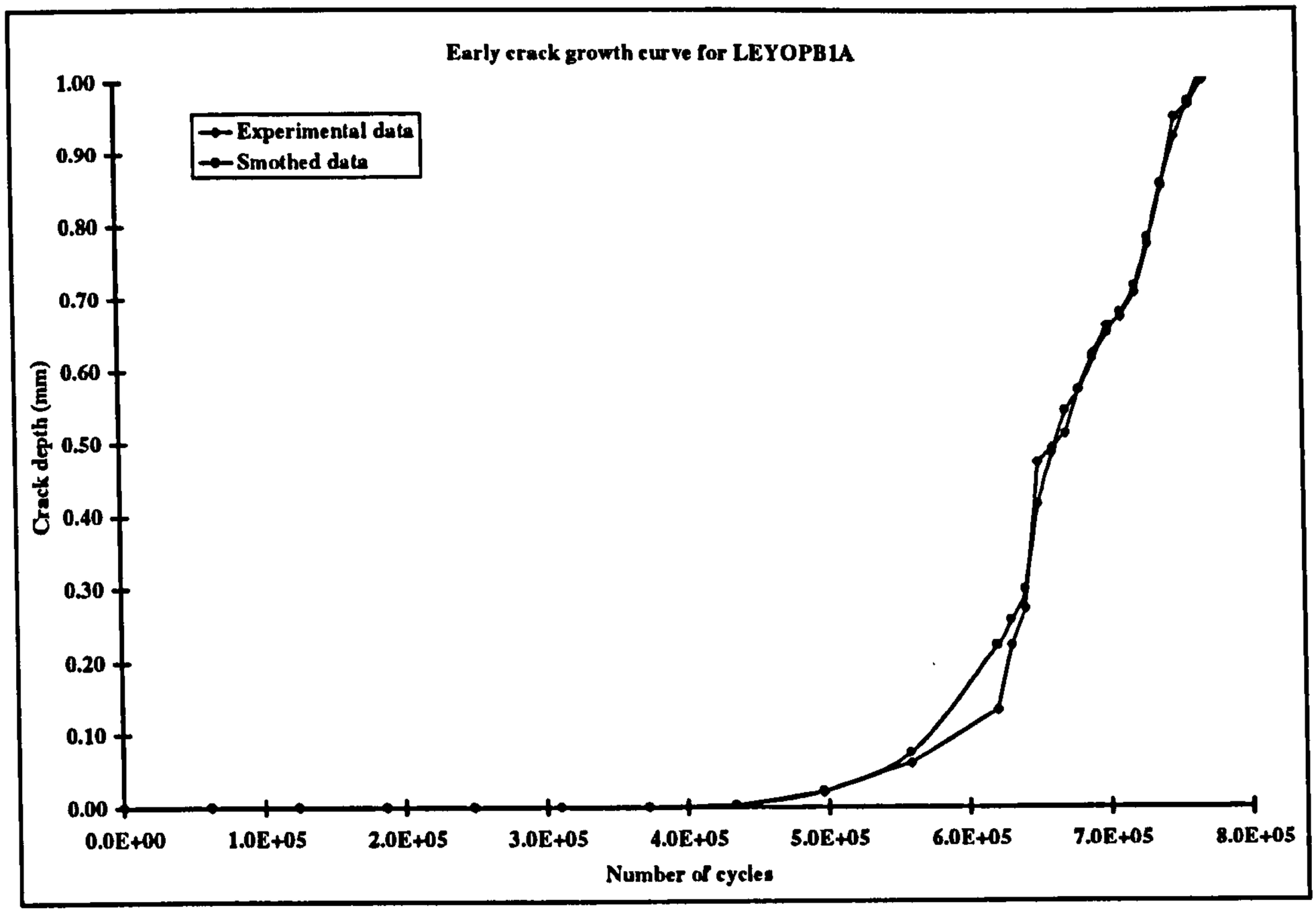

Figure 3.23: Early crack growth data for LEYOPB1A

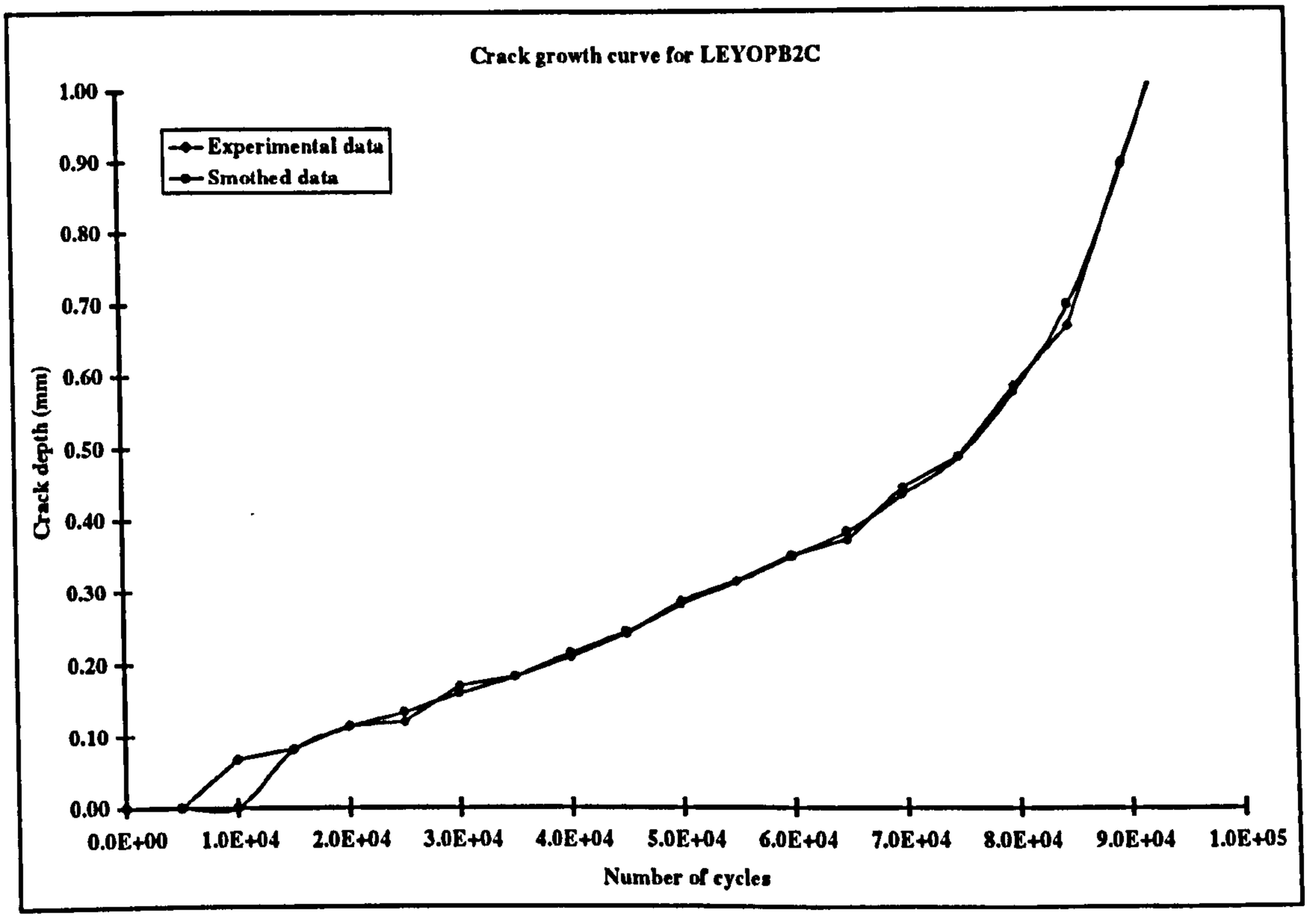

Figure 3.24: Early crack growth data for LEYOPB2C

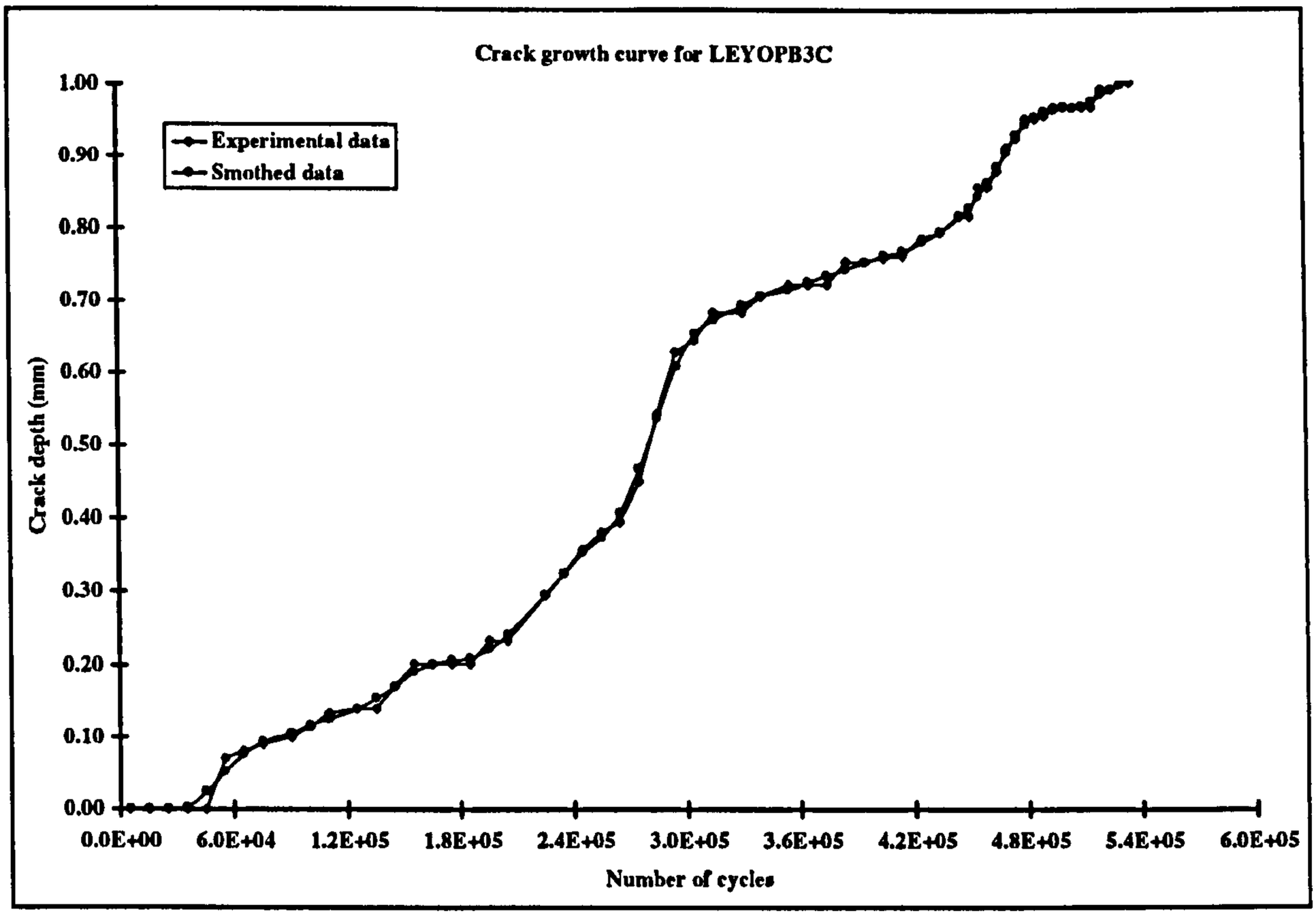

Figure 3.25: Early crack growth data for LEYOPB3C

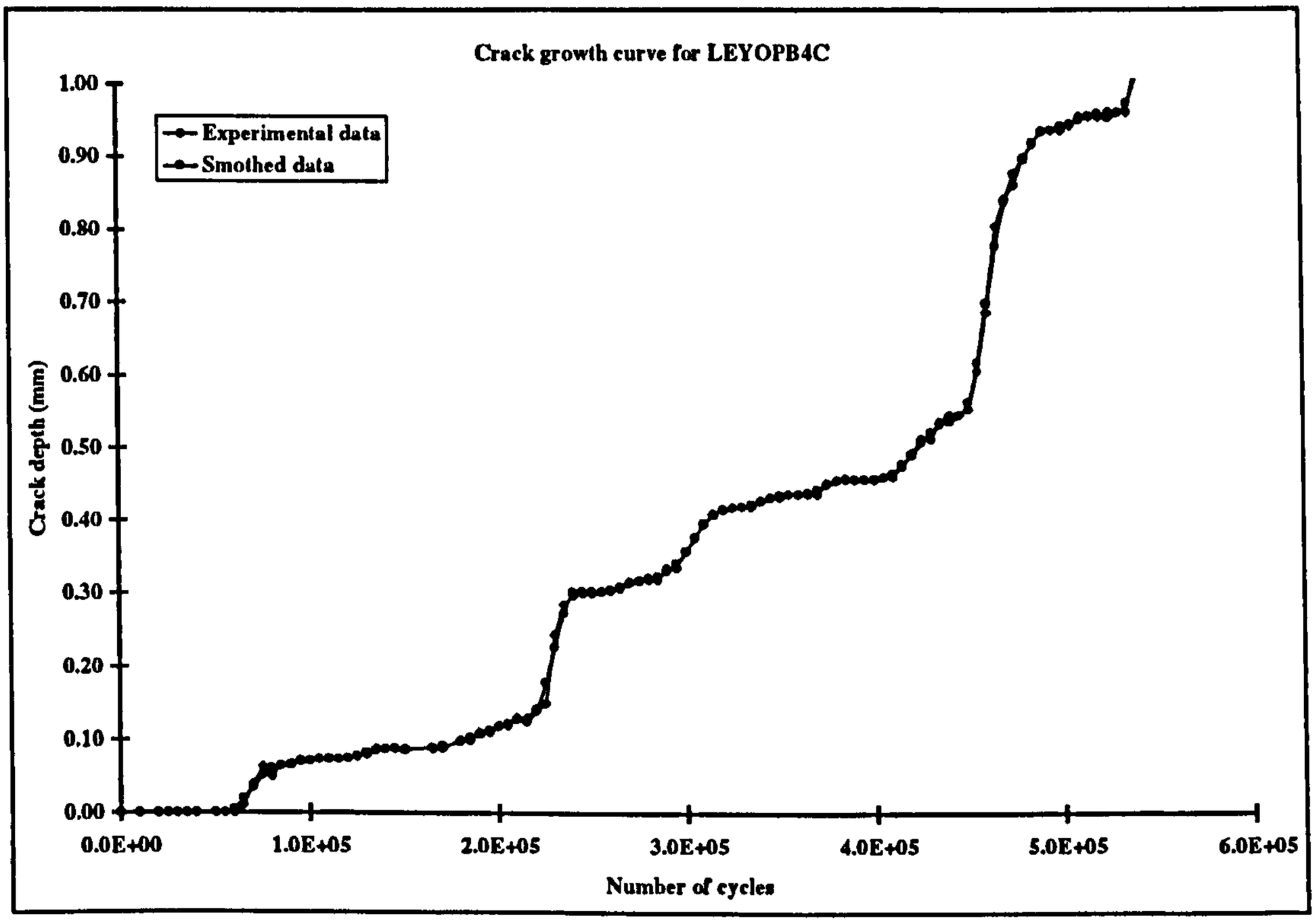

Figure 3.26: Early crack growth data for LEYOPB4C

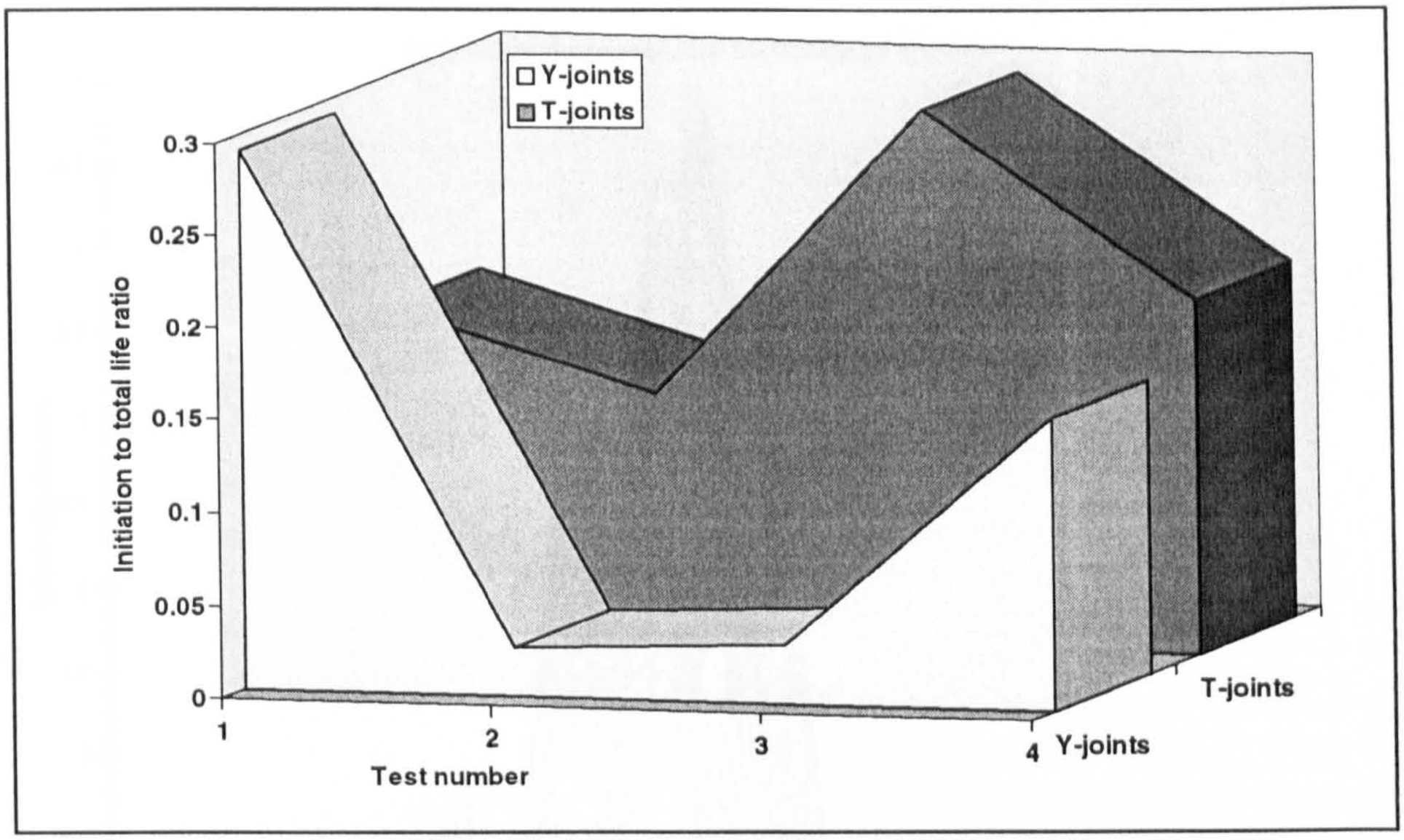

Figure 3.27: Comparison of N_1/N_3 ratio for Y and T-joints

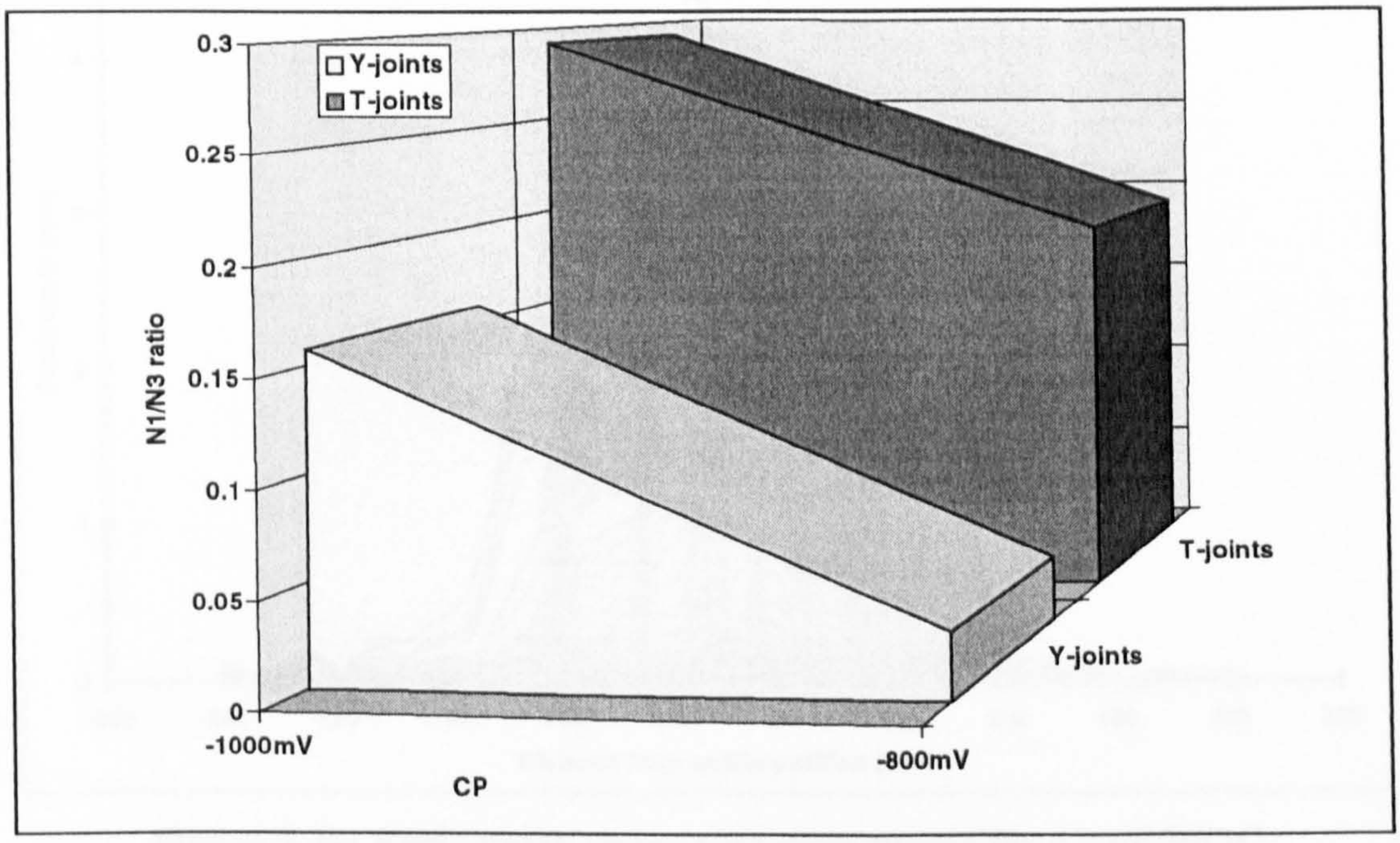

Figure 3.28: Effect of CP on N_1/N_3 ratio for Y and T-joints

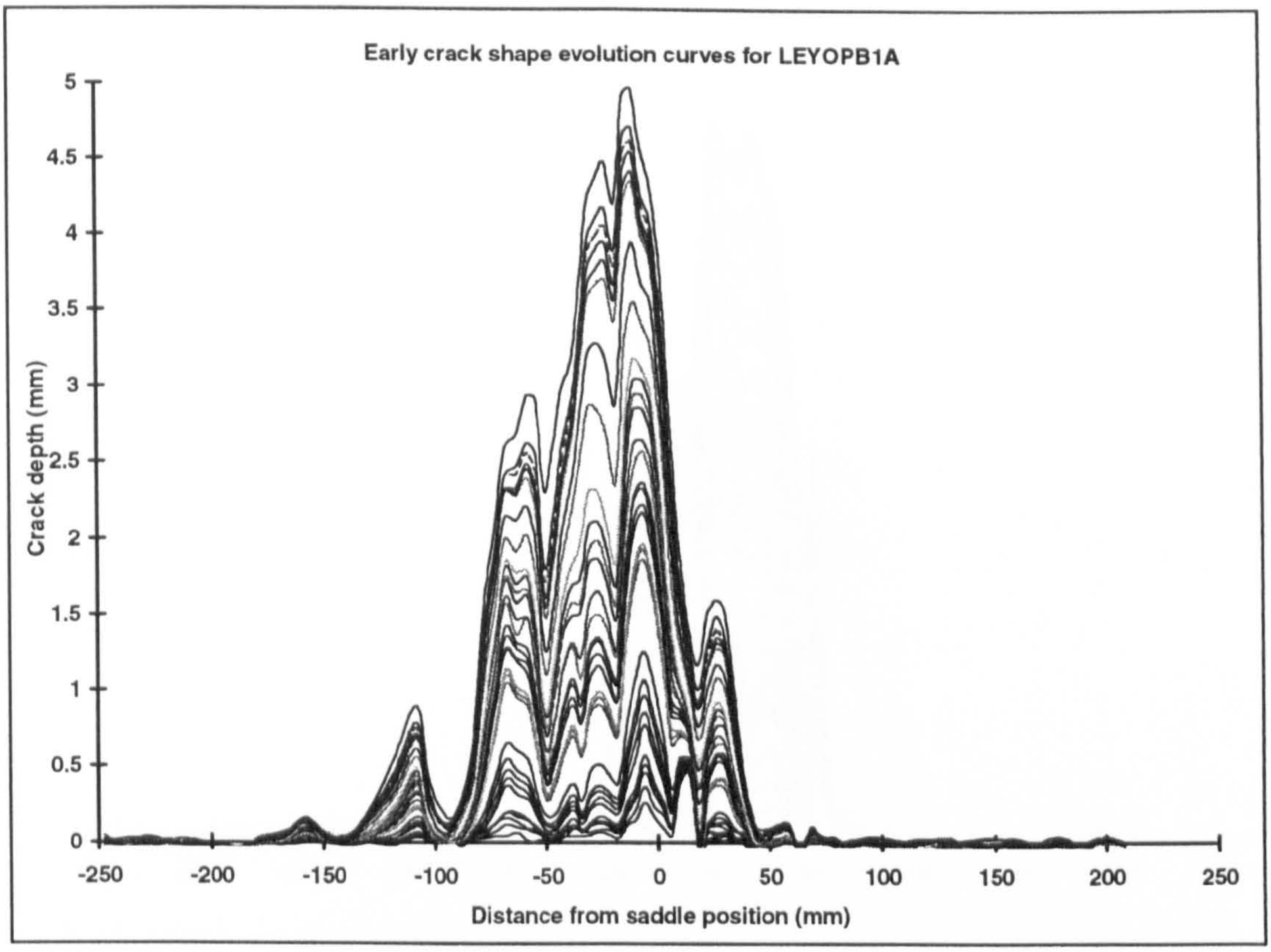

Figure 3.29: Early crack shape evolution curves for LEYOPB1A

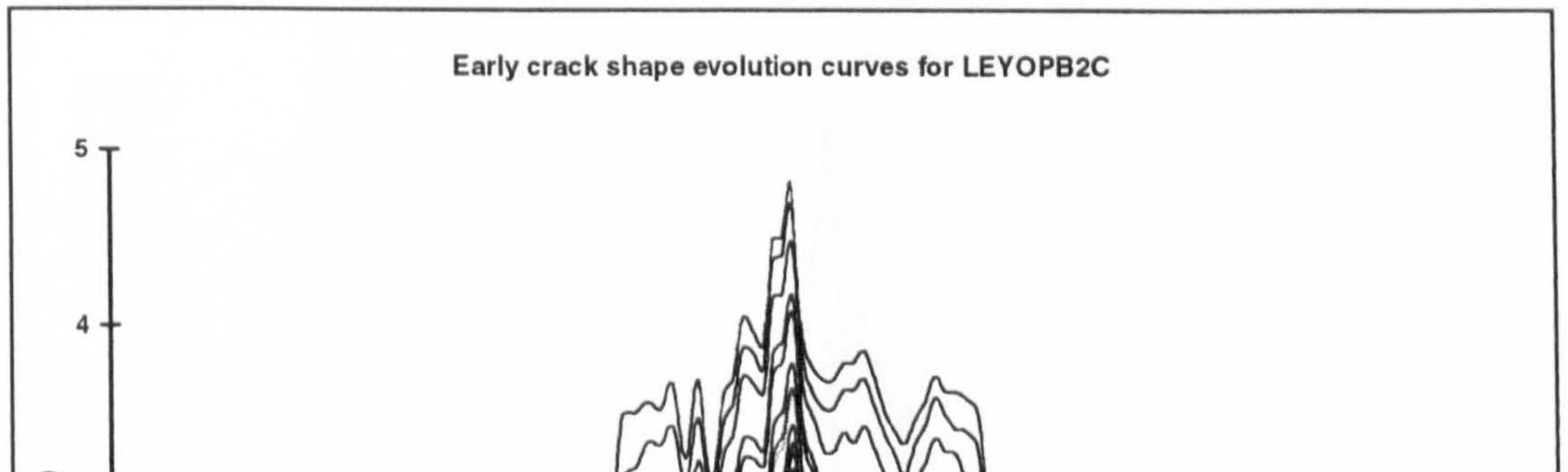

Figure 3.30: Early crack shape evolution curves for LEYOPB2C

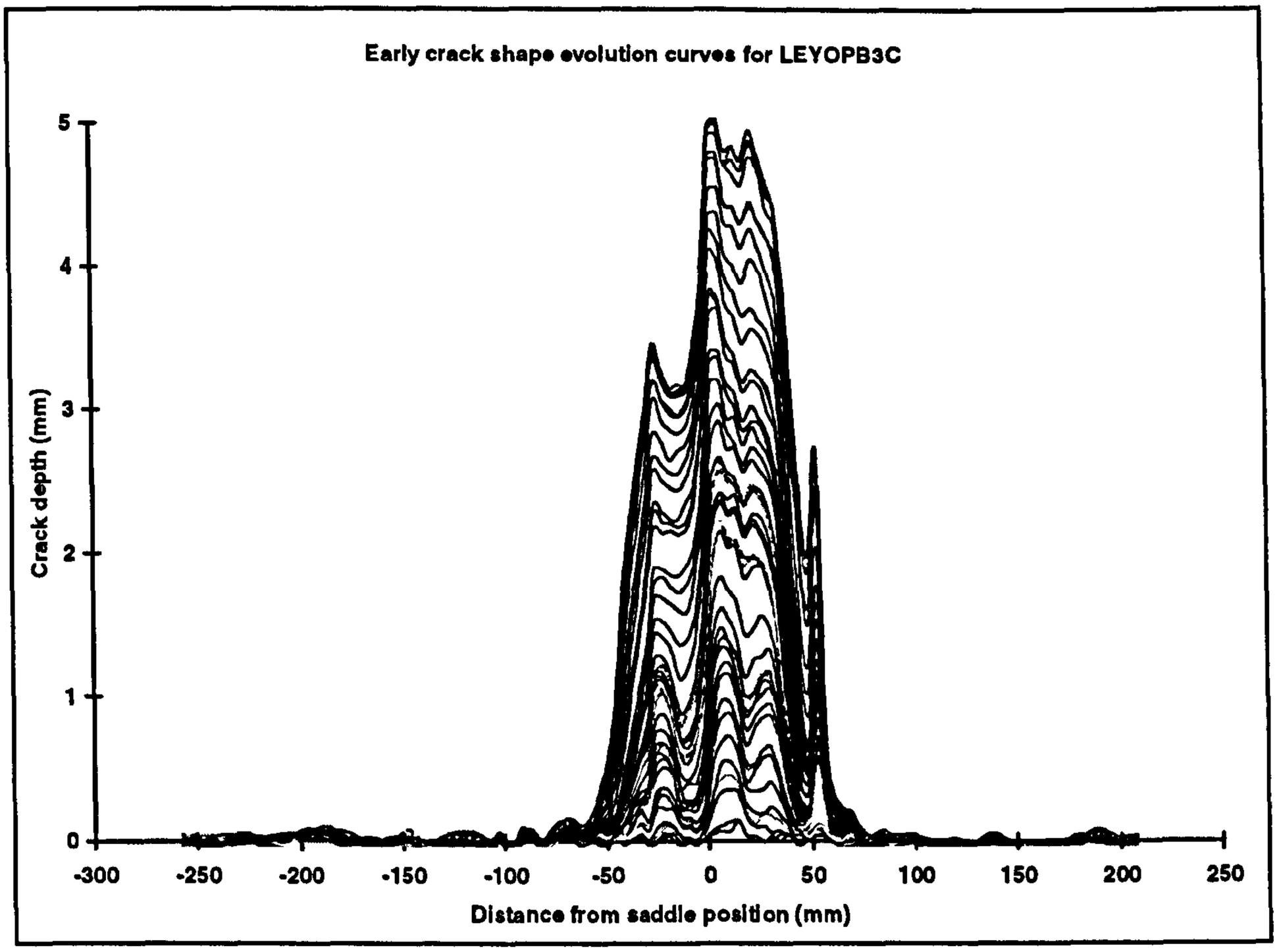

Figure 3.31: Early crack shape evolution curves for LEYOPB3C

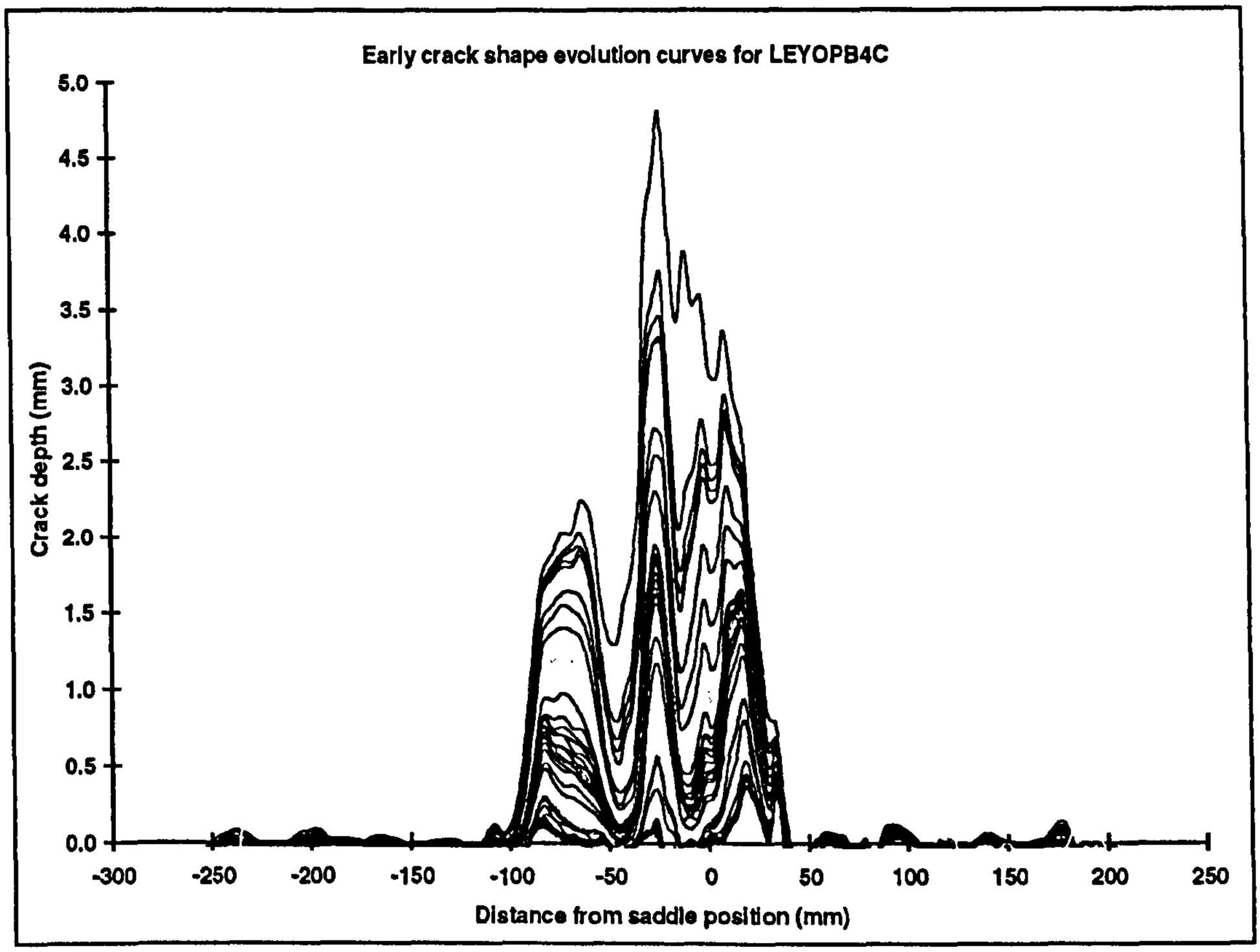

Figure 3.32: Early crack shape evolution curves for LEYOPB4C

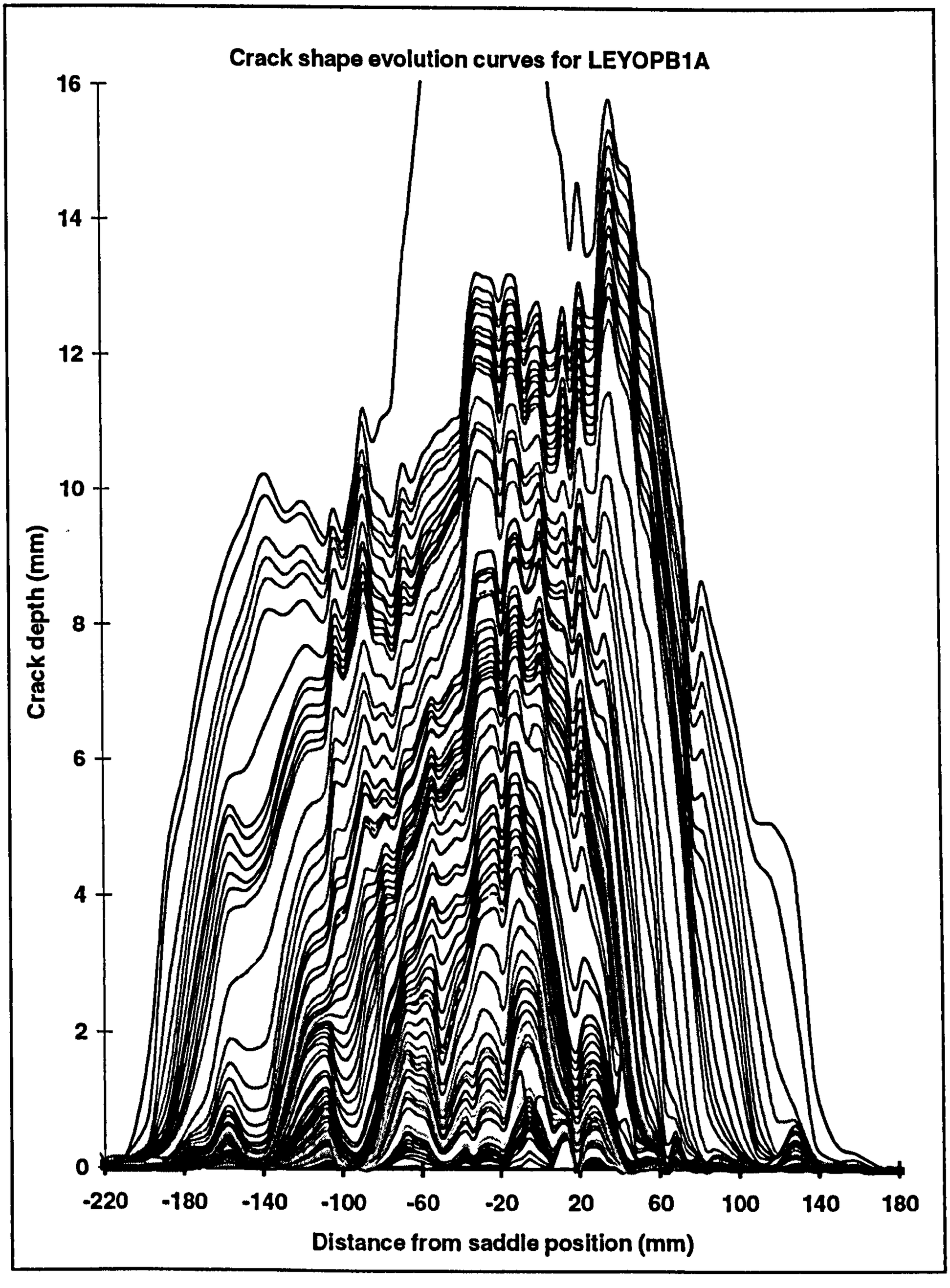

Figure 3.33: Crack shape evolution curves for LEYOPB1A

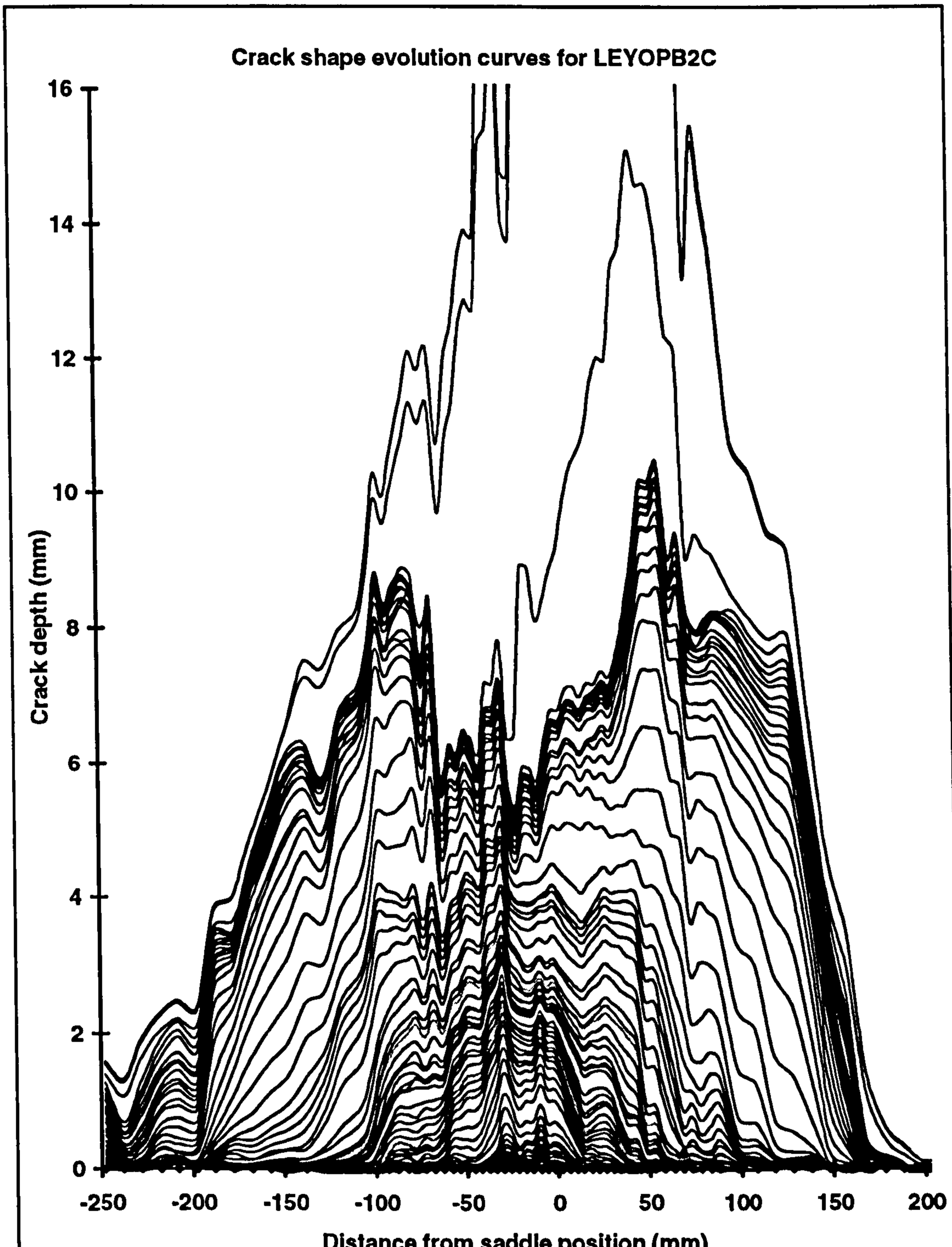

Figure 3.34: Crack shape evolution curves for LEYOPB2C

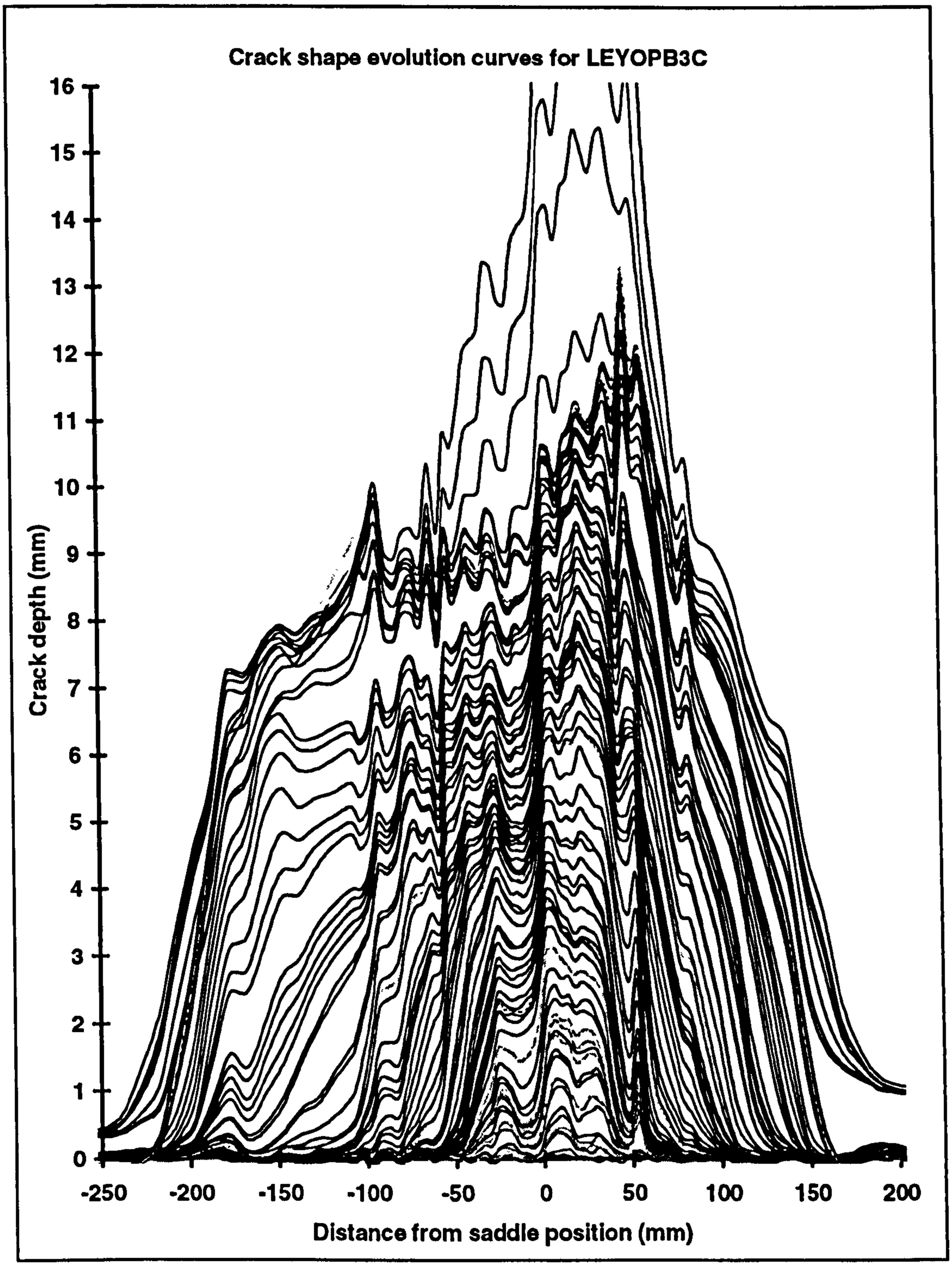

Figure 3.35: Crack shape evolution curves for LEYOPB3C

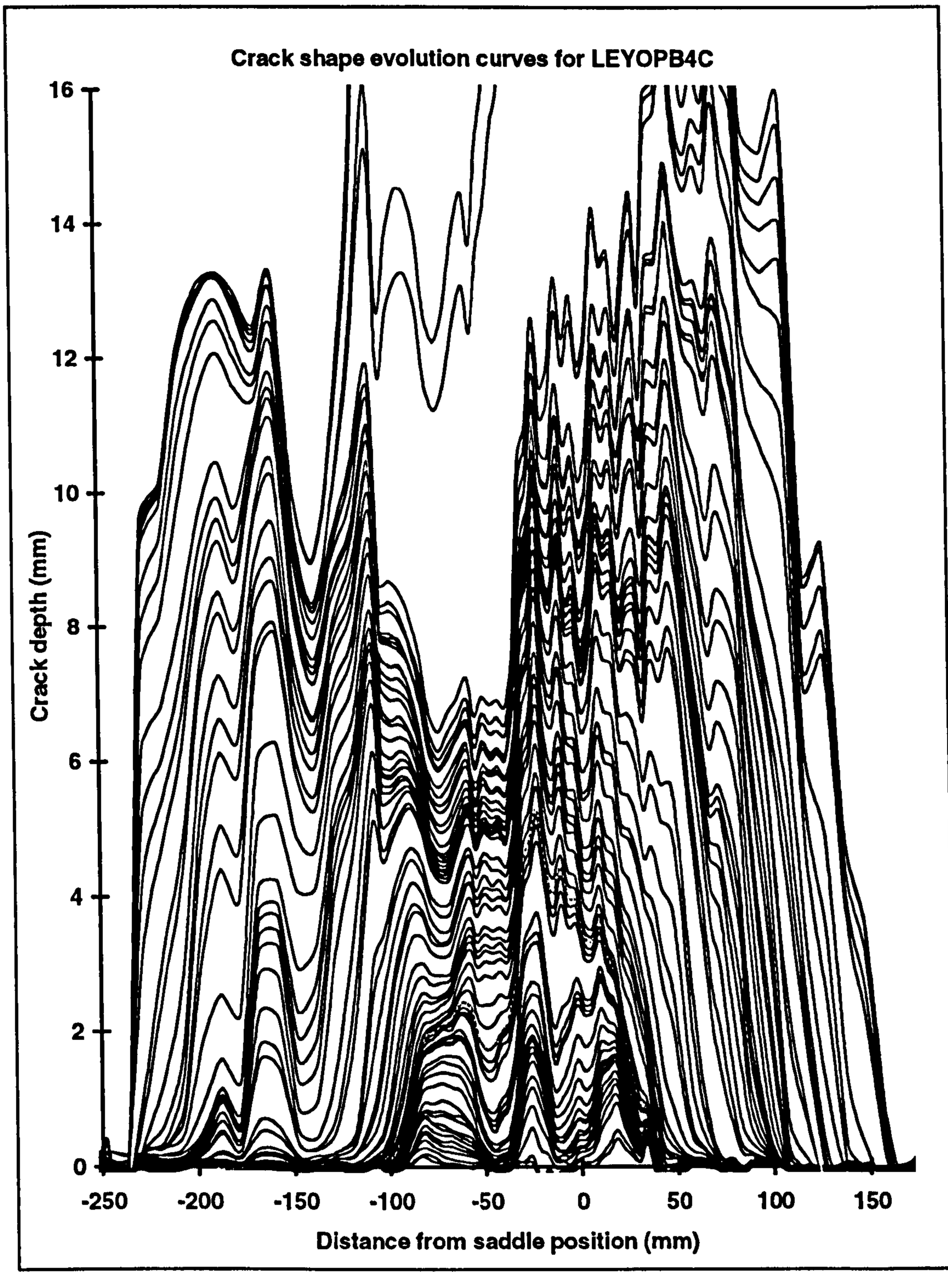

Figure 3.36: Crack shape evolution curves for LEYOPB4C

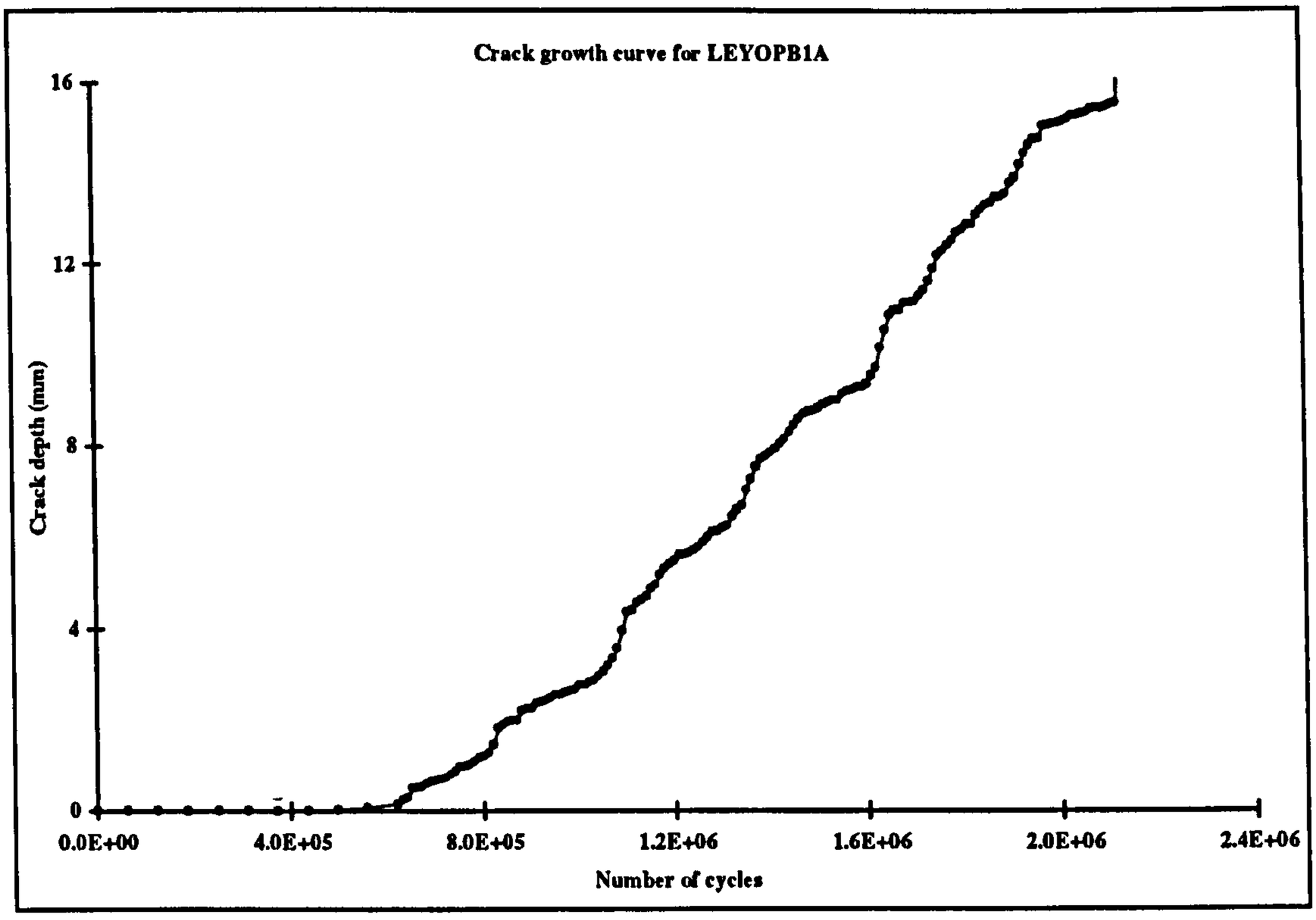

Figure 3.37: Crack growth curve for LEYOPB1A

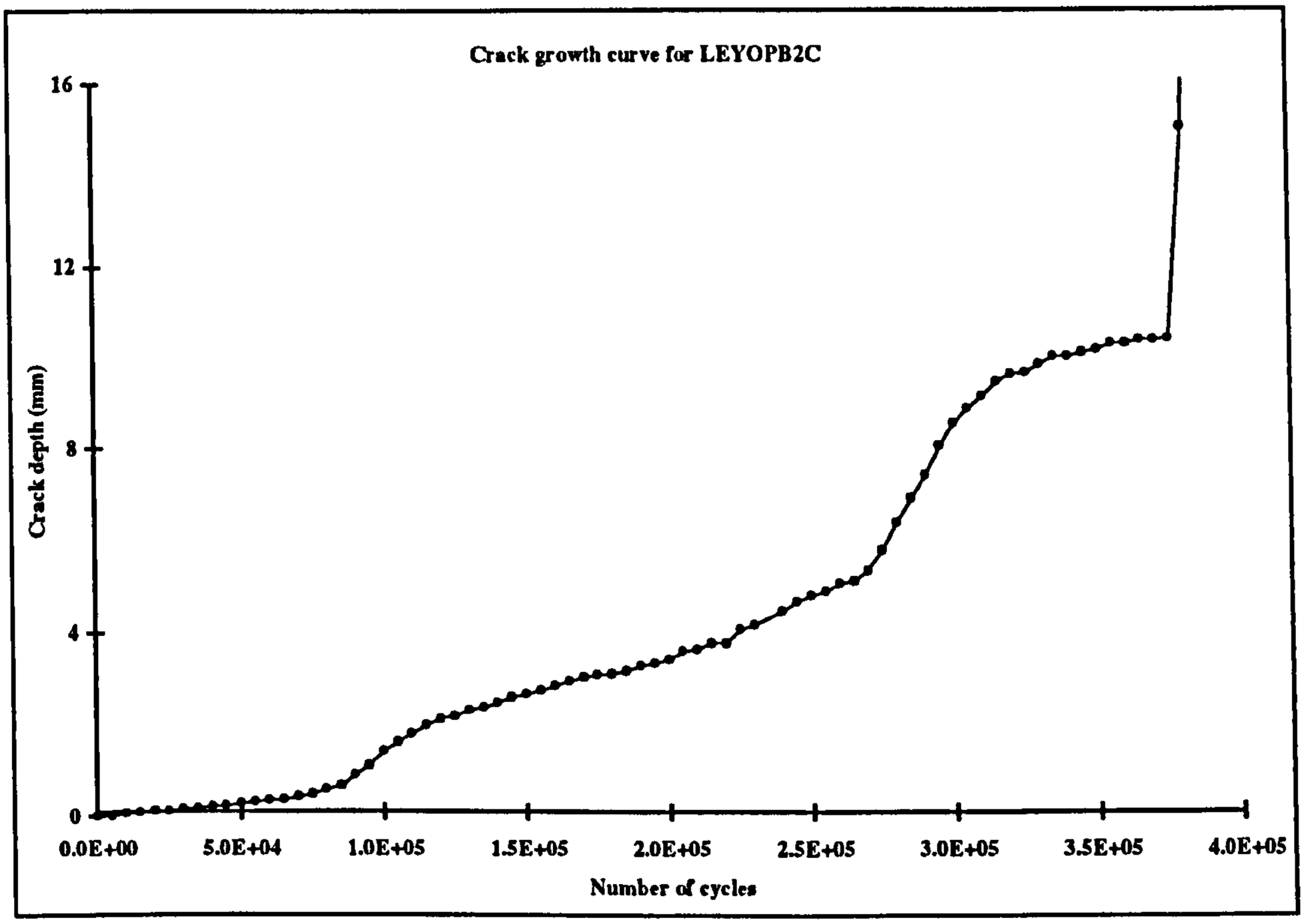

Figure 3.38: Crack growth curve for LEYOPB2C

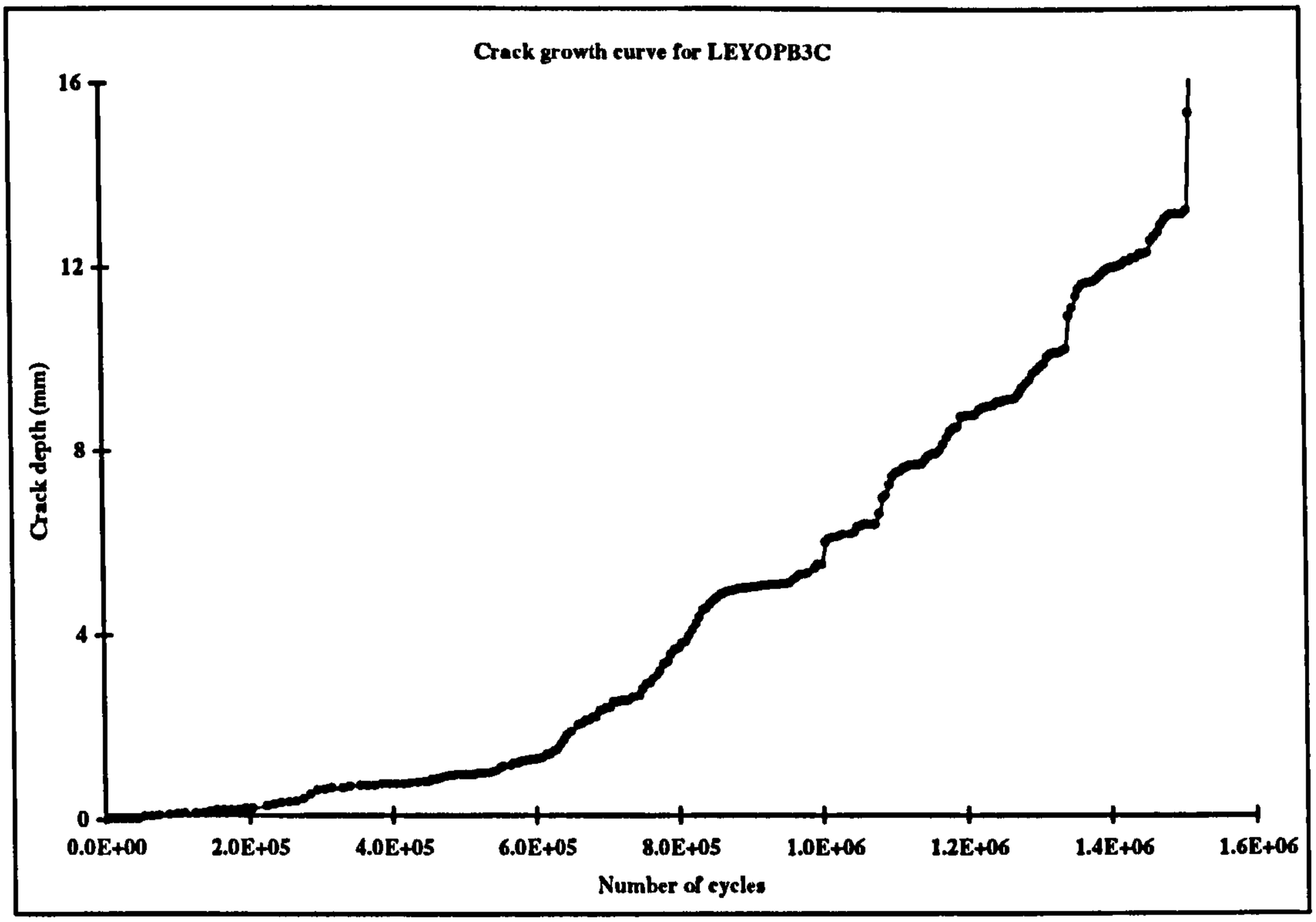

Figure 3.39: Crack growth curve for LEYOPB3C

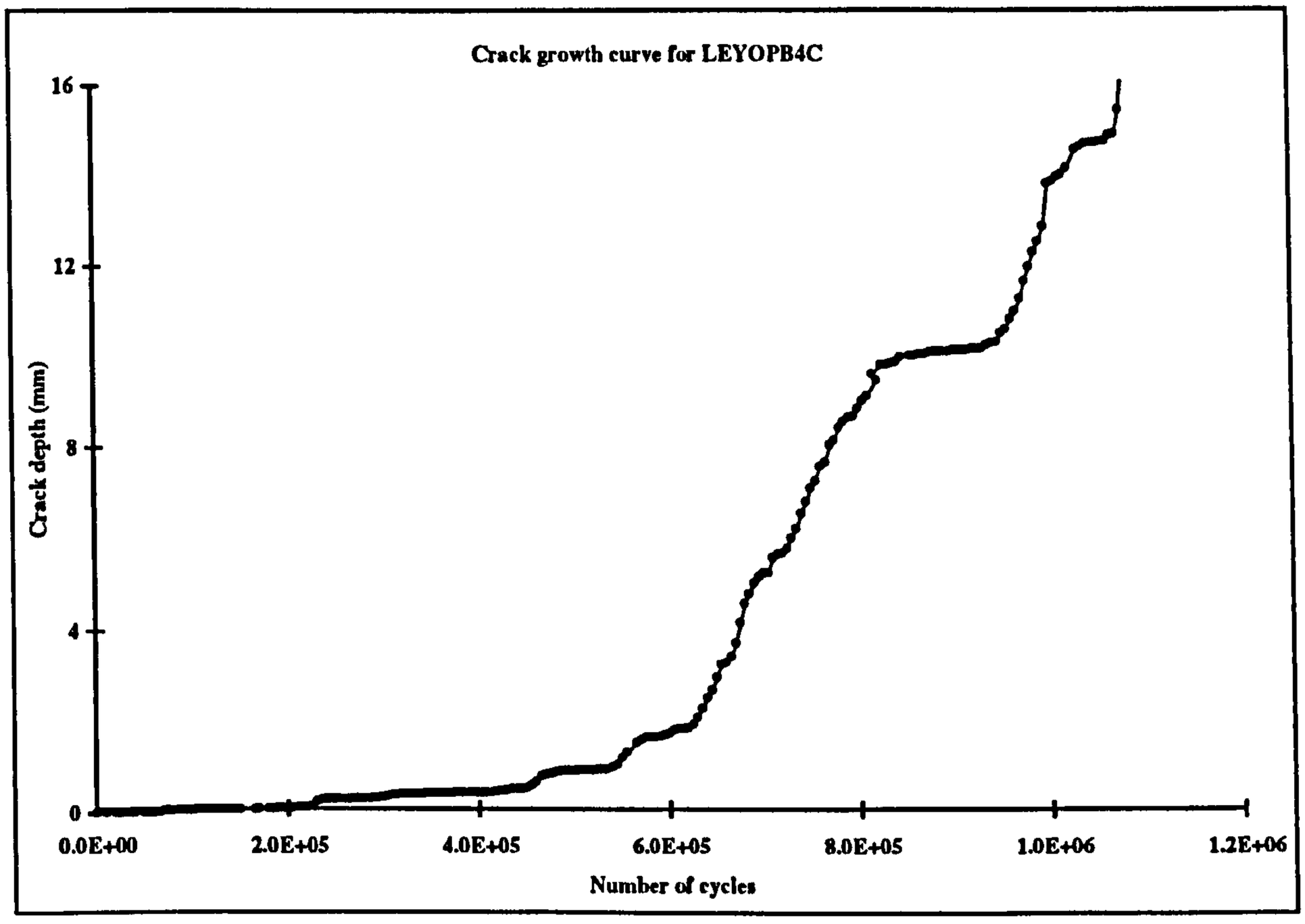

Figure 3.40: Crack growth curve for LEYOPB4C

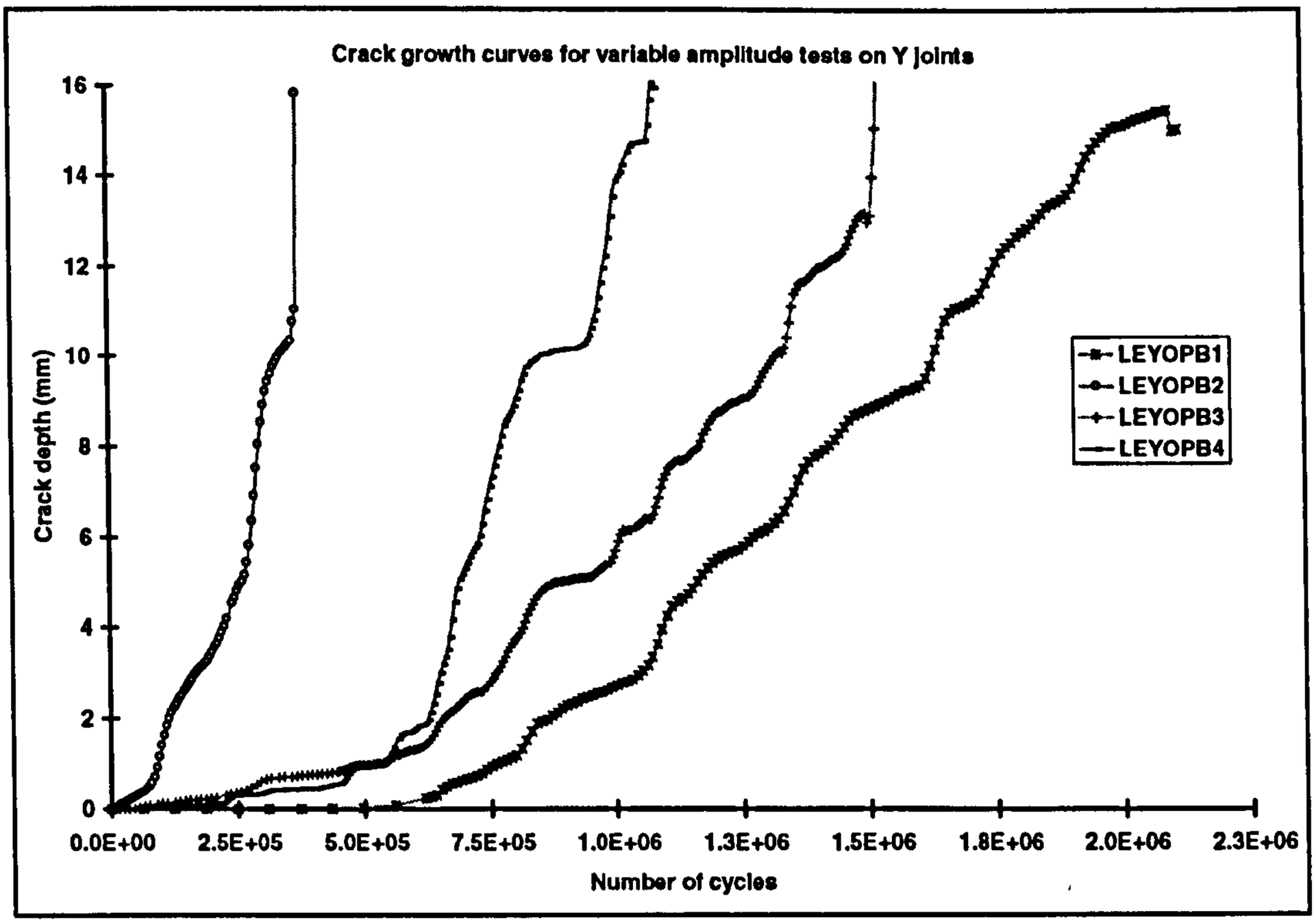

Figure 3.41: Comparison of variable amplitude fatigue crack growth curves

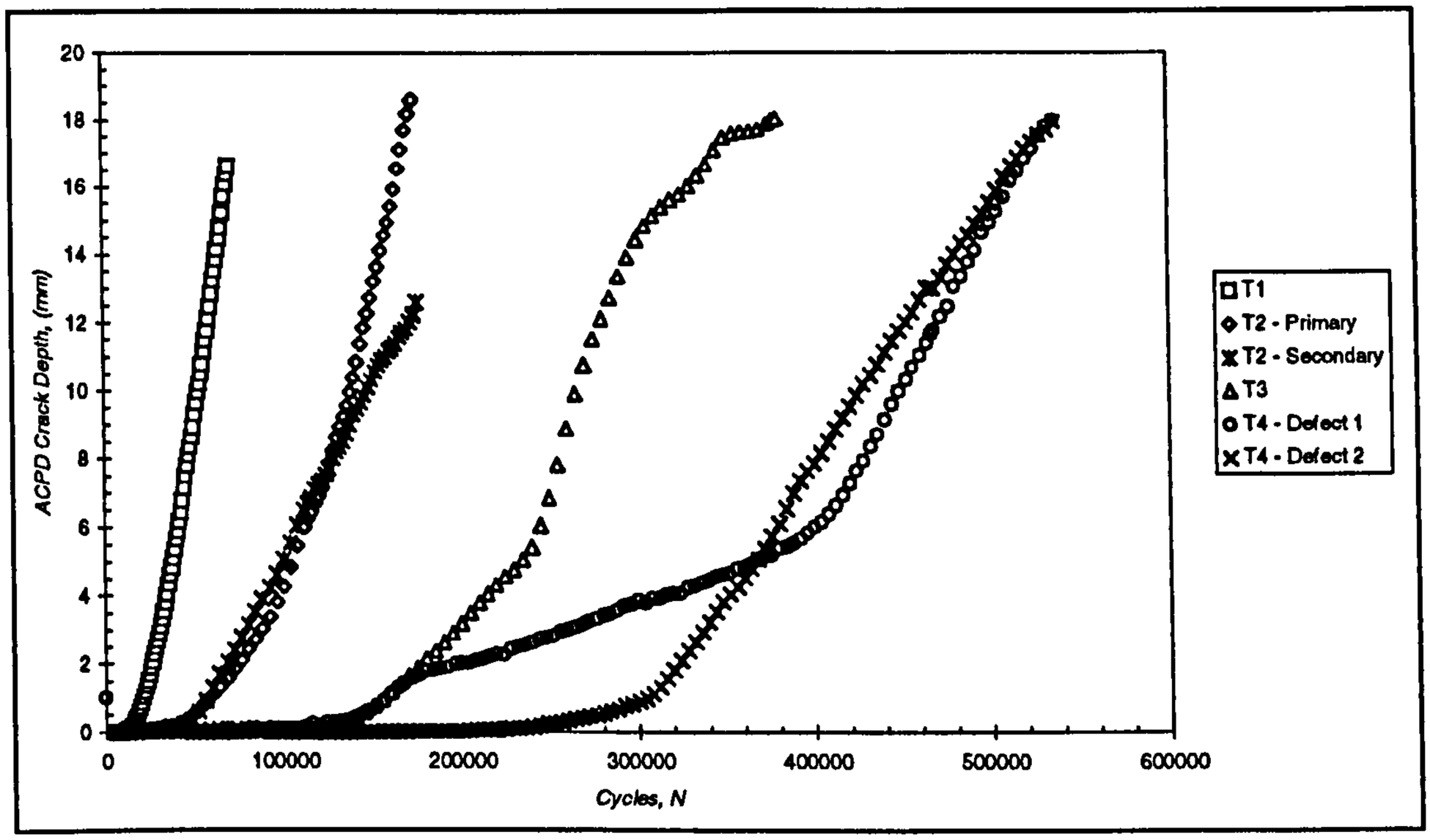

Figure 3.42: Comparison of constant amplitude fatigue crack growth curves

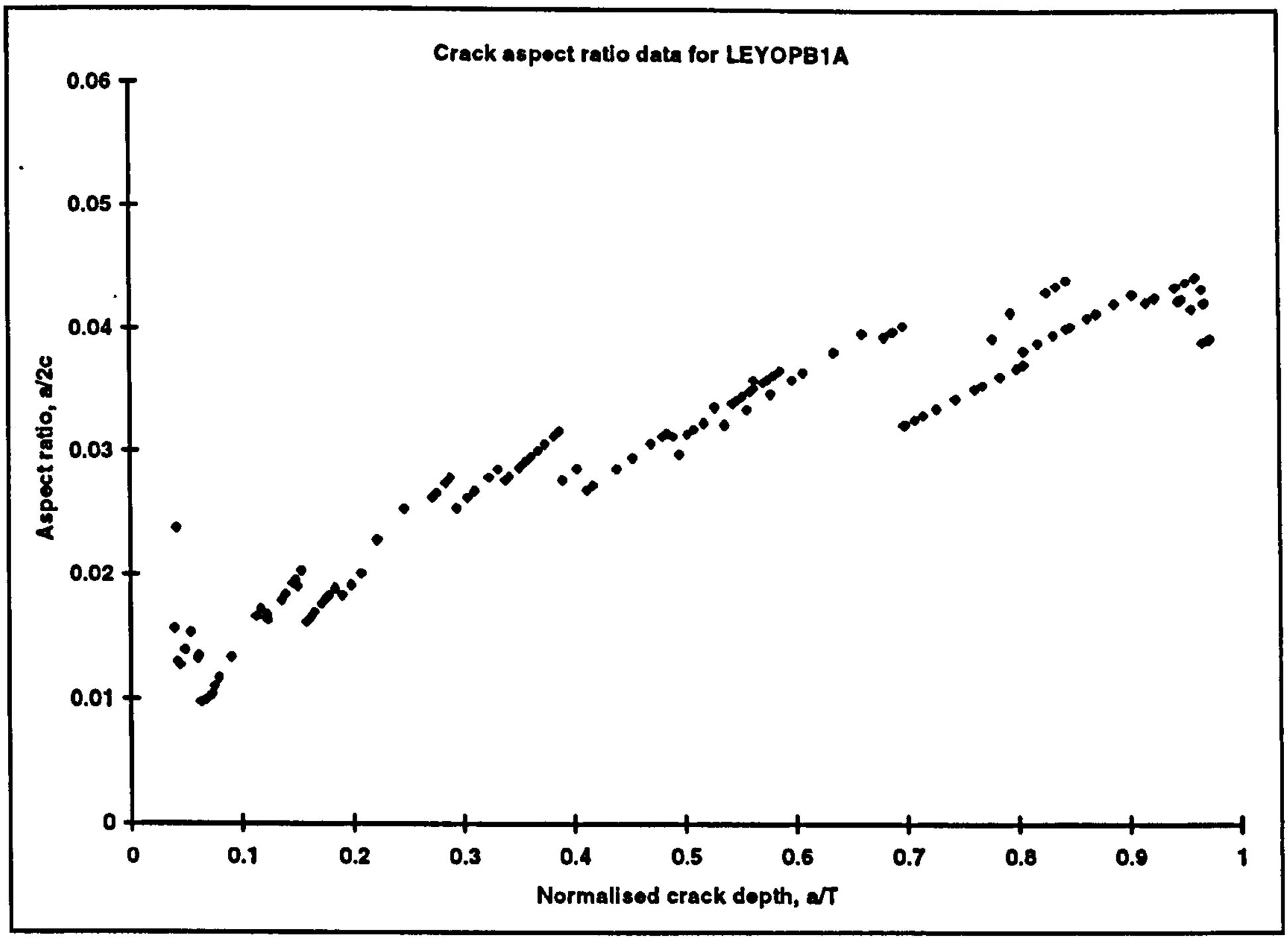

Figure 3.43: Crack aspect ratio data for LEYOPB1A

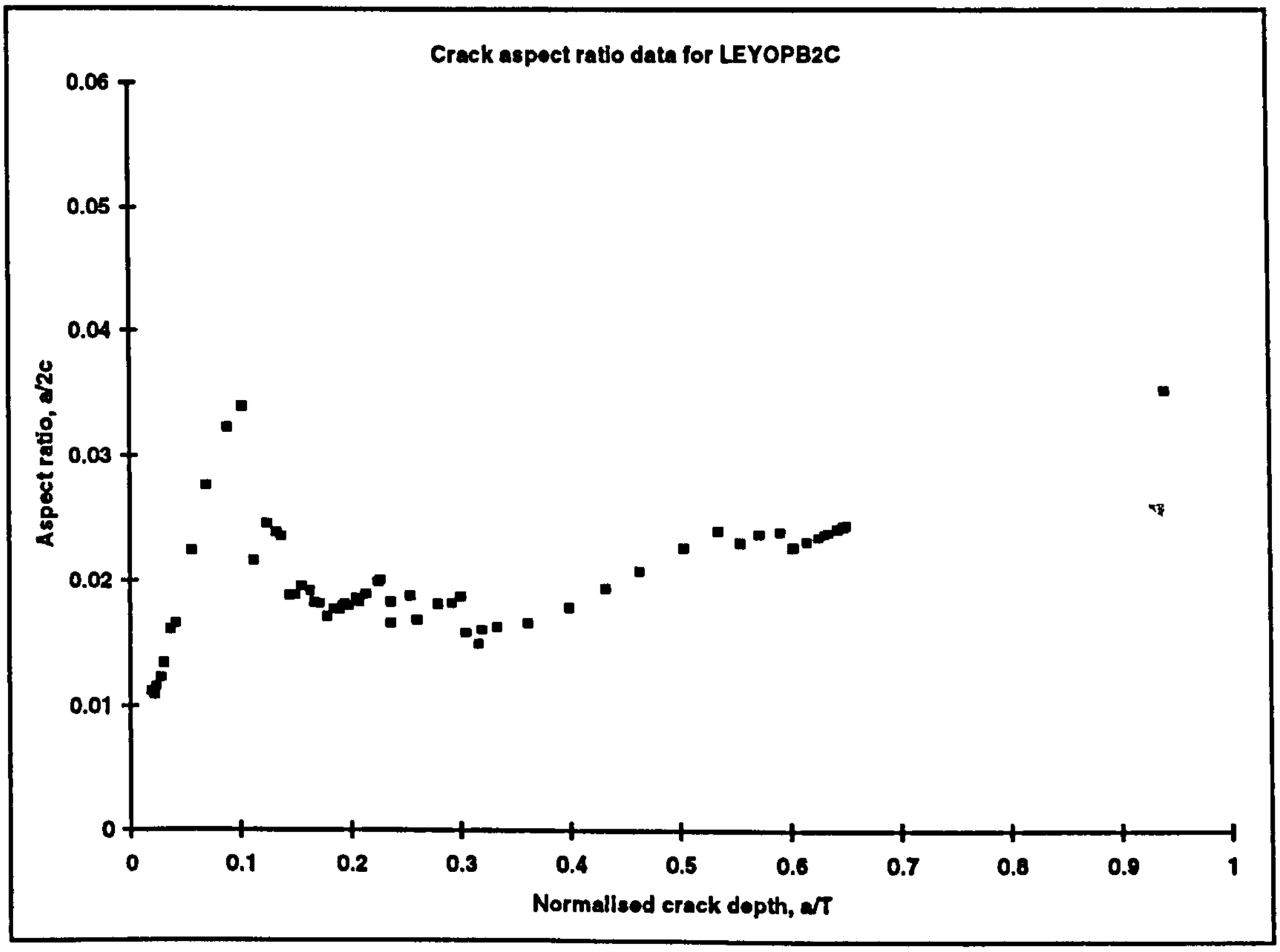

Figure 3.44: Crack aspect ratio data for LEYOPB2C

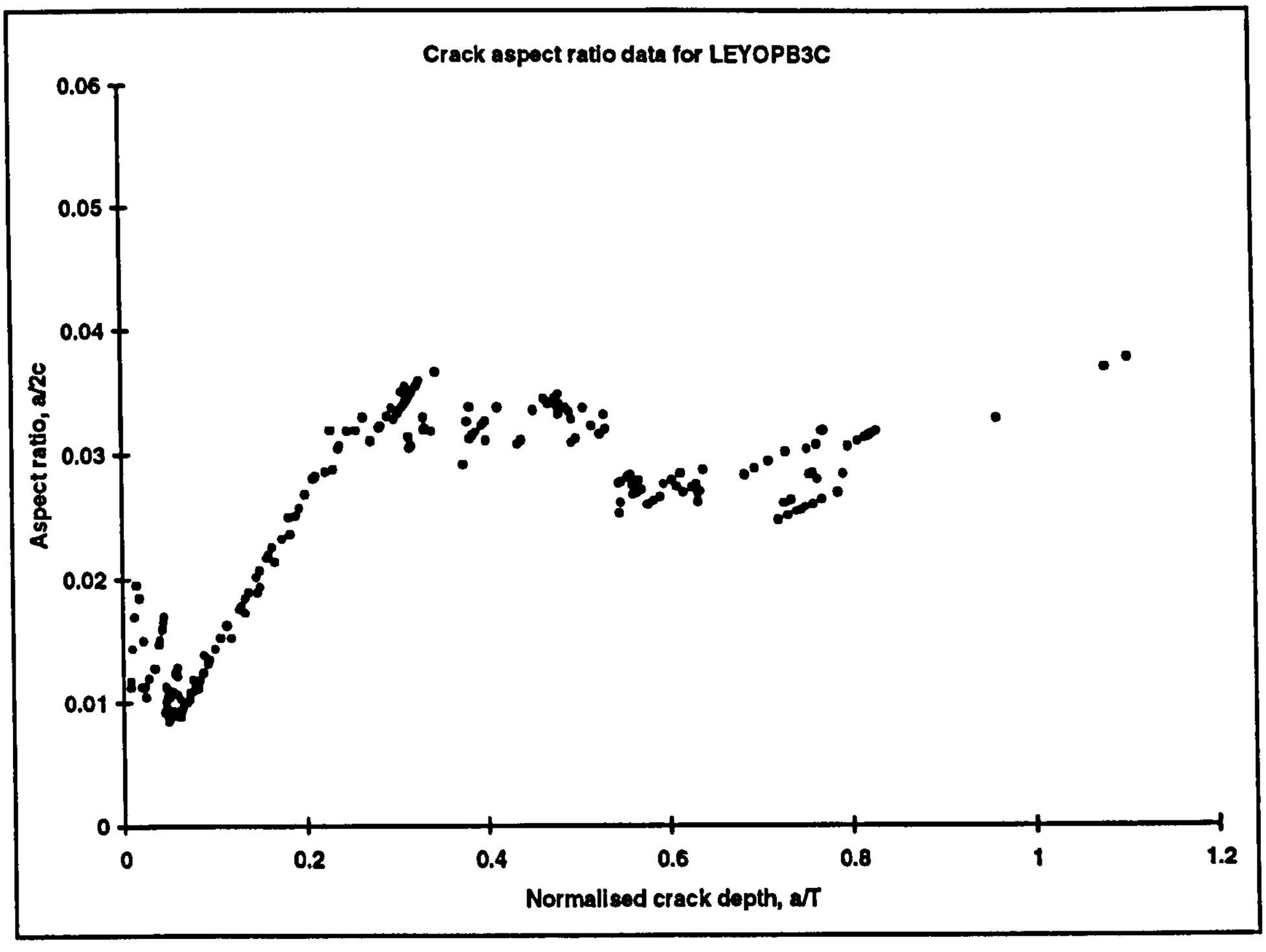

Figure 3.45: Crack aspect ratio data for LEYOPB3C

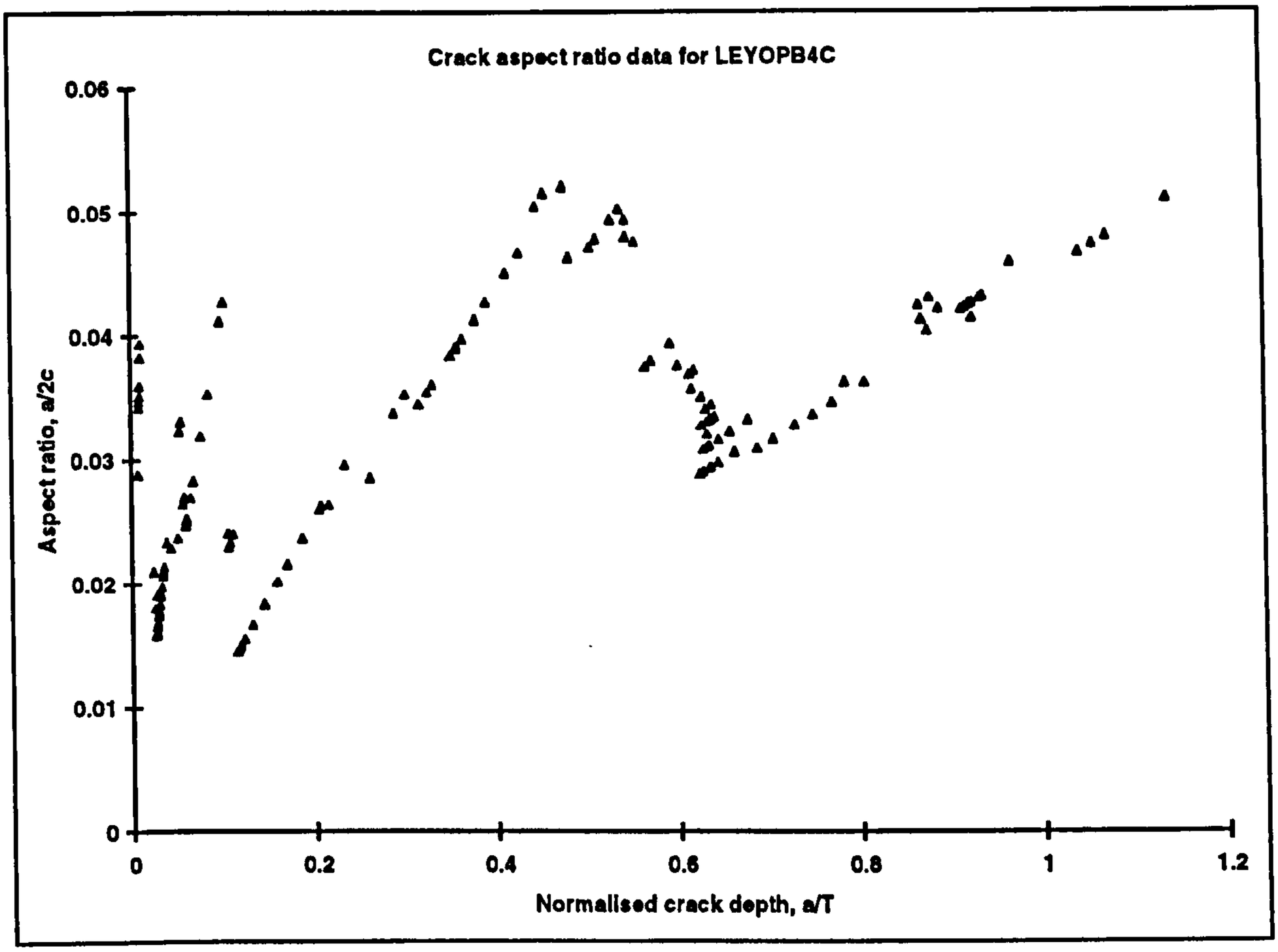

Figure 3.46: Crack aspect ratio data for LEYOPB4C

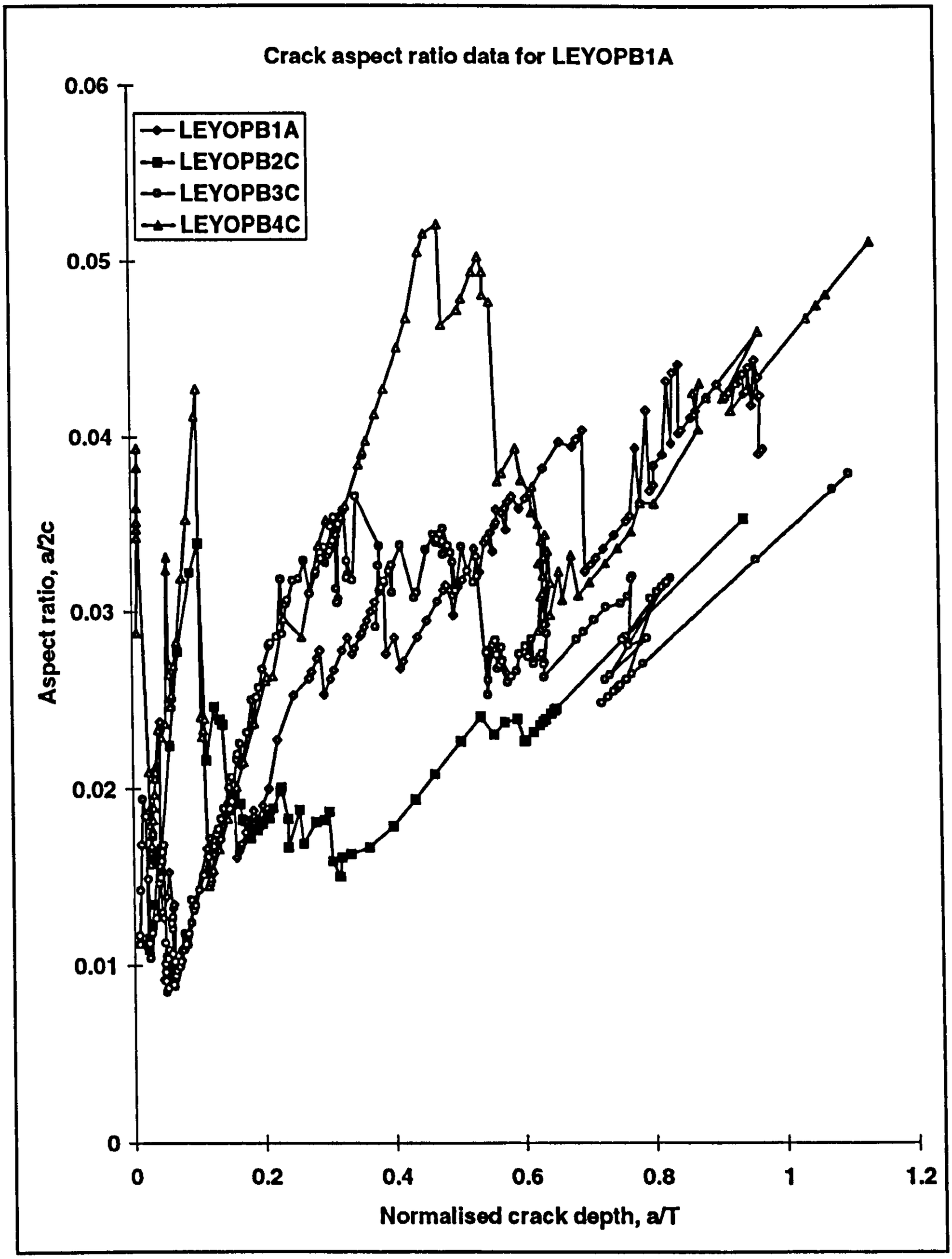

Figure 3.47: Comparison of crack aspect ratio data for Y-joint tests

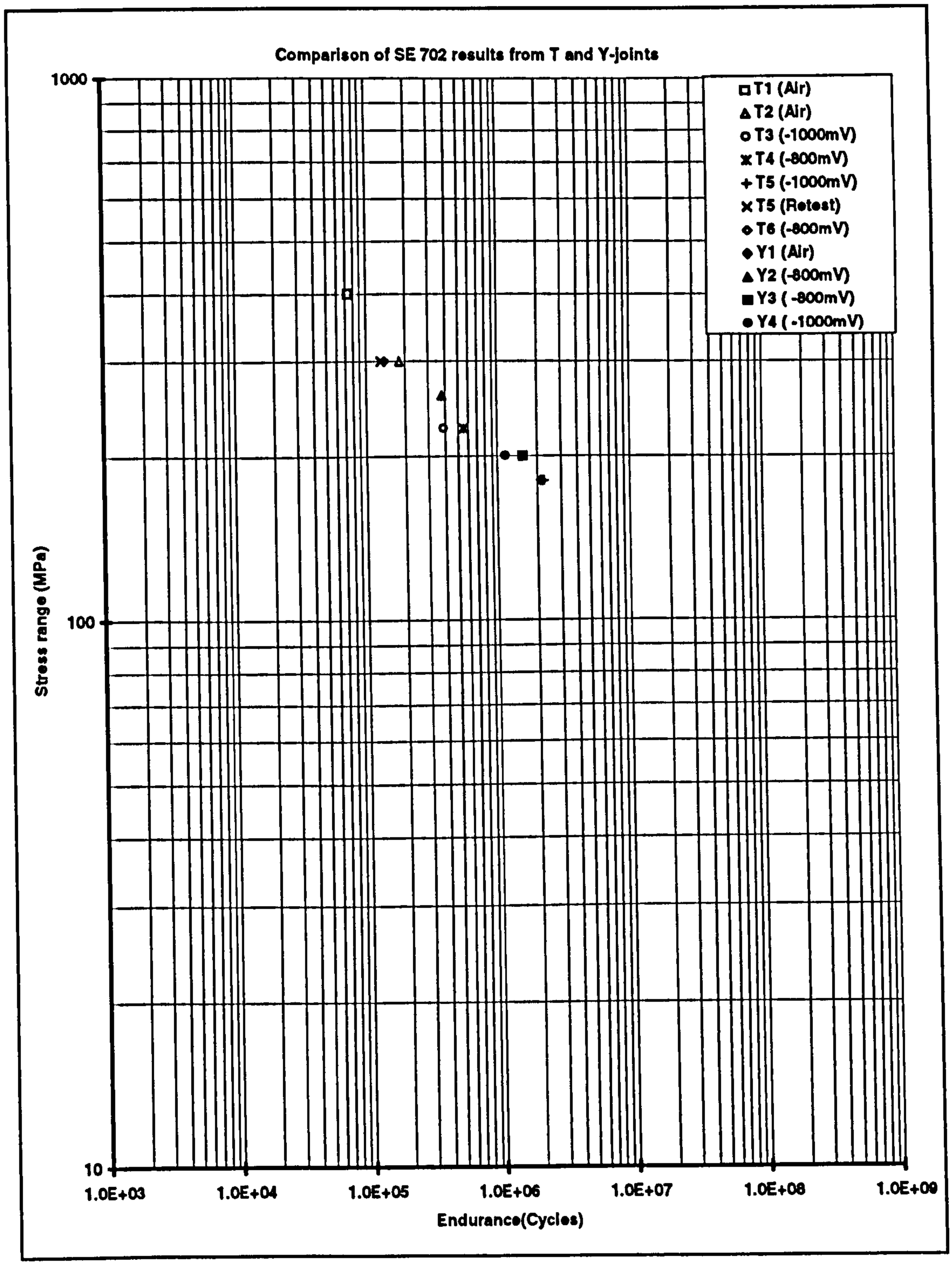

Figure 3.48: Y-joint fatigue endurance data

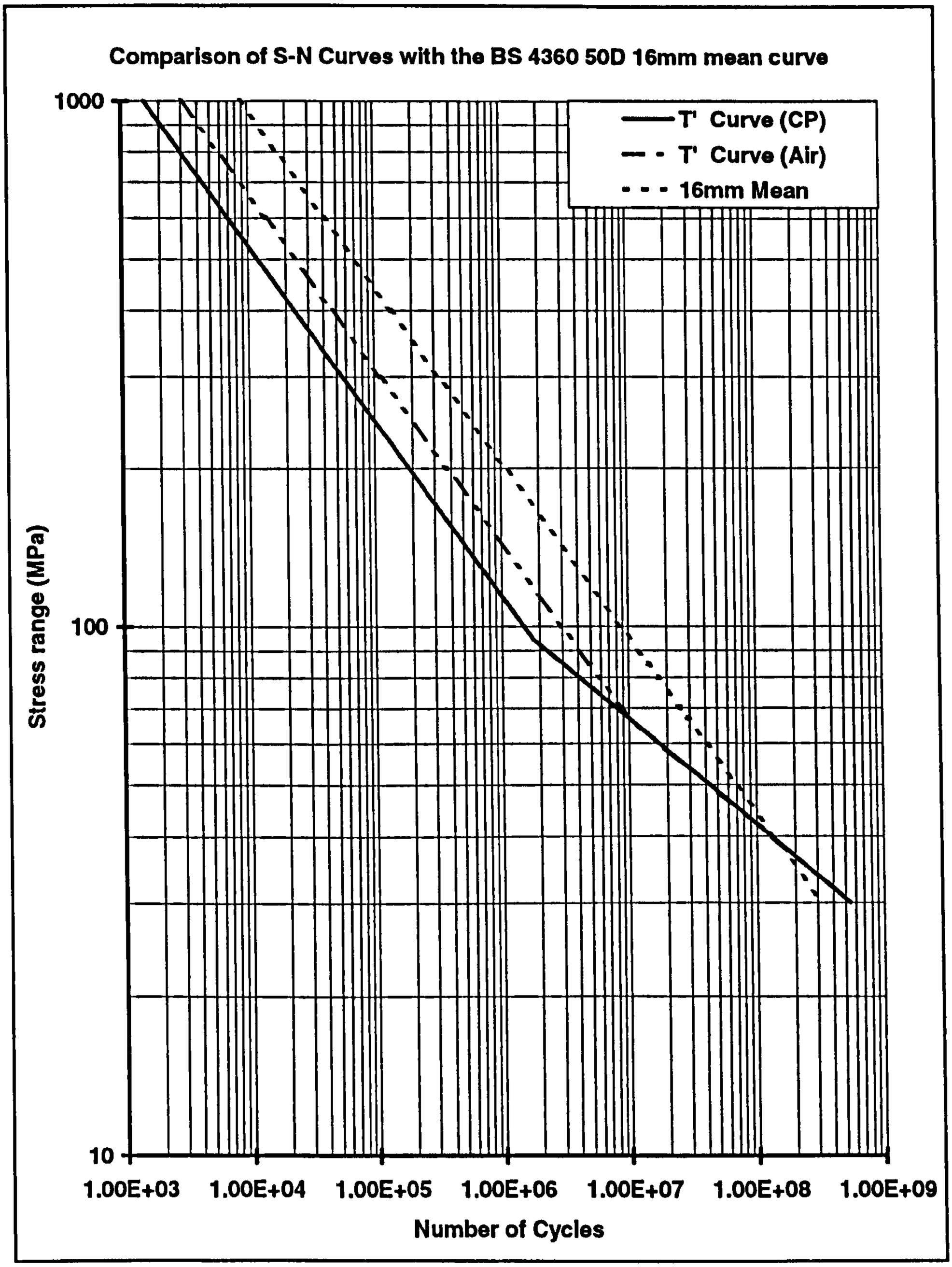

Figure 3.49: S-N curves used for the comparison of results

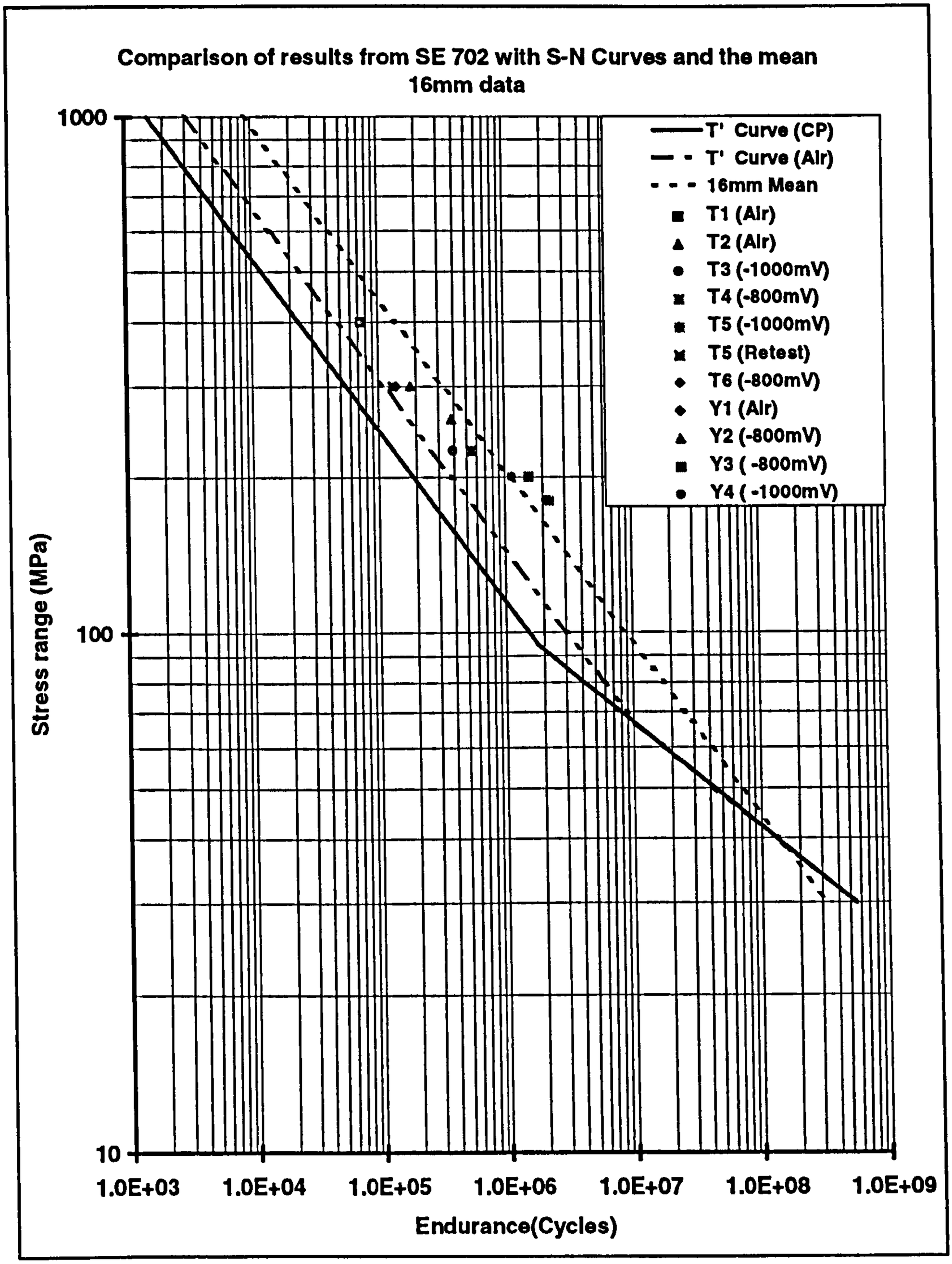

Figure 3.50: Comparison of SE 702 data with design S-N curves

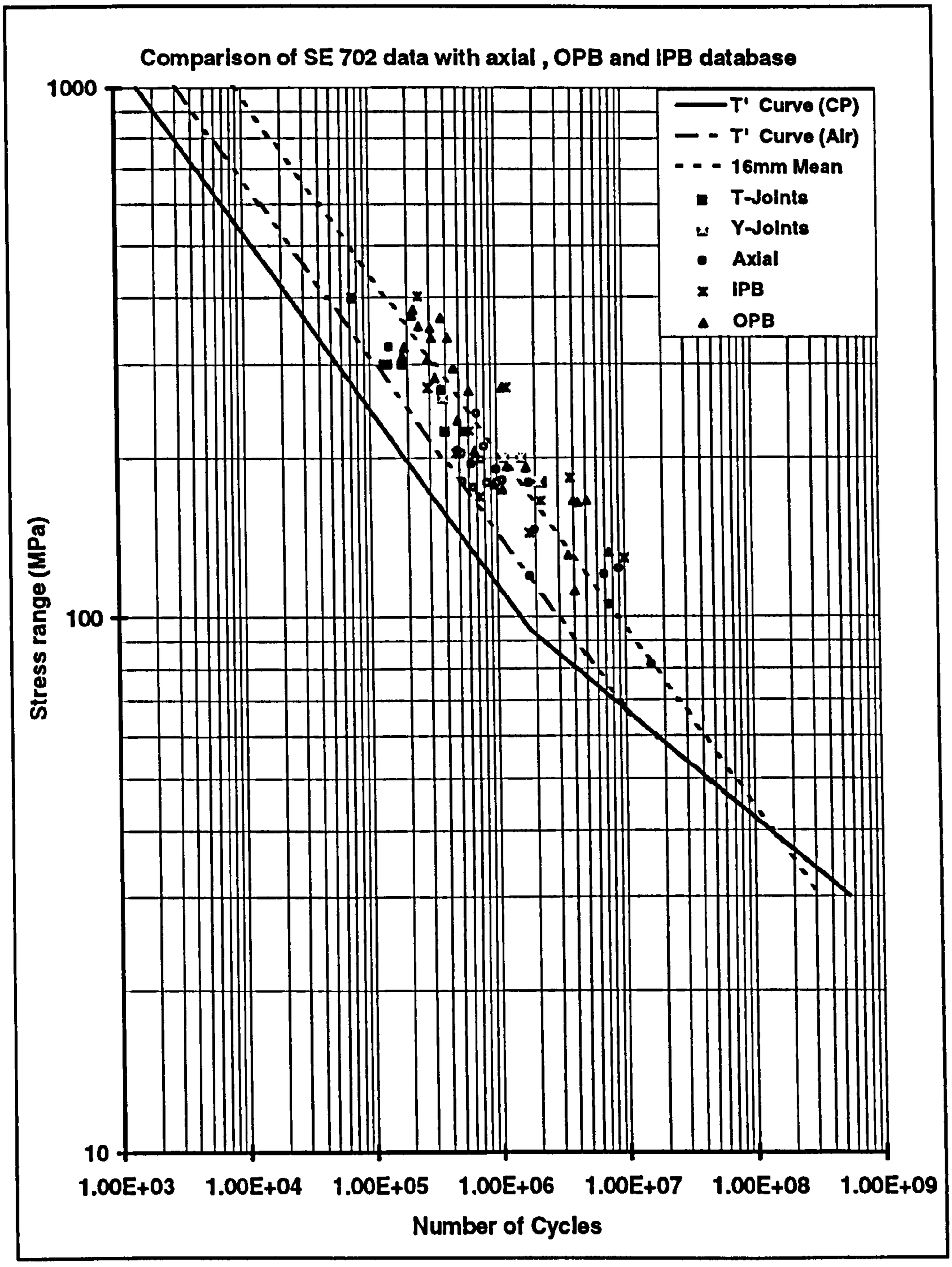

Figure 3.51: Effect of loading mode on S-N data

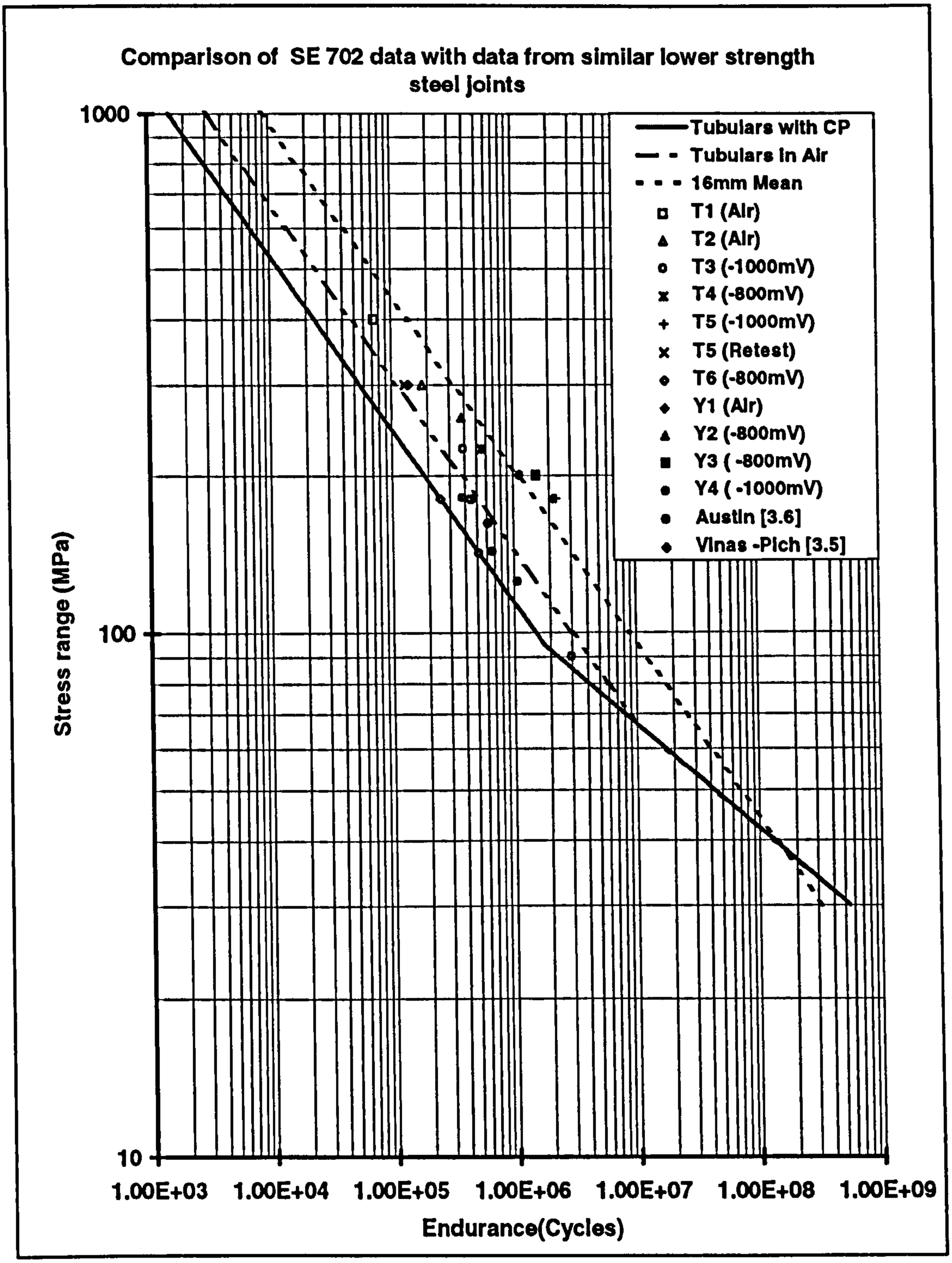

Figure 3.52: Comparison of SE 702 with lower strength steels (same geometry)

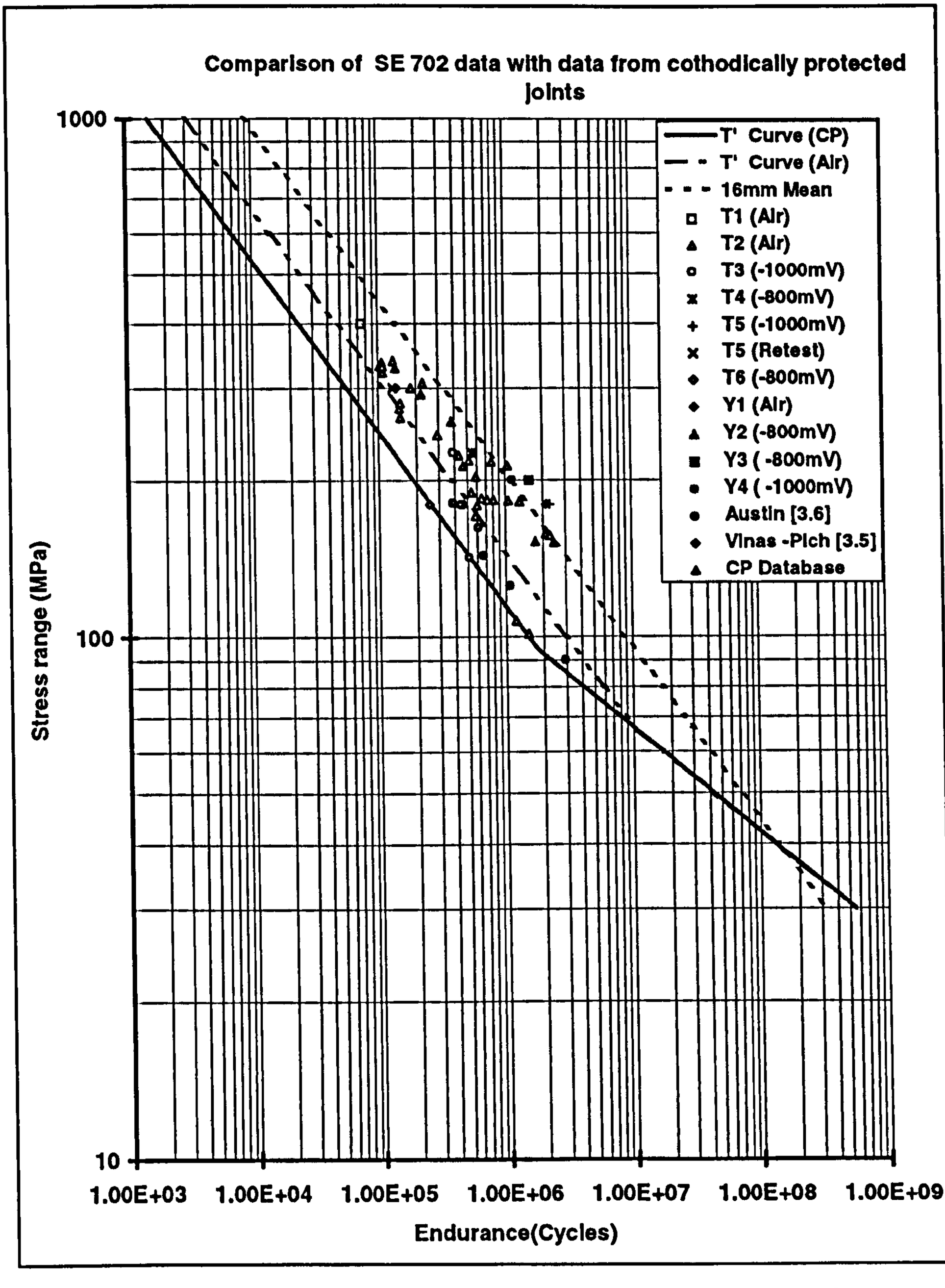

Figure 3.53: Comparison of SE 702 data with data from a database of protected joints

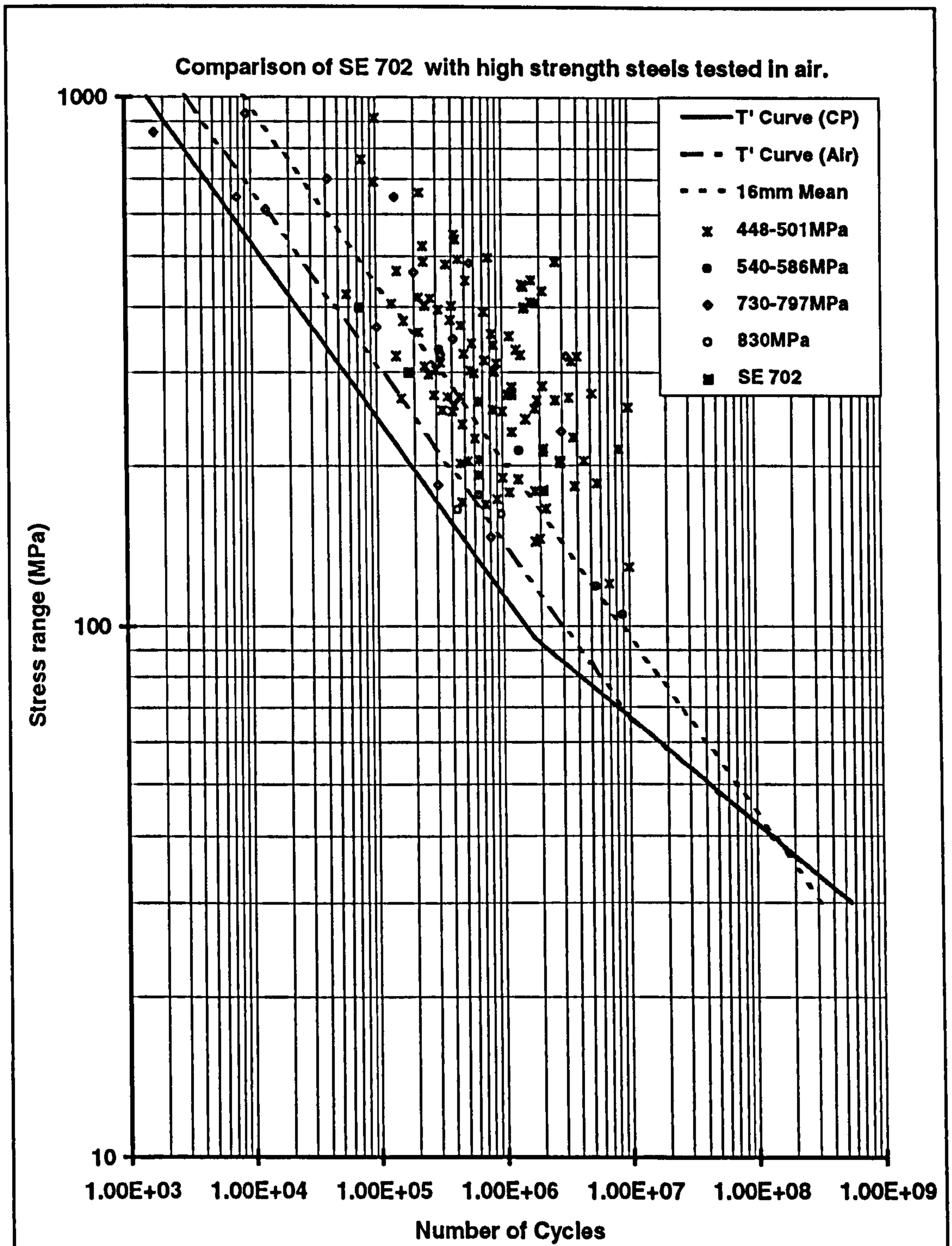

Figure 3.54: SE 702 compared with other high strength steels tested in air

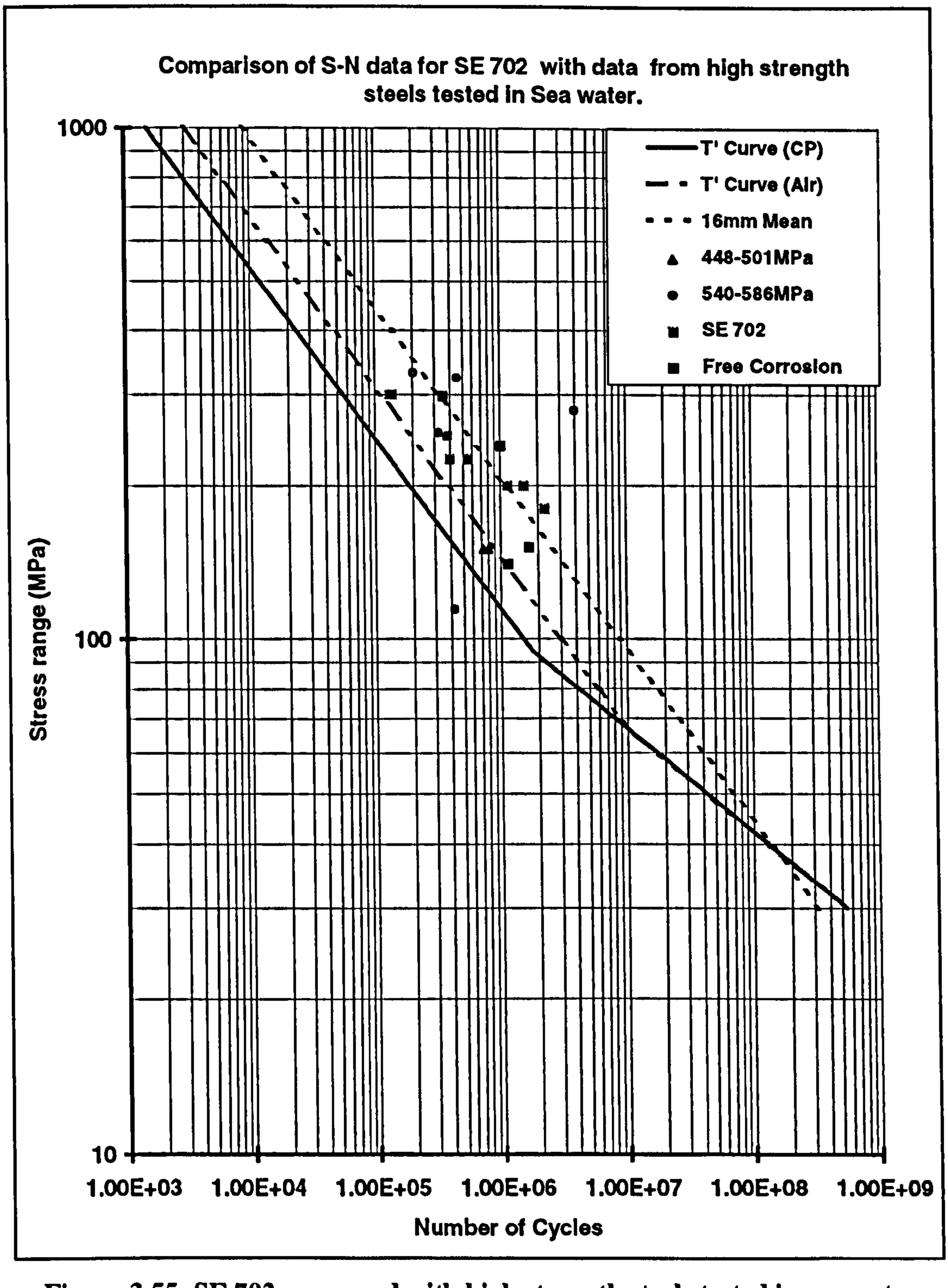

Figure 3.55: SE 702 compared with high strength steels tested in sea water

CHAPTER 4

4. FRACTURE MECHANICS ANALYSIS OF RESULTS

4.1 INTRODUCTION

The S-N approach has been used extensively to design welded Offshore tubular joints and other welded connections for Offshore applications. However the S-N approach can not be used in assessing the structural integrity of cracked tubular joints in service. In this regard fracture mechanics is used and at present, it is the most powerful and useful technological tool available for describing and solving fatigue crack problems.

The practical use of fracture mechanics has been established for use on large turbine and electric generator rotor components, the atomic power generation and the aircraft industry. Application areas in the Offshore industry have also been identified [4.1, 4.2, 4.3] and this is highlighted in this Chapter. Fracture mechanics is currently used at the design stage of Offshore facilities. It provides the basis for fatigue life prediction, steel selection and tolerance setting on allowable weld imperfections. Fracture mechanics is also used during the operational stage of a structure to make important decisions on inspection scheduling and repair strategies. It is also used as a tool for establishing limits on operational conditions.

Some of the existing fracture mechanics models used in the prediction of fatigue crack growth in Offshore welded tubular joints are presented in this Chapter. These models include empirical and semi-empirical models, adapted flat plate solutions and those based on results obtained from finite element analysis. The accuracy of these models in the prediction of fatigue crack growth in welded tubular joints is assessed by comparing the results obtained by using each of the models presented with experimental results. Emphasis is placed on the effect of service loading and a consideration of sequence effects on the accuracy of existing models when used for fatigue crack growth prediction in Offshore structures.

4.2 THE CONCEPT OF STRESS INTENSITY FACTOR

Irwin is one of the many researchers who has made a great deal of contribution to the development of fracture mechanics concepts. He extended Griffith's [4.4] theory

(*crack propagation will occur if the change in elastic strain energy due to crack extension is larger than the energy required to create new crack surfaces*) for ductile materials [4.5] and postulated that energy due to plastic deformation should be taken into account in evaluating the energy associated with the creation of a new crack surface. He also defined a quantity, G, the strain energy release rate or "crack driving force", which is the total energy absorbed during cracking per unit increase in crack length and per unit thickness.

Perhaps his most significant contribution came in the mid 1950s [4.6], when he showed that the local stresses near the crack tip can be expressed in the form;

$$\sigma_{ij} = \frac{K}{\sqrt{2\pi r}} f_{ij}(\theta) + \ldots \tag{4.1}$$

Where r and θ are the cylindrical co-ordinates of a point with respect to the crack tip. Based on the philosophy of the "crack driving force" and the crack tip stresses, Irwin [4.7] proposed the following expression for the stress intensity factor (SIF) for an embedded elliptical crack in a uniform tensile stress field (figure 4.1) after accounting for the flaw shape.

$$K = \frac{\sigma\sqrt{\pi a}}{\Phi}\left(\sin^2\phi + \frac{a^2}{c^2}\cos^2\phi\right)^{\frac{1}{4}} \tag{4.2}$$

Where the crack dimensions are described by a for crack depth and c for crack surface length and ϕ is the angle of orientation. The elliptical integral, Φ, is given by;

$$\Phi = \int_0^{\frac{\pi}{2}}\left(1 - \frac{c^2 - a^2}{c^2}\sin^2\phi\right)^{\frac{1}{2}} d\phi \tag{4.3}$$

In general the mode I stress intensity factor for a centre crack of length $2a$ in an infinite plate subjected to a uniform stress field, σ, (figure 4.2) is given by;

$$K = \sigma\sqrt{\pi a} \tag{4.4}$$

Equation 4.3 gives the stress intensity factor in the absence of all boundaries of a form applicable to the mode of loading and specimen geometry. Cracks in welded tubular

joints are usually in a complex stress field which is different from the case of a uniform stress field in an infinite plate. SIF solutions for cracks in tubular welded joints must therefore include various correction functions to account for boundary effects due to loading and specimen and crack geometries, such that the SIF is given by;

$$K = Y\sigma\sqrt{\pi a} \tag{4.5}$$

Where Y is the stress intensity factor correction function with a general recommended [4.8] form given by;

$$Y = Y_s Y_w Y_e Y_g Y_k Y_m \tag{4.6}$$

where Y_s = Correction for a free front surface

Y_w = Correction for finite plate width

Y_e = Correction for crack geometry

Y_g = Correction for non-uniform stress field

Y_k = Correction for the presence of geometrical discontinuity

Y_m = Correction for changes in structural restraint

Over the years, different analysis methods have been used to determine the Y factors for cracked tubular welded joints. This has led to the development of several SIF solutions for semi-elliptical surface cracks. Some of these are semi-empirical and empirical solutions obtained from experimental results and those based on finite element analysis results.

4.3 EXPERIMENTAL RESULTS

Calculation of experimental stress intensity factors can be carried out using experimental crack growth data. With the increasing accuracy in the measurement of experimental fatigue crack growth rates using data from ACPD crack depth measurements, it is possible to determine experimental stress intensity Y factors with reasonable accuracy. This method has been used in the past to develop empirical Y factor models.

Fatigue crack growth data presented in Chapter 3 has been used to determine experimental Y factors. These experimental values are used as a benchmark for comparing the accuracy of other models presented in this Chapter. The procedure adopted in determining the experimental Y factors is presented here.

The determination of experimental Y factor relies on the use of a suitable crack growth law such as Paris law;

$$\frac{da}{dN} = C(\Delta K)^m \tag{4.7}$$

$$C = 2.72 \times 10^{-12},\ m = 3.532 \text{ and } \Delta K = Y\Delta S\sqrt{\pi a}$$

Where a is the crack size, ΔK is the stress intensity factor range and ΔS is the hot spot stress range. By assuming that Paris law applies, experimental Y factors may be obtained from;

$$Y = \left(\frac{1}{\Delta S\sqrt{\pi a}}\right)\left(\frac{\left(\frac{da}{dN}\right)}{\mathrm{C}}\right)^{1/m} \tag{4.8}$$

The experimental crack growth rates obtained from the fatigue test conducted for this study are shown in figures 4.3, 4.4, 4.5 and 4.6 for tests LEYOPB1A, LEYOPB2C, LEYOPB3C and LEYOPB4C respectively. These experimental crack growth rates are similar to those reported in [4.10] for tests conducted on CT specimens. The corresponding experimental Y factor curves obtained for the tests are shown in figures 4.7, 4.8, 4.9 and 4.10 respectively.

The accuracy of the experimental Y factors depend on the Paris law material constants C and m. The C and m values shown above were obtained from compact tension tests performed on parent plate in air by Creusot Loire Industrie (CLI) [4.9]. A summary of the data supplied for both parent plate and the heat affected zone is given in table 4.1.

Table 4.2 shows other values of C and m for free corrosion and for corrosion tests conducted with CP. As shown in table 4.2, the CP levels used in the tests conducted to generate the data are not identical to those used for the large scale tests in this study. Comparing the results from CLI [4.9] with those from tests conducted on the same steel at Cranfield University [4.10] suggests that there is scatter on the C and m values under CP conditions. It is important to note that the accuracy of the experimental Y factors presented depends greatly on the values of C and m used in analysing the experimental results. The data shown in table 4.2 was used for the corrosion tests for comparing experimental results with those predicted using available Y factor models.

4.4 USE OF EMPIRICAL SIF SOLUTIONS

Empirical models were developed for rapid and accurate analysis of crack growth data. Some of these models have gained wide acceptance and have been successfully used for fast assessment of crack growth in tubular welded joints. These models which include the two phase, the average stress and the modified average stress models are presented here and their performance is compared with experimental results.

4.4.1 Equations of Dover et al

Irwin's infinite plate solution given by equation 4.2 predicts that the stress intensity factor at the deepest point for a semi-elliptical crack is always greater than that at the surface. However it has been observed experimentally that, crack growth on the surface may be higher than crack growth at the root as the crack aspect ratio changes. It was therefore necessary to derive correction for the finite dimension effects on the surface cracks in a semi-infinite body.

Holdbrook and Dover [4.11] carried out a series of fatigue tests on flat plate specimens of finite dimension containing semi-elliptical cracks in a tensile stress field.

This led to the development of equations which accounted for effects arising from, finite cross section area, finite second moment of area, load eccentricity and any changes in the position of the neutral axis. These equations were found to provide good correlation with crack growth data for surface cracks in plates.

Dover and Dharmavasan [4.12] extended their work to tubular joints using an experimentally based method for the determination of stress intensity factors of cracks in tubular joints. The approach adopted was based on a stress intensity factor expression of the form;

$$\Delta K = Y \Delta S_{HS} \sqrt{\pi a} \tag{4.9}$$

Where Y is the stress intensity correction factor and ΔS_{HS} is the hot-spot stress range.

The correction factor was obtained using the approach outlined in section 4.3. The values of the correction factor were obtained for various tubular joint tests. Five Y, T and K joints were used for this study and based on the results obtained, the following equation was recommended for deriving stress intensity factor correction factors for tubular joints.

$$Y = (1.18 - 0.32S)T^{(0.13-0.02S)}\left(\frac{T}{a}\right)^{(0.24+0.06S)} \tag{4.10}$$

S is a non dimensional factor which is taken as the ratio of the average stress concentration factor, SCF_{av}, to the hot spot stress concentration factor, SCF_{HS}, at any location of the joint intersection. It is given by;

$$S = \frac{SCF_{av}}{SCF_{HS}} \tag{4.11}$$

$$SCF_{av} = \frac{1}{\pi}\int_0^{\pi} SCF(\phi)d\phi \quad (\textit{for axial loading and OPB})$$

$$SCF_{av} = \frac{1}{\pi}\int_{-\frac{\pi}{2}}^{\frac{\pi}{2}} SCF(\phi)d\phi \quad (\textit{for IPB})$$

This set of equations assumed that the stress intensity factor only depends on one dimension of the crack and the average stress concentration factor was taken over the entire joint intersection instead of over the instantaneous crack length. This made the predictions of stress intensity correction factors using these equations not to be as accurate as desired. In a later investigation by Dover and Connolly good predictions were obtained for crack shape development in plates subjected to bending loads. Other more accurate models have since been developed by Dover et al to predict the Y factor. The more recent models are the average stress model [4.12], the modified average stress model [4.13] and the two phase model [4.14, 4.15] which accounts for size effects on the early growth and the propagation phases of crack propagation.

4.4.2 The Average Stress Model

The average stress (AVS) model [4.12] was proposed after testing large scale 16mm tubular joints. This model made use of several stress intensity modification (Y) factors and assumed a thickness correction for joints other than 16mm. The Y factor predicted by this model is given by;

$$Y = A\left(\frac{T}{a}\right)^{j} \tag{4.12}$$

$$A = 0.73 - 0.18S \text{ and } j = 0.24 + 0.06S$$

Where T is the chord wall thickness, a is the crack depth and S is the average stress parameter as previously defined.

This model has been used to predict experimental crack growth rates in tubular welded joints with discrepancies only occurring during early growth where the crack depth is less than 25% of the chord wall thickness. The Y factor predicted by this model is shown in figure 4.11 and compared with experimental results in figure 4.12.

4.4.3 The Two Phase Model (TPM)

The two phase model [4.14] was based on published crack growth data and was developed mainly to consider crack growth affected by joint size. It is given in the form;

$$Y = M_1 B\left(\frac{T}{a}\right)^k \tag{4.13}$$

Where B and k are functions of size and average stress parameter, S, and p is the early crack growth phase controlling parameter. M_1 is taken as 1 for the propagation phase ($a/T > 0.25$) and $\left(\frac{0.25T}{a}\right)^{-p}$ for the early crack growth phase ($a/T < 0.25$).

Where

$$p = 0.231\left(\frac{T}{0.016}\right)^{-1.71} \beta^{0.31} S_{HS}{}^{0.18} \tag{4.14}$$

$$B = (0.669 - 0.1625S)\left(\frac{T}{0.016}\right)^{0.11} \tag{4.15}$$

$$k = (0.353 + 0.057S)\left(\frac{T}{0.016}\right)^{-0.099} \tag{4.16}$$

The early crack growth phase controlling parameter was produced by assuming that early crack growth behaviour can be treated as an extrapolation of the propagation phase modified by an exponentially decaying effect determined by the wall thickness, the diameter ratio and the hot spot stress. It has been argued [4.13] that the thickness correction exponent which determines the value of the early crack growth phase controlling parameter, p, is such that it imposes a very severe dependence of crack growth on thickness. Therefore making this model more sensitive to thickness effects than has been observed experimentally. The predicted Y factor curve obtained using this model is shown in figure 4.13. The accuracy of this model is compared with experimental results in figure 4.14.

4.4.4 The Modified Average Stress Model

The modified average stress model (MAVS) [4.13] is the most recent empirical stress intensity factor solution for cracked tubular welded joints proposed by Austin et al [4.13]. It was proposed after testing large scale 16mm tubular joints. This model was developed by applying a 15% reduction factor to the original AVS model. The reduction factor was based on the assumption that rainflow cycle counting provided a higher degree of correlation with constant amplitude data than range counting on which the original AVS model was based. Austin [4.13] suggested the 15% reduction factor after noting that the equivalent stress determined from rainflow counting were higher than that obtained when simple range counting was used for the representative double peaked spectrum originally used to develop the AVS model. This factor was found to be 1.15. A modification to the AVS model was then proposed based on this difference which required that the Y factor predicted by the AVS model be reduced by 15%. The Y factor predicted by this model is given as;

$$Y = 0.85A\left(\frac{T}{a}\right)^{l} \qquad 4.17$$

All the variables are as defined for the AVS model. The degree of accuracy obtainable from this model depends largely on the accuracy of the original experimental data on which it is based. Under variable amplitude conditions this may equally be affected by the method of cycle counting used and the detail contained in the crack growth data. Figure 4.15 shows the predicted Y factor based on this model. The prediction is compared with experimental data in figure 4.16.

4.5 ADAPTED PLATE SOLUTIONS

Stress intensity factor solutions for plates can not be applied directly to tubular welded joints. This is as a result of the differences in the existing boundary conditions. They are however important in that plate solutions can be used to provide estimates of stress intensity factors for other geometries by applying the appropriate boundary correction functions. For instance flat plate solutions may be used to obtain stress

intensity factors for semi-elliptical cracks in T-plates by introducing a correction function to account for the influence of the weld detail and the attached plate.

Different researchers have used different approaches over the years to model the effect of the weld detail on the flat plate solutions and develop stress intensity factor solutions for welded connections. These range from methods based on weight functions to those based on finite element analysis carried out on welded joints. These approaches fall within three broad categories of methods generally used to determine stress intensity factors. These include classical solutions for idealised geometries, numerical methods and semi-empirical solutions based on a combination of experimental and analytical data. The more widely used of these solutions is that due to Newman Raju.

4.5.1 Newman-Raju SIF Solution for Surface Cracks

Newman and Raju (NR) derived a stress intensity factor solution for a semi-elliptical crack in a flat plate. The proposed solution gave the stress intensity factor for a surface crack of depth, a, and surface length, $2c$, in the form;

$$K_I = Y_{NR}\sqrt{\pi a} \tag{4.18}$$

$$Y_{NR} = \frac{F_m\sigma_m + F_b\sigma_b}{\Phi} \tag{4.19}$$

F_m and F_b are the correction functions for the tension and bending stresses, σ_m and σ_b, respectively. Φ is an elliptical integral approximated by;

$$\Phi = \sqrt{1 + 1.464\left(\frac{a}{c}\right)^{1.65}} \tag{4.20}$$

The correction functions for tension, F_m, and for bending, F_b, are given as;

$$F_m = \left[M_1 + M_2\left(\frac{a}{t}\right)^2 + M_3\left(\frac{a}{t}\right)^4\right]f_w \tag{4.21}$$

$$F_b = \left[1 + G_1\left(\frac{a}{t}\right) + G_2\left(\frac{a}{t}\right)^2\right]\left[M_1 + M_2\left(\frac{a}{t}\right)^2 + M_3\left(\frac{a}{t}\right)^4\right] f_w \qquad (4.22)$$

where

$$G_1 = -1.22 - 0.12\left(\frac{a}{c}\right),\ G_2 = 0.55 - 1.05\left(\frac{a}{c}\right)^{0.75} + 0.47\left(\frac{a}{c}\right)^{1.5}$$

$$M_1 = 1.13 - 0.09\left(\frac{a}{c}\right),\ M_2 = -0.54 + \left(\frac{0.89}{0.2 + \left(\frac{a}{c}\right)}\right)$$

$$M_3 = 0.5 - \left(\frac{1.0}{0.65 + \left(\frac{a}{c}\right)}\right) + 14\left(1.0 - \left(\frac{a}{c}\right)\right)^{24} \text{ and } f_w = \sqrt{\sec\left(\frac{\pi c}{w}\sqrt{\frac{a}{c}}\right)}$$

f_w is the plate width correction function for a plate with a finite width, w. Even though this flat plate solution can not be applied directly to tubular welded joints, it is very important in that it can be used to provide estimates of stress intensity factors for other geometries by applying the appropriate boundary correction functions.

The Newman-Raju solution has been shown [4.16] to yield results which agree closely with experimental tubular joint Y factors for cracks of a/T>0.15, by applying the moment release function to account for the stress redistribution which accompanies crack propagation in tubular joints.

Different researchers have used different approaches over the years to model the effect of the weld detail and crack geometry on the flat plate solutions and develop stress intensity factor solutions for use in the analysis of cracks in tubular welded connections. These range from methods based on weight functions [4.17] to those based on finite element analysis carried out on welded joints. These approaches fall within three broad categories of methods generally used to determine stress intensity factors. These include classical solutions for idealised geometries, numerical methods and semi-empirical solutions based on experimental data.

A semi-analytical model based on the Newman and Raju flat plate solution for predicting Y factors in welded tubular joints was proposed by Monahan [4.18]. This model included the following;

1. A non uniform stress correction (*NSC*) to account for weld geometry,
2. A linear moment release (*LMR*) to account for load shedding and
3. A crack shape correction (*CSC*) factor.

The proposed equation is given by;

$$Y_{NR+NSC+LMR+CSC} = \frac{\left(F_m Y_g\left(1-\frac{B}{T}\right)+F_b Y_g\left(\frac{B}{T}\right)\left(1-\frac{a}{t}\right)\right)\Psi}{\Phi} \tag{4.23}$$

Where

Y_g = non uniform stress correction factor.

Ψ = crack shape correction factor.

$\frac{B}{T}$ = bending to total stress ratio.

The non uniform stress correction factor, Y_g, accounts for the influence of the stress concentration produced by the weld detail. This factor can be obtained using a method proposed by Albrecht and Yamada [4.19]. Using Albrecht's method, this factor is given by;

$$Y_g = \frac{2}{\pi}\sum_{i=1}^{n}\frac{\sigma_{x_i}}{\sigma}\left(\sin^{-1}\left(\frac{x_{i+1}}{a}\right)-\sin^{-1}\left(\frac{x_i}{a}\right)\right) \tag{4.24}$$

This was derived for a non uniform stress distribution, $\sigma(x)$, that remains symmetrical about the crack centre line as shown in figure 4.17.

The crack shape correction factor, Ψ, introduced by Monahan was included to account for the influence of crack aspect ratio. This factor was obtained by comparing experimental Y factors with those obtained by the Newman and Raju flat plate solution which included a non uniform stress correction factor and the linear moment release model such that;

$$\Psi = \frac{Y_{Exp.}}{Y_{NR+NSC+LMR}} \tag{4.25}$$

Monahan [4.18] used curve fitting through the values given by equation 4.24 and showed that Ψ could be approximated by the following equations.

$$\left.\begin{aligned} &\Psi = 1 \text{ for } \frac{a}{2c} \leq 0.05 \\ &\Psi = \frac{1}{1+0.7\left(\frac{a}{2c}-0.05\right)^{0.4}} \text{ for } 0.05 < \frac{a}{2c} < 0.26 \end{aligned}\right\} \tag{4.26}$$

The above crack shape correction factor was derived from experimental data obtained from tests conducted on a combination of X and multi-braced tubular joints. This means that it may not be directly applicable to other joint geometries. The reason for this is that the crack shape evolution curve depends greatly on both the joint geometry and the mode of loading. This is also demonstrated by the fact that the crack shape correction factor shown above is unity for the range of crack aspect ratios obtained for the Y-joints tested for this study. This is shown in figure 4.18. It is possible that a wide range of crack shape correction factors are obtainable depending on the geometry of the specimens tested This was shown to be the case in a recent study [4.20] on T-joints under axial loading. Myers [4.20] used a similar approach adopted by Monahan [4.18] and obtained a crack shape correction factor applicable to T-joints under axial loading given by;

$$\left.\begin{aligned} &\Psi = 0.9 \text{ for } \frac{a}{2c} \leq 0.05 \\ &\Psi = \left(\frac{1}{1+0.7\left(\frac{a}{2c}-0.04\right)^{0.4}}\right) - 1 \text{ for } \frac{a}{2c} > 0.05 \end{aligned}\right\} \tag{4.27}$$

The data from which this correction factor was derived are shown in figure 4.19 and the relevant crack shape correction factor curve is shown in figure 4.20. The first part of the curve can be considered to represent an upper boundary for a/2c $\leq$ 0.05. However as shown in figure 4.19, the crack shape correction factor (CSC) used for

a/2c > 0.05, is outside the scatter band for the data used. This would make it difficult to use this type of semi empirically derived solution for other joint geometries.

The brace and chord thickness of the Y-joints used in this study are the same as that used by Myers [4.20]. However both the geometry and mode of the loading are different. As a result, the crack shape evolution curves obtained from the two studies are different. This difference is shown in figure 4.21 where the best fit curves obtained for the two geometries are compared. The predicted Y factors obtained by using the correction factors given in equations 4.26 and 4.27 are compared in figure 4.22 and with experimental results from Y-joints in figure 4.23. Figures 4.22 and 4.23 show that the Y factor curve obtained depends on the crack shape correction factor used. This sensitivity is due to the semi-empirical nature of the model. As a result, there is some degree of uncertainty in the applicability of the model to the prediction of Y factors for cases other than those from which the crack shape correction factors were derived. In other to avoid this uncertainty, a crack shape correction function which also accounts for the effect of joint dimensional parameters and the mode of loading employed needs to be introduced.

There is a lack of solutions available for predicting crack aspect ratio evolution. This has been identified [4.21] to represented the greatest hindrance to good predictions of remaining life of cracked components. Different researchers have used different approaches to incorporate the effect of crack aspect ratio into stress intensity factor models used for fatigue crack growth prediction. One approach highlighted by Brennan [4.22] is based on the use of a root mean square (RMS) or average stress intensity factor for the transverse and longitudinal directions of crack growth. This approach was proposed by Cruse and Besuner [4.23] and it has been used by Dedhia and Harris [4.24] in analysing fatigue cracks in pipes. The use of this method for the prediction of Y factors in welded joints is outside the scope of work presented in this thesis and will not be discussed in any further detail. However a new semi-empirical model which accounts for the effect of crack aspect ratio is presented below. This new model is for predicting average Y factors in tubular welded Y-joints under variable amplitude loading.

4.6 NEW SEMI-EMPIRICAL Y FACTOR SOLUTION

Figure 4.24 shows the Y factor curves predicted by various existing Y factor models. Those shown in figure 4.24 include the TPM, AVS, modified AVS and the adapted flat plate solution based on the Newman & Raju equations. As shown in figure 4.24, the experimental Y factors obtained for this study are all below those predicted by the above equations.

The importance of crack shape evolution in the accurate prediction of crack growth in cracked components has been highlighted in the previous section. The TPM, AVS and modified AVS models do not account for this effect. It is therefore possible that their accuracy in predicting Y factors in tubular welded joints will depend on whether the crack shape evolution in the welded joint of interest is representative of those originally used to derive the respective equations. The main reason for this is that crack shape evolution will be influenced by both joint geometry and mode of loading as discussed in the previous section.

Figure 4.25 shows the crack shape evolution curves for all the 4 Y-joint tests conducted for this study. Curve fitting was used with the data shown in figure 4.25 to obtain an average crack shape evolution curve for Y-joint under out-of-plane bending as shown in figure 4.26. The best fit average curve obtained is given by;

$$2c = 58.533a^{0.7194} \tag{4.28}$$

This curve has been compared with that obtained by Myers [4.20] for axial T-joint tests conducted under constant amplitude loading conditions in figure 4.21. The difference in the two curves is most likely due to the differences in the mode of loading and joint geometry. This gap can only be breached by using a Y factor model which also accounts for these observed effects due to differences in the mode of loading and joint geometry.

Figure 4.27 shows how the best fit experimental Y factors compare with the predicted values based on the modified Newman and Raju equations. This prediction method was used as a basis for comparison because it was identified to give the best correlation with experimental results obtained for the investigation reported in [4.18].

The appropriate crack shape correction factor given in equation 4.26 was used together with equation 4.28 to obtain the results shown in figure 4.27. The Gumbel distribution was then used to model the deviation, δ, of the predicted results from the experimental data. This deviation is shown in figure 4.28 and is given by;

$$\delta = Exp\left[-Exp\left(A-\frac{a}{c}\right)\left(\frac{a}{T}\right)\right] \tag{4.29}$$

Where $A = 0.56-0.18S$ and the rest of the variables are as previously defined for the AVS model.

The flat plate solution was then modelled using curve fitting to obtain an equation which is similar to the AVS model. The reason for using this form of equation is because it is a function of parameters which have been established to be important in influencing the predicted Y factor. This modified AVS solution is given by;

$$Y_{VA.AVS} = A\left(\frac{T}{a}\right)^{j} \tag{4.30}$$

$$A = 0.56-0.18S \text{ and } j = 0.22+0.06S$$

The proposed Y factor solution, Y_{VA}, is then obtained by combining the modified solution with the deviation from the experimental data such that,

$$Y_{VA} = Y_{VA.AVS} - \delta \tag{4.31}$$

$$Y_{VA} = A\left(\frac{T}{a}\right)^{j} - Exp\left[-Exp\left(A-\frac{a}{c}\right)\left(\frac{a}{T}\right)\right] \tag{4.32}$$

This proposed solution is more accurate in predicting the average Y factor for the Y-joints used for this study. It also takes into account the effect of crack aspect ratio. It is compared with the experimental data and predictions from existing models in figure 4.29.

The prediction of crack aspect ratio has been identified to represent a major source of uncertainty in the fatigue crack growth prediction. This is mainly as a result of the large scatter on crack aspect ratio obtainable from experimental data at the current

state of the art in fatigue testing. This scatter is shown in figure 4.30 for the Y-joint results. As shown in figure 4.30 a ±25% error in the predicted crack length is still within the scatter obtained from the experimental results. In absolute terms, this is quite significant. However this level of error leads to very little change in the predicted Y factor as demonstrated in figure 4.31.

4.7 VARIABLE AMPLITUDE CRACK GROWTH MODELS

The derivation of accurate stress intensity factor solutions is imperative if fatigue crack growth prediction models are to be reliable. However there are other important factors which are often ignored, partly due to the lack of sufficient data and partly due to the inherent difficulty which is often encountered in reducing the level of uncertainty to a reasonable level. One of these factors is the effect of variable amplitude loading and the associated sequence effects.

Different statistical models have been developed in recent years to predict crack growth rates under variable amplitude conditions. These models do not account for sequence effects and have been shown to be applicable to load spectra in which such effects are minimal. Some of the more popular statistical models which have been applied to crack growth prediction in Offshore structures are discussed below.

4.7.1 Equivalent Stress Range Approach

The equivalent stress range approach is an extension of the equivalent fatigue damage concept first proposed by Paris to relate the effects of variable amplitude stress histories to constant amplitude fatigue crack growth data. This extension was proposed by Dover [4.25] as the weighted average stress range or the equivalent stress range approach for the fatigue crack growth analysis in tubular welded joints. Like the original equivalent fatigue damage concept, this method does not account for any load interaction effects in the random sequence as it relies on the assumption that

such effects are negligible. Using this approach and assuming that Paris law applies, variable amplitude fatigue crack growth rates can be predicted from;

$$\frac{da}{dN} = C\left(Y\sqrt{\pi a}\right)^m S_h{}^m \tag{4.33}$$

$$S_h = \left[\int_0^\infty \Delta S^m p(\Delta S) d(\Delta S)\right]^{(1/m)} = \left[\sum \Delta S^m P(\Delta S)\right]^{(1/m)} \tag{4.34}$$

where S_h is the equivalent or weighted average stress range, ΔS an individual stress range, m Paris crack growth exponent, $p(\Delta S)$ the probability density of ΔS and $P(\Delta S)$ is the probability of occurrence of ΔS.

This approach and definition of the equivalent stress range concept has been demonstrated [4.15] to be procedurally equivalent and applicable for both crack growth analysis and conventional S-N approach using Miners cumulative damage summation method. It has also been successfully used together with the rainflow counting method to predict variable amplitude fatigue crack growth in air.

However, despite the successful application of this model to air fatigue crack growth data, it was thought that it required modification for corrosion fatigue data where crack growth was controlled mainly by two competing factors. Corrosion fatigue unlike air fatigue crack growth is controlled by a combination of the mechanical action due to cyclic stressing and the electrochemical action of the corrosive environment. Also the 'no load interaction assumption' has not been established for typical multi-sea state load spectra experienced by structures in the North Sea. For these sort of load sequences with very high clipping ratios (in excess of 7), it is possible that sequence effects may become more significant. This has been discussed in Chapter 3 in conjunction with the results obtained from this study.

The implication for not adequately modelling sequence effects is that unconservative results may be obtained when this model is used to predict crack growth under variable amplitude conditions. This aspect of crack growth prediction in Offshore structures is discussed further in Chapter 5 where a new model which predicts crack

growth under realistic loading conditions and accounts for sea state interaction effects is proposed.

4.7.2 Equivalent Crack Growth Concept

The equivalent crack growth concept was proposed by Kam et al [4.26, 4.27] as a modification to the equivalent stress range concept for the prediction of variable amplitude corrosion fatigue crack growth. This model was based on multiple segment Paris type linear representation of corrosion fatigue crack growth as shown in figure 4.32. Each segment shown in figure 4.32 was taken to represent the material response which covers all relevant stress intensity factor ranges for which the material's constants, C and m are pertinent. This model is covered in great detail in references [4.26] and [4.27] but in simple terms it states that the average crack growth rate for a multi-segment $\frac{da}{dN}$ versus ΔK curve such as that depicted in figure 4.32, which has k segments with material constants C_j and m_j over segment j can be given as;

$$\left(\frac{da}{dN}\right)_{AV} = \sum_{j=1}^{k} C_j \left(Y\sqrt{\pi a}\right)^{m_j} \int_{\Delta S_{j-1}}^{\Delta S_j} \Delta S^{m_j} p(\Delta S) d(\Delta S) \qquad (4.35)$$

The equivalent crack growth concept has been verified with experimental data [4.26] and it was shown to give good agreement with the experimental results. It however has not been possible to asses the accuracy of this model due to the lack Paris law data for SE 702.

The main problem with this model is that it involves the lengthy procedure of signal generation and cycle counting before any analysis can be carried out. To overcome this problem and bypass the signal generation and cycle counting before analysis, an alternative prediction procedure was proposed in the form of an extended version of the Kam and Dover equation. This modified version was based on the original idea behind the Chaudhury and Dover equation for predicting the equivalent stress range directly from the PSD without going through the lengthy cycle counting process. It is

important to note here that the solution determined by this equation for the distribution of peaks can be expressed as the sum of the Gaussian and Rayleigh distributions as presented in Chapter 1. It is not clear whether all representative sequences for Offshore structures will exhibit a distribution of peaks which can be sufficiently described by these two distributions combined in this way. It is therefore possible that a better prediction procedure may be obtained which is based on a more appropriate distribution relevant to a particular sequence. This aspect is discussed in greater detail Chapter 5 with respect the JOSH sequence which has power spectral density properties significantly different from fixed jacket structures.

Apart from the fast assessment equations which can be used to calculate equivalent stresses directly, all the models discussed above rely on one form of cycle counting or another the implementation of which has been covered in Chapter 1.

4.8 CONSIDERATION OF SEQUENCE EFFECTS

As discussed in the previous section, The prediction of fatigue crack growth under variable amplitude loading conditions is still in its infancy as there is a lack of suitable fatigue crack growth prediction models which account for all the relevant effects which are unique to variable amplitude loading conditions. Apart from the statistical models presented above, other models have been proposed for use in analysing variable amplitude loading. These are presented below.

4.8.1 Models Based on Crack Tip Plasticity

Crack tip plasticity models used to explain variable amplitude fatigue crack growth are based on the assumption that crack growth rates can be related to the evolution of the crack tip plastic zones. The more popular models which have attempted to explain the variability in crack growth rates observed under variable amplitude loading conditions using crack tip plasticity are those of Wheeler and Willenborg.

4.8.1.1 The Wheeler Model

The Wheeler [4.28] model predicts that crack growth following an overload may be estimated by modifying the constant amplitude growth rate using an empirical retardation parameter, C_p, such that;

$$\frac{da}{dN} = (C_p)_i \left(\frac{da}{dN}\right)_{CA_i} \tag{4.36}$$

The constant amplitude growth rate appropriate to the stress intensity factor range, ΔK_i, associated with the i_{th} cycle is given by $\left(\frac{da}{dN}\right)_{CA_i}$ and the retardation parameter is taken to be a function of the ratio of the current plastic zone size to the overload plastic zone size and give by;

$$(C_p)_i = \left(\frac{r_{yi}}{a_p - a_i}\right)^p \tag{4.37}$$

where r_{yi} is the i_{th} loading cyclic plastic zone size, a_p is the sum of overload crack length and overload plastic zone size, a_i is the crack length at i_{th} loading cycle. These parameters are shown schematically in figure 4.33 and p is an empirically determined shaping parameter.

This model was proposed for analysing crack growth on a cycle by cycle basis and it can be used to sum crack growth after r cycles as follows.

$$a_r = a_o + \sum_{i=1}^{r} \left(\frac{da}{dN}\right)_i \tag{4.38}$$

where a_o and a_r are the initial crack length and crack length after r cycles respectively.

Although this model can be used to predict the effect of overloads on a cycle by cycle basis it has some inherent disadvantages. One of the main disadvantages of this model is that it relies on the use of an empirically determined constant, p, required to shape the constant amplitude crack growth retardation parameter. The wheeler model also

predicts that maximum retardation resulting from an overload occurs immediately after the application of the overload as the retardation parameter turns to zero. This however contrasts with the phenomenon of delayed retardation observed [4.29, 4.30] during overloads and depicted in figure 4.34. The model also neglects the counteracting effect of negative peak loads in crack retardation. The main disadvantage of the model lies in its limited capability in analysing variable amplitude loading sequences such as those experienced by Offshore structures. Its cycle by cycle approach to obtain the summed crack growth makes it very difficult to account for any retardation effects which may be present in very long sequences typical for Offshore structures. The fact that it also relies on an empirically determined parameter makes it inappropriate for use in structural integrity assessment procedures. The use of this method for analysing the results obtained from this study was therefore not considered appropriate. An alternative approach to the prediction of crack growth in Offshore structures which attempts to account for overall sea state interaction effects is presented in Chapter 5.

4.8.1.2 The Willenborg Model

Willenborg's model [4.31] is based on the assumption that retardation in crack growth rate following an overload is caused by compressive residual stresses acting on the crack tip. The model relies on the use of an effective stress which is the applied stress reduced by the compressive residual stress developed around the crack tip as a result of the elastic body surrounding the overload plastic zone.

Based on the effective stresses, the calculated effective stress intensity factor range can be used together with an appropriate crack growth law to give the crack growth rate for the i_{th} cycle as;

$$\frac{da}{dN_i} = C\left(\Delta K_{eff}\right)_i \qquad 4.39$$

The main difference between this model and the Wheeler model is that it uses only constant amplitude crack growth data and does not require the derivation of any

empirical shaping constants. Like the Wheeler model, this model also predicts maximum retardation immediately after the application of an overload and fails to predict the observed retardation effects and the decrease in retardation observed due to the application of underloads. The Willenborg model is also limited in its application to fatigue loads such as those experienced by Offshore structures due to its cycle by cycle approach which is very difficult to use in analysing very long sequences encountered under realistic service conditions.

4.8.2 Crack Closure Models

The concept of crack closure is used to describe a situation where the crack tip for a crack fails to open immediately on application of a tensile load. This phenomenon was discovered by Elber. He suggested that the driving force for crack extension is reduced by the development of plasticity induced crack closure and proposed the effective stress intensity factor range concept which allowed fatigue crack growth rates to be estimated under crack closure conditions. Once the crack opening stress, σ_{op}, has been determined and the effective stress intensity factor range calculated, this model can be used to predict crack growth rate using an appropriate crack growth law.

$$\Delta a_i = \frac{da}{dN_i} = C_0\left(\Delta K_{eff}\right)_i^m \tag{4.40}$$

$$C_o = C\left[\frac{K_{\max} - K_{op}}{K_{\max} - K_{\min}}\right]^{-m} \tag{4.41}$$

where the crack growth coefficient, C_o, and effective stress intensity factor range, ΔK_{eff} correspond to the same closure level.

A number of different crack closure models have been developed in recent years [4.32, 4.33 and 4.34]. Some of these are based on plasticity induced crack closure mechanisms, roughness induced crack closure, oxide induced crack closure and crack closure resulting from the effect of calcareous deposits on the crack surfaces. Crack

closure is not a major subject of this thesis and these different mechanisms have not been covered in detail as a comprehensive review is widely available in the literature.

Crack closure based models also have problems on grounds of practicality similar to the Wheeler and the Willenborg models. The main difference between this model and the two previous models is that it accounts for delayed retardation and the effects of underloads by the variation of the crack tip opening stress, σ_{op}. This stress is however very difficult to implement for variable amplitude loading conditions and this represents a major limitation of the model.

4.9 SUMMARY

The results obtained from the variable amplitude fatigue tests conducted for this study have been analysed using existing fracture mechanics models. The use of different fracture mechanics models to predict fatigue crack growth and to model the different observations of crack growth retardation and acceleration observed during variable amplitude loading conditions have been assessed and possible areas for modification and improvement highlighted.

Through this Chapter, it is apparent that one of the main difficulties in trying to quantify corrosion fatigue crack growth under variable amplitude loading conditions is the large number of variables involved which almost always operate as a combination to influence corrosion fatigue crack growth at any one time. Some of these variables include material properties determined by the alloying elements present, nature of the corrosive environment determined mainly by its chemical composition and other additional factors. Crack shape evolution has also been identified as an important parameter which influences the stress intensity factor.

A new Y factor model has been proposed. The proposed semi-empirical function depends on crack aspect ratio and loading mode which are important parameters thought to influence the nature of Y factors obtained.

4.10 CONCLUSIONS

The performance of several Y factor models has been assessed in this Chapter by comparing the Y factors predicted by each of the models with experimental data. These included the TPM, AVS and modified AVS models. The adapted flat plate solution based on the Newman & Raju equations were also assessed.

It was noted that the average experimental Y factor curve was below the curves predicted by the above solutions. Based on this observation it was concluded that there may be other important factors which affect crack propagation under variable amplitude conditions which may have been ignored in previous models. Also importantly, crack shape evolution was not accounted for in the models apart from that based on the Newman & Raju equations.

A new Y factor model has been proposed which accounts for these important factors such as the crack shape evolution (crack aspect ratio), geometry and mode of loading. Its semi-empirical nature may however introduce a certain degree of uncertainty when applied to other geometries other than Y-joints under out-of-plane bending.

It was also noted that fatigue crack growth models for the analysis of fatigue crack growth under variable amplitude conditions are limited and that most of the existing models do not allow for interaction effects to be accounted for. Those which attempt to model interaction effects are based on a cycle by cycle analysis with emphasis on single overloads or underloads. This makes their application to Offshore structures impractical. To overcome these difficulties a new approach has been proposed based on the sea state equivalent stress concept. Details of this are presented in the next Chapter 5.

4.11 REFERENCES

[4.1] Rhee H C and Salama M M, "*Opportunities for application of fracture mechanics for Offshore structures*", Fracture Mechanics in Offshore Industry, Reprinted from Applied Mechanics Reviews, Vol. 41, No. 2, February 1988, ASME Book No. AMR032.

[4.2] Dharmavasan S and Dover W D, "*Nondestructive evaluation of Offshore structures using fracture mechanics*", Fracture Mechanics in Offshore Industry, Reprinted from Applied Mechanics Reviews, Vol. 41, No. 2, February 1988, ASME Book No. AMR032.

[4.3] Machida S, Yajima H, Toyosada M, Hagiwara Y and Kajimoto K, "*Japanese research activities in Offshore fracture mechanics applications*", Fracture Mechanics in Offshore Industry, Reprinted from Applied Mechanics Reviews, Vol. 41, No. 2, February 1988, ASME Book No. AMR032.

[4.4] Griffith A A, Philos. Trans R. Soc. London, Vol. A221, 1920, P163 (republished with additional commentary in Trans. Am. Soc. Metals, Vol. 61, 1968, p871)

[4.5] Irwin G R, "*Fracture of Metals*", American Society of Metals, Cleveland, Ohio, 1968, p871.

[4.6] Irwin G R, "*Analysis of stresses and strains near theend of a crack traversing a plate*", Trans. ASME, Journal of Applied Mechanics, Vol. E24, P361.

[4.7] Irwin G R, "*The crack extension force for a part through crack in a plate*", Trans. Journal of Applied Mechanics, 1962, pp651-654.

[4.8] BS PD 6493: 1991, *Guidance on Methods for Assessing the Acceptability of Flaws in Welded Structures,* British Standards Institution, London 1991.

[4.9] Balladon P and Coudert E, "*TPG 500 Structural Assessment*", Rapport Technique 95072 C, September 1995.

[4.10] Billingham J, Spurier J, Healy, J and Kilgallon P, "*Corrosion Fatigue Fracture Mechanics of Jack-up Steels*", Project Report, University of Cranfield 1998.

[4.11] Holdbrook S J and Dover W D, "*The stress intensity factors for a deep surface crack in a finite plate*", Engineering Fracture Mechanics, Vol. 12, pp347-364 (1979)

[4.12] Dover W D and Dharmavasan S, "*Fatigue Fracture Mechanics analysis of T and Y joints*", Paper OTC 4404 of Offshore Technology Conference, Texas, 1982.

[4.13] Austin J A, *The Role of Corrosion Fatigue crack growth Mechanisms in Predicting Fatigue life of Offshore Tubular Joints.*, Ph.D. Thesis, Department of Mechanical Engineering, University College London, October 1994.

[4.14] Kam J C P, Topp D A and Dover W D, "*Fracture Mechanics Modelling and Structural Integrity of Welded Tubular Joints in Fatigue*", Proceedings, 6th International Offshore Mechanics and Arctic Engineering Symposium, ASME, Vol. 3, pp. 395-402, 1987

[4.15] Kam J C, *Structural Integrity of Offshore Tubular Joints Subject to Fatigue*, Ph.D. Thesis ,Department of Mechanical Engineering, University College London, 1989

[4.16] Aaghaakouchaka, Glinka G, and Dharmavasan S, "*A load shedding model for fracture mechanics analysis of fatigue cracks in tubular joints*", Proceedings of the 8th International Conference on Offshore Mechanics and Arctic Engineering, The Hague, 1989.

[4.17] Nui X and Glinka G, "*The weld profile effect on stress intensity factors in weldments*", International Journal of Fracture, Vol. 35, pp. 3-20 (1987).

[4.18] Monahan C C, "Early Fatigue Crack Growth in Offshore Structure", PhD Thesis, Department of Mechanical Engineering, University College London, May 1994.

[4.19] Albrecht P and Yamada K, "*Rapid Calculation of Stress Intensity Factors*", Journal of the Structural Division, ASCE, Vol. 103, 1977, pp. 377-389,

[4.20] Myers P, *Corrosion Fatigue Fracture Mechanics of High Strength Jack Up Steels*, Ph.D. Thesis submitted to London University, February 1998.

[4.21] Brennan F P, "Fatigue and Fracture - Discussion", Proceedings of the 13th International Ship and Offshore Structures Congress, Vol. 3, Ed. Moan T and Berge S, 1997.

[4.22] Brennan F P and Dover W D, "Fatigue & Fracture Mechanics Assessment Models for RODS", RODS (Primmer), Progress Report December 1997, University College London.

[4.23] Cruse T A and Besuner P M, "*Residual Life Prediction for Surface Cracks in Complex Structural Details*", Journal of Aircraft, Vol. 12 No. 4, pp. 369-375, April 1975

[4.24] Dedhia D D and Harris D O, "*Improved Influence Functions for Part Circumferential Cracks in pipes*", ASME Pressure Vessel and Piping Conference, Portland, Oregon, June 1983.

[4.25] Dover W D "*Variable amplitude fatigue of welded structures*", Fracture mechanics, current status, future prospects, Cambridge, UK, 1979.

[4.26] Kam J C P and Dover W D, "*Fatigue crack growth in Offshore welded tubular joints under real life variable amplitude loading*", Proceedings International Conference on Fatigue Crack Growth Under Variable Amplitude Loading, June 1988.

[4.27] Kam J C P and Dover W D, "Corrosion fatigue of welded tubular joints: Fracture mechanics modeling and data interpretation2, Proceedings of the 8th International Conference on Offshore mechanics and Arctic Engineering, The Hague, 1989.

[4.28] Wheeler O E, "*Spectrum loading and crack growth*", Journal of Basic Engineering Transactions. ASME Vol. D94, No. 1, 1972 pp. 181-186.

[4.29] Bannantine J A, Comer J J and Handrock J L, *Fundamentals of Metal Fatigue Aanalysis*, Published by Prentice Hall, Inc., 1990.

[4.30] Von Euw E J F, Hertzberg R W and Roberts R, "Delay effects in Fatigue Crack Propagation", ASTM STP 513, American Society for Testing and Materials, Philiadelphia, 1972.

[4.31] Willenborg J, Engle R M and Wood H A, "*A crack growth retardation model using an effective stress concept*", AFFDL TM-71-1-FBR, Jan. 1971

[4.32] Newman J C Jr., "*A crack closure model for predicting fatigue crack growth under aircraft spectrum loading*", Methods and models for predicting fatigue crack growth under random loading, ASTM STP 748, American Society for Testing and Materials, Philadelphia, 1981, PP 53-84.

[4.33] Newman J C Jr., "*Prediction of fatigue crack growth under variable amplitude and spectrum loading using a closure model*", Design of fatigue and fracture resistant structures, ASTM STP 761, American Society for Testing and Materials, Philadelphia, 1982, PP 255-277.

[4.34] Dill H D, Saff C R and Potter J M, "*Effects of fighter attack spectrum on crack growth*", ASTM STP 714, American Society for Testing and Materials, Philadelphia, 1980, PP 205-217.

4.12 TABLES AND FIGURES

Table 4.1: Paris law air data for SE 702 [4.9]

	C	m
Parent Metal (PM)	2.715×10^{-9}	3.5320
Heat Affected Zone (HAZ)	3.872×10^{-9}	3.1687

Table 4.2: Paris law sea water data for SE 702 [4.9]

CP		-830mV/ECS
Temperature		20°C
	C	m
Parent Metal (PM)	2.715×10^{-9}	3.5320
Heat Affected Zone (HAZ)	3.872×10^{-9}	3.1687

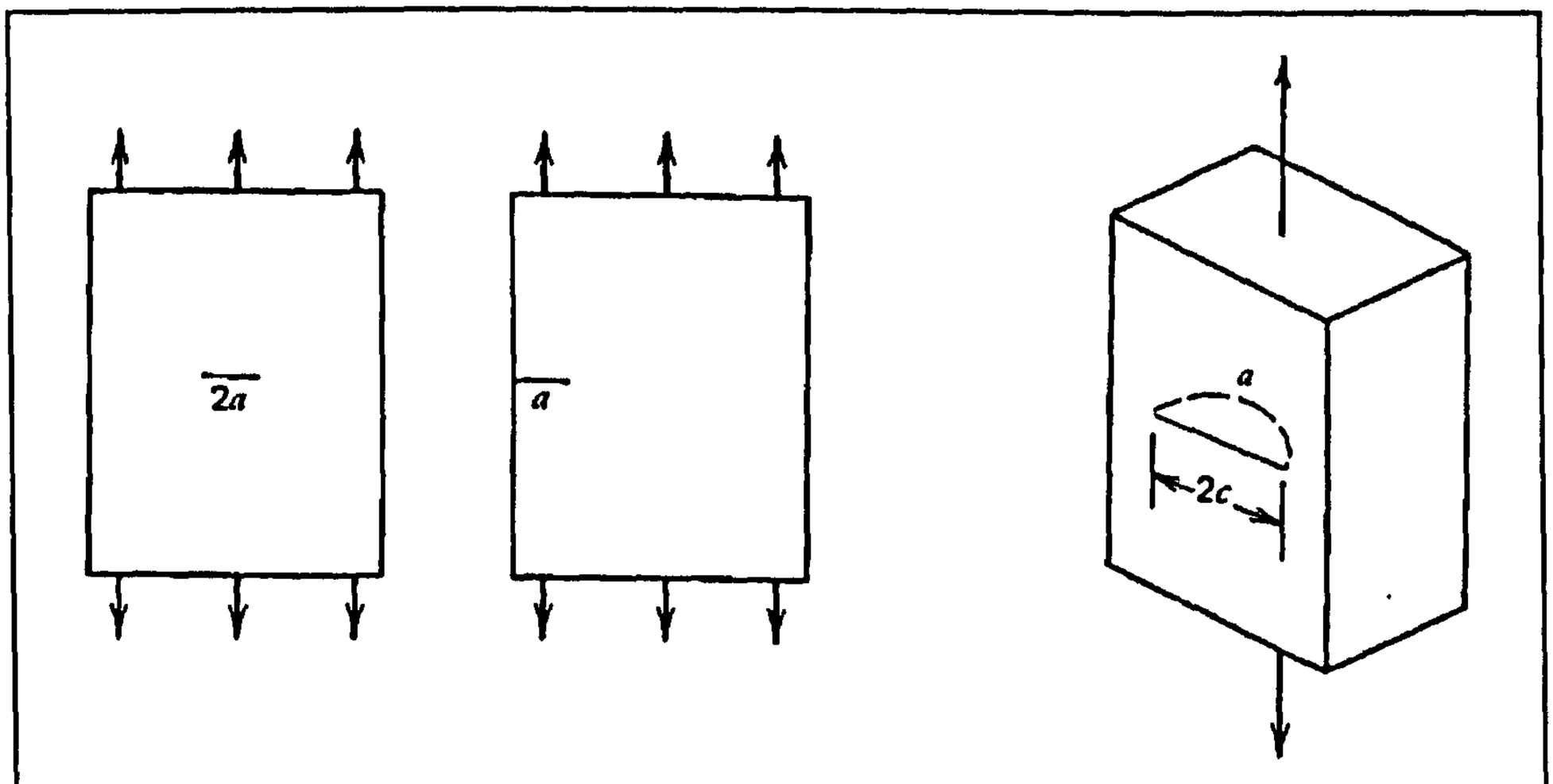

Figure 4.1: Embedded elliptical crack In a uniform tensile stress field

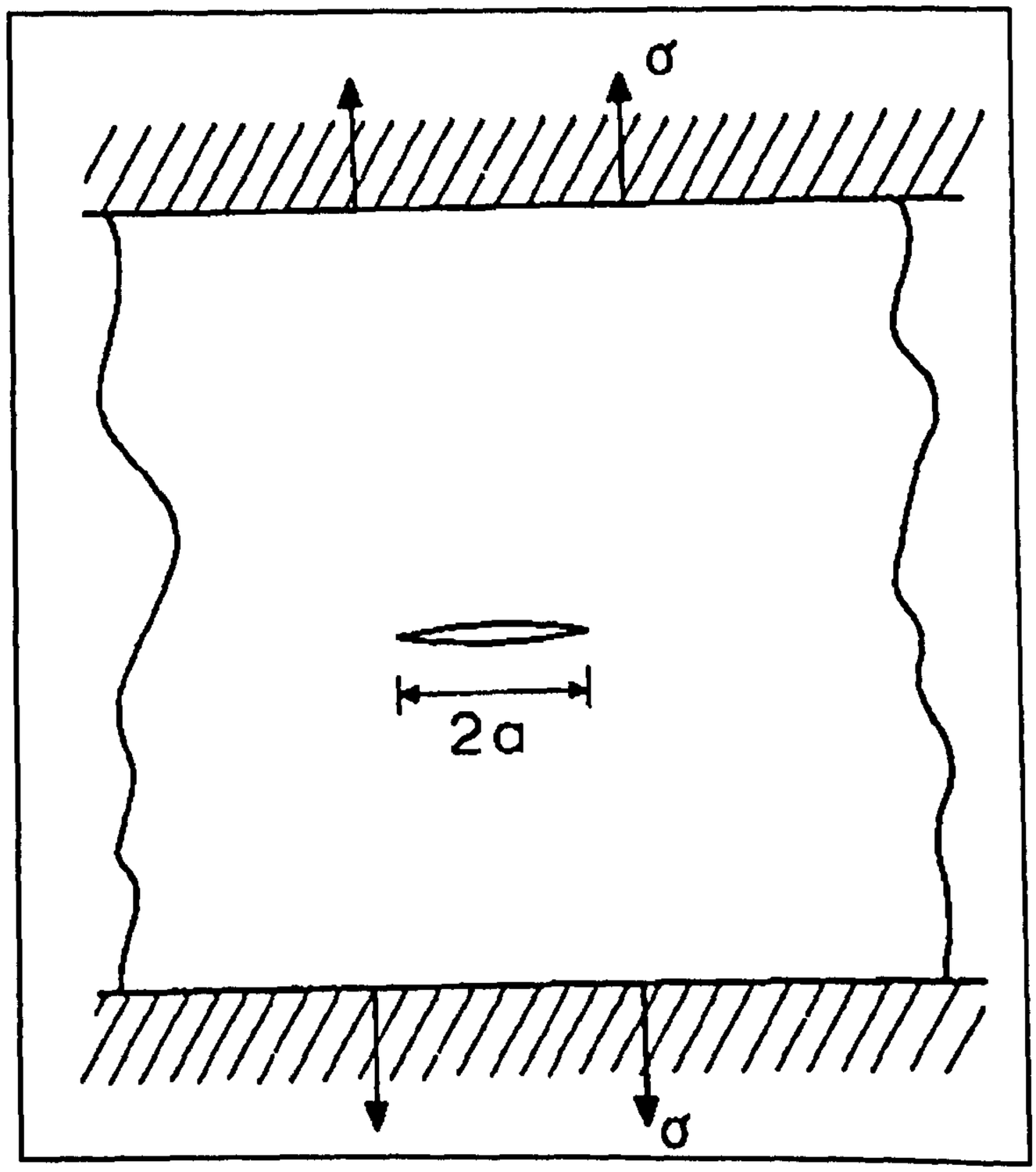

Figure 4.2: Crack in an infinite plate subjected to a uniform stress field

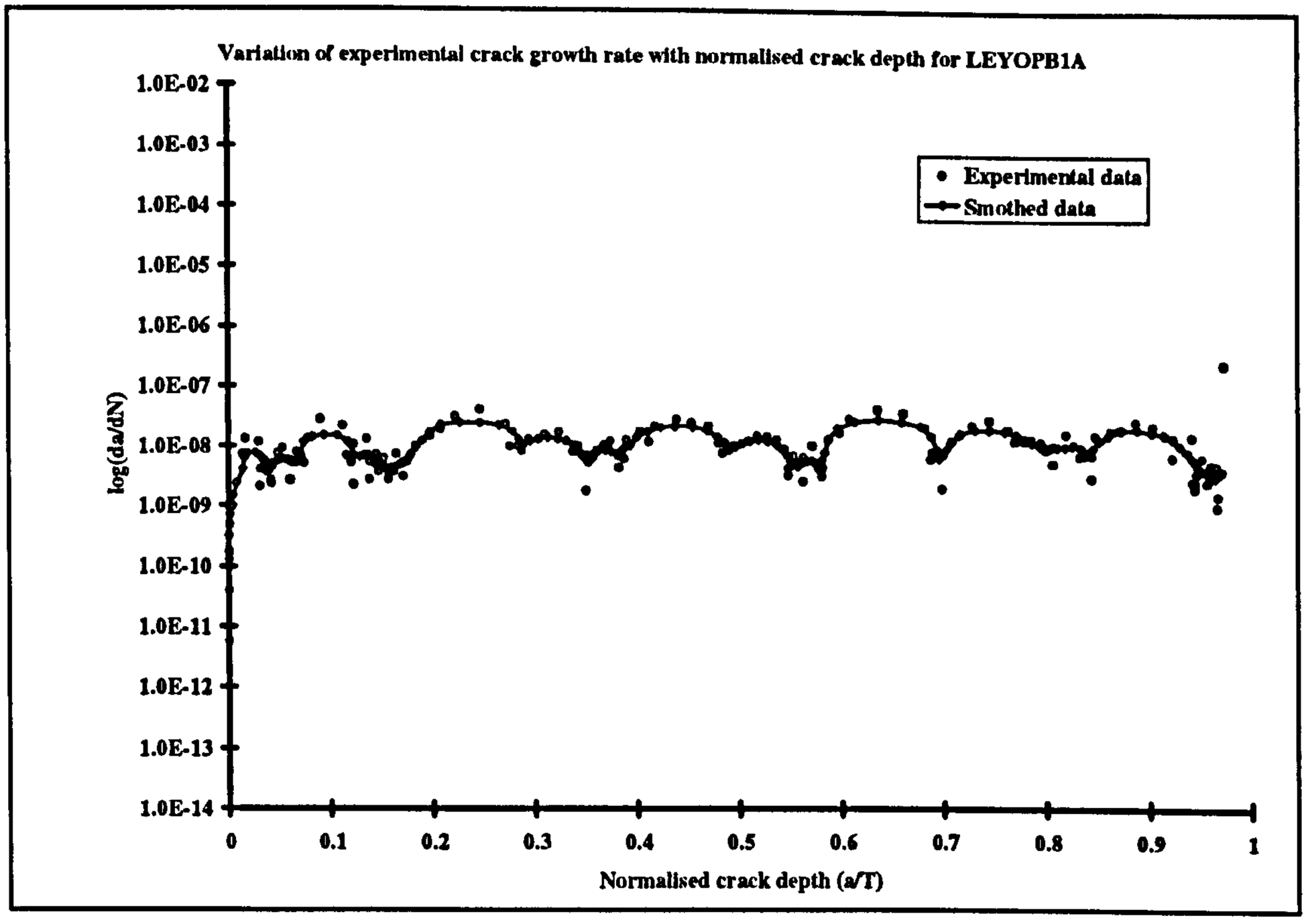

Figure 4.3: Experimental fatigue crack growth rate for LEYOPB1A

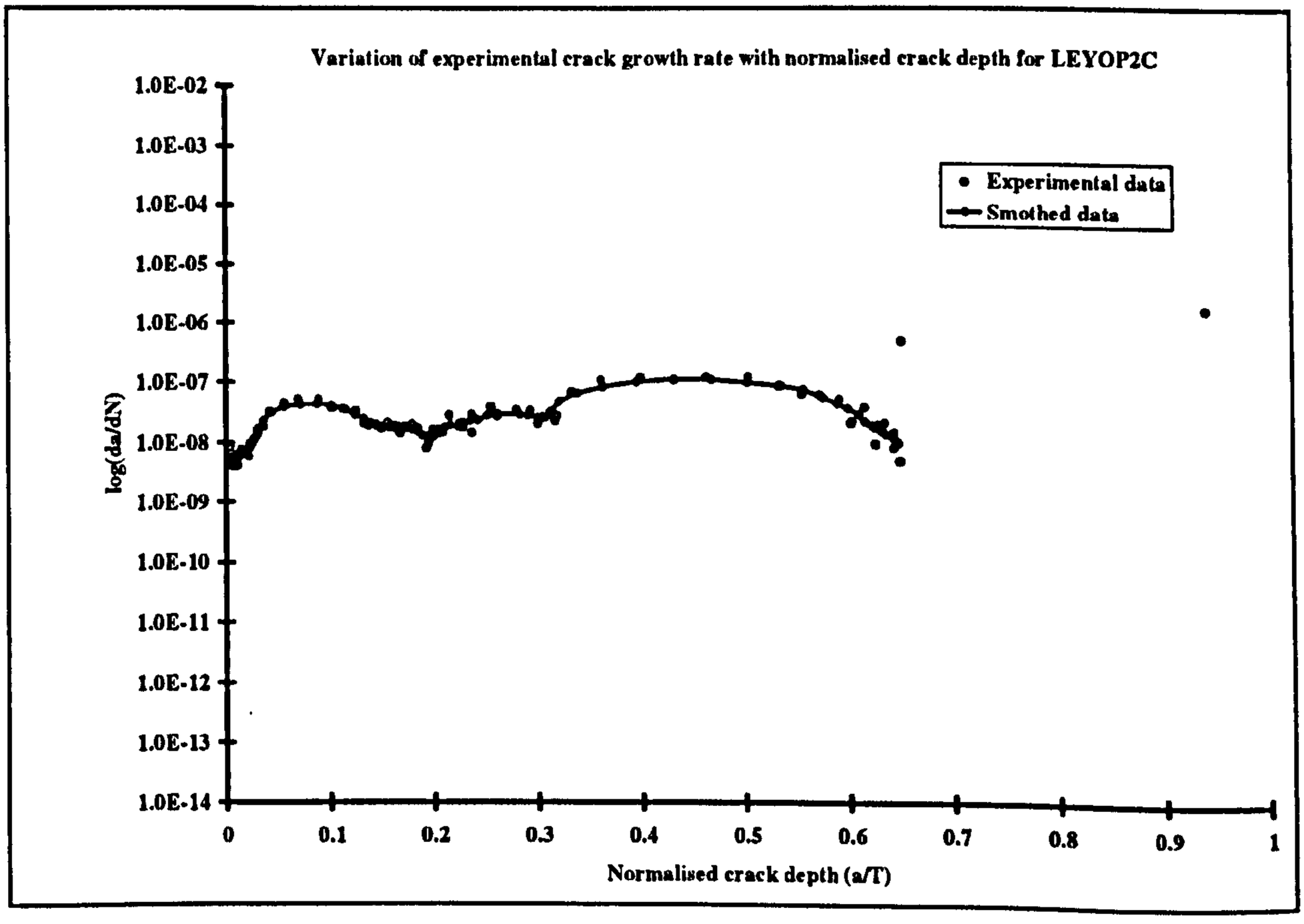

Figure 4.4: Experimental fatigue crack growth rate for LEYOPB2C

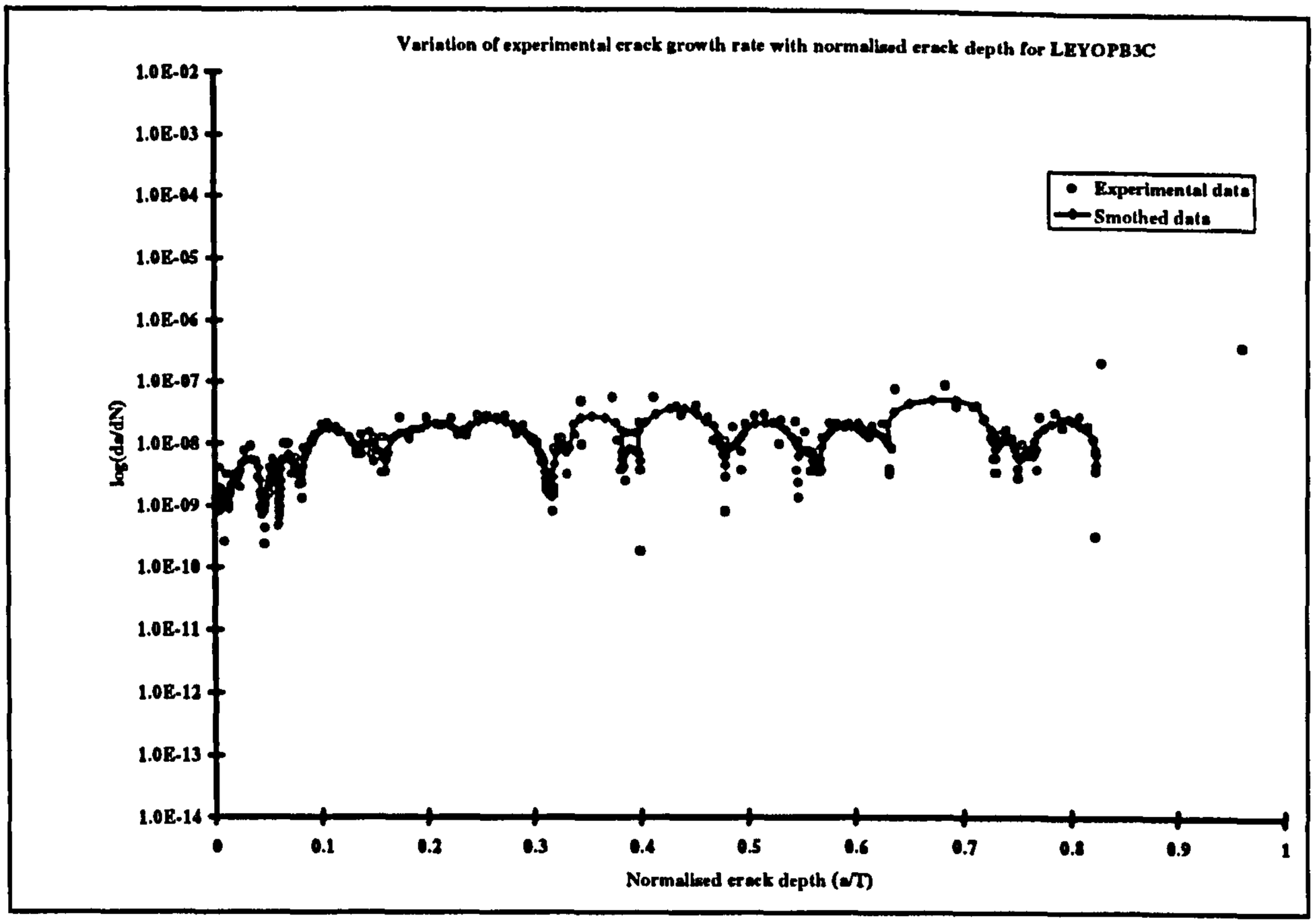

Figure 4.5: Experimental fatigue crack growth rate for LEYOPB3C

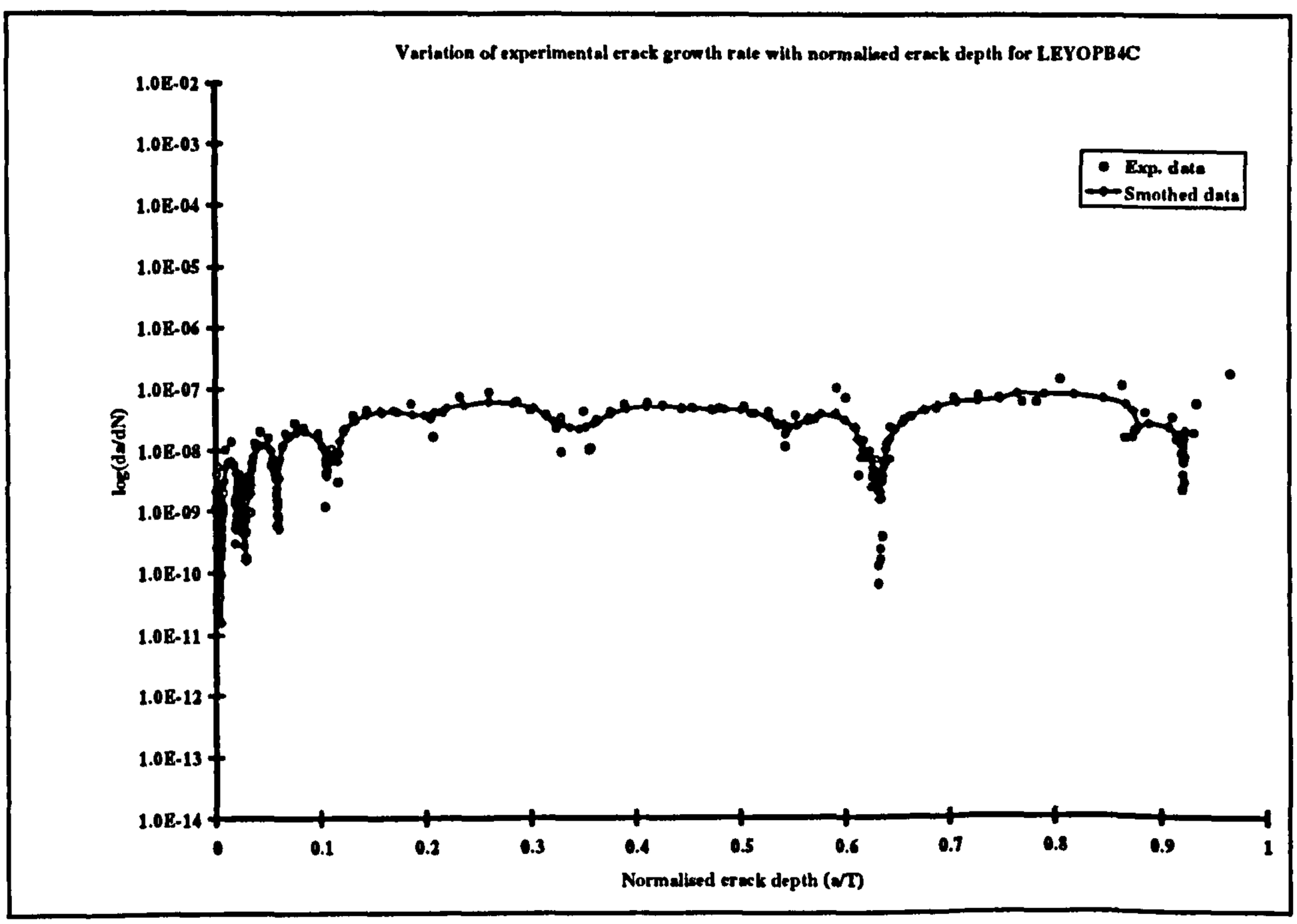

Figure 4.6: Experimental fatigue crack growth rate for LEYOPB4C

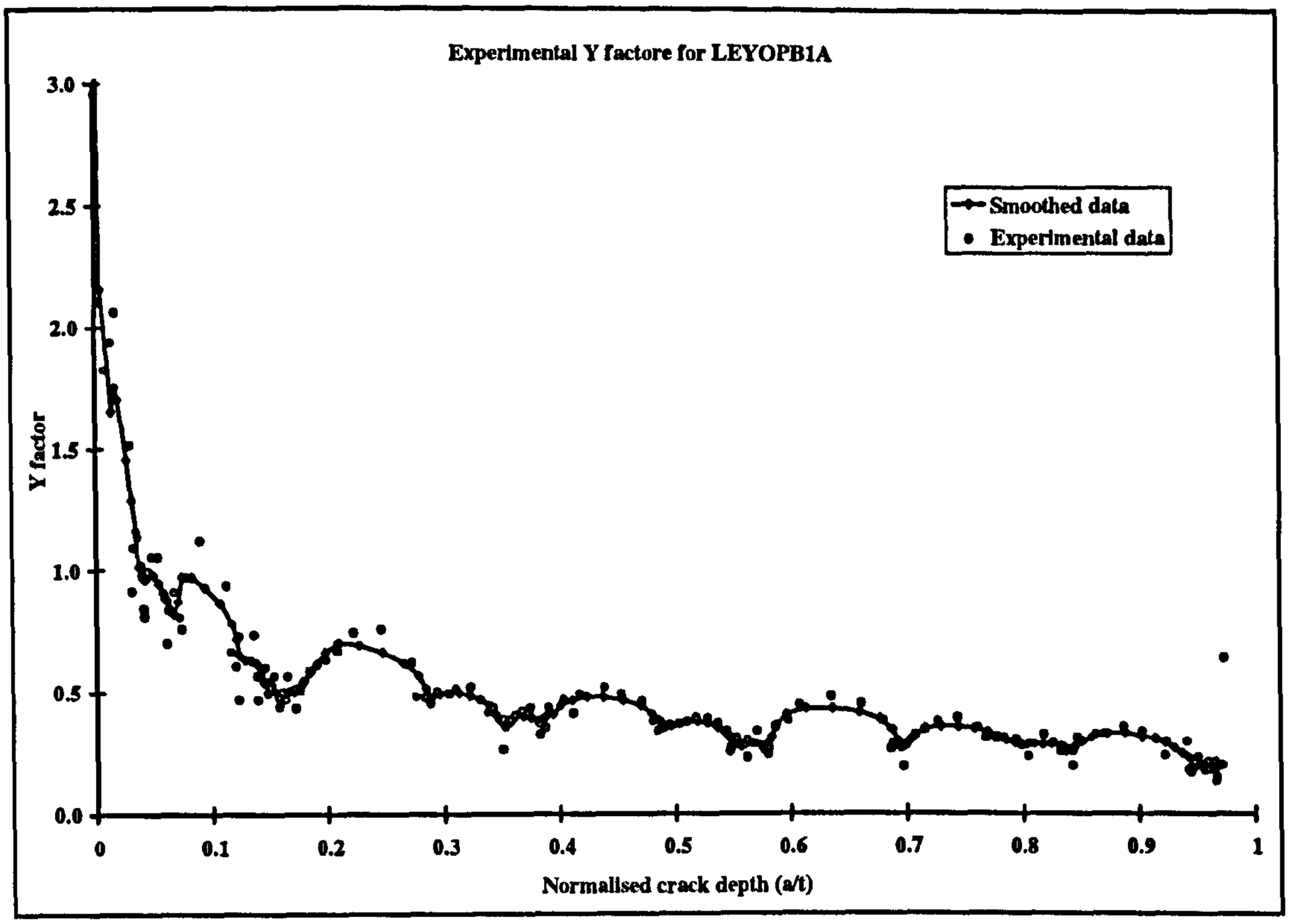

Figure 4.7: Experimental Y factors for LEYOPB1A

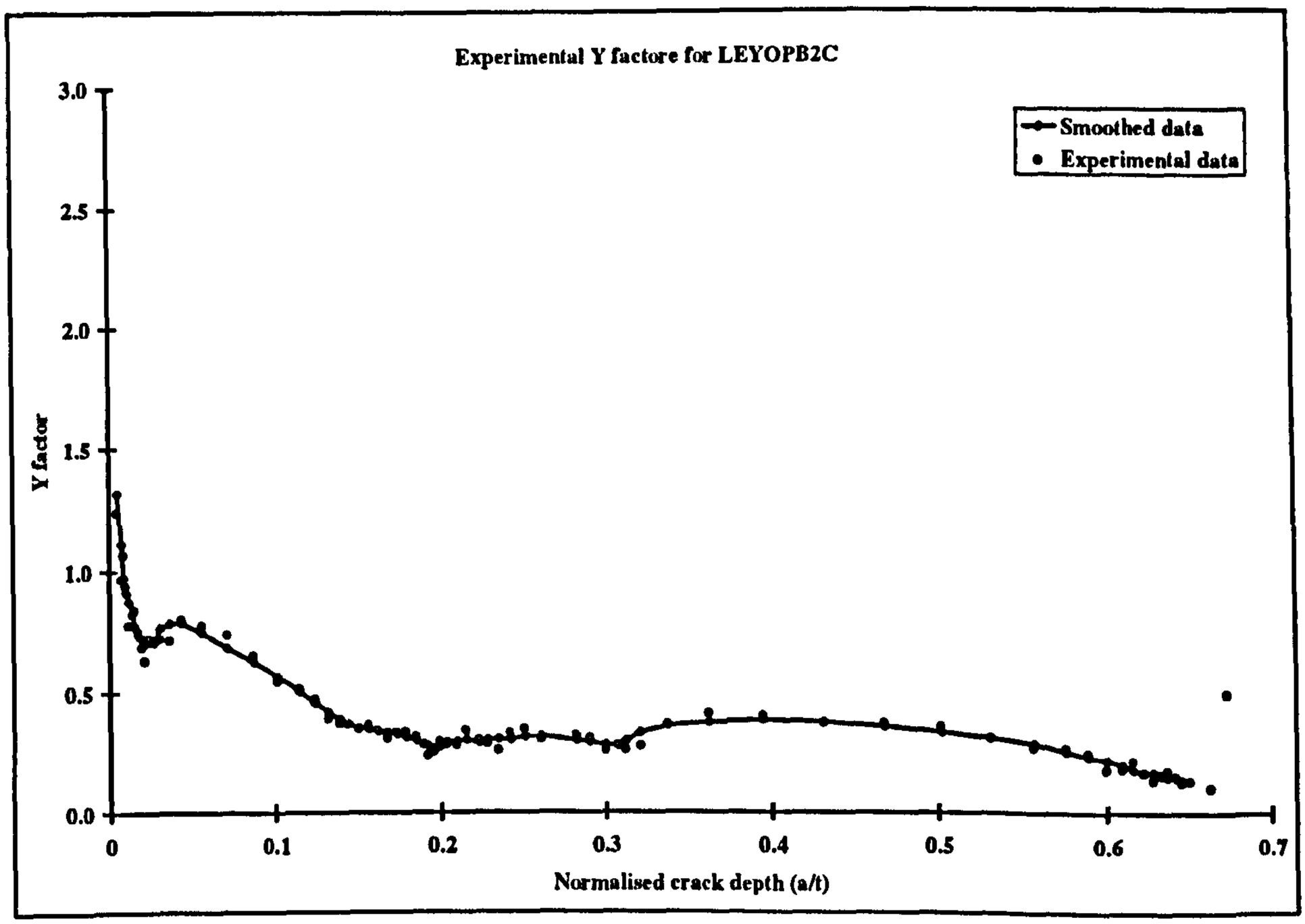

Figure 4.8: Experimental Y factors for LEYOPB2C

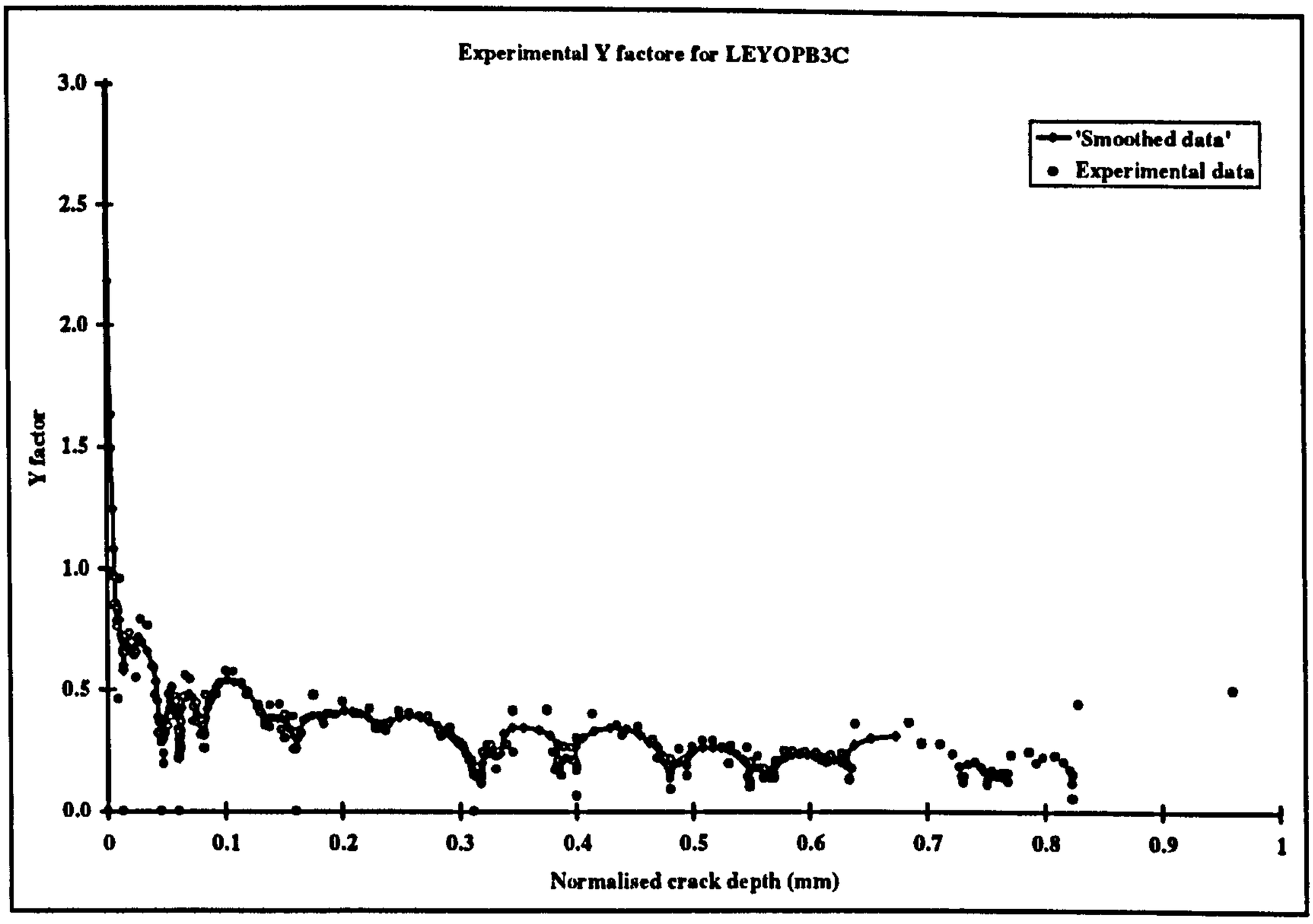

Figure 4.9: Experimental Y factors for LEYOPB3C

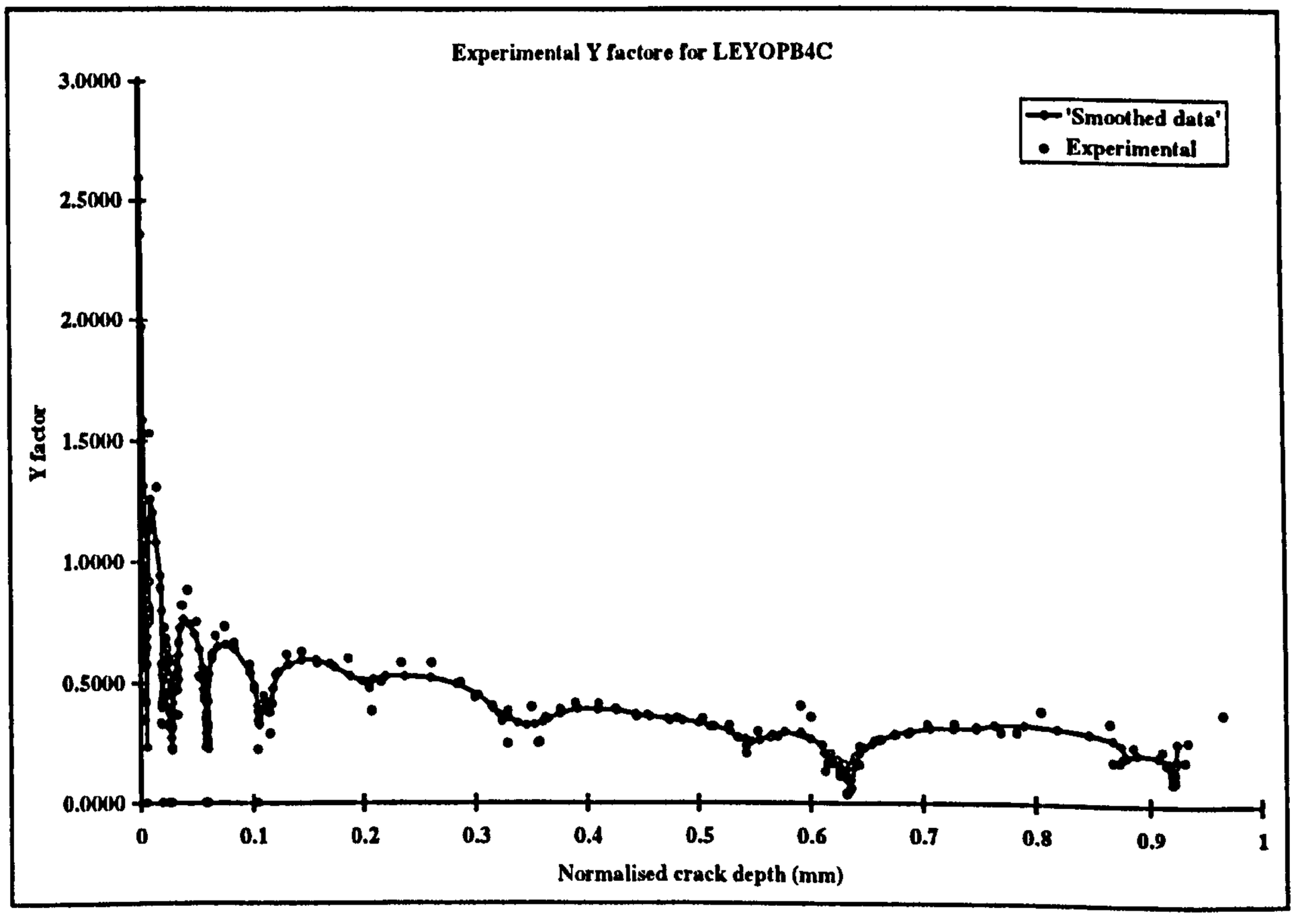

Figure 4.10: Experimental Y factors for LEYOPB4C

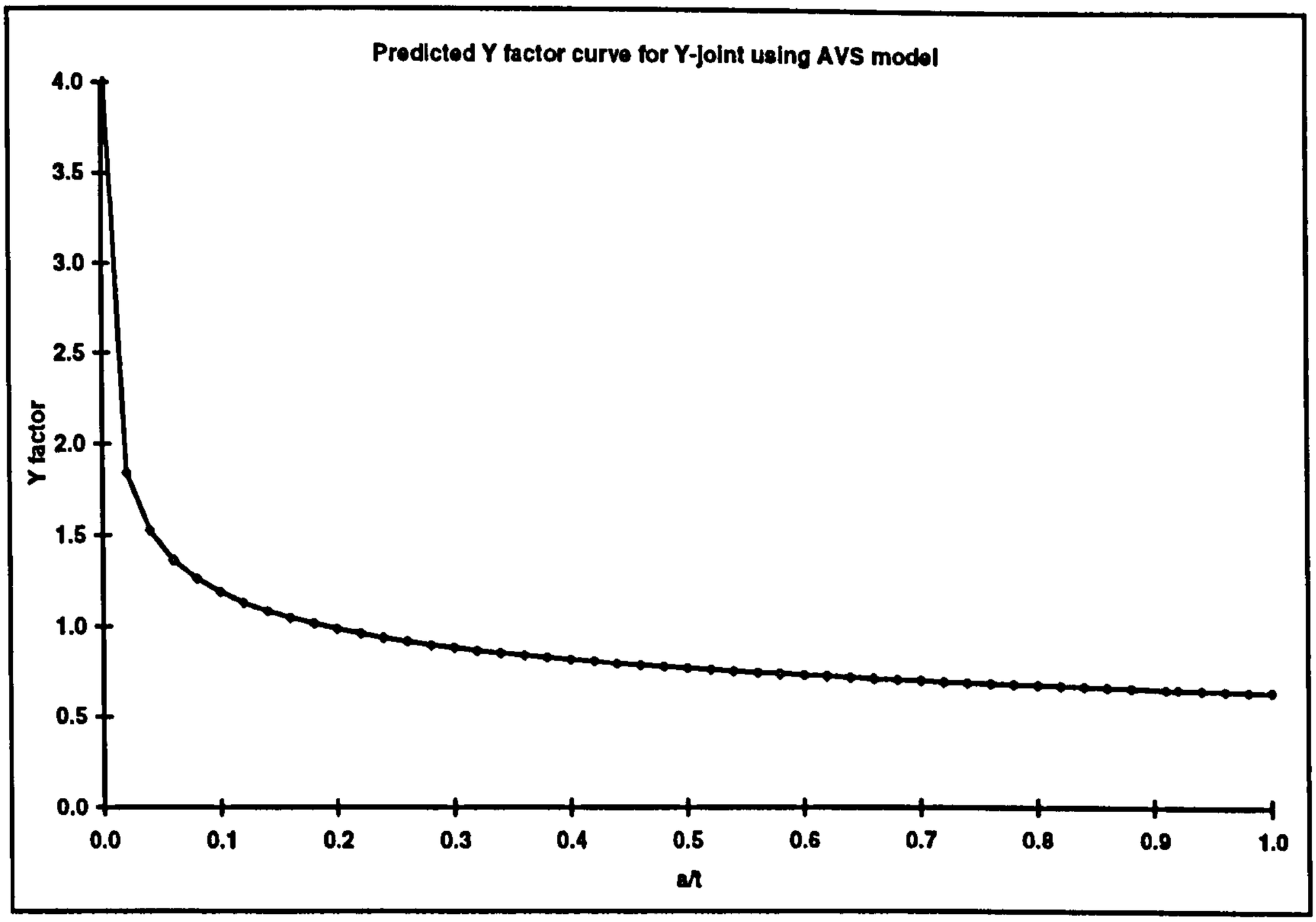

Figure 4.11: Predicted Y factor for Y-joints using the AVS model

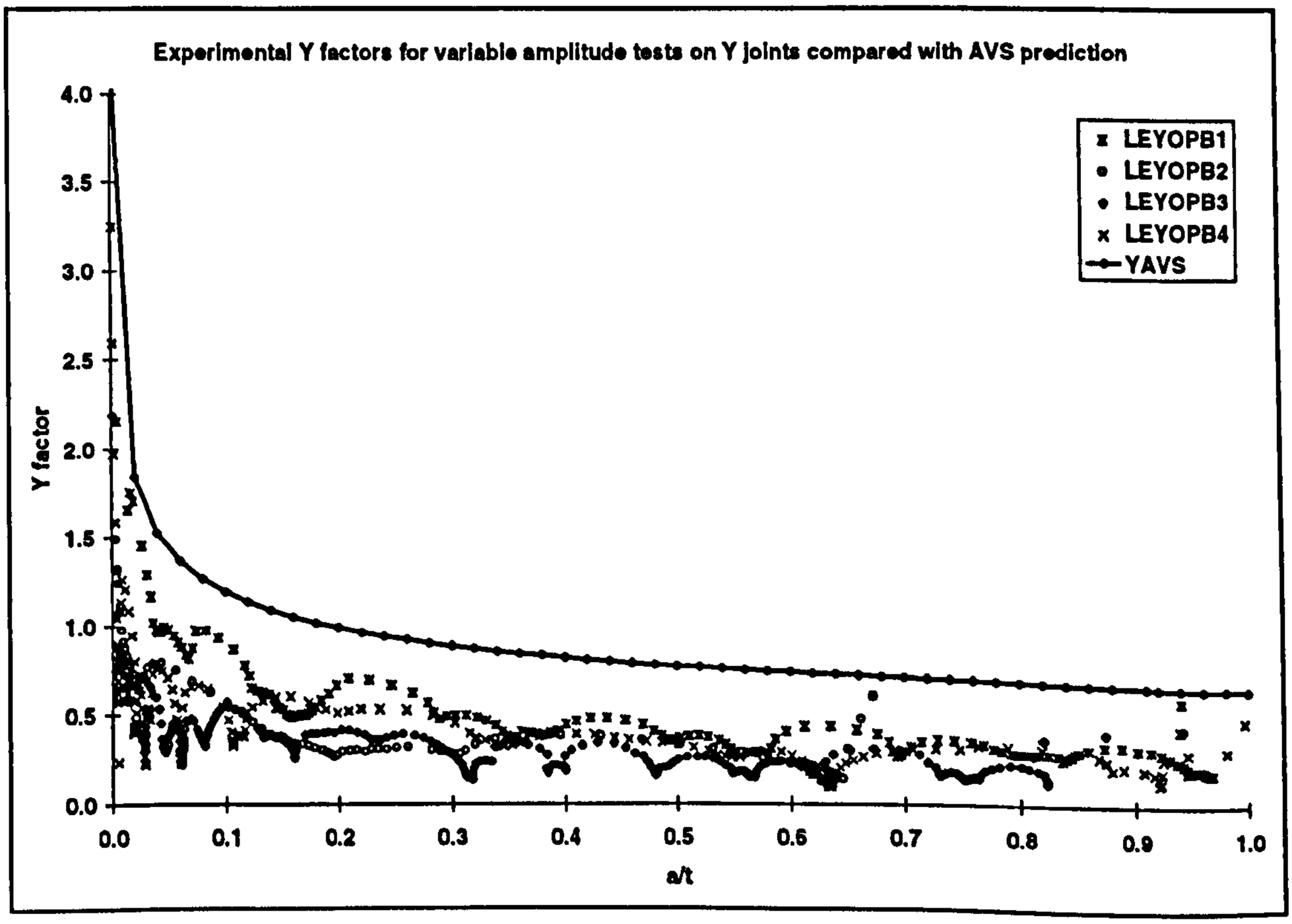

Figure 4.12: Comparison of experimental Y factors with AVS prediction

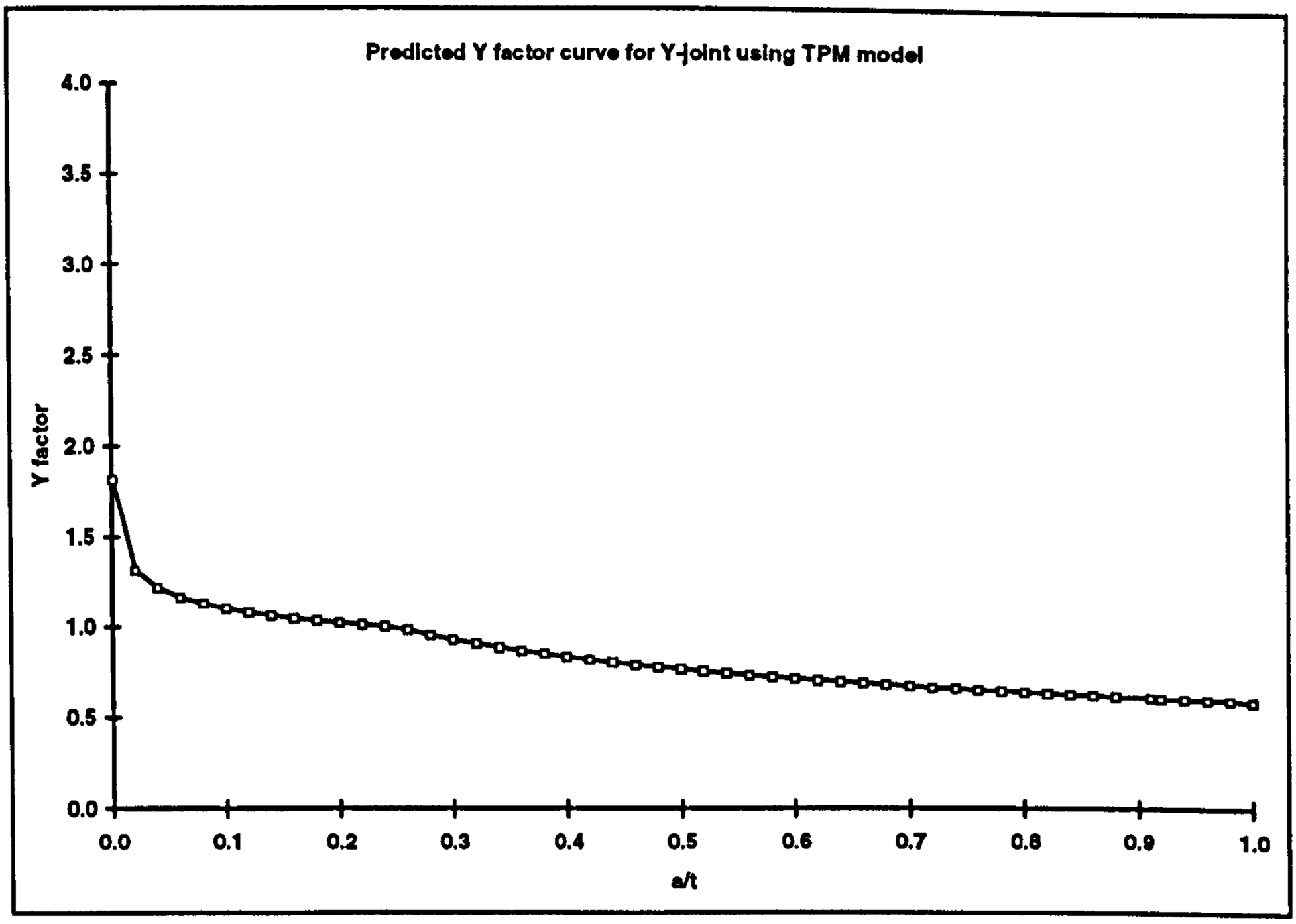

Figure 4.13: Predicted Y factor for Y-joints using the TPM model

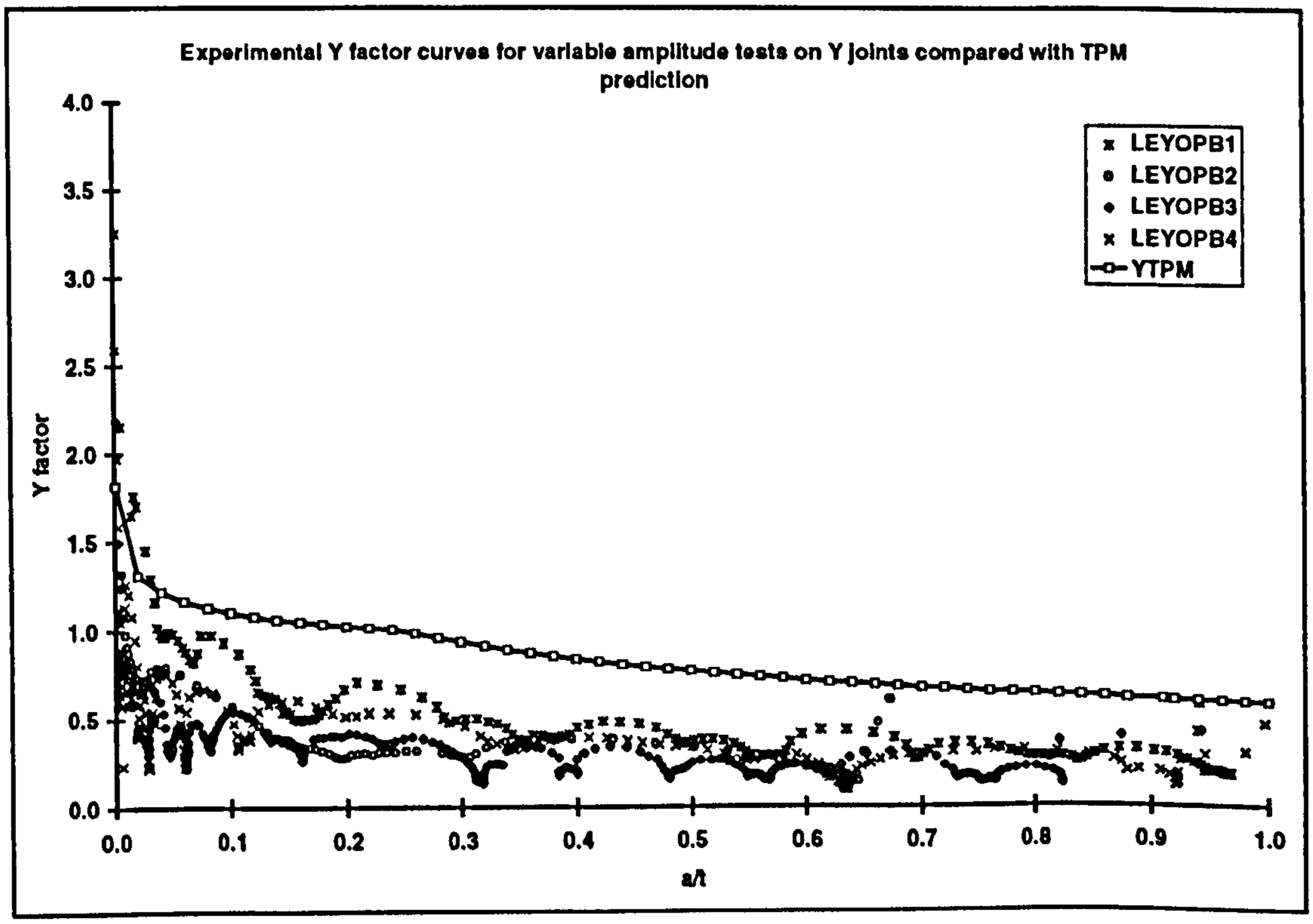

Figure 4.14: Comparison of experimental Y factor with TPM prediction

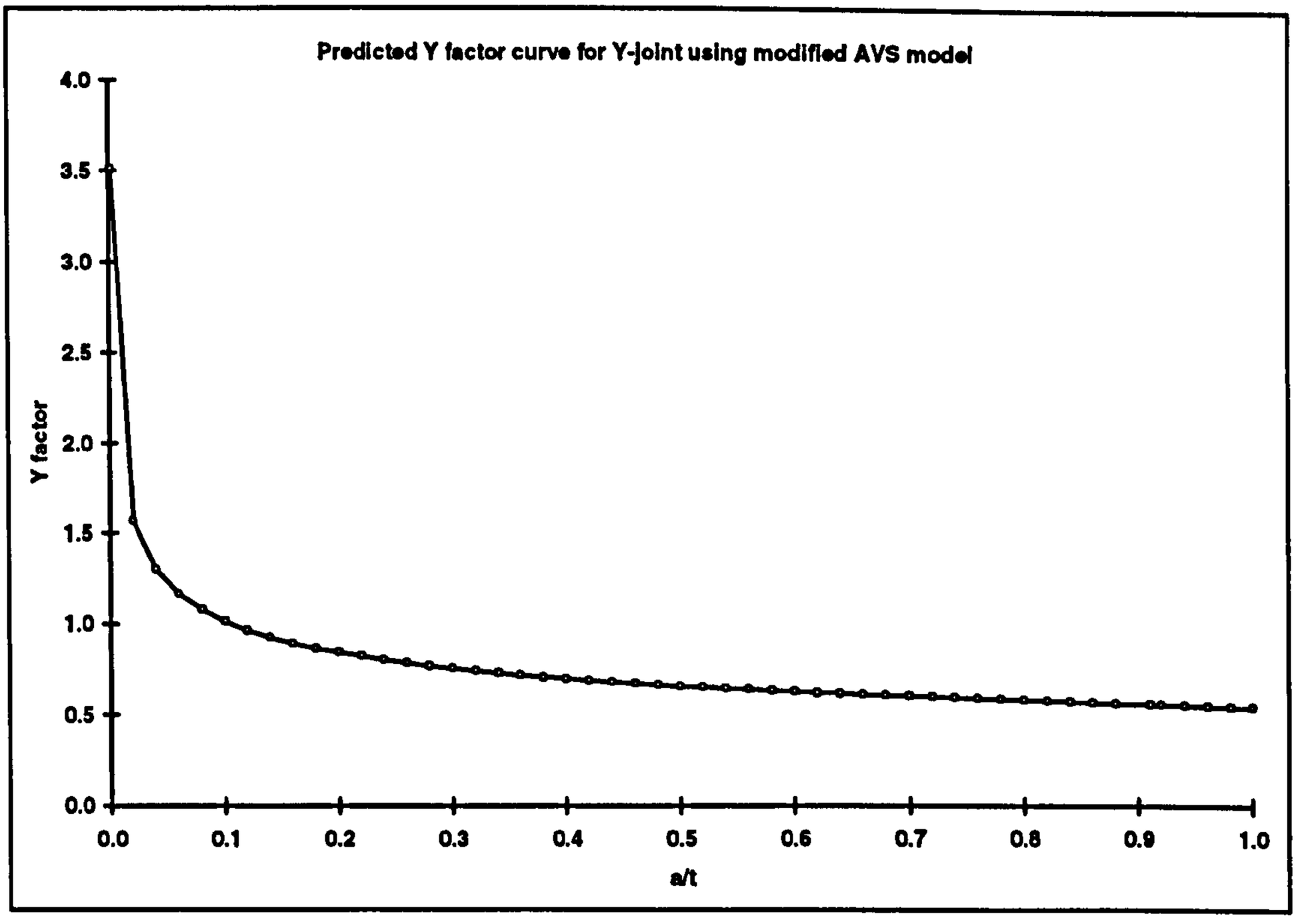

Figure 4.15: Predicted Y factor for Y-joints using the modified AVS model

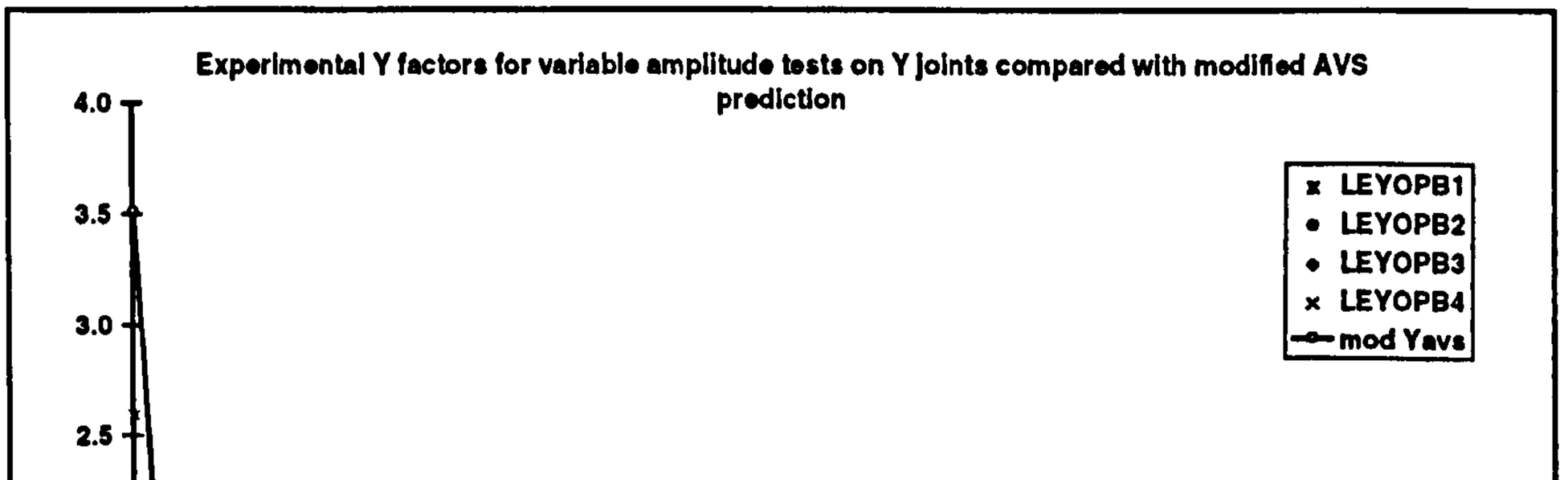

Figure 4.16: Comparison of experimental Y factor with modified AVS prediction

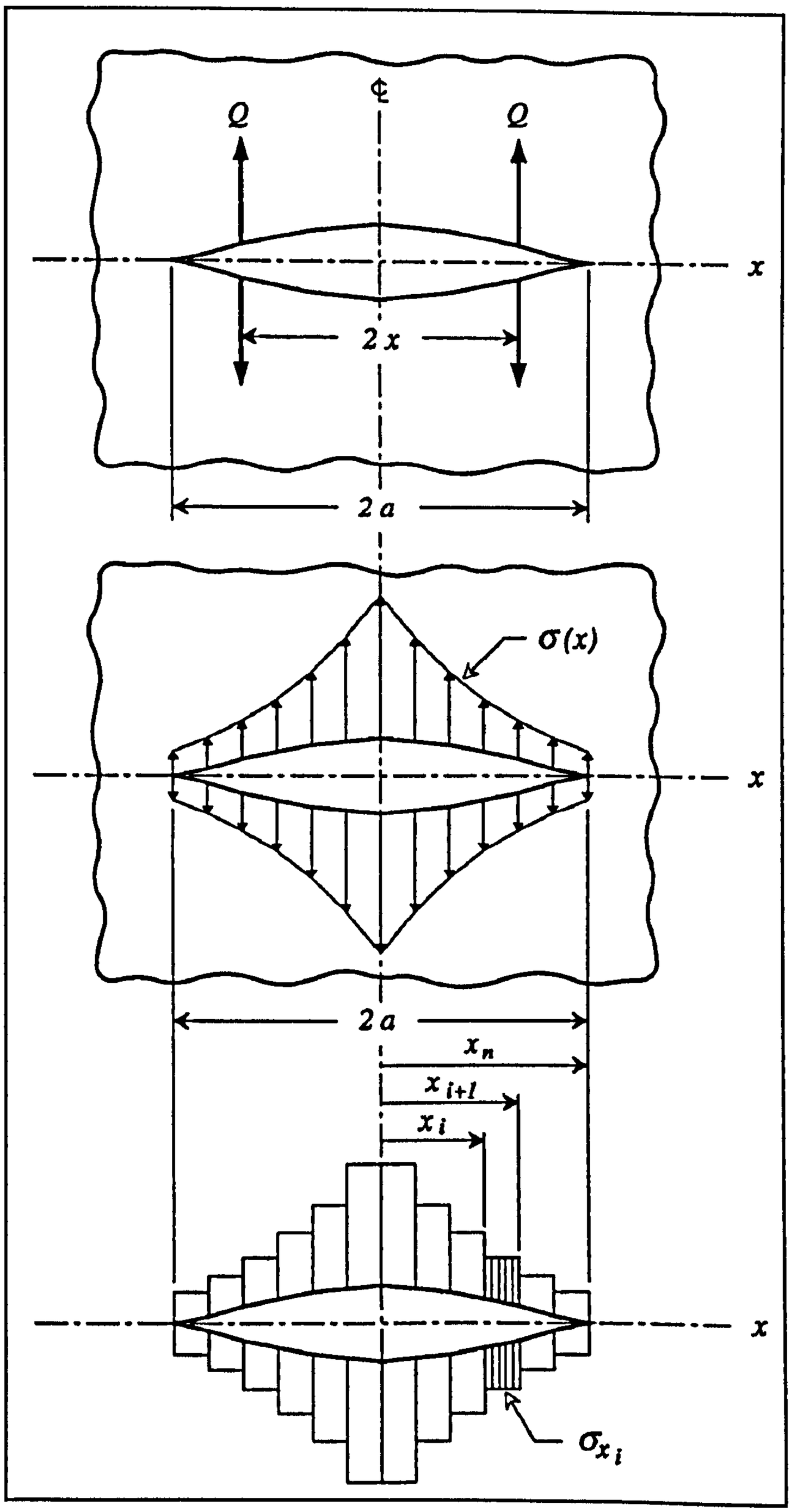

Figure 4.17: Schematic illustration of Albrecht's method for determining *Yg*

[4.18]

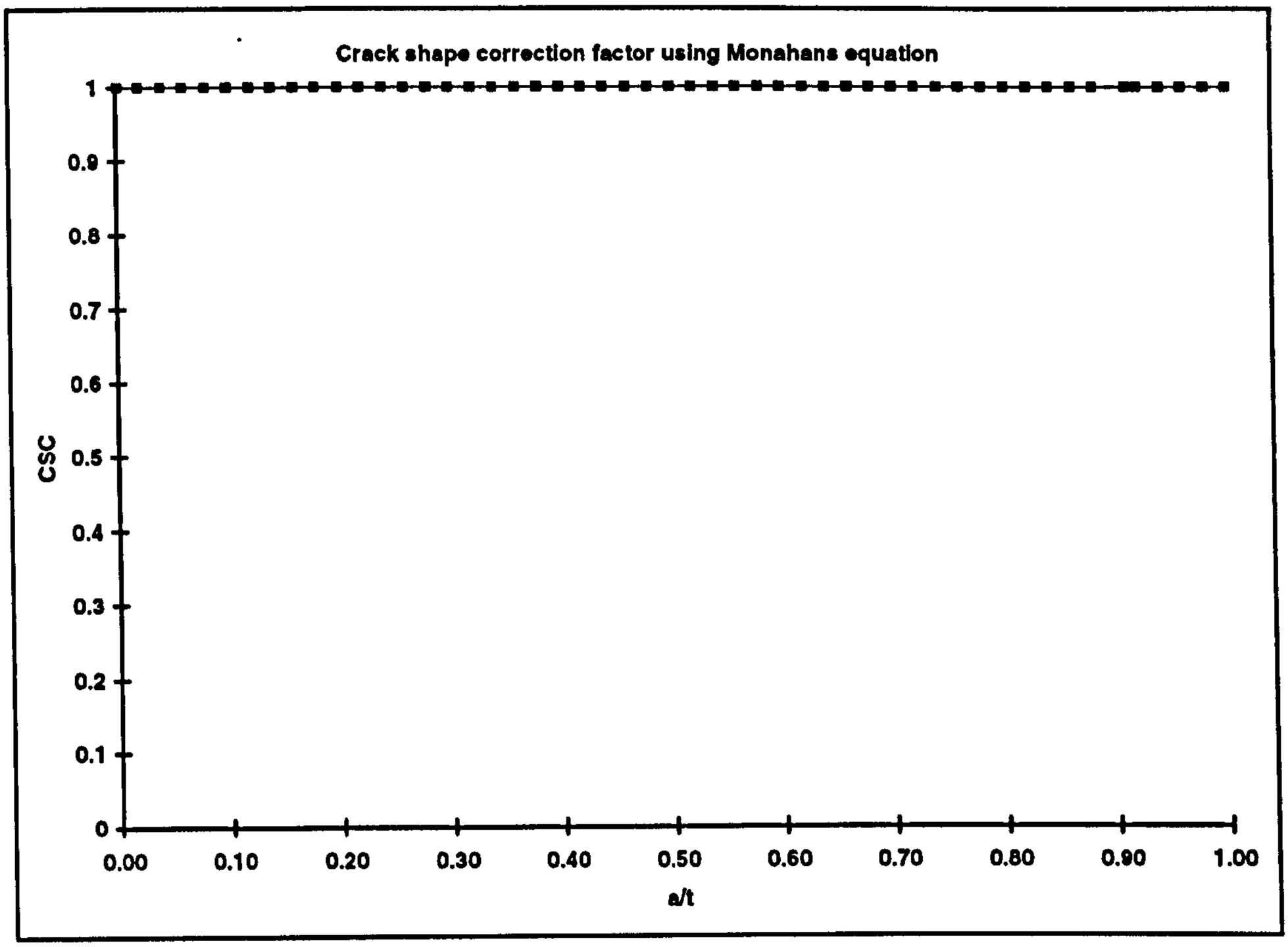

Figure 4.18: Monahan's CSC factors for use with the NR solution

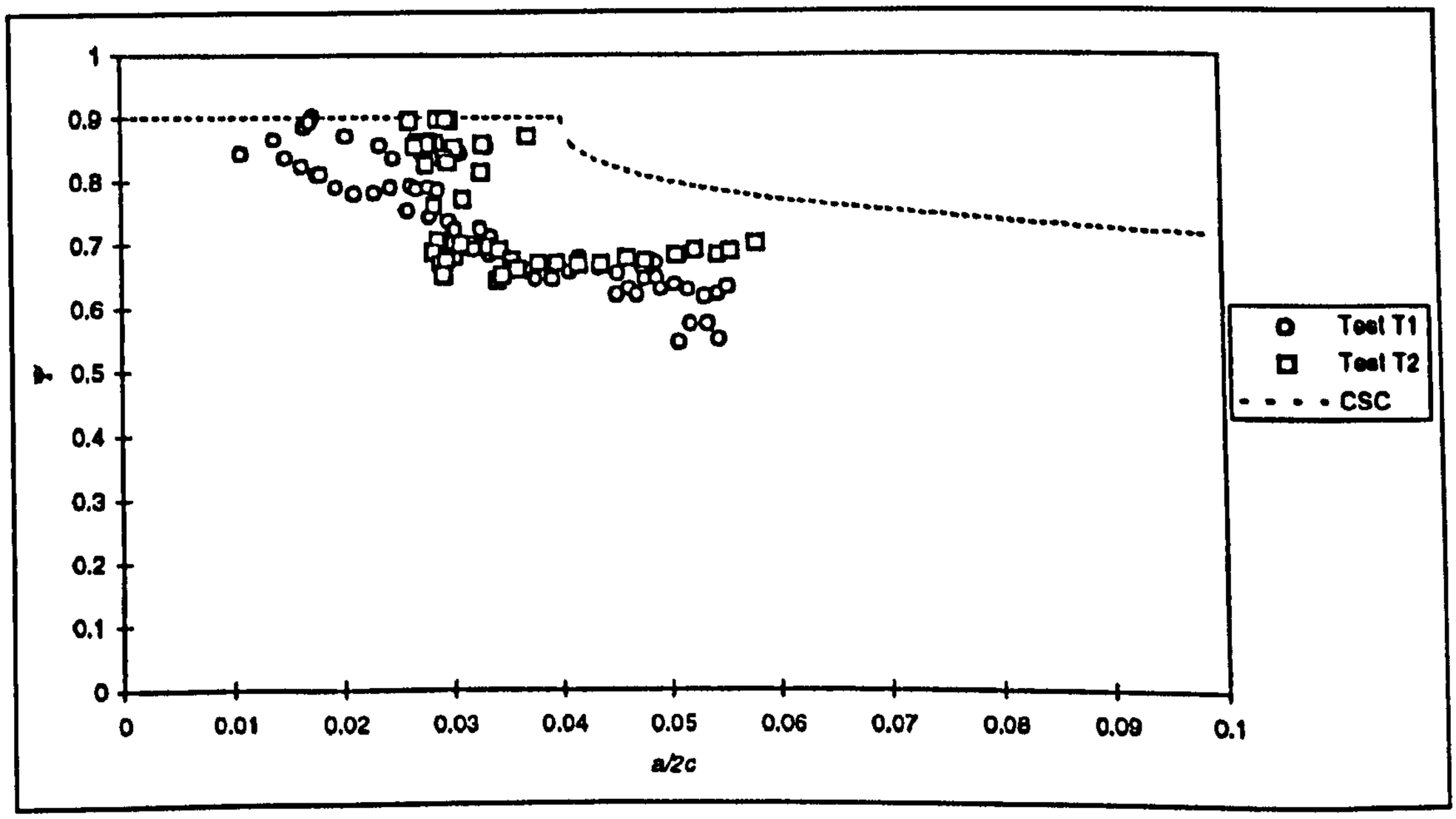

Figure 4.19: Myers' data used in deriving CSC factors for NR solution [4.20]

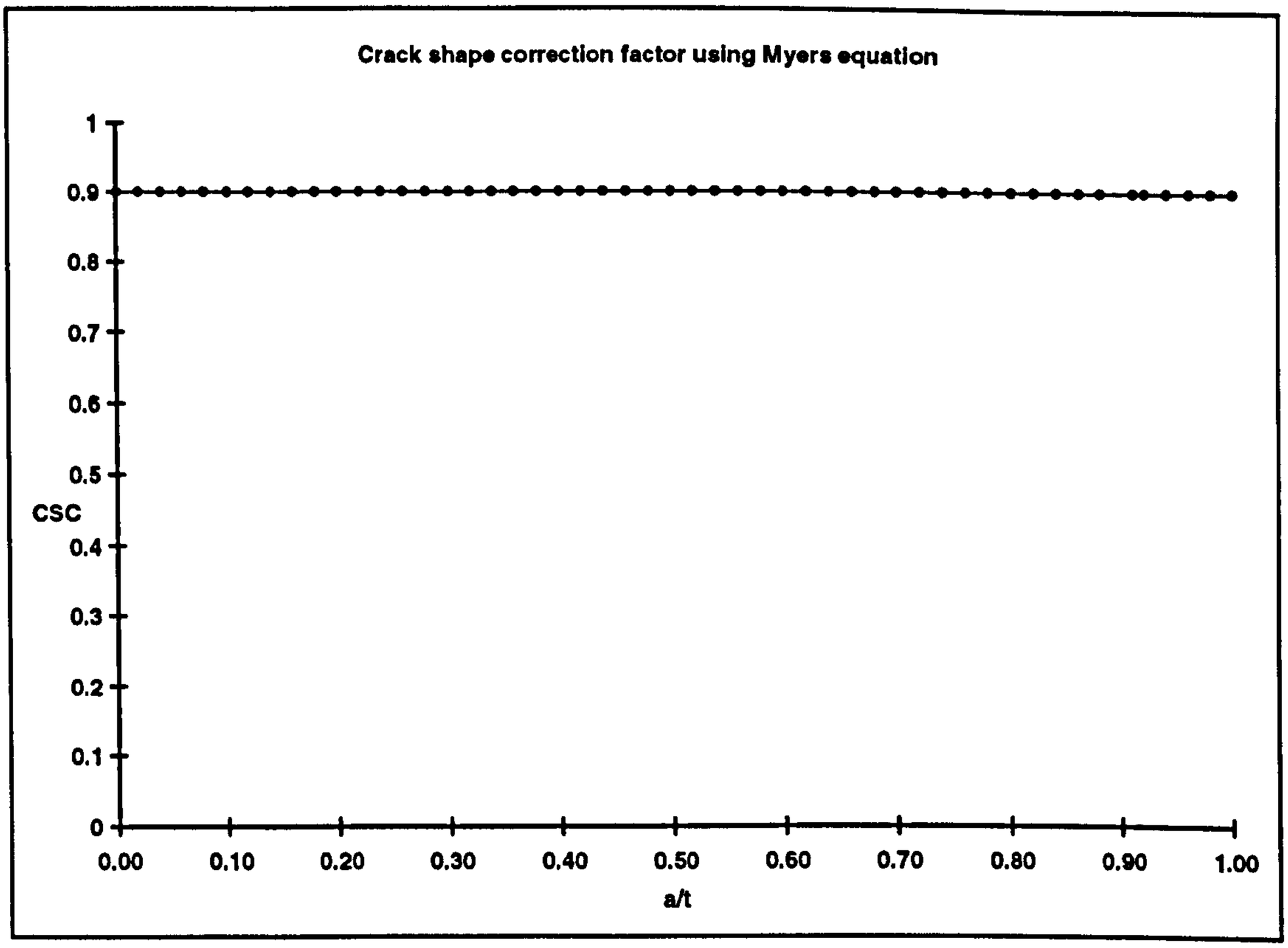

Figure 4.20: Myers' CSC factors for use with the NR solution

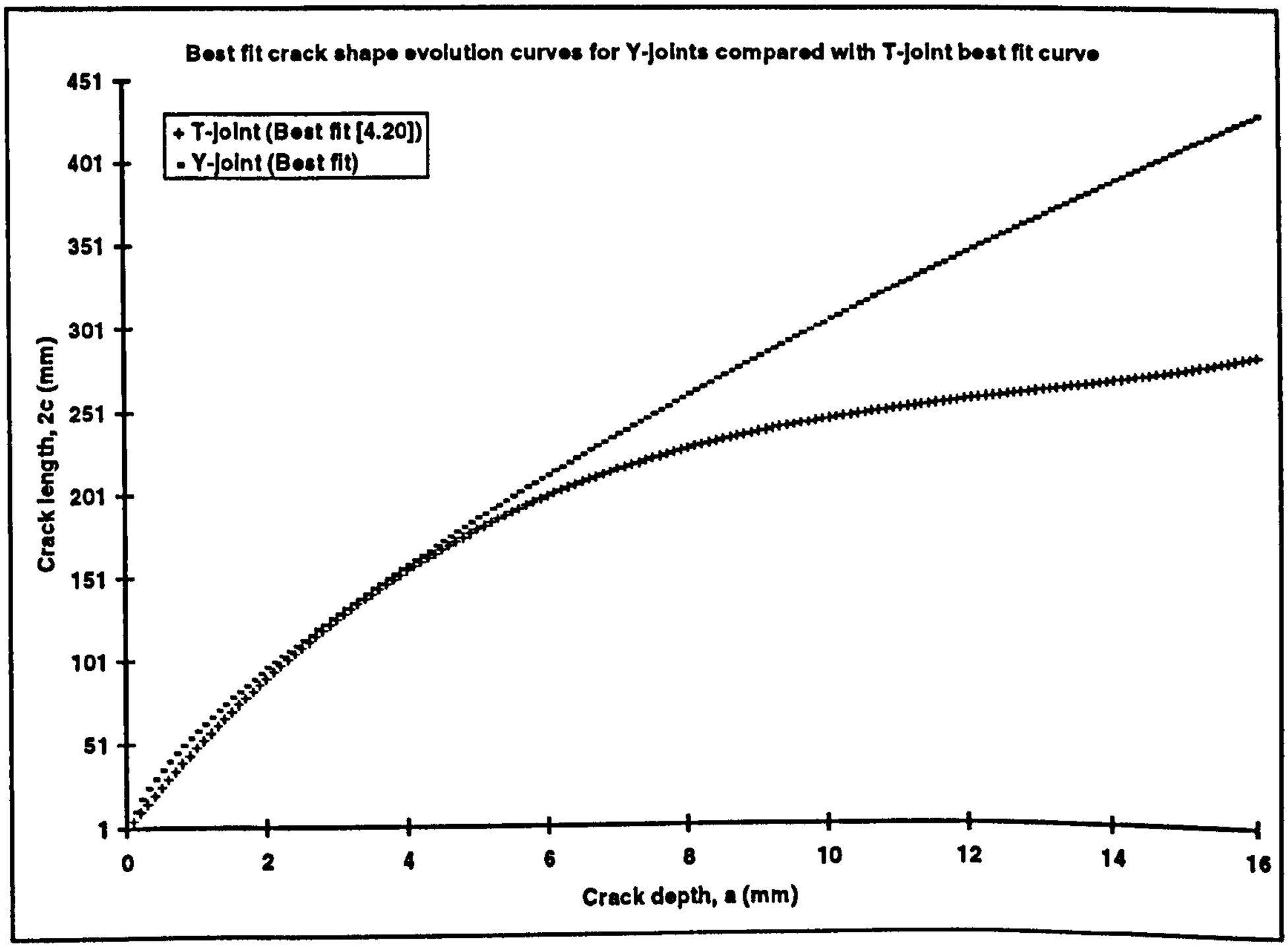

Figure 4.21: Comparison of crack shape evolution curves for Y and T-joints

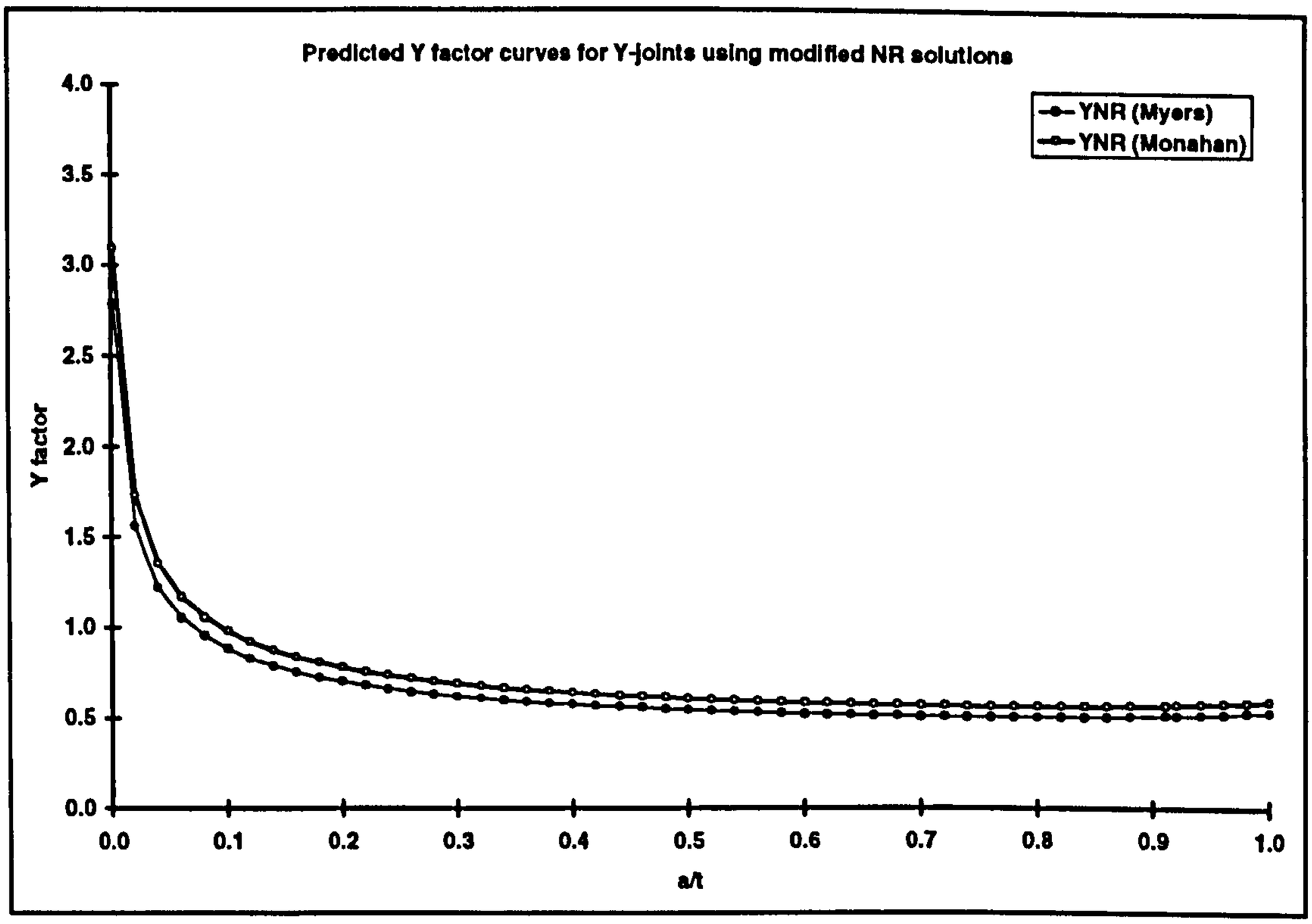

Figure 4.22: Comparison of Myers' Y factors with Monahan's

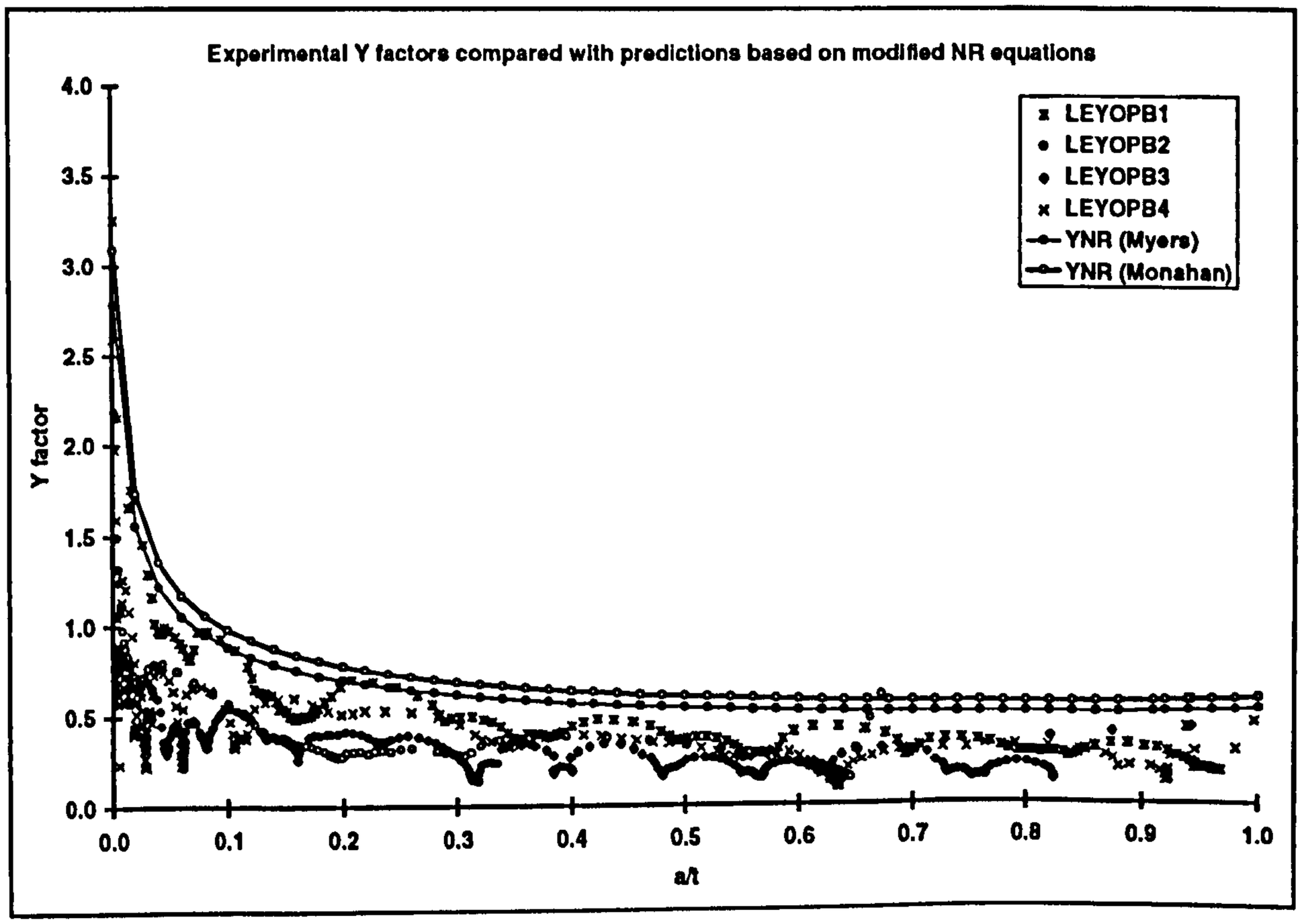

Figure 4.23: Comparison of Myers' and Monahan's solution with Y-joint data

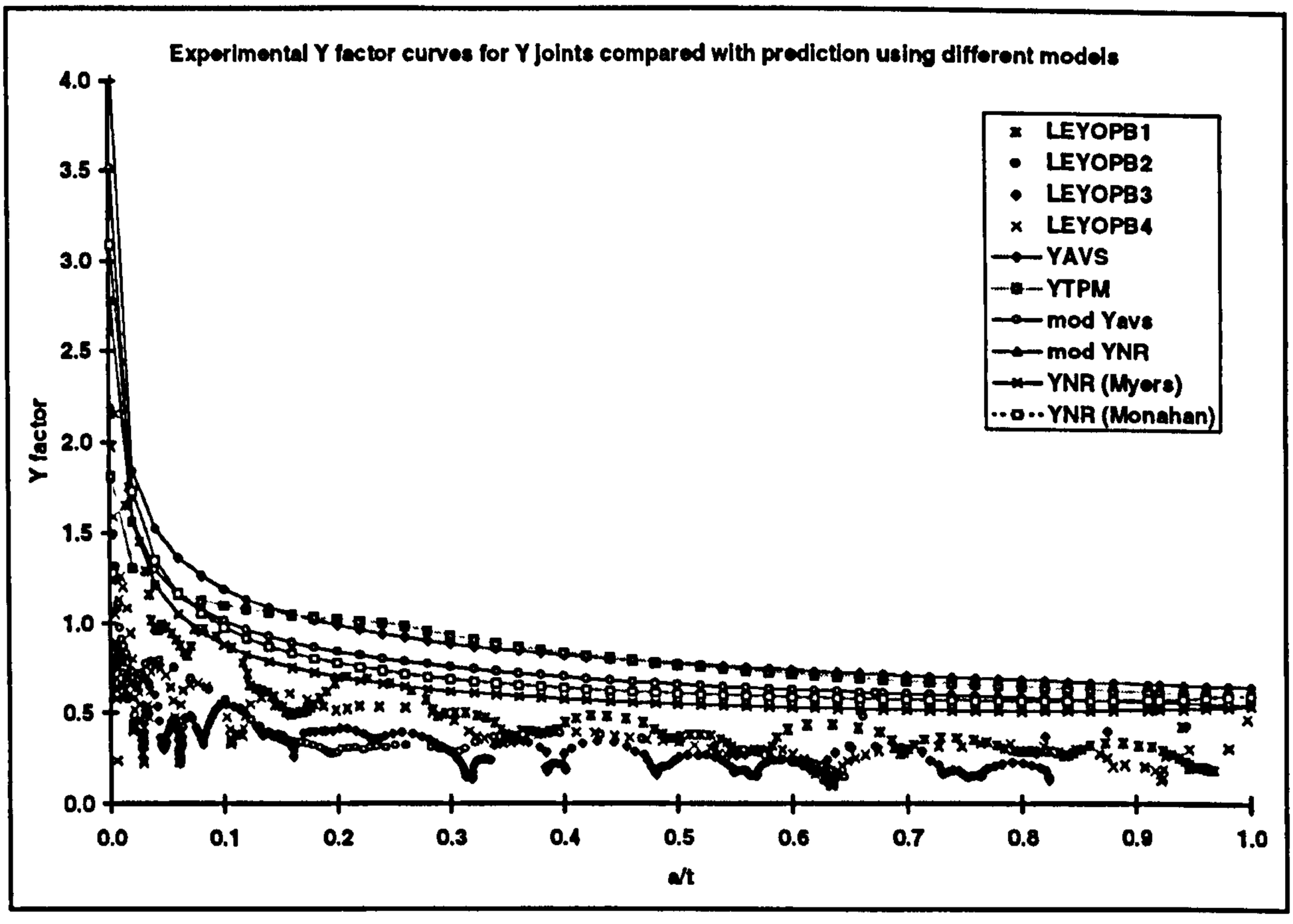

Figure 4.24: Comparison of Y factors from different models with Y-joint data

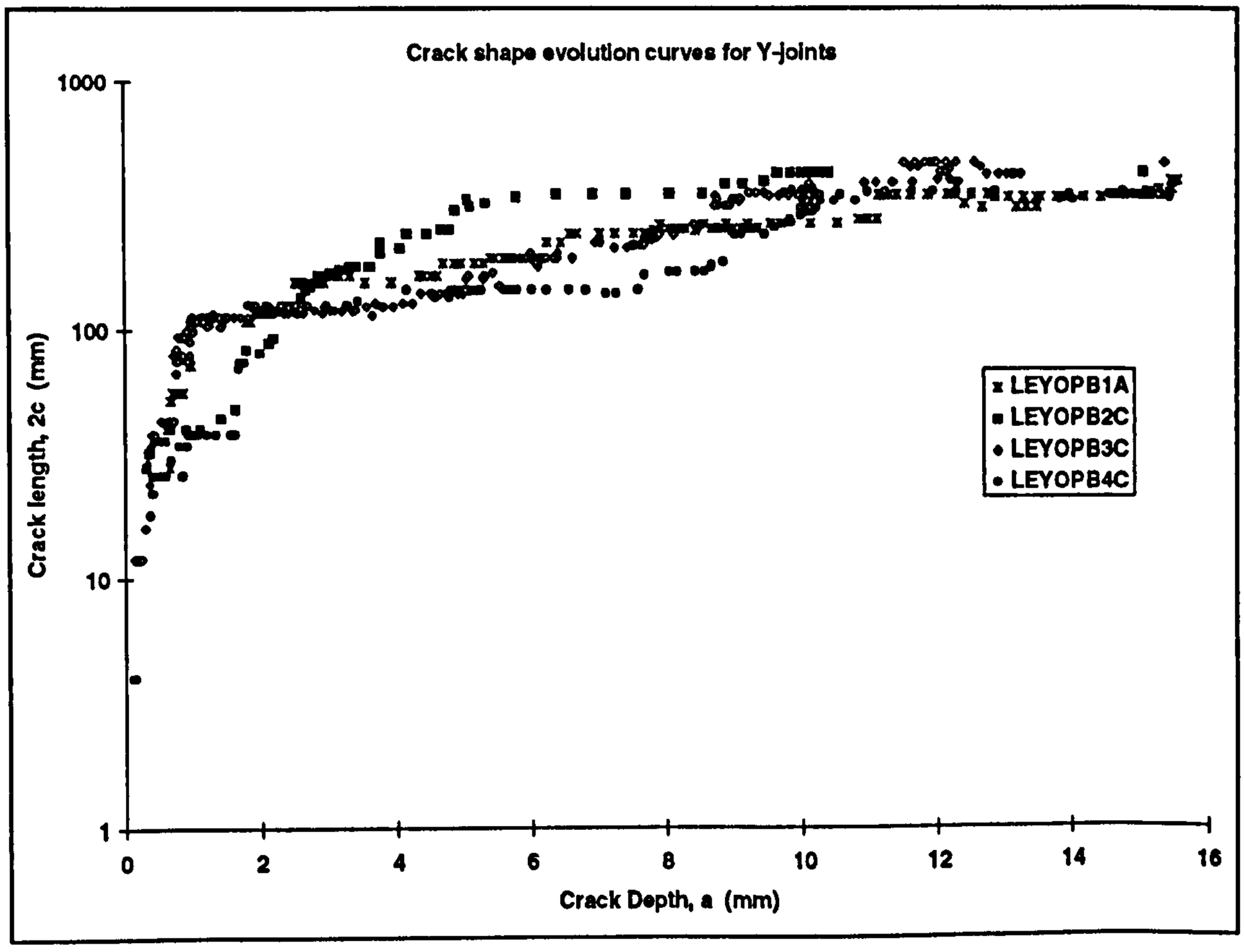

Figure 4.25: Variation of crack length with crack depth for Y-joints (OPB)

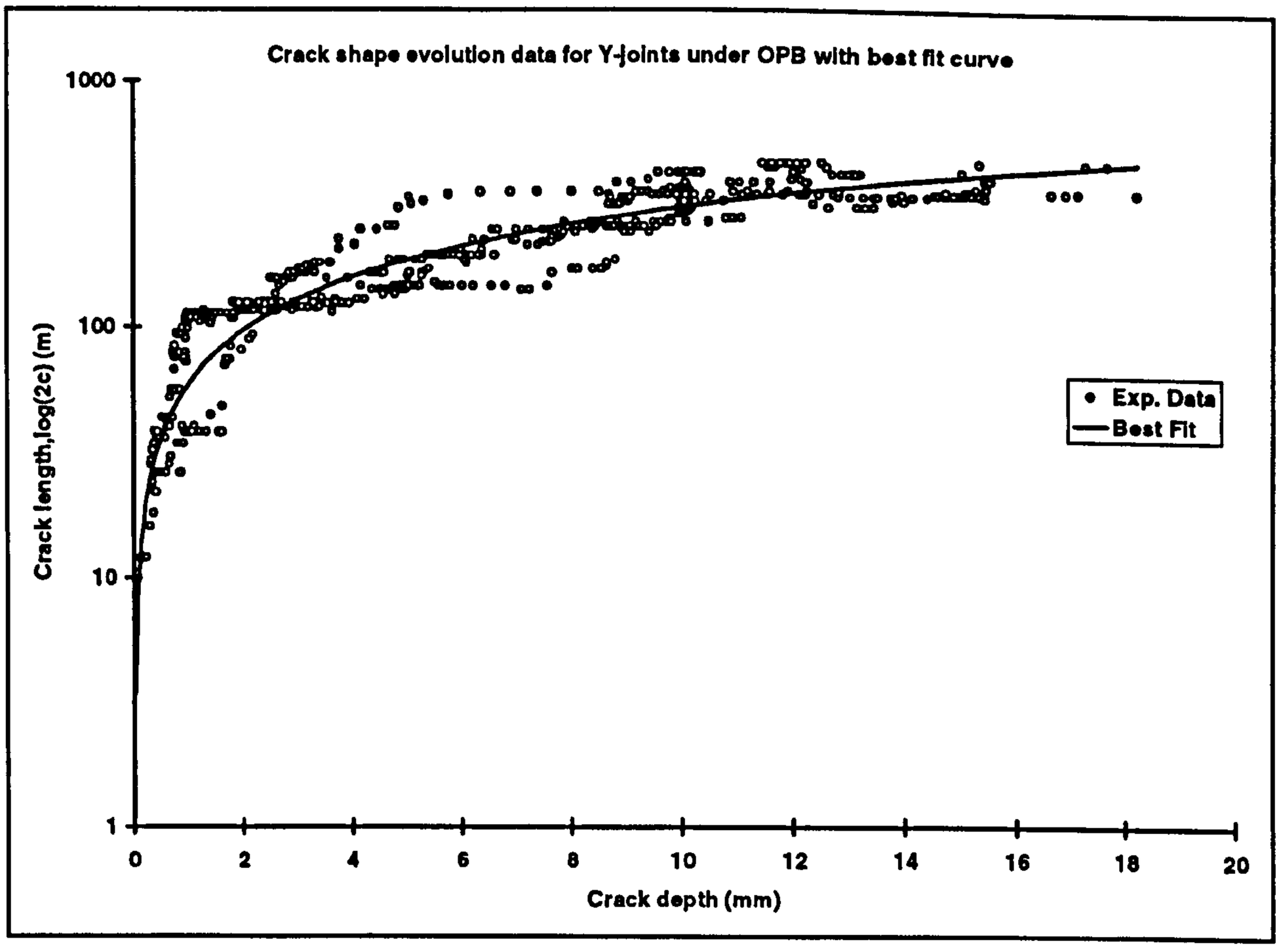

Figure 4.26: Illustration of curve fitting to experimental crack shape data

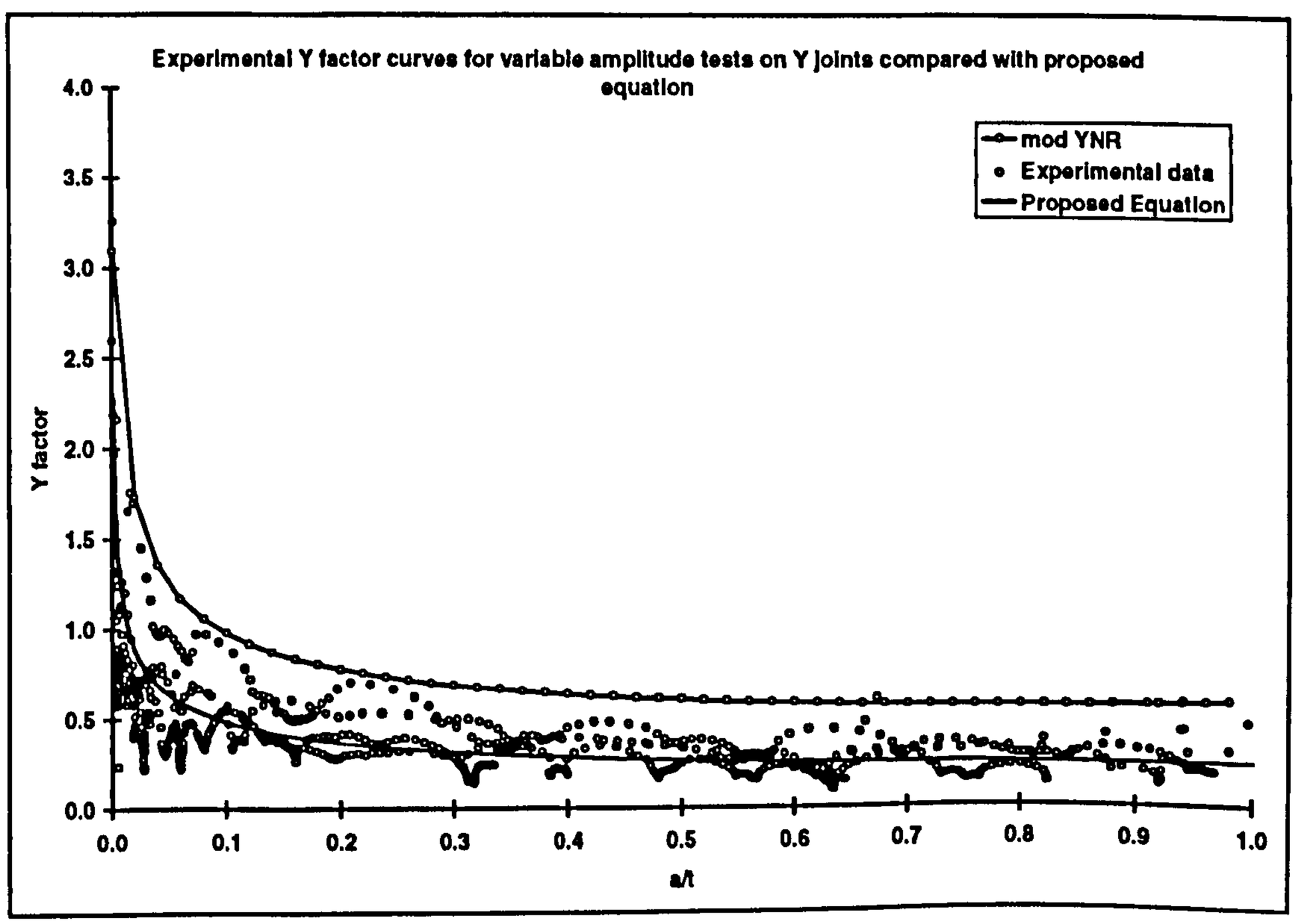

Figure 4.27: Comparison of best fit curve with the modified NR solution

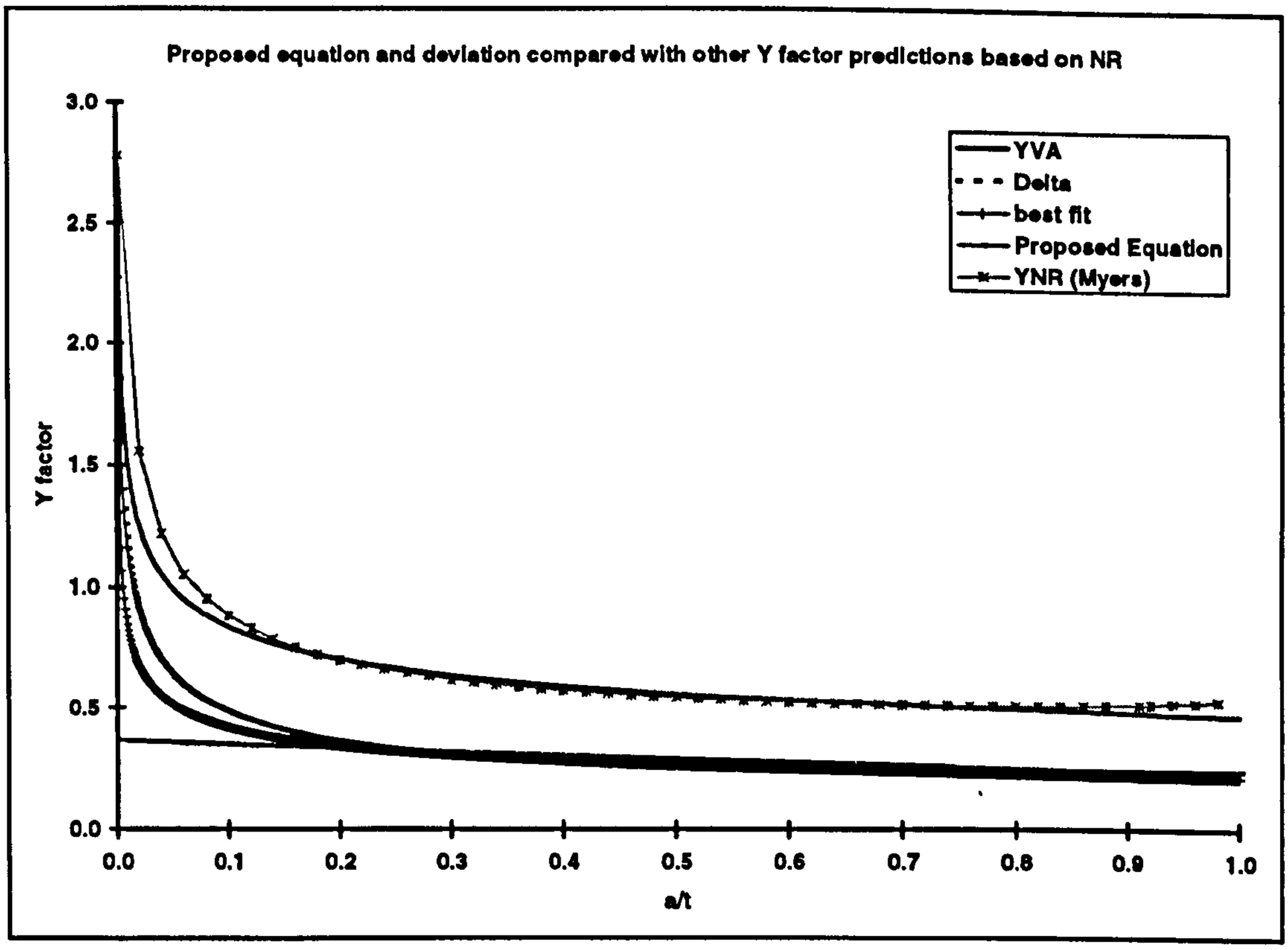

Figure 4.28: Modeled deviation (δ) of predicted results from experimental data.

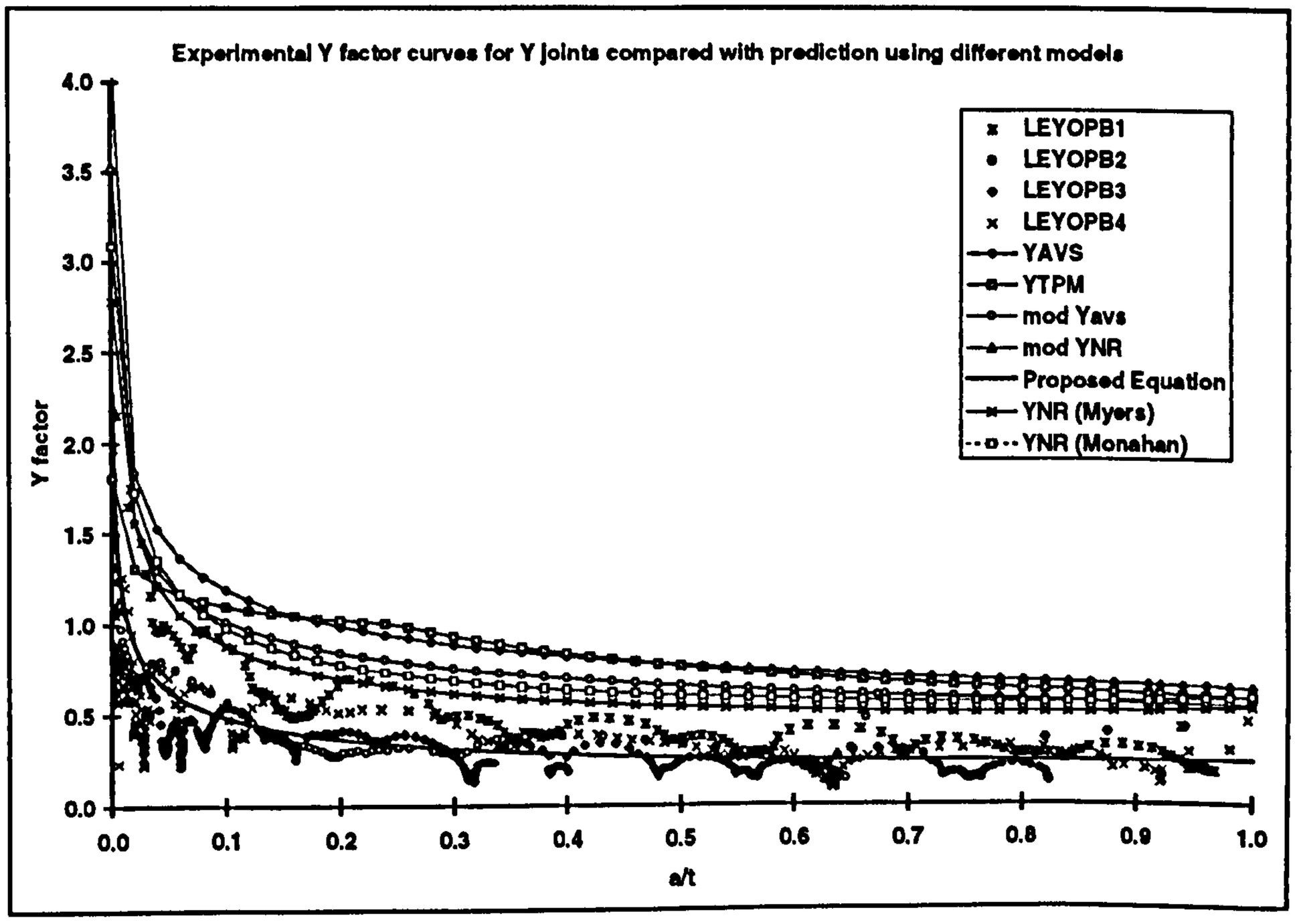

Figure 4.29: Comparison of proposed Y factor solution with other solutions

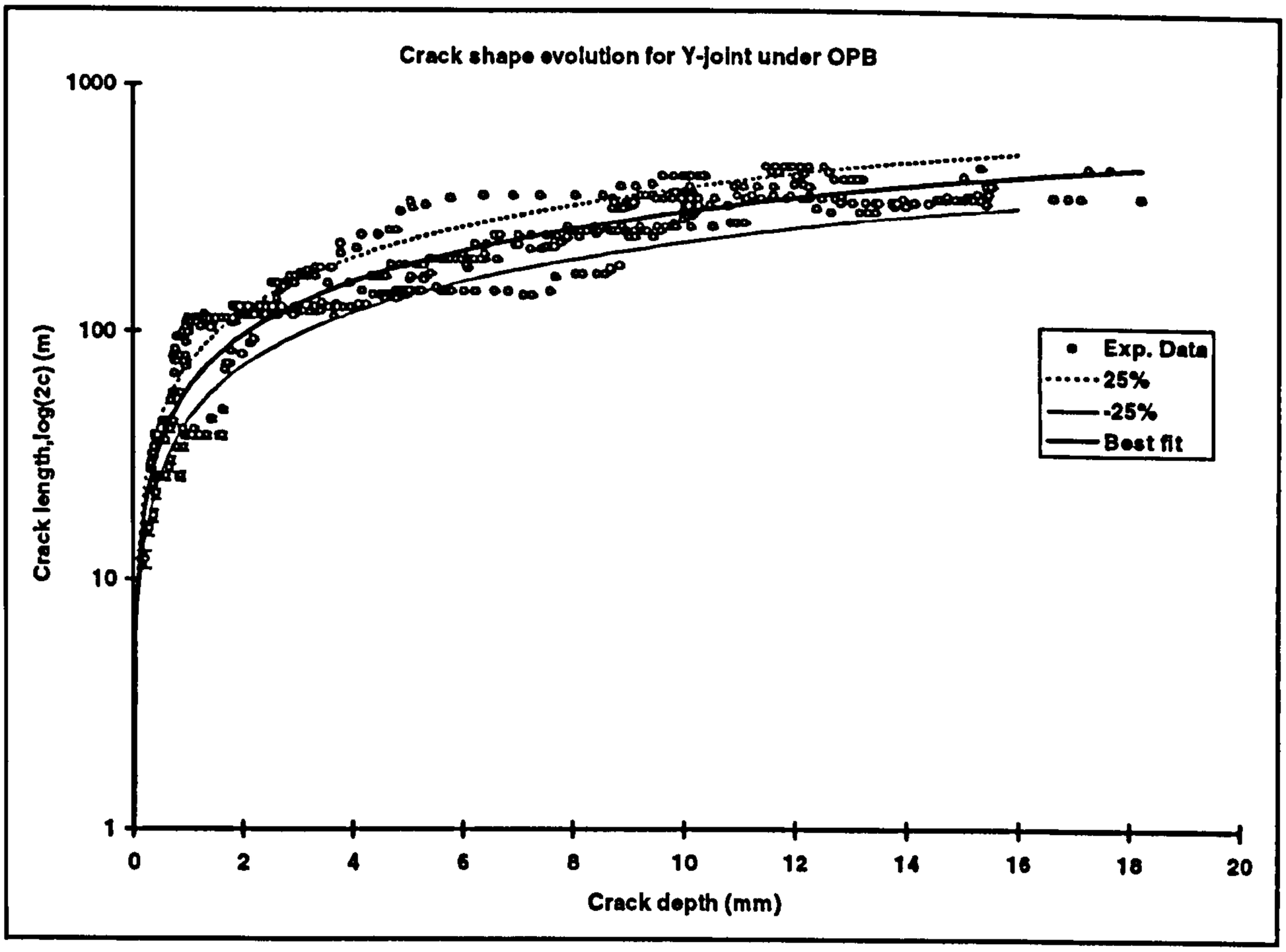

Figure 4.30: Effect of wide scatter on crack shape evolution data

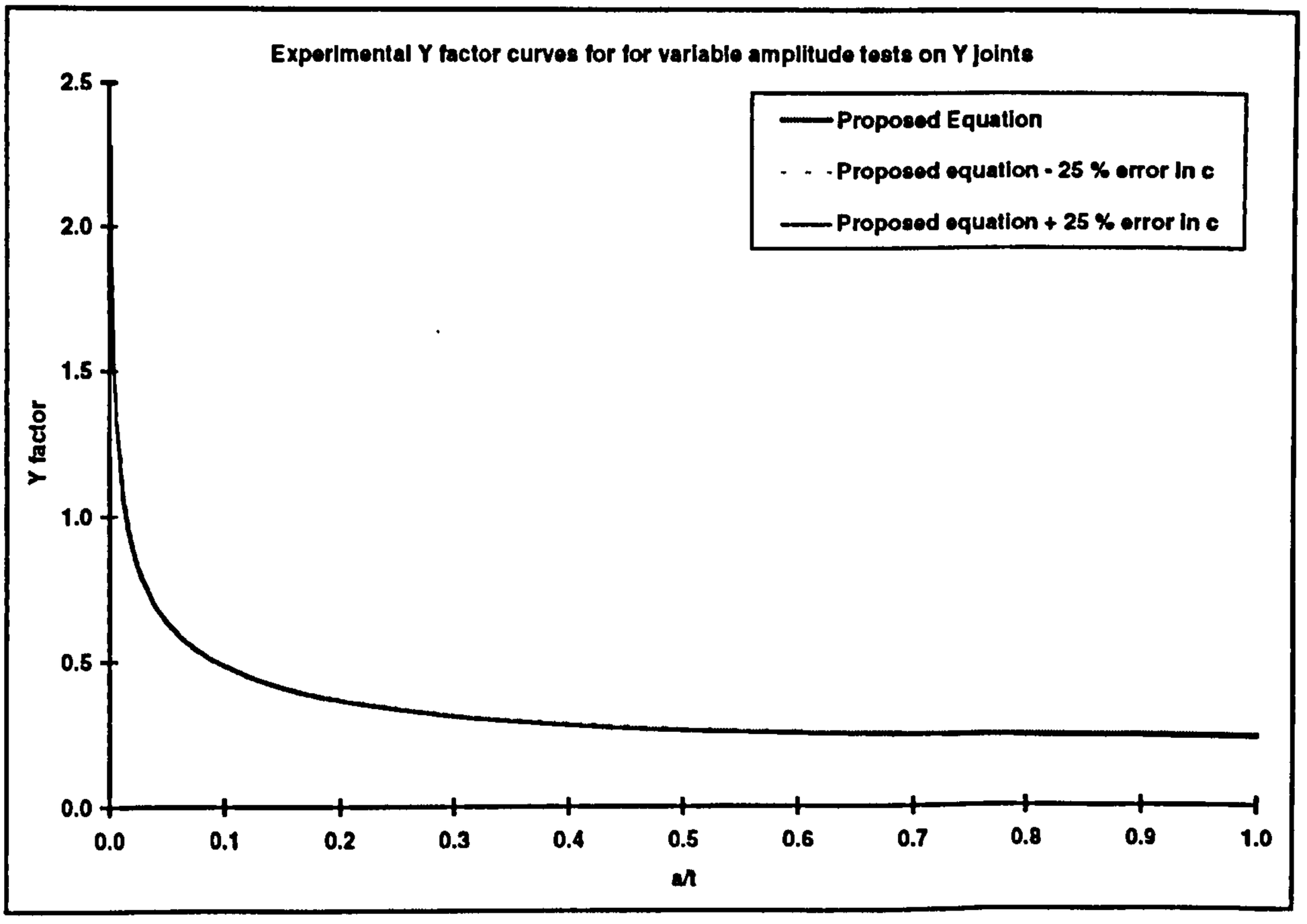

Figure 4.31: Effect of ±25% error in predicted crack length on Y factor

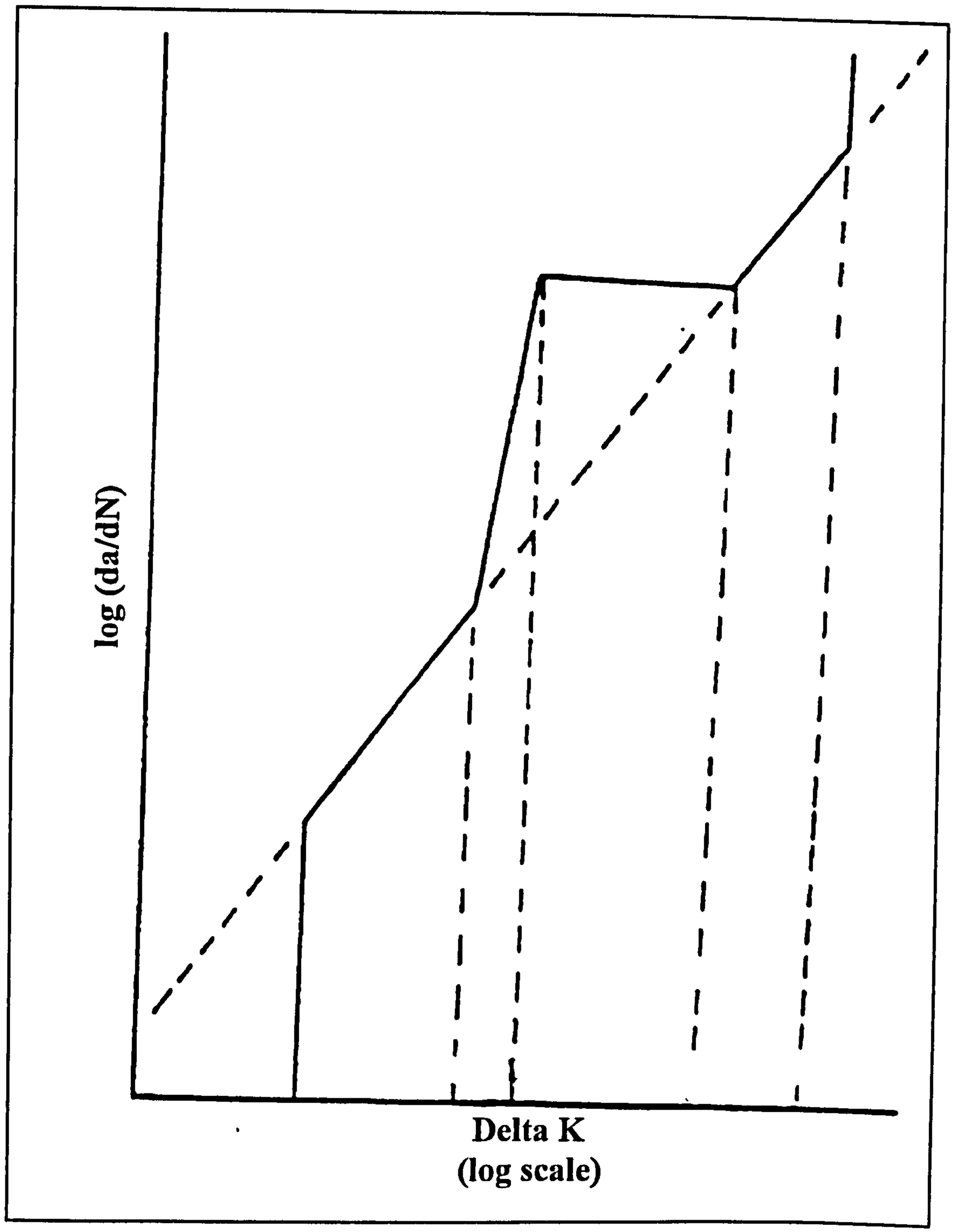

Figure 4.32: Typical multi-segment corrosion fatigue crack growth rate curve

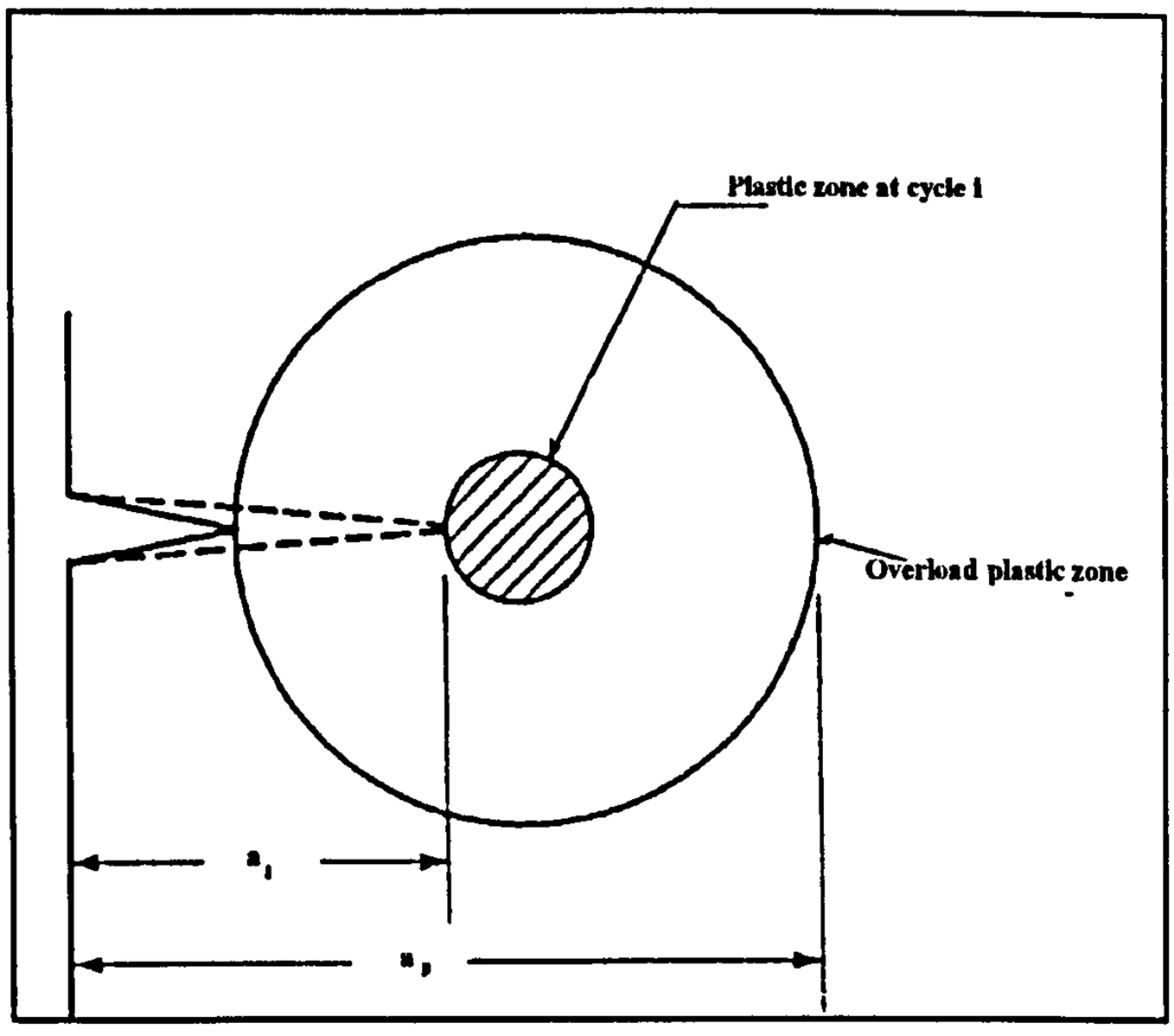

Figure 4.33: Schematic illustration of Wheeler model parameters [4.29]

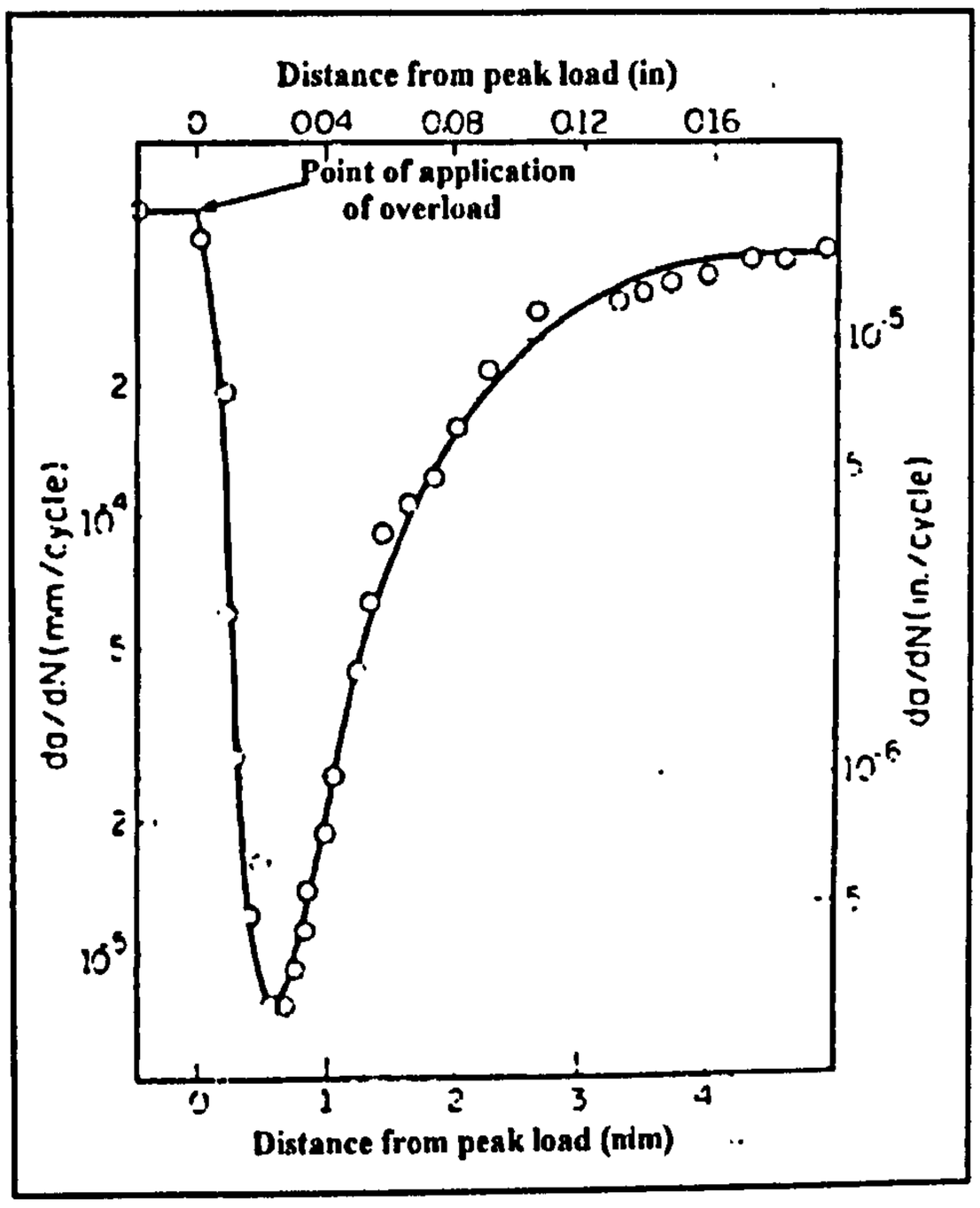

Figure 4.34: Schematic illustration of delayed retardation [4.30]

CHAPTER 5

5. MODELS FOR FATIGUE ANALYSIS OF OFFSHORE STRUCTURES

5.1 INTRODUCTION

Service loading of Offshore structures is mainly due to wave and wind action with variable amplitude and frequency content. Fatigue failure of structural components under these conditions is a major concern in the maintenance of Offshore structures. This is all the more so since the process of fatigue in Offshore structures in the North Sea for example is influenced by very many factors which may be different in each application area depending on the complex interaction between the loading and the environment.

The characteristics of fatigue loading which apply to Offshore structures such as Jack-up platforms have been covered in detail in Chapter 2. The way they were modelled to produce realistic results for this study has been presented in Chapter 3 where details of the fatigue testing programme are also given. Fatigue testing under simulated service conditions has advantages over constant amplitude tests. For example the variability in both amplitude and frequency content of service loading can be reproduced by carrying out tests under simulated service conditions. This means that the complex interactions between environment and loading which govern fatigue crack growth mechanisms in Offshore structures are taken into account.

Existing fracture mechanics models and fatigue crack growth prediction methods generally rely on using the overall equivalent stress range together with a suitable crack growth law for fatigue crack growth prediction under variable amplitude loading. For S-N type analysis this method is by far the best when dealing with variable amplitude sequences. However, for fracture mechanics (FM) crack growth prediction employed after an in-service inspection schedule, the use of the overall sequence equivalent stress range will not allow for sequence effects to be accounted for. These effects can be significant under service loading conditions as crack growth is largely dependent on the stress intensity factor range-which is a function of stress range and crack size. It is possible that the use of the overall sequence equivalent stress concept in a fracture mechanics analysis procedure may not be robust enough to handle the high degree of variability observed in service as crack growth acceleration

and retardation can not be accounted for using this approach. A different and more realistic fracture mechanics based approach is required.

This Chapter seeks to address this problem. It presents a fast assessment procedure for the determination of load spectra for fatigue analysis of Offshore structures. It also presents a proposed fracture mechanics based model for predicting fatigue crack growth in Offshore structures.

Due to the fact that fatigue is sensitive to many factors, extrapolating fatigue behaviour, obtained by studying crack growth under constant amplitude loading conditions, to in-service loading is not easy. As a result fatigue testing of Offshore structures has been performed in more recent years by use of simulated service loads under simulated environmental conditions [5.1, 5.2, 5.3, 5.4]. The use of this approach requires the generation of real time multi-sea state sequences so that equivalent stress ranges can be found by counting fatigue cycles in the sequences with standard counting techniques such as rainflow counting.

The process of signal generation and cycle counting is often a very lengthy one. Theoretical equations such as Wirsching [5.5, 5.6], Chaudhury and Dover [5.7], Hancock [5.8] and Kam and Dover [5.9] have been proposed which have made it possible to avoid this lengthy signal generation and cycle counting process. These however have been limited to discrete spectra where only the equivalent stress for a particular sea state for example can be obtained. This Chapter presents a methodology that can be used to calculate the crack growth associated with any particular sea state by using these theoretical methods. It then illustrates how a proposed probability distribution function can be used together with fast assessment equations to predict the behaviour of cracked Offshore structures under service loading conditions. This approach relies on the use of a sea sate probability distribution function together with a sea state equivalent stress concept to characterise fatigue crack growth in Offshore structures.

This Chapter gives details of how the sea state equivalent stress concept can be applied to Offshore structures using a conventional cycle counting methodology. It further introduces a sea state probability distribution function and illustrates how it

can be used to calculate equivalent stresses for typical Offshore loading for use in fatigue assessment.

5.2 IMPLICATIONS OF RESULTS OBTAINED FROM SE702

Four variable amplitude tests conducted on Y-joints in this study have been presented in Chapter 3. The joints were fabricated from SE702, a 700MPa yield steel. The results presented in Chapter 3 have also been compared with those obtained from similar studies and especially those conducted under constant amplitude conditions using T-joints [5.10] made from the same steel. Both air and sea water tests were compared and the one significant difference observed in terms of fracture mechanics analysis, was the fundamental difference in the nature of fatigue crack growth under the two loading conditions.

Characteristic 'stair case' type crack growth curves were consistently obtained for the Y-joint tests. This experimental observation suggests that crack growth under variable amplitude conditions is not uniform. The non uniform crack growth under variable amplitude loading conditions will make the prediction of fatigue crack growth in Offshore structures where multi sea state type loading prevails more difficult. It is therefore recommended [5.11] that a sea state based fracture mechanics approach is used to allow for this variations in crack growth within individual sea states to be accounted for. The implementation of this methodology is presented in subsequent sections of this Chapter.

5.2.1 Limitations of Conventional FM Approaches

The results obtained from the variable amplitude fatigue tests conducted for this study were analysed using existing fracture mechanics models. The results obtained have been presented in Chapter 4. It was noted in Chapter 4 that fatigue crack growth models for the analysis of fatigue crack growth under variable amplitude conditions are limited and that most of the existing models do not allow for interaction effects to

be accounted for. It was also concluded that those models which attempt to model interaction effects are based on a cycle by cycle analysis with emphasis on single overloads or underloads. This makes their application to Offshore structures impractical.

In order to overcome these difficulties a new approach is required which will allow for the experimentally observed crack growth behaviour to be adequately analysed.

5.3 FAST ASSESSMENT OF OFFSHORE STRUCTURES

The sea state PSDs generated from the structural dynamic transfer function approach outlined in Chapter 2 can be presented in normalised form. The advantage of using normalised spectra is that it can facilitate the process of comparison of PSDs resulting from different sea states. This method was used to compare the model transfer function with the service measurements obtained from the Maersk Guardian Jack-Up platform. As a result suitable scaling factors were applied to the normalised PSDs to investigate the effect of the scaling factor on the stress range probability distribution for the generated sequence. The results obtained are shown in figure 5.1. There is a clear indication that the effect on the SRPD due to any changes in the magnitude of the scaling factor is negligible for any chosen output range normally determined by the load requirement for any particular test. This is not surprising as the output scales used to generate the distribution of turning points are weighted with respect to the parameters of the extreme PSD [5.12, 5.13] which is normally that which corresponds to the extreme sea state. The scale for any sea state *i* is then given as;

$$Scale_i = A\left(\frac{(Sum\ of\ weight_i)\sqrt{f_{P_i}}}{(Max\ sum\ of\ weight)\sqrt{f_{P_n}}}\right) \tag{5.1}$$

Where A is the calibration factor determined by the required maximum output amplitude. This is governed by the load requirement for any particular test. f_{P_i} is the peak frequency for sea state *i*. It depends on the fourth and second spectral moments of the power spectrum and given by;

$$f_P = \sqrt{\frac{M_4}{M_2}} \tag{5.2}$$

$$M_j = \int_0^{\infty} S(f) f^j df \tag{5.3}$$

This method of scaling has been shown [5.12] to be applicable to power spectra of similar shape such as those shown in figures 5.2 and 5.3.

Based on this philosophy, an equation is proposed which uses non dimensional parameters to estimate the normalised PSD for any structure under wave excitation in the North Sea for any given set of sea states. The basic form of this equation is given as;

$$S(f)_N = \frac{4H_r^2 T_r^{-4} \Omega^{-5} \xi^2}{\left[\left(1-\Omega^2\right)^2 + \left(2\xi\Omega\right)^2\right]} Exp\left[\frac{1}{\pi}\left(\left(f_n T_{z_{ext.}}\right)^{-4} - \left(fT_z\right)^{-4}\right)\right] \tag{5.4}$$

Where f_n is the natural frequency of the structure and ξ is the damping ratio. H_r, T_r and Ω, are non dimensional parameters given by;

$$H_r = \frac{H_s}{H_{s_{ext.}}} \tag{5.5}$$

$$T_r = \frac{T_z}{T_{z_{ext.}}} \tag{5.6}$$

$$\Omega = \frac{f}{f_n} \tag{5.7}$$

The derivation of this equation is based on the assumption that normalising the PSDs for each sea state with respect to the extreme or most severe sea state does not change the stress range probability distribution for that particular structure under the given set of sea states. This is demonstrated below.

5.3.1 Proposed Normalised PSD Equation

The derivation starts with the complex structural dynamic transfer function and the wave excitation spectrum given by equations 5.8 and 5.9 respectively and uses the solution given by equation 5.10 below.

$$H(f) = \frac{\left(1/K\right)}{\sqrt{\left(1-\left(\frac{f}{f_n}\right)^2\right)^2 + \left(2\xi\frac{f}{f_n}\right)^2}} \tag{5.8}$$

$$S_{yy}(f) = \frac{H_s{}^2 T_z}{8\pi^2}(fT_z)^{-5}\exp\left[-\frac{1}{\pi}(fT_z)^{-4}\right] \tag{5.9}$$

$$S_{xx}(f) = \left|H(f)\right|^2 S_{yy}(f) \tag{5.10}$$

By applying the transfer function approach outlined in Chapter 2 and given by equation 5.10, the response spectrum for a structure with known natural frequency under an extreme sea state with significant wave height, $H_{s_{ext.}}$ and mean zero crossing period, $T_{z_{ext.}}$ can be calculated from equation 5.10 to give;

$$S_{xx}(f)_{ext.} = \left[\frac{\left(\frac{1}{K}\right)^2}{\left(1-\left(\frac{f}{f_n}\right)^2\right)^2 + \left(2\xi\frac{f}{f_n}\right)^2}\right]\frac{H_{s_{ext.}}{}^2 T_{z_{ext}}}{8\pi^2}\left(fT_{z_{ext}}\right)^{-5}\exp\left[-\frac{1}{\pi}\left(fT_{z_{ext.}}\right)^{-4}\right] \tag{5.11}$$

Since the natural frequency of the structure is a property of the structure and can be evaluated more easily when damping is not modelled the response can be sufficiently normalised with respect to the resonant peak which is a maximum when $f = f_n$. The resonant response is therefore given by;

$$S_{xx}(f)_{ext.|f=f_n} = \left[\frac{\left(\frac{1}{K}\right)^2}{(2\xi)^2}\right]\frac{H_{s_{ext.}}{}^2 T_{z_{ext}}}{8\pi^2}\left(f_n T_{z_{ext}}\right)^{-5}\exp\left[-\frac{1}{\pi}\left(f_n T_{z_{ext.}}\right)^{-4}\right] \qquad 5.12$$

In a similar manner as demonstrated by equation 5.11, the response spectrum for any other sea state with significant wave height H_s and mean zero crossing period T_z, can be obtained by replacing $H_{s_{ext.}}$ and $T_{z_{ext.}}$ with H_s and T_z, respectively to give the sea state response, $S_{xx}(f)_i$, for sea state i as;

$$S_{xx}(f)_i = \left[\frac{\left(\frac{1}{K}\right)^2}{\left(1-\left(\frac{f}{f_n}\right)^2\right)^2+\left(2\xi\frac{f}{f_n}\right)^2}\right]\frac{H_s^2 T_z}{8\pi^2}(fT_z)^{-5}\exp\left[-\frac{1}{\pi}(fT_z)^{-4}\right] \qquad (5.13)$$

This is then normalised with respect to the extreme resonant peak response obtained from equation 5.12 to give the normalised PSD for that sea state as;

$$S_{xx}(f)_{Ni} = \frac{S_{xx}(f)_i}{S_{xx}(f)_{ext.|f=f_n}} \qquad (5.14)$$

By substituting the response, $S_{xx}(f)_i$, for any sea state i and the resonant response, $S_{xx}(f)_{ext.|f=f_n}$, of the structure into equation 5.14, the normalised PSD can be obtained. This equation simplifies to the form;

$$S(f)_N = \frac{4H_r^2 T_r^{-4}\Omega^{-5}\xi^2}{\left[\left(1-\Omega^2\right)^2+\left(2\xi\Omega\right)^2\right]}Exp\left[\frac{1}{\pi}\left(\left(f_n T_{z_{ext.}}\right)^{-4}-\left(fT_z\right)^{-4}\right)\right] \qquad (5.15)$$

The PSDs obtained for a typical Jack-up platform using this equation and the JOSH sea states given in table 5.2 are shown in figure 5.2. They can be compared with those obtained using Wirsching's equation and given in figure 5.3. This comparison is shown in figure 5.4 for sea states 11 and 12.

The main advantage of the proposed normalised PSD equation is that it relies only on the use of non dimensional parameters and the natural frequency of the structure to predict its PSD. It will therefore represent a fast analytical tool for evaluating the behaviour of structures in the North Sea. It can also be adapted very easily for different locations by using the appropriate wave energy spectrum for the location of

interest. For example instead of using equation 5.9, the corrected version presented in Chapter 2 (section 2.7) can be used. This equation given below was demonstrated in Chapter 2 to be more accurate in predicting the measured wave energy spectrum after introducing a frequency correction parameter, β.

$$S_{yy}(f) = \frac{H_s^2 T_z}{8\pi^2}\left((f-\beta)T_z\right)^{-5}\exp\left[-\frac{1}{\pi}\left((f-\beta)T_z\right)^{-4}\right] \tag{5.16}$$

The difference between the above equation and equation 5.9 is that the variable f in equation 5.9 is replaced by $f-\beta$ in equation 5.16. The solution given by equation 5.15 can therefore be modified by introducing the same variable. This modification leads to the following solution.

$$S(f)_N = \frac{4H_r^2 T_r^{-4}\Omega_\beta^{-5}\xi^2}{\left[\left(1-\Omega^2\right)^2+\left(2\xi\Omega\right)^2\right]}Exp\left[\frac{1}{\pi}\left(\left(f_{n\beta}T_{z_{est.}}\right)^{-4}-\left(f_\beta T_z\right)^{-4}\right)\right] \tag{5.17}$$

Where $f_{n\beta}$, f_β and Ω_β are all frequency corrected non dimensional parameters given by;

$$f_{n\beta} = f_n - \beta \tag{5.18}$$

$$f_\beta = f - \beta \tag{5.19}$$

$$\Omega_\beta = \frac{f_\beta}{f_{n\beta}} \tag{5.20}$$

The rest of the variables are as previously defined.

The accuracy of this model depends on the accuracy of the sea state data used. However, since it only uses non dimensional sea state parameters, its overall sensitivity is reduced and depends largely on the extreme sea state. It is therefore recommended that service data where available is used in determining the normalised PSDs. However, where service data is not available, a suitable theoretical sea state distribution model can be used.

5.4 PROPOSED SEA STATE PROBABILITY MODEL

A detailed examination of oceanographic data for the North Sea, observed over a period of several years has shown that the distribution of significant wave height, H_s, is accurately described by the Gumbel distribution. The Gumbel distribution is given as;

$$P(x) = 1 - \exp[-\exp(-x)] \tag{5.21}$$

Where $P(x)$ is the exceedance of the variable x. Observed sea state data has been demonstrated [5.13] to be well fitted by the following expression:

$$P(H_s) = 1 - \exp\left[-\exp\left(\frac{\alpha - H_s}{\beta}\right)\right] \tag{5.22}$$

This modelled distribution agrees very closely with sea state data observed at typical locations in the North Sea (table 5.1). The sea states used to generate JOSH as presented in Chapter 2 and [5.14] were selected from these observed data and after consideration of the correlation between these measured data and the distribution of sea states obtained on assumption of the Gumbel distribution.

Equation 5.22 gives the sea state exceedance which really represents the probability that the significant wave height, H_s, for any particular sea state exceeds a certain value. It can also be written for all sea states with wave heights up to H_s such that;

$$P(H \le H_s) = \exp\left[-\exp\left(\frac{\alpha - H_s}{\beta}\right)\right] \tag{5.23}$$

The implication of using equation 5.23 is that it can be integrated over the specified limits to give;

$$\int_0^{H_s} p(H_s)dH_s = \exp\left[-\exp\left(\frac{\alpha - H_s}{\beta}\right)\right] \tag{5.24}$$

$$p(H_s) = \frac{d}{H_s}\left\{\exp\left[-\exp\left(\frac{\alpha - H_s}{\beta}\right)\right]\right\} \tag{5.25}$$

$$p(H_s) = \frac{1}{\beta}\exp\left(\frac{\alpha - H_s}{\beta}\right)\exp\left[-\exp\left(\frac{\alpha - H_s}{\beta}\right)\right] \tag{5.26}$$

Since equation 5.26 represents a continuous probability distribution function for an infinite range of possible wave heights, there is always a constant γ for which the integral of its product with the probability function is always unity. That is, equation 5.26 can also be expressed as a function of γ such that,

$$\int_0^{\infty} \frac{\gamma}{\beta}\exp\left(\frac{\alpha - H_s}{\beta}\right)\exp\left[-\exp\left(\frac{\alpha - H_s}{\beta}\right)\right]dH_s = 1 \tag{5.27}$$

The integral function of equation 5.27 is given by I such that;

$$I = \gamma\left[1 - \exp\left[-\exp\left(\frac{\alpha}{\beta}\right)\right]\right] \tag{5.28}$$

Now looking at equation 5.22 more closely, it is clear that substituting zero in place of H_s gives the probability that the significant wave height at any one time exceeds 0. This implies;

$$P(0) = P(H > 0) = 1 - \exp\left[-\exp\left(\frac{\alpha}{\beta}\right)\right] \tag{5.29}$$

Equations 5.28 and 5.29 are equivalent as they both represent the same cumulative probability distribution. This condition is only true for a continuous function and requires that γ is unity as expected. The implication of using the constant, γ, only becomes very important when dealing with discontinuous probability functions such as those encountered under service conditions for example.

Equation 5.27 will give the exact solution for the long term probability distribution of sea states over an infinite range based on the Gumbel distribution. This gives a probability distribution function of the form;

$$p(H_s) = \frac{\gamma}{\beta}\exp\left(\frac{\alpha - H_s}{\beta}\right)\exp\left[-\exp\left(\frac{\alpha - H_s}{\beta}\right)\right] \tag{5.30}$$

Where α, β and γ are site dependent parameters. In practice the long term probability distribution of wave heights across the entire infinite range of likely occurring sea states is not used since the sea states used for any fatigue analysis of Offshore structures will depend on oceanographic data (Table 1) based on measurements and observations carried out over a finite length of time. Under this scenario, often the total probability of occurrence of sea states is known and can be expressed such that;

$$\int_0^{\infty} \frac{\gamma}{\beta}\exp\left(\frac{\alpha - H_s}{\beta}\right)\exp\left[-\exp\left(\frac{\alpha - H_s}{\beta}\right)\right]dH_s = P(H_s)_T \tag{5.31}$$

Where $P(H_s)_T$ is the known cumulative probability. This can also be written as a discontinuous function for n discrete sea states such that;

$$\sum_{i=1}^{n}\left[\frac{\gamma}{\beta}\exp\left(\frac{\alpha - H_i}{\beta}\right)\exp\left[-\exp\left(\frac{\alpha - H_i}{\beta}\right)\right]\right] = \mathrm{P(H_s)_T} \tag{5.32}$$

The cumulative probability $P(H_s)_T$, is normally taken as 1 while γ is a constant which has to be evaluated. α and β are also constants which will vary for typical sites. Data from the Silver Pit and Ekofisk regions of the North Sea show that α and β are 1.55 and 1.06 respectively.

5.4.1 Use of Sea State Probability Distribution Model

The use of fast assessment equations to determine sea state equivalent stresses was discussed in Chapter 1. This approach does not require cycle counting and can be applied directly to structures in service. Where necessary the overall long term equivalent stress can be determined using the following procedure.

Suppose a sea state, *i*, with a significant wave height H_{s_i} and equivalent stress S_{h_i}, has a long term probability of occurrence $P(H_{s_i})$, then its long term contribution to

fatigue damage or the overall long term equivalent stress can be given by σ_{h_i}, such that;

$$(\sigma_{h_i}) = (S_{h_i})P(H_{s_i}) \tag{5.33}$$

The overall equivalent stress, σ_h, can then be given by;

$$\sigma_h = \sum_{i=1}^{n}\left[\sigma_{h_i}\right] = \sum_{i=1}^{n}\left[(S_{h_i})(\Delta H_{s_i})p(H_{s_i})\right] \tag{5.34}$$

When ΔH_{s_i} is infinitesimally small, then the long term equivalent stress is give as;

$$\sigma_h = \int\left[\sigma_{h_i}\right] = \int\left[(S_h)p(H_s)\right]\mathrm{dH_s} \tag{5.35}$$

For simulated service load histories (SLH), used for testing structural materials in the laboratory, this approach can equally be applied. A second and alternative approach to this method for an existing SLH is to use conventional cycle counting as described in Chapter 1. This method would normally allow for the overall sequence equivalent stress to be determined.

Irrespective of the method used to calculate the overall equivalent stress for any particular load history, it is very important to point out at this stage that using the overall equivalent stress concept to predict crack growth in structures under variable amplitude loading conditions will lead to inaccuracies in the results for the following reason;

Firstly, the fatigue crack growth rate at any time is dependent on the stress intensity factor range. This is a function of crack geometry, loading mode and stress range. The actual stress range applied to the fatigue crack within an individual sea state will be largely different from the overall equivalent stress range. Therefore using the overall equivalent stress range to characterise crack growth within an individual sea state may lead inaccurate results.

Secondly the element of time is very important especially for Offshore structures where frequency effects under corrosion fatigue conditions have been demonstrated.

Using the overall equivalent stress concept excludes this element of time. Another reason for caution is that the equivalent stress concept is inapplicable and meaningless as long as it applies to an entire sequence which may never be fully utilised before a structural integrity assessment exercise is carried out.

Thirdly because this approach does not include the element of time and the necessary interaction between different sea states it does not provide the necessary capability to model any interaction effects. Most of these sources of error associated with fatigue crack growth prediction using the overall equivalent stress approach will be minimised by adopting a sea state equivalent stress approach. This concept is presented in the following section.

5.4.2 Formulation of The Sea State Equivalent Stress Concept

The sea state equivalent stress concept is introduced here using a similar approach to that on which the overall equivalent stress approach is based. The overall equivalent stress approach has been presented in detail in Chapter 4 (section 4.7.1).

By using the overall sequence equivalent stress approach (section 4.7.1), crack growth under variable amplitude loading conditions is given by [5.15];

$$\frac{da}{dN} = C\left(Y\sqrt{\pi a}\right)^m S_h{}^m \tag{5.36}$$

$$S_h = \left[\int_0^\infty \Delta S^m p(\Delta S) d(\Delta S)\right]^{(1/m)} = \left[\sum \Delta S^m P(\Delta S)\right]^{(1/m)} \tag{5.37}$$

where all the parameters are as previously defined.

The sea state equivalent stress range concept is based on the same philosophy as that of the overall equivalent stress range approach. It however relies on using sea state parameters to determine the sea state equivalent stress range which is then used to calculate fatigue crack growth associated with that sea state. This is implemented by assuming an appropriate crack growth law. Using Paris law for example, the crack

growth rate within a particular sea state, i, with equivalent stress, S_{h_i}, can be calculated from

$$\frac{da}{dN_i} = C\left(Y\sqrt{\pi a}\right)^m S_{h_i}{}^m \tag{5.38}$$

$$S_{h_i} = \left[\int_0^\infty \Delta S^m p(\Delta S) d(\Delta S)\right]^{(1/m)} = \left[\sum \Delta S^m P(\Delta S)\right]^{(1/m)} \tag{5.39}$$

The number of fatigue cycles required to propagate a fatigue crack from an initial depth , a_o, to a final depth , a_f ,within a particular sea state is then given by;

$$N_{h_i} = \int_{a_o}^{a_f} \left(\frac{1}{C\left(YS_h(\pi a)^{\left(\frac{1}{2}\right)}\right)^m} \right) da \tag{5.40}$$

This procedure is then carried out over the entire sequence of expected sea states. This sequence of sea states will be determined mainly by their long term probability of occurrence, duration and transition period. Using this information, the total number of fatigue cycles required to propagate a fatigue crack after n sea state transitions can be given as;

$$N = \sum_{i=1}^{n} N_{h_i} = \sum_{i=1}^{n} \left[\int_{(a_o)_i}^{(a_f)_i} \left(\frac{1}{C\left(YS_{h_i}(\pi a)^{\left(\frac{1}{2}\right)}\right)^m} \right) da \right] \tag{5.41}$$

The sea state equivalent stress range concept is likely to be more accurate in predicting fatigue crack growth under variable amplitude loading conditions in Offshore structures than the overall equivalent stress range approach. The main reason for this is that the variability in the instantaneous stress range or stress intensity factor range is far less within any particular sea state than the equivalent variation in the overall sequence put together. The method also has the added advantage of allowing the inclusion of any sequence or sea state interaction effects. This effect is

omitted when the overall sequence equivalent stress is used to determine crack growth in Offshore structures.

5.5 DISCUSSION

The results of fatigue crack growth predictions under variable amplitude conditions presented here are based on the simulated Jack-Up Standard load History, JOSH. The sea state equivalent stress approach is compared with both the conventional overall equivalent stress range approach and experimental data obtained under variable amplitude loading conditions.

The JOSH sequence was generated using realistic service data. This was presented in Chapters 2 and 3. The sea state equivalent stress concept relies on the use of a suitable sea state probability distribution function. The probability distribution used to derive this function is the Gumbel distribution. The sea state exceedance and cumulative probability obtained from this distribution are shown in figure 5.5. It was necessary to ascertain the accuracy of this distribution used to develop the model. This was done by comparing sea state cumulative probability and exceedance curves obtained from the Gumbel distribution with those calculated from the measured data used to generate the JOSH sequence. This comparison is shown in figure 5.6. The agreement between the variation in the predicted and measured curves is good. This agreement provided a suitable starting point in developing the sea state probability distribution model for use in the prediction of fatigue crack growth in Offshore structures under variable amplitude multi-sea state loading conditions.

The JOSH sequence used was generated using advanced simulation techniques from 12 different sea state PSDs. It consists of 1064050 turning points generated from 4000 transitions of the 12 sea states. This has been presented in Chapters 2 and 3. Figure 5.7 shows the SRPDs for three variants of the sequence used in the large scale fatigue testing programme. The sequence was generated such that the long term statistical properties of the PSDs were reproduced. This is shown in figure 5.7 since the partly used sequence (used(2C)) has the same SRPD as the other variants of

JOSH based on the entire simulated sequence. The partly used sequence was 380,000 cycles long compared to the whole sequence which consisted of 530,000 rainflow cycles.

The stress range probability distribution curves for the different sea states used in JOSH (2C) are shown in figure 5.8 while the sea state exceedance curves are shown in figure 5.9. These curves were obtained after employing rainflow cycle counting. The cycle counting data was also used to calculate sea state equivalent stresses. The equivalent stresses due to each of the 12 sea states used was calculated for the different variants of JOSH used in the fatigue testing programme. These are plotted in figure 5.10 for three of the four tests carried out. Results from the fourth test are not shown in figure 5.10 because they are identical to those obtained from the third test as they were conducted at the same overall equivalent stress range.

The probability of occurrence of each sea state was used together with the sea state equivalent stresses shown in figure 5.10 to calculate the long term contribution of each sea state to the overall sequence equivalent stress. These values are compared in figure 5.11 with those obtained by using the conventional cycle counting method. In figure 5.11 the results from both the cycle counting and the probability based method are so close that the curves are virtually coincident. Figure 5.11 also shows that sea states 3, 4 and 5 have a major contribution to the overall long term equivalent stress. This is due to the combination of sea state equivalent stresses shown in figure 5.10 and their duration as discussed in Chapters 2 and 3.

The sequence of 4000 sea state transitions used to generate JOSH is shown in figure 5.12. The calculated sea state equivalent stresses can be seen to follow a trend similar to the sea state transition sequence as expected. This trend is shown in figure 5.13 for the air test (LEYOPB1A). Figure 5.13 also compares the sea state equivalent stresses with the overall sequence equivalent stress. As seen in this figure there is consideration variation in the sea state equivalent stress. This variation will have significant effects on fatigue crack growth and therefore needs to be adequately accounted for.

All the corrosion tests were conducted using a variant of JOSH (JOSH2C). This was based on the same sea states and sea state PSDs as JOSH1A. However the detailed sea state transition sequence for JOSH2C was different and is shown in figure 5.14. Tests LEYOPB2C, LEYOPB3C and LEYOPB4C were conducted using this sequence.

Even though the same sequence was used for the corrosion tests, the individual tests were conducted under the required loading conditions by using different amplitude and load ranges. This made the overall equivalent stresses different apart from tests LEYOPB3C and LEYOPB4C which were carried out the same equivalent stress level. The variation in the sea state equivalent stress for the test conducted at an equivalent stress level of 250 MPa is shown in figure 5.15. Figure 5.15 also compares this variation in sea state equivalent stress with the overall sequence equivalent stress of 250 MPa. Again the variation in sea state equivalent stress follows the same trend as the sea state transition sequence given in figure 5.14. This observed variation in sea state equivalent stress was consistent for all the tests and the data obtained for tests LEYOPB3C and LEYOPB4C are shown in figures 5.16 and 5.17 respectively.

From these results it is evident that the stress intensity factor range which is a function of crack geometry and stress range will be different for the cases where an overall equivalent stress range is used when compared with results obtained using a sea state equivalent stress. The way this difference affects the accuracy of crack growth rate predictions is very important. This was investigated for this study.

The sea state equivalent stress concept was used to predict crack growth in the high strength steel (SE702) used in the fatigue testing programme. The crack growth curve obtained is compared with experimental data for the air test together with results obtained using the overall equivalent stress range method in figures 5.18 to 5.21. In each figure the smooth curve is that obtained with the overall equivalent stress range method. The other two curves show the predicted crack growth curve based on the sea state equivalent stress concept and experimental crack growth data from LEYOPB1A.

One of the problems encountered in predicting crack growth using this approach is that information on the crack initiation point within the sequence is required for accurate prediction. If it is assumed that the crack growth analysis starts from the beginning of the sequence then the resulting curves are as shown figure 5.18. Here it would appear that the prediction based on the overall equivalent stress is not very different from that based on the sea state equivalent stress concept. Figure 5.18 shows that under this scenario, the crack growth period (0.1-16.0mm) is roughly equivalent for both methods and is as shown in figure 5.19 after correcting for the crack initiation life. However if the sea state calculation is started at the appropriate moment during the sequence then the overall and sea state approaches diverge (as shown in figure 5.20). Finally if the initiation period is reintroduced for both predictions then figure 5.21 indicates that the sea state approach is more accurate.

Figures 5.22 to 5.27 show comparisons between the two methods for the test conditions used for LEYOPB2C, LEYOPB3C and LEYOPB4C. In all cases the effect of correlating the point of crack initiation on the predicted results was assessed. Figures 5.22 and 5.23 show the uncorrelated and correlated results respectively for LEYOPB2C. The corresponding results for the test conditions for LEYOPB3C are shown in figures 5.24 and 5.25 respectively while those for LEYOPB4C are given in figures 5.26 and 5.27. In all cases the effect of correlating the point of crack initiation (onset of crack propagation) in the sequence is shown to be important as this will determine whether conservative results are obtained (figures 5.23 and 5.25) or not (figure 5.27). This shows principally the effect of sea state interaction on the accuracy of the predicted results and not the dependence of the method on the sequence used. In practice severe sea states will lead to higher crack growth rates than would normally be predicted by the overall equivalent stress approach. In this case results obtained may appear to be too conservative when compared with the overall equivalent stress prediction.

It should be noted that the individual sea state approach has the added capability of modelling interaction effects which can not be included if the overall sequence equivalent stress approach is used. It can also be applied using an arbitrary sea state transition sequence. This is demonstrated in figures 5.28 to and 5.30 where the sea

state transition sequence shown in figure 5.28 is used to predict crack growth for test LEYOPB1A as shown in figure 5.29. The results obtained are shown in figure 5.30 after accounting for the crack initiation life.

This approach can therefore be used as long as a good approximation to the expected sea state transition sequence can be obtained. This can be obtained from oceanographic data. Knowledge of the long term distribution of sea states and their duration is important in the use of the sea state equivalent stress approach.

The accuracy of this method however like any other fracture mechanics based method relies very much on the accuracy in the material constants used in the model.

5.6 SUMMARY

This Chapter has introduced a fast assessment approach to the analysis of Offshore structures. The methodology relies on the use of non dimensional sea state parameters together with the fundamental mode of structural response. The advantages associated with using the proposed equation have been highlighted and discussed.

A sea state probability distribution model has also been presented. This model relies on the Gumbel distribution and it has been verified with service measurements from a typical location in the North Sea. Based on this model a sea state equivalent stress concept has been formulated and its mathematical background presented.

A generalised fracture mechanics approach for the assessment of fatigue crack growth in Offshore installations is proposed. This approach is based on the sea state equivalent stress concept and has been demonstrated to be more consistent with experimental observations of crack propagation under variable amplitude conditions.

5.7 CONCLUSIONS

From the analysis presented in this Chapter the following conclusions can be drawn;

A fast assessment equation has been proposed which can be used to analyse Offshore structures to obtain PSDs. These PSDs can be used for fatigue analysis.

A sea state probability distribution model has been proposed. This model is based on the Gumbel distribution and it has been demonstrated that it can be used to characterise the distribution of sea states in service.

It has also been demonstrated that a suitable sea state probability distribution function can be used to determine long term sea state equivalent stresses.

A sea state equivalent stress concept has been formulated and it has been successfully used to predict fatigue crack growth in a typical high strength Offshore steel. This approach predicts fatigue crack propagation more realistically than the overall equivalent stress range approach and shows the potential to model sea state interaction effects.

5.8 REFERENCES

[5.1] IABG Report TF-1892, "*The Common Load Sequence for Fatigue Evaluation of Offshore Structures -Background and Generation*", 1985

[5.2] Schutz W and Pook L P, "*WASH (Wave Action Standard History) A Standardised Stress-time History for Offshore Structures*", Elsevier, Amsterdam 1987, pp 161-178

[5.3] Etube L S, Brennan F P and Dover W D, '*Service Load simulation for Fatigue Testing of Jack-up steels*', Recent Advances in Corrosion Fatigue, Sheffield, April 1997.

[5.4] Etube L S, Brennan F P and Dover W D, '*Modelling of Jack-up response for fatigue testing of weldable high strength Jack-up steels under simulated service conditions*', Sixth International Conference on the Jack-up Platform, City University, September 1997.

[5.5] Wirsching P W, "*Probability-based fatigue design criteria for Offshore structures*", International Journal of Fatigue 2, April 1980 pp 77-83

[5.6] Wirsching P H, "*Fatigue Under Wide Band Random Stresses*", Journal of the Structural Division, July 1980, pp 1593-1606, ASCE.

[5.7] Chaudhury G K and Dover W D, "*Fatigue Analysis of Offshore Platforms Subject to Sea Wave Loading*", Int. Journal of Fatigue, Vol. 7, No. 1, 1985, pp 13-19.

[5.8] Hancock J W and Gall D S, "*Fatigue Under Narrow and Broad Band Stationary Loading*", Part I and II, Cohesive Programme of Research and Development into the Fatigue of Offshore Structures, 1983-85, Final Reports.

[5.9] Kam J C P, "*Structural Integrity of Offshore Tubular Joints Subject to Fatigue*", PhD Thesis ,Department of Mechanical Engineering, University College London, 1989

[5.10] Myers P, *Corrosion Fatigue Fracture Mechanics of High Strength Jack Up Steels*, Ph.D. Thesis submitted to London University, February 1998

[5.11] Etube L S, Brennan F P and Dover W D, "*Prediction of Fatigue Crack Growth in Offshore structures Using a Sea State Equivalent Stress Concept*", International Offshore and Polar Engineering Conference, Montreal, Canada, May 1998.

[5.12] Kam J C P and Dover W D, "*Procedure to generate the wave action standardised history (WASH)*", Draft manual, Version 1.0, October 1988.

[5.13] Pook L P and Dover W D, "*Progress in the development of a Wave Action Standard History (WASH) for fatigue testing relevant to tubular structures in the North Sea.*", American Society for Testing and Materials: Symposium on the Development of Standard Load Spectra, 29 April 1987.

[5.14] Etube L S, Brennan F P and Dover W D, '*Service Load simulation for Fatigue Testing of Jack-up steels*', Recent Advances in Corrosion Fatigue, Sheffield, April 1997.

[5.15] Kam J C P, "*Structural Integrity of Offshore Tubular Joints Subject to Fatigue*", PhD Thesis ,Department of Mechanical Engineering, University College London, 1989.

5.9 TABLES AND FIGURES

Table 5.1: Scatter diagram for a typical North Sea site

	Zero crossing period (s)							
Hs	2.5	3.5	4.5	5.5	6.5	7.5	8.5	9.5
0.25		1	1					
0.75	3	32	34	13	6	1		
1.25		30	82	46	17	4	1	
1.75		3	66	67	28	13	1	1
2.25			21	77	37	45	3	
2.75			2	49	40	16	4	1
3.25				19	48	16	7	1
3.75				4	39	17	7	2
4.25					15	19	5	2
4.75					4	19	5	1
5.25					1	19	5	1
5.75						6	4	1
6.25						4	6	
6.75						1	3	1
7.25							2	1
7.75							1	1
8.25							1	

Table 5.2: Sea states used in the generation of JOSH

Sea state number	Significant wave height (m)	Mean zero crossing period (s)	Fraction of time (%)
1	1.25	5.5	38.5000
2	1.75	5.9	28.5000
3	2.25	6.2	17.5000
4	2.75	6.5	7.1800
5	3.25	6.8	3.4000
6	3.75	7.1	2.1600
7	4.25	7.4	1.3100
8	4.75	7.7	0.6780
9	5.25	7.9	0.3340
10	6.25	8.4	0.1540
11	7.25	8.9	0.0797
12	8.00	9.2	0.0043

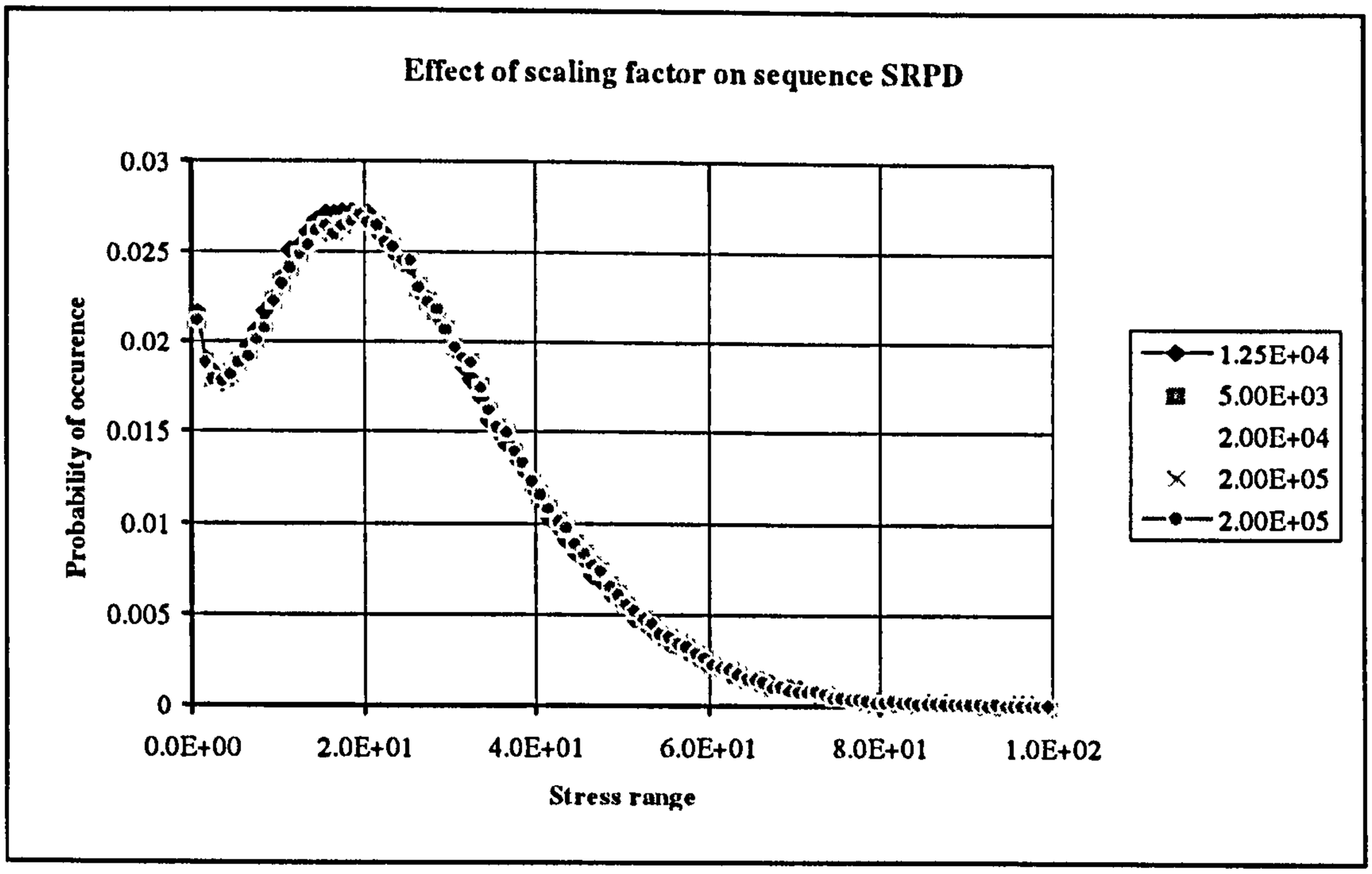

Figure 5.1: Effect of scaling factor on stress range probability distribution

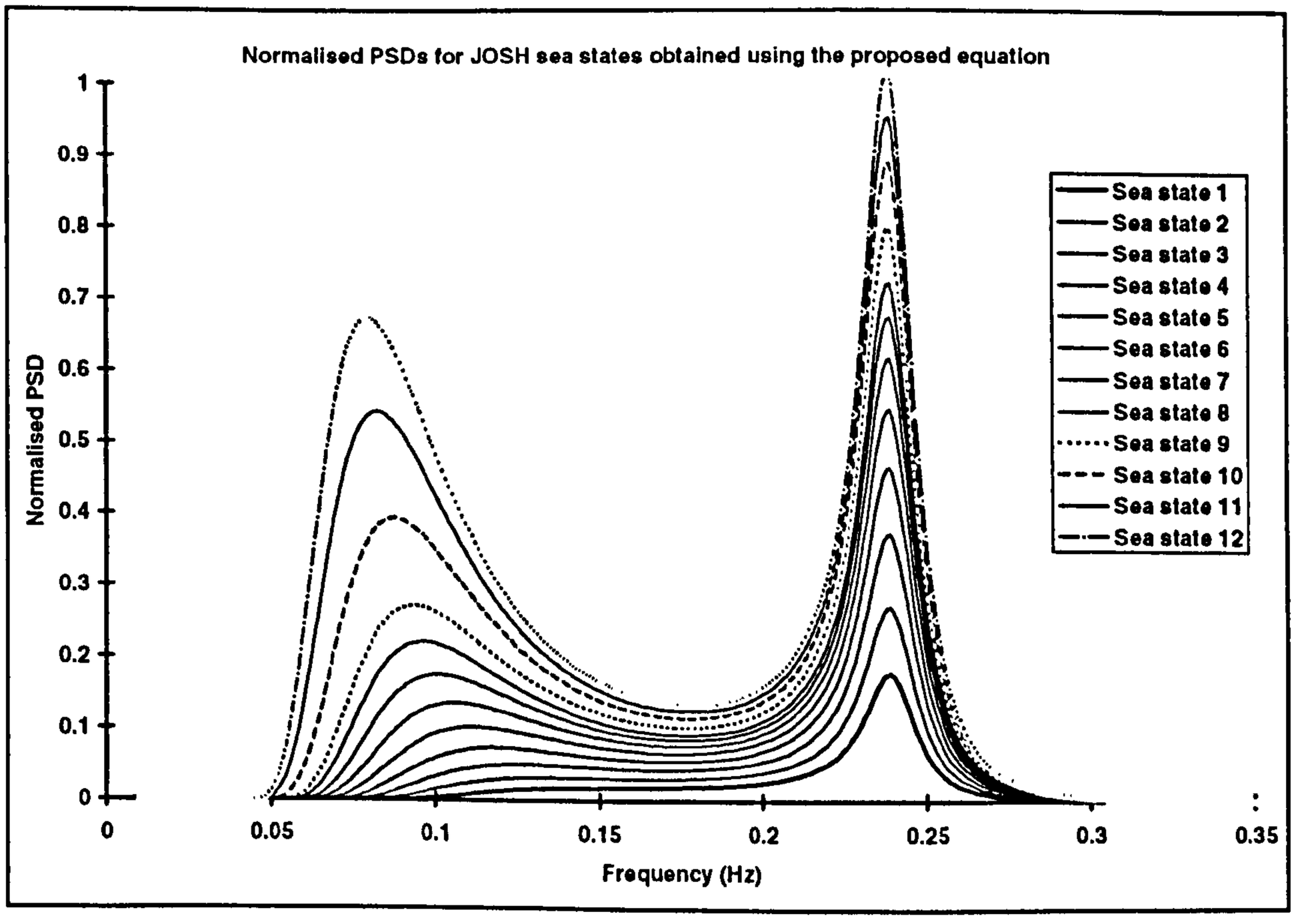

Figure 5.2: Sea state PSDs obtained using proposed equation

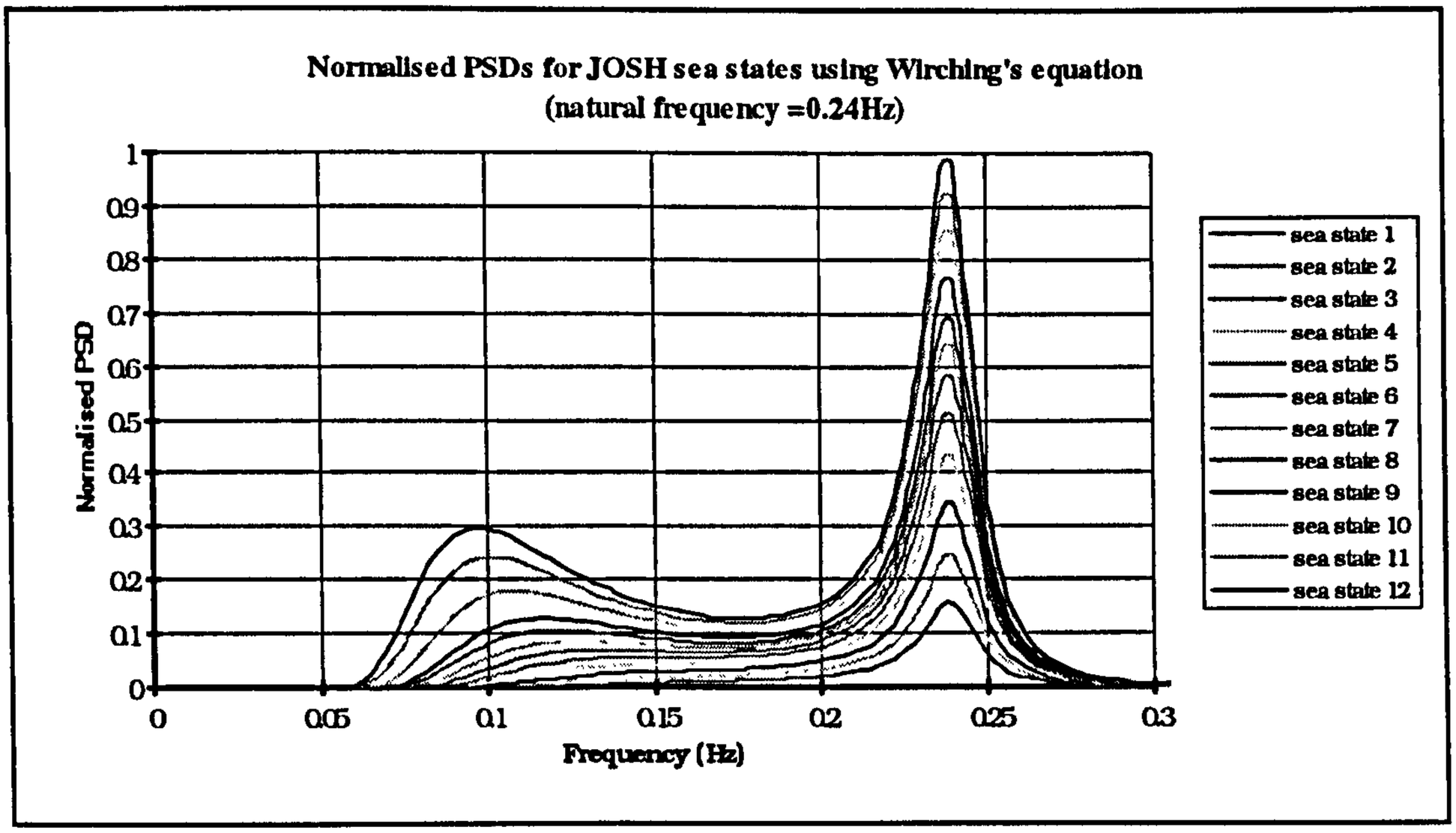

Figure 5.3: Sea state PSDs obtained using Wirsching's equation

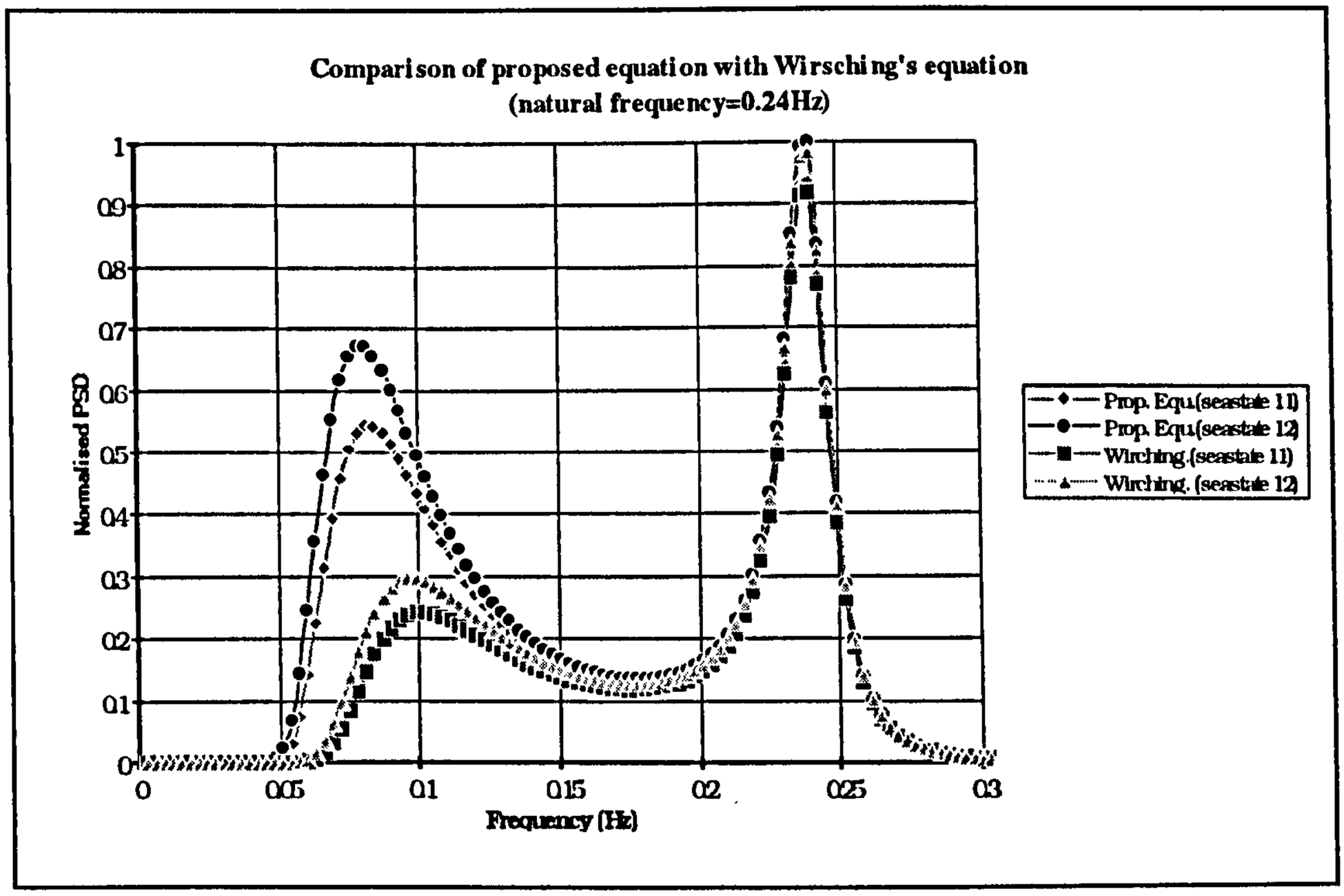

Figure 5.4: Comparison of proposed equation with Wirsching's equation.

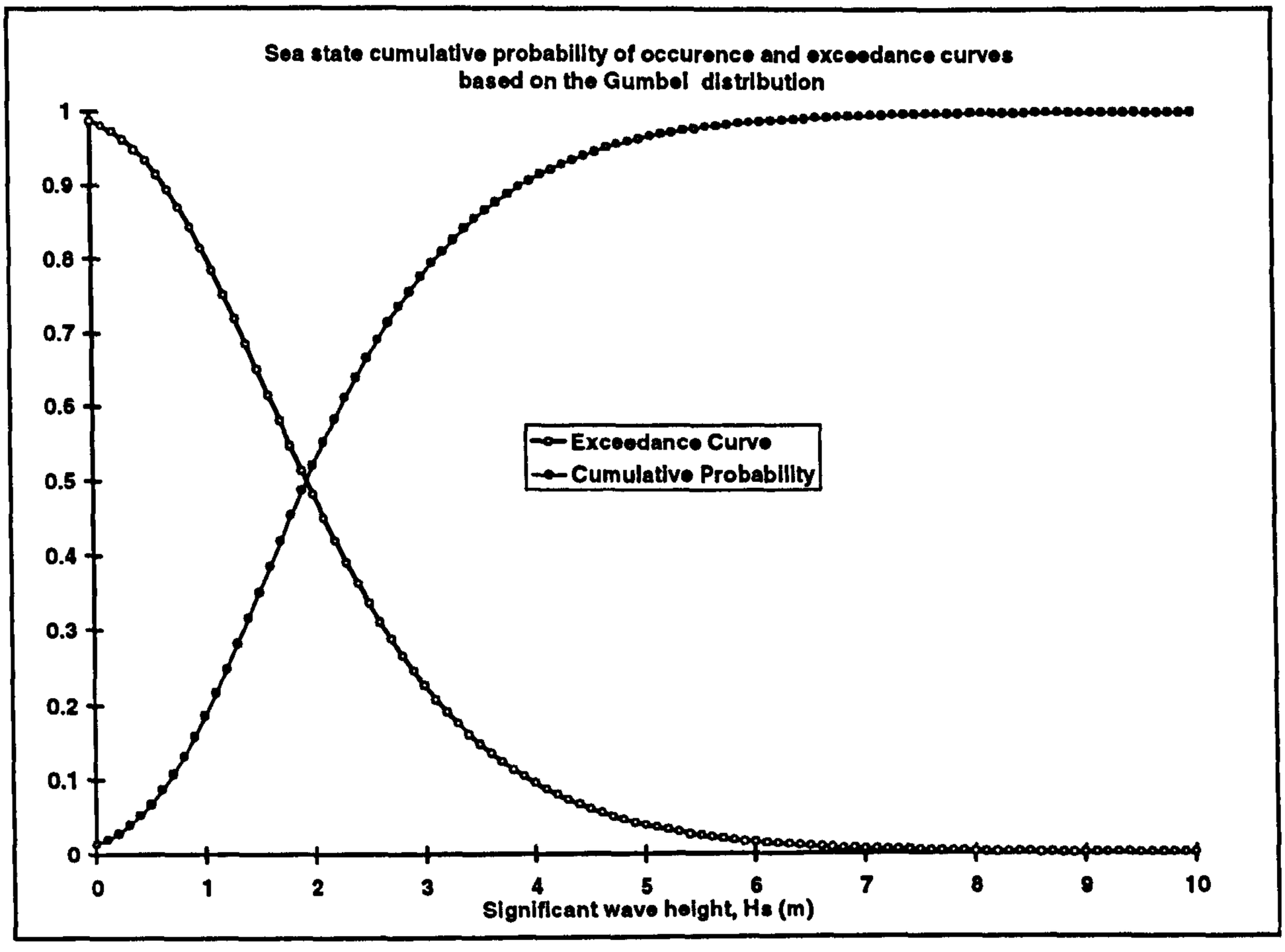

Figure 5.5: Theoretical Cumulative probability and exceedance curves

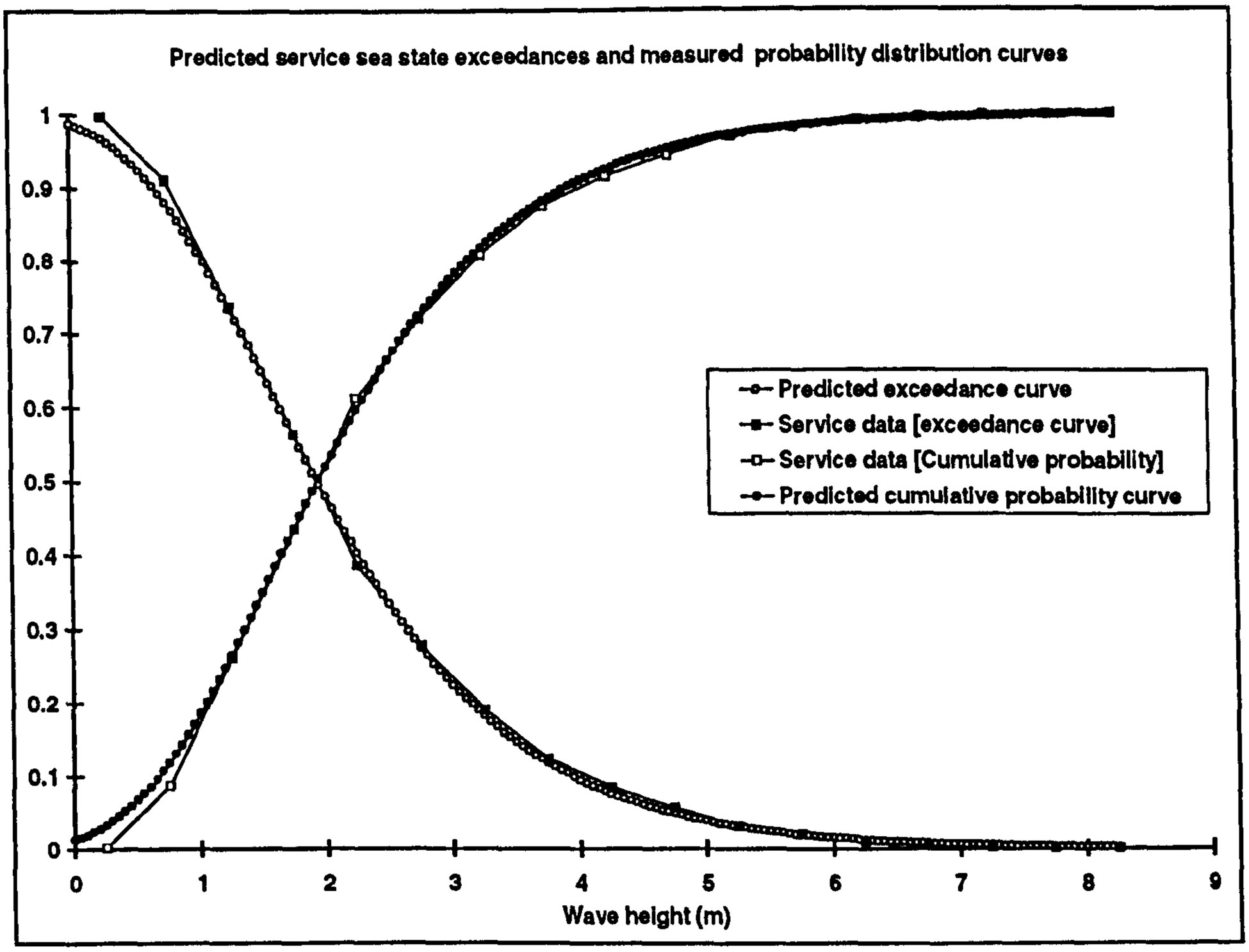

Figure 5.6: Measured and predicted exceedance curves for JOSH sea states

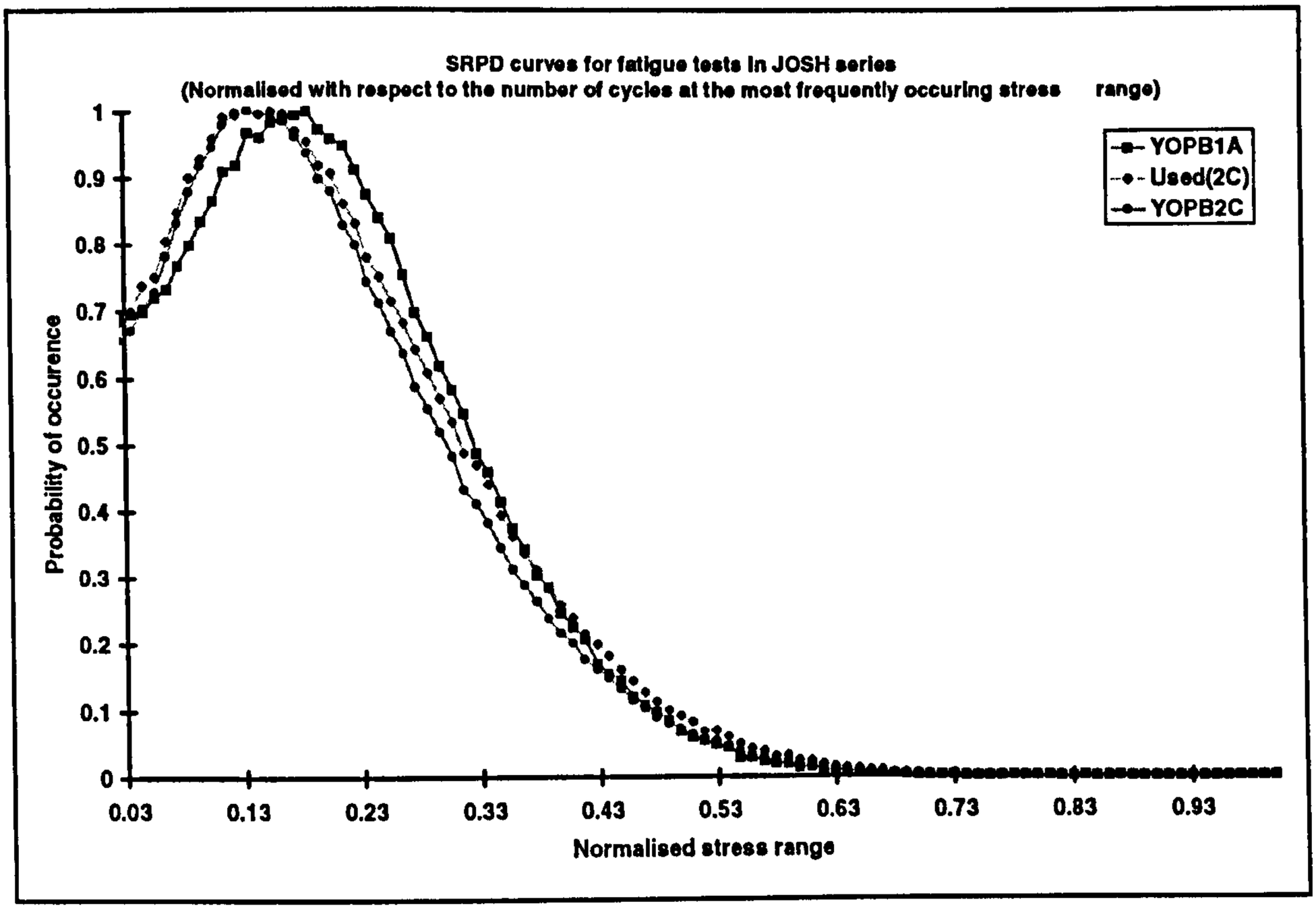

Figure 5.7: Stress range probability distribution curves for JOSH

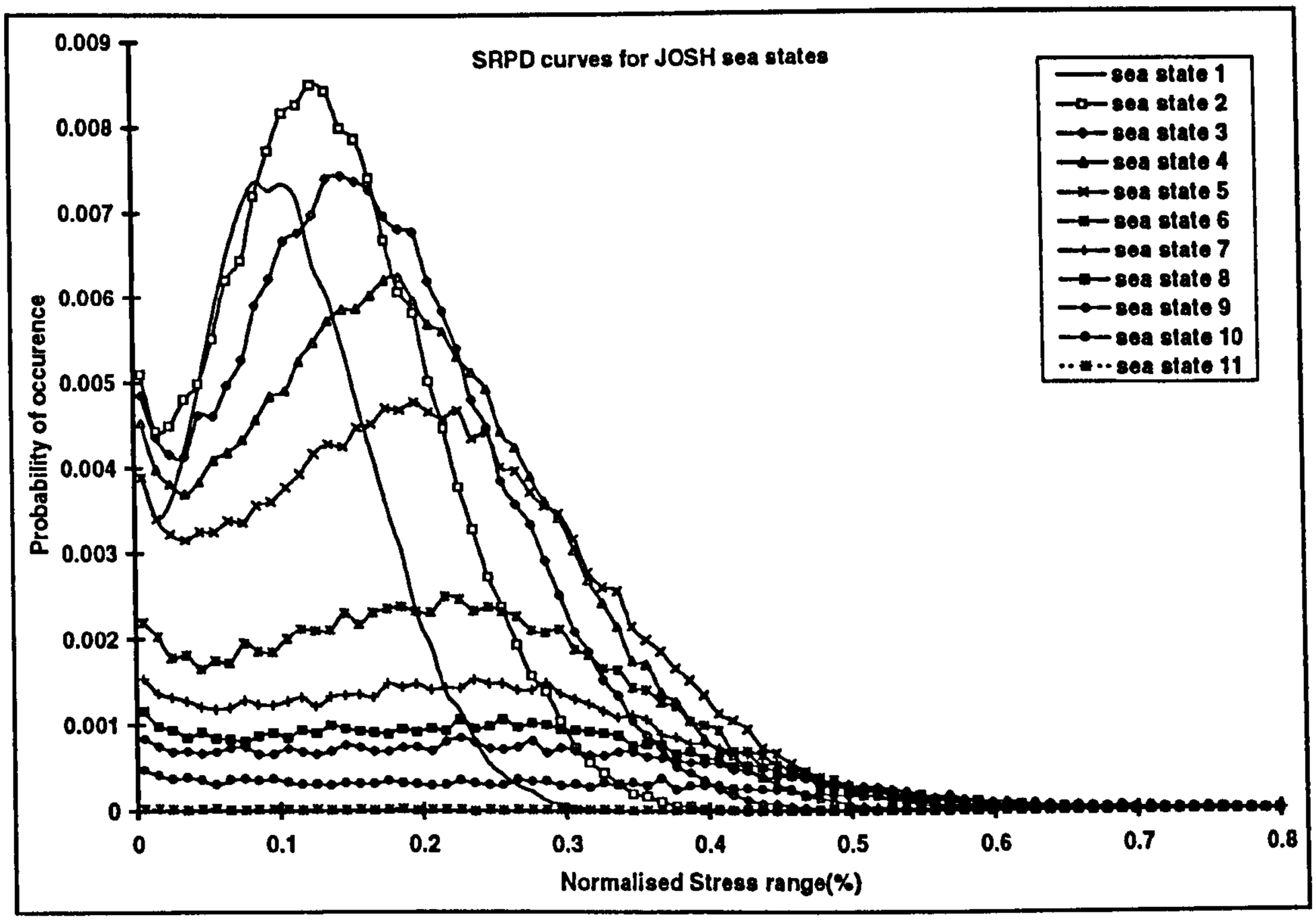

Figure 5.8: SRPD curves for JOSH sea states

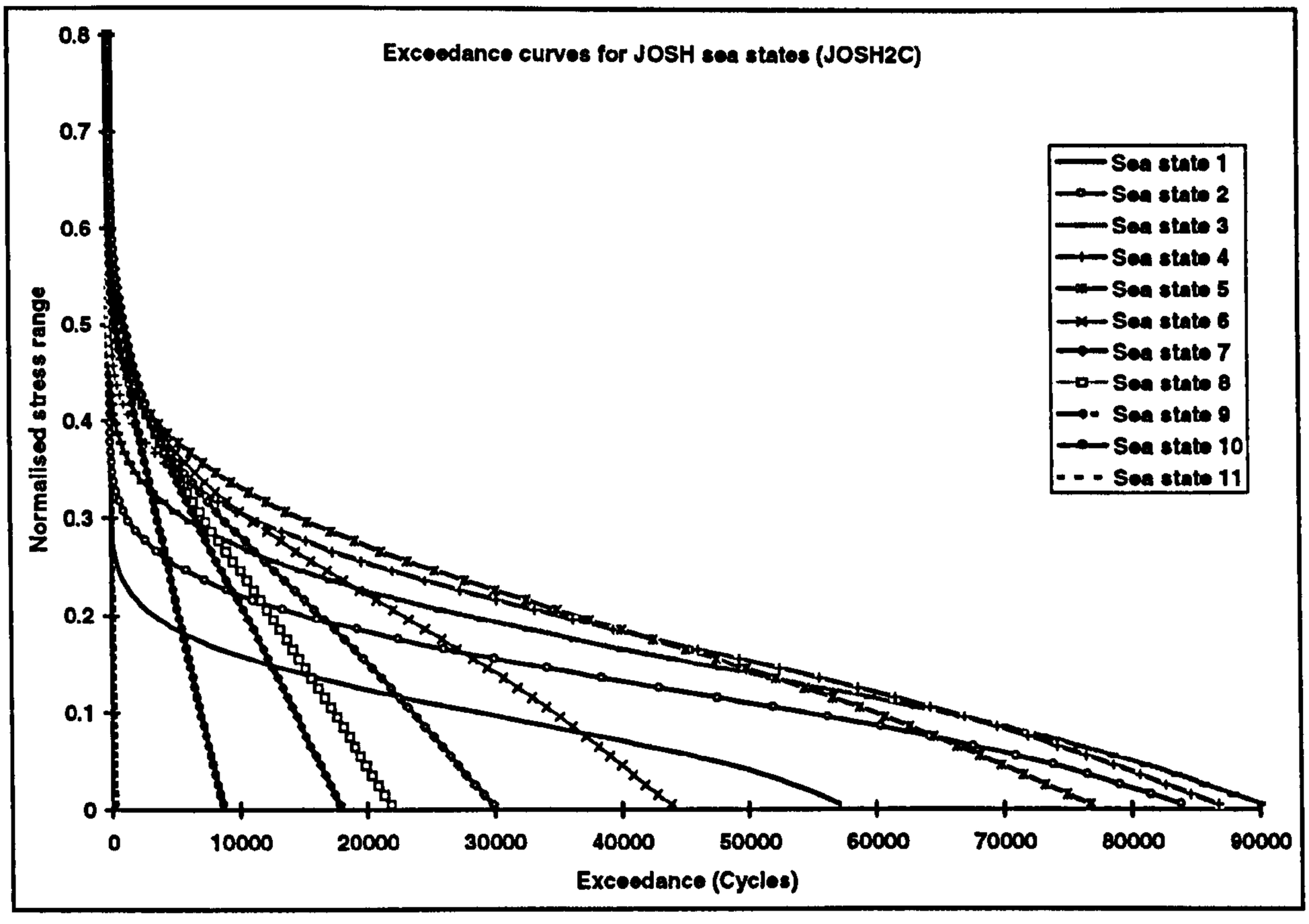

Figure 5.9: Exceedance curves for JOSH sea states

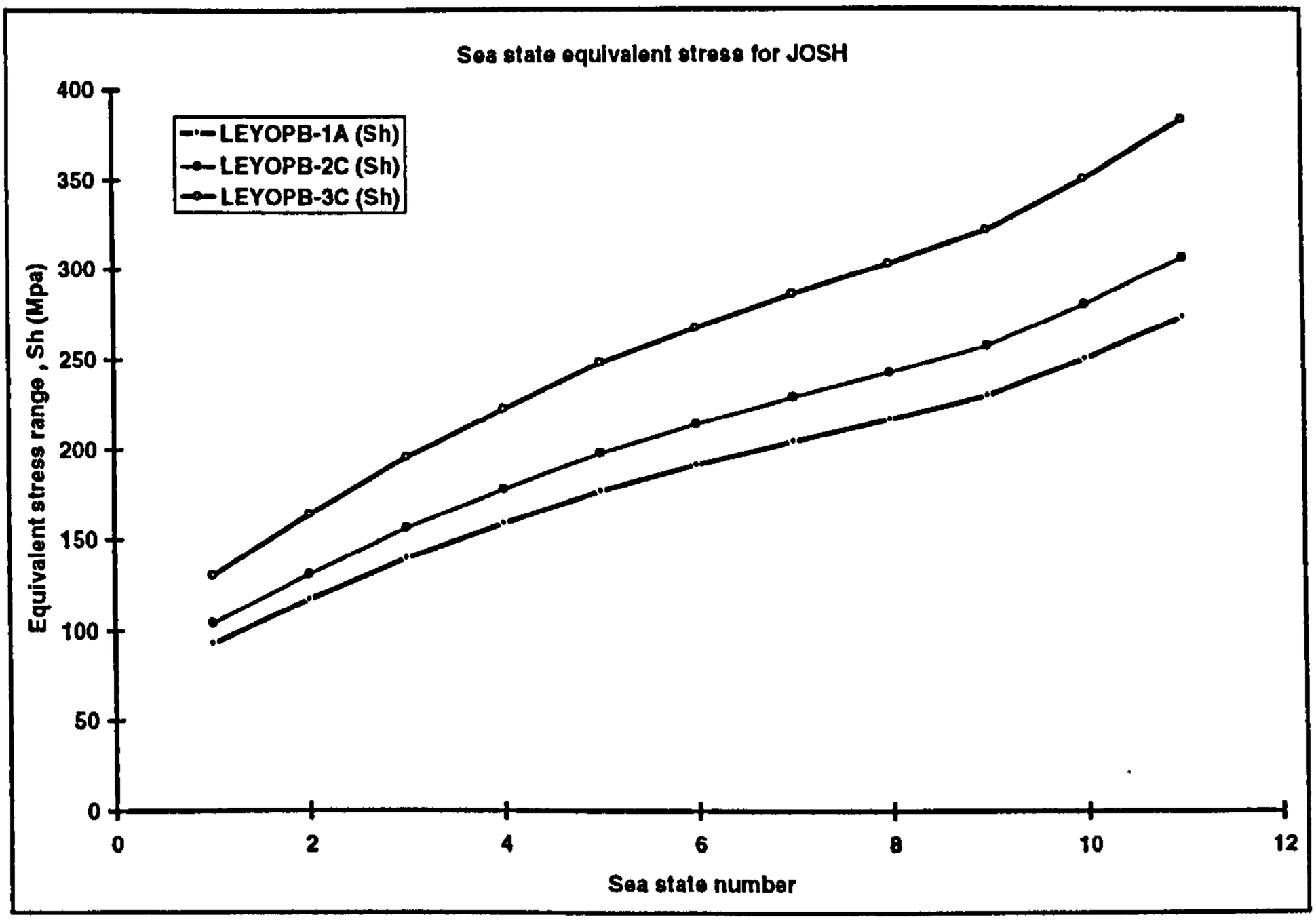

Figure 5.10: Sea state equivalent stresses for different tests

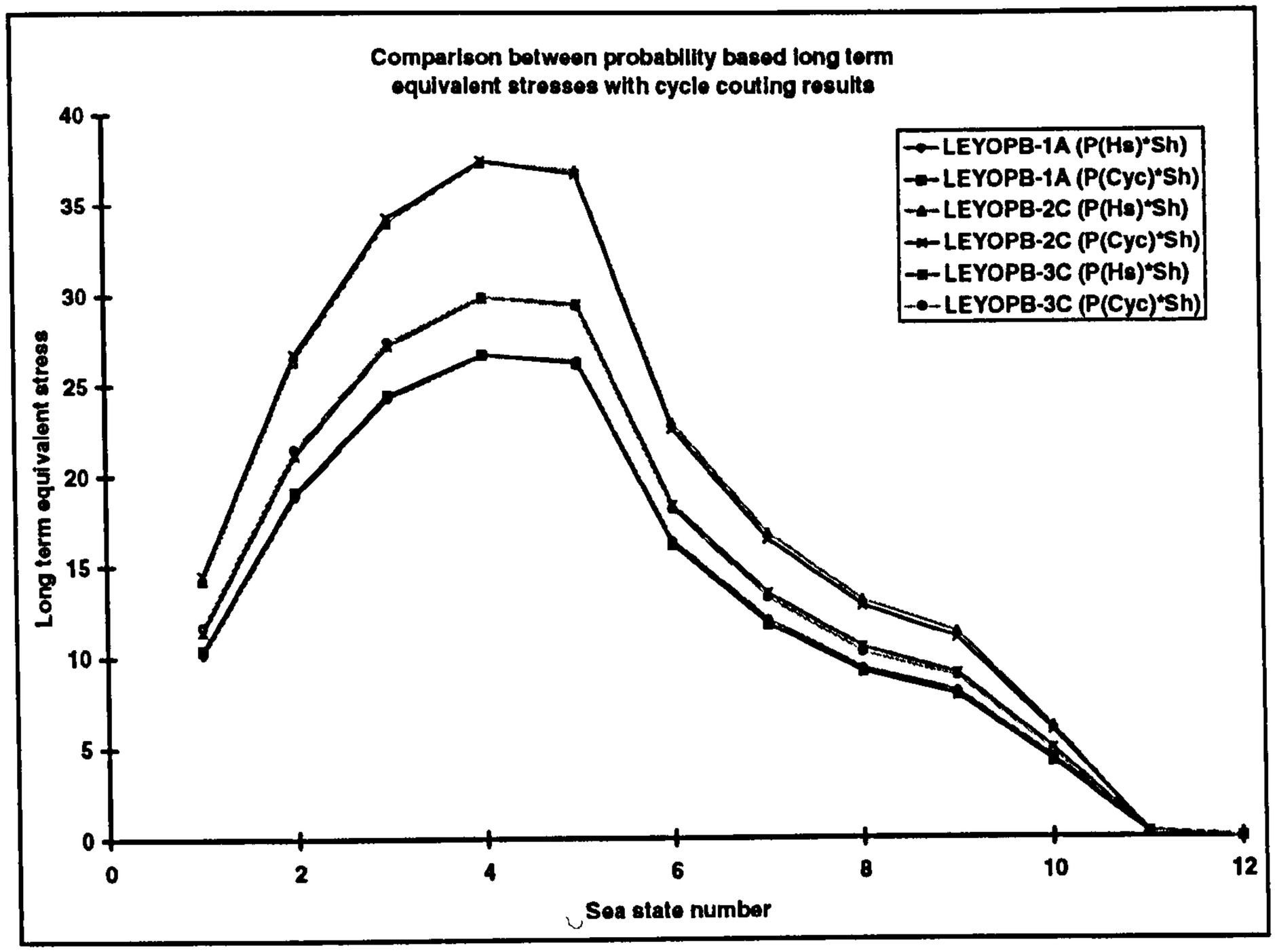

Figure 5.11: Comparison of probability and cycle counting methods for calculating S_h

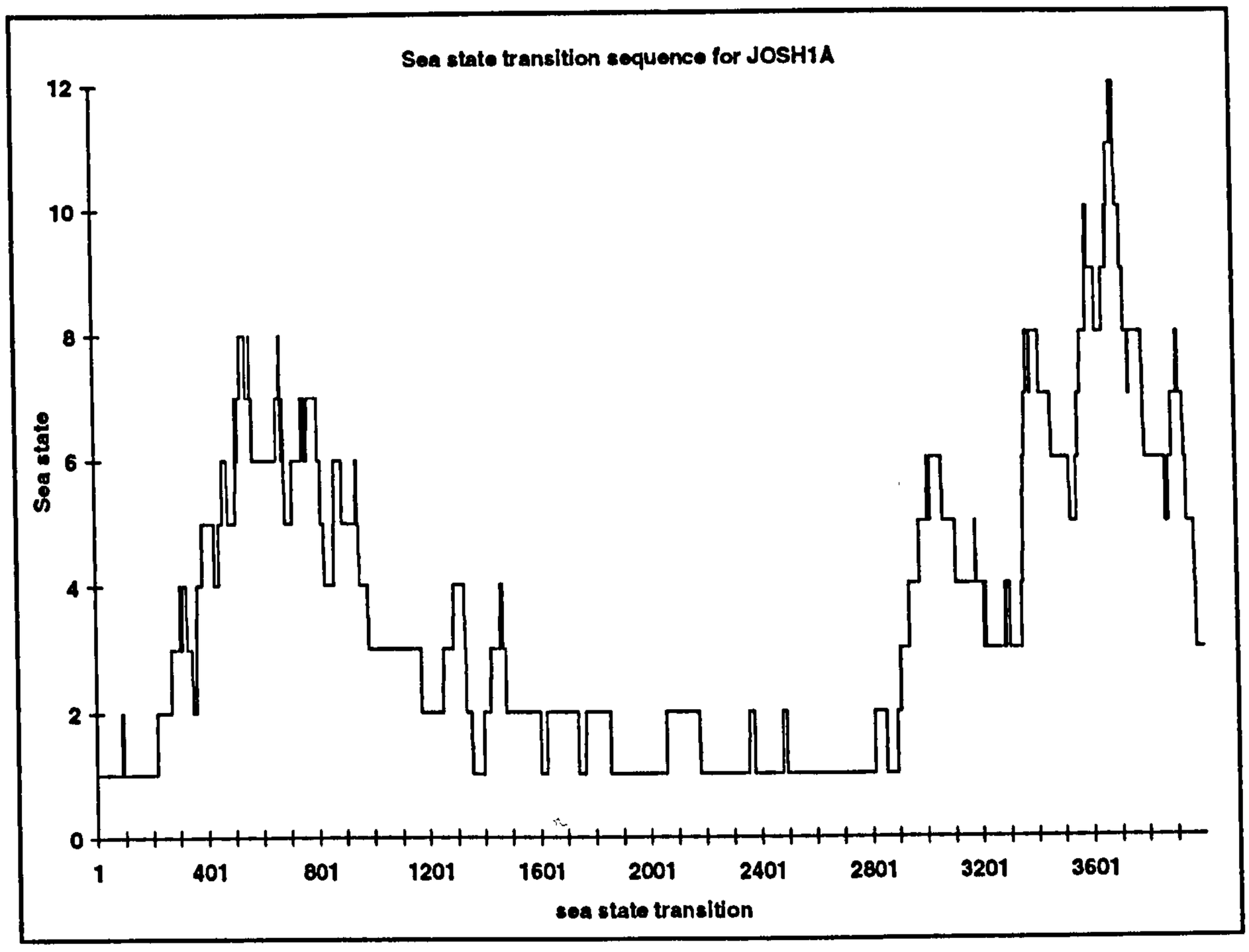

Figure 5.12: Sea state transition sequence for JOSH1A

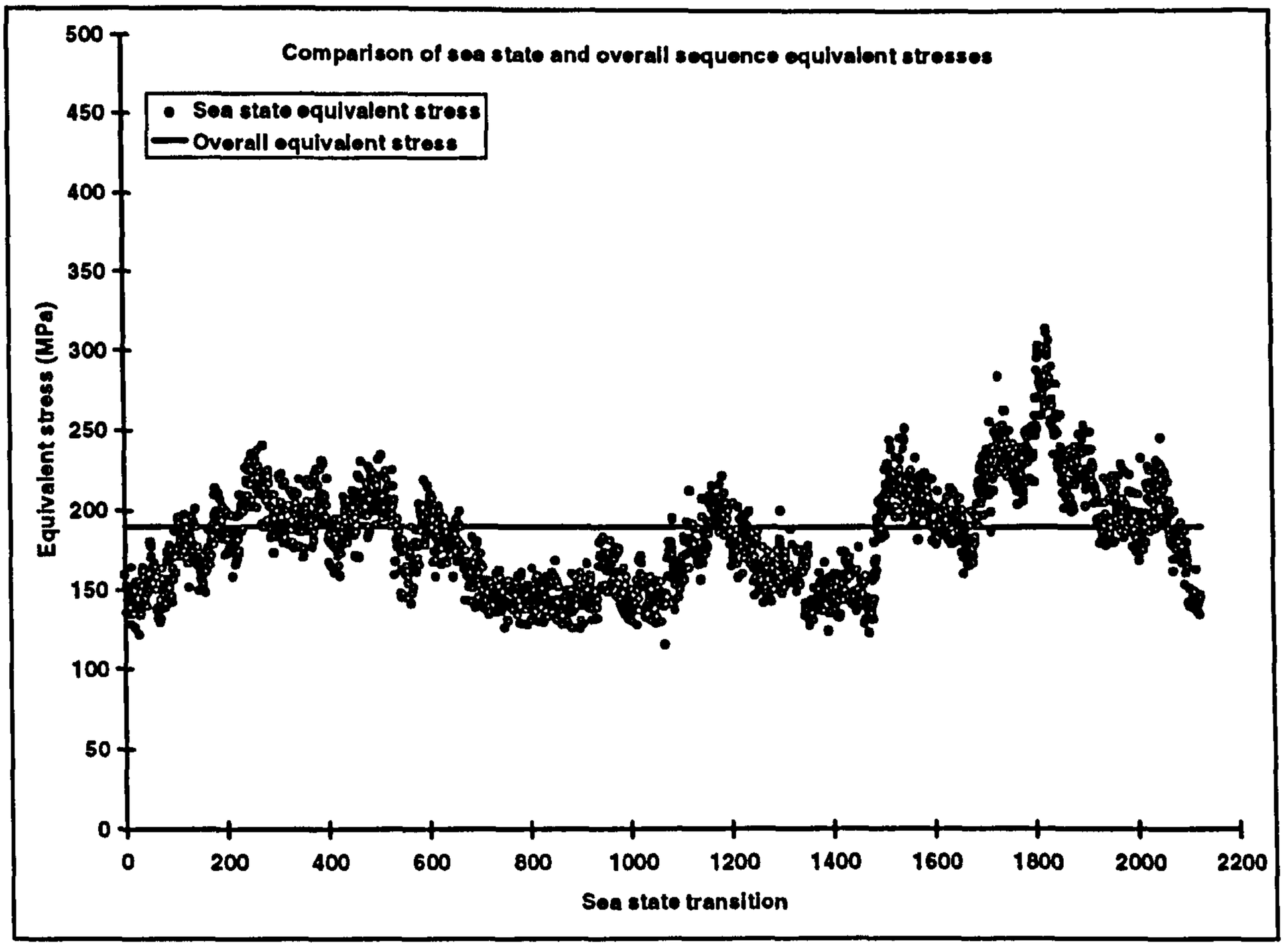

Figure 5.13: Comparison of overall and sea state equivalent stresses for LEYOPB1A

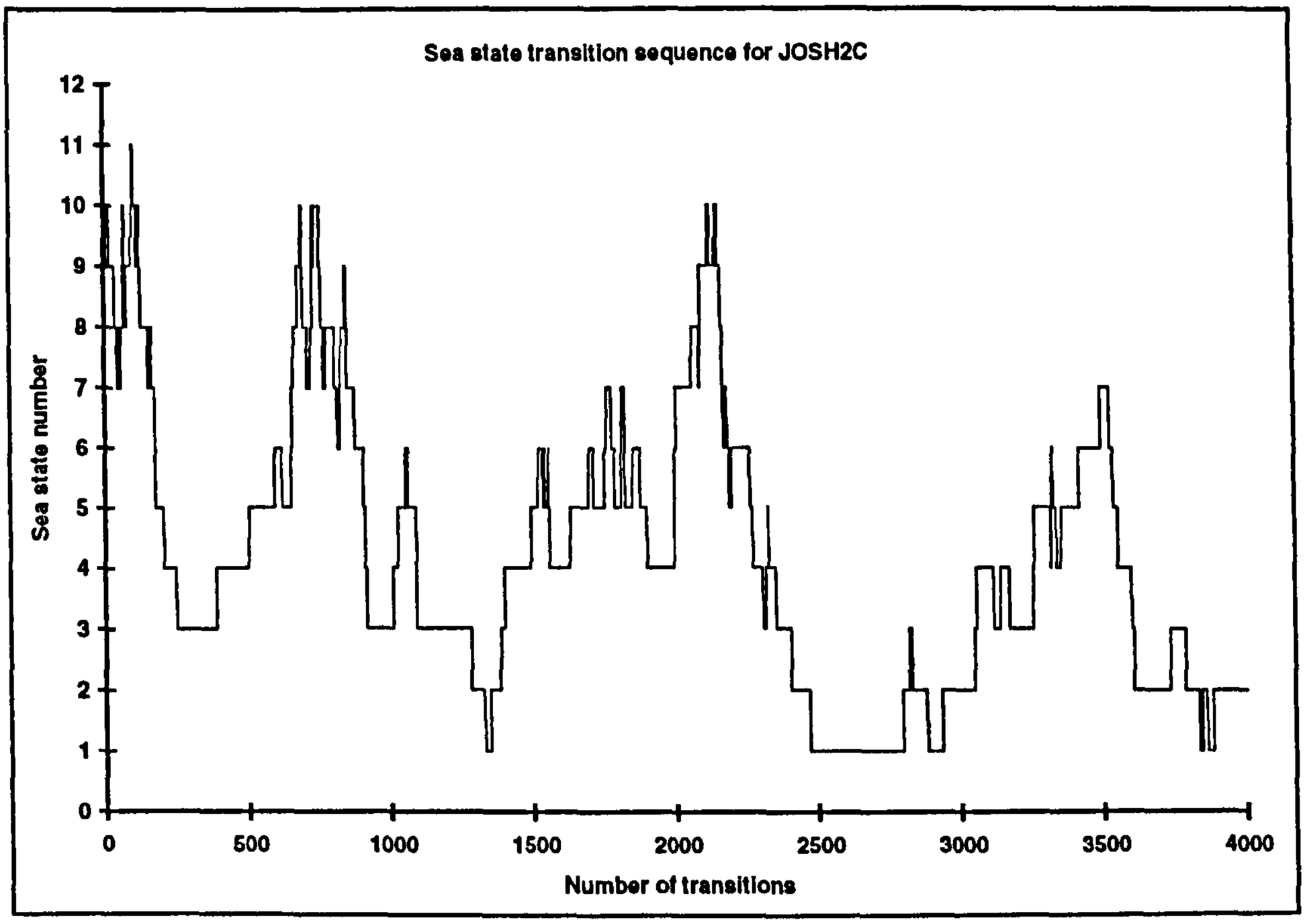

Figure 5.14: Sea state transition sequence for JOSH2C

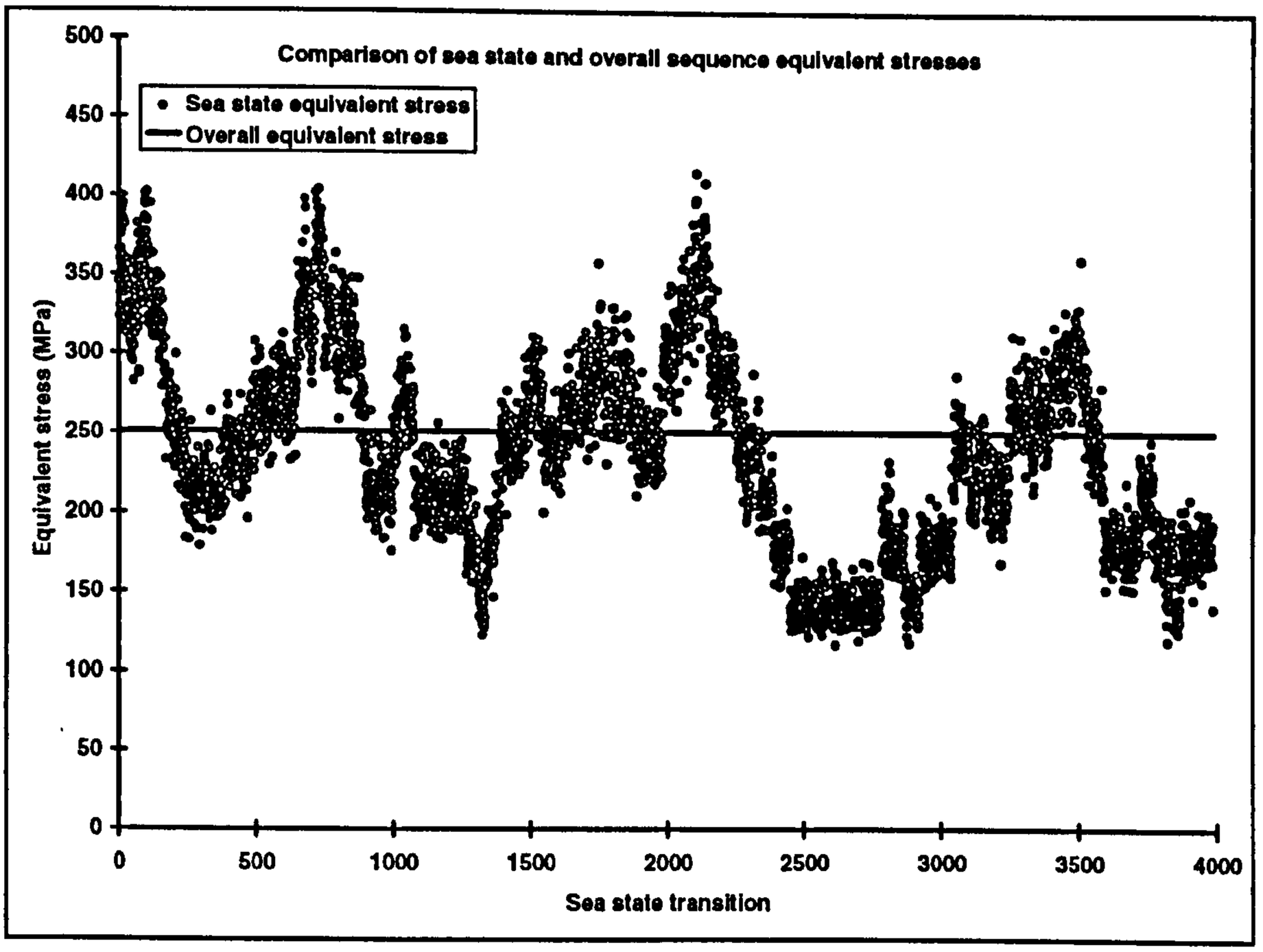

Figure 5.15: Comparison of overall and sea state equivalent stresses for LEYOPB2C

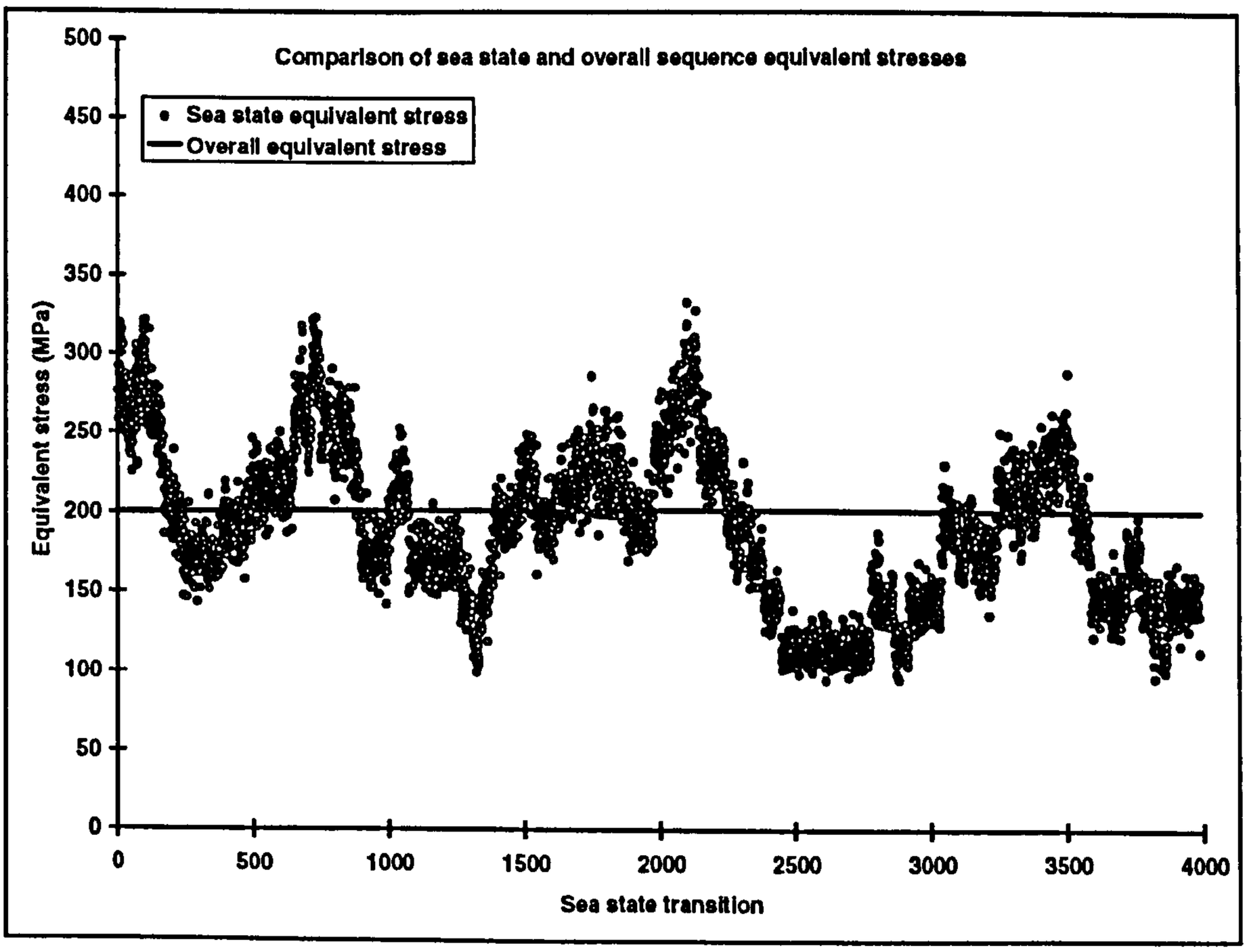

Figure 5.16: Comparison of overall and sea state equivalent stresses for LEYOPB3C

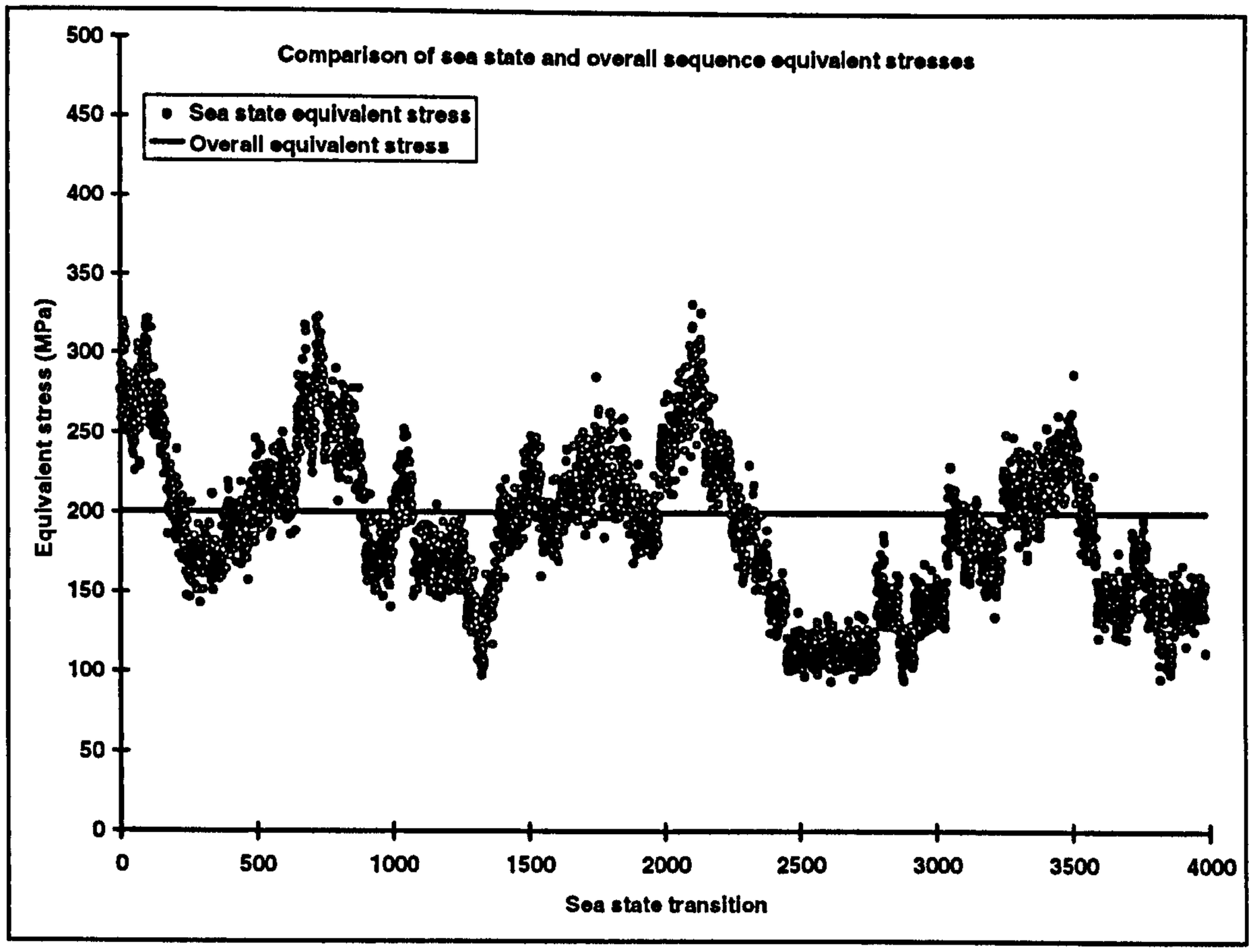

Figure 5.17: Comparison of overall and sea state equivalent stresses for LEYOPB4C

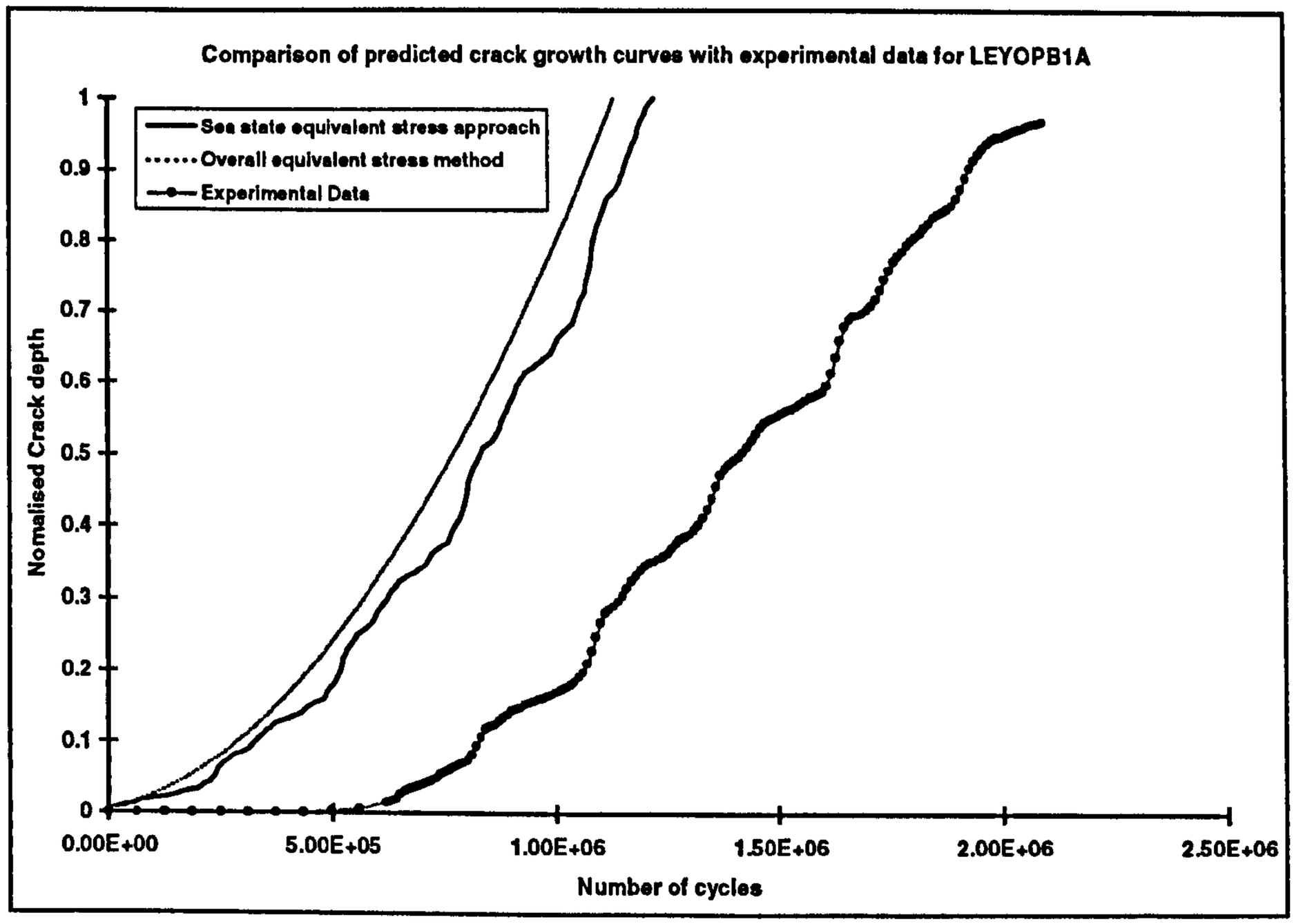

Figure 5.18: Comparison of prediction methods without consideration for crack initiation period

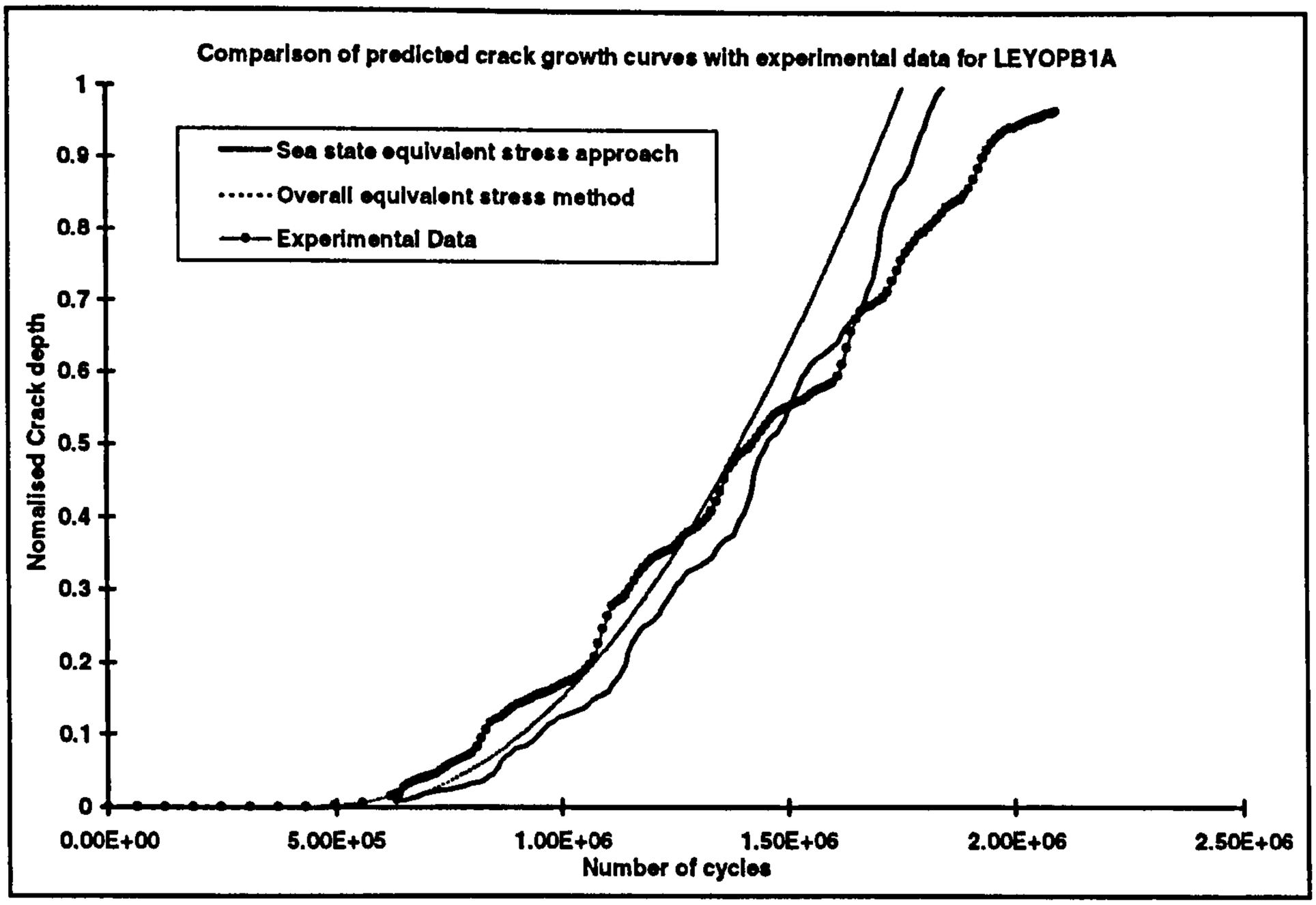

Figure 5.19: Prediction with consideration for initiation -no correlation for initiation point

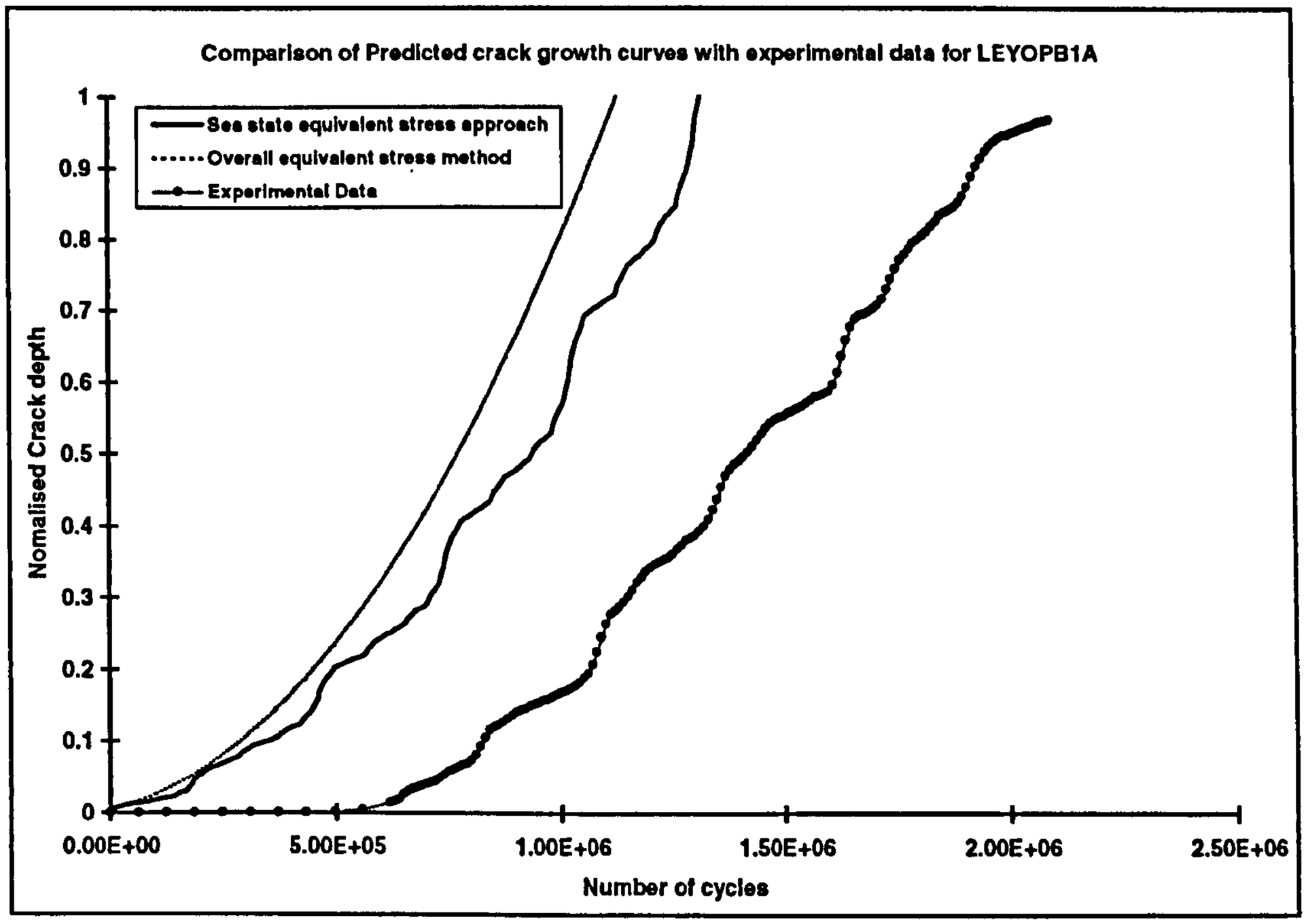

Figure 5.20: Prediction without consideration for crack initiation- correlated initiation point

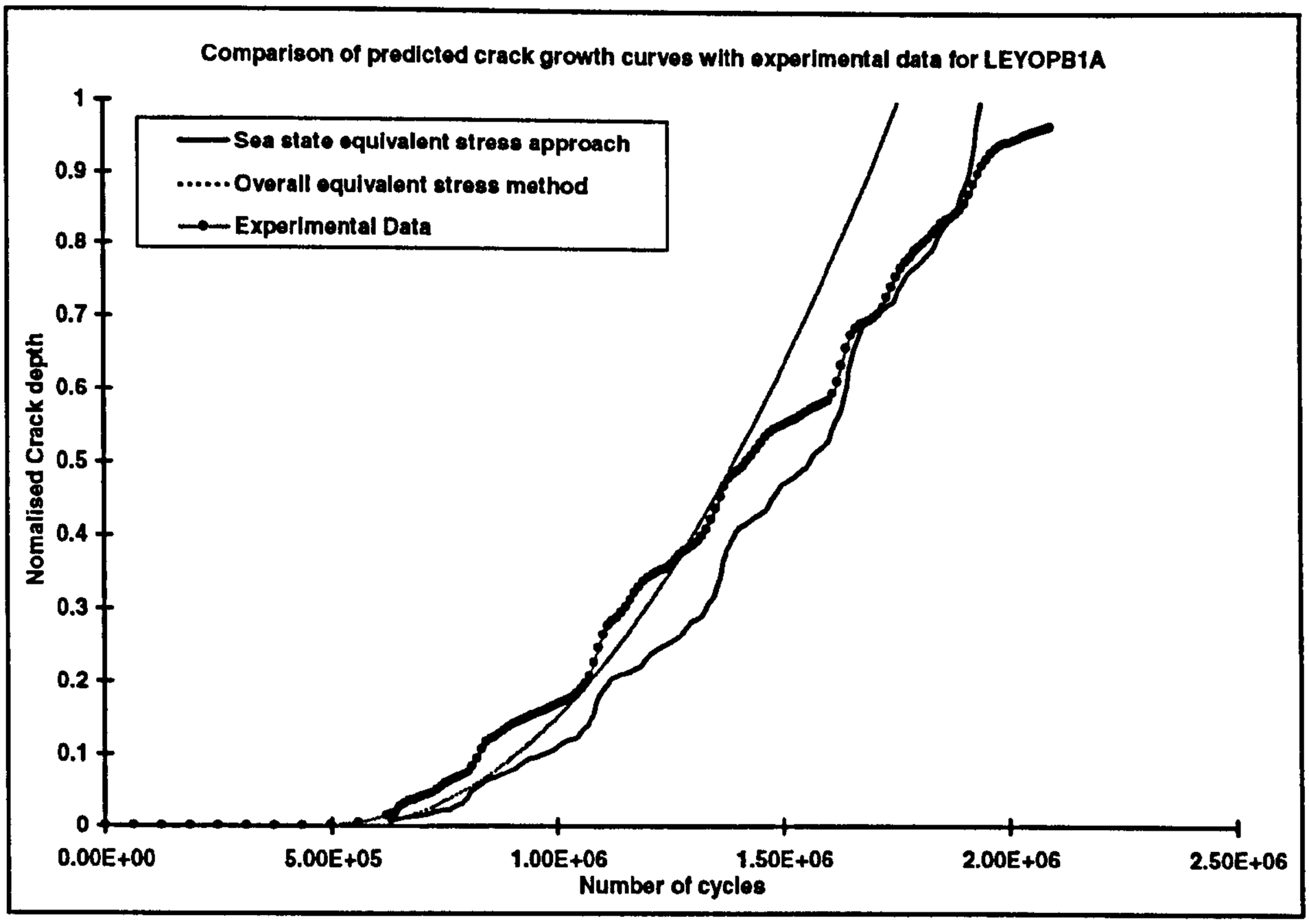

Figure 5.21: Prediction with consideration for initiation and correlated initiation point

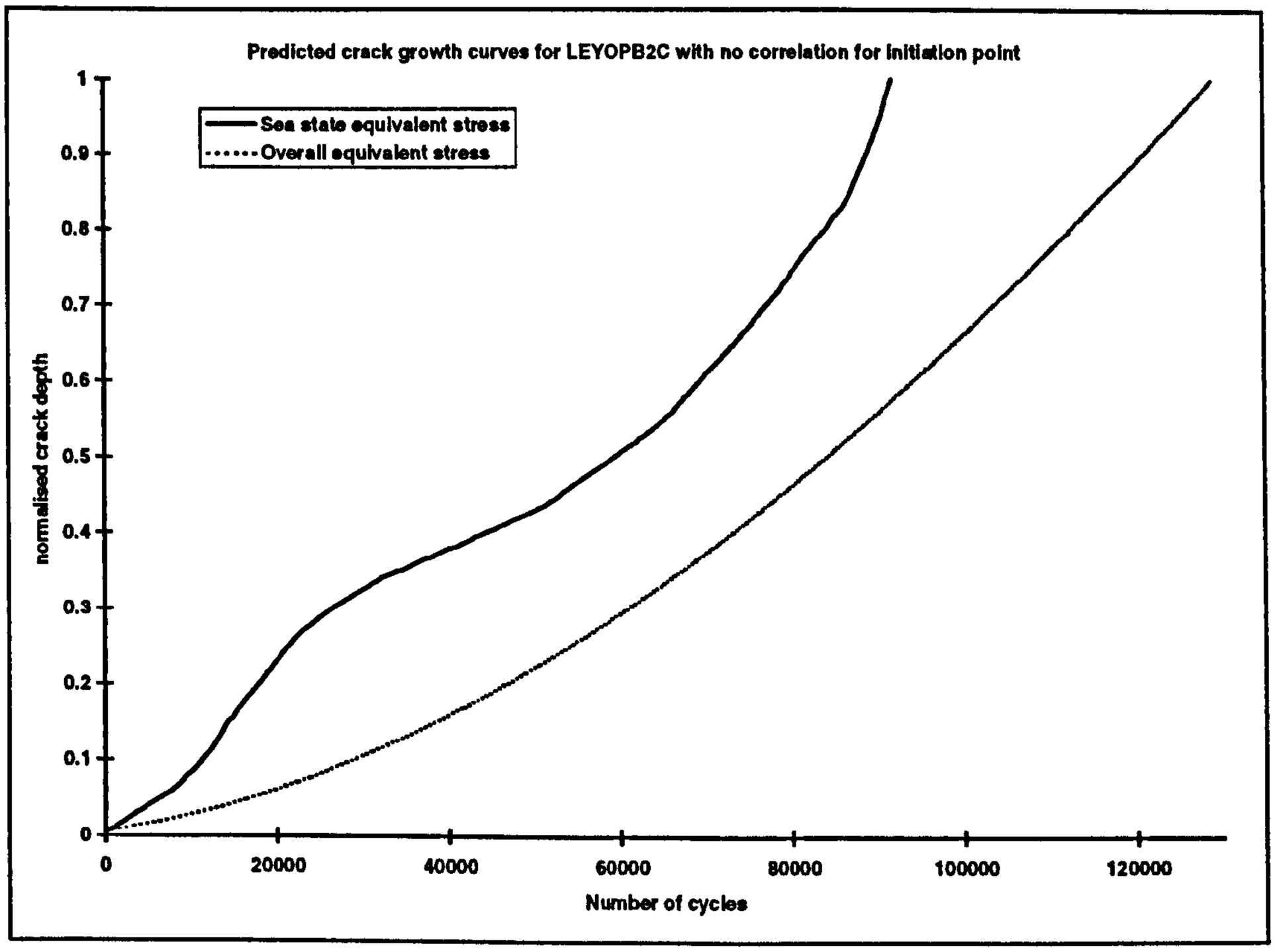

Figure 5.22: Predictions for LEYOPB2C without correlating initiation point

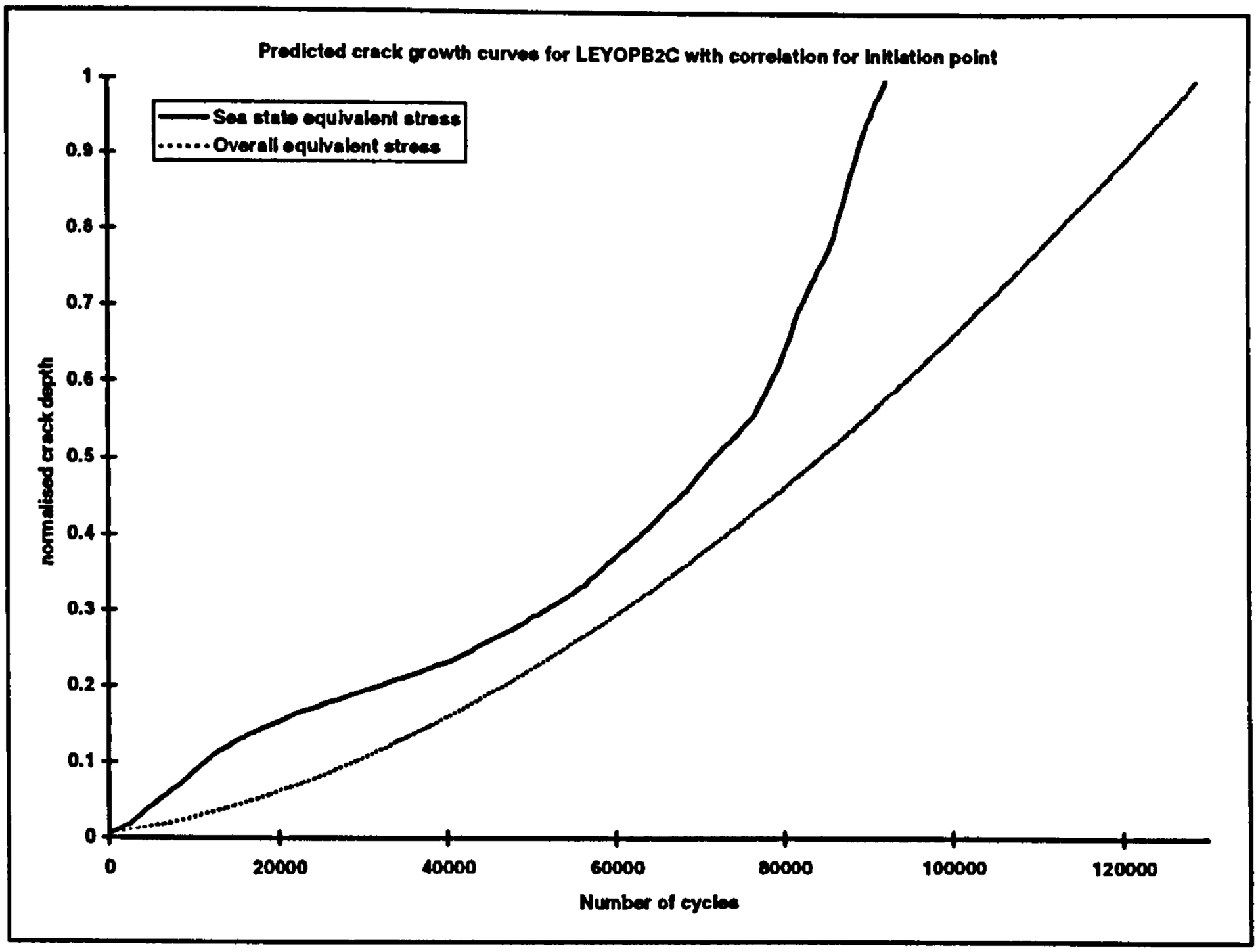

Figure 5.23: Predictions for LEYOPB2C with correlated initiation point

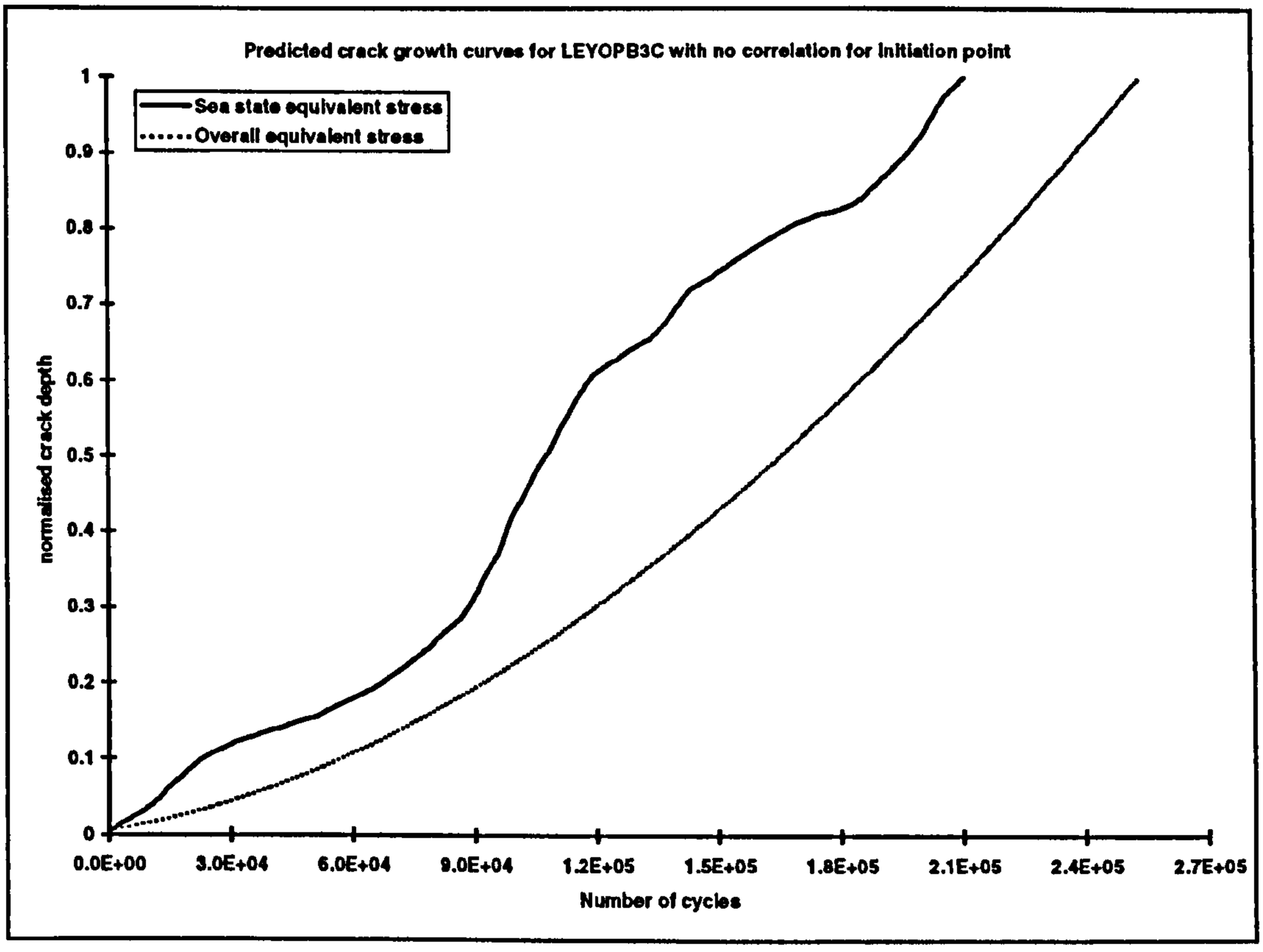

Figure 5.24: Prediction for LEYOPB3C without correlating initiation point

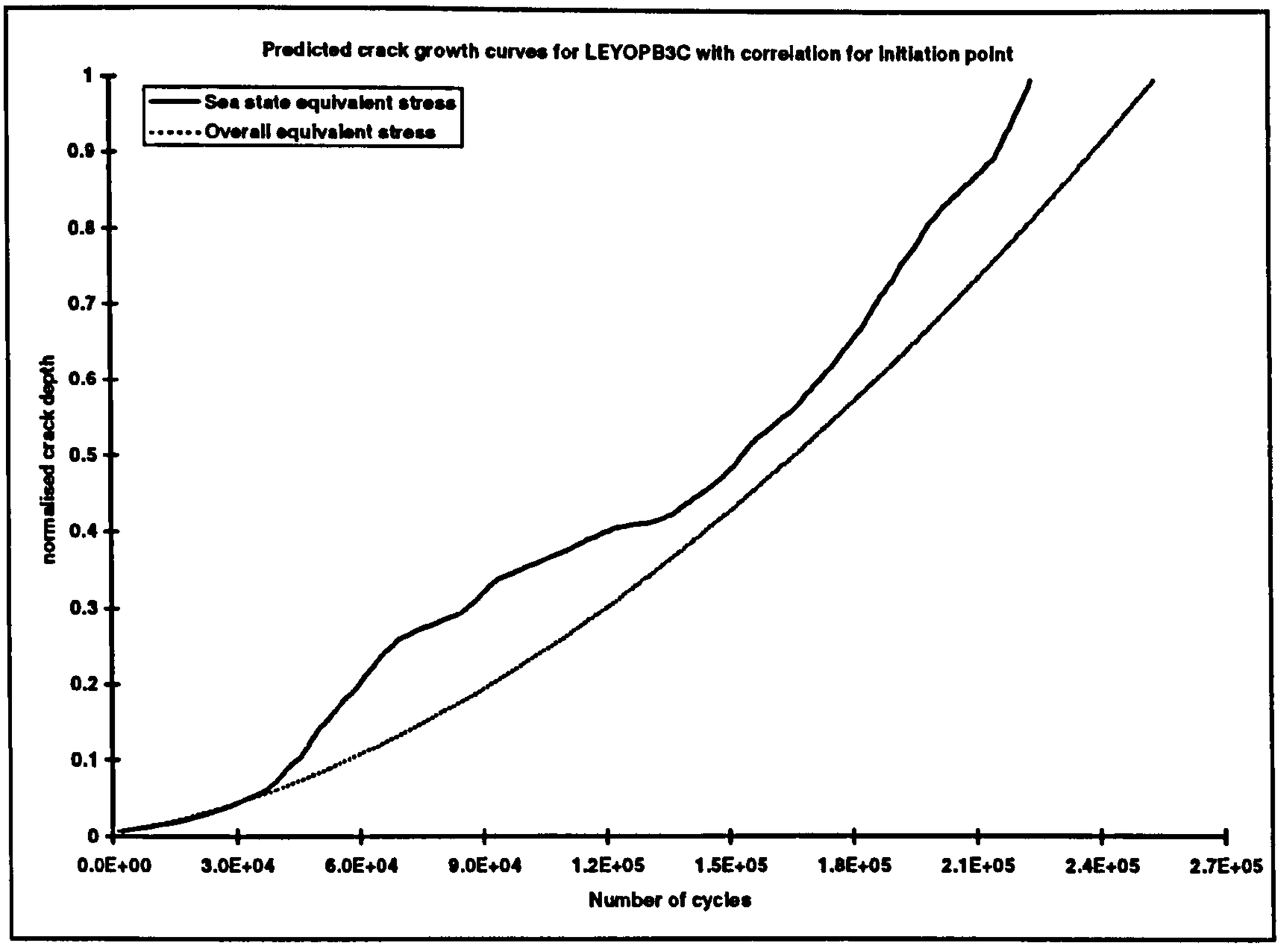

Figure 5.25: Predictions for LEYOPB3C with correlated initiation point

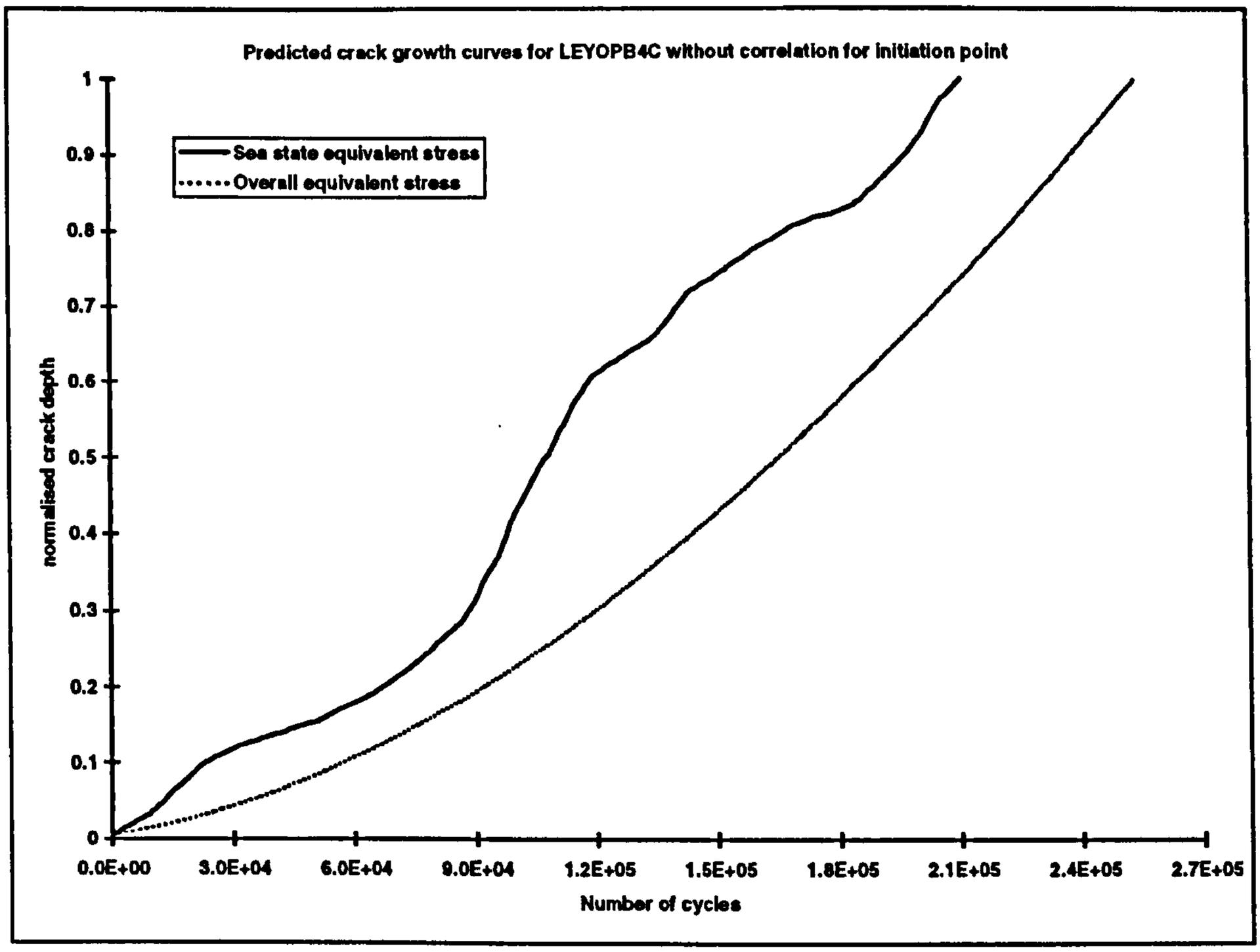

Figure 5.26: Predictions for LEYOPB4C without correlating initiation point

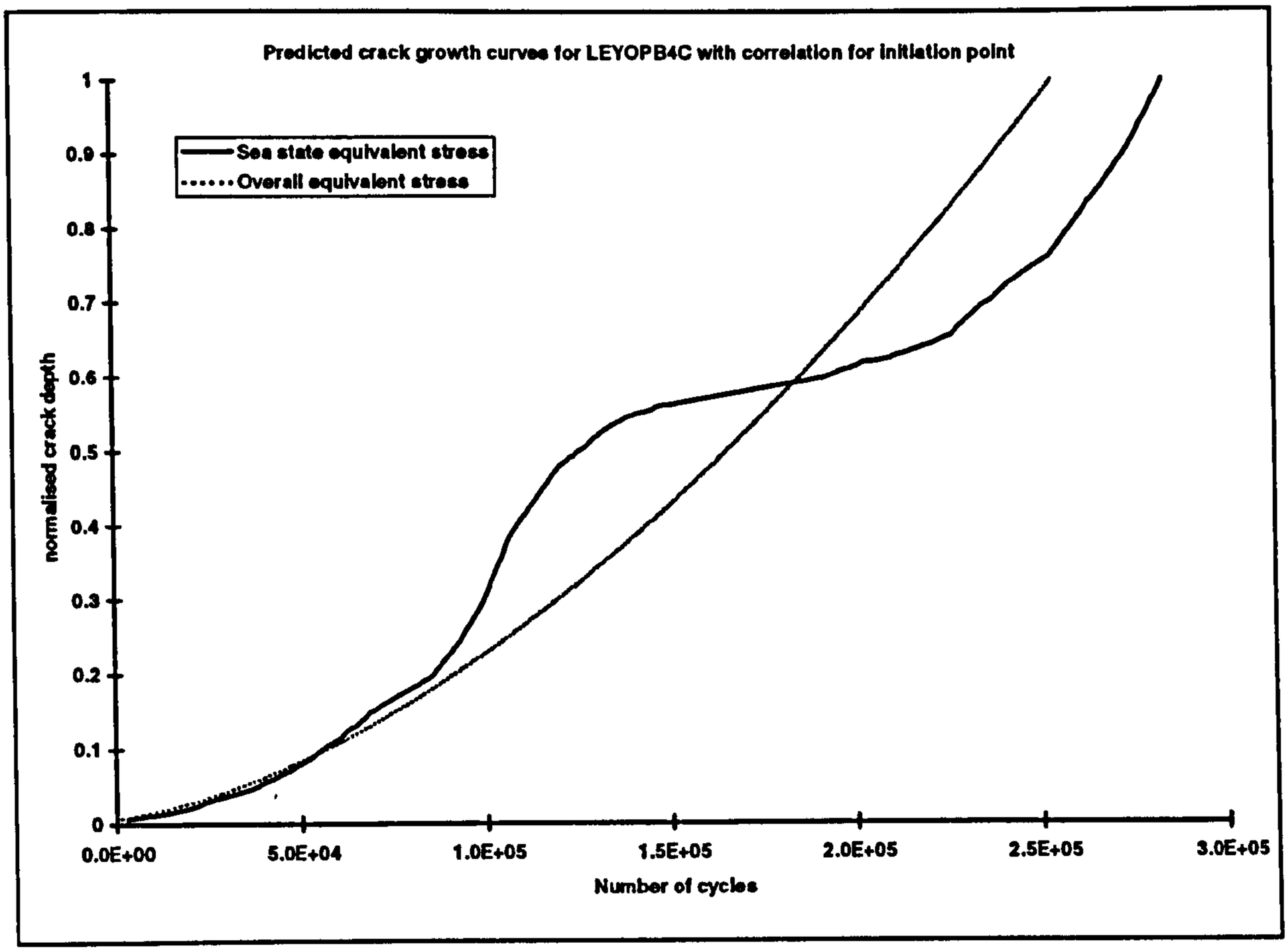

Figure 5.27: Prediction for LEYOPB4C with correlated initiation point

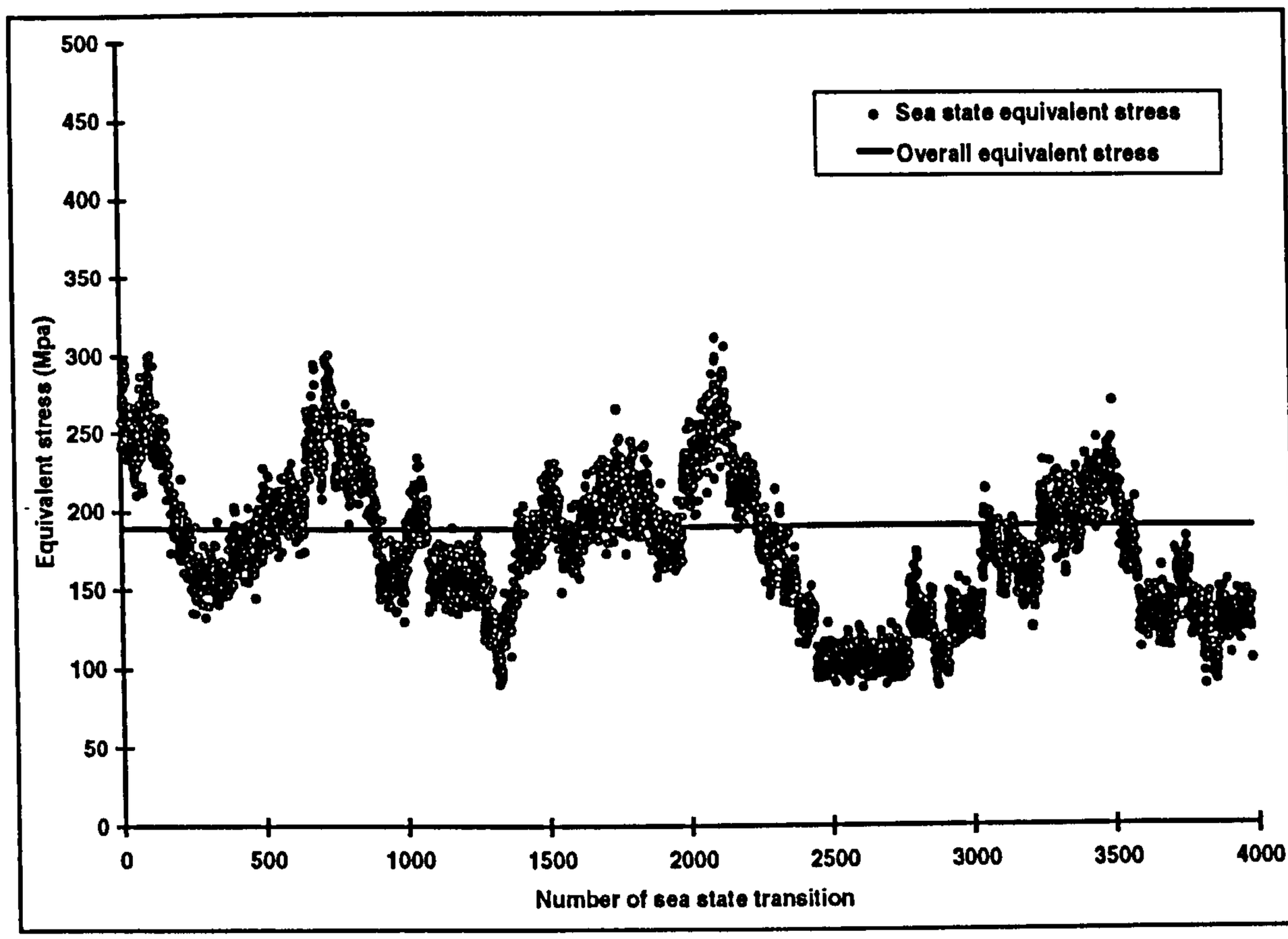

Figure 5.28: Comparison of overall and sea state equivalent stresses for JOSH2C (based on parameters for test LEYOPB1A)

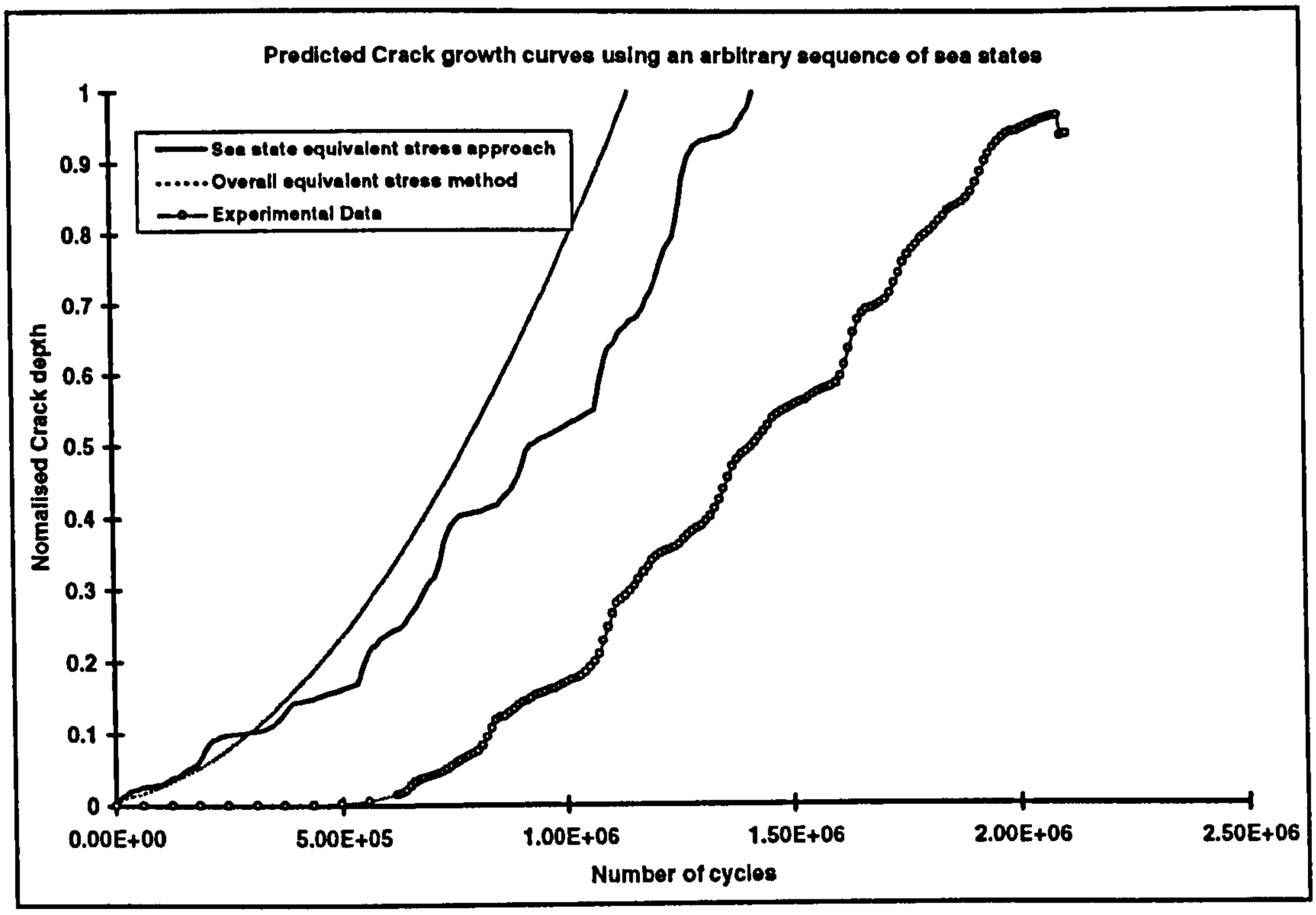

Figure 5.29: Comparison of prediction methods without correlating initiation point in an arbitrary sequence (JOSH2C)

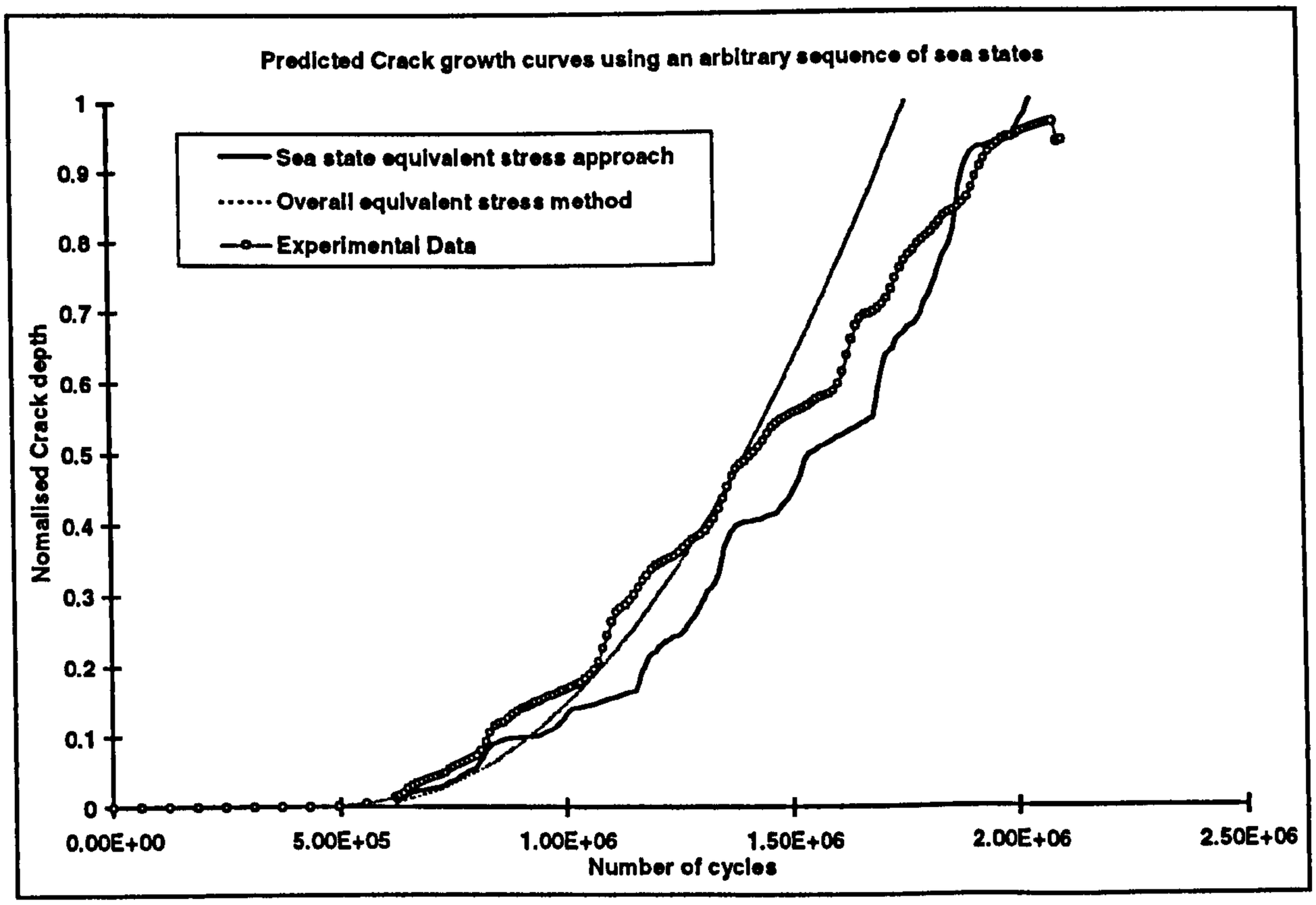

Figure 5.30: Comparison of prediction methods with consideration for initiation and correlated initiation point in an arbitrary sequence.

CHAPTER 6

6. CONCLUSION OF THESIS

6.1 SUMMARY OF THESIS

This thesis has presented results of an investigation undertaken to assess the performance of a typical high strength weldable Jack-up steel under realistic loading and environmental conditions. Details of the methodology employed to develop a typical Jack-up Offshore Standard load History (JOSH) have been presented.

Results and details of experimental variable amplitude corrosion fatigue (VACF) tests conducted using JOSH have been presented and discussed with respect to results obtained from other high strength steels and conventional fixed platform steels. Different fracture mechanics models for VACF crack growth prediction have also been compared in terms of the accuracy of predicted Y factors. An improved methodology for fast assessment of Offshore structural welded joints has been proposed and a sea state equivalent stress concept formulated.

The following sections present the main conclusions drawn from this study. Areas of further work which will contribute to the general body of knowledge in this field are also identified.

6.2 CONCLUSIONS AND RECOMMENDATIONS

One of the main objectives of this study was to simulate service loading on a typical Jack-up platform. This was successfully achieved by use of a representative Jack-up transfer function which was validated by use of service data obtained from a Jack-up platform operating under service conditions. A sensitivity analysis carried out suggests that Jack-up response is very sensitive to water depth. As a result of this sensitivity it was concluded that there are difficulties associated with producing a single load history that can be considered to be representative of all service loading conditions for Jack-ups operating in different water depths and locations. However most operating sites in practice cover extensive areas of similar water depth. For these reasons, the JOSH model provides a suitable frame work for generating any representative service load history applicable to all sites within a range of water depths. In this regard a fast assessment approach has been proposed based on results

obtained from this study which is expected to eliminate the lengthy analysis procedure normally required to generate the load PSDs for Offshore structures. This approach relies on the use of non dimensional parameters to describe the normalised stress PSD of any particular structure for any set of sea states.

The results obtained from the large scale fatigue testing programme on SE 702 under simulated loading and environmental conditions are very encouraging. The fatigue life results suggest that tubular joints fabricated from SE 702 are at least as good as conventional fixed platform steels. Under cathodic protection conditions, the results show that an increase in the cathodic protection level from $-800mV$ to $-1000mV$ may lead to a reduction in fatigue life by up 30%.

There was no evidence to suggest that SE 702 is more susceptible to corrosion fatigue in the presence of hydrogen produced under cathodic protection conditions than other high strength steels of similar grade. There was an apparent trend showing a potential for better performance with longer fatigue lives at lower stress levels. This implies that the existing slope of -3 for the T' curve may not be applicable to high strength steels.

On the whole, the results from the investigation presented in this thesis suggest that there may be advantages to be gained by using high strength steels but further tests at lower stress levels need to be performed to confirm any existing trends. The existence of a more negative slope for the design curve for example will have wide implications on inspection scheduling for high strength steel installations. This will lead to a reduction in operational costs especially for Jack-ups used as production platforms. Jack-up structures used for short term drilling operations may be designed with less safety margins when compared with those used for long term operations. The added significance of these results is that, with a better understanding of high strength Jack-up steels under realistic loading and environmental conditions, it will be possible to narrow down these safety margins during the design process. It is recommended that further fatigue tests be carried out on SE 702 and other high strength steels to quantify the benefits associated with their use Offshore. These further tests are

required so that any trends in the fatigue performance of high strength steels can be clearly defined and quantified for incorporation into a suitable design guidance.

After comparing existing fracture mechanics models with experimental results, the inherent limitations of the models when applied under variable amplitude loading conditions have been identified. It was noted that the average experimental Y factor curve lies below the curves predicted by the existing solutions. Based on this observation it can be concluded that there may be other important factors which affect crack propagation under variable amplitude conditions which may have been ignored in previous models. A new Y factor model has been proposed which accounts for important factors such as the crack shape evolution (crack aspect ratio), geometry and mode of loading. Its semi-empirical nature may however introduce a certain degree of uncertainty when applied to other joint geometries. Its performance on other joint geometries therefore needs to be checked with further experimental data obtained from tests conducted under realistic loading conditions. More accurate and reliable crack growth prediction in high strength steels will have significant implications on the safety and reliability of production Jack-ups. These structures are more susceptible to long term fatigue problems when compared with Jack-ups used as mobile drilling units with the possibility of dry dock inspection. Inspection scheduling for production Jack-ups is therefore an important aspect in the risk reduction and safety enhancement process required for their reliable operation. It is especially in this area that some of the models developed as results of this study can be used as tools for the assessment of high strength steel offshore installations to enhance safety and structural reliability.

A generalised fracture mechanics approach for the assessment of fatigue crack growth in Offshore installations has been proposed. This model relies on the use of a sea state probability distribution function which has been verified with service data. However the data used in the development of the model was obtained from specific regions of the North Sea. In order to increase confidence in the use of this model and reduce the level of uncertainty associated with its use, it is important to check its accuracy against further service data from different locations. This will help in establishing the validity of using the proposed probability distribution model to analyse structures at different locations other than the North Sea region.

A sea state equivalent stress concept has been mathematically formulated for the first time and used to predict fatigue crack growth in a typical high strength Offshore steel. This approach has been shown to have certain advantages over the conventional overall equivalent stress range approach, one of which is the potential to model sea state interaction effects. It can also be used for more accurate inspection scheduling and also for the structural reliability analysis after an inspection schedule to ensure a high level of safety.